UNIVERSIDAD COMPLUTENSE DE MADRID
FACULTAD DE FARMACIA

TESIS DOCTORAL

Synthesis, biophysical and biological evaluation of N -phenylbenzamide derivatives targeting the mitochondrial DNA of kinetoplastid parasites

Síntesis, evaluación biofísica y biológica de derivados de N-fenilbenzamida dirigidos al ADN mitocondrial de parásitos cinetoplástidos

MEMORIA PARA OPTAR AL GRADO DE DOCTOR

PRESENTADA POR

Jorge Jonathan Nué Martinez

Directores

Christophe Dardonville
Alicia Gómez Barrio

Madrid

UNIVERSIDAD COMPLUTENSE DE MADRID
FACULTAD DE FARMACIA

DOCTORAL THESIS

Synthesis, biophysical and biological evaluation of *N*-phenylbenzamide derivatives targeting the mitochondrial DNA of kinetoplastid parasites / Síntesis, evaluación biofísica y biológica de derivados de *N*-fenilbenzamida dirigidos al ADN mitocondrial de parásitos cinetoplástidos

THESIS SUBMITTED FOR THE DEGREE OF DOCTOR OF PHYLOSOPHY

PRESENTED BY

Jorge Jonathan Nué Martinez

SUPERVISORS

Christophe Dardonville, PhD.
Alicia Gómez Barrio, PhD.

Acknowledgements / Agradecimientos

I really wish to thank the following people because I would not be where I am now without their help, support and friendship. Firstly, I would like to thank Dr. Christophe Dardonville for allowing me to rejoin his group after an amazing master year and, especially, for his invaluable advice, support and enthusiasm over the years. You may have wished that I spent more time in the lab and less time doing networking Fridays, but this thesis is a testament to the freedom you gave me to pursue my own interests in science. Thank you!

Me gustaría agradecer de forma muy especial a "las chicas de la complu". Primero a mi codirectora Alicia, por estar siempre atenta y dispuesta a ayudarme con la burocracia, por su buen hacer y sus ánimos para seguir siempre adelante. A Cristina y Sandra, por ser tan activas y colaboradoras, por trabajar con pandemia, nieve o incluso en navidades, muchas gracias por todo.

I wish to thank Dr. Isabel Rozas and Cristina Trujillo, for all the support and patience in organizing and planning the stay in Dublin. Despite the COVID and all the situations I finally manage to be there and learn from you both. Thanks to all the people I met, specially mentions to Nikolina, Helene, Danielle, Lorenzo, Pierre (not French), Ian and from the bottom of my heart to Iñigo for make me feel at home.

I would also want to thank Dr. Harry de Koning and his research group, for the biological evaluation of the compounds. Thank you for your dedication and patience in the review of the manuscript.

También me gustaría agradecer a las Dras. Lourdes Campos y Nuria Saperas por enseñarme el maravilloso mundo de la cristalografia. Quiero agradecer a Lourdes por dedicarme innumerables fines de semana, gracias por todo lo compartido, realmente aprendí muchas cosas, no solo de ciencia. A Nuria quiero agradecerle el estar siempre pendiente. A todos los chicos del laboratorio, especialmente a Hamidreza, Jordi, Brenda, e Irene, por recibir a "Jordi el peruano". Moltes gràcies!

Una mención especial también para la Dra. Ana González sin cuya ayuda no habría sido possible el capítulo de nanopartículas, que guerra te he dado Ana, muchas gracias por todo.

To Dr. Godwin Ebiloma, for his kindly support not only in the evaluation of compounds but also in planning future experiments.

A Francisco Gamarro e Ignacio Manzano por su invaluable apoyo en la evaluación biológica de los compuestos.

A la Dra. Laura Lagartera por la realización de los ensayos de SPR y al Dr. Tomás Herraiz por su apoyo para el Desarrollo de esta tesis.

Al grupo del Dr. Carlos González del IQFR-CSIC, de manera muy especial al Dr. Miguel Garavís por su apoyo en la realización de los experimentos de RMN del compuesto 3a. También mencionar a Cris e Isra, por su ayuda muchas veces en el laboratorio.

Como no mencionar a todas las personas que han pasado por el IQM, 4 años da para conocer a mucha gente. Me gustaría agradecer de manera especial a los miembros de mi grupo de investigación: Vicente Arán, Maite Molina, Eduardo, Ramón, Rebeca, Tania, Valle, Marianne, Teresa, Román, Valentina, Rejanne, Sergio, Miguel, Hristo y finalmente a Damien Kraeutler por su invaluable apoyo con la medición de los pK_{as} y David Cisneros, por su pasión en la investigación, por su ayuda constante y por ser tan buen compañero de labo, creo que tuve mucha suerte de teneros a cada uno de vosotros en el momento indicado. También mencionar a Carlos Rios y Paco Fueyo, porque aprendí mucho de vosotros, y de Paco también tuvimos mucha suerte de compartir las noches de Madrid.

Me gustaría agradecer también a las personas con las que he podido compartir durante estos 4 años, de manera muy especial a Cristina Martin, Marta Gargantilla, Jessy, Ma. Angeles, Marta Leo, Eva, Maxime, Carolina, Olia, Sonia, Ana, Dani, Miguel, Jesús, Aitor, Chema, Rocio, Carlos, Kike, Rocio (Salamanca), Laura, Javi, Alba, Julia, Natalia, Angela.

(Teresa, Rosalva y Rosalvita), gracias por acogerme con tanto cariño, nunca olvidaré mi estancia en México, ni la plaza Garibaldi.

No quiero terminar sin agradecer a otra parte de mi familia, la que Dios me regalo, mi familia parroquial, esa que hace que uno se sienta en casa esté donde esté. Gracias al P. Santiago que motive mi inquietud sobre España y a Jorgito, que siempre estuvo apoyándome y sé que continuas haciéndolo. Gracias a, Chema, Esteban, Graciela, Carlos, Keyla, Victor y todos los demás miembros de la comunidad, me habéis hecho sentir en casa durante toda mi estancia en Madrid. Y a todos los miembros de la Fraternidad del Diaconado Permanente de Madrid, especialmente a Orlando y D. Javier.

Finalmente, deseo agradecer a las personas más importantes en la vida, mi familia: mis padres Jorge y Maria, por su apoyo constante y ánimo para crecer cada día. A mi hermana, que he tenido la suerte de compartir con ella estos últimos meses, como cuando éramos peques. A Mary la he dejado al final, porque todo esto ha sido posible gracias a que ha estado conmigo, en toda la amplitud de la palabra, gracias por apoyarme, ayudarme, animarme y sobre todo soportarme (que no debe ser cosa fácil) gracias por estar a mi lado y ser mi apoyo. Y a Fede, que siempre me espera alegre al volver a casa.

A todos y cada uno de vosotros, quiero expresaros mi gratitud.

A Dios, por todo, siempre.

A mis padres Jorge y Maria, por todo su amor y esfuerzo, por todo lo que la distancia ha significado.

A Mary, mi esposa, por ser mi amor, compañera y cómplice.

"The first gulp from the glass of natural sciences will turn you into an atheist, but at the bottom of the glass God is waiting for you."

Werner Karl Heisenberg
Nobel prize in Physics.

"Nothing in life is to be feared, it is only to be understood."
Marie Curie.
Nobel Prize in Physics and Chemistry.

Synthesis, biophysical and biological evaluation of *N*-phenylbenzamide derivatives targeting the mitochondrial DNA of kinetoplastid parasites

Introduction

Kinetoplastid parasites are responsible for three most common and neglected vector-borne human diseases, which are the focus of this Thesis: leishmaniasis*,* which is caused by *Leishmania spp.*, human African trypanosomiasis caused by *Trypanosoma brucei spp.*, and Chagas disease caused by *Trypanosoma cruzi*. All of them display high morbidity and mortality rates mainly in developing countries.

Kinetoplastid parasites are characterised by the presence of a disk-shaped mitochondrial DNA, named as "kinetoplast DNA" (kDNA), comprising > 70% AT base pairs. Kinetoplastid cell shapes change during the complex differentiation processes that occur in their life cycles. These differentiations are key to the successful transfer of the parasite between vector and host, and vice versa.

Despite the social and economic burden of kinetoplastid diseases, the chemotherapeutic arsenal to treat them remains underdeveloped. Hence, there is an urgent need for new safe antitrypanosomal and leishmanicidal treatments.

Previous studies showed that dicationic bisguanidine and bis(2-aminoimidazoline) compounds are DNA minor groove binders (MGB) selective for AT-rich DNA sequences. In particular, the *N*-phenylbenzamide bis(2-aminoimidazoline) lead compound **I** showed 100% curative activity by oral dosage in a mouse model of acute *T. b. rhodesiense* infection. In contrast, this compound was mostly inactive against the intracellular parasites *T. cruzi* and *Leishmania*.

Since compound **I** is an excellent DNA MGB with proven *in vivo* efficacy and kDNA is a common target of *T. brucei*, *T. cruzi* and *Leishmania*, this Thesis work aimed at optimizing the biological activity of compound **I** towards the endoparasites *Leishmania* and *T. cruzi*.

Objectives

The main goal of this research was to discover new kDNA-targeting compounds active against the kinetoplastid parasites *Leishmania, T. cruzi*, and *T. brucei*.

The objective was to prepare three families of dicationic compounds having the common *N*-phenylbenzamide scaffold of lead compound **I**, which is known to interact favourably with the minor groove of kDNA. Different chemical modifications of this scaffold were tested to improve the membrane permeability, and hence, the anti-*T. cruzi* and leishmanicidal activity of the new molecules.

The antiprotozoal activity of the new compounds was evaluated *in vitro* and the unspecific cytotoxicity towards mammalian cells was tested to calculate the selectivity indexes (SI). The DNA binding affinity, sequence selectivity and binding mode of the new compounds was assessed carefully using different biophysical techniques (Surface Plasmon Resonance (SPR), circular dichroism (CD), flow linear dichroism (LD), UV-Vis titrations, ^{1}H-Nuclear Magnetic Resonance (NMR), crystallization and X-ray diffraction) and computational studies. Finally, nanostructured lipid carriers (NLC) loaded with compound **3a** were synthesised as drug delivery strategy to improve its leishmanicidal activity.

Results

Seven bis(imidazolidin-2-imine) analogues (**1b–h**) were synthesised in two steps from dianiline precursors using di-*tert*-butyl 2-thioxoimidazolidine-1,3-dicarboxylate (**5**). Thermal melting experiments and SPR-biosensor assays showed that these compounds bind selectively to AT DNA sequences. The presence of induced CD and LD signals upon titration with (AT)$_4$-containing DNA (**1b–h**) and unspecific DNA (i.e., compound **1e**) showed that the compounds are MGB. This series showed micromolar range activity against *T. brucei* (5.71 to 78.5 μM) with SI from 1.3 to >35. Chlorine derivative **1c** was the most active and selective from this series. Compound **1g** was the only molecule active against promastigotes of *L. donovani* (EC$_{50}$ = 7.64 μM). The whole series was inactive against *T. cruzi* and *T. vaginalis.*

Nine bis(2-aminobenzimidazole) derivatives (**2a–e**, **2h**, **30**, **31**, **34**) were synthesised in three steps from dianiline precursors. Thermal melting experiments with (AT)$_4$-containing DNA and UV-Vis titrations with unspecific DNA showed that these compounds bind to DNA. Even though some experiments reveal these compounds are presumably MGB, more evidences will be necessary in order to clearly state the binding mode. This series displayed micromolar activity on *T. brucei* whereas it was mainly inactive against *T. cruzi* and *Leishmania* parasites. Compound **30** was the sole compound to be active against *L. donovani* promastigotes (EC$_{50}$ =

8.67 µM), albeit with a poor selectivity (SI = 1.6). Furthermore, **34** had weak trichomonacidal efficacy and poor selectivity (EC$_{50}$ = 33.2 µM, SI ≈ 1.5).

Eleven bis(arylimidamide) derivatives (**3a–e**, **3g–i**, **36**, **37**, **53**) were synthesised from dianiline precursors. A novel protocol using *N*-(*tert*-butoxycarbonyl)pyridine-2-carbimidothioate (**44**) was developed for the synthesis of halogen-containing bis(arylimidamides). Thermal melting experiments and/or SPR-biosensor assays showed that these compounds bind selectively (except the fluorene analogue **53**) to AT DNA sequences. The presence of induced CD and LD signals upon titration with (AT)$_4$-containing DNA (**3b**, **3g–i**, **37**, and **53**) and unspecific DNA (i.e., compound **3a**) showed that the compounds are MGB. The biophysical data (SPR, CD, LD, and ^{1}H-NMR) conclusively showed that **3a** is an AT-specific DNA MGB. Docking studies were performed to rationalize these results. The bis(arylimidamide) derivatives were very potent and selective inhibitors of *T. brucei*, *T. cruzi* and *Leishmania* growth. Compounds **3a**, a close analogue of **I**, was the best antiparasitic compound with submicromolar activity and high selectivity against these 3 kinetoplastid parasites.

Crystals of compounds **1c**, **3a** and **36** complexed with AT-containing DNA were obtained and diffracted at ALBA Synchrotron. Some diffraction patterns were obtained for compound **3a** crystallized with d(AAATATATTT) oligonucleotide.

NLC loaded with compound **3a** were successfully prepared and their storage stability was evaluated. Blank NLC were very stable at room temperature (60 days), whereas folic acid-functionalized NLC had limited stability (<21 days).

Conclusions

The bis(arylimidamide) derivatives (**3a–e**, **3g–i**, **36**, **37**, **53**) are very promising anti-kinetoplastid compounds. In particular, **3a** is an AT-specific DNA MGB which is active in the submicromolar range against bloodstream form trypomastigotes of *T. brucei* (EC$_{50}$ = 0.40 µM, SI > 500) and intracellular amastigotes of *L. donovani* (EC$_{50}$ = 0.65 µM, SI > 76.9) and *T. cruzi* (EC$_{50}$ =1.28 µM, SI = 69.6). This compound is selective towards these parasites and it is metabolically stable towards human and mouse liver metabolism, and in human serum. Therefore, **3a** is a good candidate to perform further *in vivo* assays.

Síntesis, evaluación biofísica y biológica de derivados de *N*-fenilbenzamida dirigidos al ADN mitocondrial de parásitos cinetoplástidos

Introducción

Los parásitos cinetoplástidos son responsables de las tres enfermedades humanas desatendidas que son transmitidas por vectores, y que son el centro de esta Tesis: la leishmaniasis, que es causada por *Leishmania* spp., la tripanosomiasis africana humana causada por *Trypanosoma brucei* spp., y la enfermedad de Chagas causada por *Trypanosoma cruzi*. Todos ellos presentan altas tasas de morbilidad y mortalidad principalmente en países en vías de desarrollo.

Los parásitos cinetoplastídicos se caracterizan por la presencia de un ADN mitocondrial en forma de disco, denominado "ADN cinetoplasto" (ADNc), que comprende > 70 % de pares de bases AT. Las formas de las células de los cinetoplastos cambian durante los complejos procesos de diferenciación que ocurren en sus ciclos de vida. Estas diferenciaciones son clave para la transferencia exitosa del parásito entre el vector y el huésped, y viceversa.

A pesar de la carga social y económica de las enfermedades cinetoplástidas, el arsenal quimioterapéutico para tratarlas sigue estando poco desarrollado. Por lo tanto, existe una necesidad urgente de nuevos tratamientos antitripanosómicos y leishmanicidas que ofrezcan seguridad y eficacia.

Estudios previos demostraron que los compuestos dicatiónicos de bisguanidina y bis(2-aminoimidazolina) son ligandos del surco menor (LSM) del ADN selectivos para secuencias de ADN ricas en AT. En particular, el compuesto **I** de *N*-fenilbenzamida bis(2-aminoimidazolina) mostró ser 100% curativo administrado por vía oral en un modelo murino de infección aguda por *T. b.* rhodesiense. Por el contrario, este compuesto fue mayormente inactivo contra los parásitos intracelulares *T. cruzi* y *Leishmania*.

Dado que el compuesto **I** es un excelente LSM del ADN con eficacia *in vivo* comprobada y que el ADNc es una diana común de *T. brucei*, *T. cruzi* y *Leishmania*, esta Tesis tuvo como objetivo optimizar la actividad biológica del compuesto **I** hacia los endoparásitos *Leishmania* y *T. cruzi*.

Objetivos

El objetivo principal fue descubrir nuevos compuestos activos dirigidos al ADNc de los parásitos cinetoplástidos *Leishmania*, *T. cruzi* y *T. brucei*.

El objetivo fue preparar tres familias de compuestos dicatiónicos que tuvieran el esqueleto común de *N*-fenilbenzamida del compuesto **I**, que interactúa favorablemente con el surco menor del ADNc. Se probaron diferentes modificaciones químicas para mejorar la permeabilidad de la membrana y, por lo tanto, la capacidad anti-*T. cruzi* y la actividad leishmanicida de las nuevas moléculas.

La actividad antiprotozoaria de los nuevos compuestos se evaluó *in vitro* y se probó la citotoxicidad inespecífica hacia células de mamíferos para calcular los índices de selectividad (IS). La afinidad de unión al ADN, la selectividad de secuencia y el modo de unión de los nuevos compuestos se evaluaron cuidadosamente utilizando diferentes técnicas biofísicas (resonancia de plasmón superficial (SPR), dicroísmo circular (CD), dicroísmo lineal de flujo (LD), valoraciones UV-Vis, Resonancia Magnética Nuclear de ^{1}H (RMN), cristalización y difracción de rayos X) y estudios computacionales. Finalmente, se sintetizaron nanopartículas lípidicas nanoestructuradas transportadoras (NLC) cargados con el compuesto **3a**, como estrategia de administración del fármaco para mejorar su actividad leishmanicida.

Resultados

Se sintetizaron siete análogos de bis(imidazolidin-2-imina) (**1b–h**) en dos pasos a partir de precursores de dianilina utilizando di-terc-butil-2-tioxoimidazolidin-1,3-dicarboxilato (**5**). Los experimentos de fusión térmica y de SPR mostraron que estos compuestos se unen selectivamente a las secuencias AT del ADN. La presencia de señales inducidas de CD y LD tras la titulación con ADN con (AT)$_4$ (**1b–h**) y ADN inespecífico (**1e**) mostraron que los compuestos son LSM. Esta serie mostró actividad micromolar contra *T. brucei* (5.71 a 78.5 µM) con IS de 1.3 a >35. El derivado clorado **1c** fue el más activo y selectivo de esta serie. El compuesto **1g** fue el único compuesto activo frente a promastigotes de *L. donovani* (CE$_{50}$ = 7.64 µM). Toda la serie fue inactiva frente a *T. cruzi* y *T. vaginalis*.

Se sintetizaron nueve derivados de bis(2-aminobenzimidazol) (**2a–e**, **2h**, **30**, **31**, **34**) en tres pasos a partir de los precursores dianilina. Los experimentos de fusión térmica con ADN

conteniendo (AT)$_4$ y valoraciones UV-Vis con ADN inespecífico mostraron que estos compuestos se unen al ADN. Aunque algunos experimentos revelan que estos compuestos son presumiblemente LSM, se necesitarán más ensayos para establecer claramente el modo de unión. Esta serie mostró actividad micromolar sobre *T. brucei* mientras que fue principalmente inactiva contra *T. cruzi* y *Leishmania*. El compuesto **30** fue el único compuesto activo frente a promastigotes de *L. donovani* (EC$_{50}$ = 8.67 μM), aunque con poca selectividad (IS = 1.6). Además, **34** fue poco eficaz y selectivo frente a *T. vaginalis* (EC$_{50}$ = 33.2 μM, SI ≈ 1.5).

Once derivados de bis(arilimidamida) (**3a–e**, **3g–i**, **36**, **37**, **53**) fueron obtenidos a partir de los precursores dianilina. Se desarrolló un nuevo protocolo utilizando *N*-(terc-butoxicarbonil)piridin-2-carbimidotioato (**44**) para la síntesis de bis(arilimidamidas) halogenadas. Los experimentos de fusión térmica y/o ensayos de SPR mostraron que estos compuestos se unen selectivamente (excepto **53**) a secuencias de ADN ricas en AT. La presencia de señales inducidas de CD y LD tras la titulación con ADN (AT)$_4$ (**3b**, **3g–i**, **37** y **53**) y ADN no específico (**3a**) mostró que los compuestos son LSM. Los datos biofísicos (SPR, CD, LD y ^{1}H-NMR) mostraron de manera concluyente que **3a** es un LSM del ADN, AT-específico. Se realizaron estudios de acoplamiento para racionalizar estos resultados. Los derivados de bis(arilimidamida) fueron inhibidores muy potentes y selectivos del crecimiento de *T. brucei*, *T. cruzi* y *Leishmania*. El compuesto **3a**, un análogo de **I**, fue el mejor compuesto antiparasitario con actividad submicromolar y alta selectividad contra estos 3 parásitos cinetoplástidos.

Se obtuvieron cristales de los compuestos **1c**, **3a** y **36** complejados con ADN rico en AT y se difractaron en el Sincrotrón ALBA. Se obtuvieron algunos patrones de difracción para el compuesto **3a** cristalizado con el oligonucleótido d(AAATATATTT).

Se prepararon con éxito NLC cargados con el compuesto **3a** y se evaluó su estabilidad. Las NLC blancas cargadas eran muy estables a temperatura ambiente (60 días), mientras que las NLC funcionalizados con ácido fólico tenían una estabilidad limitada (<21 días).

Conclusiones

Los derivados de bis(arilimidamida) (**3a–e**, **3g–i**, **36**, **37**, **53**) son compuestos prometedores con actividad anti cinetoplastos. Particularmente, **3a** es un LSM de AND, AT específico, activo en el rango submicromolar contra las formas tripomastigotes de *T. brucei* (EC$_{50}$ = 0.40 μM, IS >

500) y amastigotes intracelulares de *L. donovani* (EC_{50} = 0.65 µM, IS > 76.9) y *T. cruzi* (EC_{50} =1.28 µM, IS = 69.6). Este compuesto es selectivo frente a estos parásitos y es metabólicamente estable frente al metabolismo hepático humano y de ratón, y en suero humano. Por lo tanto, **3a** es un excelente candidato para realizar futuros ensayos *in vivo*.

Abbreviatures

μM	micro molar
$^{13}\text{C-NMR}$	carbon nuclear magnetic resonance
$^{1}\text{H-NMR}$	proton nuclear magnetic resonance
Å	angstrom units
AT	Adenine Timine bases
BBB	blood-brain barrier
Boc	*tert*-butyloxycarbonyl protecting group
CC_{50}	half maximal cytotoxic concentration
CD	circular dichroism
CDC	Centers for Disease Control and Prevention
CH_2Cl_2	dichloromethane
CL	cutaneous leishmaniasis
DIPEA	*N,N*-diisopropylethylamine
DMF	dimethylformamide
DMSO	dimethyl sulfoxide
DMSO-*d₆*	deuterated dimethyl sulfoxide
DNA	desoxyribonucleic acid
EC_{50}	half maximal effective concentration
Et2O	diethyl ether
Et_3N	trimethylamine
FA	folic acid
g	gram
GC	Guanine Citosine bases

H_2O	water
HAT	human African trypanosomiasis
H-bond	hydrogen bond
HBs	hydrogen bonds
HCl	hydrochloric acid
HEK	human kidney cells
HEPES	2-[4-(2-hydroxyethyl)piperazin-1-yl]ethanesulfonic acid
HIFBS	heat-inactivated fetal bovine serum
hiFCS	heat-inactivated calf bovine serum
IR	infrared spectroscopy
kbp	kilobase pair
K_d	binding affinity constant
kDNA	kinetoplastid DNA
LD	flow linear dichroism
LiOH	lithium hydroxide
logP	partition coefficient
M	molar
MeOH	methanol
mg	miligram
MGB	minor grove binder
ML	mucocutaneous leishmaniasis
mM	mili molar
MPD	2-methyl-2,4-pentanediol
MW	microwave irradiation

NADPH	Reduced nicotinamide adenine dinucleotide phosphate
NaPi	sodium phosphate
NH$_3$ sat	ammonia saturated
NLC	nanostructured lipid carrier
NOESY	Nuclear Overhauser Effect Spectroscopy
NTD	neglected tropical diseases
PBS	phosphate buffered saline
PDB	Protein data bank
pK_a	acid dissociation constant
PKDL	post Kala-azar dermal leishmaniasis
rt	room temperature
RU	binding response units
SD	standard deviation
SDS	sodium dodecyl sulphate
SI	selectivity index
SPR	surface plasmon resonance
TFA	trifluoro acetic acid
THF	tetrahydrofuran
T$_m$	thermal melting
TOCSY	Total Correlation Spectroscopy
UDPGA	Uridine diphosphate glucuronic acid
UGT	Uridine Glucuronosyl-Transfererase
VL	visceral leishmaniasis
WHO	World Health Organization

CHAPTER 1

1. Chapter 1: Introduction

1.1. Neglected Tropical Diseases

Neglected tropical diseases (NTDs) are defined by the World Health Organization (WHO) as a group of 20 diseases mainly prevalent in the tropics (Africa, Asia and Latin America) affecting the disadvantaged populations (disproportionately affecting women and children). More than one billion people are affected by these diseases. NTDs cause serious physical, social, and economic consequences, which allow to consider them as a public-health problem. The epidemiology of NTDs is complex and is often associated with environmental factors.[1, 2]

NTDs cause billions of dollars of harm to communities in developing countries each year due to direct health care costs, reduced productivity, and lower socioeconomic and educational standards. They also lead to other consequences such as disability, stigma, social exclusion, and discrimination, and impose a significant economic burden on patients and their families.[1]

NTDs do not just affect impoverished nations.[3] Some essential parasitic illnesses and other infections are common everywhere there is poverty, including in rich nations such as the United States and European countries, and have a significant detrimental influence on mother and child health.[3, 4]

Among these diseases, exist a group of vector-borne kinetoplastid diseases comprising Chagas disease, leishmaniasis and human African trypanosomiasis (HAT, also known as sleeping sickness).[1, 2, 5]

1.2. Kinetoplastid diseases

Kinetoplastids are a group comprised by flagellated protozoans that are responsible for distinct human illnesses transmitted by different vectors.[6] Kinetoplastid parasites are responsible for the three most common and neglected human diseases which are the focus of this Thesis: *leishmaniasis,* which is caused by *Leishmania spp.*, human African trypanosomiasis caused by *Trypanosoma brucei spp.*, and Chagas disease caused by

Trypanosoma cruzi. All of them display high morbidity and mortality rates mainly in developing countries.[3, 5, 7]

Kinetoplastid pathogens share genomic organization and cellular structural features. The main characteristic of kinetoplastid parasites is the presence of a DNA-containing region in their single large mitochondrion, named as "kinetoplast DNA" (kDNA), comprising > 70% AT base pairs. Kinetoplastid cell shapes change during the complex cell type differentiation processes in their life cycles, intimately linked to interactions with mammalian hosts or insect vectors. These differentiations are key to the successful transfer of the parasite between vector and host, and vice versa. The structural differences between *T. brucei*, *T. cruzi* and *Leishmania* cells during their life cycle stages have been reported in the literature.[8, 9]

Despite the social and economic burden of diseases caused by kinetoplastid protozoa, efforts to discover new drugs for them remain underdeveloped.[10, 11] Hence, there is an urgent need for new treatments that have trypanocidal and leishmanicidal properties.[12]

1.2.1. Leishmaniasis

The etiologic agent of leishmaniasis is the intracellular protozoan parasite of the genus *Leishmania*. It is estimated that each year 700 000 to 1.2 million new cases arise.[13, 14] Leishmaniasis is currently found in both the Eastern and the Western hemisphere. In the Eastern hemisphere, this disease is found in some parts of Asia, tropical regions of Africa and north of Africa and, over the last years, in southern Europe. In the Western hemisphere, leishmaniasis is spread over central and south America except Chile and Uruguay, and some regions of Mexico. However, it is also possible to find cases in non-listed countries due to the current travel and immigration patterns.[13]

There are three main forms of leishmaniasis: (i) visceral (VL), (ii) cutaneous (CL) and (iii) mucocutaneous (ML). Visceral leishmaniasis, also known as kala-azar, is the most serious form of the disease and results lethal if not treated. Moreover, individuals who get treatment are at risk of developing a disfiguring skin form of relapsing illness termed post kala-azar dermal leishmaniasis (PKDL), which may also contribute to disease transmission.[13, 15]

CL has a greater worldwide incidence (> 1 000 000 cases per year) than VL (30 000 cases per year),[14] with the highest frequency in Africa, the Mediterranean, and South America. It does not cause systemic morbidity or mortality, but it can inflict severe disfigurement and stigma.[13, 14]

The clinical manifestations of leishmaniasis depend on the illness form. CL is characterised by producing skin sores. Characteristic features are observed such as plaques, papules and nodule formation with the addition of skin thickening at multiple sites on the facial skin and the outer surface of the membranous tissue.[16] ML develops metastatic lesions, resulting in the progressive destruction of the nasal mucosa, as well as the soft and hard palate, and eventually the nasal septum.[17] Facial disfigurement and crippling injuries result in social discrimination.[18] The clinical symptoms of VL are anaemia, progressive cachexia, intermittent fever, hepatomegaly and splenomegaly. Other symptoms, such as lymphadenopathy and persistent diarrhoea, are also common.[19] Remarkably, as *Leishmania* parasites directly affect cells of the phagocytic mononuclear system (e.g., macrophages) the disease progresses to cause alterations in the immune system.[20] VL is affecting several internal organs (e.g., spleen, liver, and bone marrow) resulting life threatening in some cases. The illness is developed within months (sometimes as long as years) of the sand fly bite.[13, 14, 21, 22]

1.2.1.1. *Leishmania* life cycle

Leishmaniasis is transmitted by sand flies and caused by obligate intracellular protozoa of the genus *Leishmania*. The *Leishmania* life cycle involves two stages: sandfly and human stages, in which two forms of the parasite (i.e., promastigote and amastigote) are observed (Figure 1.1).

As first step, female phlebotomine sand flies inject infective promastigote stages from their proboscis into the skin of the human during blood meals. Promastigotes that reach the puncture wound are phagocytized by macrophages and other types of mononuclear phagocytic cells in the host. Promastigotes transform into amastigotes (i.e., the tissue stage) inside these mononuclear phagocytic cells, multiply by simple division, and proceed to infect other mononuclear phagocytic cells. Different factors, including the parasite species and/or subspecies and the host, influence whether the infection becomes symptomatic and whether cutaneous or visceral leishmaniasis results. To close the life

cycle, sand flies become infected by ingesting infected cells during blood meals. In sand flies, amastigotes transform into promastigotes, divide in the gut (in the hindgut for *Viannia* subgenus; in the midgut for *Leishmania* subgenus), and migrate to the proboscis.[13]
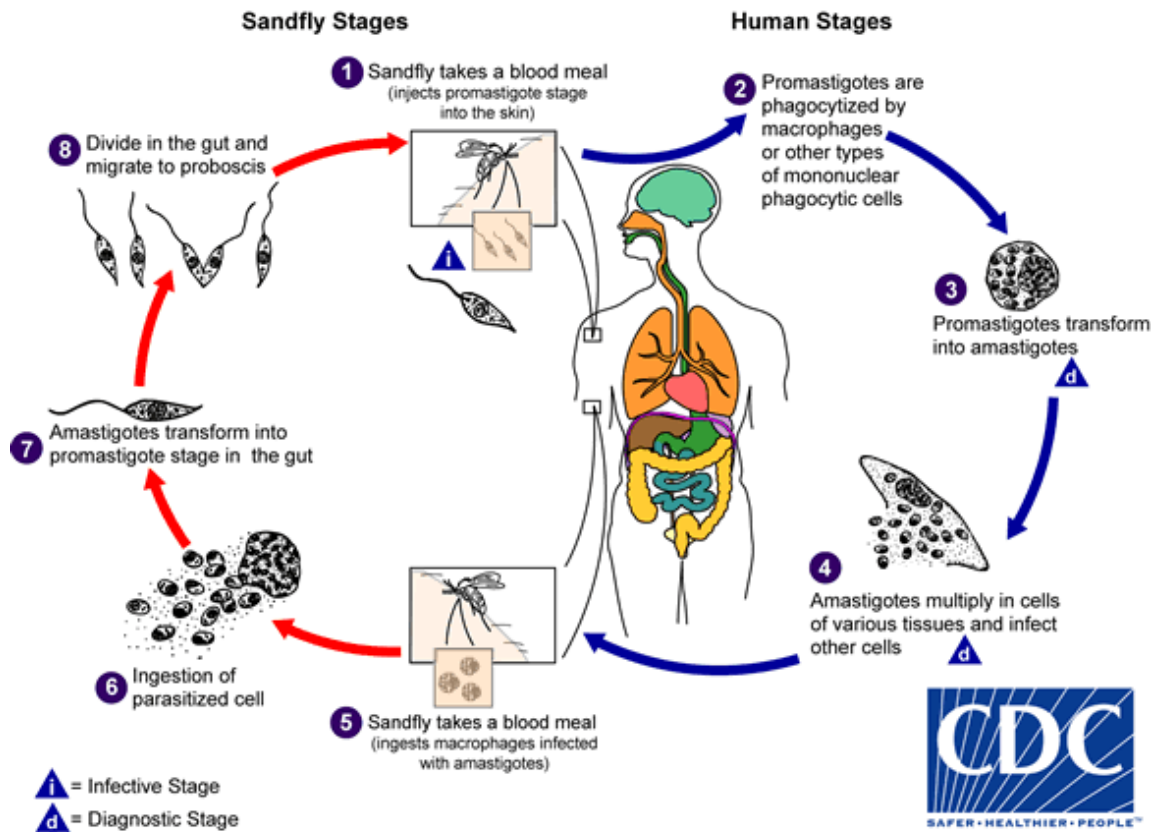
Figure 1.1: *Leishmania* life cycle. Taken from Centers for Disease Control and Prevention (CDC). Parasites - Leishmaniasis.[13]

1.2.1.2. Current treatments

Despite their toxicity and varied effectiveness, antimonials were the only treatment for the previous 60 years, until alternative therapies were developed and introduced at the beginning of the 21st century.[21, 23] Recent advances in the treatment of VL, such as the combination of sodium stibogluconate and paramomycin, the oral formulation of miltefosine, and the combination of liposomal amphotericin B and pentamidine isethionate, provide improved safety profiles, shorter treatment durations, and a lower risk of drug-resistance (Figure 1.2).[21, 23, 24]
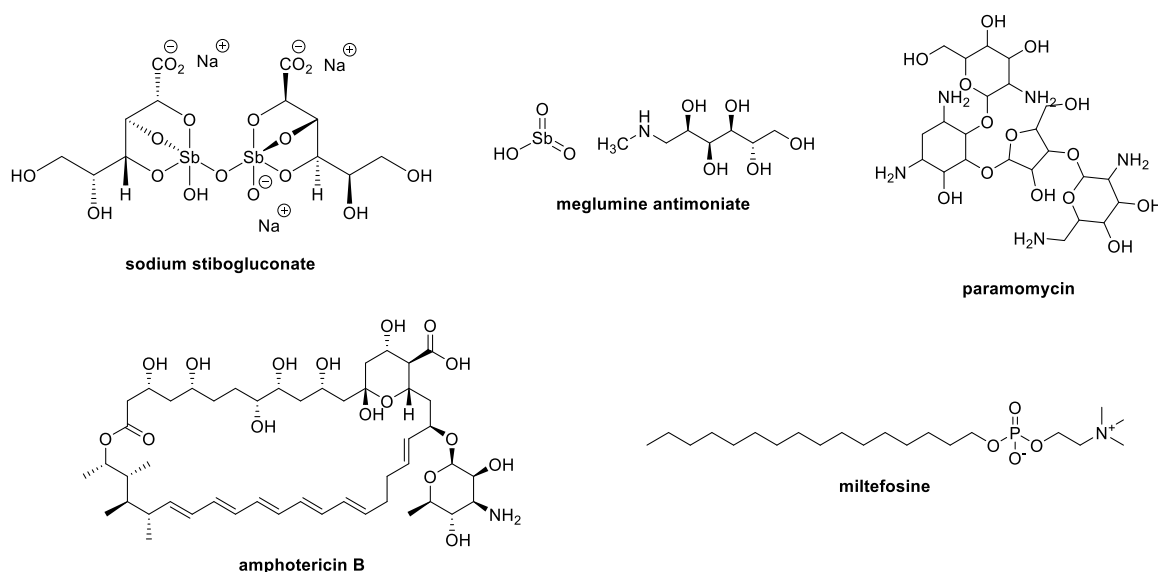
Figure 1.2: Drugs for the treatment of leishmaniasis.

Current approved therapeutic arsenal for leishmaniasis treatment has important limitations regarding access and affordability. The medicines available for first-line VL treatment involves a combination of liposomal amphotericin B and pentamidine isethionate, or a combination of pentavalent antimonials (i.e., sodium stibogluconate and meglumine antimoniate) and paromomycin. For the first-line CL treatment the use of pentavalent antimonials in both local or systemic administration is recommended. Furthermore, the use of miltefosine and pentavalent antimonials is prescribed for the treatment of PKDL. Antimonials, amphotericin B, paromomycin sulphate, and miltefosine have variable efficacy against the more than 20 *Leishmania* species responsible of this disease.[5] WHO treatment guidelines propose different doses and combination based on the geographical distribution of the disease. As an example, WHO recommendation treatment regimen for VL on the Indian subcontinent should include liposomal amphotericin B or miltefosine (oral administration). However, these medicines are poorly effective in patients in other countries. Treatment regimens are generally long, requiring hospitalization, and have significant toxicities. Hence, monitoring the process is necessary. Regional differences in treatment protocols, high costs, and the low availability of some medicines stretch the limits of underfunded health-care systems in countries where these diseases are endemic.[5, 13]

1.2.2. American trypanosomiasis

American trypanosomiasis (Chagas disease) is caused by *Trypanosoma cruzi* and is transmitted to animals and humans by insect vectors (triatomine bugs, family Reduviidae).[25] This disease is endemic in the American continent, especially spread in rural areas of Latin America where it is associated to poverty factors.

It is estimated that $\approx$ 8 million people in Mexico, Central America, and South America is infected by *T. cruzi*. However, most of them do not know they are infected, due to the lack of serological controls. If left untreated, this infection is lifelong and can be life threatening.[26]

The impact of Chagas disease is not limited to rural areas of Latin America in which vector-borne transmission occurs.[27] A major problem is related to large-scale population movements from rural to urban areas, not only in Latin America but also to other regions of the world, which provokes the spreading of the parasite outside its endemic area. This results in a changeable epidemiology of the disease. Hence, Chagas is now an emerging disease in non-endemic countries such as the United States and Europe.[28, 29]

Chagas disease has an acute and a chronic phase. Acute Chagas disease occurs immediately after infection, and can last up to a few weeks or months. During the acute phase, parasites may be found in the circulating blood. This phase of infection is usually mild (fever or swelling around the inoculation area) or asymptomatic. Even though, acute infection may result in severe inflammation of the heart muscle or the brain in a few cases. Most infected people that remain untreated enter into a prolonged asymptomatic form of the disease ("chronic indeterminate"). These people may remain asymptomatic for life and never develop Chagas-related symptoms. However, an estimated 20–30% of infected people will develop severe and sometimes life-threatening medical problems over the course of their lives.[26]

Chronic Chagas disease may develop cardiomyopathy, digestive mega syndromes, or both. Clinic manifestations include heart rhythm abnormalities leading to sudden death, a dilated heart that does not pump blood adequately, and a dilated oesophagus or colon, leading to difficulties with eating or passing stool, respectively. In immunocompromised patients

(i.e., AIDS or chemotherapy patients), Chagas disease can reactivate with parasites found in the circulating blood, leading to severe disease.[26]

1.2.2.1.   *Trypanosoma cruzi* life cycle

This life cycle involves two stages: human and triatomine bug stages (Figure 1.3). Common triatomine vector species belong to the genera *Triatoma*, *Rhodnius*, and *Panstrongylus*.
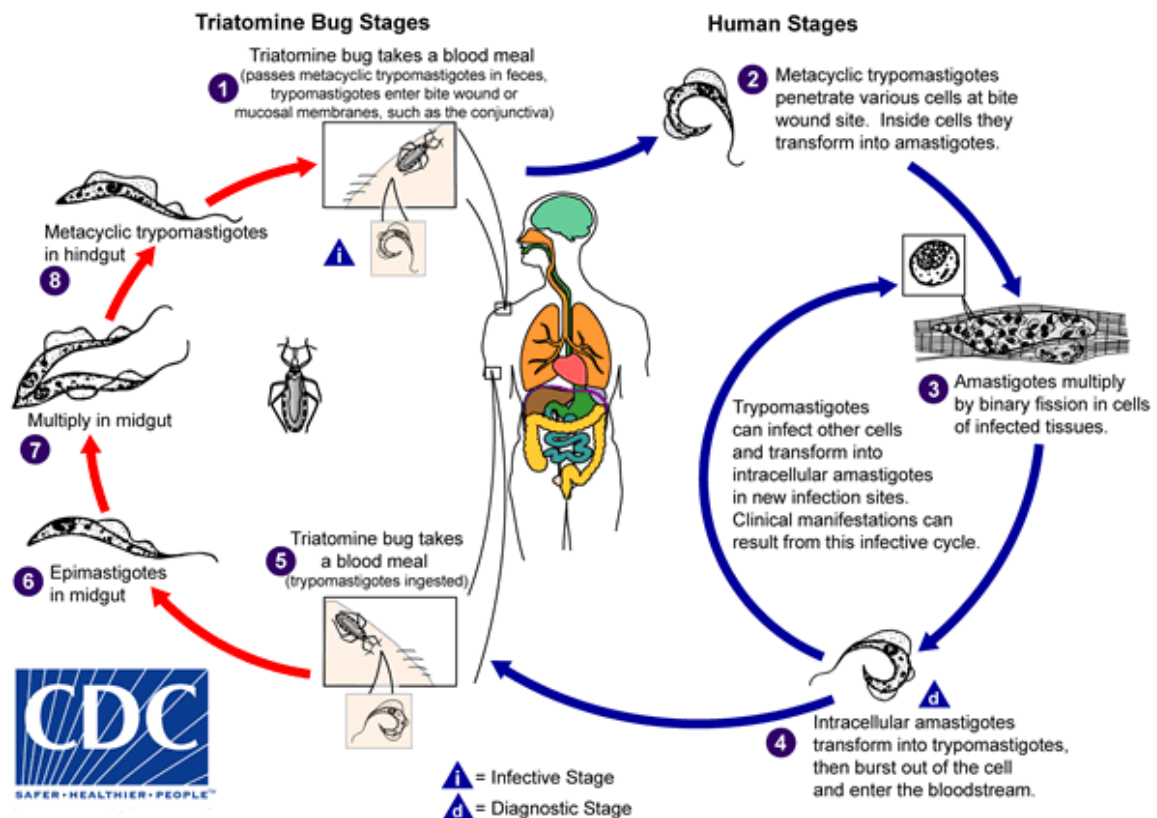
Figure 1.3: *Trypanosoma cruzi* life cycle. Taken from Centers for Disease Control and Prevention (CDC). Parasites – American trypanosomiasis.[26]

An infected triatomine insect vector (or "kissing bug") ingests a blood meal releasing trypomastigotes in its faeces near the site of the bite wound. These trypomastigotes enter the host through the wound or through mucosal membranes. Inside the host, the trypomastigotes invade cells near the site of inoculation and differentiate into intracellular amastigotes. The amastigotes multiply and differentiate into trypomastigotes, and then are released into the circulation as bloodstream trypomastigotes. Trypomastigotes infect cells from a variety of tissues and transform into intracellular amastigotes in new infection sites.

Replication resumes only when the parasites enter another cell or are ingested by another vector.

To complete the cycle, a new insect vector becomes infected by feeding on human or animal blood containing bloodstream parasites. The ingested trypomastigotes transform into epimastigotes in the vector's midgut. The parasites multiply and differentiate in the midgut, then differentiate into infective metacyclic trypomastigotes in the hindgut reinitializing the cycle.

T. cruzi can also be transmitted through blood transfusions, organ transplantation, transplacentally (from mother to unborn baby), orally (contaminated food or drink), and in laboratory accidents.[26]

1.2.2.2. Current treatments

Currently, only two nitroheterocyclic drugs – benznidazole and nifurtimox – are available. These treatments decrease parasite load and can result in parasite clearance from blood in both acute and chronic *T. cruzi* infections.[5] However, both of them, which were developed decades ago, present serious adverse effects and are contraindicated during pregnancy (Figure 1.4).

benznidazole   **nifurtimox**
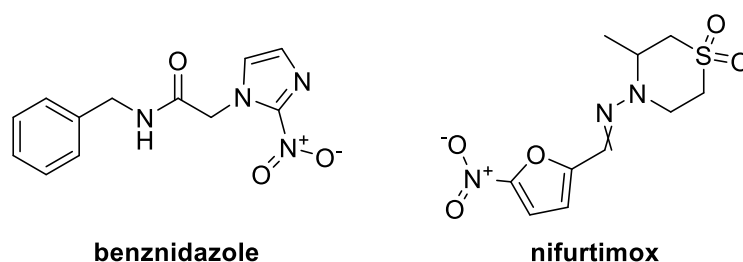
Figure 1.4: Nitroheterocyclic drugs available for the treatment of Chagas disease.

Available medications are insufficient because they fail too frequently due to dormant amastigotes which are exceptionally resistant to extended drug treatments *in vivo* (and *in vitro*) allowing the re-establishment of infection.[30] Benznidazole is well tolerated in adults, despite skin and nervous system complications, whereas nifurtimox is the common treatment for kids. However, WHO recommends the use of benznidazole off-label for the treatment of persistently infected individuals, despite the fact that its efficacy in later stages

of the disease is disputed. The BENEFIT trial, a comprehensive investigation of individuals with chronic Chagas cardiomyopathy, found that benznidazole therapy lowered parasite load but did not significantly improve disease progression.[5] Hence, the search of better treatments for Chagas disease remains a necessity and a priority in tropical medicine.

1.2.3. African trypanosomiasis

Human African trypanosomiasis, popularly known as "sleeping sickness," is caused by subspecies of the parasite of the *Trypanosoma brucei*. It is transmitted by the tsetse fly (*Glossina* species) which is found in Sub-Saharan Africa. There are two morphologically indistinguishable forms of African trypanosomiasis; each is named after the historical area of Africa where it was discovered. The parasite *Trypanosoma brucei rhodesiense* causes East African trypanosomiasis, whereas the parasite *Trypanosoma brucei gambiense* causes West African trypanosomiasis. Sleeping sickness is treatable, but it is lethal if untreated.

Control measures have lowered the number of yearly cases, and the number of recorded cases went below 10,000 for the first time in 50 years in 2009. Less than 2000 cases were reported to WHO in the 2017–2018 period. In recent years, the use of the nifurtimox–eflornithine combination therapy (NECT) and fexinidazole has contributed to the decline of the number of cases with fewer than 700 combined cases reported to WHO in 2020, with more than 85% caused by *T. b. gambiense* and roughly 15% caused by *T. b. rhodesiense*.[31]

1.2.3.1. *Trypanosoma brucei* life cycle

T. brucei has two hosts: the *tsetse* fly and the mammalian host (human or animal). The cycle begins when metacyclic trypomastigotes from fly saliva are injected into the human blood during a blood meal (Figure 1.5). In the mammalian host, the infection occurs in two stages, an initial haemolymphatic stage, with bloodstream trypomastigotes that multiply by binary fission, and a meningoencephalitic stage after the trypanosomes invade the central nervous system.

When a *tsetse* fly feeds of blood of an infected mammal, it receives trypomastigotes that are converted into procyclic trypomastigotes in the fly midgut. Finally, they leave the

midgut and change into epimastigotes which multiply in salivary gland and transform into metacyclic trypomastigotes.
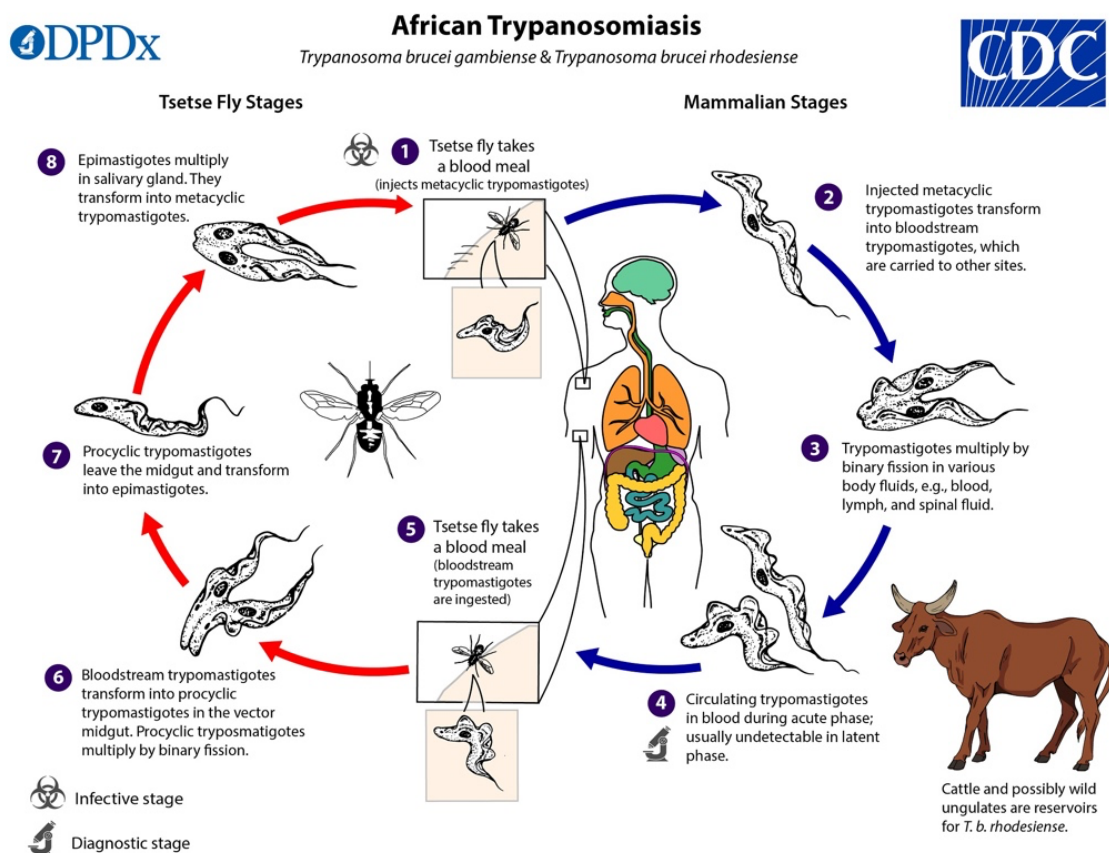
Figure 1.5: Life cycle of *T. brucei*. Taken from Centers for Disease Control and Prevention (CDC). Parasites – African Trypanosomiasis.[32]

1.2.3.2.   Current treatments

The treatments of human African trypanosomiasis (HAT) (Figure 1.6) depend on the parasite involved (*T. b. gambiense* or *T. b. rhodesiense*) and the illness stage (i.e., presence or absence of central nervous system involvement). For first-stage of *T. b. gambiense* infection, pentamidine is the recommended treatment whereas suramin is chosen for *T. b. rhodesiense*. For the second stage, melarsoprol and eflornithine are also used. However, the administration regimen and availability of the drugs remain as significant problems.[32, 33] The introduction since 2009 of the nifurtimox-eflornithine combination therapy (NECT) for *T. b. gambiense* HAT was a milestone, followed by the recently demonstrated efficacy of oral fexinidazole.[5] Fexinidazole, which was included in 2019 as oral treatment (i.e., 10 days regimen), is indicated as first line drug for first stage and non-severe second stage of

gambiense HAT.[34] With fexinidazole, oral pills can be administered to patients making the chemotherapy of *gambiense* sleeping sickness much easier and affordable.[35]
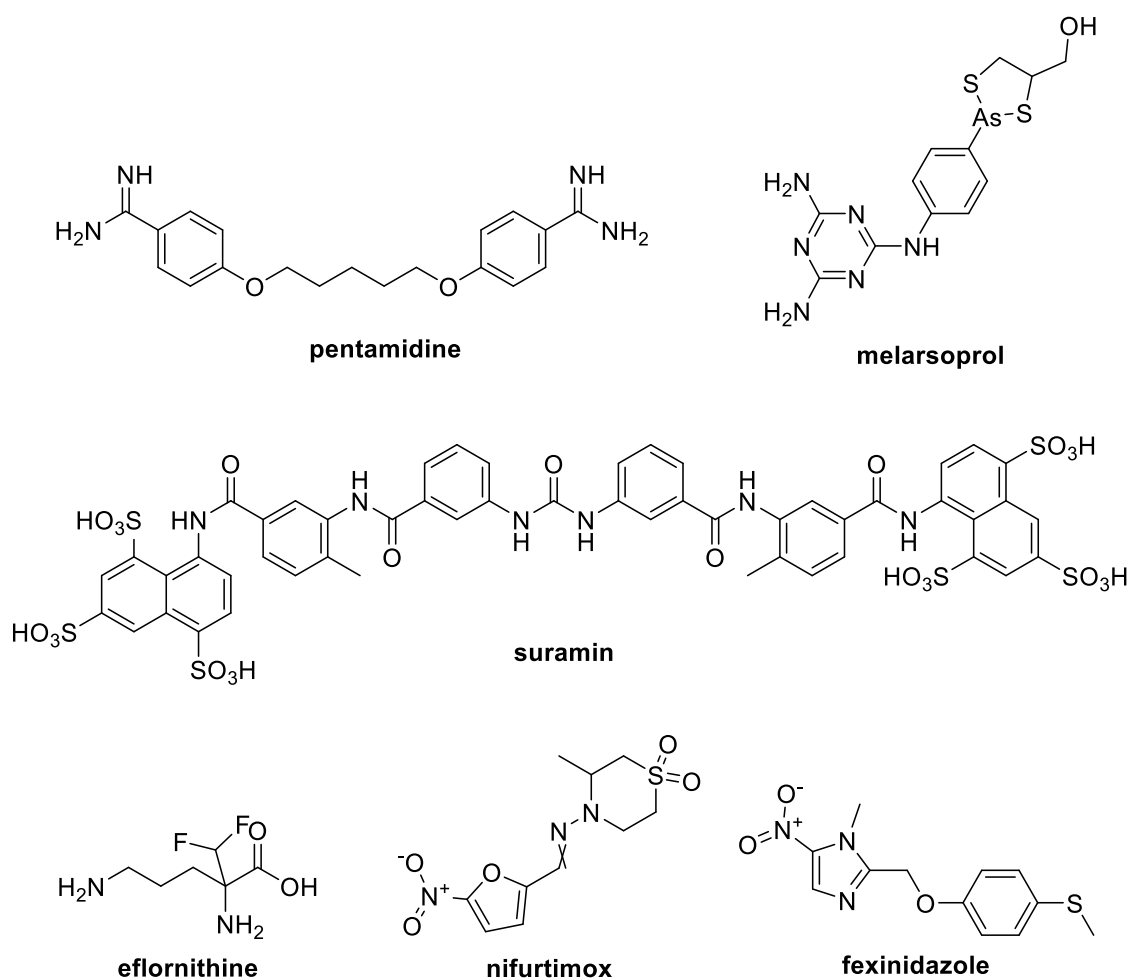
Figure 1.6: Available drugs for the treatment of sleeping sickness.

1.3. DNA as therapeutic target: structure and function

Molecules that bind to the DNA double helix can be used as chemotherapeutic agents for the treatment of parasitic diseases which are dependent on cellular division.[36] Chemotherapeutic compounds mainly bind to DNA through three different modes, i.e., alkylation, intercalation or groove binding. It is also possible to observe a dual binding mode in which two binding modes are observed. The mentioned binding modes occur through hydrophobic forces, electrostatic interactions (intercalators and groove binders), $\pi - \pi$ stacking (intercalators) or ionic interactions.[37-41]

1.3.1. The structure of DNA

DNA encodes the genetic information needed for the correct development and functioning of living organisms. A knowledge of the DNA structure is fundamental to understand the interactions of the DNA–ligand complexes involved in DNA binding.

The DNA structure consists in two helical chains coiled round the same axis as first described by Watson and Crick.[42] Helixes are formed by repeating units named nucleotides, composed of substructures known as nucleosides. These nucleosides are formed by a nitrogenous base covalently bound to a five-carbon sugar (i.e., 2'-deoxyribose). If this nucleoside holds a phosphate group attached to the structure, it is named nucleotide (Figure 1.7).
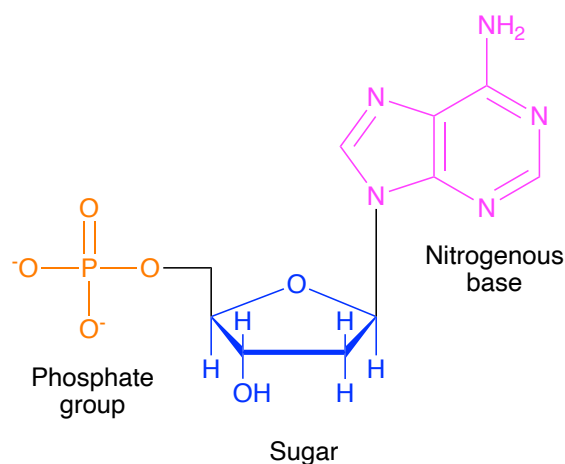
Figure 1.7: Schematic structure of the adenine (purine) nucleotide

The unmodified, natural four DNA bases are classified into two groups based on their heterocyclic structure: (i) purines: adenine (A), guanine (G), and (ii) pyrimidines: cytosine (C) and thymine (T). These bases associate in pairs through hydrogen bonds connecting the two DNA strands. Guanines associate with cytosines with three Watson−Crick H-bonds, and adenines with thymines through the formation of two H-bonds (Figure 1.8).[43, 44]
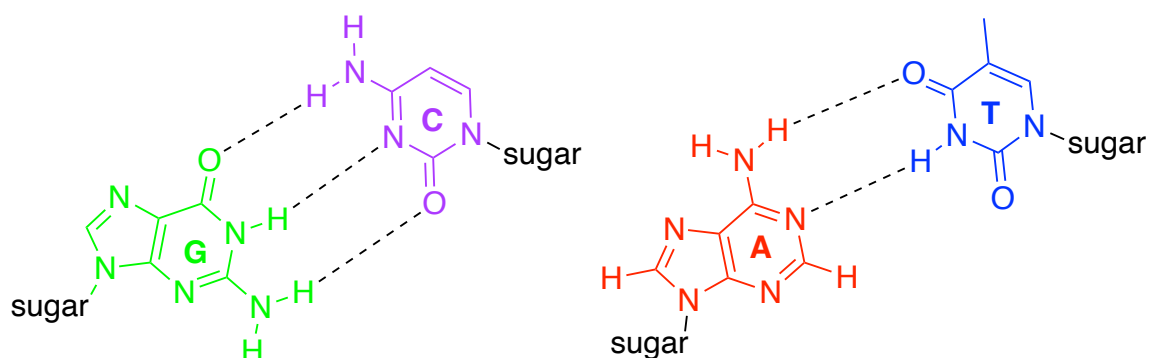
Figure 1.8: Watson−Crick base pairing of canonical nucleic acids showing hydrogen bonding between guanine (G) and cytosine (C), and adenine (A) and thymine (T).

The importance of the sugar rings in nucleotides is due to their structural features, being a five atoms ring, at least one of the atoms must be out of the plane, meaning there is a non-planar structure.[43, 45]

1.3.2. DNA polymorphs A, B and Z-DNA

Different forms of DNA (referred as polymorphs) exist depending on the base sequence and the surrounding environment. The most commonly observed structures are the A-DNA, B-DNA and Z-DNA.[46] The best known model is the B-form. It was first described by Watson and Crick for the right-handed double-helical form.[42, 46] The right-handed B-form is the standard form in biological systems (Figure 1.9).
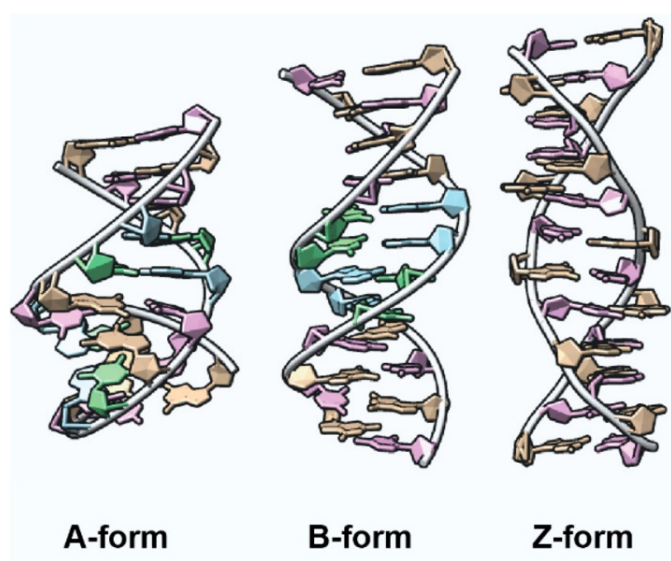
Figure 1.9: **A**, **B** and **Z** forms of DNA. Right-handed forms **A** (left) and **B** (middle). Left-handed **Z**-form (right). (Adapted from Largy et al. *Chem. Rev.* **2022**, *122*, 7720-7839).[44]

The main difference between the polymorphs of DNA is that A-DNA and B-DNA are both right-handed, uniform double-helical structures, while Z-DNA is a left-handed double helix with a repeating dinucleotide and a backbone following a zig-zag path. Low humidity is necessary to observe A-form DNA whereas Z-DNA requires an alternating sequence of poly(dC-dG). High salt concentration (> 2.5 M NaCl) is believed to be necessary to allow the formation of the Z-DNA structure.[43, 46]

1.3.3. DNA function

Two main functions are described for DNA:

- Transcription is based on the retrieving of information from the DNA by ribonucleic acid (RNA) in order to synthesise complex molecules (i.e., proteins, tRNA, rRNA, siRNA, etc.) essentials in the organism. Such proteins are part of biological processes and have different roles (e.g., hormones, enzymes, carriers, structural proteins, receptors, etc.).
- Replication: this function involves DNA self-replication.[47]

These two functions are key for cell survival, proliferation and maintaining the correct functioning of all biological systems. The initiation of transcription and replication requires a signal given by the binding of a regulatory substance (e.g., protein) to a particular region of DNA. Thus, mimicking the regulatory substance in both specificity and strength, the function can be activated, inhibited or modified. On the one hand, activation would lead to DNA replication or over production of the regulatory substance. On the other hand, inhibition would avoid synthesis of the activating substance or replication process, which could finally produce cell death. Hence, a small molecule can act as both activator or inhibitor, controlling or being able to cure a disease.

As regards to antiparasitic chemotherapy, DNA is mostly targeted in an inhibitory mode in order to prevent parasites replication.[48]

1.3.4. DNA targeting compounds

Based on the double-stranded DNA structure, four different modes of interaction with the DNA have been proposed in the literature: intercalation, alkylation, strand-cleaving and binding to the major or minor groove.[36]

1.3.4.1. Alkylating agents

Alkylating compounds interact non-specifically with DNA by transferring an alkyl group to the heterocyclic bases of DNA. They are highly electrophilic species that can react with nucleophiles forming covalent bonds. The development of alkylating substances designed after the nitrogen mustards produced numerous treatments, especially in cancer therapy. Some examples of these compounds are the cyclophosphamide, cisplatin, carboplatin and oxaliplatin (Figure 1.10).[49-51]

Cyclophosphamide

Cisplatin

Carboplatin
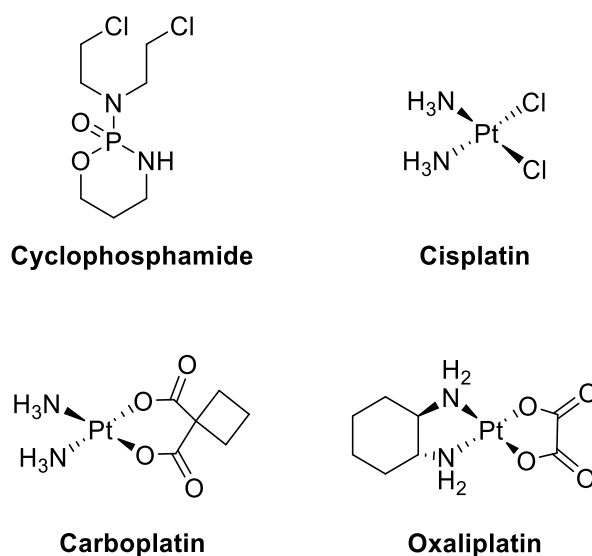
Oxaliplatin

Figure 1.10: Chemical structures of alkylating agents: cyclophosphamide, cisplatin, carboplatin and oxaliplatin.[51]

1.3.4.2. Intercalating agents

Intercalators are characterised by being large, hydrophobic and planar molecules (Figure 1.11). They insert themselves in between DNA bases using a combination of hydrophobic and $\pi - \pi$ stacking interactions.[36, 52] This insertion leads to structural changes in the helix (i.e., lengthening and unwinding). Non-covalent bonds formed by the interaction between intercalating aromatic system and the two base pairs perpendicular to the axis produces the distortion of the polysaccharide backbone leading to potential deletions in the coding region.[52, 53]

Daunomycin HCl   **Acridine**
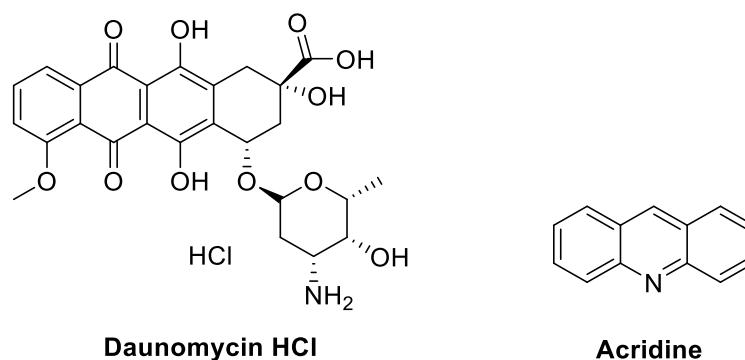
Figure 1.11: Chemical structures of common intercalators: daunomycin hydrochloride and acridine.

1.3.4.3.   Cleaving agents

These compounds break the DNA strands probably with the involvement of hydroxide and superoxide free radicals. Bleomycin (Figure 1.12) is the most widely known cleaving agent. It is obtained from *Streptomyces verticillus* and used clinically for the treatment of a wide variety of cancers usually as a co-adjuvant.[36, 54]
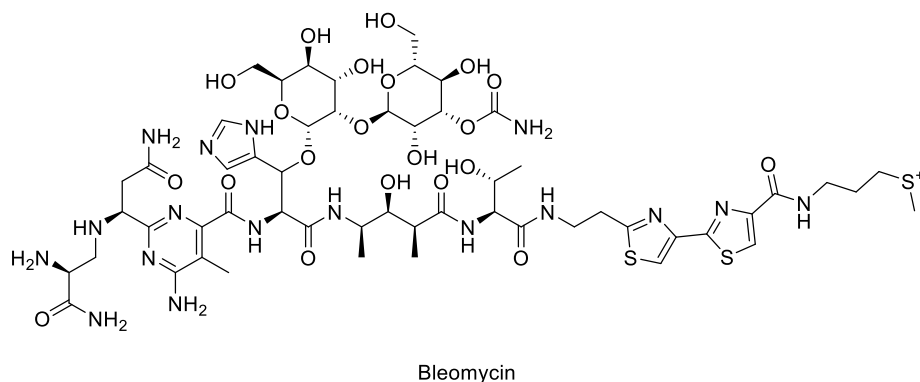
Bleomycin

Figure 1.12: Chemical structure of Bleomycin

1.3.4.4.   Major and minor groove binding agents

The sugar phosphate backbone of DNA spirals around the outer surface of DNA. Between these backbones are two different sized grooves known as the major and minor grooves. The larger one (major groove) measures 11.6 Å wide and 8.5 Å deep. This major groove is mainly formed by G:C base pairs and possess the greatest positive potential compared to the negative electrostatic potential observed in the minor groove. Contrary to the major groove, the minor groove is rich in A:T base pairs (Figure 1.13).[55, 56]
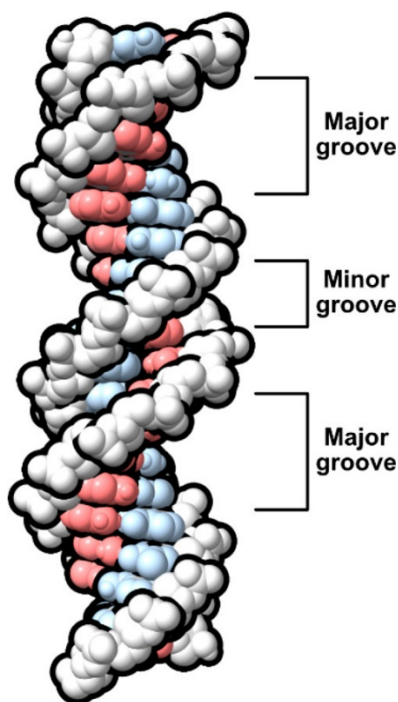
Figure 1.13: Major and minor grooves in a B helix (Taken from Largy et al. *Chem. Rev.* **2022**, *122*, 7720-7839).[44]

As regard of the environment, both grooves are surrounded by Na^+, K^+, Ca^{2+}, Mg^{2+} and polyamines which are physiological essential cations that neutralize the negatively charged sugar-phosphate backbone. These counterions bind the phosphate groups of the DNA backbone, exposed to the solution, and the electronegative pockets in the grooves of the double helix. The presence of water molecules within the grooves allows water-mediated interactions (i.e., hydrogen bonds) supporting the organisation of cations.[57] Polyamine molecules such as putrescine^{2+}, spermidine^{3+} and spermine^{4+} prefer the narrowest part of A-tract regions of the minor groove.[58]

Many replication and repair enzymes necessary for the transcription of proteins bind to the major and minor grooves of DNA. Generally, proteins tend to bind the major groove while small molecules show interaction within the minor groove. However, a few small molecules (e.g., methyl green) also bind to the major groove.[59] Binding of proteins to the major groove is favoured by the larger size of the groove and the higher number of potential hydrogen bonding interactions that can occur with a minimum alteration of the DNA structure.[60-62]

The minor groove of the DNA duplex has a greater negative electrostatic potential than the major groove, as previously stated. Extensive studies have been performed on the molecular electrostatic potential of the sugar-phosphate backbone of the B-DNA helix and the geometric factors that control the negative electrostatic potential within the groove.[62] The overall shape of the grooves and the electric potential is differently affected by the position of the base pairs within the grooves relative to the double helix.[63]

Base pairs arrangement within the minor groove is key for determining the preference for electrostatic interactions with ligands. Research in this area has led to determining that CG base pairs in the major groove and AT base pairs in the minor groove are more likely to interact with ligands.[64, 65]

1.3.5. DNA minor groove binders as anti-protozoal agents

In this Thesis, we have concentrated our efforts towards the study of DNA minor groove binders (MGB) that can be useful in the treatment of kinetoplastid diseases.

The minor groove of DNA is an excellent target for compounds acting as sequence-specific drugs.[66] Minor groove binders usually show a planar and concave structure to fit the groove curvature. Usually, these aromatic derivatives contain hydrophobic regions, which remove the hydration spine along the groove. Furthermore, cationic groups allow ionic interactions with the negative potential of the minor groove (at physiological pH) and to form hydrogen bonds (HBs) with specific DNA base sequences at the groove floor. Since (di)cationic compounds accumulate to high levels in the parasite's single mitochondrion driven by the mitochondrial membrane potential and binding to kDNA,[67] MGBs can disrupt essential protein or transcription factor–DNA interactions by causing structural alterations in the DNA helix.[68]

The most important DNA minor groove binder (MGB) clinically used is pentamidine (Figure 1.6), which was suggested to inhibit pathogens growth by targeting the protozoan topoisomerases.[55] Kahvedžić demonstrated that pentamidine binds to AT-rich regions along four base pairs.[69] The H-bonds observed between the amidinium groups and the adenine and thymine of the DNA stabilise the formed complex.[70]
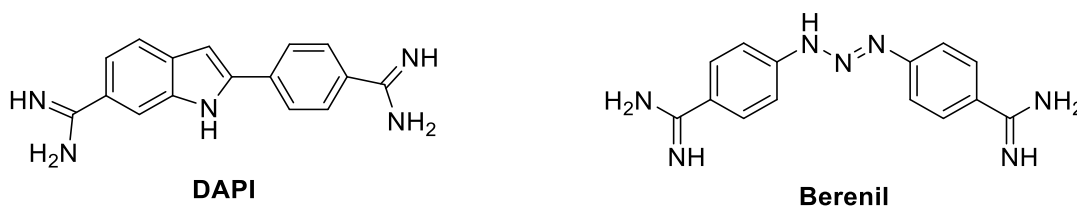
Figure 1.14: Chemical structure of antiprotozoal MGBs.

The well-known diarylamidine 4′,6-diamidino-2-phenylindole (DAPI) has been reported to be active against *Trypanosoma congolense* (Figure 1.14).[71] However, the appearance of undesirable side effects *in vivo* limited its clinical use as trypanocide. DAPI was shown to inhibit DNA and RNA polymerases trough specific AT-rich binding in the double-stranded DNA.[72, 73] The presence of amidine groups at the ends of the molecule is hypothesised to stabilise the complex DNA–DAPI through H-bonding and electrostatic interactions.

The aromatic diamidine diminazene, also known as Berenil,[74] is widely used for the treatment of animal trypanosomiasis under veterinarian prescriptions.[75] Berenil displays trypanocidal activity selectively against extranuclear DNA.[75, 76] Berenil also displayed babesicidal[77] and bactericidal[78] activity. This compound is also characterized by a high affinity for AT-rich sequences.[79]

1.3.5.1. Kinetoplast DNA (kDNA) as target

Kinetoplast DNA (kDNA) is an important structural characteristic of the flagellated protozoa of the order Kinetoplastida. kDNA is different from other DNA in nature because it is a network of interconnected DNA rings. This network has a topology that resembles medieval chain mail. kDNA represents approximately 30% of the total quantity of DNA in the parasite cell.[80, 81] The understanding of the kDNA network replication, which is rather complex, was analysed by studying the proteins involved.[82-86]
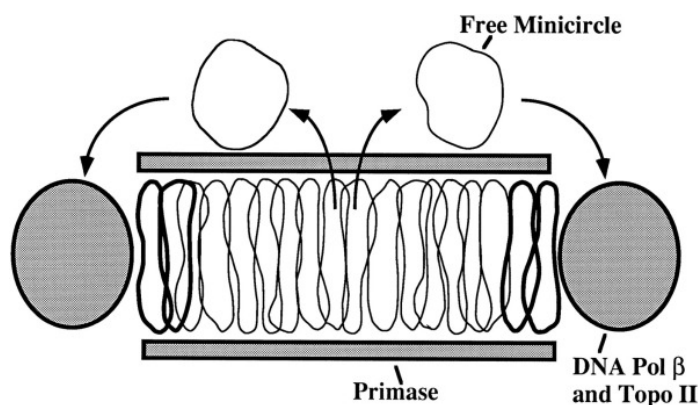
Figure 1.15: Section through the kinetoplast disc, with interlocked minicircles aligned in a monolayer. The disc is flanked by two antipodal protein complexes containing DNA polymerase β and topoisomerase II. Primase is localized above and below the kinetoplast disc. Covalently closed free minicircles are released from the central region of the disc. After replication, the progeny minicircles, containing gaps, are attached to the network periphery adjacent to the two protein complexes. The newly replicated minicircles are drawn in bold (Taken from J. *Biol. Chem.* **1997,** 272, 20787-20792).[87]

The kDNA structure network consists of two kind of DNA rings: (i) a few thousand minicircles (0.45 to 2.5 kbp) and (ii) few dozen maxicircles (13 to 40 kbp).[80] The minicircles encode guide RNAs that take part in the editing of transcripts produced by the maxicircles, which are responsible for making rRNAs and proteins of the respiratory chain.[88] Minicircles and maxicircles can be visualised after decatenation of the network under topoisomerase II action.[82, 89, 90] Each parasite cell has one mitochondrion containing a single kDNA network condensed into a disk-shaped structure (Figure 1.15). The kDNA slice is positioned in a specialized region of the mitochondrial matrix near the flagellar basal body. The minicircles in the kDNA disk are extended parallel to the disk axis, the configuration is stabilized by histone-like proteins.[91]

Since kDNA is a hallmark of kinetoplastids and mitochondrial functions are indispensable to their life cycle, it is a valuable chemotherapeutic target against these parasites.[92]

1.3.6. Dicationic compounds as antikinetoplastid drugs

Dicationic antiprotozoal compounds have been known for decades. Synthalin, a well-known diguanidine trypanocidal drug was discovered more than 80 years ago.[67, 93-95] Further development of trypanocides with dicationic nature (e.g., diguanidines, diamidines) led to the discovery of treatments for human and animal trypanosomiasis.[93, 96-99] Diminazene (Berenil) and isometamidium are the most representative veterinary drugs

of this class.[74, 99, 100] Pentamidine, which was discovered more than 90 years ago,[74, 99, 100] is still in use today for the treatment of stage 1 HAT despite many side effects.[101-105]

Aromatic diamidines employed as antiprotozoal drugs has been previously reported in several research papers by Tidwell and by Boykin and their co-workers over the past 20 years (Figure 1.16).[106-124]

R = H: **furamidine (DB75)**
R = OMe: **pafuramidine (DB289)**

CGP 40215A

DB911

DB820

DB921

DB829
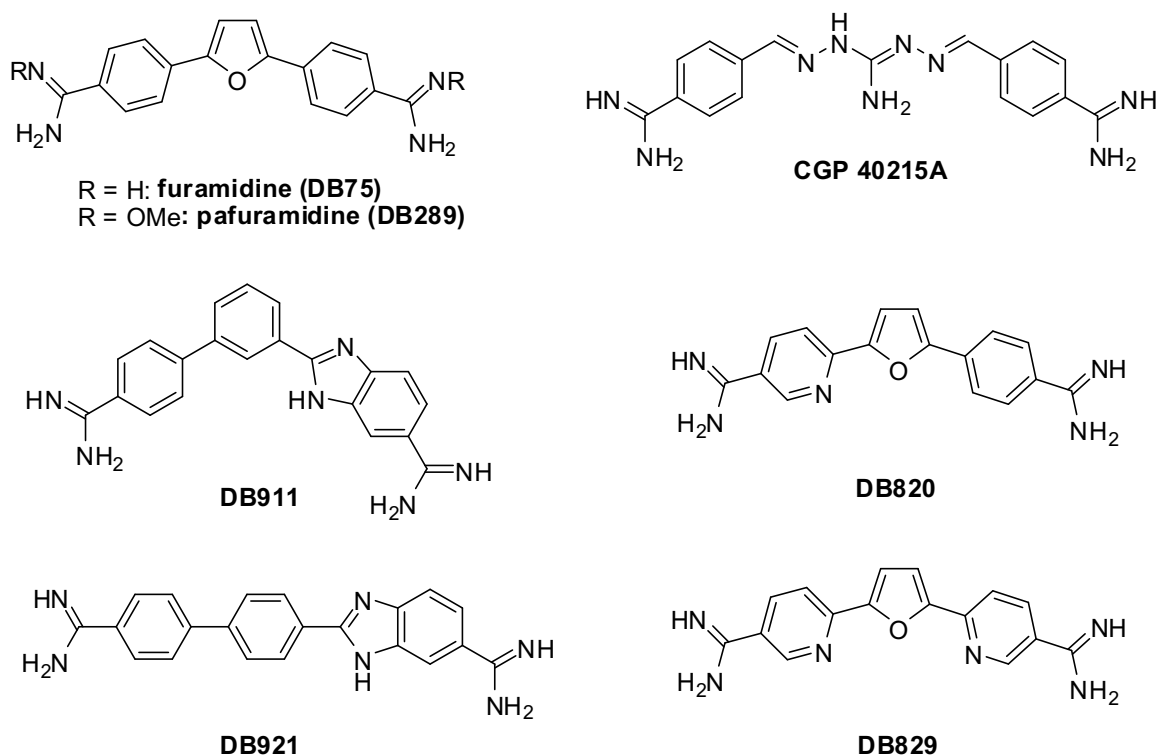
Figure 1.16: Chemical structures of some diamidines synthesised by Boykin and co-workers.

Pafuramidine (DB289), a prodrug of furamidine (DB75), is the most representative example of this class.[107, 125-129] This compound was advanced to phase III clinical trials for the oral treatment of stage 1 HAT. However, unexpected nephrotoxicity impeded clinical implementation of DB289 and the structurally related aza derivatives DB820 and DB829.[67, 130]

Another class of very effective dicationic antiprotozoal agents are the so-called "bisarylimidamide"[131-147] derivatives which are active against kinetoplastid (*T. cruzi*, *T. brucei*, *Leishmania*)[133-135, 137, 139-141, 143, 145, 146, 148, 149] and apicomplexan parasites (e.g.

Neospora caninum, Besnoitia besnoiti).[136, 138, 142] Bisarylimidamide compounds were also reported to display antifungal, antimicobacterial, or anti-inflammatory activity (Figure 1.17).[112, 150]
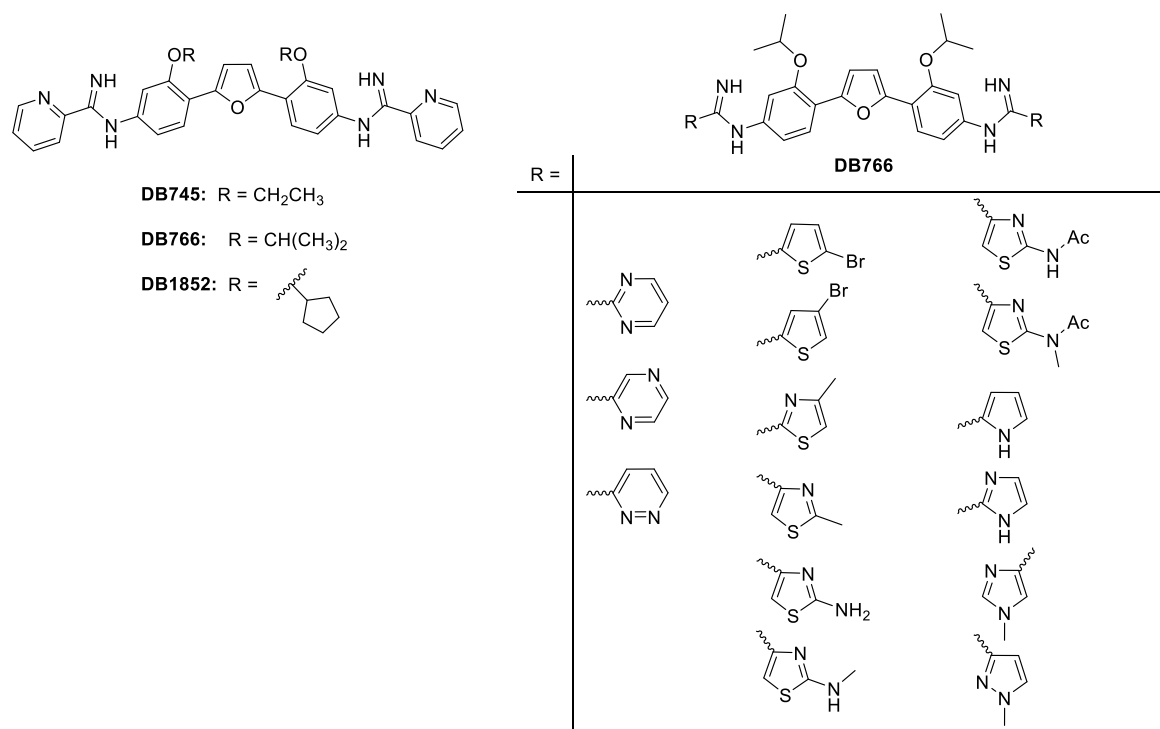
Figure 1.17: Chemical structure of bis(arylimidamide) minor groove binders active against kinetoplastid parasites.

Bis(2-aminoimidazolines) compounds are a class of DNA minor groove binders with established *in vitro* and *in vivo* efficacy against *T. brucei* (Figure 1.18).[151-157] A major difference between these compounds and the diamidines (e.g., furamidine) is the presence of different cationic functionalities. The replacement of the amidine with a guanidine-derived functional group allows an extra point of contact (i.e., polar imino N, H-Bond donor) and an increased hydrophobic character (i.e., ethylene bridge for the cyclic 2-aminoimidazoline groups) that potentially increase the DNA binding affinity.[152, 158]

X = CH$_2$, CH$_2$CH$_2$, NH, CO, CONH
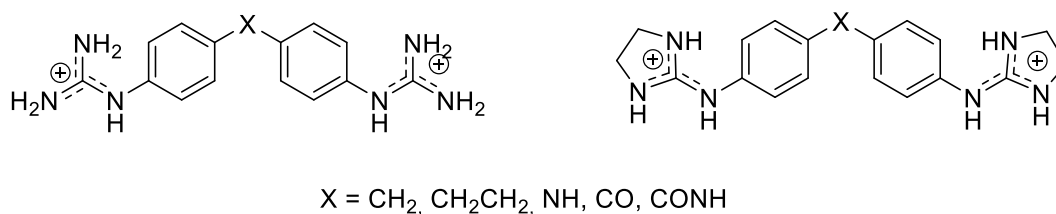
Figure 1.18: Bisguanidinium (left) and bis(2-aminoimidazolidinium) (right) MGBs with antitrypanosomal activity.

1.4. Previous work that constitutes the basis of this research

Previous studies in Dr. Dardonville's group on bisguanidine and bis(2-aminoimidazoline) compounds have shown the *N*-phenylbenzamide derivative **I**, which was orally active in an acute mouse model of *T. b. rhodesiense* infection, is the prototype of this series (Figure 1.19).[153, 155] They showed that the introduction of one halogen atom into the *N*-phenylbenzamide scaffold of **I** would reduce the pK_a and improve the trypanocidal activity of the same (e.g., compound **II**, Figure 1.19).[159] Studies of the binding mode of lead compounds **I** and **II** to DNA showed that these compounds are minor groove binders, with selectivity for the AT-rich DNA sequences. This mode of interaction was studied on the crystallised drug–DNA complexes.[160]

I: R = H
II: R = Cl

III: R = H, Me, Et, Bn
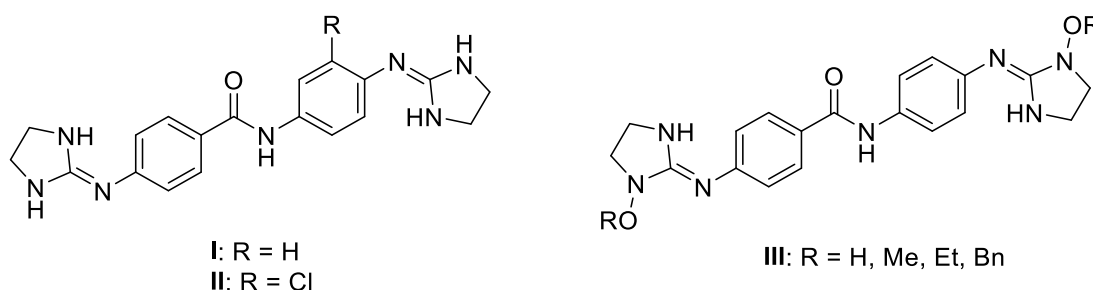
Figure 1.19: Chemical structure of the *N*-phenylbenzamide derivative lead **I** and analogues **II** and **III**.

Strong experimental evidences suggested that compound **I** can displace HMG-box-containing proteins that are essential for kDNA function from their DNA binding sites. This interaction led to the disruption of kinetoplast DNA (kDNA) and eventually to the death of the parasite.[160]

Modification of the pending imidazoline rings with alkoxy groups also reduced the basicity of these bis(2-aminoimidazoline) compounds by approximately 2 pK_a units. The *N*-hydroxy-substituted compound (**III**, R = H) showed efficacy in models of first- and

second-stage *T. brucei* infection in mice (Figure 1.19). However, these compounds were inactive against *L. donovani* and *T. cruzi*.[153]

In spite of their action on kDNA and their excellent trypanocidal activity, bis(2-aminoimidazolines) are much less active or inactive against other kinetoplastid endoparasites such as *Leishmania* or *T. cruzi*.[154, 156] For instance, lead compound **I** displays a 5-fold lower activity against promastigotes of *L. donovani* ($EC_{50} = 4.29$ µM) than against bloodstream form *T. b. brucei* ($EC_{50} = 0.83$ µM).[159] This difference is attributed to a poor passive permeation of these dicationic compounds across biological membranes. In fact, a drug targeting the kDNA of *Leishmania* amastigotes will have to cross 4 membranes (host cell membrane, parasitophorous vacuole membrane, parasite cell membrane, and mitochondrial membrane) to reach its target. Boykin and co-workers showed that bis(arylimidamides) are interesting analogues of diamidine drugs with lower basicity ($pK_a \approx 7$) and higher lipophilicity, which makes them especially active against intracellular parasites such as *Leishmania* and *T. cruzi*.[122, 131, 134, 135, 141, 145] In particular, they showed that compounds with 2-pyridyl terminal groups and fairly large hydrophobic substituents on the diphenylfuran linker were very effective against intracellular *L. amazonensis*.[135]

Since compound **I** is an excellent DNA MGB with proven *in vivo* efficacy, and kDNA is a common target shared by *T. brucei*, *T. cruzi* and *Leishmania* parasites, this Thesis work aimed at optimizing the biological activity of compound **I** towards the endoparasites *Leishmania* and *T. cruzi*. To do so, three new families of dicationic derivatives were synthesised [i.e., bis(imidazolidine-2-imines) (series **1**), bis(2-aminobenzimidazoles) (series **2**) and bis(arylimidamides) (series **3**)] and their antiprotozoal activity and DNA binding affinity were studied by biological and biophysical assays.

In the context of kinetoplastid diseases, the target product profile for Chagas disease and leishmaniasis is shown in Table 1.1.

Table 1.1 Ideal Target Product Profiles for the kinetoplastid diseases (modified from DND$_i$)[161-163]

	Chagas disease	Cutaneous leishmaniasis	Visceral leishmaniasis combination therapies
Target	Chronic and acute	One treatment for all species of *Leishmania*	Patients with visceral leishmaniasis and PKDL Immunocompetent and immunosuppressed Active against all species and resistant strains
Geographic distribution	All regions	All regions	All areas
Efficacy	Superiority to benznidazole standard dose in acute and chronic phases of disease	>95% patients with complete clinical cure, defined as 100% epithelialization/flattening of lesion(s) at 3 months from treatment onset Minimal scar No relapse or development of *Leishmania recidivans* or mucocutaneous leishmaniasis (MCL) Parasitological endpoint not required	≥ 95%
Safety/tolerability	Superiority to benznidazole* in the frequency of definitive treatment discontinuations for medical indication** No genotoxicity, no teratogenicity, no pro-arrhythmic potential	Well tolerated All adverse reactions (AR)s ≤ grade 1	No adverse events (AEs) requiring monitoring
Contraindications	No contraindications	None	None
Drug-drug interactions	No clinically significant interactions	—	No interactions between the drugs to be combined for visceral leishmaniasis treatment, or with those used for other common comorbidities (malaria, TB, HIV)
Formulation	Oral (Age adapted)	Topical/oral	Oral/oral
Stability	5 yearas, climatic zone IV	No cold chain At least 3 years at 37 °C	3 years in climatic zone IV
Treatment regimen	< 30 days	Topical ≤ 14 days Oral < 7 days	Single dose treatment or fixed-dose combination tablet/paediatric formulation up to 7 days
Cost	Lowest possible	To be defined	To be defined

*As per WHO recommendation. ** No genotoxicity is a condition only for NCEs. *** Need for parenteral treatment for severe disease*

1.5. References

1. World Health Organization (WHO). Neglected Tropical Diseases. https://www.who.int/health-topics/neglected-tropical-diseases#tab=tab_1 (18 April, 2022).

2. Centers for Disease Control and Prevention (CDC). Neglected Tropical Diseases. https://www.cdc.gov/globalhealth/ntd/diseases/index.html (18 April 2022).

3. Hotez, P. J.; Molyneux, D. H.; Fenwick, A.; Kumaresan, J.; Sachs, S. E.; Sachs, J. D.; Savioli, L. Control of Neglected Tropical Diseases. *N. Engl. J. Med.* **2007,** 357, 1018-1027.

4. Hotez, P. J. One World Health: Neglected Tropical Diseases in a Flat World. *PLoS Negl. Trop. Dis.* **2009,** 3, e405.

5. Rao, S. P. S.; Barrett, M. P.; Dranoff, G.; Faraday, C. J.; Gimpelewicz, C. R.; Hailu, A.; Jones, C. L.; Kelly, J. M.; Lazdins-Helds, J. K.; Mäser, P.; Mengel, J.; Mottram, J. C.; Mowbray, C. E.; Sacks, D. L.; Scott, P.; Späth, G. F.; Tarleton, R. L.; Spector, J. M.; Diagana, T. T. Drug Discovery for Kinetoplastid Diseases: Future Directions. *ACS Infect. Dis.* **2019,** 5, 152-157.

6. Stuart, K.; Brun, R.; Croft, S.; Fairlamb, A.; Gürtler, R. E.; McKerrow, J.; Reed, S.; Tarleton, R. Kinetoplastids: related protozoan pathogens, different diseases. *J. Clin. Invest.* **2008,** 118, 1301-1310.

7. Barrett, M. P.; Burchmore, R. J.; Stich, A.; Lazzari, J. O.; Frasch, A. C.; Cazzulo, J. J.; Krishna, S. The trypanosomiases. *Lancet* **2003,** 362, 1469-1480.

8. Gull, K. The biology of kinetoplastid parasites: insights and challenges from genomics and post-genomics. *Int. J. Parasitol.* **2001,** 31, 443-452.

9. Gull, K. The Cytoskeleton of Trypanosomatid Parasites. *Annu. Rev. Microbiol.* **1999,** 53, 629-655.

10. Cerecetto, H.; González, M. Synthetic medicinal chemistry in Chagas' disease: Compounds at the final stage of "hit-to-lead" phase. *Pharmaceuticals* **2010,** 3, 810-838.

11. Richard, J. V.; Werbovetz, K. A. New antileishmanial candidates and lead compounds. *Curr. Opin. Chem. Biol.* **2010,** 14, 447-455.

12. Motta, M. C. Kinetoplast as a potential chemotherapeutic target of trypanosomatids. *Curr. Pharm. Des.* **2008,** 14, 847-854.

13. Centers for Disease Control and Prevention (CDC). Parasites - Leishmaniasis. https://www.cdc.gov/parasites/leishmaniasis/gen_info/faqs.html (April 28, 2022).

14. World Health Organization (WHO). Leishmaniasis. https://www.who.int/health-topics/leishmaniasis#tab=tab_1 (April 29, 2022).

15. World Health Organization (WHO). Skin NTDs: prioritizing integrated approaches to reduce suffering, psychosocial impact and stigmatization. https://www.who.int/news/item/29-10-2020-skin-ntds-prioritizing-integrated-approaches-to-reduce-suffering-psychosocial-impact-and-stigmatization (April 29, 2022).

16. Machado, P. R. L.; Rosa, M. E. A.; Guimarães, L. H.; Prates, F. V. O.; Queiroz, A.; Schriefer, A.; Carvalho, E. M. Treatment of disseminated Leishmaniasis with liposomal Amphotericin B. *Clin. Infect. Dis.* **2015,** 61, 945-949.

17. Berman, J. D. Human Leishmaniasis: Clinical, Diagnostic, and Chemotherapeutic Developments in the Last 10 Years. *Clin. Infect. Dis.* **1997,** 24, 684-703.

18. Kassi, M.; Kassi, M.; Afghan, A. K.; Rehman, R.; Kasi, P. M. Marring Leishmaniasis: The Stigmatization and the Impact of Cutaneous Leishmaniasis in Pakistan and Afghanistan. *PLoS Negl. Trop. Dis.* **2008,** 2, e259.

19. Ashkan, M. M.; Rahim, K. M. Visceral leishmaniasis in paediatrics: a study of 367 cases in southwest Iran. *Trop. Doct.* **2008,** 38, 186-188.

20. Stanley, A. C.; Engwerda, C. R. Balancing immunity and pathology in visceral leishmaniasis. *Immunol. Cell Biol.* **2007,** 85, 138-147.

21. Choi, H. L.; Jain, S.; Ruiz Postigo, J. A.; Borisch, B.; Dagne, D. A. The global procurement landscape of leishmaniasis medicines. *PLoS Negl. Trop. Dis.* **2021,** 15, e0009181.

22. Zulfiqar, B.; Shelper, T. B.; Avery, V. M. Leishmaniasis drug discovery: recent progress and challenges in assay development. *Drug Discov. Today* **2017,** 22, 1516-1531.

23. Alves, F.; Bilbe, G.; Blesson, S.; Goyal, V.; Monnerat, S.; Mowbray, C.; Ouattara, G. M.; Pécoul, B.; Rijal, S.; Rode, J.; Solomos, A.; Strub-Wourgaft, N.; Wasunna, M.; Wells, S.; Zijlstra, E. E.; Arana, B.; Alvar, J. Recent Development of Visceral Leishmaniasis Treatments: Successes, Pitfalls, and Perspectives. *Clin. Microbiol. Rev.* **2018,** 31, e00048-18.

24. Musa, A.; Khalil, E.; Hailu, A.; Olobo, J.; Balasegaram, M.; Omollo, R.; Edwards, T.; Rashid, J.; Mbui, J.; Musa, B.; Abuzaid, A. A.; Ahmed, O.; Fadlalla, A.; El-Hassan, A.; Mueller, M.; Mucee, G.; Njoroge, S.; Manduku, V.; Mutuma, G.; Apadet, L.; Lodenyo, H.; Mutea, D.; Kirigi, G.; Yifru, S.; Mengistu, G.; Hurissa, Z.; Hailu, W.; Weldegebreal, T.; Tafes, H.; Mekonnen, Y.; Makonnen, E.; Ndegwa, S.; Sagaki, P.; Kimutai, R.; Kesusu, J.; Owiti, R.; Ellis, S.; Wasunna, M. Sodium Stibogluconate (SSG) & Paromomycin Combination Compared to SSG for Visceral Leishmaniasis in East Africa: A Randomised Controlled Trial. *PLoS Negl. Trop. Dis.* **2012,** 6, e1674.

25. Bellini, M. F.; Silistino-Souza, R.; Varella-Garcia, M.; de Azeredo-Oliveira, M. T. V.; Silva, A. E. Biologic and Genetics Aspects of Chagas Disease at Endemic Areas. *J. Trop. Med.* **2012,** 2012, 357948.

26. Centers for Disease Control and Prevention (CDC). Parasites - American Trypanosomiasis (also known as Chagas Disease). https://www.cdc.gov/parasites/chagas/ (April 28, 2022).

27. Stanaway, J. D.; Roth, G. The burden of Chagas disease: estimates and challenges. *Glob Heart* **2015,** 10, 139-144.

28. World Health Organization (WHO). *Investing to overcome the global impact of neglected tropical diseases. Third WHO Report on Neglected Tropical Diseases. Department of Control of Neglected Tropical Diseases, WHO, Geneva.*; 2015.

29. Dubner, S.; Schapachnik, E.; Riera, A. R.; Valero, E. Chagas disease: state-of-the-art of diagnosis and management. *Cardiol. J.* **2008,** 15, 493-504.

30. Sánchez-Valdéz, F. J.; Padilla, A.; Wang, W.; Orr, D.; Tarleton, R. L. Spontaneous dormancy protects Trypanosoma cruzi during extended drug exposure. *eLife* **2018,** 7, e34039.

31. World Health Organization (WHO). Trypanosomiasis, human African (sleeping sickness). https://www.who.int/news-room/fact-sheets/detail/trypanosomiasis-human-african-(sleeping-sickness) (May 2, 2022).

32. Centers for Disease Control and Prevention (CDC). Parasites - African Trypanosomiasis (also known as Sleeping Sickness). https://www.cdc.gov/parasites/sleepingsickness/index.html (April 28, 2022).

33. Steverding, D. The development of drugs for treatment of sleeping sickness: a historical review. *Parasites Vectors* **2010,** 3, 15.

34. World Health Organization (WHO). Trypanosomiasis, human African sleeping sickness - Key facts. https://www.who.int/news-room/fact-sheets/detail/trypanosomiasis-human-african-(sleeping-sickness (May 2, 2022).

35. Maxmen, A. Sleeping sickness can now be cured with pills. *Nature* **2017,** 550, 441-441.

36. Rahman, A.; O'Sullivan, P.; Rozas, I. Recent developments in compounds acting in the DNA minor groove. *MedChemComm* **2019,** 10, 26-40.

37. Kennard, O. DNA-drug interactions. *Pure Appl. Chem.* **1993,** 65, 1213-1222.

38. Khan, G. S.; Shah, A.; Zia ur, R.; Barker, D. Chemistry of DNA minor groove binding agents. *J. Photochem. Photobiol., B* **2012,** 115, 105-118.

39. Baraldi, P. G.; Bovero, A.; Fruttarolo, F.; Preti, D.; Tabrizi, M. A.; Pavani, M. G.; Romagnoli, R. DNA minor groove binders as potential antitumor and antimicrobial agents. *Med. Res. Rev.* **2004,** 24, 475-528.

40. Denny, W. A. Chemotherapeutic effects of acridine derivatives. *Med. Chem. Rev.-Online* **2004,** 1, 257-266.

41. Nelson, S. M.; Ferguson, L. R.; Denny, W. A. Non-covalent ligand/DNA interactions: Minor groove binding agents. *Mutat. Res., Fundam. Mol. Mech. Mutagen.* **2007,** 623, 24-40.

42. Watson, J. D.; Crick, F. H. C. Molecular structure of nucleic acids. *Nature* **1953,** 171, 737-738.

43. Neidle, S. *Principles of Nucleic Acid Structure.* 1st edition ed.; Elsevier: 2008.

44. Largy, E.; König, A.; Ghosh, A.; Ghosh, D.; Benabou, S.; Rosu, F.; Gabelica, V. Mass Spectrometry of Nucleic Acid Noncovalent Complexes. *Chem. Rev.* **2022,** 122, 7720-7839.

45. Rich, A. The double helix: a tale of two puckers. *Nat. Struct. Mol. Biol.* **2003,** 10, 247-249.

46. Ghosh, A.; Bansal, M. A glossary of DNA structures from A to Z. *Acta Crystallogr. D.* **2003,** 59, 620-626.

47. Clayton, D. A. Transcription and replication of mitochondrial DNA. *Hum. Reprod.* **2000,** 15, 11-17.

48. Neidle, S.; Thurston, D. E. Chemical approaches to the discovery and development of cancer therapies. *Nat. Rev. Cancer* **2005,** 5, 285-296.

49. Hirsch, J. An Anniversary for Cancer Chemotherapy. *JAMA* **2006,** 296, 1518-1520.

50. Cheson, B. D.; Rummel, M. J. Bendamustine: rebirth of an old drug. *J. Clin. Oncol.* **2009,** 27, 1492-1501.

51. Griffith, D.; P Parker, J.; J Marmion, C. Enzyme inhibition as a key target for the development of novel metal-based anti-cancer therapeutics. *Anti-Cancer Agents Med. Chem.* **2010,** 10, 354-370.

52. Sriram, D.; Yogeeswari, P.; Thirumurugan, R.; Ratan Bal, T. Camptothecin and its analogues: a review on their chemotherapeutic potential. *Nat. Prod. Res.* **2005,** 19, 393-412.

53. Ashley, N.; Poulton, J. Mitochondrial DNA is a direct target of anti-cancer anthracycline drugs. *Biochem. Biophys. Res. Commun.* **2009,** 378, 450-455.

54. Chen, J.; Stubbe, J. Bleomycins: towards better therapeutics. *Nat. Rev. Cancer* **2005,** 5, 102-112.

55. Neidle, S. *Nucleic Acid Structure and Recognition*. Oxford University Press: 2002.

56. Dickerson, R. E.; Drew, H. R.; Conner, B. N.; Wing, R. M.; Fratini, A. V.; Kopka, M. L. The Anatomy of A-, B-, and Z-DNA. *Science* **1982,** 216, 475-485.

57. Hud, N. V.; Polak, M. DNA–cation interactions: the major and minor grooves are flexible ionophores. *Curr. Opin. Struct. Biol.* **2001,** 11, 293-301.

58. Perepelytsya, S.; Uličný, J.; Laaksonen, A.; Mocci, F. Pattern preferences of DNA nucleotide motifs by polyamines putrescine^{2+}, spermidine^{3+} and spermine^{4+}. *Nucleic Acid Res.* **2019,** 47, 6084-6097.

59. Kim, S. K.; Nordén, B. Methyl green: A DNA major-groove binding drug. *FEBS Lett.* **1993,** 315, 61-64.

60. Breitkreuz, C. J.; Zadmard, R.; Schrader, T. DNA recognition with large calixarene dimers and varying spacers. *Supramol. Chem.* **2008,** 20, 109-115.

61. Pindur, U.; Fischer, G. DNA complexing minor groove-binding ligands: perspectives in antitumour and antimicrobial drug design. *Curr. Med. Chem.* **1996,** 3, 379-406.

62. Morávek, Z.; Neidle, S.; Schneider, B. Protein and drug interactions in the minor groove of DNA. *Nucleic Acid Res.* **2002,** 30, 1182-1191.

63. Pullman, B.; Lavery, R.; Pullman, A. Two aspects of DNA polymorphism and microheterogeneity: molecular electrostatic potential and steric accessibility. *Eur. J. Biochem.* **1982,** 124, 229-238.

64. Perahia, D.; Pullman, A.; Pullman, B. Molecular electrostatic potential of the B-DNA helix. V. Poly(dG·dC) and poly(dA·dT). *Int. J. Quantum Chem.* **1979,** 16, 353-363.

65. Corbin, S.; Lavery, R.; Pullman, B. The molecular electrostatic potential of DNA: The effect of countercation screening on various allomorphic forms. *Int. J. Quantum Chem.* **2009,** 22, 103-110.

66. Bailly, C.; Helbecque, N.; Hénichart, J. P.; Colson, P.; Houssier, C.; Rao, K. E.; Shea, R. G.; Lown, J. W. Molecular recognition between oligopeptides and nucleic acids. DNA sequence specificity and binding properties of an acridine-linked netropsin hybrid ligand. *J. Mol. Recognit.* **1990,** 3, 26-35.

67. De Koning, H. P. The Drugs of Sleeping Sickness: Their Mechanisms of Action and Resistance, and a Brief History. *Trop. Med. Infect. Dis.* **2020,** 5, 14.

68. Neidle, S. DNA minor-groove recognition by small molecules. *Nat. Prod. Rep.* **2001,** 18, 291-309.

69. Kahvedžić, A. New families of Minor Groove Binders: Synthesis, Biophysical and Biochemical Evaluation and their Role in Apoptosis. Trinity College, Dublin, Ireland, Trinity College Dublin, 2011.

70. Fox, K. R.; Sansom, C. E.; Stevens, M. F. Footprinting studies on the sequence-selective binding of pentamidine to DNA. *FEBS Lett.* **1990,** 266, 150-154.

71. Dann, O.; Fernbach, R.; Pfeifer, W.; Demant, E.; Bergen, G.; Lang, S.; Lürding, G. Trypanocide Diamidine mit drei Ringen in zwei isolierten Ringsystemen. *Justus Liebigs Ann. Chem.* **1972,** 760, 37-87.

72. Chandra, P.; Mildner, B.; Dann, O.; Metz, A. Influence of 4′-6-diamidino-2-phenylindole on the secondary structure and template activities of DNA and polydeoxynucleotides. *Mol. Cell. Biochem.* **1977,** 18, 81-86.

73. Mildner, B.; Metz, A.; Chandra, P. Interaction of 4′-6-diamidino-2-phenylindole to nucleic acids, and its implication to their template activity in RNA-polymerase reaction of E. coli bacteria and of friend-virus infected mouse spleen. *Cancer Lett.* **1978,** 4, 89-98.

74. Jensch, H. 4,4'-Diamidino-diazoaminobenzene, a new agent in the treatment of trypanosomiasis and babesiasis. *Arzneimittel-Forsch.* **1955,** 5 (11), 634-635.

75. Newton, B. A. Berenil: a trypanocide with selective activity against extranuclear DNA. In *Mechanism of Action of Antimicrobial and Antitumor Agents*, Springer: 1975; pp 34-47.

76. Newton, B. A. Preferential inhibition of extranuclear deoxyribonucleic acid synthesis by the trypanocide berenil. *Proc. Biochem. Soc. (475th Meeting)* **1967,** 105.

77. Botha, H. Berenil: efficacy against *Babesia canis* and comparison with phenamidine. *J. S. Afr. Vet. Assoc.* **1964,** 35, 23-26.

78. Wu, S. Y.; Park, G. Y.; Kim, S. H.; Hulme, J.; An, S. S. Diminazene aceturate: an antibacterial agent for Shiga-toxin-producing *Escherichia coli* O157:H7. *Drug Des., Dev. Ther.* **2016,** 10, 3363-3378.

79. Wierenga, W. Sequence-selective DNA-interactive antitumor agents. *Drugs Future* **1991,** 16, 741-750.

80. Vickerman, K. On The Surface Coat and Flagellar Adhesion in Trypanosomes. *J. Cell Sci.* **1969,** 5, 163-193.

81. Vargas-Parada, L. Kinetoplastids and their networks of interlocked DNA. *Nature Education* **2010,** 3, 63.

82. Liu, B.; Liu, Y.; Motyka, S. A.; Agbo, E. E. C.; Englund, P. T. Fellowship of the rings: the replication of kinetoplast DNA. *Trends Parasitol.* **2005,** 21, 363-369.

83. Riou, G.; Delain, E. Electron microscopy of the circular kinetoplastic DNA from *Trypanosoma cruzi*: occurrence of catenated forms. *Proc. Natl. Acad. Sci. U. S. A.* **1969,** 62, 210-217.

84. Laurent, M.; Steinert, M. Electron microscopy of kinetoplastic DNA from *Trypanosoma mega. Proc. Natl. Acad. Sci. U.S.A.* **1970,** 66, 419-424.

85. Simpson, L.; da Silva, A. Isolation and characterization of kinetoplast DNA from *Leishmania tarentolae. J. Mol. Biol.* **1971,** 56, 443-473.

86. Klingbeil, M. M.; Drew, M. E.; Liu, Y.; Morris, J. C.; Motyk, S. A.; Saxowsky, T. T.; Wang, Z.; Englund, P. T. Unlocking the Secrets of *Trypanosome* Kinetoplast DNA Network Replication. *Protist* **2001,** 152, 255-262.

87. Li, C.; Englund, P. T. A Mitochondrial DNA Primase from the Trypanosomatid *Crithidia fasciculata *. *J. Biol. Chem.* **1997,** 272, 20787-20792.

88. Zuma, A. A.; Cavalcanti, D. P.; Zogovich, M.; Machado, A. C. L.; Mendes, I. C.; Thiry, M.; Galina, A.; de Souza, W.; Machado, C. R.; Motta, M. C. M. Unveiling the effects of berenil, a DNA-binding drug, on *Trypanosoma cruzi*: implications for kDNA ultrastructure and replication. *Parasitol. Res.* **2015,** 114, 419-430.

89. Chen, J.; Rauch, C. A.; White, J. H.; Englund, P. T.; Cozzarelli, N. R. The topology of the kinetoplast DNA network. *Cell* **1995,** 80, 61-69.

90. Rauch, C. A.; Perez-Morga, D.; Cozzarelli, N. R.; Englund, P. T. The absence of supercoiling in kinetoplast DNA minicircles. *Embo J.* **1993,** 12, 403-411.

91. Lukeš, J.; Hines, J. C.; Evans, C. J.; Avliyakulov, N. K.; Prabhu, V. P.; Chen, J.; Ray, D. S. Disruption of the *Crithidia fasciculata* KAP1 gene results in structural rearrangement of the kinetoplast disc. *Mol. Biochem. Parasitol.* **2001,** 117, 179-186.

92. Das, B. B.; Ganguly, A.; Majumder, H. K. DNA topoisomerases of *Leishmania*: the potential targets for anti-leishmanial therapy. In *Drug targets in Kinetoplastid parasites*, Majumder, H. K., Ed. Springer, New York, NY: 2008; pp 103-115.

93. Lourie, E. M.; Yorke, W. Studies in Chemotherapy. *Ann. Trop. Med. Parasitol.* **1937,** 31, 435-445.

94. von Jancsó, N.; von Jancsó, H. Chemotherapeutic effects and carbohydrate metabolism: The healing effects of guanidine derivatives on trypanosome infection. *Z. Immunitätsforsch. Exper. Ther.* **1935,** 86, 1-30.

95. Schern, K.; Artagaveytia-Allende, R. Zur glykopriven therapie und prophylaxe mit sowohl toxisch als auch atoxisch wirkenden substanzen bei der experimentellen trypanosomen und treponemeninfektion. . *Z. Immunitätsforsch. Exper. Ther.* **1936,** 89, 21-64.

96. Ashley, J. N.; Barber, H. J.; Ewins, A. J.; Newbery, G.; Self, A. D. H. 20. A chemotherapeutic comparison of the trypanocidal action of some aromatic diamidines. *J. Chem. Soc.* **1942**, 103-116.

97. King, H.; Lourie, E. M.; Yorke, W. Studies in Chemotherapy. *Ann. Trop. Med. Parasitol.* **1938,** 32, 177-192.

98. King, H.; Lourie, E. M.; Yorke, W. New trypanocidal substances. *Lancet* **1937,** 230 (5963), 1360-1363.

99. Lourie, E. M.; Yorke, W. Studies in Chemotherapy. *Ann. Trop. Med. Parasitol.* **1939,** 33 (3-4), 289-304.

100. Wragg, W. R.; Washbourn, K.; Brown, K. N.; Hill, J. Metamidium: A new trypanocidal drug. *Nature* **1958,** 182 (4641), 1005-1006.

101. Vardanyan, R. S.; Hruby, V. J. 37 - Drugs for Treating Protozoan Infections. In *Synthesis of Essential Drugs*, Vardanyan, R. S.; Hruby, V. J., Eds. Elsevier: Amsterdam, 2006; pp 559-582.

102. Scholar, E. Pentamidine. In *xPharm: The Comprehensive Pharmacology Reference*, Enna, S. J.; Bylund, D. B., Eds. Elsevier: New York, 2009; pp 1-7.

103. Franco, J.; Scarone, L.; Comini, M. A. Chapter Three - Drugs and Drug Resistance in African and American Trypanosomiasis. In *Annu. Rep. Med. Chem.*, Botta, M., Ed. Academic Press: 2018; Vol. 51, pp 97-133.

104. Tiwari, N.; Kumar, A.; Singh, A. K.; Bajpai, S.; Agrahari, A. K.; Kishore, D.; Tiwari, V. K.; Singh, R. K. 8 - Leishmaniasis control: limitations of current drugs and prospects of natural products. In *Discovery and Development of Therapeutics from Natural Products Against Neglected Tropical Diseases*, Brahmachari, G., Ed. Elsevier: 2019; pp 293-350.

105. Jacobs, R. T.; Ding, C. Chapter 17 - Recent Advances in Drug Discovery for Neglected Tropical Diseases Caused by Infective Kinetoplastid Parasites. In *Annu. Rep. Med. Chem.*, Macor, J. E., Ed. Academic Press: 2010; Vol. 45, pp 277-294.

106. Neidle, S.; Kelland, L. R.; Trent, J. O.; Simpson, I. J.; Boykin, D. W.; Kumar, A.; Wilson, W. D. Cytotoxicity of bis(phenylamidinium)furan alkyl derivatives in human tumour cell lines: Relation to DNA minor groove binding. *Bioorg. Med. Chem. Lett.* **1997,** 7, 1403-1408.

107. Boykin, D. W.; Kumar, A.; Xiao, G.; Wilson, W. D.; Bender, B. C.; McCurdy, D. R.; Hall, J. E.; Tidwell, R. R. 2,5-Bis[4-(*N*-alkylamidino)phenyl]furans as Anti-*Pneumocystis carinii* Agents. *J. Med. Chem.* **1998,** 41, 124-129.

108. Del Poeta, M.; Schell, W. A.; Dykstra, C. C.; Jones, S.; Tidwell, R. R.; Czarny, A.; Bajic, M.; Kumar, A.; Boykin, D.; Perfect, J. R. Structure-*in vitro* activity relationships of pentamidine analogues and dication-substituted bis-benzimidazoles as new antifungal agents. *Antimicrob. Agents Chemother.* **1998,** 42, 2495-502.

109. Feichtinger, K.; Zapf, C.; Sings, H. L.; Goodman, M. Diprotected Triflylguanidines: A New Class of Guanidinylation Reagents. *The Journal of Organic Chemistry* **1998,** 63, 3804-3805.

110. Hopkins, K. T.; Wilson, W. D.; Bender, B. C.; McCurdy, D. R.; Hall, J. E.; Tidwell, R. R.; Kumar, A.; Bajic, M.; Boykin, D. W. Extended Aromatic Furan Amidino Derivatives as Anti-*Pneumocystis carinii* Agents. *J. Med. Chem.* **1998,** 41, 3872-3878.

111. Francesconi, I.; Wilson, W. D.; Tanious, F. A.; Hall, J. E.; Bender, B. C.; Tidwell, R. R.; McCurdy, D.; Boykin, D. W. 2,4-Diphenyl Furan Diamidines as Novel Anti-*Pneumocystis carinii* Pneumonia Agents. *J. Med. Chem.* **1999,** 42, 2260-2265.

112. Stephens, C. E.; Tanious, F.; Kim, S.; Wilson, W. D.; Schell, W. A.; Perfect, J. R.; Franzblau, S. G.; Boykin, D. W. Diguanidino and "Reversed" Diamidino 2,5-Diarylfurans as Antimicrobial Agents. *J. Med. Chem.* **2001,** 44, 1741-1748.

113. Tidwell, R. R. B., W. D. Dicationic DNA Minor Groove Binders as Antimicrobial Agents. In Small Molecule DNA and RNA Binders: From Synthesis to Nucleic Acid Complexes. In Wiley-VCH: Weinheim, Germany, 2002; Vol. 2, pp 414-460.

114. Ismail, M. A.; Brun, R.; Wenzler, T.; Tanious, F. A.; Wilson, W. D.; Boykin, D. W. Dicationic biphenyl benzimidazole derivatives as antiprotozoal agents. *Bioorg. Med. Chem.* **2004,** 12, 5405-5413.

115. Arafa, R. K.; Brun, R.; Wenzler, T.; Tanious, F. A.; Wilson, W. D.; Stephens, C. E.; Boykin, D. W. Synthesis, DNA Affinity, and Antiprotozoal Activity of Fused Ring Dicationic Compounds and Their Prodrugs. *J. Med. Chem.* **2005,** 48, 5480-5488.

116. Ismail, M. A.; Batista-Parra, A.; Miao, Y.; Wilson, W. D.; Wenzler, T.; Brun, R.; Boykin, D. W. Dicationic near-linear biphenyl benzimidazole derivatives as DNA-targeted antiprotozoal agents. *Bioorg. Med. Chem.* **2005,** 13, 6718-6726.

117. Wilson, W. D.; Nguyen, B.; Tanious, F. A.; Mathis, A.; Hall, J. E.; Stephens, C. E.; Boykin, D. W. Dications that target the DNA minor groove: compound design and preparation, DNA interactions, cellular distribution and biological activity. *Curr. Med. Chem.: Anti-Cancer Agents* **2005,** 5, 389-408.

118. Wilson, W. D.; Tanious, F. A.; Mathis, A.; Tevis, D.; Hall, J. E.; Boykin, D. W. Antiparasitic compounds that target DNA. *Biochimie* **2008,** 90, 999-1014.

119. Hu, L.; Kully, M. L.; Boykin, D. W.; Abood, N. Optimization of the central linker of dicationic bis-benzimidazole anti-MRSA and anti-VRE agents. *Bioorg. Med. Chem. Lett.* **2009,** 19, 3374-3377.

120. Pacheco, M. G.; da Silva, C. F.; de Souza, E. M.; Batista, M. M.; da Silva, P. B.; Kumar, A.; Stephens, C. E.; Boykin, D. W.; Soeiro Mde, N. *Trypanosoma cruzi*: activity of heterocyclic cationic molecules *in vitro*. *Exp. Parasitol.* **2009,** 123, 73-80.

121. Farahat, A. A.; Paliakov, E.; Kumar, A.; Barghash, A.-E. M.; Goda, F. E.; Eisa, H. M.; Wenzler, T.; Brun, R.; Liu, Y.; Wilson, W. D.; Boykin, D. W. Exploration of larger central ring linkers in furamidine analogues: Synthesis and evaluation of their DNA binding, antiparasitic and fluorescence properties. *Bioorg. Med. Chem.* **2011,** 19, 2156-2167.

122. Soeiro, M. N. C.; Werbovetz, K.; Boykin, D. W.; Wilson, W. D.; Wang, M. Z.; Hemphill, A. Novel amidines and analogues as promising agents against intracellular parasites: a systematic review. *Parasitology* **2013,** 140, 929-951.

123. Harika, N. K.; Paul, A.; Stroeva, E.; Chai, Y.; Boykin, D. W.; Germann, M. W.; Wilson, W. D. Imino proton NMR guides the reprogramming of A•T specific minor groove binders for mixed base pair recognition. *Nucleic Acid Res.* **2016,** 44, 4519-4527.

124. Farahat, A. A.; Ismail, M. A.; Kumar, A.; Wenzler, T.; Brun, R.; Paul, A.; Wilson, W. D.; Boykin, D. W. Indole and Benzimidazole Bichalcophenes: Synthesis, DNA Binding and Antiparasitic Activity. *Eur. J. Med. Chem.* **2018,** 143, 1590-1596.

125. Mdachi, R. E.; Thuita, J. K.; Kagira, J. M.; Ngotho, J. M.; Murilla, G. A.; Ndung'u, J. M.; Tidwell, R. R.; Hall, J. E.; Brun, R. Efficacy of the Novel Diamidine Compound 2,5-Bis(4-Amidinophenyl)- Furan-Bis-*O*-Methylamidoxime (Pafuramidine, DB289) against *Trypanosoma brucei rhodesiense* Infection in Vervet Monkeys after Oral Administration. *Antimicrob. Agents Chemother.* **2009,** 53, 953-957.

126. Nyunt, M. M.; Hendrix, C. W.; Bakshi, R. P.; Kumar, N.; Shapiro, T. A. Phase I/II Evaluation of the Prophylactic Antimalarial Activity of Pafuramidine in Healthy Volunteers Challenged with *Plasmodium falciparum* Sporozoites. *Am. J. Trop. Med. Hyg.* **2009,** 80, 528-535.

127. Thuita, J. K.; Karanja, S. M.; Wenzler, T.; Mdachi, R. E.; Ngotho, J. M.; Kagira, J. M.; Tidwell, R.; Brun, R. Efficacy of the diamidine DB75 and its prodrug DB289, against murine models of human African trypanosomiasis. *Acta Trop.* **2008,** 108, 6-10.

128. Hall, J. E.; Kerrigan, J. E.; Ramachandran, K.; Bender, B. C.; Stanko, J. P.; Jones, S. K.; Patrick, D. A.; Tidwell, R. R. Anti-*Pneumocystis* Activities of Aromatic Diamidoxime Prodrugs. *Antimicrob. Agents Chemother.* **1998,** 42, 666-674.

129. Bajic, M.; Kumar, A.; Boykin, D. W. Synthesis of 2,5-Bis-(4-cyanophenyl)-furan. *Heterocycl. Commun.* **1996,** 2, 135-140.

130. Paine, M.; Wang , M.; Boykin, D.; Wilson, W. D.; De Koning, H. P.; Olson, C.; Polig, G.; Burri, C.; Brun, R.; Murilla, G. A.; Thuita, J. K.; Barrett, M. P.; Tidwell, R. R. Diamidines for human African trypanosomiasis. *Current Opinion in Investigational Drugs* **2010**, 876-883.

131. Stephens, C. E.; Brun, R.; Salem, M. M.; Werbovetz, K. A.; Tanious, F.; Wilson, W. D.; Boykin, D. W. The activity of diguanidino and 'reversed' diamidino 2,5-diarylfurans versus *Trypanosoma cruzi* and *Leishmania donovani. Bioorg. Med. Chem. Lett.* **2003,** 13, 2065-2069.

132. Boykin, D.; Hu, L. A Novel and Convenient Synthesis of 'Reversed' Diamidino 2,5-Aryl- and 2,5-Azaheterocycle-Substituted Furans. *Synthesis* **2009,** 13, 2143-2145.

133. Batista Dda, G.; Batista, M. M.; de Oliveira, G. M.; do Amaral, P. B.; Lannes-Vieira, J.; Britto, C. C.; Junqueira, A.; Lima, M. M.; Romanha, A. J.; Sales Junior, P. A.; Stephens, C. E.; Boykin, D. W.; Soeiro Mde, N. Arylimidamide DB766, a potential chemotherapeutic candidate for Chagas' disease treatment. *Antimicrob. Agents Chemother.* **2010,** 54, 2940-2952.

134. Wang, M. Z.; Zhu, X.; Srivastava, A.; Liu, Q.; Sweat, J. M.; Pandharkar, T.; Stephens, C. E.; Riccio, E.; Parman, T.; Munde, M.; Mandal, S.; Madhubala, R.; Tidwell, R. R.; Wilson, W. D.; Boykin, D. W.; Hall, J. E.; Kyle, D. E.; Werbovetz, K. A. Novel Arylimidamides for treatment of visceral Leishmaniasis. *Antimicrob. Agents Chemother.* **2010,** 54, 2507-2516.

135. Collar, C. J.; Zhu, X.; Werbovetz, K.; Boykin, D. W.; Wilson, W. D. Molecular factors governing inhibition of arylimidamides against *Leishmania*: Conservative computational modeling to improve chemotherapies. *Bioorg. Med. Chem.* **2011,** 19, 4552-4561.

136. Cortes, H. C. E.; Muller, N.; Boykin, D.; Stephens, C. E.; Hemphill, A. *In vitro* effects of arylimidamides against *Besnoitia besnoiti* infection in Vero cells. *Parasitology* **2011,** 138, 583-592.

137. Da Silva, C. F.; Daliry, A.; PB, D. A. S.; Akay, S.; Banerjee, M.; Farahat, A. A.; Fisher, M. K.; Hu, L.; Kumar, A.; Liu, Z.; Stephens, C. E.; Boykin, D. W.; Correia Soeiro, M. D. The efficacy of novel arylimidamides against *Trypanosoma cruzi in vitro*. *Parasitology* **2011,** 138, 1863-1869.

138. Debache, K.; Guionaud, C.; Kropf, C.; Boykin, D.; Stephens, C. E.; Hemphill, A. Experimental treatment of *Neospora caninum*-infected mice with the arylimidamide DB750 and the thiazolide nitazoxanide. *Exp. Parasitol.* **2011,** 129, 95-100.

139. Banerjee, M.; Farahat, A. A.; Kumar, A.; Wenzler, T.; Brun, R.; Munde, M. M.; Wilson, W. D.; Zhu, X.; Werbovetz, K. A.; Boykin, D. W. Synthesis, DNA binding and antileishmanial activity of low molecular weight bis-arylimidamides. *Eur. J. Med. Chem.* **2012,** 55, 449-454.

140. da Silva, C. F.; Batista Dda, G.; Oliveira, G. M.; de Souza, E. M.; Hammer, E. R.; da Silva, P. B.; Daliry, A.; Araujo, J. S.; Britto, C.; Rodrigues, A. C.; Liu, Z.; Farahat, A. A.; Kumar, A.; Boykin, D. W.; Soeiro Mde, N. *In vitro* and *in vivo* investigation of the efficacy of arylimidamide DB1831 and its mesylated salt form-DB1965-against *Trypanosoma cruzi* infection. *PLoS One* **2012,** 7, e30356.

141. Reid, C. S.; Farahat, A. A.; Zhu, X.; Pandharkar, T.; Boykin, D. W.; Werbovetz, K. A. Antileishmanial bisarylimidamides: DB766 analogs modified in the linker region and bisarylimidamide structure-activity relationships. *Bioorg. Med. Chem. Lett.* **2012,** 22, 6806-6810.

142. Schorer, M.; Debache, K.; Barna, F.; Monney, T.; Müller, J.; Boykin, D. W.; Stephens, C. E.; Hemphill, A. Dicationic arylimidamides act against *Neospora caninum* tachyzoites by interference in membrane structure and nucleolar integrity and are active against challenge infection in mice. *Int. J. Parasitol.: Drugs Drug Resist.* **2012,** 2, 109-120.

143. Zhu, X.; Liu, Q.; Yang, S.; Parman, T.; Green, C. E.; Mirsalis, J. C.; de Nazare Correia Soeiro, M.; Mello de Souza, E.; da Silva, C. F.; da Gama Jaen Batista, D.; Stephens, C. E.; Banerjee, M.; Farahat, A. A.; Munde, M.; Wilson, W. D.; Boykin, D. W.; Wang, M. Z.; Werbovetz, K. A. Evaluation of arylimidamides DB1955 and DB1960 as candidates against visceral leishmaniasis and Chagas' disease: *in vivo* efficacy, acute toxicity, pharmacokinetics, and toxicology studies. *Antimicrob. Agents Chemother.* **2012,** 56, 3690-3699.

144. Chai, Y.; Munde, M.; Kumar, A.; Mickelson, L.; Lin, S.; Campbell, N. H.; Banerjee, M.; Akay, S.; Liu, Z.; Farahat, A. A.; Nhili, R.; Depauw, S.; David-Cordonnier, M. H.; Neidle, S.; Wilson, W. D.; Boykin, D. W. Structure-

dependent binding of arylimidamides to the DNA minor groove. *ChemBioChem* **2014,** 15, 68-79.

145. Liu, Z. Y.; Wenzler, T.; Brun, R.; Zhu, X.; Boykin, D. W. Synthesis and antiparasitic activity of new bisarylimidamides: DB766 analogs modified in the terminal groups. *Eur. J. Med. Chem.* **2014,** 83, 167-173.

146. Zhu, X.; Farahat, A. A.; Mattamana, M.; Joice, A.; Pandharkar, T.; Holt, E.; Banerjee, M.; Gragg, J. L.; Hu, L.; Kumar, A.; Yang, S.; Wang, M. Z.; Boykin, D. W.; Werbovetz, K. A. Synthesis and pharmacological evaluation of mono-arylimidamides as antileishmanial agents. *Bioorg. Med. Chem. Lett.* **2016,** 26, 2551-2556.

147. da Silva, C. F.; Batista, D.; de Araújo, J. S.; Cunha-Junior, E. F.; Stephens, C. E.; Banerjee, M.; Farahat, A. A.; Akay, S.; Fisher, M. K.; Boykin, D. W.; Soeiro, M. N. C. Phenotypic evaluation and *in silico* ADMET properties of novel arylimidamides in acute mouse models of *Trypanosoma cruzi* infection. *Drug Des., Dev. Ther.* **2017,** 11, 1095-1105.

148. Guedes-da-Silva, F. H.; Batista, D. G.; Meuser, M. B.; Demarque, K. C.; Fulco, T. O.; Araujo, J. S.; Da Silva, P. B.; Da Silva, C. F.; Patrick, D. A.; Bakunova, S. M.; Bakunov, S. A.; Tidwell, R. R.; Oliveira, G. M.; Britto, C.; Moreira, O. C.; Soeiro, M. N. *In vitro* and *in vivo* Trypanosomicidal Action of Novel Arylimidamides against *Trypanosoma cruzi. Antimicrob. Agents Chemother.* **2016,** 60, 2425-2534.

149. Timm, B. L.; da Silva, P. B.; Batista, M. M.; da Silva, F. H.; da Silva, C. F.; Tidwell, R. R.; Patrick, D. A.; Jones, S. K.; Bakunov, S. A.; Bakunova, S. M.; Soeiro Mde, N. *In vitro* and *in vivo* biological effects of novel arylimidamide derivatives against *Trypanosoma cruzi. Antimicrob. Agents Chemother.* **2014,** 58, 3720-3726.

150. Arya, S.; Kumar, N.; Roy, P.; Sondhi, S. M. Synthesis of amidine and bis amidine derivatives and their evaluation for anti-inflammatory and anticancer activity. *Eur. J. Med. Chem.* **2013,** 59, 7-14.

151. Dardonville, C.; Brun, R. Bisguanidine, Bis(2-aminoimidazoline), and Polyamine Derivatives as Potent and Selective Chemotherapeutic Agents against *Trypanosoma brucei rhodesiense.* Synthesis and *in Vitro* Evaluation. *J. Med. Chem.* **2004,** 47, 2296-2307.

152. Dardonville, C.; Nué Martinez, J. J. Bis(2-aminoimidazolines) and Bisguanidines: Synthetic Approaches, Antiparasitic Activity and DNA Binding Properties. *Curr. Med. Chem.* **2017,** 24, 3606-3632.

153. Ríos Martínez, C. H.; Miller, F.; Ganeshamoorthy, K.; Glacial, F.; Kaiser, M.; de Koning, H. P.; Eze, A. A.; Lagartera, L.; Herraiz, T.; Dardonville, C. A new nonpolar *N*-hydroxy imidazoline lead compound with improved activity in a murine model of late-stage *Trypanosoma brucei brucei* infection is not cross-resistant with diamidines. *Antimicrob. Agents Chemother.* **2015,** 59, 890-904.

154. Montalvo-Quiros, S.; Taladriz-Sender, A.; Kaiser, M.; Dardonville, C. Antiprotozoal activity and DNA binding of dicationic acridones. *J. Med. Chem.* **2015,** 58, 1940-1949.

155. Rodríguez, F.; Rozas, I.; Kaiser, M.; Brun, R.; Nguyen, B.; Wilson, W. D.; García, R. N.; Dardonville, C. New Bis(2-aminoimidazoline) and Bisguanidine DNA Minor Groove Binders with Potent *in Vivo* Antitrypanosomal and Antiplasmodial Activity. *J. Med. Chem.* **2008,** 51, 909-923.

156. Nieto, L.; Mascaraque, A.; Miller, F.; Glacial, F.; Ríos Martínez, C.; Kaiser, M.; Brun, R.; Dardonville, C. Synthesis and Antiprotozoal Activity of N-Alkoxy Analogues of the Trypanocidal Lead Compound 4,4′-Bis(imidazolinylamino)diphenylamine with Improved Human Blood−Brain Barrier Permeability. *J. Med. Chem.* **2011,** 54, 485-494.

157. Dardonville, C.; Barrett, M. P.; Brun, R.; Kaiser, M.; Tanious, F.; Wilson, W. D. DNA Binding Affinity of Bisguanidine and Bis(2-aminoimidazoline) Derivatives with *in vivo* Antitrypanosomal Activity. *J. Med. Chem.* **2006,** 49, 3748-3752.

158. Dardonville, C.; Rozas, I.; Alkorta, I. Similarity studies on guanidinium, imidazolinium, and imidazolium cations: toward new bradykinin antagonists. *J. Mol. Graphics Modell.* **1998,** 16, 150-156.

159. Ríos Martínez, C. H.; Nué Martinez, J. J.; Ebiloma, G. U.; de Koning, H. P.; Alkorta, I.; Dardonville, C. Lowering the pK_a of a bisimidazoline lead with halogen atoms results in improved activity and selectivity against *Trypanosoma brucei in vitro*. *Eur. J. Med. Chem.* **2015,** 101, 806-817.

160. Millan, C. R.; Acosta-Reyes, F. J.; Lagartera, L.; Ebiloma, G. U.; Lemgruber, L.; Nué Martinez, J. J.; Saperas, N.; Dardonville, C.; de Koning, H. P.; Campos, J. L. Functional and structural analysis of AT-specific minor groove binders that

disrupt DNA-protein interactions and cause disintegration of the *Trypanosoma brucei* kinetoplast. *Nucleic Acid Res.* **2017,** 45, 8378-8391.

161. Drugs for Neglected Diseases *initiative,* D. Chagas disease - Target Product Profiles. https://dndi.org/diseases/chagas/target-product-profile/ (May 26, 2022).

162. Drugs for Neglected Diseases *initiative,* D. Cutaneous leishmaniasis - Target Product Profiles. https://dndi.org/diseases/cutaneous-leishmaniasis/target-product-profile/ (May 26, 2022).

163. Drugs for Neglected Diseases *initiative,* D. Visceral lesihmaniasis - Target Product Profiles. https://dndi.org/diseases/visceral-leishmaniasis/target-product-profile/ (May 26, 2022).

CHAPTER 2

2. Chapter 2 : Objectives

2.1. Main objectives

The main goal of this research is to discover new mitochondrial DNA-targeting compounds active against kinetoplastid parasites, namely *Leishmania, T. cruzi*, and *T. brucei*.

To do so, we will prepare three families of dicationic compounds having a common *N*-phenylbenzamide scaffold known to interact favourably with the DNA minor groove of kDNA. Different chemical modifications will be introduced to improve the membrane permeability of the compounds and their activity, especially toward intracellular amastigotes of *Leishmania* and *T. cruzi* parasites. Then, their antiprotozoal activity and unspecific cytotoxicity will be evaluated. Finally, the DNA binding affinity, sequence selectivity and mode of binding of the new compounds will be assessed carefully using different biophysical techniques.

The specific goals pursued in this research can be summarised as follows:

2.1.1. Design and synthesis of dicationic derivatives of lead compounds I and II

Three new families of derivatives (i.e., series 1–3) with structural characteristics related to dicationic lead compounds **I** and **II** will be prepared as potential DNA minor groove binders (Figure 2.1). The rationale behind this synthesis is to optimise the access of these compounds to their intracellular target (i.e., kDNA) in *Leishmania* and *T. cruzi* parasites. To achieve this goal, three chemical strategies will be used to modify the physicochemical properties of leads **I** and **II** in order to improve their antiparasitic activity against intracellular parasites: (1) bioisosteric replacement of the imidazoline heterocycle with less basic benzimidazole (series 2) or pyridine-2-carboxamidine groups (series 3), (2) modification of the central scaffold incorporating lipophilic and/or electronegative substituents, and (3) drug delivery optimization using nanoparticles (e.g. receptor–mediated drug delivery).
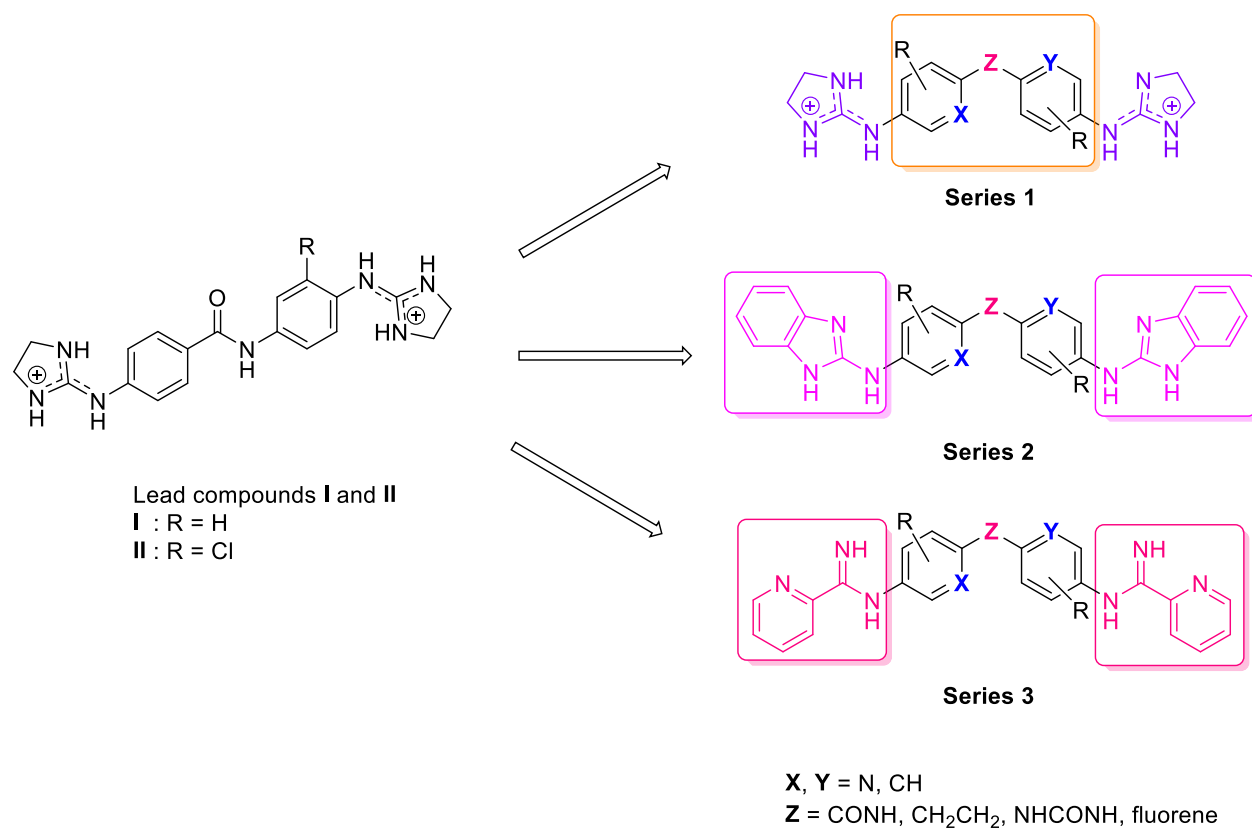
Figure 2.1: Dicationic DNA MGB lead compounds previously developed in our group and bioisosteric replacements proposed to improve the activity and selectivity towards intracellular parasites.

(1) Bioisosteric replacement of the imidazoline heterocycles represents an interesting tool to modulate the biostructural properties (i.e., size, shape, lipophilicity, electronic distribution) of lead compounds **I** and **II**. Introduction of less basic moieties such as benzimidazole or pyridine-2-carboxamide shall decrease the pK_a of the planned derivatives.

(2) Scaffold modifications introducing electronegative atoms (e.g., chlorine atoms) in both phenyl rings is also proposed in order to reduce the basicity and increase the lipophilicity of the molecules. In addition, the introduction of isopropoxy groups in the central scaffold has been reported previously[1-6] as a successful strategy to improve the activity of diamidines compounds against *Leishmania* and *T. cruzi*. Other strategies such as replacing the amide linkage by ethylene, urea, or fluorene groups, will be studied as well.

(3) Biologically active compound(s) will be encapsulated into lipophilic nanoparticles to facilitate their internalization into macrophages. A receptor–mediated drug delivery

strategy using folic acid-coated nanoparticles will be used to improve the internalization of nanoparticles. This strategy will take advantage of the folate receptors present in macrophages to boost the internalization and antileishmanial activity of the compounds. This work will be carried out in collaboration with Dr. Ana González Paredes from the Medicinal Chemistry Institute (IQM–CSIC).

Once all the molecules are prepared, their DNA binding affinity and their antiparasitic activity will be analysed by means of biophysical and biochemical assays, to determine structure–activity relationships (See objectives 2.1.2, 2.1.3). These results will be compared with that of the lead compounds **I** and **II**, which DNA binding affinity and antiparasitic activity has been previously determined.[7, 8]

2.1.2. Evaluation of the DNA binding affinity of synthesized molecules using different biophysical techniques and computational studies

The second objective of this research is to study the DNA binding affinity and the mode of binding (intercalation vs. minor groove binding, or both) of the prepared molecules to different types of DNA (i.e., AT–rich, GC–rich and unspecific DNA). This will be carried out using different biophysical experiments such as:

1) Thermal denaturation experiments, which provide a fast and qualitative method for ranking compounds according to their binding affinity.[9]

2) Surface plasmon resonance (SPR)–biosensor experiments with AT–rich and GC–rich oligonucleotides, which will provide the binding affinity (K_d) of the compounds to different DNA sequences, allowing the selection of the best DNA MGBs.

3) UV titration experiments will be carried out using salmon testes DNA to measure binding affinity for mixed (unspecific) sequences.

4) Circular (CD) and linear dichroism (LD) will be used to confirm the mode of binding of these molecules. This technique is used to estimate the mode of binding to DNA, being able to distinguish minor groove binding and intercalation.

Once the best DNA MGB molecules are selected, further experiments will be performed to analyse the binding mode of these compounds in details and determine the selective interaction with AT–rich sequences of the most suitable molecule–oligonucleotide complexes. These studies will include:

5) Nuclear magnetic resonance (NMR) experiments to characterize the interaction of the molecule–oligonucleotide complex in solution. These studies will be performed in collaboration with Prof. Carlos González and Dr. Miguel Garavís from Rocasolano Institute of Physical Chemistry (IQFR–CSIC).

6) Crystallographic studies to characterize the interaction of the molecule–oligonucleotide complex in the solid state will also be carried out, in collaboration with Prof. Lourdes Campos and Prof. Núria Saperas at the Polytechnic University of Catalonia (Barcelona Tech).

7) Computational experiments: docking studies of the new ligands into the minor groove of a previously DNA co-crystalised with lead compound **I** will be performed. The top-scoring poses will be evaluated based on its ability to superimpose to the crystal structure of **I** complexed with the d(AAATTT)$_2$ DNA duplex [PDB: 5LIT],[8] to understand the possible interactions between the new ligands and the minor groove. This work will be carried out at Trinity College of Dublin, the University of Dublin, in collaboration with Prof. Isabel Rozas and Dr. Cristina Trujillo.

2.1.3. Biological and biochemical assays to determine the cytotoxic activity of the compounds on *Leishmania donovani*, *Trypanosoma cruzi*, *Trypanosoma brucei* and *Trichomonas vaginalis*

In collaboration with Dr. Francisco Gamarro and Dr. José Ignacio Manzano from the Institute of Parasitology and Biomedicine "López–Neyra" (IPBLN–CSIC) we will carry out the evaluation of the synthesised compounds against promastigote and intracellular amastigote forms of *Leishmania donovani*. The antiparasitic activity will be reported by means of EC$_{50}$ values. Unspecific cytotoxicity against macrophages (human monocytic cell line, THP-1) will be evaluated to calculate the selectivity index (SI) of the compounds versus mammalian cells.

In vitro evaluation against *Trypanosoma brucei* wild–type and drug–resistant strains will be performed in collaboration with Prof. Harry de Koning, from the Institute of Infection, Immunity and Inflammation of the University of Glasgow. The activity against $T. b. brucei$ cell lines will be reported by means of EC_{50} values. Unspecific cytotoxicity against human embryonic kidney cells (HEK) will be evaluated to calculate the selectivity index (SI) of the compounds versus mammalian cells.

The biological evaluation against *Trypanosoma cruzi* and *Trichomonas vaginalis* will be performed by members (Dr. Cristina Fonseca Berzal and Dr. Alexandra Ibañez Escribano) of the Group "Epidemiology, Diagnostic and Antiparasite Therapy" lead by my co-supervisor, Prof. Alicia Gómez Barrio, from the Department of Microbiology and Parasitology, School of Pharmacy, Complutense University of Madrid (UCM). The activity will be informed by means of IC_{50} values. Nonspecific cytotoxicity against murine L929 fibroblasts (CCL-1) will be assayed to calculate the SI of the synthesised compounds versus mammalian cells.

2.1.4. Preliminary pharmacokinetic studies of the most active lead(s) compound(s)

Metabolic stability will be studied in collaboration with Dr. Tomas Herraiz (ICTAN–CSIC). The microsomal stability toward metabolism by cytochrome P450 (Phase-I metabolism) and Uridine Glucuronosyl-Transfererase (UGT) (Phase-II metabolism) will be studied in presence of the cofactors NADPH and UDPGA, respectively. Metabolic stability results will be reported as intrinsic clearance, from which secondary pharmacokinetic parameters such as bioavailability and half-life can be calculated.[10]

2.2. References

1. Liu, Z.-y.; Wenzler, T.; Brun, R.; Zhu, X.; Boykin, D. W. Synthesis and antiparasitic activity of new bis-arylimidamides: DB766 analogs modified in the terminal groups. *Eur. J. Med. Chem.* **2014,** 83, 167-173.

2. Zhu, X.; Liu, Q.; Yang, S.; Parman, T.; Green, C. E.; Mirsalis, J. C.; de Nazare Correia Soeiro, M.; Mello de Souza, E.; da Silva, C. F.; da Gama Jaen Batista, D.; Stephens, C. E.; Banerjee, M.; Farahat, A. A.; Munde, M.; Wilson, W. D.; Boykin, D. W.; Wang, M. Z.; Werbovetz, K. A. Evaluation of arylimidamides

DB1955 and DB1960 as candidates against visceral leishmaniasis and Chagas' disease: *in vivo* efficacy, acute toxicity, pharmacokinetics, and toxicology studies. *Antimicrob. Agents Chemother.* **2012,** 56, 3690-3699.

3. Reid, C. S.; Farahat, A. A.; Zhu, X.; Pandharkar, T.; Boykin, D. W.; Werbovetz, K. A. Antileishmanial bisarylimidamides: DB766 analogs modified in the linker region and bisarylimidamide structure-activity relationships. *Bioorg. Med. Chem. Lett.* **2012,** 22, 6806-6810.

4. da Silva, C. F.; Batista Dda, G.; Oliveira, G. M.; de Souza, E. M.; Hammer, E. R.; da Silva, P. B.; Daliry, A.; Araujo, J. S.; Britto, C.; Rodrigues, A. C.; Liu, Z.; Farahat, A. A.; Kumar, A.; Boykin, D. W.; Soeiro Mde, N. *In vitro* and *in vivo* investigation of the efficacy of arylimidamide DB1831 and its mesylated salt form-DB1965-against *Trypanosoma cruzi* infection. *PLoS One* **2012,** 7, e30356.

5. Wang, M. Z.; Zhu, X.; Srivastava, A.; Liu, Q.; Sweat, J. M.; Pandharkar, T.; Stephens, C. E.; Riccio, E.; Parman, T.; Munde, M.; Mandal, S.; Madhubala, R.; Tidwell, R. R.; Wilson, W. D.; Boykin, D. W.; Hall, J. E.; Kyle, D. E.; Werbovetz, K. A. Novel Arylimidamides for treatment of visceral Leishmaniasis. *Antimicrob. Agents Chemother.* **2010,** 54, 2507-2516.

6. Batista Dda, G.; Batista, M. M.; de Oliveira, G. M.; do Amaral, P. B.; Lannes-Vieira, J.; Britto, C. C.; Junqueira, A.; Lima, M. M.; Romanha, A. J.; Sales Junior, P. A.; Stephens, C. E.; Boykin, D. W.; Soeiro Mde, N. Arylimidamide DB766, a potential chemotherapeutic candidate for Chagas' disease treatment. *Antimicrob. Agents Chemother.* **2010,** 54, 2940-2952.

7. Ríos Martínez, C. H.; Nué Martinez, J. J.; Ebiloma, G. U.; de Koning, H. P.; Alkorta, I.; Dardonville, C. Lowering the pK_a of a bisimidazoline lead with halogen atoms results in improved activity and selectivity against *Trypanosoma brucei in vitro*. *Eur. J. Med. Chem.* **2015,** 101, 806-817.

8. Millan, C. R.; Acosta-Reyes, F. J.; Lagartera, L.; Ebiloma, G. U.; Lemgruber, L.; Nué Martinez, J. J.; Saperas, N.; Dardonville, C.; de Koning, H. P.; Campos, J. L. Functional and structural analysis of AT-specific minor groove binders that disrupt DNA-protein interactions and cause disintegration of the *Trypanosoma brucei* kinetoplast. *Nucleic Acid Res.* **2017,** 45, 8378-8391.

9. Nagle, P. S.; Rodriguez, F.; Kahvedžić, A.; Quinn, S. J.; Rozas, I. Asymmetrical Diaromatic Guanidinium/2-Aminoimidazolinium Derivatives: Synthesis and DNA Affinity. *J. Med. Chem.* **2009,** 52, 7113-7121.

10. Masimirembwa, C. M.; Bredberg, U.; Andersson, T. B. Metabolic Stability for Drug Discovery and Development. *Clin. Pharmacokinet.* **2003,** 42, 515-528.

CHAPTER 3

3. Chapter 3 : Synthesis of bis(imidazolidin-2-imines), bis(2-aminobenzimidazoles) and bis(arylimidamides)

3.1. Synthesis of bis(imidazolidin-2-imino) derivatives

3.1.1. Introduction

Bis(imidazolidin-2-imino) derivatives are a series of promising antiprotozoal compounds which are curative in murine models of stage 1 human African trypanosomiasis (haemolymphatic phase) but fail to cure the late–stage disease affecting the central nervous system (CNS).[1] This lack of activity in the meningoencephalitic stage of HAT was attributed to the intrinsic dicationic nature of the compounds at physiological pH, which is responsible for the poor distribution across the blood–brain barrier (BBB).[2] We have shown previously that the chemical modification of (di)cationic compounds to lower their pK_a can lead to a notable improvement in membrane permeability and antitrypanosomal activity.[2-4] In particular, we showed that it was possible to reduce the pK_a of the basic 2-iminoimidazolidine groups (approximately 0.5–1 pK_a unit) though the introduction of a chlorine or fluorine atom in the *N*-phenylbenzamide scaffold of lead compound **I** (Figure 3.1).[2] Replacement of the phenyl ring by an electron-poor pyridine ring was also effective at reducing the pK_a values of the adjacent 2-aminoimidazoline ring by 0.6 pK_a units.[5]

I : R = H
II : R = Cl
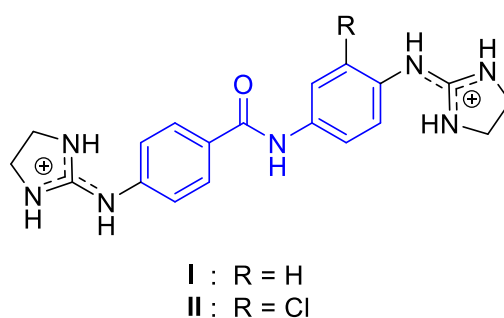
Figure 3.1: Previous antiprotozoal lead compounds identified in our group.[2, 4, 6] The *N*-phenylbenzamide scaffold is shown in blue.

Incorporation of one fluorine, chlorine, or nitrogen atom in the scaffold of **I** gave bisimidazoline compounds with reduced basicity that resulted active and selective against *T. brucei in vitro*. Compound **II**, a chlorinated analogue closely related to **I**, was more potent than **I** *in vitro* (EC$_{50}$ = 0.22 μM versus 0.83 μM for lead compound **I**) against bloodstream form trypomastigotes of *T. b. brucei* s427.[2] Furthermore, these derivatives

exhibited submicromolar activities against drug-resistant *T. b. brucei* strains.[2] Since the medicinal chemistry strategy to improve the antiparasitic activity of lead compound **I** with halogen atoms gave encouraging results, the first objective of this thesis was to synthesize new bis(imidazolidin-2-imino) derivatives of **I** with two halogen or nitrogen atoms in the *N*-phenylbenzamide scaffold.

Synthetic methodologies for the preparation of 2-aminoimidazolines (formally: 4,5-dihydro-1*H*-imidazol-2-ylamino) are similar to (or derive from) the methods developed for the synthesis of guanidine-like derivatives.[7-9] They were reviewed previously by Dardonville & Nué-Martínez,[1] and Crouch.[10]

Scheme 3.1: Different synthetic approaches to obtain 2-(arylimino)imidazolidine (adapted from Dardonville & Nué, *Curr. Med. Chem.* **2017**, *24*, 1–28)[1]

R$_1$ = SMe, Cl, SO$_3$H
PG = protecting group (COR, CO$_2$R)
4: PG = CO$_2$Me, R$_1$ = SMe
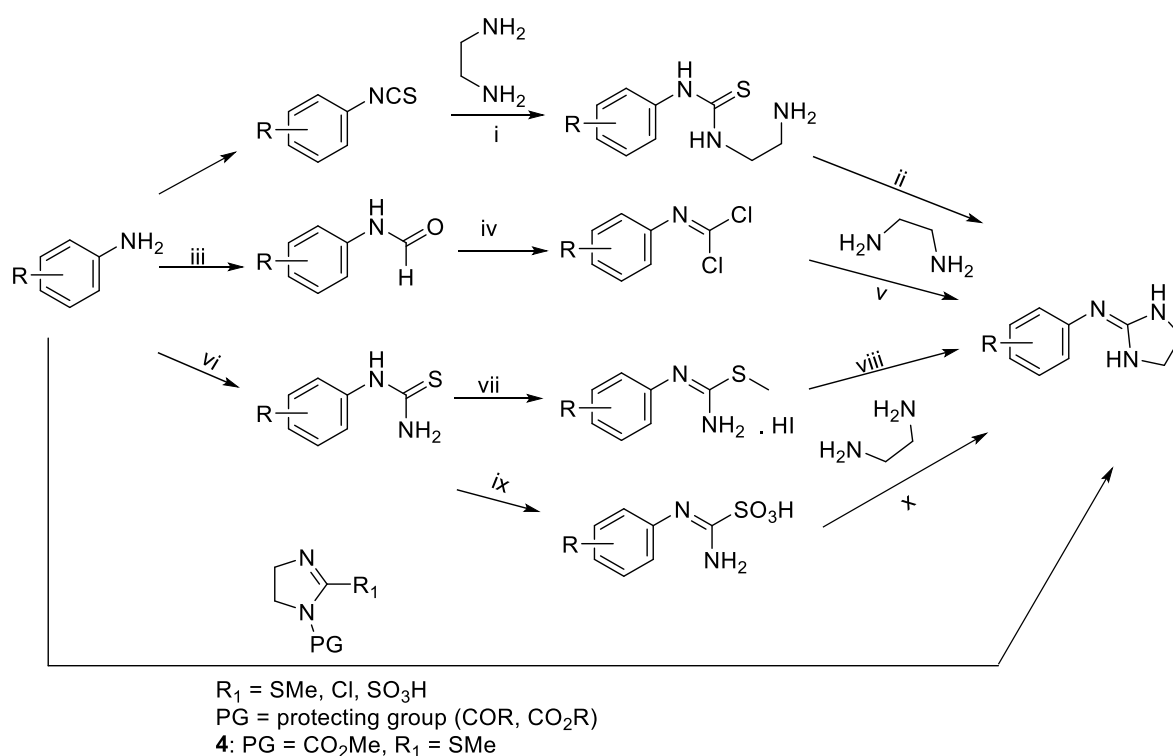
Reagents and conditions: (i) THF, rt; (ii) TsCl, NaOH, THF, H$_2$O; (iii) HCHO, Ac$_2$O, 50 ºC, 5 h; (iv) SOCl$_2$ (excess), SO$_2$Cl$_2$ (1 equiv), 50–60 ºC, 10 h; (v) Et$_3$N, EtOAc, rt; (vi) benzoylisothiocyanate then OH$^-$; (vii) CH$_3$I, MeOH, reflux, 2 h; (viii) neat, 130–170 ºC; (ix) H$_2$O$_2$, MoNa$_2$O$_4$, NaCl, H$_2$O; (x) 2-propanol or H$_2$O, 4 h, 60 ºC.

For example, the 2-aminoimidazoline heterocycle can be obtained by reacting an amine with a 2-substituted imidazoline ring (e.g. reagent **4**) or by reaction of ethylenediamine

with arylisothiocyanates,[11] *N*-aryldichloroimines[12, 13] or dibromoimines,[14] *N*-aryl-*S*-methylisothiouronium iodides[12] or aminoiminomethanesulfonic acid derivatives[15] (Scheme 3.1).[1]

A relevant methodology proposed previously by Dardonville & col.[16] is generally applicable to the synthesis of (2-arylimino)imidazolidines, in particular from electron-poor anilines. This approach involves the reaction of an aromatic diamine with di-*tert*-butyl 2-thioxoimidazolidine-1,3-dicarboxylate **5** in the presence of mercury (II) chloride (HgCl$_2$) with an excess of triethylamine (Et$_3$N). This procedure provides the fully *tert*-butoxycarbonyl (Boc)-protected 2-iminoimidazoline (Scheme 3.2). Then, Boc-protecting groups are removed by hydrolysis with trifluoroacetic acid (TFA), and the imidazoline compounds are isolated as trifluoroacetate salts. Finally, a treatment with strongly basic anion exchange resins (e.g., Amberlite IRA 400, Cl$^-$ ion) yields the 2–aminoimidazolinium chloride salts (Scheme 3.2).[16]

Scheme 3.2: Example of synthesis of bis(imidazolin-2-imino) derivatives using di-*tert*-butyl 2-thioxoimidazolidine-1,3-dicarboxylate (**5**).[16]
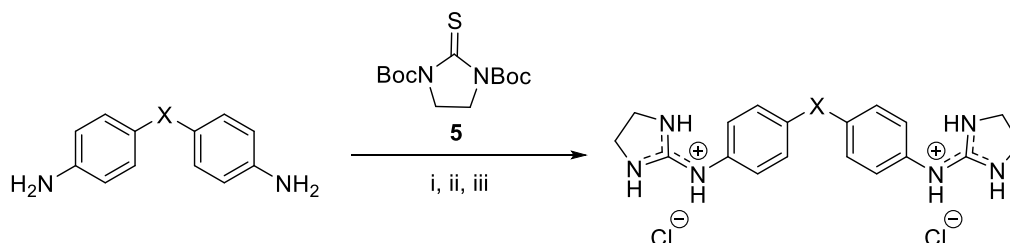
Reagents and conditions: i) HgCl$_2$/ Et$_3$N. ii) TFA /CH$_2$Cl$_2$. iii) Amberlite IRA400 (Cl$^-$), H$_2$O/THF.

3.1.2. Synthesis of bis(imidazolidin-2-imino) derivatives 1b–h

The preparation of the target compounds (**1b–h**) involved first the synthesis of the common di-nitro precursors **9** from the corresponding substituted benzoic acids and 4-nitroanilines following a known protocol (Scheme 3.3).[2] Then, the di-nitro intermediates **9** were reduced to di-anilines **15** that were used as starting material for the synthesis of the *N*-protected bis(imidazolidin-2-imino) derivatives using either 1-carbomethoxy-2-methylthio-2-imidazoline (**4**) or di-*tert*-butyl 2-thioxoimidazolidine-1,3-dicarboxylate (**5**).

Scheme 3.3: Synthetic route proposal to obtain bis(imidazolidin-2-imino) derivatives **1b–h**.
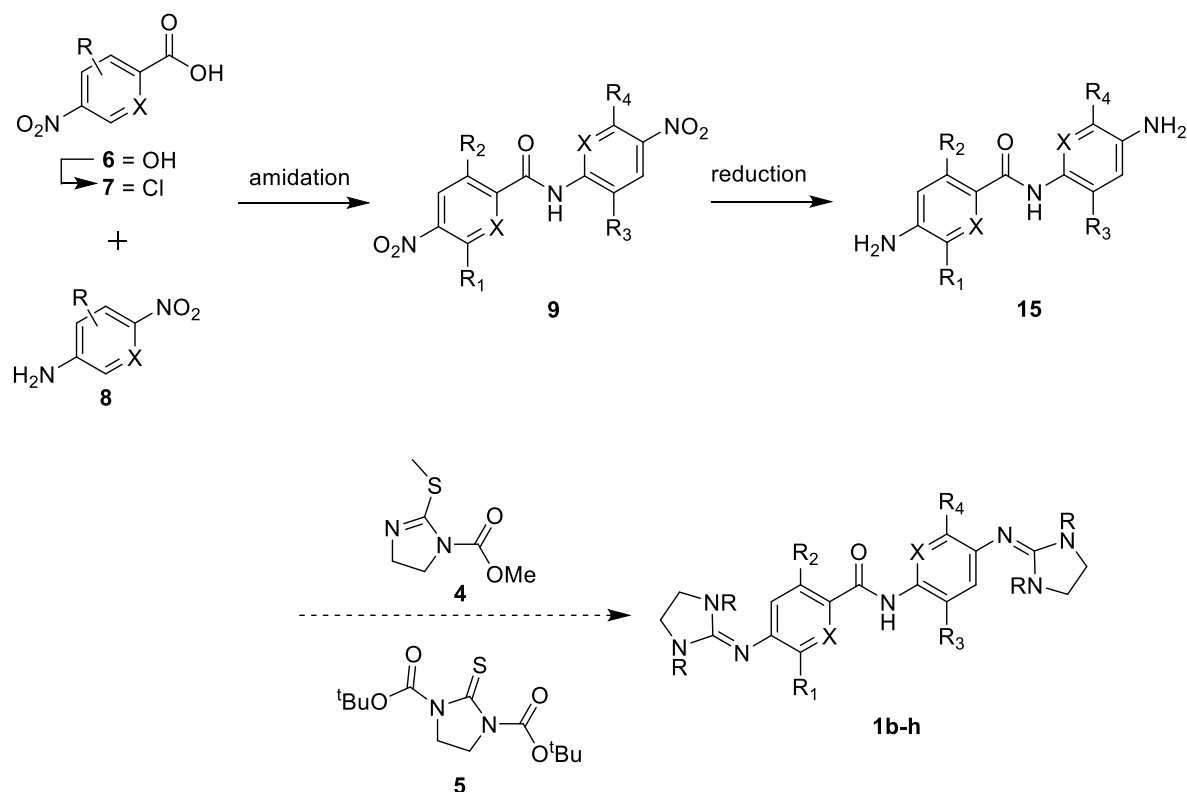
3.1.3. Synthesis of 4-nitro-*N*-(4-nitrophenyl)benzamide derivatives (9a–i)

Syntheses of the 4-nitro-*N*-(4-nitrophenyl)benzamide derivatives **9a**–**h** were carried out using the same general protocol, except for the heating mode which was either conventional (**9a**–**h**) or by microwave irradiation (**9i**). This reactions sequence comprises the acylation at room temperature of commercially available 4-nitroanilines **8a**–**g** with 4-nitrobenzoyl chlorides **7a**–**g**, respectively, using *N*,*N*-diisopropylethylamine (DIPEA) as base and anhydrous toluene as solvent (Scheme 3.4). 4-Nitrobenzoyl chlorides **7a**–**g** were obtained by reaction of the corresponding acid precursors **6a**–**g** with an excess of thionyl chloride at 80 °C. They were used without further purification after removal of the solvents under reduced pressure. 5-Nitro-*N*-(5-nitropyridin-2-yl)picolinamide (**9h**) was prepared by reaction of 5-nitropyridin–2-amine (**8h**) and 5-nitropicolinoyl chloride (**7h**) (Scheme 3.4). Compound **7h** was obtained by reaction of commercial 5-nitropicolinic acid (**6h**) with an excess of oxalyl chloride and a catalytic amount of dimethylformamide (DMF) in dichloroethane at 0 °C. 4-Nitro-*N*-(5-nitropyridin-2-yl)benzamide (**9i**) was synthesized by reaction of 5-nitropyridin-2-amine (**8i**) with 4-nitrobenzoyl chloride (**7i**) and DIPEA in

toluene at 100 °C under microwave (MW) irradiation for one hour. Compounds **9a**–**i** were isolated in good yield and high purity by filtration and successive washings with 0.1 M HCl and methanol (Scheme 3.4).

Scheme 3.4: Synthesis of 4-nitro-*N*-(4-nitrophenyl)benzamide) derivatives **9a**–**i**
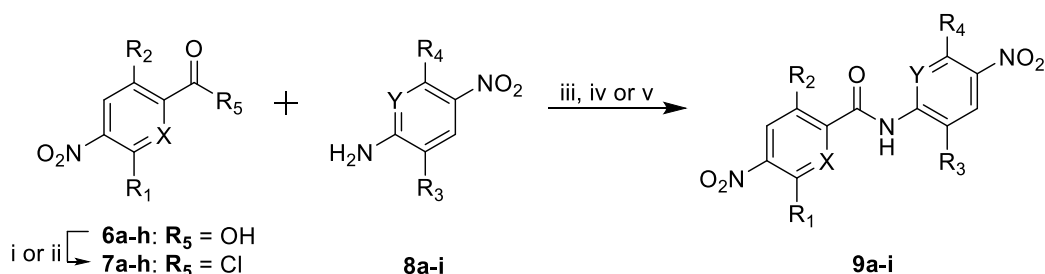
Cmpd	X	Y	R_1	R_2	R_3	R_4	Yield
a	CH	CH	H	H	H	H	80%
b	CH	CH	Cl	H	Cl	H	76%
c	CH	CH	Cl	H	H	Cl	77%
d	CH	CH	H	Cl	Cl	H	83%
e	CH	CH	H	Cl	H	Cl	65%
f	CH	CH	F	H	F	H	96%
g	CH	CH	H	O^{i}Pr	O^{i}Pr	H	69%
h	N	N	H	H	H	H	81%
i	CH	N	H	H	H	H	80%

Reagents and conditions: i) **6a–g**, SOCl$_2$, 80 °C. ii) **6h**, (COCl)$_2$, CH$_2$Cl$_2$, DMF$_{cat}$, 0 °C. iii) **7a–g**, DIPEA, dry toluene, rt. iv) **7h**, Et$_3$N, DMF, 0 °C. v) **7i**, DIPEA, dry toluene, MW, 100 °C, 1 h.

The synthesis of 2-isopropoxy-*N*-(2-isopropoxy-4-nitrophenyl)-4-nitrobenzamide (**9g**) involved two previous steps in order to obtain the acid and aniline precursors **6g** and **8g**, respectively. Initially, the synthesis of known compound **6g** was attempted following a reported procedure.[17] However, disappointing results were obtained and an azoxybenzene compound (**13**) was isolated instead (see section 3.2.2). Hence, an improvement of the reported protocol was worked out. Commercially available 2-hydroxy-4-nitrobenzoic acid (**10**) was reacted with isopropyl iodide under basic conditions in DMF (Scheme 3.5).[18] The intermediate isopropyl 2-isopropoxy-4-nitrobenzoate (**11**), which was used without further

purification, was hydrolysed with LiOH in a mixture $Et_2O:H_2O$ to give the desired 2-isopropoxy-4-nitrobenzoic acid (**6g**) with 82% yield (Scheme 3.5).

Scheme 3.5: Synthesis of 2-isopropoxy-4-nitrobenzoic acid (**6g**)[18]
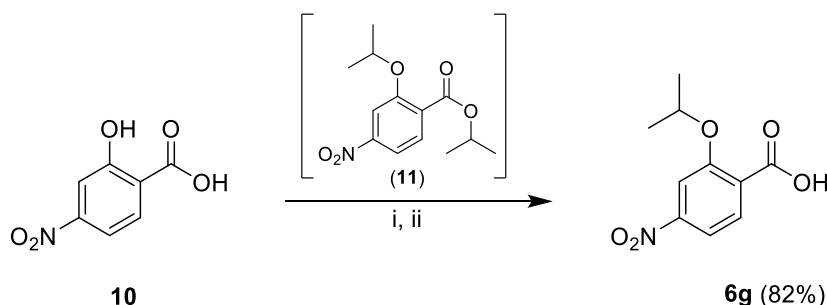
Reagents and conditions: i) $(CH_3)_2CHI$, K_2CO_3, DMF, rt. ii) LiOH, $THF:H_2O$ (1:1), rt.

In order to obtain the 2-isopropoxy-4-nitroaniline precursor **8g**, commercially available 2-hydroxy-4-nitroaniline (**12**) was reacted with isopropyl iodide in basic conditions to obtain **8g** with 86% yield (Scheme 3.6).

Scheme 3.6: Synthesis of 2-isopropoxy-4-nitroaniline (**8g**).
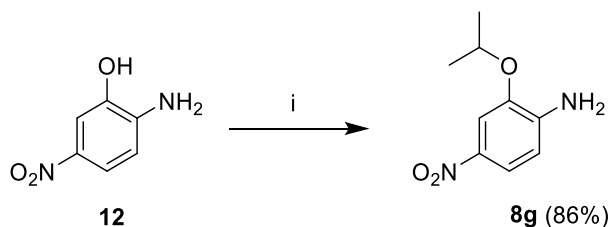
Reagents and conditions: i) $(CH_3)_2CHI$, K_2CO_3, DMF, rt.

3.1.4. Synthesis of (*Z*)-1,2-bis(4-carboxy-3-isopropoxyphenyl)diazene-1-oxide (13)

The synthesis of 2-isopropoxy-4-nitrobenzoic acid (**6g**) from commercially available 2-hidroxy-4-nitrobenzoic acid (**10**) had been previously reported by Adler & Hamilton,[17] using isopropyl iodide, potassium bicarbonate (K_2CO_3), and subsequent hydrolysis of the isopropyl 2-isopropoxy-4-nitrobenzoate intermediate (**11**) with 45% aq. NaOH in THF:EtOH at 80 °C.

Our repeated attempts to synthesize **6g** using the two-step protocol reported previously[17] led to the formation of the unknown (*Z*)-1,2-bis(4-carboxy-3-isopropoxyphenyl)diazene-1-oxide (**13**) as major product, and a minor by-product possibly corresponding to 4-amino-2-isopropoxybenzoic acid (**14**) (Scheme 3.7). The latter, which was stained as pink spot by TLC, had molecular mass of *m/z* 195 as detected by HPLC–MS. The main reaction product **13** was isolated (92%) and characterized by IR, ^{1}H, ^{13}C, and ^{15}N NMR spectroscopy as we recently reported.[18]

Scheme 3.7: Main compounds isolated following the Adler & Hamilton two-step strategy to synthesize **6g**.[17]

10   **13** (92%)   **14**
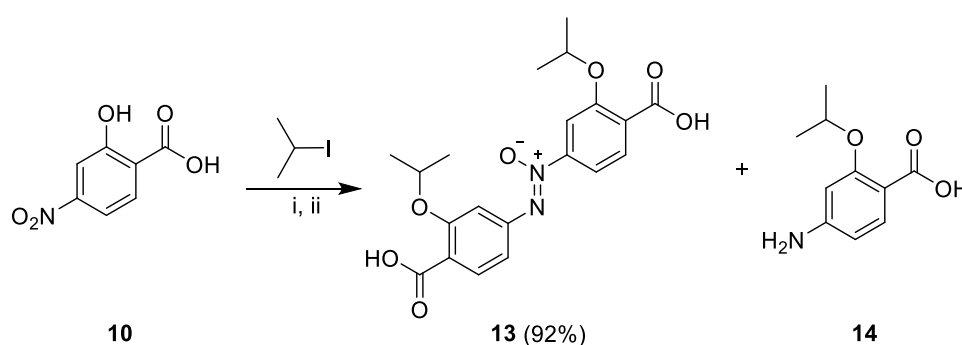
Reagents and conditions: i) K$_2$CO$_3$, DMF, 80 °C, 16 h; ii) 45% aq. NaOH, THF:EtOH (1:2), 80 °C, 15 h.

Since azoxybenzene **13** was formed in the second step of the reaction, different conditions of hydrolysis (i.e., base, concentration, temperature) of the benzoate intermediate **11** were tested (Table 3.1). When the reaction was performed with 45% aq. NaOH at 60 °C and 40 °C, the expected acid **6g** was obtained as major product (70 and 81% detected by HPLC–MS, respectively). However, **6g** was not detected with temperature ≥80 °C (entries 3–4), whereas **13** and **14** were obtained predominantly (Scheme 3.7).

Table 3.1: Conditions tested and products formed during the hydrolysis of benzoate **11** with concentrated aqueous sodium hydroxide solution.
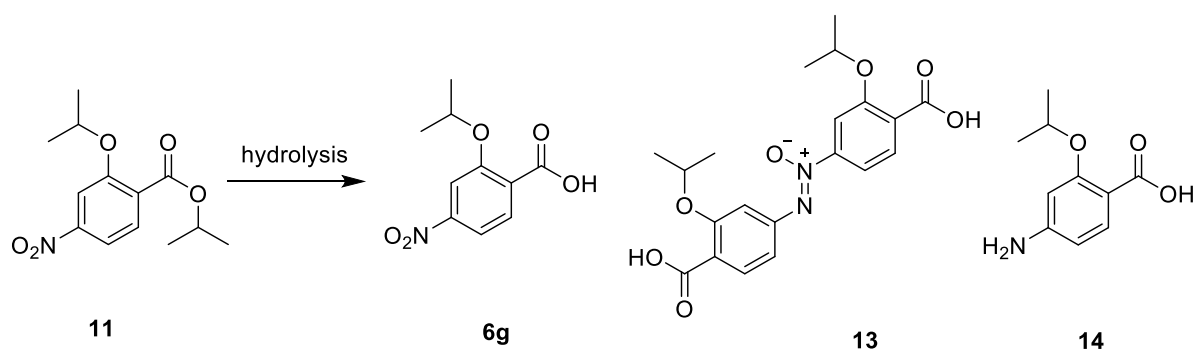
Entry	Conditions[a]		Detected product[b] (%)		
	Base	T (°C)[c]	**6g**	**13**	**14**
1	45% aq. NaOH	40	81	19	0
2		60	70	23	7
3		80	0	96	4
4		100	0	49	51
5	10% aq. NaOH	40	76	24	0
6		60	76	24	0
7		100	79	21	0
8	45% aq. KOH	80	39	61	0

[a] Reactions were performed at 1 mmol scale following the same protocol as reported[17] with the conditions indicated in the Table. [b] The products were detected by HPLC–MS. [c] The internal temperature of the reaction mixture was controlled with a thermometer.

When the reaction was performed with 10% aq. NaOH solution (entries 5–7), acid **6g** was obtained as major product (approximately 77%) regardless of the temperature used in the reaction. Altogether, azoxybenzene **13** was obtained as major by-product (≥ 19%) in all cases. Of note, the use of 45% aq. KOH instead of 45% NaOH (entry 8) was less efficient in producing azoxybenzene **13**.[18]

The main conclusion of this work is that the control of temperature and base concentration is key to the formation of the desired product **6g**, stating that possible misreading or bad control temperature were performed in Adler's protocol to synthesize **6g**.

It is quite remarkable to mention that this method appears to be a good strategy to obtain azoxybenzene derivatives in high yield. Thus, this synthetic protocol may be useful for the gram scale synthesis of 2-alkoxy trans-azoxybenzene derivatives.

3.1.5. Synthesis of 4-amino-*N*-(4-aminophenyl)benzamide derivatives (15b–i)

The reduction of the halogenated 4-nitro-*N*-4-(4-nitrophenyl)benzamide derivatives **9b–f** was carried out with tin (II) chloride dihydrate, with catalytic drops of HCl, in EtOAc at 50 °C (Scheme 3.8).[19]

Scheme 3.8: Synthesis of 4-amino-*N*-(4-aminophenyl)benzamide derivatives (**15b–i**)
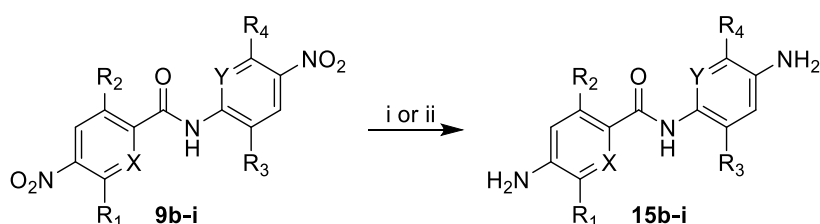
Cmpd	X	Y	R_1	R_2	R_3	R_4	Yield
b	CH	CH	Cl	H	Cl	H	90%
c	CH	CH	Cl	H	H	Cl	90%
d	CH	CH	H	Cl	Cl	H	59%
e	CH	CH	H	Cl	H	Cl	71%
f	CH	CH	F	H	F	H	59%
g	CH	CH	H	O^{i}Pr	O^{i}Pr	H	92%
h	N	N	H	H	H	H	99%
i	CH	N	H	H	H	H	88%

Reagents and conditions: i) **9b–f**, SnCl$_2$.2H$_2$O, EtOAc, HCl$_{cat}$, 50 °C. ii) **9g–i**, Pd–C 5%, EtOAc, rt.

Diamines **15b–f** were isolated by basification of the reaction mixture (pH = 8), extraction with EtOAc, and recrystallization from EtOAc. Diamines **15g–i** were obtained by Parr hydrogenation of **9g–i**, respectively; they were isolated by filtration and purified by recrystallization from hexane:EtOAc or EtOAc:MeOH.

3.1.6. Attempted synthesis of bis(imidazolidin-2-imino) derivatives

The subsequent step in the preparation of the target compounds was the introduction of the imidazoline rings from diamines **15b–i** to generate bis(imidazolin-2-imino) derivatives. Bearing in mind the low nucleophility of aromatic amines – especially **15b–f** that contain two halogen atoms – we first tried the reagent (**4**) developed by Mundla & col.[20] for the large scale, high yielding, synthesis of 2-arylamino-2-imidazolines (Scheme 3.9 and 3.10). Among the advantages of this protocol is the direct formation of the acetate salt of the product in a one-pot procedure avoiding the use of toxic reagents and harsh reaction conditions.[20] The synthesis of 1-carbomethoxy-2-methylthio-2-imidazoline (**4**) was carried out in 90% yield (Scheme 3.9).

Scheme 3.9: Synthesis of 1-carbomethoxy-2-methylthio-2-imidazoline (**4**).[20]
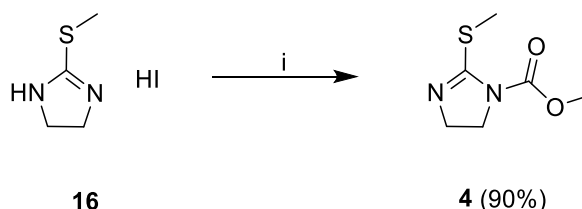
Reagents and conditions: i) $ClCO_2CH_3$, Et_3N, CH_2Cl_2, 0 °C to rt.

Different conditions were tried in order to obtain the bis(imidazolidin-2-imino) target compounds **1b–h** using an excess of **4** (2.5 – 4.0 equiv.) (Table 3.2, Scheme 3.10). However, the reaction did not go to completion and only low yields of disubstituted products **1b–c** were detected by HPLC–MS in the crude reaction mixtures. The presence of a high content of mono-substituted compound (**17b–c** and/or **18b–c**) and the fact that the products are obtained as bis(imidazolidin-2-iminium) salts represented a hardship in the purification process. The attempts of purification by silica column chromatography were unsuccessful, giving mixtures containing a 30:70 ratio of mono:disubstituted compounds after purification as observed by HPLC–MS. The attempts of purification by circular chromatography resulted in lower purity of the product (40:60 ratio of mono:disubstituted).

Since the reaction progress was slow– taking between 2 to 7 days for incomplete conversions – a different approach was deemed necessary.

Scheme 3.10: First synthetic attempt to obtain bis(imidazolidin-2-imino) derivatives **1b–c**[a]

15b: R$_1$, R$_3$ = Cl; R$_2$, R$_4$ = H
15c: R$_1$, R$_4$ = Cl; R$_2$, R$_3$ = H
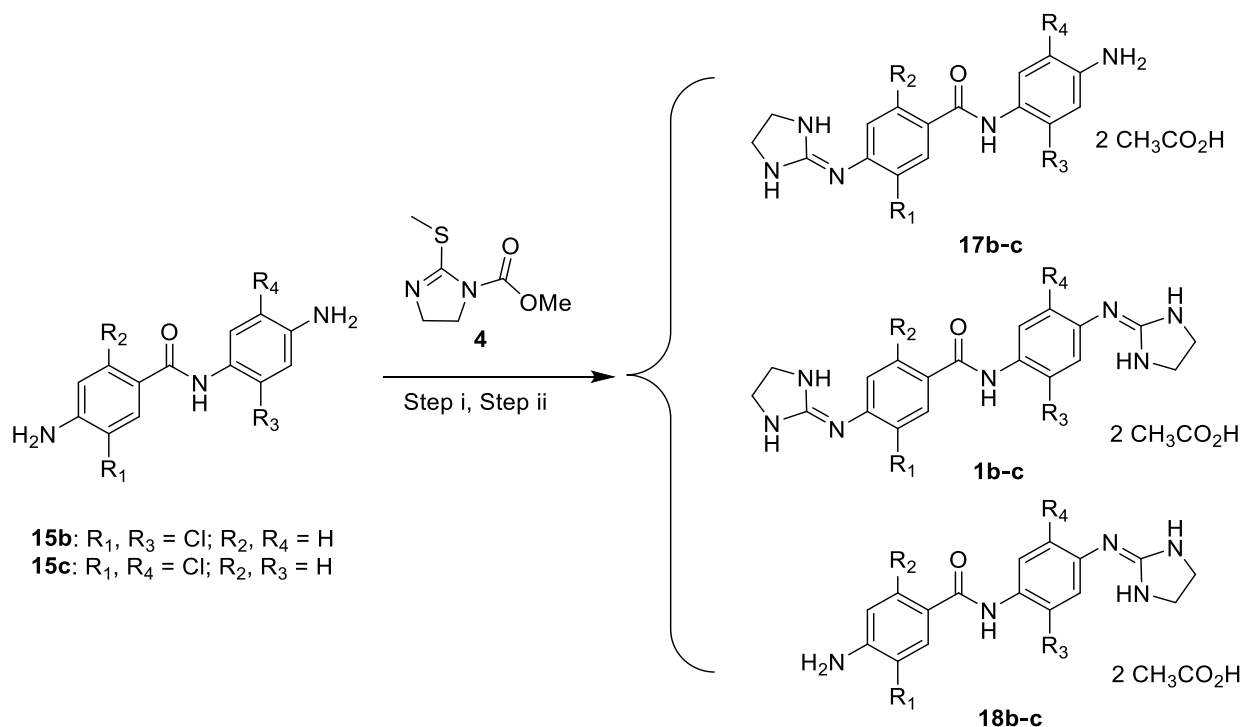
[a]See conditions in Table 2

Table 3.2: Reagents, conditions and % of product **1b–c** formed when using reagent **4**.

Substrate	Reaction conditions		Product[a]
	Step 1	Step 2	1b–c
15b	AcOH, 70 ºC, overnight	MeOH, 70 ºC, (1 – 6 days)	22.3 – 33.9 %
15b	AcOH, 70 ºC, (1–3 days)	[b]	20.7%
15c	AcOH, 65 ºC, overnight	MeOH:H$_2$O (3:1), reflux, (1 – 7 days)	19.9 – 37.5 %
15c	AcOH:MeOH (9:1), 65 ºC,	Reflux, overnight	1.0 – 1.5 %
15c	AcOH, MW, 60 ºC, (20 – 100 min)	[b]	1.1 %
15c	AcOH, MW, 60 ºC, (1 – 15 h)	[b]	10.0 – 19.2 %
15c	AcOH, 80 ºC, (1 – 3 days)	MeOH, 80 ºC, (1 – 3 days)	21.2 – 28.9 %

[a] Detected by HPLC–MS. [b] The reaction was performed in one-step.

A different approach was proposed to obtain the desired bis(imidazolidin-2-imino) derivatives (Scheme 3.11). This approach was tested with unsubstituted

bis(arylisothiocyanates) **19** and **20**,[4] which were reacted with ethane-1,2-diamine to obtain thiourea **21** and **22**, the formation of which was monitored by HPLC–MS. Once completed, attempts of cyclization of the thiourea intermediates using *N,N′*-dicyclohexylcarbodiimide (DCC) were performed as indicated in Table 3.3.

Scheme 3.11: Synthetic attempt to obtain bis(imidazolidin-2-imine) **I** and **23**.

19 = CONH
20 = NHCONH

21 = CONH
22 = NHCONH

I = CONH
23 = NHCONH
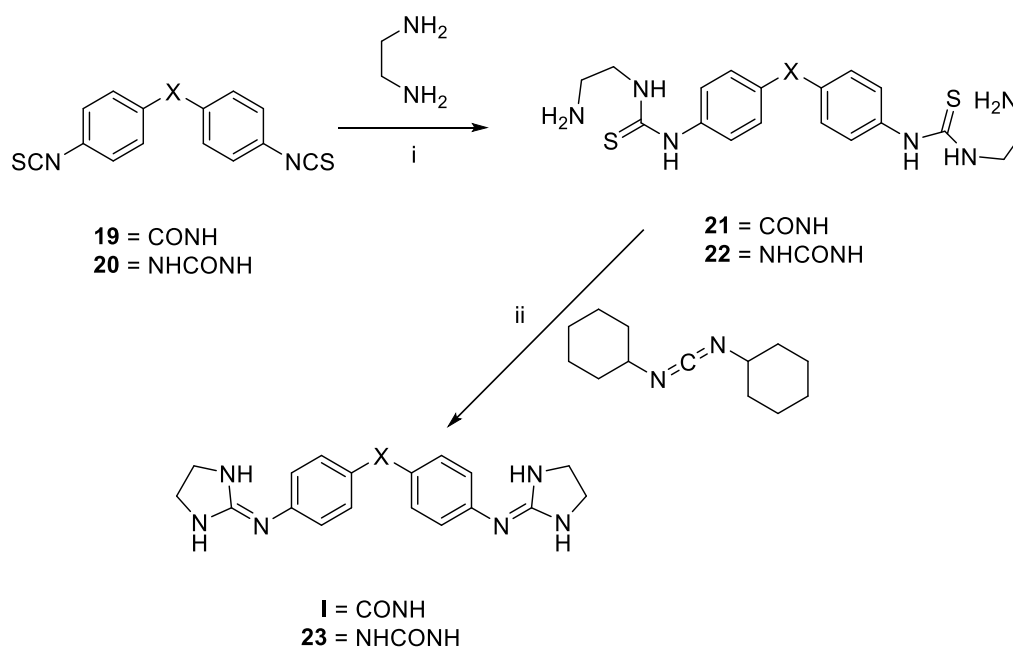
Reagents and conditions: i) 1,2-ethylenediamine, CH₃CN, rt. ii) DCC, DMF, 60 °C.

The HPLC–MS analysis of the crude reaction mixtures showed that the formation of the thiourea intermediates (**21**, **22**) proceeded in a clean way, giving > 95% conversion. In contrast, the cyclization step did not work properly, giving very complex crudes along with low conversion yields to **I** and **23** (18–38%) in most cases (Table 3.3). When mild conditions but longer reaction time were used (7 days), a 51.3% conversion of **19** to **I** was detected by HPLC–MS (Table 3.3). Even though other cyclization-promoting agent exist to carry out this kind of reaction (e.g. EDC.HCl, polymer–bound TsCl/NaOH[11]), we did not make any further attempt and this synthetic strategy was abandoned.

Table 3.3: Reagents, conditions and % of product formed in the synthesis of **I** and **23** from isothiocyanates **19** and **20**.

Substrate	Step 1 conditions	Product[a] 21, 22	Step 2 conditions	Product[a] I, 23
19 (1 eq.)		> 95 % m/z 431	DCC (2.1 eq.), DMF, 60 °C, 3 days.	21.3 %
19 (1 eq.)	ethane-1,2-diamine (4 eq.)	> 95 % m/z 431	DCC (3.1 eq.), DMF, 60 °C, 6 days.	51.3 %
20 (1 eq.)	CH$_3$CN overnight	> 95 % m/z 446	DCC (2.1 eq.), DMF, 60 °C, 24 h	18.1 %
20 (1 eq.)	room temperature	> 95 % m/z 446	DCC (3.1 eq.), DMF, MW, 120 °C, 1.5 h	38.0 %

[a]Detected by HPLC–MS.

To overcome this obstacle and obtain the desired bis(imidazolidin-2-imino) compounds, we revisited the methodology using the previously reported di-*tert*-butyl 2-thiooximidazolidine-1,3-dicarboxylate reagent (**5**) (Scheme).[16] Previous work from our group[2, 21, 22] and from Rozas' group[6, 23-25] showed that this two-steps method is usually quite efficient and results in medium to high overall yield with reactive anilines. Conveniently, the Boc-protected derivatives can be separated by chromatography to yield the fully protected imidazoline intermediates (**27b–h**) which will be easily deprotected in the last step of the synthesis.

This approach was inspired by the use of Boc-protected thiourea as a guanidylating agent proposed by Kim & Qian.[26] The introduction of Boc-protecting groups on the thiourea nitrogens increases the electrophilic character of the central carbon atom, thus activating it towards nucleophilic attack. Hence, reagent **5** proved to be useful for the synthesis of bis(imidazolidin-2-imines) from poorly nucleophilic amines containing one chlorine atom (Scheme 3.12).[2]

Scheme 3.12: Example of synthesis of Boc-protected bis(imidazolidin-2-imines) from deactivated anilines using reagent **5**.[2]

R₁ = H, R₂ = Cl
R₁ = Cl, R₂ = H

R₁ = H, R₂ = Cl
R₁ = Cl, R₂ = H
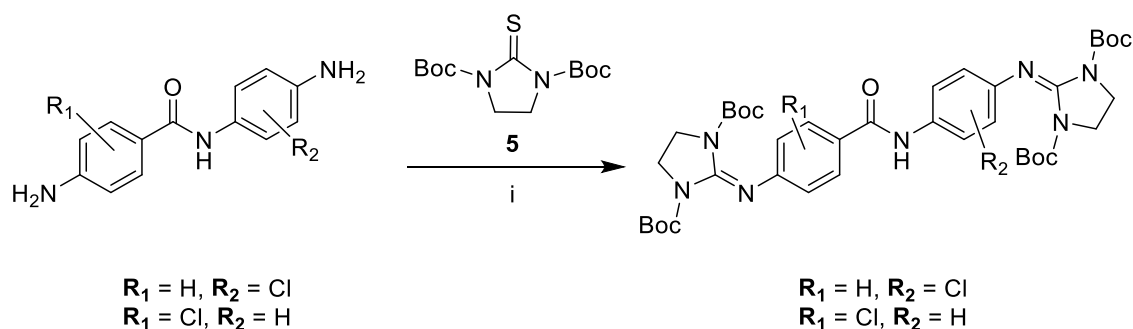
Reagents and conditions: i) $HgCl_2$, Et_3N, DMF, 0 °C to 60 °C.

Reagent **5** was synthesized in high yield (95%) from imidazolidine-2-thione (**24**) using di–*tert*–butyldicarbonate (Boc₂O) in dry tetrahydrofuran (THF) in the presence of sodium hydride (Scheme 3.13).[16]

Scheme 3.13: Synthesis of di-*tert*-butyl 2-thioxoimidazolidine-1,3-dicarboxylate (**5**).[16]

24

5 (95%)
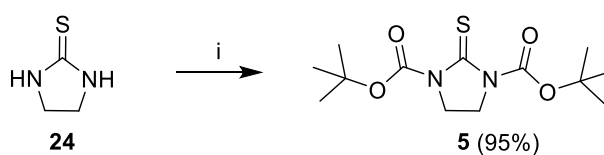
Reagents and conditions: i) NaH, Boc₂O, THF, 0 °C.

The reaction mechanism for the formation of the Boc-protected 2-thioxoimidazolidine (**5**) involves both of the amino groups on the imidazoline being irreversibly deprotonated by NaH expelling H_2 gas (Scheme 3.14). The highly basic and reactive thioimidazoline salt attacks di-*tert*-butyldicarbonate to yield the relevant mono-*tert*-butoxycarbonyl protected imidazolinethione, CO_2, and sodium *tert*-butoxide. As there is a further thioamide group on the mono-Boc–protected imidazolinethione, the two steps previously mentioned are repeated, resulting in the formation of **5**.

Scheme 3.14: Proposed reaction mechanism for the formation of **5**.
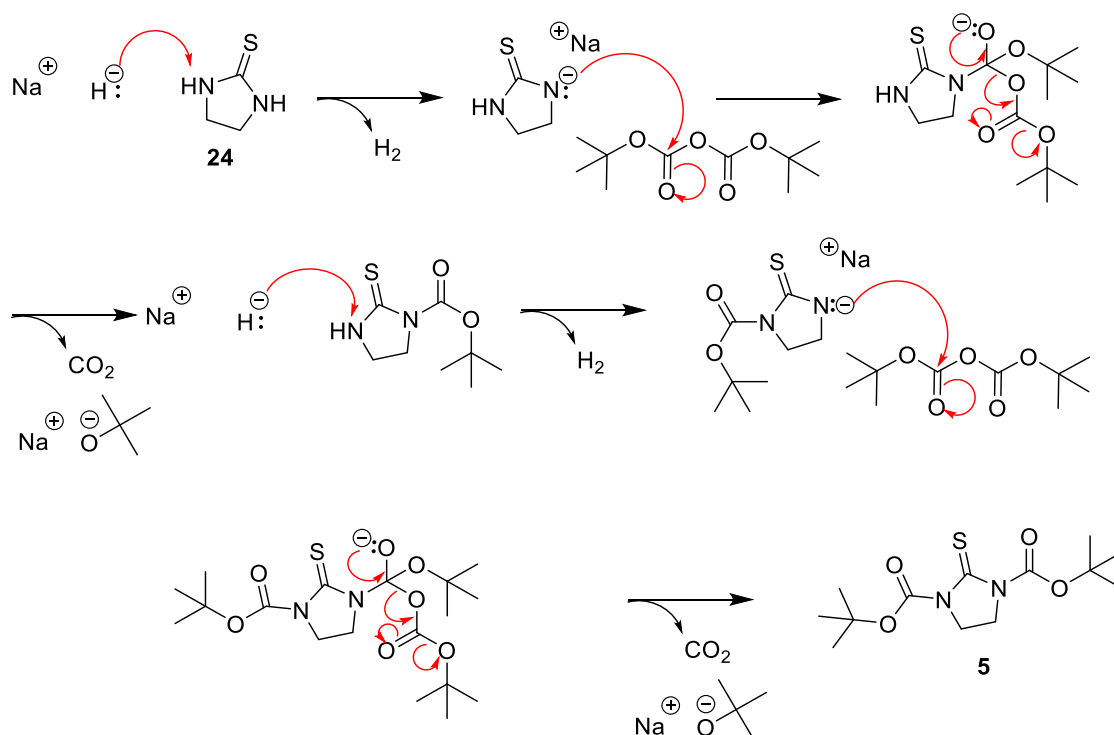
3.1.7. Synthesis of Boc-protected bis(imidazolidin-2-imine) derivatives (25b–h)

Guanidylating agent **5** was used for the synthesis of Boc-protected bis(imidazolidin-2-imine) derivatives **25b–h** (Scheme 3.15). The diamines (**15b–h**) were reacted with **5** (3 eq.) in the presence of an excess of triethylamine (7 eq., Et_3N) and $HgCl_2$ (3 eq.) in dry DMF. A 3:1 ratio of diamine: guanidylating agent was used in order to obtain a full conversion into the bis(imidazolidin-2-imine) derivatives **25b–h**. Since $HgCl_2$ was used, a characteristic black precipitate (HgS) normally formed upon reaction with the amines. The mild reaction conditions involved an initial stirring at 0 °C, and then overnight at 60 ºC under argon atmosphere. The progress and completion of the reaction was monitored by thin layer chromatography (TLC) and by HPLC–MS.

Scheme 3.15: Synthesis of Boc-protected bis(imidazolidin-2-imine) derivatives **25b**–**h**.
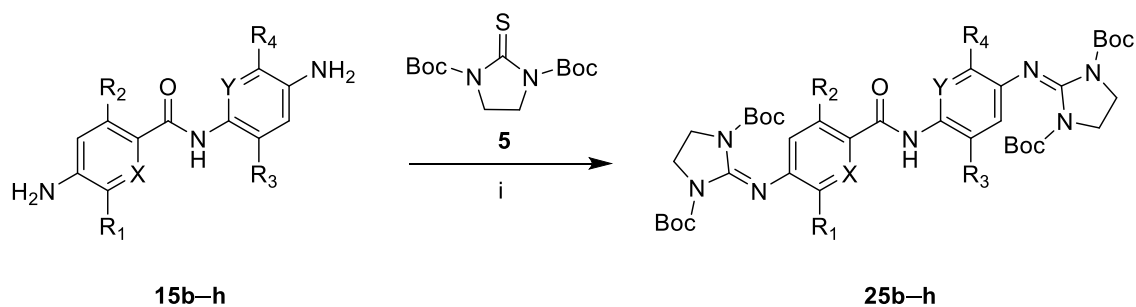
Cmpd	X	Y	R$_1$	R$_2$	R$_3$	R$_4$	Yield
b	CH	CH	Cl	H	Cl	H	54%
c	CH	CH	Cl	H	H	Cl	47%
d	CH	CH	H	Cl	Cl	H	78%
e	CH	CH	H	Cl	H	Cl	88%
f	CH	CH	F	H	F	H	20%
g	CH	CH	H	O^{i}Pr	O^{i}Pr	H	45%
h	N	N	H	H	H	H	47%

Reagents and conditions: i) HgCl$_2$, Et$_3$N, DMF, 0 °C to 60 °C.

In most cases, the reaction did not go to completion and a mixture of mono and di-substituted compounds was obtained. This reaction proceeds slowly at room temperature (e.g., low conversion rate was observed by HPLC–MS after 7 days) and heating at 60 ºC was required to reduce the reaction time. A workup involving dilution of the crude reaction mixture with dichloromethane (CH$_2$Cl$_2$), filtration through a pad of Celite, and partition between CH$_2$Cl$_2$ and water was performed. The crude products were purified by circular chromatography on silica plates previously deactivated with a 9:1 hexane:Et$_3$N mixture (**25b**–**e**, **25g**–**h**), or by column chromatography using neutral aluminium oxide (**25f**) (Scheme 3.15). Using this method, the Boc-protected target compounds **25b**–**h** were obtained in moderate to good yields: 47–88% for the dichlorinated derivatives (**25b**–**e**), 20% for the difluorinated compound (**25f**), 45% for the di-isopropoxi derivative (**25g**) and 47% for the di-pyridyl derivative (**25h**). Compound **25h** was purified twice by circular chromatography, which resulted in lower yield possibly due to product being stuck on the plate.

To conclude, we found that the use of an excess of **5** (3 eq.)/ Et$_3$N (7 eq.)/ HgCl$_2$ (3 eq.)/ DMF/ 60 ºC is useful for the synthesis of Boc-protected bis(imidazolidin-2-imine) derivatives (**25b**–**h**) from poorly nucleophilic anilines. Importantly, these intermediates are stable compounds that can be purified by column chromatography on neutral aluminium oxide or circular chromatography on deactivated silica.

As regards to the mechanism of this reaction, it must be different from the one proposed by Kim and Qian[26] (Scheme 3.16A). Since our guanidilating agent lacks of free H atoms, no carbodiimide intermediate (i.e., the proposed electrophilic species attacked by the amine nucleophile) can be formed upon desulfurization of reagent **5** in the presence of HgCl$_2$. Our hypothesis is that the formation of the Boc-protected imidazolidin-2-imine derivatives goes through a tetrahedral intermediate (Scheme 3.16B, b) formed by the C-2 carbon of the imidazoline ring. This putative mechanism involves the coordination of the sulphur atom of **5** to the thiophilic mercury atom of HgCl$_2$. This is followed by a nucleophilic attack of the amine to the C-2 atom of the imidazoline ring generating the tetrahedral intermediate (Scheme 3.16B).

Scheme 3.16: (A) Kim & Qian proposed mechanism[26] and (B) putative reaction mechanism for the formation of the Boc-protected imidazolidin-2-imines.
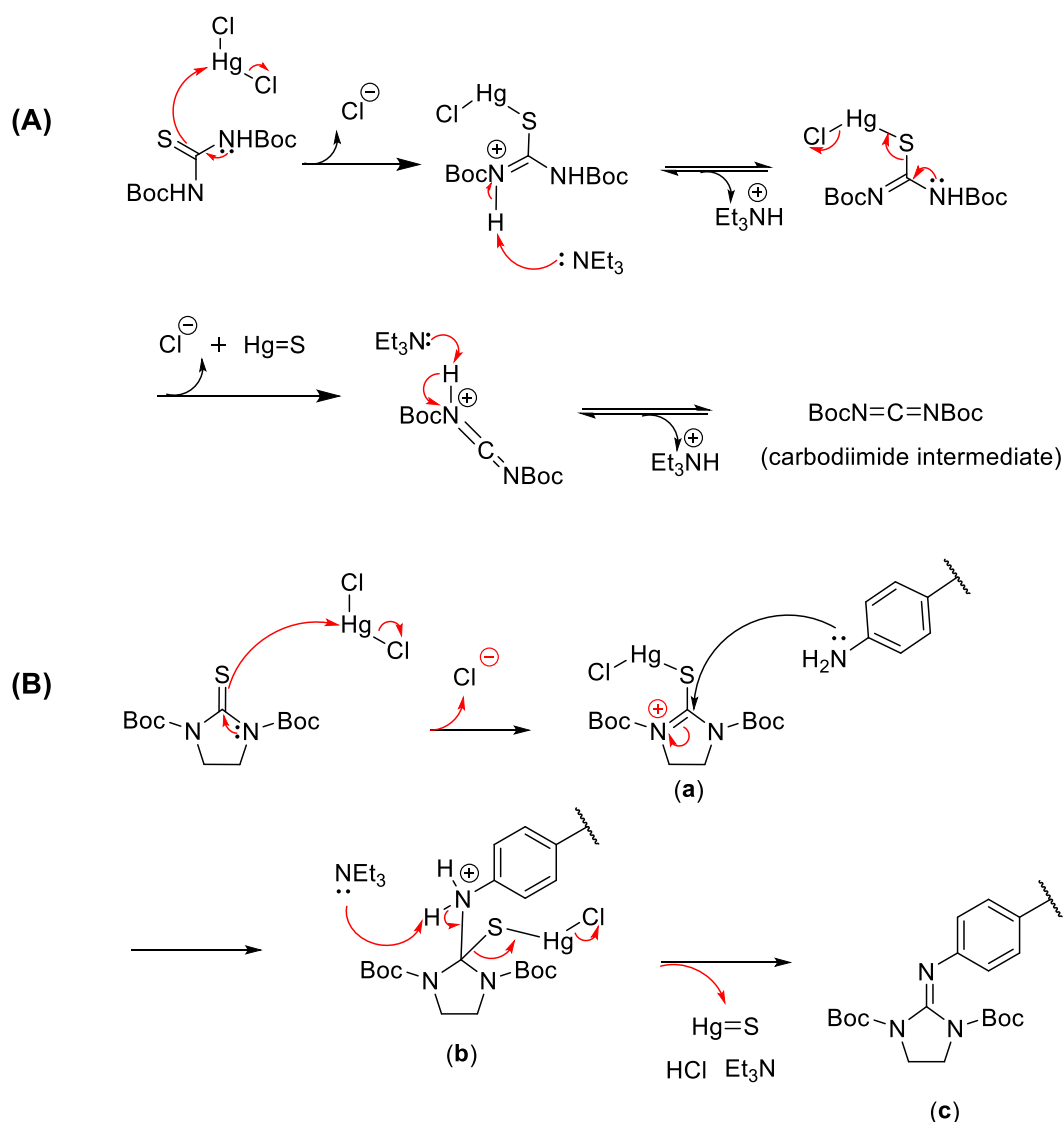
3.1.8. Synthesis of bis(imidazolidin-2-imine) salts (1b–h)

Trifluoroacetic acid (TFA), either neat or in DCM solution, is the standard reagent to remove Boc-protecting groups.[27] The typical reaction followed in our laboratory involves treatment with 1:1 TFA/DCM at 0 °C (ice-bath) for 2 hours followed by solvent removal under vacuum.[2]

Deprotection of the synthesized compounds **25b–h** was carried out with TFA at 0 ºC to yield the corresponding bis(imidazolidin-2-imine) compounds **1b–h** as trifluoroacetate salts after evaporation of the solvents (Scheme 3.17). Working at low temperature in the

absence of protic solvent (e.g., using CH_2Cl_2) was important to avoid the rupture of the PhN=C bond resulting in the loss of the imidazoline ring and generation of the amine starting material. Purification was carried out crushing the crude products with Et_2O to yield the trifluoroacetate salts as off-white solids. The products were isolated in moderate to good yields. Compound **1f** was obtained in low yield because several recrystallizations were necessary to remove traces of the mono-substituted compound (Scheme 3.17).

Scheme 3.17: Synthesis of bis(imidazolidin-2-imine) target compounds **1b–h**.
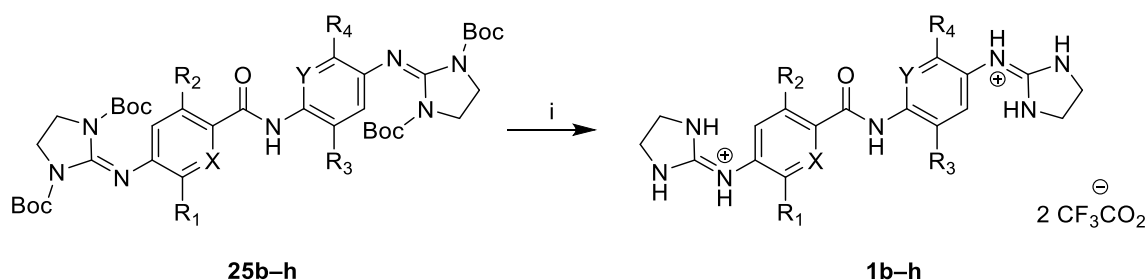
Cmpd	X	Y	R_1	R_2	R_3	R_4	Yield
b	CH	CH	Cl	H	Cl	H	28%
c	CH	CH	Cl	H	H	Cl	85%
d	CH	CH	H	Cl	Cl	H	60%
e	CH	CH	H	Cl	H	Cl	81%
f	CH	CH	F	H	F	H	23%
g	CH	CH	H	O^iPr	O^iPr	H	51%
h	N	N	H	H	H	H	35%

Reagents and conditions: i) CH_2Cl_2, TFA, 0 °C, 2 h.

The mechanism of the deprotection reaction (Figure 3.2) involves protonation of the carbonyl group by TFA; the electrons then migrate so that the positively charged carbonyl is quenched. This is followed by the movement of the lone pair of electrons from the O to reform the carbonyl bond and CO_2 is expelled to form the deprotected amine.
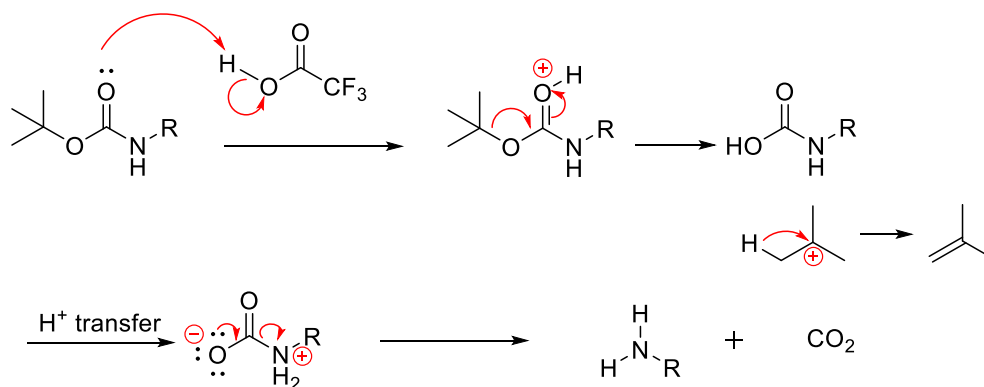
Figure 3.2: Mechanism of Boc-deprotection using TFA

3.1.9. Predominant tautomeric forms of compounds 1b–h in solution

Due to the presence of two endocyclic and one exocyclic nitrogen atoms, two possible tautomeric forms exist in the synthesized compounds, namely the "2-amino" and "2-imino" tautomers (Figure 3.3). Determining the predominance of any of them is important to properly name the synthesized compounds.

"4,5-dihydro-1*H*-imidazol-2-ylamino"
"amino" tautomer

"imidazolidin-2-imino"
"imino" tautomer
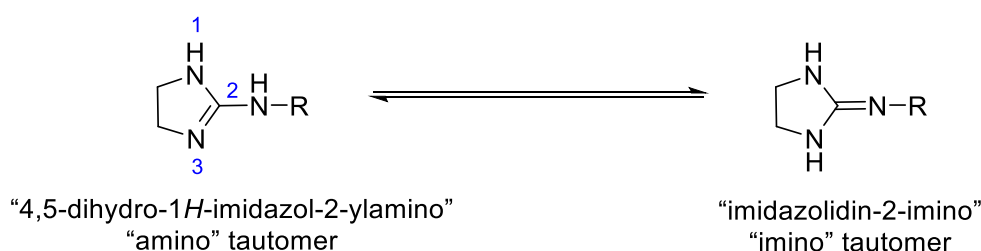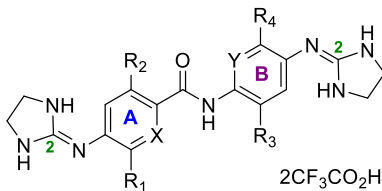
Figure 3.3: Tautomeric forms of the 2-aminoimidazoline group.

In order to describe the major tautomer in solution for compounds **1b–h**, the ^{13}C NMR chemical shifts of the imidazoline C-2 carbon was gathered in Table 3.4.

The nature of the R substituent on the exocyclic nitrogen (N-2) exerts an influence on the type of tautomer observed in solution; generally, the imino tautomer is favoured by the presence of phenyl groups at N-2, but substituents on the phenyl rings of the scaffold also exert an influence.[28] A previous work[29] from our group analysed this topic in related bis(imidazolidin-2-imine) derivatives where the signals for the quaternary C-2 of the imino tautomer exhibit a chemical shift at ~155–160 ppm. In contrast, the chemical shift for the amino tautomer is around ~130 ppm. The chemical shifts for the quaternary C-2 atom of

the imidazoline rings shown in Table 3.4 (i.e. ~157–160 ppm) indicate that the major tautomer of **1b**–**h** in DMSO solution is the imino tautomer.

Table 3.4: ^{13}C NMR chemical shift (DMSO–d_6) for the C-2 carbon of the imidazoline rings

Cpd	Structure	Imidazoline ring A δ ppm	Imidazoline ring B δ ppm
1b		157.8	158.1
1c		158.1	158.6
1d		158.0	158.3
1e		157.5	158.6
1f		158.6	160.1
1g		157.6	158.2
1h		157.8	158.5

3.2. Synthesis of bis(2-aminobenzimidazole) derivatives

3.2.1. Introduction

Benzimidazole rings can undergo electrophilic, nucleophilic and cyclocondensation reactions giving rise to stable compounds. This ability has made possible the synthesis of a large variety of substituted benzimidazoles and benzimidazole heterocycles, resulting in effective drugs for treating not only human infections but also animal diseases.[30, 31]

The therapeutic potential of benzimidazole in the treatment of parasitic diseases was only taken into account since the 60's when the first anthelmintic drugs appeared.[30] The most common benzimidazole derivatives used in antiparasitic chemotherapy are mebendazole and albendazole (Figure 3.4), due to their efficacy and low side–effects reports for the treatment of gastrointestinal infections (e.g., *Necator americanus* or *Ancylostoma duodenale*, *Ascaris lumbricoides*, *Enterobius vermicularis* and *Trichuris trichiura)* or intestinal nematode infection (e.g., *Echinococcus granulosus*, *Trichinella spiralis*).[32]

Albendazole   Mebendazole
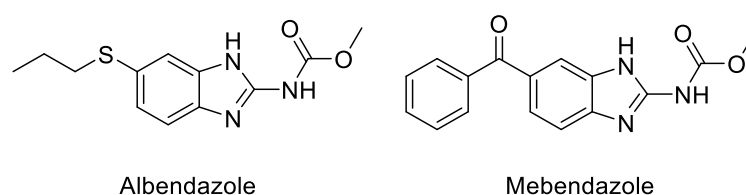
Figure 3.4: Albendazole and Mebendazole chemical structures.

Synthetically the most known method to obtain benzimidazole derivatives involves the reaction of *o*–phenylenediamine (OPD) with orthoesters in the presence of catalytic amounts of Lewis acid (Scheme 3.18).[33, 34] This reaction is performed at room temperature, under mild reaction conditions, resulting in high conversions and clean reaction profiles, as the main attractive features.[34]

Scheme 3.18: Synthesis of benzimidazole derivatives from orthoesters using Lewis acids.[34]

$$R = H, Me, Cl, NO_2$$
$$R_1 = H, Me, Et, CH_3(CH_2)_3$$
$$R_2 = Me, Et$$
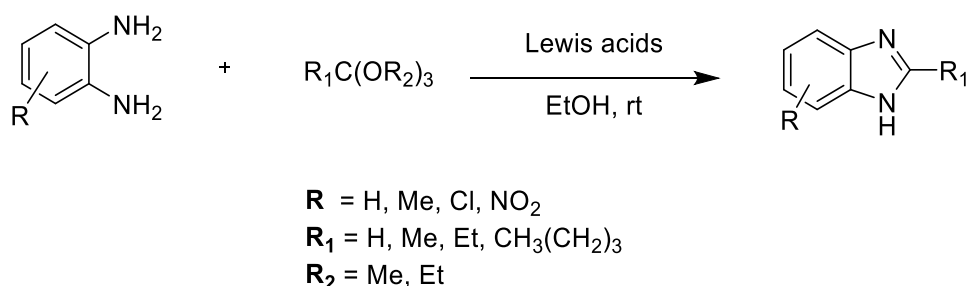
The most useful strategy to obtain 2-substituted benzimidazoles involves the reaction of substituted aromatic/aliphatic aldehydes with OPD. As this reaction involves oxidation of the aldimine intermediate trough H_2O elimination, the process can be carried out in the presence of air or other oxidizing agents such as iodobenzene diacetate $PhI(OAc)_2$ (Scheme 3.19a). On the other hand, carrying out the reaction between OPD and an aldehyde in the absence of a specific oxidizing agent results to either 2-substituted benzimidazoles or aldimines product formation (Scheme 3.19b).

Scheme 3.19: Synthesis of substituted benzimidazole derivatives a) catalyzed by oxidizing agent [$PhI(OAc)_2$] and b) via aldiminine intermediate in the absence of catalyst.
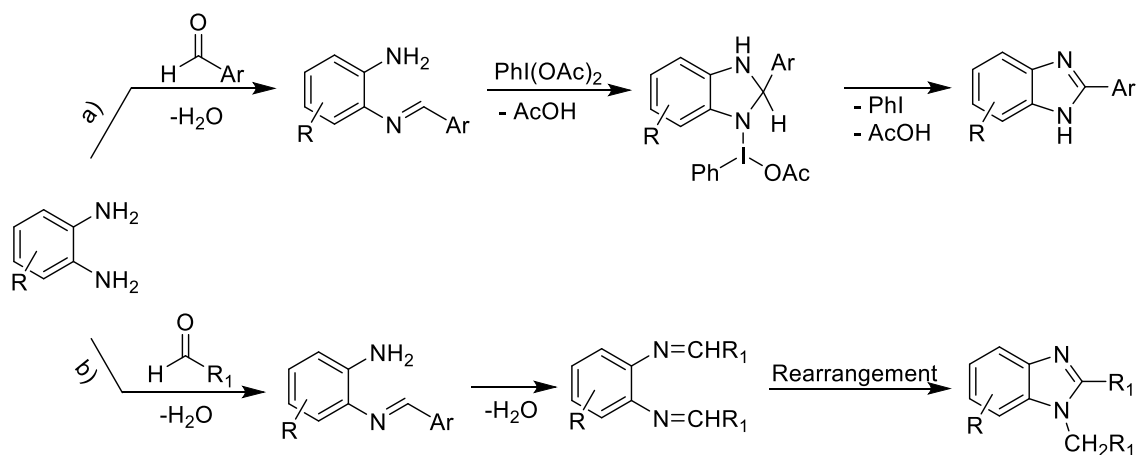
In order to prepare 2-aminobenzimidazoles, several conventional routes have been described previously.[35] This includes the a) cyclization of *o*-nitrothioureas (with prior reduction to aminothioureas), b) nucleophilic aromatic substitution reaction of chlorobenzimidazole, c) one-pot cyclization of diamines and isothiocyanates (Scheme 3.20).

Scheme 3.20: Conventional routes to 2-aminobenzimidazoles.[35]
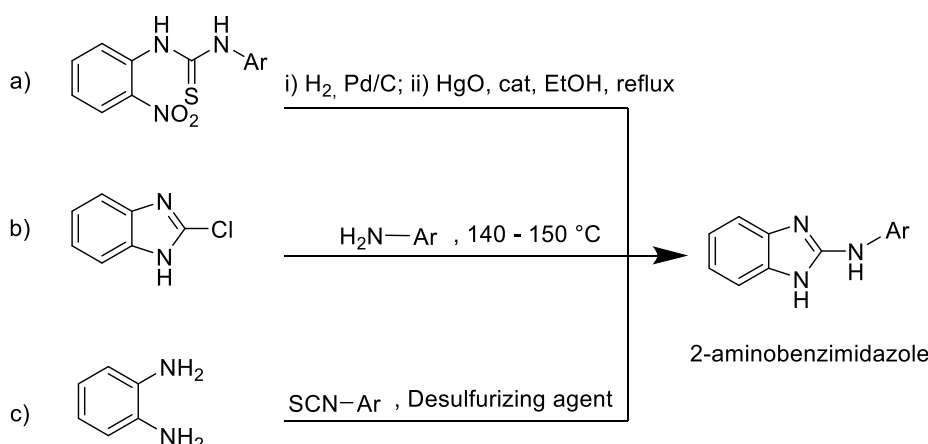
Low yields are reported with method a) where the reduction of the nitro group is the limiting step.[35] Method b) requires elevated temperatures and usually yields self-arylation products.[36] To obtain 2-aminobenzimidazole derivatives with higher yield, a one-pot synthesis from OPD and isothiocyanates (method c) has been used.[35] In this case, the use of a desulfurizing agent is compulsory, being the most common: HgO, $HgCl_2$, CuCl, MeI, tosyl chloride or carbodiimide reagents [e.g. DCC, EDC, diisopropylcarbodiimide (DIC)].[35, 36]

3.2.2. Synthesis of 4-((1,3-dihydro-2*H*-benzo[*d*]imidazol-2-ylidene)amino)-*N*-(4-((1,3-dihydro-2*H*-benzo[*d*]imidazol-2-ylidene)amino)phenyl)benzamide derivatives (2a–e, 2h)

The strategy to synthesise our target bisbenzimidazole derivatives was based on the reaction between OPD and isothiocyanate precursors to give a thiourea intermediate which was cyclized *in situ* using EDC.HCl (Scheme 3.21). The first-step involved the formation of a thiourea intermediate, in which a total conversion rate was observed by HPLC–MS. This intermediate was not isolated and the reaction was performed in one pot. The overall yields of bisbenzimidazole compounds were moderate due to the difficulty of the purification process. Chloro-derivatives (Scheme 3.21, R = Cl) were most of the time difficult to separate by column chromatography, due to product binding to the silica gel. Hence, the use of 10% of polar solvents (e.g., MeOH, MeOH/NH$_{3sat}$) in the eluent mixture was required to recover the products.

Scheme 3.21: Synthetic route to bis(2-aminobenzimidazoles)

Isothyocyanate derivatives **26a–e** and **26h** were prepared following the methodology described below (Scheme 3.22). Previously synthesized diamines **15b–e** and **15h** (Scheme 3.8) were reacted with thiophosgene in H_2O/Et_2O at room temperature overnight (Scheme 3.22).[4] Diamine **15a** was commercially available. Isothiocyanate **26a** was prepared as reported earlier.[4]

Scheme 3.22: Synthesis of bisbenzimidazole derivatives **2a–e** and **2h**
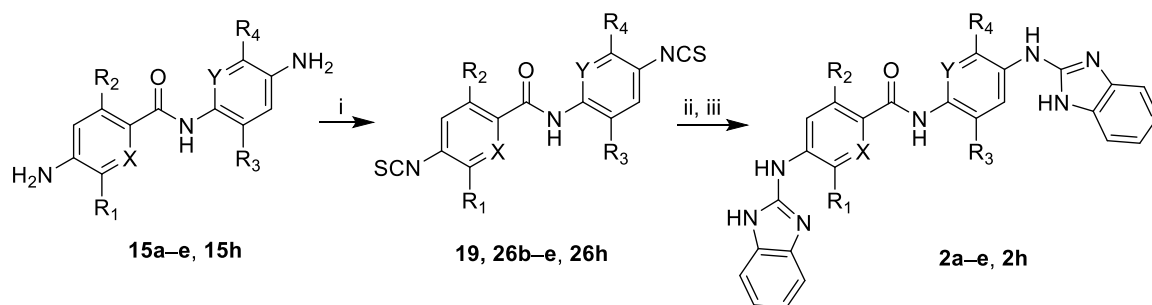
Cmpd	X	Y	R₁	R₂	R₃	R₄	Yield (26)	Yield (2)
19	CH	CH	H	H	H	H	92%	61%
26b	CH	CH	Cl	H	Cl	H	44%	43%
26c	CH	CH	Cl	H	H	Cl	83%	15%
26d	CH	CH	H	Cl	Cl	H	66%	31%
26e	CH	CH	H	Cl	H	Cl	24%	59%
26h	N	N	H	H	H	H	52%	44%

Reagents and conditions: i) Cl_2CS, $Et_2O:H_2O$ (3:1), rt. ii) *o*-phenylenediamine, DMF, rt; iii) EDC.HCl, 60 °C.

The isothiocyanate derivatives were obtained in moderate to good yield in most cases. Despite of high conversion rates (as observed by HPLC–MS and TLC), the isolated yields were lower for compound **26e** due to purification issues. For all of the compounds, the purification process involved a filtration of the crude reaction mixture over a filtration funnel, using water to remove excess of thiophosgene. The product was obtained as a solid precipitate. One reason for the low yield is possibly due to this first filtration step in which some crude is lost in the aqueous phase. Another reason could be pointed to the chromatographic separation when product was jammed to the silica and high polarity solvent mixtures were required (i.e., CH$_2$Cl$_2$:MeOH, 90:10→80:20).

Bisbenzimidazoles **2a–e** and **2h** were synthesized by reaction of OPD with isothiocyanate **26a–e** and **26h**, respectively, followed by *in situ* cyclization of the thiourea intermediate using EDC.HCl as promoting agent. Low to moderate yields were obtained for the final products **2a–e** and **2h** despite of high conversion rates to the thiourea intermediate (> 90% detected by HPLC–MS) and the bisbenzimidazole products ($\geq$ 50%); however, column chromatography purification of the crude products **2a–e** and **2h** was complicated due to the products jammed into the silica gel. To increase the yields of isolated compound, the products were purified by circular chromatography using previously deactivated silica plates (i.e., hexane:Et$_3$N, 90:10) and high polarity solvent mixtures (i.e., containing 10% MeOH or 10% MeOH:NH$_{3sat}$).

3.2.3. Synthesis of 4-((1,3-dihydro-2*H*-benzo[*d*]imidazol-2-ylidene)amino)-*N*-(4-((1,3-dihydro-2*H*-benzo[d]imidazol-2-ylidene)amino)phenyl)benzamide derivatives 30, 31, and 34.

Diamines **27** and **32** were commercially available whereas **28** was prepared by Parr hydrogenation of commercial 1,3-bis(4-nitrophenyl)urea (89%). Isothiocyanates **29**, **20**, and **33** were prepared as reported earlier.[4] Bisbenzimidazoles **30, 31**, and **34** were synthesized by reaction of the isothiocyanate precursors (**29**, **20**, and **33**, respectively) with OPD, followed by *in situ* cyclization of the thiourea intermediate as described in Scheme 3.23.

Scheme 3.23: Synthesis of bisbenzimidazole derivatives (**30**, **31**, and **34**) with different scaffolds.

R = NH₂
27 : X = CH₂CH₂
28 : X = NHCONH

R = NCS
29 : X = CH₂CH₂ (79%)
20 : X = NHCONH (64%)

30 = CH₂CH₂   (54%)
31 = NHCONH (25%)

32: R = NH₂
33: R = NCS (86%)

34 (61%)
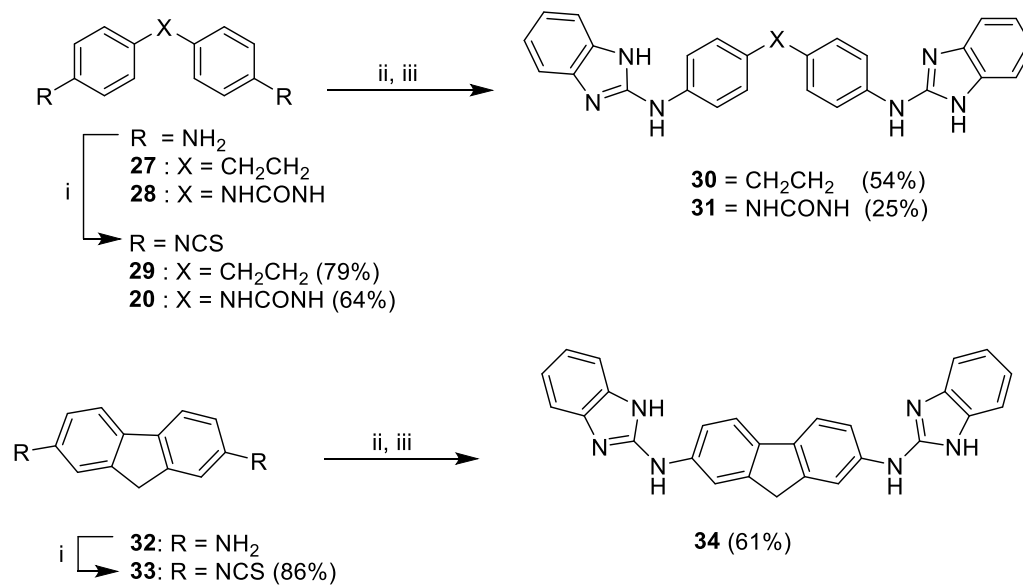
Reagents and conditions: i) Cl₂CS, Et₂O:H₂O (3:1), rt. ii) *o*-phenylenediamine, DMF, rt; iii) EDC.HCl, 60 °C.

3.3. Synthesis of bis(pyridine-2-carboxamidine) ["bis(arylimidamide)"] derivatives

3.3.1. Introduction

The synthesis of *N*-phenylpyridinecarboxamidines (**III**, Scheme 3.24a) can be achieved by reaction of substituted anilines with 2-cyanopyridine catalysed by different bases (e.g. NaH, NaOMe, BuLi, LDA, NaN(SiMe$_3$)$_2$, DBU)[37, 38] or in the presence of Lewis acid (e.g. AlCl$_3$, TiCl$_4$ or SnCl$_4$).[39-41] One of the main problem of the direct synthesis of bis(pyridine-2-carboxamidines) using 2-cyanopyridine with AlCl$_3$ or sodium hexamethyldisilazide in tetrahydrofuran lies in the difficult isolation of pure amidines from complex reaction mixtures. This is due in part to the poor solubility of these products in organic solvents. The low solubility of the mono-amidine intermediates could also be responsible for the failure of this method.[42]

The synthesis of bis(pyridine-2-carboxamidines) using the Pinner method was successful with aliphatic or biphenyl diamines.[43] An alternative protocol based on the modification of the classical Pinner method via S-(2-naphthylmethyl)thioimidates (**35**) was developed Collins *et al*[44] for the reaction with non-nucleophilic amines such as substituted anilines (Scheme 3.24b). This protocol was used later by Boykin and co-workers to prepare different series of bis(arylimidamides).[45-50]

Scheme 3.24: Classical routes to prepare *N*-aryl-pyridin-2-carboxamidines from anilines.
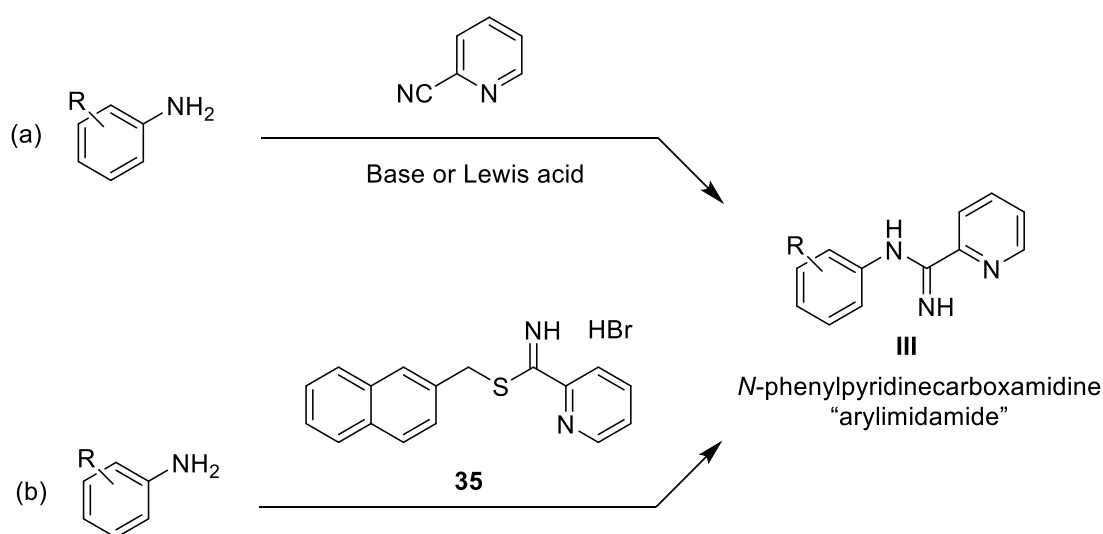
3.3.2. Attempted synthesis

Previous reports have shown that the reaction between *S*-(2-naphthylmethyl)-2-pyridylthioimidate hydrobromide (**35**) and aryl diamines yielded the expected bis(arylimidamides) in good yield as long as the diamines were reasonably electron-rich.[45] In contrast, this reaction failed with diamines containing halogen substituents on the phenyl rings or electron-deficient rings (e.g. 2,7-diamino-9*H*-fluoren-9-one, 2,7-diaminoanthracene-9,10-dione, acridine-3,6-diamine, etc.)[42, 45, 51]

The classical synthetic protocol using reagent **35** was tried with diamines **15a**, **27** and **28**, yielding bis(pyridine-2-carboxamidines) **3a**, **36** and **37** which were isolated as free bases (Scheme 3.25). The reaction of unsubstituted diamine **15a** with a small excess of **35** (2.5 eq.) yielded bis(pyridine-2-carboxamidine) **3a** (23%) after purification by circular chromatography on deactivated silica (i.e. the plate was deactivated with a mixture of hexane:Et₃N (90:10) before use). Other electron rich scaffolds **27** and **28** were reacted following this method to obtain the desired compounds **36** and **37** in moderate yields, 24% and 39%, respectively.

Scheme 3.25: Synthesis of bis(pyridine-2-carboxamidines) **3a**, **36** and **37**.
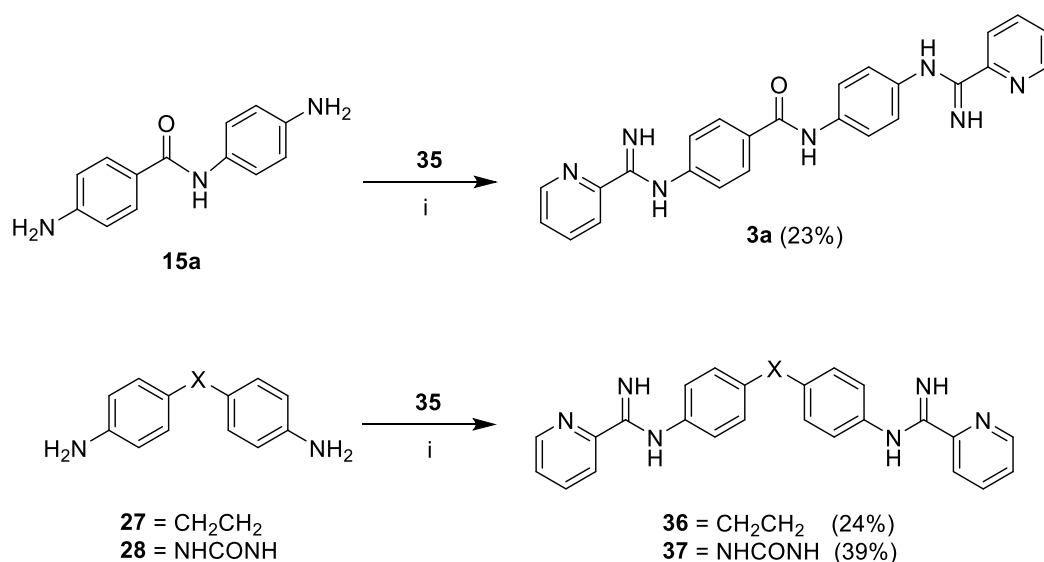
Reagents and conditions: (i) EtOH, CH₃CN (3:1), rt, 72 h.

When we tried to synthesize **3b–e** with reagent **35** using the electron-deficient diamine precursors containing chlorine substituents (**15b–e**) we could not isolate the bis(pyridine-2-carboxamidine) products **3b–e** (Scheme 3.26).

Scheme 3.26: Attempts to synthesize bis(pyridine-2-carboxamidines) **3b–e** and **3h–i**
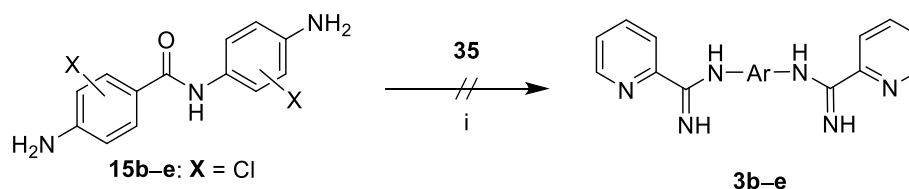
Reagents and conditions: (i) EtOH, CH$_3$CN (3:1), rt.

When the reaction was performed with the pyridine–containing starting materials 5-amino-*N*-(5-aminopyridin-2-yl)picolinamide (**15h**) and 4-amino-*N*-(5-aminopyridin-2-yl)benzamide (**15i**), only little amount of the mono-substituted products (**38** and **39**, respectively) were isolated by silica chromatography (Scheme 3.27). HPLC–MS analysis of the crude reaction mixtures showed that the reaction did not go to completion even after prolonged time (i.e., more than 7 days) or using higher temperature (i.e., 40 °C and 60 °C). Polar aprotic solvents (i.e., DMF, THF) were also tried, but the same results were obtained. Nevertheless, small quantities of bis(arylimidamide) **3h** (97 mg, 36%) and **3i** (10 mg, 6.1%) could be isolated by silica chromatography together with the mono-substituted product **38** (63 mg, 23%) and **39** (20 mg, 12.2%).

To determine the substitution pattern of compounds **38** and **39**, we compared the experimental and predicted ^{1}H NMR shifts of the free NH$_2$ group in the starting material diamines and the product (Table 3.5). ^{1}H NMR shift prediction was performed using MestReNova. Experimental data were collected for both compounds using deuterated DMSO as solvent.

Scheme 3.27: Synthesis of **3h**, **3i**, **38** and **39**
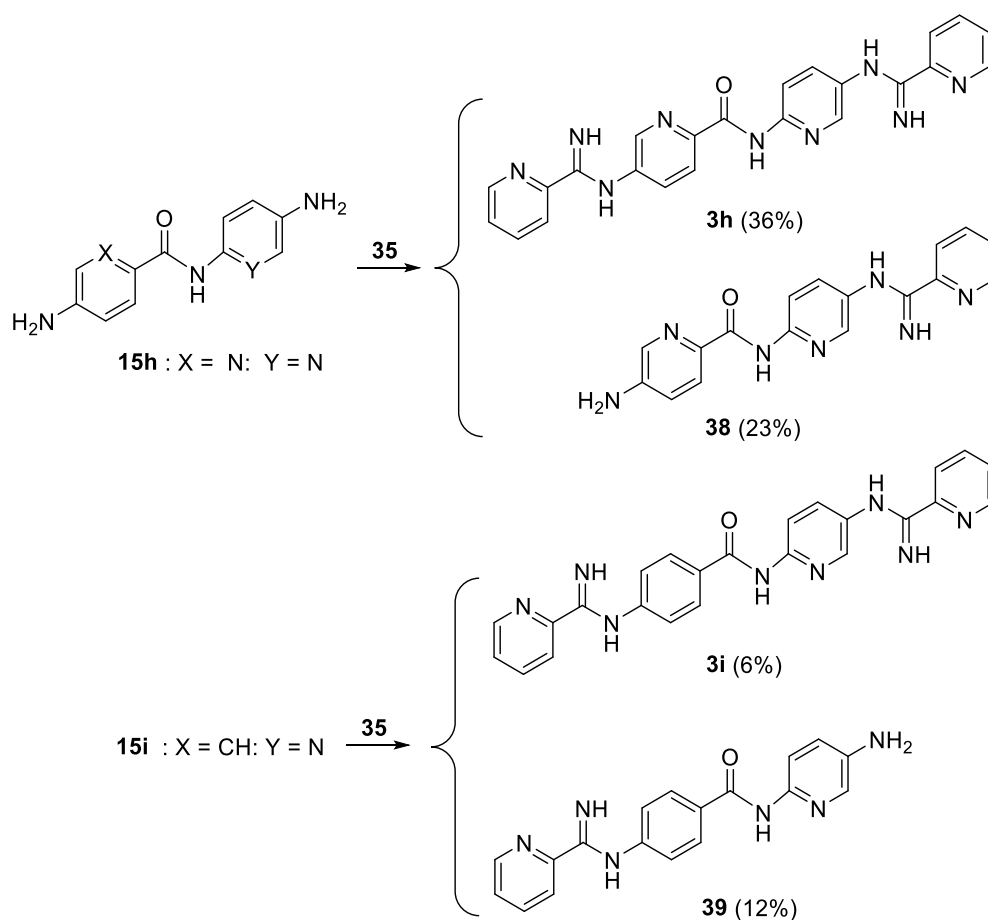
The ^{1}H NMR spectrum of compound **39** shows a broad peak integrating for 2H at 5.21 ppm. This value is almost identical to the experimental value of NH$_2$(b) in diamine **15i** (5.06 ppm), suggesting that **39** is substituted on the NH(a) group. Compound **38** shows a broad peak integrating for 2H at 6.21 ppm. This value is close to the experimental value of NH$_2$(a) in diamine **15h** (6.12 ppm), which implies that compound **38** is substituted on the NH(b) group. Of note, the chemical shift predictions for **15a** are in excellent agreement with the experimental values. In contrast, the predicted values of the compounds containing aminopyridine groups (**15h**, **15i**, **38**, **39**) are disconnected from the experimental ones.

Table 3.5: ^{1}H NMR chemical shifts of the free amino (NH$_2$) groups in the starting material diamines and compounds **38–39**

Cmpd	Structure	Predicted^a (δ, ppm)	Experimental^b (δ, ppm)
15a		5.80 (a) 4.73 (b)	5.67 4.86
15i		5.80 (a) 6.72 (b)	5.70 5.06
39		6.72 (b)	5.10 (br s, 2H)
15h		6.72 (a) 6.72 (b)	6.12 5.13
38		6.72 (a)	6.21 (br s, 2H)

^{a} Mestrenova 14.2.1-27684. ^{b} Solution in DMSO-d_6

As we use electron-deficient diamine precursors, we tested an alternative synthetic route to obtain the chlorine-containing bis(pyridine-2-carboxamidine) derivatives **15b–e**. This approach was tried with the previously synthesized isothiocyanate **26b** as probe (Scheme 3.28). The proposal involves the conversion of 2-bromo pyridine into the organolithium reagent as first-step, followed by the nucleophilic addition to isothiocyanate **26b** to form

secondary thioamide intermediate.[52] The last step consists in the transformation of the thioamide group into the carboxamidine.[53-55]

Scheme 3.28: Proposed synthetic route of pyridine-2-carboxamidine derivatives using 2-bromo pyridine and an isothiocyanate precursor.[52]
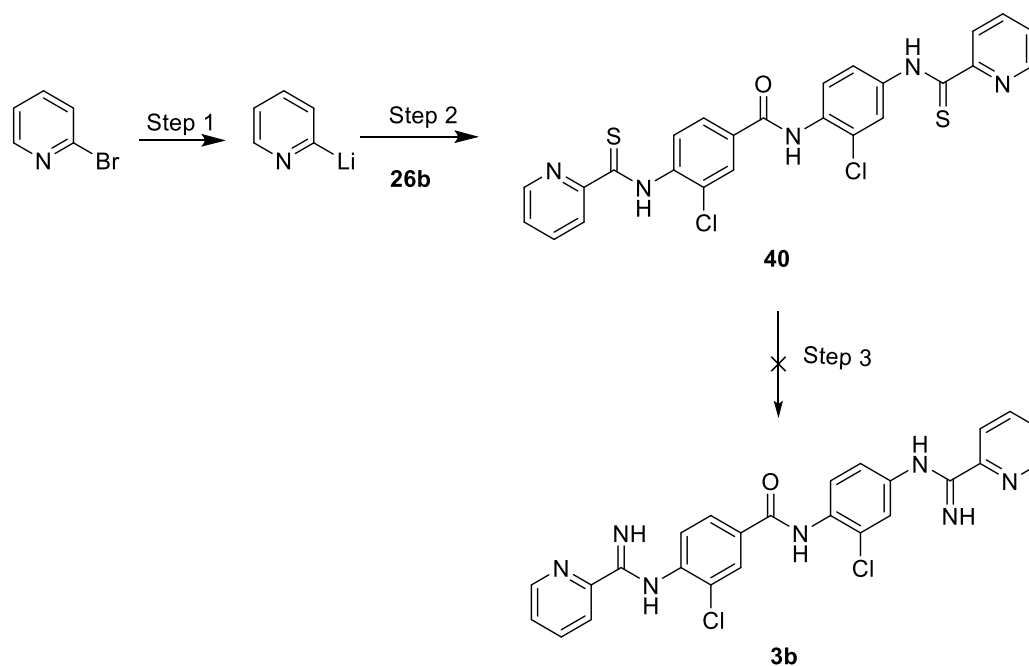
Reagents and conditions: Step 1: *n*-BuLi, CMPE, -78 °C, 3 h; Step 2: CMPE, -78 °C, 2 h (See Table); Step 3: aq. NH$_3$, EtOH:CH$_2$Cl$_2$ (2:1), rt, 2 h.

The synthesis of the organolithium reagent was easily achieved following the conditions previously reported.[52] However, compound **40** was not obtained when cyclopentyl methyl ether (CPME) was used as solvent,[30] probably due to the low solubility of the isothiocyanate **26b**. Different attempts using other solvents (i.e., CH$_2$Cl$_2$, DMF) which solubilized **26b** were unsuccessful and the starting material (i.e., isothiocyanate) was recovered in all the cases (Table 3.6). These disappointing results could be related to the instability of the organometallic intermediate even though dry solvents and inert conditions were used. Additionally, it could be related to an incomplete solubilisation of the organometallic derivative – solubilized in CMPE – in the final reaction mixture containing the co-solvent used in Step 2 (Table 3.6). All these attempts under the conditions shown in Table 3.6 yielded the mono-substituted product in low yield in a mixture difficult to separate.

Table 3.6: Conditions evaluated to synthesize pyridine-2-carboxamidine derivatives using 2-bromo pyridine and an isothiocyanate precursor

Step 1				Step 2		
Reagent	Solvent	Temp.	Time	Solvent	Temp.	Time
n-BuLi	CPME	-78 °C	3h	CPME	-78 °C	2h
n-BuLi	CPME	-78 °C	3h	CH$_2$Cl$_2$	-78 °C	2h
n-BuLi	CPME	-78 °C	3h	DMF	-78 °C	3h

A different approach to obtain bis(arylimidamide) **3a** via the formation of picolinamide intermediate **41** was proposed (Scheme 3.29). The reaction of 4-amino-*N*-(4-aminophenyl)benzamide with picolinoyl chloride hydrochloride gave **41** in high yield (94%) by precipitation from MeOH. Then, different conditions were tested to transform **41** into bis(arylimidamide) **3a** (Scheme 3.29, conditions ii, iii, iv or v).

Scheme 3.29: Proposed synthetic route to **3a** using picolinoyl chloride hydrochloride.
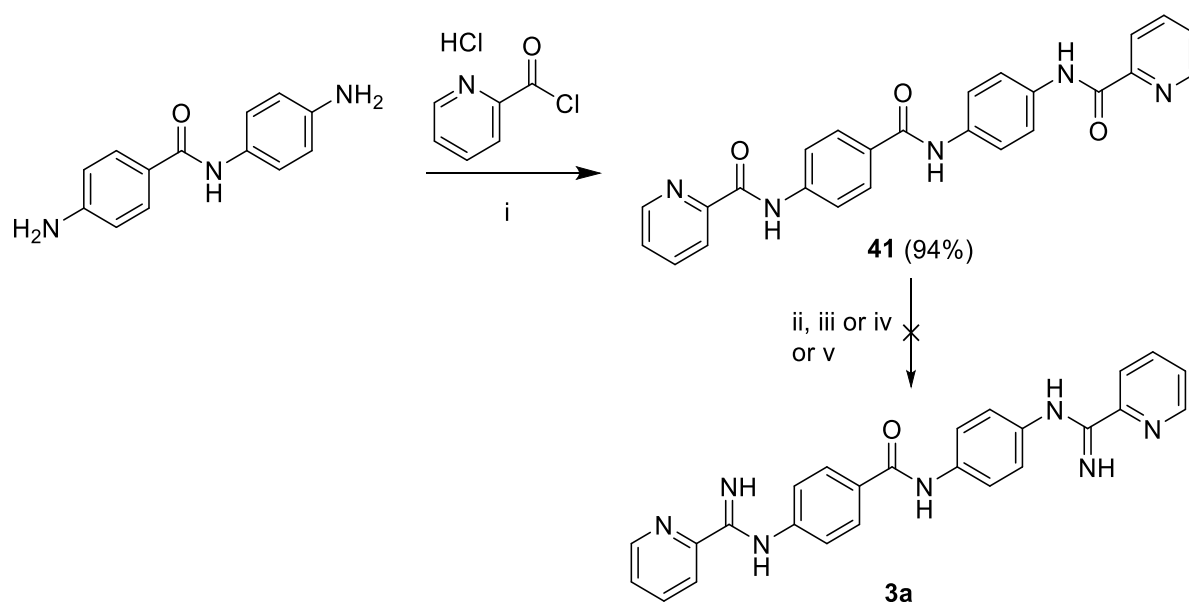
Reagents and conditions: i) Et$_3$N, THF, 2 h, rt. ii) SOCl$_2$, 80 °C, 14 h. iii) aq. NH$_3$, THF, CH$_2$Cl$_2$. iv) PCl$_5$, aq. NH$_3$. v) PCl$_5$, NH$_3$ in dioxane.

In all the attempts, compound **3a** was not obtained and the starting material was always recovered. The HPLC–MS spectra showed a compound with a mass similar to the desired product (i.e., m/z = 436 [M+H]). Even though the conversion rate detected by HPLC–MS was low (~12%), the different attempts to purify it using column chromatography or circular chromatography were unsuccessful due to the complexity of the reaction mixtures. Hence, we were unable to confirm that the observed mass corresponded to the desired product.

Due to the failure of this approach, we proposed the synthesis of a new pyridine-2-carboxamide-containing reagent (**42**, Scheme 3.30). Commercially available pyridine-2-carboximidamide hydrochloride was reacted with Boc$_2$O to obtain the Boc-protected intermediate **43** in good yield (74%). The next step, consisting in the protection of the remaining amino group with trifluoromethanesulfonic anhydride, did not go to completion and **42** was obtained in very low proportion (~15%) as detected by HPLC–MS. Compound **42** could not be isolated from the starting material (**43**) by column chromatography.

Scheme 3.30: Proposed synthesis of **42**
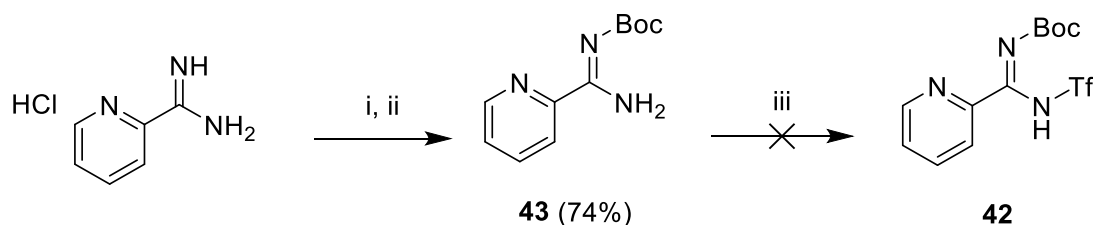
Reagents and conditions: i) Boc$_2$O, MeOH/THF, NaHCO$_3$. ii) Tf$_2$O, Et$_3$N, CH$_2$Cl$_2$, -78 °C to rt.

Next, a different attempt to obtain the pyridine-2-carboxamidine derivative **3b** from the deactivated chlorine-containing diamine **15b** was performed using 2-cyanopyridine as reagent (Scheme 3.31). Nonetheless, starting material was recovered in each attempt and compound **3b** was not obtained.

Scheme 3.31: Proposed synthetic route to **3b** using 2-cyanopyridine
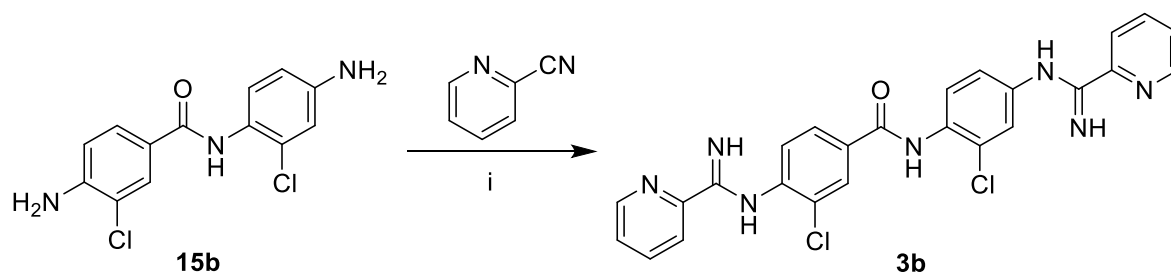
Reagents and conditions: i) AlCl$_3$, 120 °C, reflux, 30 min, ClCH$_2$CH$_2$Cl

Since all the previous attempts to achieve the synthesis of bis(pyridine-2-carboxamidine) derivatives from electron-deficient diamines were unsuccessful, we turned our attention to a new electrophilic carbimidothioate derivative, methyl *N*-(*tert*-butoxycarbonyl)pyridine-2-carbimidothioate (**44**). With the imido nitrogen protected by a Boc group, this reagent was expected to be more reactive towards poorly nucleophilic amines. Its synthesis was accomplished in two high yielding steps (94 and 59%, respectively) from pyridine-2-carbothioamide (Scheme 3.32). Compound **44** was obtained as a free base as reported by elemental analysis.

Scheme 3.32: Synthesis of methyl *N*-(*tert*-butoxycarbonyl)pyridine-2-carbimidothioate (**44**)
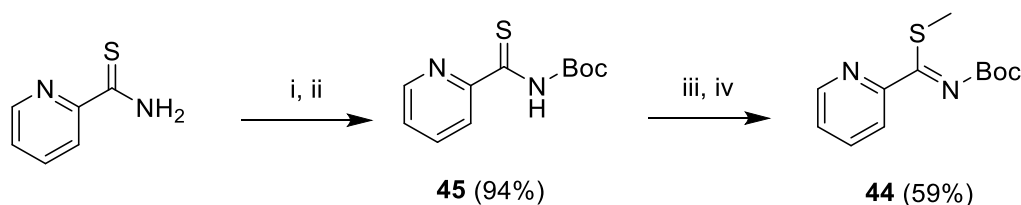
Reagents and conditions: i) NaH, THF, 0 °C to rt., ii) Boc$_2$O, iii) NaH, THF, 0 °C to rt., iv) CH$_3$I.

With this new reagent in hands, we tested its potential for the synthesis of pyridine-2-carboxamidine derivatives from deactivated amines (Scheme 3.33). Compound **44** reacted with 2,4-dichloroaniline (**46**), 2-chloro-4-nitroaniline (**47**) and 3-chloro-4-nitroaniline (**48**) in the presence of either HgCl$_2$ (1.2 equiv.) or CuCl (1.2 equiv.), and Et$_3$N (2 equiv.), to give the Boc-protected pyridine-2-carboxamidine derivatives **49, 50** and **51** smoothly (70–76% of conversion).

As shown in Table 3.7, the reaction was faster when $HgCl_2$ was used instead of CuCl. For instance, a 75 % conversion rate of dichloroaniline **46** was achieved in 4 hours with $HgCl_2$ (as detected by HPLC-MS) whereas 24 hours were needed to obtain a similar conversion rate (76 %) using CuCl. Similar trends were observed with more deactivated anilines containing one chlorine atom and a *para*-nitro group (**47**, **48**). Although similar conversion rates were obtained with both reagents, we decided to use $HgCl_2$ in further studies to reduce the reaction time.

Scheme 3.33: Synthesis of Boc-protected *N*-phenylpyridinecarboxamidines using **44** (1.5 equiv.)

46 : R_1 = Cl; R_2 = H; R_3 = Cl
47 : R_1 = NO_2; R_2 = H; R_3 = Cl
48 : R_1 = NO_2; R_2 = Cl; R_3 = H

49 : R_1 = Cl; R_2 = H; R_3 = Cl
50 : R_1 = NO_2; R_2 = H; R_3 = Cl
51 : R_1 = NO_2; R_2 = Cl; R_3 = H
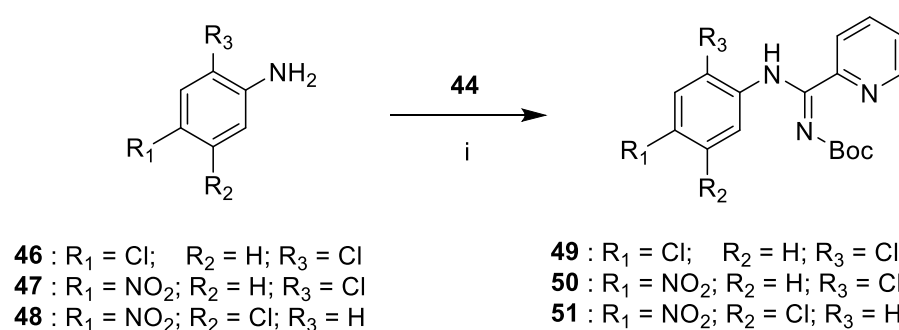
Reagents and conditions: (i) $HgCl_2$ (1.2 equiv.) or CuCl (1.2 equiv.), Et_3N (2 equiv.), CH_2Cl_2, 30 ºC.

Table 3.7: Synthesis of Boc-protected *N*-phenylpyridinecarboxamidines with reagent **44** using $HgCl_2$ or CuCl

Aniline	Reagent	Time	% conversion[a]
46	$HgCl_2$	4 hours	75 %
46	CuCl	24 hours	76 %
47	$HgCl_2$	4 days	72 %
47	CuCl	4 days	72 %
48	$HgCl_2$	4 days	68 %
48	CuCl	4 days	67%

[a] Detected by HPLC–MS

More assays were performed with 3-chloro-4-nitroaniline (**48**) in order to optimize the conditions. When we ran the reaction at room temperature and 40 ºC, 7 to 10 days were necessary to achieve conversion into *N*-Boc protected pyridine-2-carboxamidine products (Table 3.8). The use of temperature (i.e., 40 °C) gave a 68% conversion rate in 8 days,

whereas running the reaction at room temperature required two more days to achieve a similar conversion rate (i.e., ~71%). In addition, the use of CuCl as desulfurizing agent always required more time to achieve similar yield (~70–80%) as the one obtained using $HgCl_2$. Furthermore, CH_2Cl_2 was found to be the best solvent as it produced the highest conversion rate (88%). Eventually, we decided to perform the reactions under microwave irradiation. This optimization process led us to reduce the reaction time from days to 1 h with a conversion rate of 85 – 96% (Table 3.8).

Table 3.8: Conditions tested in the synthesis of **51** with reagent **44** using $HgCl_2$ or CuCl.
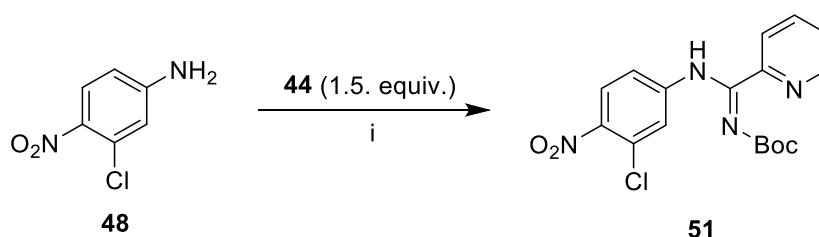
Reagent	Base	Solvent	Temp	Reaction time	% conversion[a] (51)
$HgCl_2$ 1.2 eq.	Et_3N 2 eq.	DMF 1 mL	rt	10 days	71 %
$HgCl_2$ 1.2 eq.	Et_3N 2 eq.	DMF 1 mL	40 °C	8 days	68 %
CuCl 2 eq.	Et_3N 2 eq.	DMF 1 mL	rt	15 days	78 %
CuCl 2 eq.	Et_3N 2 eq.	DMF 1 mL	40 °C	15 days	86 %
CuCl 2 eq.	K_2CO_3 4 eq.	THF 1 mL	40 °C	15 days	82 %
$HgCl_2$ 1.2 eq.	Et_3N 2 eq.	CH_2Cl_2 1 mL	rt	10 days	51 %
$HgCl_2$ 1.2 eq.	Et_3N 2 eq.	CH_2Cl_2 1 mL	rt	15 days	88 %
$HgCl_2$ 1.2 eq.	Et_3N 2 eq.	CH_2Cl_2 1 mL	MW 50 °C	1 hour	85 – 96 %

[a] Detected by HPLC–MS.

Using this optimized method with halogen-containing di-anilines, we observed that the reaction proceeded with slow conversion rates. In all the HPLC chromatograms of the crude reaction mixtures, the presence of a significant amount of the mono-substituted product (i.e., mono-arylimidamide) and of the demethylated reagent (**45**) was detected. However, compound **45** (Scheme 3.32) does not react with deactivated di-anilines to form the arylimidamide product under the reaction conditions used in our experiments (data not shown). Therefore, its presence indicates a degradation of reagent **44** in the reaction medium.

To improve the conversion rates to the desired bis(arylimidamides), we increased the number of equivalents of reagent **44** (from 1.5 to 2.0 equivalents per amino group) to push the reaction forward. This resulted in higher conversion rates ($\geq 60\%$) even though the demethylated reagent **45** was still present in the reaction mixture.

In summary, the best conditions to synthesise bis(arylimidamides) was achieved with 2 equivalents of reagent **44**, $HgCl_2$, and Et_3N per reactive amino group, CH_2Cl_2 as solvent, and microwave irradiation at 50 ºC during 1 hour (Scheme 3.34).

Scheme 3.34: Best conditions for the synthesis of bis(arylimidamides) using **44**
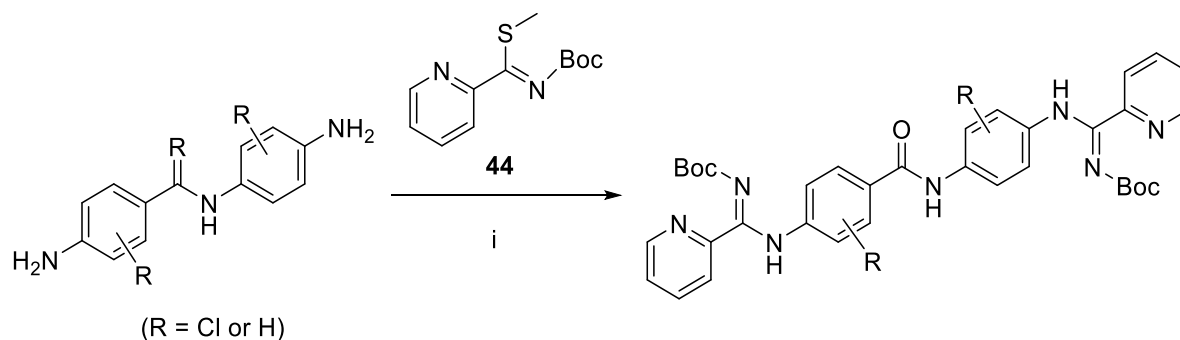
Reagents and conditions: di-aniline (1 equiv.)/ **44** (4 equiv.)/ $HgCl_2$ (4 equiv.)/ Et_3N (4 equiv.)/ CH_2Cl_2/ MW (50 °C)/ 1 h.

3.3.3. Synthesis of bis(*N*-aryl-pyridin-2-carboxamidines) (3b–h)

With this new protocol in hands, we were able to synthesize Boc-protected bis(*N*-aryl-pyridin-2-carboxamidines) **52b–e** and **52g–h** in low to moderate yields (12–67%, Scheme 3.35). Removal of the Boc-protecting groups using TFA/CH_2Cl_2 at 0 ºC yielded the pure bis(pyridine-2-carboxamidines) **3b–h** in good yield after crystallization (65–90%).

As stated before, the synthesis of bis(*N*-aryl-pyridin-2-carboxamidines) starting from highly deactivated dianilines required the use of 4 equivalents of reagent **44** (i.e., 2 equiv. per amino group). However, despite of the excess of reagent **44**, the reaction did not go to completion and the mono-substituted products were always obtained in the reaction crude. The high polarity of the bis(pyridine-2-carboxamidines) made them difficult to purify by silica chromatography. Reverse phase chromatography was attempted using a C18 flash cartridge. However, only low yields of pure product were obtained. Finally, circular chromatography on silica appeared to be the best purification method, although work is in progress to improve the purification method via reverse phase chromatography.

Scheme 3.35: Synthesis of bis(*N*-aryl-pyridin-2-carboxamidines) **3b**–**h** with **44**
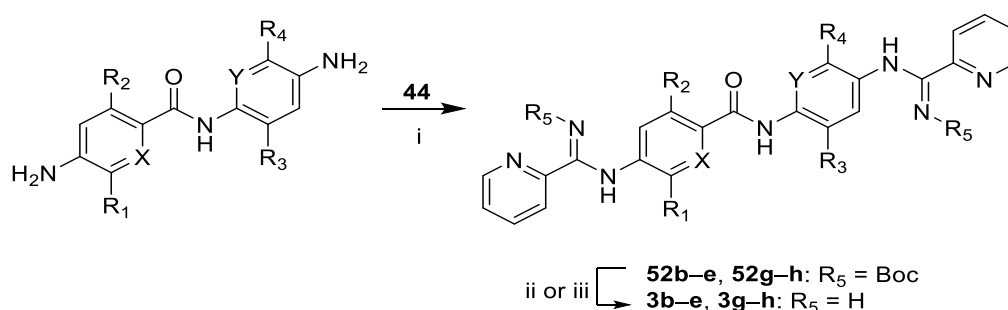
Cmpd	X	Y	R_1	R_2	R_3	R_4	Yield (52)	Yield (3)	Salt
b	CH	CH	Cl	H	Cl	H	44%	88%	$2CF_3CO_2H$
c	CH	CH	Cl	H	H	Cl	32%	76%	$2CF_3CO_2H$
d	CH	CH	H	Cl	Cl	H	67%	67%	2HCl
e	CH	CH	H	Cl	H	Cl	12%	82%	$2CF_3CO_2H$
g	CH	CH	H	O^{i}Pr	O^{i}Pr	H	50%	65%	2HCl
h	N	N	H	H	H	H	36%	90%	$2CF_3CO_2H$

Reagents and conditions: i) **44** (4 eq.), Et$_3$N (4 eq.), HgCl$_2$ (4 eq.), CH$_2$Cl$_2$, MW, 50 °C, 1 h. ii) CH$_2$Cl$_2$, TFA, 0 °C; iii) CH$_2$Cl$_2$, 4 M HCl, 0 °C.

To sum up, the relatively low yields obtained in this synthesis were related to the difficulty of the purification process of the first step of the reaction, and to an incomplete conversion rate. Work is ongoing to solve these issues. We have recently hypothesized that more equivalents of base (Et$_3$N) and HgCl$_2$ may be necessary to push the reaction forward, which would facilitate the product formation and purification.

3.4. References

1. Dardonville, C.; Nué Martinez, J. J. Bis(2-aminoimidazolines) and Bisguanidines: Synthetic Approaches, Antiparasitic Activity and DNA Binding Properties. *Curr Med Chem* **2017,** 24, 3606-3632.

2. Ríos Martínez, C. H.; Nué Martinez, J. J.; Ebiloma, G. U.; de Koning, H. P.; Alkorta, I.; Dardonville, C. Lowering the pK_a of a bisimidazoline lead with halogen atoms results in improved activity and selectivity against *Trypanosoma brucei in vitro*. *Eur. J. Med. Chem.* **2015,** 101, 806-817.

3. Nieto, L.; Mascaraque, A.; Miller, F.; Glacial, F.; Ríos Martínez, C.; Kaiser, M.; Brun, R.; Dardonville, C. Synthesis and Antiprotozoal Activity of N-Alkoxy Analogues of the Trypanocidal Lead Compound 4,4′-Bis(imidazolinylamino)diphenylamine with Improved Human Blood−Brain Barrier Permeability. *J. Med. Chem.* **2011,** 54, 485-494.

4. Ríos Martínez, C. H.; Miller, F.; Ganeshamoorthy, K.; Glacial, F.; Kaiser, M.; de Koning, H. P.; Eze, A. A.; Lagartera, L.; Herraiz, T.; Dardonville, C. A new nonpolar *N*-hydroxy imidazoline lead compound with improved activity in a murine model of late-stage *Trypanosoma brucei brucei* infection is not cross-resistant with diamidines. *Antimicrob. Agents Chemother.* **2015,** 59, 890-904.

5. Caine, B. A.; Dardonville, C.; Popelier, P. L. A. Prediction of Aqueous pKa Values for Guanidine-Containing Compounds Using Ab Initio Gas-Phase Equilibrium Bond Lengths. *ACS Omega* **2018,** 3, 3835-3850.

6. Rodríguez, F.; Rozas, I.; Kaiser, M.; Brun, R.; Nguyen, B.; Wilson, W. D.; García, R. N.; Dardonville, C. New Bis(2-aminoimidazoline) and Bisguanidine DNA Minor Groove Binders with Potent in Vivo Antitrypanosomal and Antiplasmodial Activity. *J. Med. Chem.* **2008,** 51, 909-923.

7. Shaw, J. W.; Grayson, D. H.; Rozas, I. Synthesis of Guanidines and Some of Their Biological Applications. In *Guanidines as Reagents and Catalysts I*, Berlin, S., Ed. Springer Berlin: Heidelberg, 2015; pp 1-51.

8. Tahir, S.; Badshah, A.; Hussain, R. A. Guanidines from 'toxic substances' to compounds with multiple biological applications – Detailed outlook on synthetic procedures employed for the synthesis of guanidines. *Bioorg. Chem.* **2015,** 59, 39-79.

9.   Castagnolo, D.; Schenone, S.; Botta, M. Guanylated Diamines, Triamines, and Polyamines: Chemistry and Biological Properties. *Chem. Rev.* **2011,** 111, 5247-5300.

10. David Crouch, R. Synthetic routes toward 2-substituted 2-imidazolines. *Tetrahedron* **2009,** 65, 2387-2397.

11. Heinelt, U.; Schultheis, D.; Jäger, S.; Lindenmaier, M.; Pollex, A.; Beckmann, H. S. g. A convenient method for the synthesis of 2-amino substituted aza-heterocycles from N,N′-disubstituted thioureas using TsCl/NaOH. *Tetrahedron* **2004,** 60, 9883-9888.

12. Timmermans, P. B. M. W. M.; van Zwieten, P. A.; Speckamp, W. N. 2-(Arylimino)imidazolidines; synthesis and hypotensive activity. *Recl. Trav. Chim. Pays-Bas* **1978,** 97, 51-56.

13. Kühle, E.; Anders, B.; Klauke, E.; Tarnow, H.; Zumach, G. Reactions of Isocyanide Dihalides and their Derivatives. *Angew. Chem. Int. Edit.* **1969,** 8, 20-34.

14. Jung, F.; Delvare, C.; Boucherot, D.; Hamon, A. Cephalosporins with C-7-isocyanide dihalides : useful synthons for the introduction of amino heterocycles at C-7 - new routes to the synthesis of amino imidazoles. *Tetrahedron Lett.* **1989,** 30, 2375-2378.

15. Mohanazadeh, F.; Nami, N.; Hosseini, S. S. Efficient Synthesis of 2-Arylamino-2-imidazolines and 2-Aminobenzimidazoles with Aminoiminomethanesulfonic Acid Derivatives. *Chin. J. Chem.* **2011,** 29, 1055-1058.

16. Dardonville, C.; Goya, P.; Rozas, I.; Alsasua, A.; Martín, M. I.; Borrego, M. J. New aromatic iminoimidazolidine derivatives as α_1-adrenoceptor antagonists: a novel synthetic approach and pharmacological activity. *Bioorg. Med. Chem.* **2000,** 8, 1567-1577.

17. Adler, M. J.; Hamilton, A. D. Oligophenylenaminones as Scaffolds for α-Helix Mimicry. *J. Org. Chem.* **2011,** 76, 7040-7047.

18. Nué Martínez, J. J.; Alkorta, I.; Dardonville, C. High yield synthesis of trans-azoxybenzene versus 2-isopropoxy-4-nitrobenzoic acid: influence of temperature and base concentration. *Arkivoc* **2021,** viii, 265-276.

19. Bellamy, F. D.; Ou, K. Selective reduction of aromatic nitro compounds with stannous chloride in non acidic and non aqueous medium. *Tetrahedron Lett.* **1984,** 25, 839-842.

20. Mundla, S. R.; Wilson, L. J.; Klopfenstein, S. R.; L. Seibel, W.; Nikolaides, N. N. A novel method for the efficient synthesis of 2-arylamino-2-imidazolines. *Tetrahedron Lett.* **2000,** 41, 6563-6566.

21. Ríos Martínez, C. H.; Lagartera, L.; Kaiser, M.; Dardonville, C. Antiprotozoal activity and DNA binding of *N*-substituted *N*-phenylbenzamide and 1,3-diphenylurea bisguanidines. *Eur. J. Med. Chem.* **2014,** 81, 481-491.

22. Taladriz, A.; Healy, A.; Flores Perez, E. J.; Herrero Garcia, V.; Rios Martinez, C.; Alkhaldi, A. A.; Eze, A. A.; Kaiser, M.; de Koning, H. P.; Chana, A.; Dardonville, C. Synthesis and structure-activity analysis of new phosphonium salts with potent activity against African trypanosomes. *J. Med. Chem.* **2012,** 55, 2606-2622.

23. Nagle, P. S.; McKeever, C.; Rodriguez, F.; Nguyen, B.; Wilson, W. D.; Rozas, I. Unexpected DNA Affinity and Sequence Selectivity through Core Rigidity in Guanidinium-Based Minor Groove Binders. *J. Med. Chem.* **2014,** 57, 7663-7672.

24. McKeever, C. Targeting DNA : synthesis, biophysical and biochemical studies of new aminoalkyl derivatives of diphenyl guanidines and acridine. PhD Thesis, Trinity College Dublin, The University of Dublin, School of Chemistry, 2012.

25. Rahman, A.; O'Sullivan, P.; Rozas, I. Recent developments in compounds acting in the DNA minor groove. *MedChemComm* **2019,** 10, 26-40.

26. Kim, K. S.; Qian, L. Improved method for the preparation of guanidines. *Tetrahedron Lett.* **1993,** 34, 7677-7680.

27. Nagle, P. S.; Rodriguez, F.; Kahvedžić, A.; Quinn, S. J.; Rozas, I. Asymmetrical Diaromatic Guanidinium/2-Aminoimidazolinium Derivatives: Synthesis and DNA Affinity. *J. Med. Chem.* **2009,** 52, 7113-7121.

28. Jackman, L. M.; Jen, T. Nuclear magnetic resonance spectroscopy. XIII. Amidines. VII. Proton and carbon-13 nuclear magnetic resonance studies on the tautomerism, geometrical isomerism, and conformation of some cyclic amidines, guanidines, and related systems. *J. Am. Chem. Soc.* **1975,** 97, 2811-2818.

29. Ríos Martínez, C. H. Synthesis and study of new antiprotozoal agents derivatives of dicationic compounds for the treatment of Human African Trypanosomiasis. PhD Thesis, Universidad Complutense de Madrid, Madrid, Spain, 2013.

30. Sharma, S.; Anand, N. Chapter 8 - Benzimidazoles. In *Pharmacochemistry Library*, Sharma, S.; Anand, N., Eds. Elsevier: 1997; Vol. 25, pp 195-238.

31. Kazimierczuk, Z.; Upcroft, J. A.; Upcroft, P.; Górska, A.; Starościak, B.; Laudy, A. Synthesis, antiprotozoal and antibacterial activity of nitro- and halogeno-substituted benzimidazole derivatives. *Acta Biochim. Pol.* **2002,** 49, 185-195.

32. Edlind, T. D.; Hang, T. L.; Chakraborty, P. R. Activity of the Anthelmintic Benzimidazoles against *Giardia lamblia In Vitro. J. Infect. Dis.* **1990,** 162, 1408-1411.

33. Kamanna, K. Synthesis and Pharmacological Profile of Benzimidazoles. In *Chemistry and Applications of Benzimidazole and its Derivatives*, IntechOpen, Ed. IntechOpen: 2019.

34. Zhang, Z.-H.; Yin, L.; Wang, Y.-M. An expeditious synthesis of benzimidazole derivatives catalyzed by Lewis acids. *Catal. Commun.* **2007,** 8, 1126-1131.

35. Xie, Y.; Zhang, F.; Li, J.; Shi, X. Novel Synthesis of 2-Aminobenzimidazoles from Isoselenocyanates. *Synlett* **2010,** 2010, 901-904.

36. Carpenter, R. D.; DeBerdt, P. B.; Lam, K. S.; Kurth, M. J. Carbodiimide-Based Benzimidazole Library Method. *J. Comb. Chem.* **2006,** 8, 907-914.

37. Khanna, I. K.; Yu, Y.; Huff, R. M.; Weier, R. M.; Xu, X.; Koszyk, F. J.; Collins, P. W.; Cogburn, J. N.; Isakson, P. C.; Koboldt, C. M.; Masferrer, J. L.; Perkins, W. E.; Seibert, K.; Veenhuizen, A. W.; Yuan, J.; Yang, D.-C.; Zhang, Y. Y. Selective Cyclooxygenase-2 Inhibitors: Heteroaryl Modified 1,2-Diarylimidazoles Are Potent, Orally Active Antiinflammatory Agents. *J. Med. Chem.* **2000,** 43, 3168-3185.

38. Gobis, K.; Foks, H.; Wisniewska, K.; Dabrowska-Szponar, M.; Augustynowicz-Kopec, E.; Napiorkowska, A. Synthesis and antimicrobial activity of novel heterocyclic sulfamoyl-phenyl-carboximidamides derived from clinically applied sulfonamides. *Arch Pharm (Weinheim)* **2012,** 345, 911-917.

39. Nandre, J.; Patil, S.; Patil, P.; Sahoo, S.; Redshaw, C.; Mahulikar, P.; Patil, U. The Amidine Based Colorimetric Sensor for Fe^{3+}, Fe^{2+}, and Cu^{2+} in Aqueous Medium. *J. Fluoresc.* **2014,** 24, 1563-1570.

40. Patil, U. D.; Mahulikar, P. P. A Convenient, $TiCl_4/SnCl_4$-Mediated Synthesis of *N*-Phenyl or *N*-Aryl Benzamidines and *N*-Phenylpicolinamidines. *Int. Scholarly Res. Not.* **2012,** 963195, 1-6.

41. Hisano, T.; Tasaki, M.; Matsuoka, T.; Ichikawa, M. An efficient synthesis of *N'*-(O-alkoxyphenyl)-pyridinecarboxamidine derivatives. *Org. Prep. Proced. Int.* **1982,** 14, 399-403.

42. Boykin, D.; Hu, L. A Novel and Convenient Synthesis of 'Reversed' Diamidino 2,5-Aryl- and 2,5-Azaheterocycle-Substituted Furans. *Synthesis* **2009,** 13, 2143-2145.

43. Arya, S.; Kumar, N.; Roy, P.; Sondhi, S. M. Synthesis of amidine and bis amidine derivatives and their evaluation for anti-inflammatory and anticancer activity. *Eur. J. Med. Chem.* **2013,** 59, 7-14.

44. Collins, J. L.; Shearer, B. G.; Oplinger, J. A.; Lee, S.; Garvey, E. P.; Salter, M.; Duffy, C.; Burnette, T. C.; Furfine, E. S. *N*-Phenylamidines as Selective Inhibitors of Human Neuronal Nitric Oxide Synthase: Structure−Activity Studies and Demonstration of *in vivo* Activity. *J. Med. Chem.* **1998,** 41, 2858-2871.

45. Stephens, C. E.; Tanious, F.; Kim, S.; Wilson, W. D.; Schell, W. A.; Perfect, J. R.; Franzblau, S. G.; Boykin, D. W. Diguanidino and "Reversed" Diamidino 2,5-Diarylfurans as Antimicrobial Agents. *J. Med. Chem.* **2001,** 44, 1741-1748.

46. Abdelhameed, A.; Feng, M.; Joice, A. C.; Zywot, E. M.; Jin, Y.; La Rosa, C.; Liao, X.; Meeds, H. L.; Kim, Y.; Li, J.; McElroy, C. A.; Wang, M. Z.; Werbovetz, K. A. Synthesis and Antileishmanial Evaluation of Arylimidamide–Azole Hybrids Containing a Phenoxyalkyl Linker. *ACS Infect. Dis.* **2021,** 7, 1901-1922.

47. Zhu, X.; Farahat, A. A.; Mattamana, M.; Joice, A.; Pandharkar, T.; Holt, E.; Banerjee, M.; Gragg, J. L.; Hu, L.; Kumar, A.; Yang, S.; Wang, M. Z.; Boykin, D. W.; Werbovetz, K. A. Synthesis and pharmacological evaluation of mono-arylimidamides as antileishmanial agents. *Bioorg. Med. Chem. Lett.* **2016,** 26, 2551-2556.

48. Liu, Z. Y.; Wenzler, T.; Brun, R.; Zhu, X.; Boykin, D. W. Synthesis and antiparasitic activity of new bisarylimidamides: DB766 analogs modified in the terminal groups. *Eur. J. Med. Chem.* **2014,** 83, 167-173.

49. Reid, C. S.; Farahat, A. A.; Zhu, X.; Pandharkar, T.; Boykin, D. W.; Werbovetz, K. A. Antileishmanial bisarylimidamides: DB766 analogs modified in the linker region and bisarylimidamide structure-activity relationships. *Bioorg. Med. Chem. Lett.* **2012,** 22, 6806-6810.

50. Banerjee, M.; Farahat, A. A.; Kumar, A.; Wenzler, T.; Brun, R.; Munde, M. M.; Wilson, W. D.; Zhu, X.; Werbovetz, K. A.; Boykin, D. W. Synthesis, DNA

binding and antileishmanial activity of low molecular weight bis-arylimidamides. *Eur J Med Chem* **2012,** 55, 449-454.

51. Arafa, R. K.; Brun, R.; Wenzler, T.; Tanious, F. A.; Wilson, W. D.; Stephens, C. E.; Boykin, D. W. Synthesis, DNA Affinity, and Antiprotozoal Activity of Fused Ring Dicationic Compounds and Their Prodrugs. *J. Med. Chem.* **2005,** 48, 5480-5488.

52. Pace, V.; Castoldi, L.; Monticelli, S.; Safranek, S.; Roller, A.; Langer, T.; Holzer, W. A Robust, Eco-Friendly Access to Secondary Thioamides through the Addition of Organolithium Reagents to Isothiocyanates in Cyclopentyl Methyl Ether (CPME). *Chem. Eur. J.* **2015,** 21, 18966-18970.

53. Lee, K.; Park, C. W.; Jung, W.-H.; Park, H. D.; Lee, S. H.; Chung, K. H.; Park, S. K.; Kwon, O. H.; Kang, M.; Park, D.-H.; Lee, S. K.; Kim, E. E.; Yoon, S. K.; Kim, A. Efficacious and Orally Bioavailable Thrombin Inhibitors Based on a 2,5-Thienylamidine at the P1 Position: Discovery of N-Carboxymethyl-d-diphenylalanyl-l-prolyl[(5-amidino-2-thienyl)methyl]amide. *J. Med. Chem.* **2003,** 46, 3612-3622.

54. Alekseeva, I. V.; Pal'chikovskaya, L. I.; Shalamai, A. S.; Ognyanik, S. S.; Morgart, N. V.; Petrusha, N. A. Synthesis of N^1-substituted 6-azacytosines and their biological activity. *Pharm. Chem. J.* **1994,** 28, 227-230.

55. Alig, L.; Edenhofer, A.; Hadvary, P.; Huerzeler, M.; Knopp, D.; Mueller, M.; Steiner, B.; Trzeciak, A.; Weller, T. Low molecular weight, non-peptide fibrinogen receptor antagonists. *J. Med. Chem.* **1992,** 35, 4393-4407.

CHAPTER 4

## 4. Chapter 4 :   Biophysical, physicochemical and computational studies

4.1. Introduction

DNA, the most important macromolecule carrying genetic information, is considered an exceptional target for diseases that depend on the division of malignant cells or microbes (e.g., parasites).[1] As mentioned in Chapter 1, di-cationic compounds such as those synthesised in this thesis possess the ability to interact with the DNA minor groove.[2] The interaction of minor groove binders (MGBs) with DNA has the potential to block important enzymes and transcription control proteins that are essential for the growth of protozoan parasites.[1] Hence, the study of this interaction may shed light on the mechanism of antiparasitic action of these series of compounds.

DNA MGBs tend to be concave in shape (isohelicity that allows the adaptation to the groove curvature), possess several aromatic rings, be cationic in nature and have the ability to form hydrogen bonds (HB).[3] The lipophilicity due to the aromatic rings performs a displacement in the structured backbone of hydration along the DNA minor groove.[4] MGBs are particularly interesting compounds for the design of antimicrobials because they are sequence-selective in contrast to intercalators. MGBs mainly bind to the double helix of AT-rich DNA.[3-6] This selectivity is especially relevant in the case of pathogenic parasites such as trypanosomatids which mitochondrial genome (kDNA) has a high percentage of AT-rich DNA sequences.[1, 7-9]

Our group has shown previously that bis(2-aminoimidazoline) compounds such as lead **I** bind AT-rich DNA with high affinity. In the crystal structure of compound **I** complexed with the d(AAATTT)$_2$ DNA duplex [PDB: 5LIT], it was observed that the drug molecules fill the central part of the minor groove of the duplexes (Figure 4.1).[10] Hence, once the synthesis of the compounds discussed in Chapter 3 was complete, we undertook biophysical and computational studies to determine their affinity and selectivity towards DNA, and deduce their mode of binding.
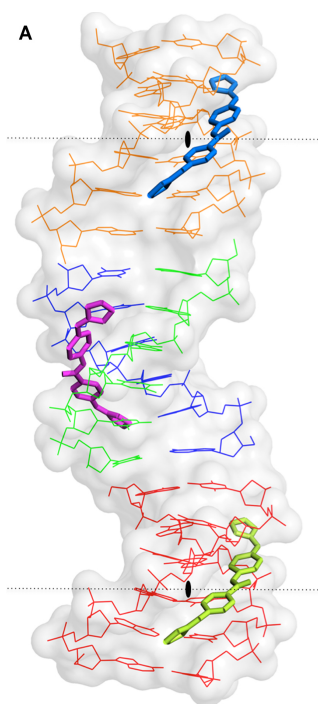
Figure 4.1: Crystallographic units of the DNA duplex d(AAATTT)$_2$ –ligand **I** complex [PDB: 5LIT]. The black lozenge indicates the dyad axes. Four independent single oligonucleotides chains are shown; two of them (blue-green) form the central duplex and the other two (orange and red) form two different DNA duplexes with their symmetrical chain. Three crystallographically independent drug molecules are indicated (pink, green and blue).[10]

Biophysical assays contribute to the determination of both affinity (e.g., K_D, kinetic and thermodynamic parameters) and mode of binding (e.g., minor groove binding and/or intercalation) of DNA ligands. In this work, we used different optical biophysical techniques including thermal denaturation assays (T_m), ultraviolet (UV) titrations, circular dichroism (CD), linear dichroism (LD), surface plasmon resonance (SPR), nuclear magnetic resonance (NMR), and X-ray crystallography.

Furthermore, we measured the acid dissociation constants (i.e., pK_a) of the new compounds by a UV-based method previously developed by our group.[11] The knowledge of this physicochemical parameter is crucial to determine whether these dibasic compounds will be protonated (i.e., cationic) at physiological pH. This is important because the di-cationic nature of MGBs is crucial for accumulation in the parasite (i.e., driven by the plasma and mitochondrial transmembrane potentials) and formation of H-bonds with A-T bases at the minor groove floor, which has negative electrostatic potential.

In this chapter, we will describe the basic theory related to each technique and discuss the results obtained in the different experiments.

4.2. Physicochemical evaluation of the protonation state of the compounds: pK_a determination

4.2.1. Background

The ionization constant (K_a), also known as protonation or acid dissociation constant is an equilibrium constant defined as the ratio of the protonated and the deprotonated form of a compound.[12] This physiochemical parameter is usually reported as the negative logarithm of K_a:

$$\mathbf{p}K_a = -\log_{10} K_a.$$

The pK_a can be defined as the ability a molecule or ion has to keep a proton (H^+) at its ionization centre(s). At pH within approximately 1.5 pH units away from the pK_a of a molecule, a fraction of both ionized and unionized species will be present in solution. At pH > 1.5 pH units away from pK_a, an acid will be charged whereas a base will be uncharged; the contrary will occur at pH < pK_a.[13]

The pK_a has biological implications because the ionization of a compound is one of the factors governing its partition between aqueous media and lipid membranes.[14, 15] The protonation state of biologically active compounds has a profound influence on their absorption, distribution, metabolism, and excretion (ADME). The pK_a of a molecule determines its pH–dependent solubility, lipophilicity (log D), permeability, stability and protein binding as well as binding to its biological target.[13, 16-18] Therefore, the accurate measurement of pK_a values is key in areas such as medicinal chemistry and drug development.[19]

In the drug design process, the protonation state of a molecule in aqueous environment at physiological pH will be critical for the biodistribution of the compound and the ligand-receptor interaction. When a compound is positively or negatively charged at physiological pH, it is expected to be soluble in body fluids. However, its entry into cells by passive diffusion may be compromised unless it is recognized by a specific cation or anion

transporter. This is the case, for example, of diamidine drugs (i.e., pentamidine, furamidine) that gain entry into the brain via the human organic cation transporter 1 (hOCT1) present on the blood-brain barrier.[20, 21]

Regarding the DNA minor groove, its environment is considerably more electron-rich than its surroundings,[22] which means that cationic compounds will have favourable interactions with the minor groove. For DNA MGBs, the (di)cationic nature of the ligand, in addition to a crescent shape matching the curve of the groove, is crucial to allow the best fitting between the MGB and the groove through van der Waals and hydrogen bonding interactions.[4] For all these reasons, the pK_a of all the compounds was measured by UV spectrophotometry using the 96–wells plate methodology developed in our group.[11, 16]

For the dibasic compounds under study, three possible protonation states exist that will depend on the pH in the acidic environment[23-25] of the minor groove (Scheme 4.1):

(1)   both basic sites of the molecule are protonated and the molecule is di-cationic,

(2)   one of the basic sites is protonated and hence the molecule is mono-cationic,

(3)   none of the basic sites are protonated and the molecule is neutral.

**Scheme 4.1**: Possible protonation states of the synthesised compounds.
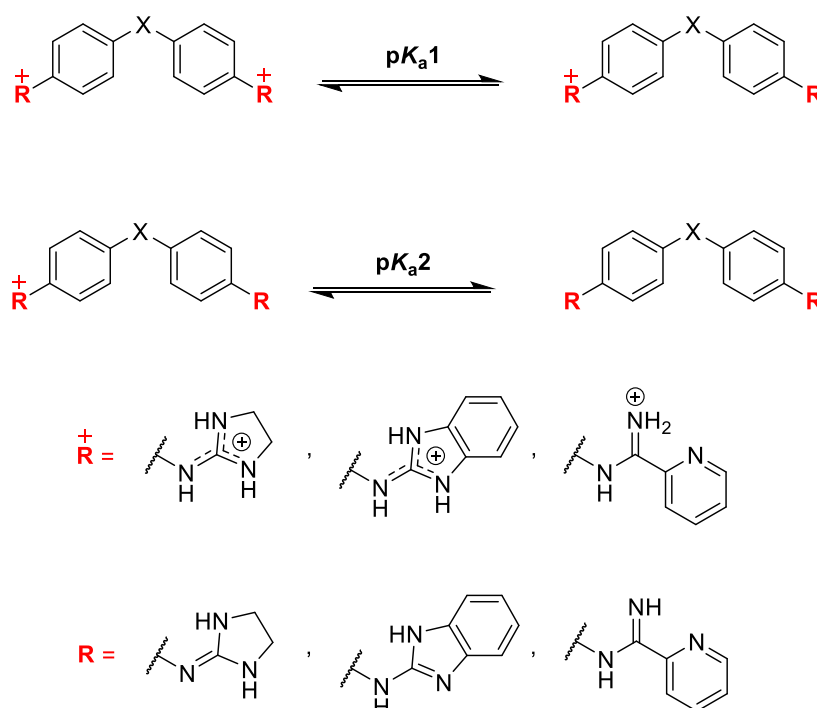
As the structure of the synthesised compounds contains two basic guanidine-like groups, our hypothesis is that two pK_a (pK_a1 and pK_a2) values shall be observed as represented in Scheme 4.1. However, we were not able to measure a distinct pK_a value for each basic group using the 96-wells UV-spectrophotometric method. In its place, an average value was observed for each molecule. These results will be discussed later in this chapter.

4.2.2. pK_a measurements by UV Spectroscopy using 96-well microtiter plates: determination of the percentage of ionization at physiological pH

4.2.2.1. Methodology

The pK_a values of the synthesised compounds were experimentally determined by UV spectroscopy following the 96-well plate protocol developed by Drs. Ríos Martinez and Dardonville.[11, 16] pK_a determination by UV spectroscopy was possible because the compounds fulfil two requisites: they hold a chromophore next to the ionisable group, for which the UV absorbance is modified as function of the ionization state of the molecule.

Firstly, different aqueous buffer solutions were prepared at variable pH and constant ionic-strength ($I = 0.1$ M, adjusted with KCl) covering a range between 3 and 12 (e.g., 2 or 3 different points per pH unit). Then, the compounds were prepared in 5 mM stock solutions in DMSO. The experiment was carried out by mixing 4 µL of test compound and 196 µL of the correspondent buffer (Figure 4.2). The spectra were collected in the UV range (200 – 500 nm) and corrected by resting the blank values (i.e., buffer + DMSO without test compound). Then, the GraphPad programme[26] was used to represent the absorbance as a function of the pH in order to calculate the pK_a of the molecule.[11, 27]
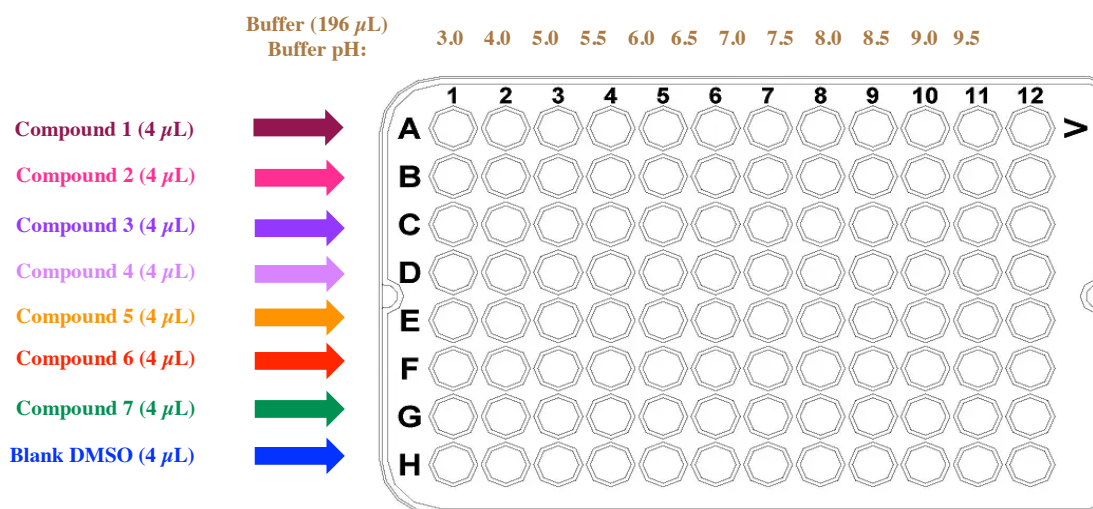
Figure 4.2: Loading of the 96 well-microtiter plate for measuring simultaneously 7 compounds pK_as. With a different loading, 3 compounds can be measured in duplicate (or 2 compounds in triplicate)

As general procedure, 12 aqueous buffer solutions are loaded in the microtiter plate (in the pH range 3 to 12) to obtain a broad pK_a value of the compound. This value can be refined as required by using more buffer solutions of ± 2 pH units around the measured pK_a.

4.2.2.2. Data processing

The UV data obtained were imported to the Excel program and processed as stated in the protocol previously reported:[11] (a) the UV spectrum was corrected by subtracting the UV spectrum of the blanks for each pH and wavelength. (b) the UV corrected spectra were normalized by subtracting from the UV spectra the absorbance at which the compound does not absorb (e.g., λ = 400 or 500 nm in most cases, (Figure 4.3a). (c) The differential spectrum was obtained subtracting the UV spectrum of the compound at the most acidic pH from the UV spectra obtained at every other pHs. (d) The analytical wavelengths were determined graphically from the wavelength of the maximum and the minimum observed in the spectral difference graph (Figure 4.3b). (e) The total absorbance for each of the pH analysed was calculated as the sum of the absolute value of the absorbances at the analytical wavelengths for each of the pHs used (Figure 4.3c). Finally, these values were represented as a function of the pH and the pK_a of each molecule was determined by nonlinear regression using equation 4.1.

Equation 4.1:
$$Total\ Absorbance = \frac{\varepsilon_{HA} - \varepsilon_{A-} * [10^{(pH-pKa)}]}{1 + 10^{(pH-pKa)}} * [S_t]$$

Where ε_{HA} and ε_{A^-} are the extinction coefficients of acid and basic forms of the compound respectively. S_t is the compound concentration.
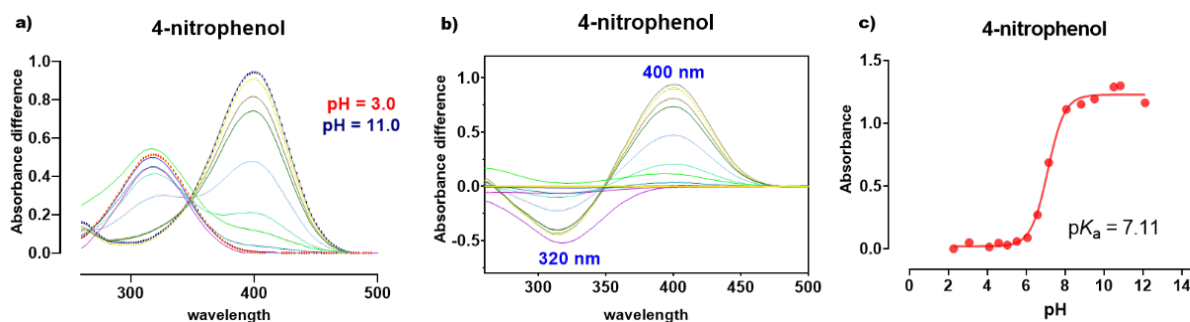
Figure 4.3: Spectra analysis and pK_a determination of 4-nitrophenol. (a) 4-nitrophenol UV spectra ($\lambda = 250 – 500$ nm) using different buffers in the pH range 3 – 11. Absorbance is normalized to zero at $\lambda = 500$ nm. (b) Differential spectra of the UV spectra at pH = 3 and the others UV spectra at different pH values. Maximum deviation occurs at 400 nm whereas minima appears at 320 nm. (c) Graphic representation of the total absorbance vs pH (the total absorbance difference is the sum of the absolute absorbance difference values at the chosen wavelengths (i.e., 320 and 400 nm). The pK_a value was determined by non-linear regression using Equation 4.1 (lit. value[11]: 7.16).[27]

4.2.2.3. Structure–pK_a relationships results

The pK_a values of the 3 series of compounds were measured and the data gathered in Tables 1–3. The percentage of ionization at physiological pH (7.4) was also calculated for each compound according to Equation 4.2:

Equation 4.2: $$\% \, ionization = \frac{100}{1+10^{(pH-pKa)}}$$

The experimental data were compared with calculated values obtained with the Chemicalize online prediction software (https://chemicalize.com/, developed by ChemAxon, https://www.chemaxon.com). This predictor uses wide databases of experimental values and involves derived Quantitative Structure–Property Relationships (QSPR) to estimate the pK_a values.[28]

As mentioned above, the synthesised compounds are non-symmetrical (except the compounds having a urea, ethylene or 9H-fluorene scaffold), which means they hold two different basic moieties and should have different – albeit relatively close – pK_a values. However, we could only determine one (average) value for these series using the 96-well

UV-spectroscopic method. This is probably due to overlapping pK_a values. As a control experiment, the pK_a of **3a** was measured by potentiometric titration using a SIRIUS T3 apparatus. Since **3a** is poorly soluble in water its pK_a was measured in H_2O/MeOH mixtures and extrapolated to 0% co-solvent using the Yasuda−Shedlovsky[29, 30] procedure as implemented in the SIRIUS T3 Refine software. The measured pK_a values (H_2O, 25 ºC) obtained for both protonation sites, which ranged within 0.5 pK_a units (6.92 ± 0.18 and 7.42 ± 0.22), were in excellent agreement with the average pK_a value obtained by UV-spectroscopy (7.18 ± 0.13).

4.2.2.4.   Structure–pK_a relationships: bis(imidazolin-2-imines)

The introduction of one halogen atom into the *N*-phenylbenzamide scaffold and its influence on the pK_a and anti-*T. brucei* activity of the molecule was previously studied by our group.[31] This structural modification led to a reduction of the pK_a and an increase in trypanocidal activity in some cases (R_1 = Cl, F or R_2 = F or R_4 = Cl, F). In this thesis, molecules bearing two halogen atoms were synthesized as a strategy to modulate their physicochemical properties (pK_a and logP), with the aim of improving their membrane permeability to target intracellular parasites.

In the next section, we analyze the structure–pK_a relationships for these series of compounds. For a better understanding, we will use the general structure shown in Figure 4.4.
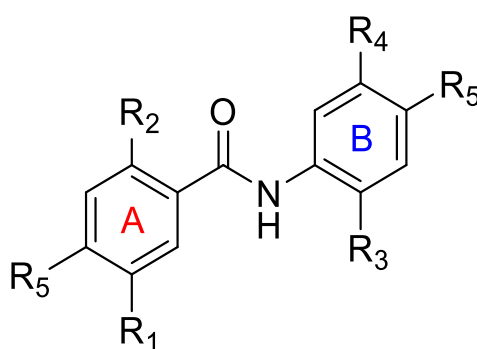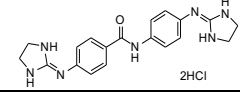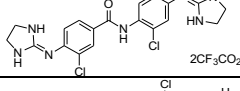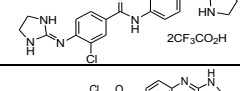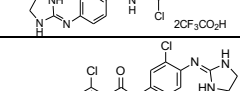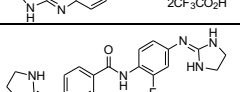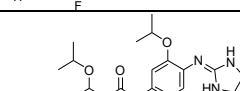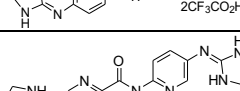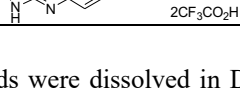

Figure 4.4: *N*-phenylbenzamide scaffold structure bearing halogen atoms (R_1–R_4) and different heterocyclic substituents for each series (R_5)

All of the newly synthesised bis(imidazolin-2-imine) compounds (Table 4.1; **1b**–**h**) displayed lower pK_a values than the unsubstituted lead **I** (pK_a = 9.29). However, the presence of isopropoxy groups as substituents (R_2 = R_4 = O*i*Pr) led to a smaller reduction

of the pK_a in comparison to lead **I** (-0.2 pK_a units for **1g**). The largest pK_a decrease (-1.09 and -1.05 pK_a units for **1b** and **1c**, respectively) was observed when one chlorine atom is placed in position *ortho* to the imidazoline heterocycle in ring A (R_1 = Cl), independently from the position of the second chlorine atom. In addition, the replacement of phenyl rings for pyridine ones also led to the reduction of 1 pK_a unit versus **I** (pK_a = 8.17 for **1h**). Within this series, the percentage of ionization ranged from 85.5 to 98.7% indicating that the bis(imidazolin-2-imine) derivatives are mostly dicationic at physiological pH.

Table 4.1: Experimental pK_a, and calculated pK_a and logP values of the synthesised bis(imidazolidin-2-imine) derivatives.[a]
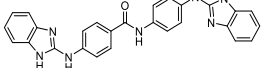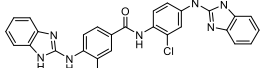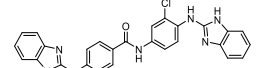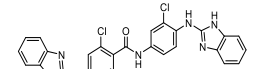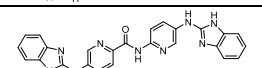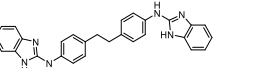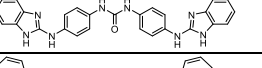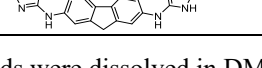
Cmpd	Structure	$pK_a \pm SD$[b] (H₂O, 25 °C)	% Ionization pH 7.4	Predicted[c] pK_a1 pK_a2	logP[d]
I		9.29 ± 0.07[e]	98.7	7.05 7.22	2.85
1b		8.20 ± 0.10	86.3	6.08 7.02	3.89
1c		8.24 ± 0.03	87.4	6.12 6.78	3.89
1d		8.60 ± 0.25	94.1	6.31 6.97	3.89
1e		8.82 ± 0.23	96.3	6.86 6.24	3.89
1f		*f*	*f*	5.88 6.95	3.13
1g		9.09 ± 0.06	98.0	6.52 7.18	3.86
1h		8.17 ± 0.07	85.5	6.45 7.11	1.32

[a]Compounds were dissolved in DMSO (5 mM stock solution) and diluted with the correspondent buffer to achieve a 0.1 mM concentration in each well (2% DMSO v/v). [b]Only one (average) pK_a value could be measured for both imidazoline rings. [c]Calculated using ChemAxon package "Chemicalize". [d]Calculated using MarvinSketch (ChemAxon method, considering tautomerization/resonance) Version 22.9.0. [e]Previously reported.[31] [f]Not measured.

4.2.2.5. Structure–pK_a relationships: bis(2-aminobenzimidazoles)

With regard to the bisbenzimidazole derivatives (Table 4.2; **2a**–**h**, **30**, **31**, and **34**), the experimental pK_a values were in the range 2.77–5.93, indicating that the compounds are mostly neutral at physiological pH (i.e. pK_a <1.5 pH unit from 7.4). This shows that the replacement of the 2-aminoimidazoline (R$_5$) with 2-aminobenzimidazole heterocycles leads to a reduction of > 4 pK_a units for this series. Of note, the measured pK_a values were much lower (i.e. approximately 3 pK_a units) than the predicted ones (6.54–7.70), highlighting the limits of pK_a prediction tools for compounds containing a large number of possible tautomeric states.[13, 18]

Table 4.2: Experimental pK_a, and calculated pK_a and logP values of the synthesised bis(2-aminobenzimidazole) derivatives[a]
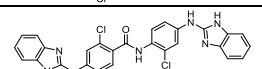
Cmpd	Structure	pK_a ± SD[b] (H$_2$O, 25 ºC)	% Ionization pH 7.4	Predicted[c] pK_a1 pK_a2	logP[d]
2a		4.49 ± 0.08	0.12	7.75 7.15	5.82
2b		3.39 ± 0.07	0.01	6.64 7.47	6.86
2c		2.77 ± 0.02	0.00	6.54 7.18	6.86
2d		3.41 ± 0.06	0.01	6.91 7.57	6.86
2e		3.38 ± 0.16	0.01	7.35 6.74	6.86
2h		3.85 ± 0.16[e]	0.03	6.56 7.20	4.30
30		5.64 ± 0.08	1.71	7.10 7.70	7.24
31		5.93 ± 0.05	3.28	7.70 7.09	6.23
34		4.12 ± 0.25	0.05	7.09 7.69	6.49
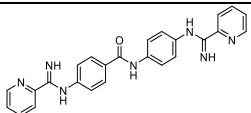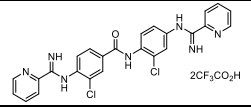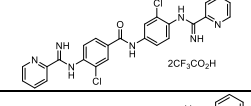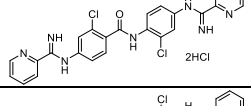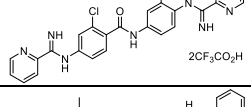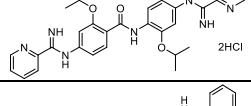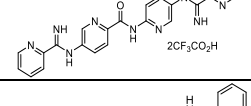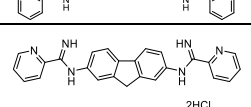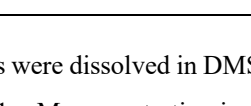
[a]Compounds were dissolved in DMSO (5 mM stock solution) and diluted with the correspondent buffer to achieve a 0.1 mM concentration in each well (2% DMSO v/v). [b]Only one pK_a value could be measured for both benzimidazole rings. [c]Calculated using ChemAxon package "Chemicalize". [d]Calculated using MarvinSketch (ChemAxon method, considering tautomerization/resonance) Version 22.9.0. [e]This pK_a is more closely related to the value predicted for the pyridine rings (0.29 & 2.58).

4.2.2.6.   Structure–pK_a relationships: bis(arylimidamides)

The pK_a determination for the bis(arylimidamide) derivatives (Table 4.3; **3a–i**, **36**, **37**, and **41**) was more troublesome and only six pK_a could be measured due to inconsistent data (i.e., **3d**, **41**) or the lack of sufficient amounts of the samples to run the analysis (i.e., **3c**, **3h**, **3i**, **37**). In this series, the 2-aminoimidazoline heterocycles of lead **I** were replaced by pyridine-2-carboxamidine substituents in position R$_5$. As a result, the pK_a of the molecules dropped by >2 pK_a units, giving values in the range 4.76 (**3g**) – 7.18 (**3a**). Similar to the other two series, the presence of chlorine atoms in the *N*-phenylbenzamide scaffold reduced the pK_a values compared to the unsubstituted **3a** (-0.72 to -1.28 for **3e** and **3b**, respectively). The most striking result was obtained with the di-isopropoxy derivative (**3g**) which displayed the lowest pK_a of this series (4.76). This behaviour differed somewhat from the bis(2-aminoimidazoline) analogue **1g** which pK_a (9.09) was close to that of lead **I** (9.26). The substitution of the amide bridge between the phenyl rings (e.g., **3a**, pK_a = 7.18) with an ethylene bridge (**36**, pK_a = 6.70) led to a significant reduction of the pK_a (-0.48 units) compared to **3a**. The 9*H*-fluorene analogue was the only compound of the series which we could measure two different pK_a values (4.23 and 6.91). To sum up, the percentage of ionization at pH 7.4 was quite disparate in this series, from 0.2% (**3g**) up to 38% for **3a**.

Table 4.3: Experimental pK_a, and calculated pK_a and logP values of the synthesised bis(arylimidamide) derivatives.[a]

Cmpd	Structure	pK_a ± SD[b] (H₂O, 25 ºC)	% Ionization pH 7.4	Calculated[c] pK_a1 pK_a2	logP[d]
3a		7.18 ± 0.13[e]	37.6	5.12 5.93	3.73
3b		5.90 ± 0.14	3.1	4.21 5.63	4.77
3c		f	f	4.14 4.94	4.77
3d		g	g	4.89 5.70	4.77
3e		6.46 ± 0.02	10.3	5.22 4.61	4.77
3g		4.76 ± 0.24	0.2	4.89 5.70	4.74
3h		f	f	4.19 4.98	2.21
3i		f	f	5.37 4.72	3.12
36		6.70 ± 0.05	16.6	5.75 6.35	5.15
37		f	f	5.49 6.10	4.13
53		4.23 ± 0.10	0.1	5.52 6.13	4.39
		6.91 ± 0.12	24.5		

[a]Compounds were dissolved in DMSO (0.5 mM stock solution) and diluted with the correspondent buffer to achieve a 0.1 mM concentration in each well (2% DMSO v/v). [b]Only one pK_a value could be measured for both arylimidamide rings. [c]Calculated using ChemAxon package "Chemicalize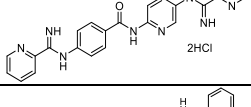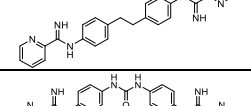". [d]Calculated using MarvinSketch (ChemAxon method, considering tautomerization/resonance) Version 22.9.0. [e]Potentiometric titration using the SIRIUS T3 apparatus allowed to measure pK_1 = 6.92 ± 0.18 and pK_2 = 7.42 ± 0.22. [f]Not measured due to lack of sample. [g]Inconsistent results not able to provide a pK_a value.

4.2.2.7. Conclusions

Bis(imidazolidin-2-imine) series (**1**) display pK_a values > 8 with a percentage of ionization ranging from 85.5 to 98.7% indicating that these derivatives are mostly dicationic at physiological pH. Calculated logP ranged from 1.82 to 3.89. As expected, the introduction of two chlorine atoms (one in each of the phenyl rings of the *N*-phenylbenzamide scaffold) reduced the pK_a (from 0.5 to 1.1 pK_a units) and increased the logP versus lead compound **I**. The introduction of pyridine rings in the scaffold led to a similar pK_a decrease (-1.1 pK_a units) and also a drop in lipophilicity.

Bis(2-aminobenzimidazole) derivatives showed much lower pK_a values in the range 2.77–5.93, indicating that the compounds are mostly neutral at physiological pH. This series showed the highest calculated logP values (4.3 – 7.24), at the limit of what is desirable for orally active compounds (logP < 5). Unsubstituted compound **2a** has a pK_a = 4.49, and the effect of the introduction of chlorine atoms modulated the reduction from 1.1 to 1.64 pK_a units. In this series, the replacement of phenyl with pyridine rings led to a subtle reduction of just -0.64 pK_a units.

Bis(arylimidamide) derivatives showed disparate percentages of ionization at pH 7.4, from 0.2% (**3g**) up to 38% for **3a**. The introduction of two chlorine atoms led to (-0.72 to -1.28 pK_a units). Calculated logP values were in the mid-range (2.21–5.15).

4.3. DNA binding studies: determination of the binding affinity of series 1–3

4.3.1. Surface Plasmon Resonance-biosensor experiments

4.3.1.1. Background

Surface Plasmon Resonance (SPR)-biosensor experiments were carried out in the laboratory of Biophysical Interactions at the Medicinal Chemistry Institute (IQM–CSIC). SPR was used to measure the binding affinities of the 3 series of compounds to different hairpin DNAs. One of the advantages of the SPR-technique is the possibility to measure binding affinities and kinetics of the interaction,[32] thus enabling the investigation of the interaction of molecules with specific DNA sequences and the evaluation of the corresponding binding constants.

To measure DNA–compound interactions, the SPR technique uses a sensor chip – normally made of a gold surface – where the DNA hairpin is immobilized. The SPR-biosensor experiment is based on a physical characteristic of this gold sensor chip, which will reflect the light with a different angle depending on whether the immobilized DNA is free or bound to a ligand (Figure 4.5). Adsorption and desorption occurring on metal surfaces change the refractive index of the near media metal–dielectric interface and therefore change the SPR angle.[33] Therefore, monitoring the changes in the SPR angle can be used to analyse adsorption–desorption activities or associations that occur on the metal surface.
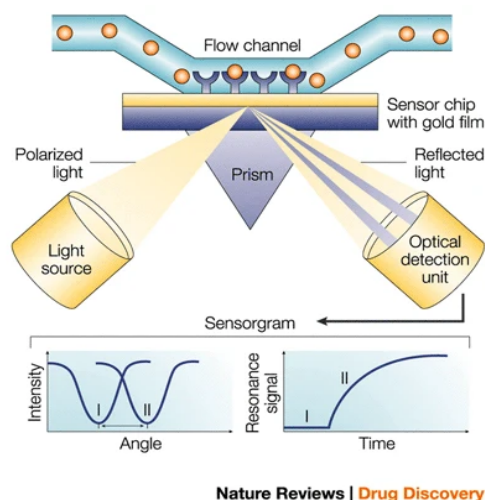
Figure 4.5: Instrument setup for an SPR experiment. Reflection of light on the sensor chip with the hairpin DNA and the influx of the ligand solution.[33]

Multiple injections of varied quantities of chemicals (ligand) into the surface of immobilized DNA are used to perform steady-state binding studies. The ligand solutions are injected via the flow cell until the reaction reaches a steady state. Then, a solution of buffer only flows over the surface of the sensor chip to separate the ligand from the DNA. The signal, displayed as RU (response unit) is directly proportional to the amount of bound compound, which is obtained when the response from the reference "empty" cell (i.e., chip + dextran matrix + streptavidin) is subtracted from the response of the cell containing DNA (Figure 4.6).[32, 34]
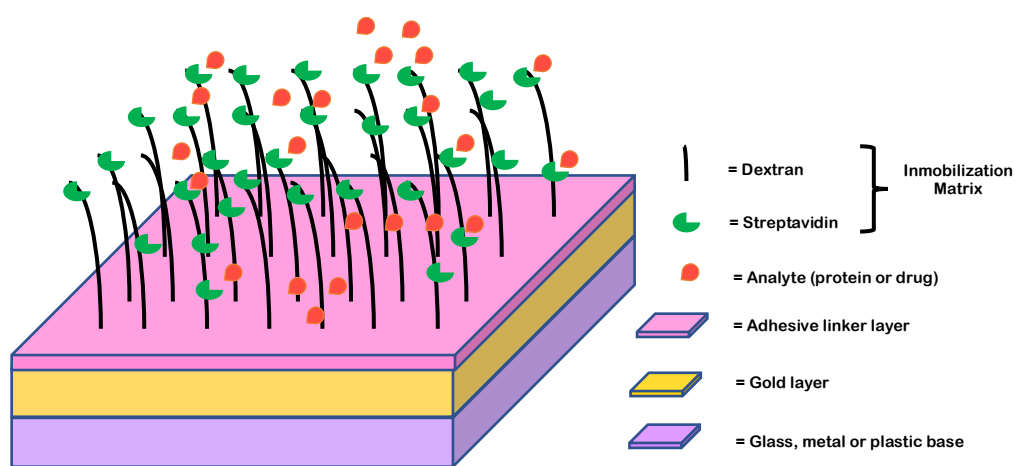
Figure 4.6: SPR sensor chip schematic representation (capture sensor chip).

The DNA molecular weight, the amount of DNA in the flow cell, the compound's molecular weight, and the refractive index gradient ratio of the compound and DNA are used to calculate the expected maximum response per bound compound in the steady-state region (RU_{max}). By registering the variations in the RU over time, a plot known as a sensorgram can be created (Figure 4.7).
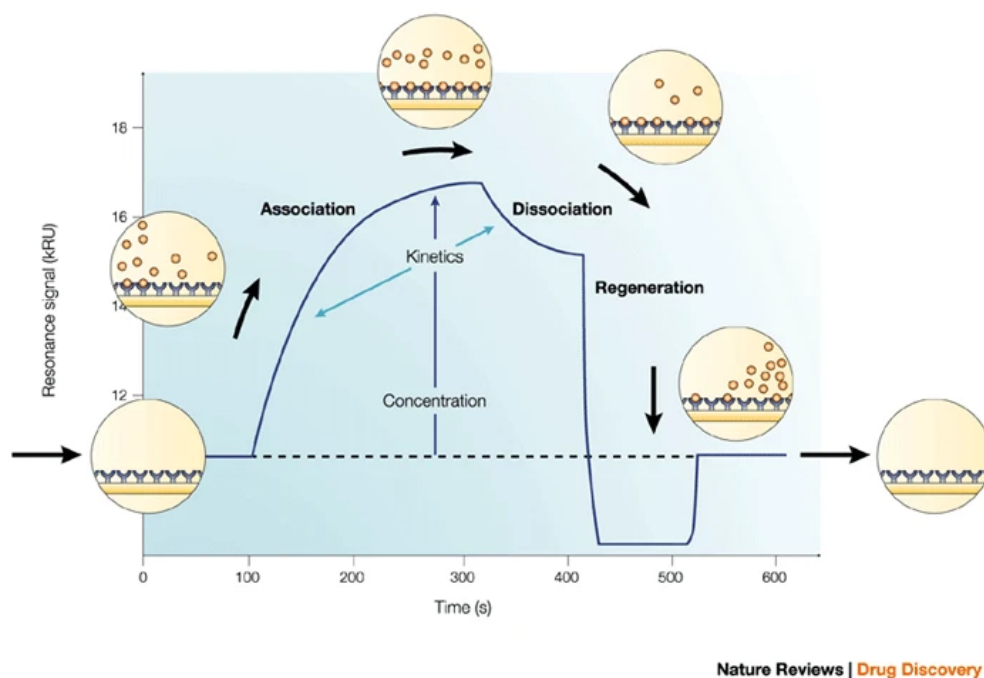
Figure 4.7: SPR sensorgram resulting from the association-dissociation of the ligand to the oligonucleotide.[33]

From the sensorgrams obtained with different concentrations of the ligand, the binding affinity can be determined by fitting the results to a one-site or two-sites binding model according to:

Equation 4.3: Determination of binding affinities by fitting to a two-sites binding model

$$r = \frac{(K_1 C_f + 2K_1 K_2 C_f^2)}{(1 + K_1 C_f + K_1 K_2 C_f^2)}$$

where *r* is the moles of bound compound per mole of DNA hairpin duplex, C_f is the free concentration at the equilibrium, and K_1 and K_2 the microscopic binding constants ($K_2 = 0$ for the one-site binding model).

4.3.1.2.   SPR results

The capacity of all the compounds (series **1**, **2** and **3**) to bind DNA hairpin duplexes containing CGAATTCG ["AATT"] and CGCGCGCG ["(CG)$_4$"] sequences was determined using a SPR-biosensor assay.[35] AT-rich sequences are abundant in the mitochondrial genome of kinetoplastid parasites.[6, 36] Hence, the study of the specific

interaction of the compounds with each oligonucleotide sequence will inform on their potential to target kDNA as selective MGBs.[32, 34]

Two biotin-labelled DNA hairpin sequences were used:

a)   5'-biotin-CGAATTCGTCTCCGAATTCG-3' [AATT], and

b)   5'-biotin-CGCGCGCGTTTTCGCGCGCG-3' [(CG)$_4$]

which was used as negative control (Figure 4.8). These two sequences were immobilised on the gold microchip using the streptavidin technique as reported in the experimental section.

5´biotin - C - G - A - A - T - T - C - G - T - C
3´- G - C - T - T - A - A - G -C - C - T

AATT

5´biotin - C - G - C - G - C - G - C - G - T - T
3´- G - C - G - C - G - C - G - C - T - T

(CG)$_4$
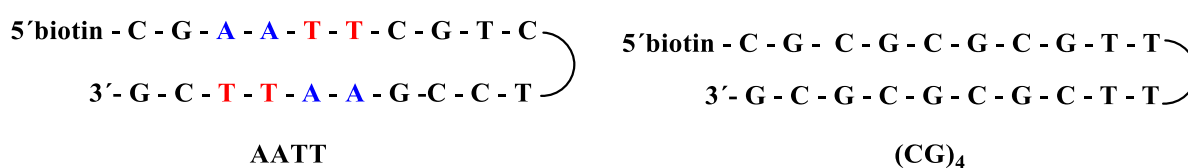
Figure 4.8: Structure of 5´-biotinilated DNA sequences (hairpin duplexes)

The compounds were initially screened at two concentrations (i.e., 5 and 100 µM) and ranked as binders/non binders. For binders, the experiments were carried out following this procedure: different concentrations of the synthetic compounds, in the range of 0.1 – 100 µM, were injected on the surface of the gold sensor chip having the immobilised DNA sequences to obtain a sensorgram for each concentration. The SPR response (RU) at equilibrium (plateau region) in the sensorgrams was converted to r (moles of bound compound per mole of DNA hairpin duplex; $r = RU/RU_{max}$) and plotted against the free compound concentration, C_f, flowing over the chip surface. The binding constants were determined by fitting the values to single-site or two-site binding models according to equation (4.3). The stoichiometry of this interaction is given by the maximum r value.

The binding constants to both DNA hairpins for the 3 series of compounds are shown in Table 4.4. For the bis(2-aminobenzimidazole) derivatives (**2a–e**, **2h**, **30**, **31**, and **34**) no binding to AATT or (CG)$_4$ oligonucleotide hairpin sequences was observed at the highest concentration tested (100 µM). Unspecific binding to the chip dextran matrix (compounds **2a–h**) or aggregation/precipitation (**30**, **31**, and **34**) was observed instead, indicating that SPR-biosensor assays are not adequate to determine the binding affinity of this class of compounds.

Among the bis(arylimidamide) derivatives, compound **3a** was the only compound with the *N*-phenylbenzamide scaffold that bound selectively to the AT-containing sequence versus the (CG)$_4$ oligonucleotide, with $K_D = 0.58 \times 10^{-6}$ M (Figure 4.9). The other compounds of this series showing DNA binding interactions were the 1,2-diphenylethane (**36**), and fluorene (**53**) derivatives, none of which possess the same central scaffold, although they share the bis(arylimidamide) moieties. Their K_D values for the AT-containing hairpin were 17- (**53**) to 40-fold (**36**) higher than the binding constant of **3a**. As shown in Figure 4.9c, compounds **3a**, **36**, and **53** displayed a binding stoichiometry (*r*) of two moles of bound compound per mole of DNA hairpin duplex.
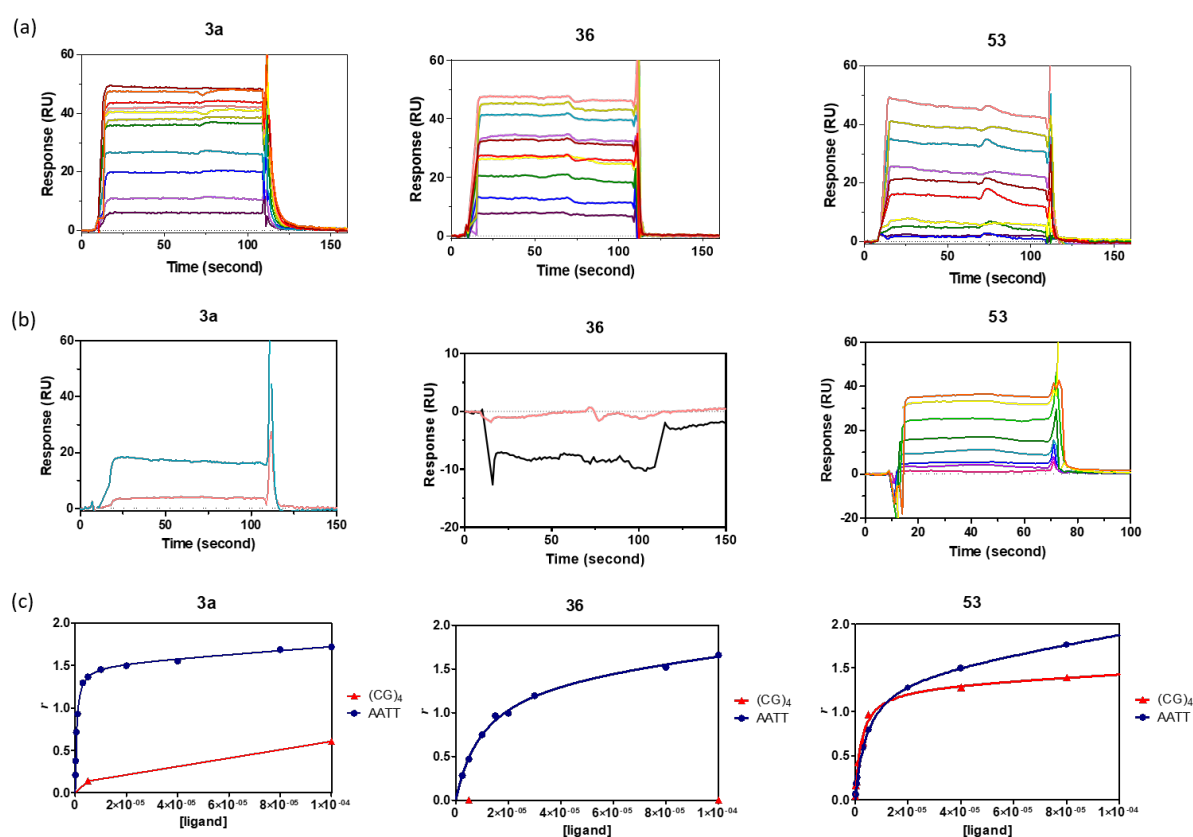
Figure 4.9: SPR binding affinity. (a) Sensorgrams for binding of bis(arylimidamides) **3a**, **36**, and **53** to AATT and (b) (CG)$_4$ hairpin duplexes using increasing concentrations of the ligand in the range (from bottom to top): 0.1–100 μM (**3a**), 2–100 μM (**36**), and 0.1–80 μM (**53**). (c) SPR binding plots of **3a**, **36**, and **53** for AATT and (CG)$_4$ hairpins: the SPR response (RU) at equilibrium (plateau) in the sensorgrams was transformed to *r* and represented against the unbound concentration of the compounds.

The chlorine (**3b–e**), isopropoxy (**3g**), and pyridine-based (**3h–i**) bis(arylimidamide) derivatives showed unspecific binding to the chip dextran matrix, making impossible the interpretation of the data.

In contrast, all of the *N*-phenylbenzamide-based bis(imidazolin-2-imine) derivatives **1f**–**h** bound to the AATT hairpin sequence with K_D values in the submicromolar to micromolar range (Table 4.4), in agreement with previous results obtained with similar compounds.[10, 31] Binding was selective for the AT-containing sequence as no binding to the $(CG)_4$ oligonucleotide sequence was observed up to 100 μM for **1f**, **1g**, and **1h** (Figure 4.10 & Figure 4.11).

Analogues with substituents on the phenyl rings were > 2-fold weaker binders than **I** (K_D = 0.17 × 10^{-6} M) as shown by primary binding constants (i.e., high affinity site) ranging from 0.38 × 10^{-6} M for the dipyridyl derivative **1h** to 45 × 10^{-6} M for the dichloro analogue **1c**. Secondary binding constants were 80- to 30-times weaker, respectively. In these experiments, secondary binding generally accounts for non-specific binding interaction with the DNA hairpin loop as previously reported.[10]

Within this *N*-phenylbenzamide-based bis(imidazolin-2-imine) series, the relative position and size of the substituents (i.e., Cl, O^{i}Pr, F) had a clear influence on the binding to the minor groove of the DNA hairpin. The compounds with chlorine (**1b**, **1d**, **1e**) or O^{i}Pr (**1g**) groups in position *ortho* to the amide bond of the scaffold had >40-times weaker binding affinity than the molecules with the Cl atoms next to the 2-aminoimidazoline group (**1c**). The presence of fluorine atoms *ortho* to the amide bond (**1f**) hardly affected the binding to DNA (K_D = 0.55 × 10^{-6} M), possibly due to the small size of the fluorine atoms (Figure 4.10 & Figure 4.11).
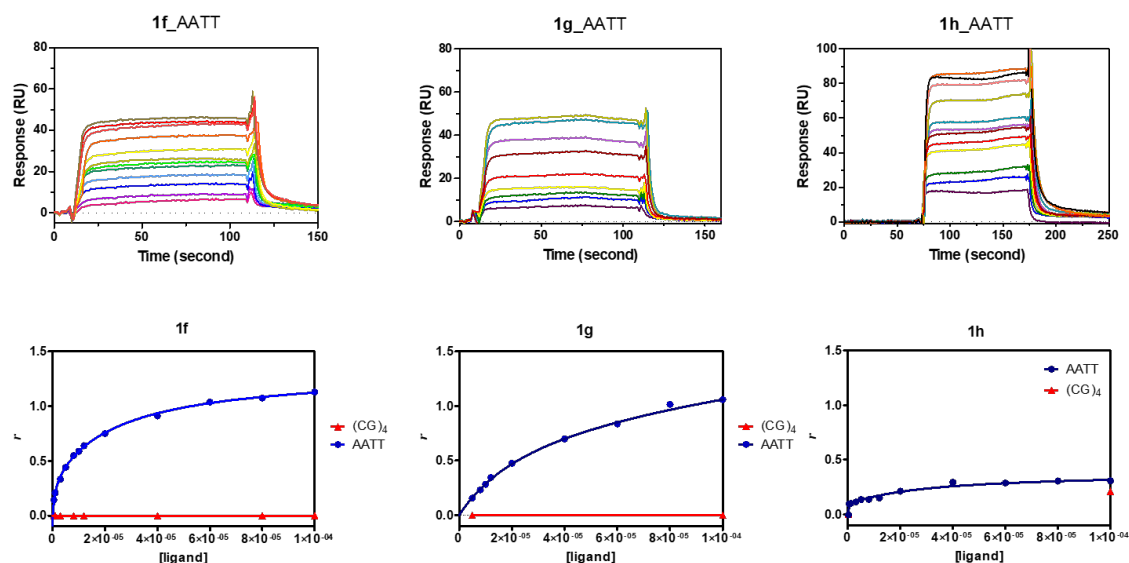
Figure 4.10: SPR binding affinity of bis(imidazolin-2-imines). (a) Sensorgrams for binding of **1f–h** to AATT hairpin duplex using increasing concentrations of the ligand in the range 0.5–100 μM (**1f**, **1g**) or 0.25–100 μM (**1h**) (from bottom to top). (b) SPR binding plots of **1f–h** for AATT and (CG)$_4$ hairpins: the SPR response (RU) at equilibrium (plateau) in the sensorgrams was transformed to r and represented against the unbound concentration of the compounds.
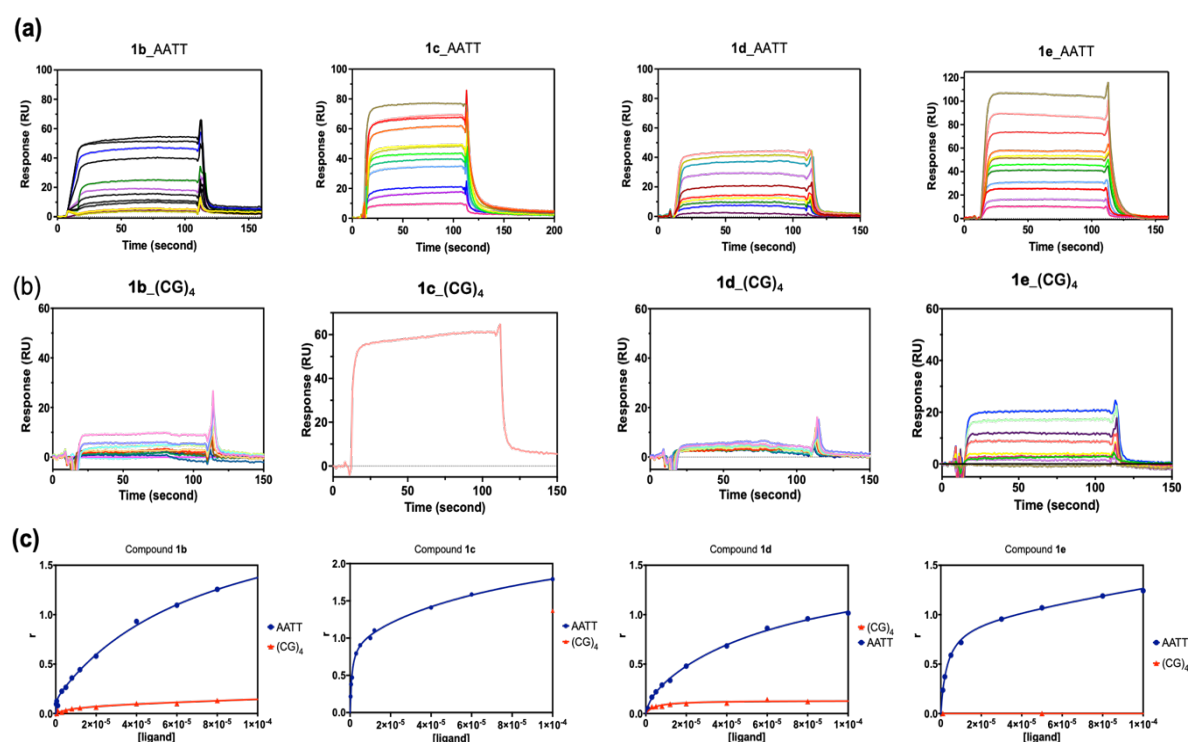
Figure 4.11: SPR binding affinity of bis(imidazolin-2-imines). Sensorgrams for binding of chloro analogues **1b–e** to (a) AATT and (b) (CG)$_4$ hairpin duplexes using increasing concentrations of the ligand in the range: 0.5–100 μM (**1b**, **1c**), 2–100 μM (**1d**), or 0.1–80 μM (**1e**) (from bottom to top).

Table 4.4: SPR results: binding constants (K_D) determined by SPR for DNA hairpins containing AATT and (CG)$_4$ sequences.

Cmpd	$K_D \times 10^{-6}$ M	
	AATT[a]	**(CG)$_4$**
I	$K_1 = 0.17$[d] $K_2 = 207$[d]	>100[b]
1b	45[f]	>100[b]
1c	$K_1 = 0.75$ $K_2 = 96.6$	>100[b]
1d	$K_1 = 3.2$ $K_2 = 95$	>100[b]
1e	$K_1 = 3.5$ $K_2 = 1150$	>100[b]
1f	$K_1 = 0.55$ $K_2 = 22.7$	>100[b]
1g	55[f]	>100[b]
1h	$K_1 = 0.38$ $K_2 = 30.6$	>5[e]
2a–e	Unspecific binding[c]	>5[e]
2h	Unspecific binding[c]	-
30, 31	Aggregate or Precipitate	-
34	Aggregate Precipitate	>100[b]
3a	$K_1 = 0.58$ $K_2 = 14620$	>100[b]
3b–e	>100[b]	>100[b]
3g	Unspecific binding[c]	>100[b]
3h–i	Unspecific binding[c]	>100[b]
36	23.6[f]	[b]
39	Unspecific binding[c]	-
53	9.82[f]	13.0

[a]Primary binding constant for fitting to a two-site binding model. [b]No binding observed at 5 and 100 μM. [c]Unspecific binding to the chip dextran matrix. [d]Taken from reference [10]. [e]No binding observed at 5 μM. [f]Fitted to a one-site binding model.

4.3.2. DNA thermal denaturation experiments

4.3.2.1. Background

The stability of a DNA–drug complex can be measured by a thermal denaturation experiment. Thermal denaturation is understood as the transition from the folded (or associated) duplex DNA to the unfolded (or dissociated) single strands (Figure 4.12), which often leads to a conformational change reflected as a change in absorbance properties (duplex denaturation leads to a hyperchromism). The temperature of melting (T_m) can also be defined in a more accurate sense as the temperature of mid-transition from the double strand conformation to the denatured single strands DNA.[37, 38]
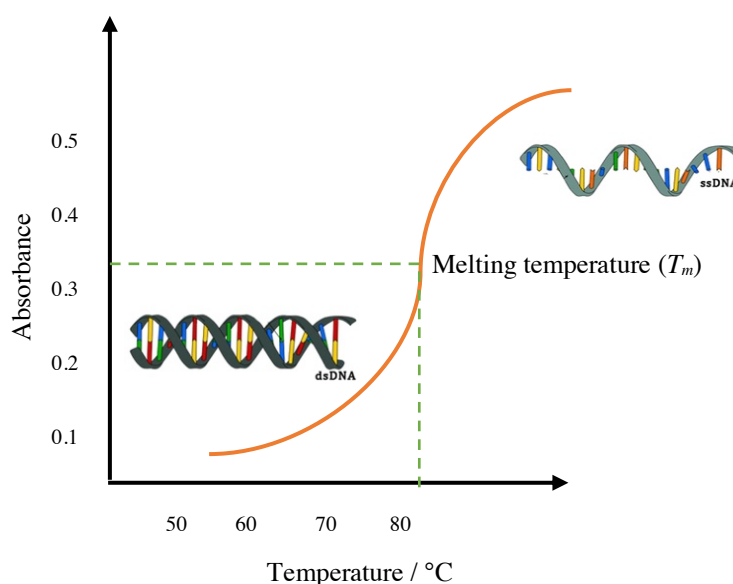
Figure 4.12: Example of experimental determination of oligonucleotide T_m. The T_m is the reading halfway between the double-stranded DNA (dsDNA) and single-stranded DNA (ssDNA) plateaus.

DNA average secondary structure is in its double helix form when placed in solution under physiological conditions. The bases are stacked away in the helix and are shielded from the light by the external phosphate groups; thus, the bases do not absorb much light. Nonetheless, as a sample of DNA is heated, the hydrogen bonds between the base pairs are given enough heat energy to break. At this point the double helix begins to split apart giving the bases freedom to rotate. Consequently, an increasing amount of light is absorbed by the DNA bases that correlate with the gradual hyperchromic effect seen in the spectrum.[37, 39]

By measuring the absorbance of a sample of DNA as a function of temperature, thermal denaturation curves can be obtained. Different spectroscopic techniques can be used to obtain these curves; e.g., fluorescence emission signals, the intensity of an NMR peak, UV-visible, Raman, or circular dichroism (CD) signals.[37, 38] Thus, thermal denaturation can be used to measure the stabilization effect (i.e., the binding affinity) produced by a molecule on binding to duplex DNA. In our case, we used circular dichroism to analyse the T_m increase for compound complexes with an $(AT)_4$-containing DNA hairpin relative to uncomplexed DNA (ΔT_m). These denaturation experiments were performed with the bis(imidazolin-2-imine), bis(2-aminobenzimidazole) and bis(arylimidamide) series.

4.3.2.2. Circular Dichroism fundamentals

Circular dichroism (CD) is a spectroscopic technique defined as the differential absorption of left and right circularly polarized light.[40] It arises from molecular electron oscillations that are driven by both the light's electric and magnetic fields, where the effects are in phase for one circular polarization and out of phase for the other (Figure 4.13).[41, 42]
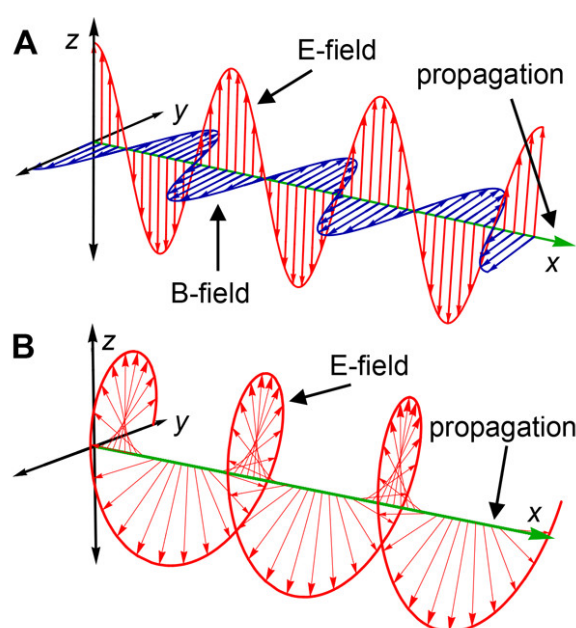
Figure 4.13: Light polarization, shown with the **E**-field (electric field) in red and **B**-field (magnetic field) in blue. (A) Vertically polarized light. (B) **E**-field of right circularly polarized light (RCP) with the **B**-field not shown for clarity. Modified from *J. Chem. Educ.* **2020**, 97, 12, 4370-4376.[41]

It is a technique that allows to get information regarding secondary structures of biological macromolecules such as DNA. A one-plane-polarized beam of light can be considered as

formed by two components circularly polarized, one to the right and the other to the left. The interaction between one-plane-polarized beam of light and the stereogenic centre of the irradiated molecule induces a differential absorbance of both components of circularly-polarized light which is irradiated. This different absorption of the two components of circularly-polarized light causes the vector sum of the electrical vectors of each component $(E_L + E_R)$ to describe an ellipse (Figure 4.13).

The CD is defined by the relationship between the semi-major and semi-minor axis of that ellipse. This relationship is the tangent of the angle θ, known as ellipticity.
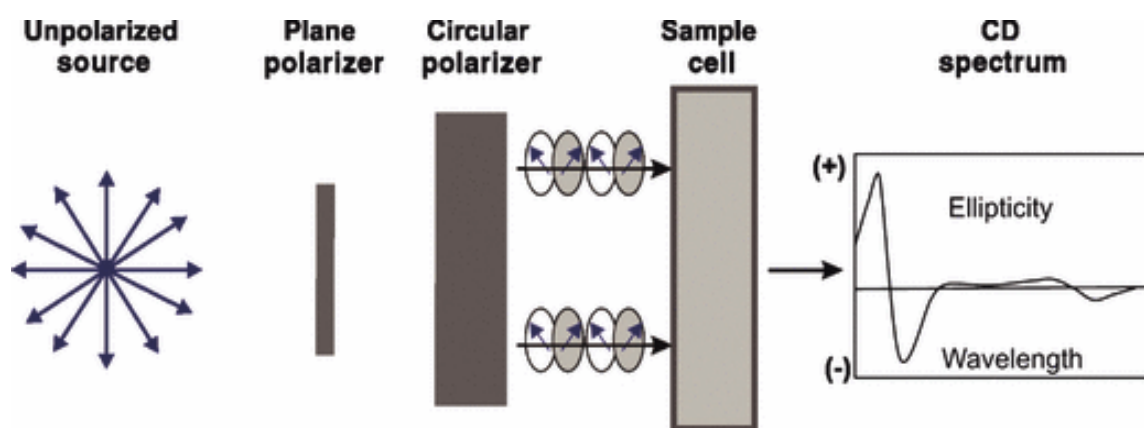
Figure 4.14: Scheme of CD in which a difference in absorption is measured (Taken from *Chem. Biol. Drug Des.*, **2009**, *74*, 101-120).[43]

In CD experiments, the difference between the absorption of circularly-polarized light to the left and to the right ($\Delta Abs = A_L - A_R$) is recorded, which is related to the ellipticity (θ) (Figure 4.14). CD data are commonly reported as ellipticity (θ), which is related to absorbance by a factor of 32.98 (θ = 32.98 ΔAbs). Ellipticity varies with wavelength, so spectra can be obtained plotting ellipticity versus wavelength. Ellipticity is usually reported in millidegrees (mdeg). Another type of experiment consists in recording the variation of ellipticity with temperature while maintaining a fixed wavelength. In this type of experiment, denaturation curves are obtained that allow the denaturation temperature of the studied structure to be determined.

Molecules analysed by CD must absorb UV–visible radiation and be chiral. The chiral character of a molecule may be due to the presence of intrinsically chiral elements or to the location of chromophores in an asymmetric environment. There will be no spectrum if

the molecule is achiral, because it will interact with the same amount of left and right-handed photons.

The CD spectrum of DNA has its origin in the asymmetry of the sugars of the sugar-phosphate backbone and in the folding that the nucleotide chain adopts. CD spectra of nucleic acids are usually performed by varying the wavelength between 200 and 320 nm. Electronic transitions of nitrogenous bases occur in this range of wavelengths. The position of the positive and negative bands in the spectrum is indicative of the type of secondary structure that the DNA or RNA molecule is forming.[44-46] Furthermore, CD is used to measure the interaction between small molecules and macromolecules (i.e., proteins or DNA).[47]

Additionally, CD measures the interaction between DNA/RNA and DNA/protein interactions which cannot be evaluated with UV spectroscopy. Achiral single stranded DNA produces little or no spectrum. Conversely, when two strands come together to form duplex DNA, this chirality is due to the DNA bases rearrangement inside the helix. When DNA is in the β-form, the CD spectrum has a positive signal at 275 nm and a negative one at 245 nm, passing zero at 258 nm.[47]

One of the main uses of CD involving DNA is to probe DNA conformational changes and its interaction with small molecules.[19,20,48] One can monitor spectrum changes that are indicative of structural alterations to the double helix by adding small amounts of achiral compounds.

4.3.2.3.   Thermal melting results

The thermal melting caused by the compounds from series **1**, **2**, and **3** were determined for their complexes with the (AT)$_4$-containing DNA hairpin (Tables 4.5–4.7). With the exception of **1c** (ΔT_m = 0.9 °C), the T_m increases measured for bis(imidazolin-2-imines) **1b–h**, which ranged from 3.1 ºC (**1g**) to 8.2 ºC (**1h**), were larger than ΔT_m of lead **I** (1.6 °C). This showed that the introduction of Cl or nitrogen atoms in the scaffold positively affected DNA binding affinity for these molecules. Binding to the (CG)$_4$ hairpin was also evaluated with one example from this series (**1e**), but no binding was observed. No correlation between pK_a and T_m values was observed.

Table 4.5: DNA binding affinity (ΔT_m) for bis(imidazolin-2-imines) **1b**–**h**.

Cmpd	Structure[a]	T_m (ºC) ± SD	ΔT_m, (AT)$_4$ hairpin (ºC)[b]
I		45.2 ± 0.4	1.6
1b		50.9 ± 0.3	7.3
1c		44.5 ± 1.3	0.9
1d		49.1 ± 0.3	5.5
1e		51.3 ± 0.7	7.7
1g		46.7 ± 0.4	3.1
1h		51.8 ± 4.8	8.2

[a]The compounds are di-trifluoroacetate salts except **I** (dihydrochloride salt). [b]The increment in DNA thermal melting (ΔT_m, ºC) was measured with the oligonucleotide hairpin (AT)$_4$. The melting temperature of (AT)$_4$ DNA in sodium phosphate buffer (10 mM) was 43.6 ± 0.7 ºC.

Bis(2-aminobenzimidazoles) **2a**–**e** showed ΔT_m values in the range 4.0–7.0 °C, indicating that these benzimidazole derivatives also bind to the (AT)$_4$-containing hairpin DNA (Table 4.6). This result is important because we were unable to observe specific DNA binding using SPR-biosensor assays (see section 4.3.1.2). With the exception of **2a** and **2c**, the binding affinities of the bis(2-aminobenzimidazoles) were lower than that of the bis(imidazolin-2-imines) counterparts. This may be related to the uncharged nature ($pK_a <$ 6) of this series of compounds at physiological pH (see section 6.2.2.5.).

The replacement of the amide bond linker of **2a**–**e** by a more flexible ethylene chain (**30**) produced an increase of 1.2 ºC with respect to **2a** (ΔT_m = 4.9 ºC). In contrast, changing the

N-phenylbenzamide skeleton with a rigid and planar fluorene scaffold (**34**) resulted in an insignificant (within the experimental error) increase in T_m versus **2a**. Binding to the (CG)$_4$ hairpin was also evaluated with compound **2a** as series lead, but no binding (T_m increase) was observed.

Table 4.6: DNA binding affinity (ΔT_m) for bis(2-aminobenzimidazoles) **2a**–**h**, **30**, **31**, and **34**.

Cmpd	Structure	T_m (ºC) ± SD	ΔT_m, (AT)$_4$ hairpin (ºC)[a]
2a		48.5 ± 0.3	4.9
2b		48.6 ± 0.4	5.0
2c		48.7 ± 0.4	5.1
2d		47.6 ± 0.3	4.0
2e		48.9 ± 0.4	5.3
2h		49.2 ± 0.3	5.6
30		49.7 ± 0.5	6.1
31		50.6 ± 0.5	7.0
34		48.7 ± 0.4	5.1

[a]The increment in DNA thermal melting (ΔT_m, ºC) was measured with the oligonucleotide hairpin (AT)$_4$. The melting temperature of (AT)$_4$ DNA in sodium phosphate buffer (10 mM) was 43.6 ± 0.7 ºC.
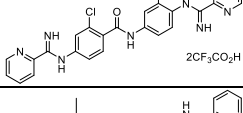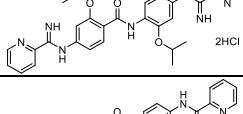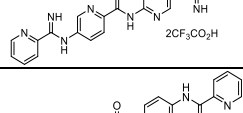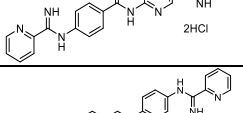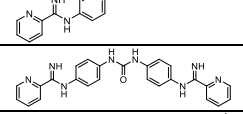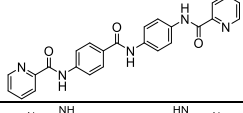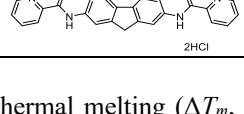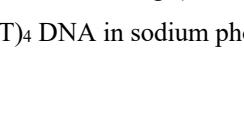
The larger thermal increases were obtained with the bis(arylimidamide) series, with ΔT_m values ranging from 1.6 to 11 ºC (Table 4.7). Most of the compounds except **3i** showed larger T_m increases than lead **I**. The strongest binder was the rigid fused ring tricyclic fluorene derivative **53** ($\Delta T_m = 11.0$ ºC). This data agreed with the reported value ($\Delta T_m =$ 15 ºC) for poly(d(A-T)$_2$).[49] In addition, the chlorinated derivatives **3b**, **3d**, and **3e** also showed good affinity with ΔT_m values in the range 5.1 to 8.9 ºC. In general, except **3e** which displayed one of the strongest binding affinities ($\Delta T_m = 8.9$ ºC) of the series, the

introduction of chlorine (**3b**–**d**) or isopropoxy (**3g**) substituents led to a drop in binding affinity with respect to the unsubstituted compound **3a**. The same trend was observed with the introduction of one or two pyridine rings into the scaffold (**3h**, **3i**). These results differed from series **1** and **2** where pyridine rings increase the ΔT_m value with respect to the unmodified scaffold.

The case of **3c** and **1c**, which have a similar substitution pattern with both chlorine atoms in position *ortho* to the *N*-pyridylcarboxamidine groups, is striking. Both compounds hardly stabilized (AT)$_4$-containing duplex DNA in these experiments (1.6 and 0.9 ºC, respectively). However, **1c** bound strongly to AATT-containing DNA duplex (K_D = 0.75×10^{-6} M), as shown by SPR-biosensor experiments, whereas **3c** did not. This may indicate that bis(imidazolin-2-imines) (**1**) and bis(arylimidamides) (**3**) interact with the DNA minor groove in a different way.

The replacement of the central amide bridge for a more flexible ethylene bridge resulted in a large T_m increase (8.0 ºC), whereas a more rigid (and larger) urea linker (**37**) provided poor affinity. This may indicate that the two-carbon length is the most adequate or reflect conformational restriction for optimum binding to DNA in our compounds. Previous studies have reported that the minor groove generally assumes a narrow width that provides for tight binding of the heterocyclic system of the dications. Also, in the narrow AT base pair sequences, the compounds can fit tightly and deeply into the minor groove allowing groups on the inner face of the compounds to interact with complementary groups on the edges of the AT base pairs (i.e., through H- bonding and van der Waals interactions).[50]

Table 4.7: DNA binding affinity (ΔT_m) for bis(arylimidamides) **3a–i**, **36**, **37**, **41**, and **53**.

Cmpd	Structure	T_m (°C) ± SD	ΔT_m, (AT)$_4$ hairpin (°C)[a]
3a		49.5 ± 0.5	5.9
3b		48.8 ± 0.4	5.2
3c		45.2 ± 0.4	1.6
3d		48.7 ± 0.4	5.1
3e		52.5 ± 0.6	8.9
3g		49.7 ± 0.4	6.1
3h		45.9 ± 0.5	2.3
3i		45.4 ± 0.4	1.8
36		51.6 ± 0.7	8.0
37		45.2 ± 0.4	1.6
41		49.5 ±0.4	5.9
53		54.6 ± 1.3	11.0

[a]The increment in DNA thermal melting (ΔT_m, °C) was measured in oligonucleotide hairpin (AT)$_4$. The melting temperature of (AT)$_4$ DNA in sodium phosphate buffer (10 mM) was 43.6 ± 0.7 °C.
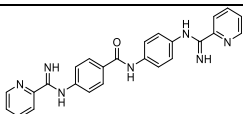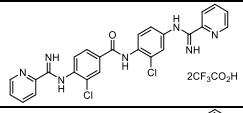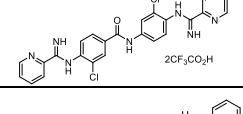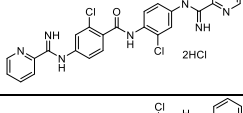
4.3.3. Ultraviolet titration experiments

As shown in section 4.3.1.2., we could not measure the binding affinity of the bis(2-aminobenzimidazoles) series (**2**) by SPR–biosensor experiments because of unspecific binding to the chip dextran matrix or precipitation/aggregation during the assay. Since series **2** compounds appear to stabilize the $(AT)_4$–containing DNA hairpin (as shown by ΔT_m values > 4 ºC), we decided to perform UV titrations with few compounds of this series (i.e., **2a–h**, **30**, **31**, and **34**) to confirm the results obtained by thermal melting experiments.

4.3.3.1. Studies of the changes in the UV-Vis spectra of ligands upon the addition of DNA

UV spectroscopy is an optical technique widely used to measure the binding affinity of different ligands to DNA. This technique has a wide range of applications including the determination of the sequence selectivity. UV titration experiments measure the binding affinity based on the observation of changes in the absorption spectra as DNA aliquots are added to the ligand to form a DNA – ligand complex (Figure 4.15).[51, 52]

$$K_a$$

DNA + Ligand ⇌ **DNA - Ligand**
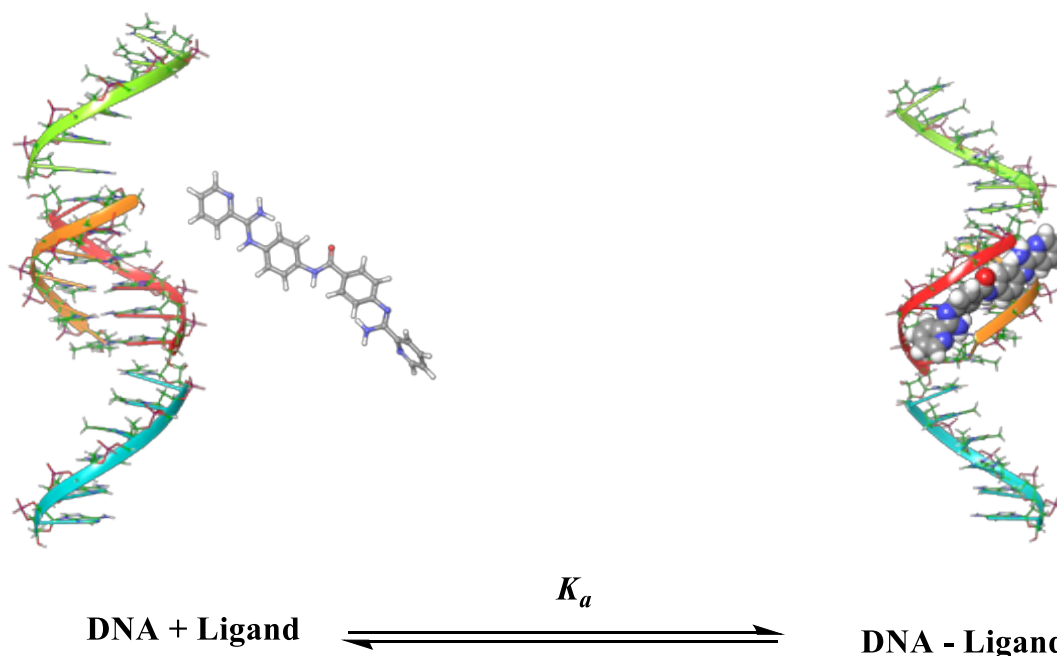
Figure 4.15: DNA – ligand binding equilibrium (Adapted from Han, F. et al. *Biochemistry*, **2005**, 44, 9785).[52]

When a molecule binds to DNA, spectral changes will be observed. Generally, a hypochromic shift will occur which represents a decrease in the concentration of the free molecule accompanied by the formation of a new band at a different wavelength representing the DNA–ligand complex.

The UV–Vis spectra of intercalating compounds binding DNA results in a characteristic shift of the absorption maximum wavelength (bathochromic or hypsochromic shift) and a decrease (hypochromicity)[53, 54] or increase (hyperchromicity) of the absorbance.[55, 56] Hyperchromic and hypochromic effects are spectral features of DNA that relate to the double helix structure. Contractions of DNA in the helix axis or conformational changes of DNA induces hypochromism; whereas hyperchromism arises when the DNA double-helix structure is damaged.[56-58]

4.3.3.2.   Results

UV titration experiments were performed by adding aliquots of salmon testes DNA (i.e., unspecific DNA containing 41.2% GC) to a fixed concentration of the ligand dissolved in phosphate-buffered saline (PBS, pH =7). After each addition, an equilibration time of 1 min was allowed and the UV spectra were registered.

For these assays, the bis(arylimidamide) compound **3a** was used as a reference because this compound proved to be an excellent DNA MGB. The binding of **3a** to salmon testes DNA provoked a small hypochromic effect with Bp/D ratio up to 1.2 (a higher hypochromic effect appeared with ratio > 1.2) and a large bathochromic shift. This showed that the free **3a** molecule formed a new DNA ligand complex (Figure 4.16).[53-55]
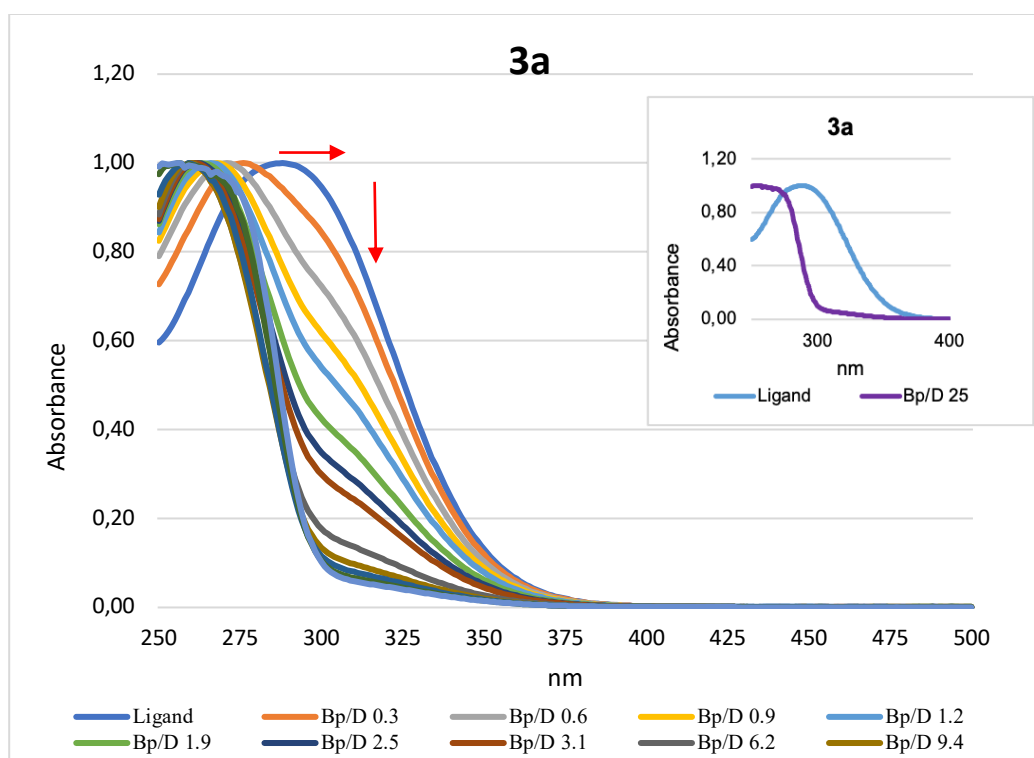
Figure 4.16: Absorption spectra of **3a** (25 μM) with increasing concentrations of FS-DNA. Red arrows indicate the hypochromic (↓) and bathochromic (→) shifts observed upon addition of aliquots of a 0.8 mM natural fish sperm DNA (FS–DNA) solution to (25 μM) the compound solution.

Titration of compound **2a** was also carried out with aliquots of a 0.8 mM natural FS-DNA solution added to the compound solution (25 μM). A high hypochromic shift observed with a Bp/D ratio = 0.9 and a red shift from 315 to 320 nm at the compound λ_{max} indicated the formation of a new DNA-ligand species (Figure 4.17). Similar spectral changes were also observed in the titration of the chloro derivatives from series 2. These results are reported in the Appendix 1.

These results confirmed that compounds **2a** and **3a** bind to DNA, in agreement with the data obtained in the thermal melting experiments. However, they do it in a clearly distinct way as shown by the differences in the UV-titration spectra. Compound **2a** seems to interact more strongly with unspecific DNA than **3a**, which may reflect a different binding mode and/or selectivity.
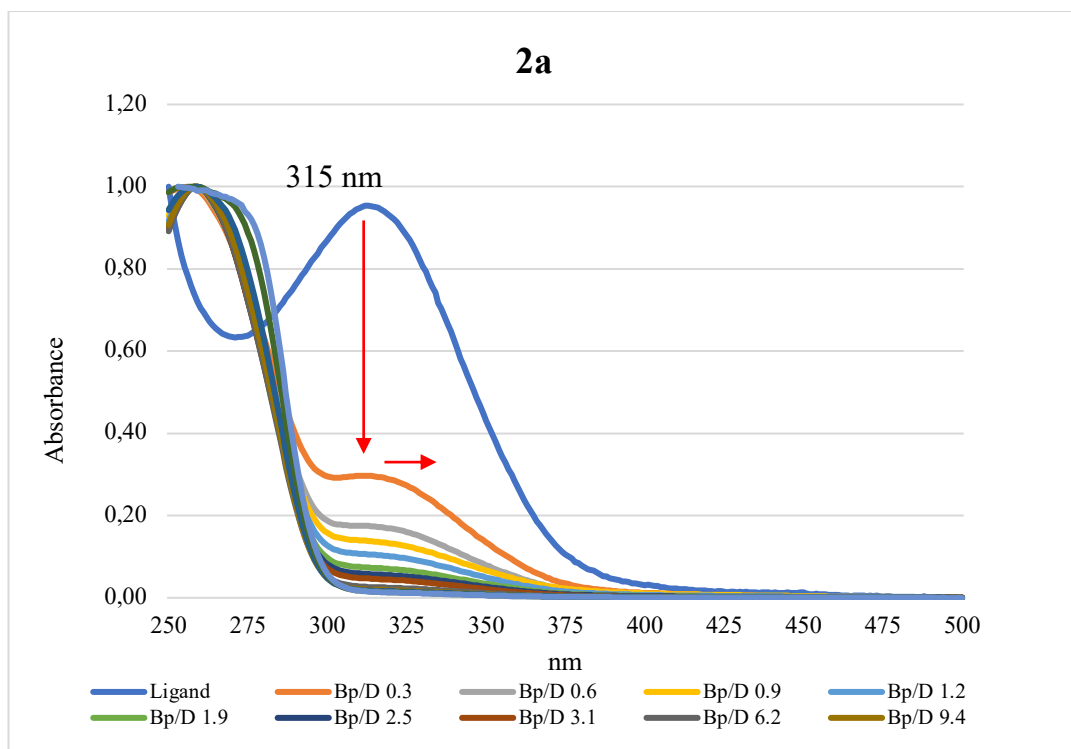
Figure 4.17: Absorption spectra of **2a** (25 μM) with increasing concentrations of FS–DNA. Red arrows refer to hypochromic (↓) and bathochromic (→) effects, respectively.

In summary, the UV-Vis results indicate that the bis(2-aminobenzimidazole) derivatives bind to DNA although they seem to do it through a different mode of binding with respect to the bis(arylimidamides). However, further experiments will be needed (e.g., DNA-intercalator displacement experiments using fluorescence spectroscopy; high resolution ^{1}H-NMR spectroscopy; linear-flow LD spectroscopy; electrophoretic mobility of circular DNA)[59] to get a better understanding of the binding mode of this series.

4.4. DNA binding studies: determination of the mode of binding of series 1–3

4.4.1. Circular Dichroism studies

CD experiments were carried on compounds from series **1**, **2** and **3** with a hairpin oligonucleotide containing CGATATATATCG [(AT)$_4$]. First, the CD spectrum of the (AT)$_4$ DNA in buffer (pH = 7.0; 10 mM Na$_2$HPO$_4$/ 100 mM NaCl) was recorded at 60 µM concentration. Following this, the synthesised compounds (C = 120 µM) were added and the corresponding CD spectra were recorded at different temperatures (5–90 ºC), the ratio compound/DNA was 2:1. The free compounds are not chiral and hence display no CD signal. On the contrary, the compounds bound to DNA have induced CD, which is usually characterized by a strong positive CD signal (at the maximum λ_{abs} of the bound compound) for MGBs.[49] Structural changes in the DNA due to the binding of the synthesised compounds were observed in the obtained spectra. For most of the compounds, a bathochromic shift (approximately +5 nm) of the positive CD signal of the DNA at 270 nm was observed when the temperature increased, with the most dramatic effect being observed at 65 and 85 ºC (Figure 4.18). Within the bis(imidazolin-2-imine) series (**I**, **1b–h**), a substantial positive induced CD signal was observed at ≈ 300–310 nm when working at 25 ºC (Figure 4.18 and appendix 2). For the bis(arylimidamide) series, a substantial positive induced CD signal was observed at ≈ 320 nm for **3a** (Figure 4.18), whereas a weak induced CD signal was perceived for **3b**, **3g–i**, **37**, and **53** (see appendix 2). In contrast, the bis(2-aminobenzimidazole) series displayed none (**2a–2d**, **2h**) or insignificant induced CD signal (**2e**, **30**, **31**, **34**). As an example, the CD spectrum of **2a** is shown in Figure 4.18.
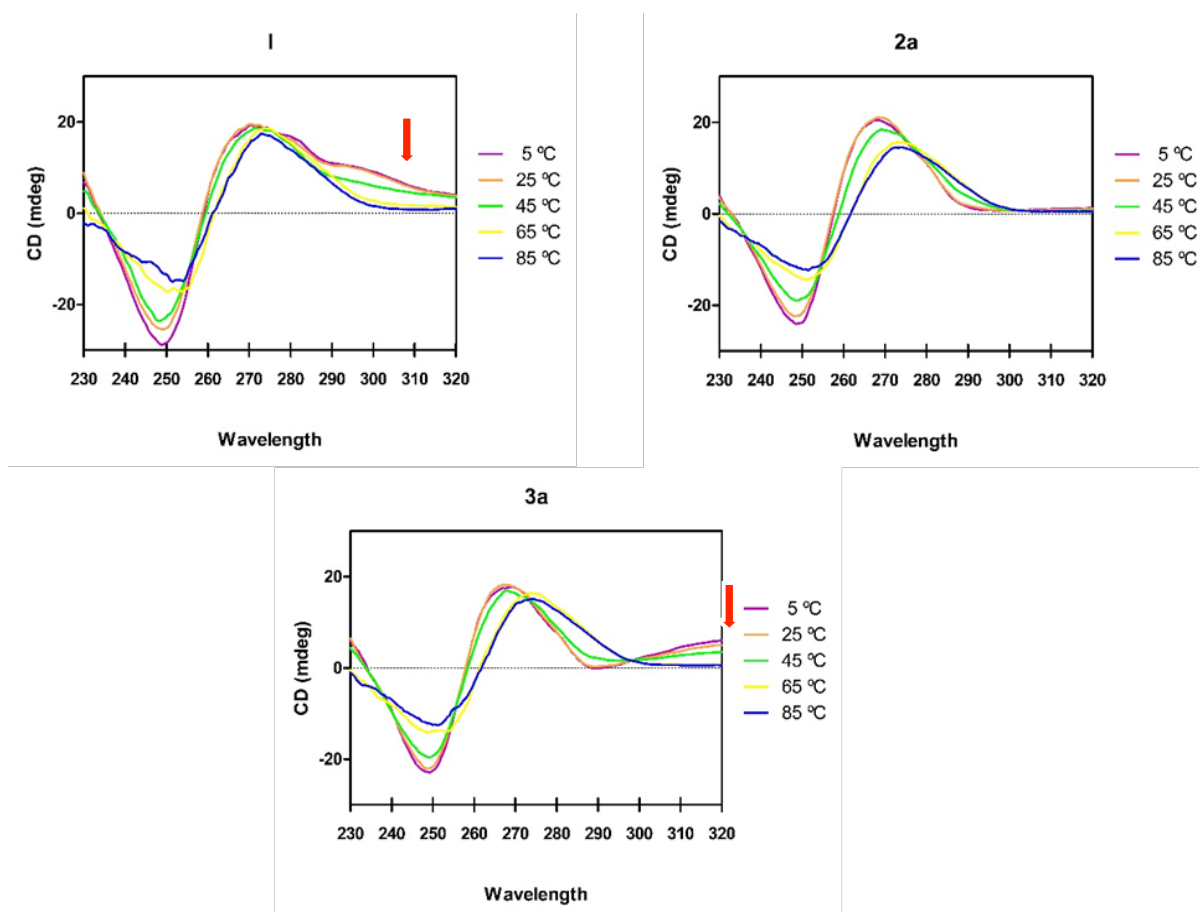
Figure 4.18: CD spectra of representative compounds of each series: spectra of **I**, **2a**, and **3a** (C = 120 μM) with (AT)$_4$ oligonucleotide (60 μM) obtained at different temperatures (from 5 to 85 ºC). The ratio of compound to DNA base pairs is 2. Red arrows indicate the presence of the positive induced CD signal.

Because the CD spectra were originally recorded for the thermal denaturation assays, where the DNA absorption band at 245 and 275 nm are the only ones of interest, the spectral window was arbitrary restricted to 230 – 320 nm during the experiments, to avoid excessive recording time. Since the observed induced CD signals appear at λ$_{max}$ > 300 nm, new experiments with a larger spectral window and different ratio compound/DNA should be performed to confirm these findings.

4.4.2. Electric Flow Linear Dichroism studies

4.4.2.1. Fundamentals of linear dichroism

Linear Dichroism (LD) is defined as the difference in the absorption of linearly polarised light ($A_{parallel}$) and perpendicularly polarised light ($A_{perpendicular}$) according to the Equation 4.4. LD methodology is used for the determination of the binding mode of small molecules to DNA.[40]

Equation 4.4: Linear Dichroism calculus for the canonical A and B forms.

$$\mathbf{LD} = A_{parallel} - A_{perpendicular} = \tfrac{3}{2}S(3Cos^2\alpha - 1)$$

where **S** is the orientation factor (**S** = 1 if the DNA is aligned whereas **S** = 0 if the DNA is not aligned), and α is the angle representing the orientation of the transition moment that is responsible for the absorption of light.[40, 60]

In this experiment, the DNA is rotated so that the bases are perpendicular to the incident light. Therefore, the bases absorb perpendicular light at 260 nm and then we observe a large negative peak at 260 nm. When a molecule intercalates between the base pairs, the intercalating molecule would be parallel to the bases, so the α angle would be 90°. By solving Equation 4.4 when α = 90°, it corresponds to a negative LD signal.

If a molecule binds to the DNA minor groove, then α would be equal to 45°, which is related to a positive induced LD signal. Therefore, LD experiments are able to provide information of the binding mode of the ligand.

As main advantage, this method can evaluate the binding mode of a molecule irrespective of its λ_{abs}. For example, if a minor groove binder absorbed strongly in the DNA region, we would observe an increase in the LD signal in that range.

4.4.2.2. Results: Linear Dichroism studies of bis(imidazolin-2-imine) 1e and bis(arylimidamide) 3a

The LD spectra were recorded for natural DNA (salmon testes) titrated with compounds **1e** and **3a** in phosphate buffer at 25 °C, following the methodology previously reported by Rozas' group.[5] Titrations were carried out with a DNA (blue line) concentration of 378.8 μM working with a Base pair / Drug (Bp/D) ratio of 0, 1 and 5, varying the Bp/D ratio from 5 to 1 over 2 additions (Figure 4.19).

According to the reported technique,[5] the concentrations of the DNA and the compounds were kept constant to avoid the dilution effect. This is because the experiment was done in a very small volume (70 μL). Each solution was then prepared individually and the corresponding spectra were recorded.
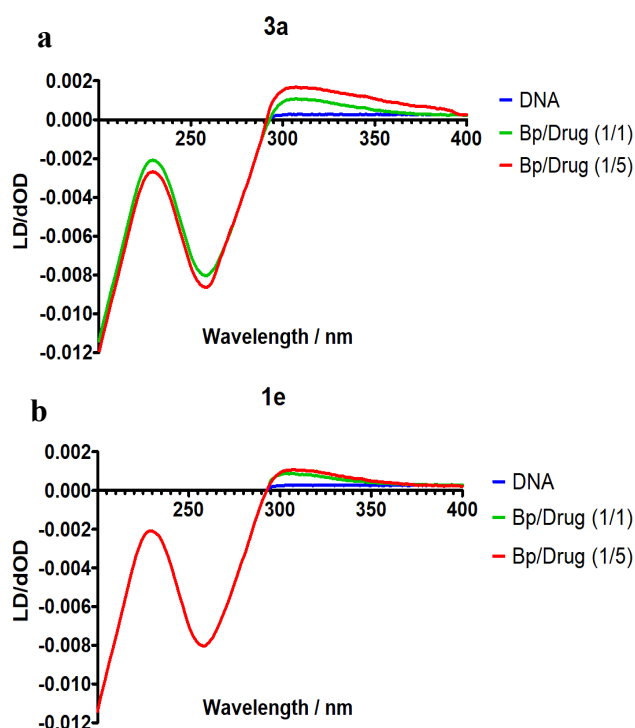
Figure 4.19: LD spectra for natural DNA salmon testes titrated with (a) **3a** and (b) **1e** using a Base pair / Drug (Bp/D) ratio of 0, 1 and 5. DNA concentration was 378.8 μM.

Both compounds showed a notable increase in the absorbance at 310 nm (where the DNA does not absorb) upon addition of increasing concentration of the compounds. Positive

induced signals are indicative of minor groove binding and, hence, these LD results with unspecific DNA indicate that the bis(arylimidamide) **3a** and the (bis(imidazolidin-2-imine) **1e** bind to the minor groove of DNA. These results are consistent with the data obtained by SPR and CD experiments with specific AT-containing DNA.

4.5. Nuclear Magnetic Resonance studies

The NMR experiments reported in this thesis have been performed in collaboration with Dr. Miguel Garavís and Dr. Carlos González at the Rocasolano Institute of Physical Chemistry – CSIC.

4.5.1. Introduction

Nuclear magnetic resonance (NMR) is based on the detection of some atomic nuclei - which have nuclear spin – under a magnetic field. Magnetic interactions between NMR-active nuclei along covalent bindings result in spin–spin couplings, which enable three-dimensional structure elucidation.[61] Hence, NMR is the most useful technique to elucidate the structure of organic and inorganic compounds.[61] It is also a great tool that can be used for the determination of biophysical interactions between small molecules and macromolecules (e.g., interaction of a MGB with DNA).[62-65]

NMR experiments consist in placing a sample in a magnetic field and expose it to high frequency radiation of the appropriate frequency so the nuclei in the sample can absorb energy. The frequency of radiation required to absorb energy depends on three factors: (1) type of nucleus, (2) chemical environment of the nucleus and (3) spatial location in the magnetic field.[66] The nuclear Overhauser effect (NOE) is used to detect through-space interactions.

The structure of DNA–ligand complexes can be determined in solution by ^{1}H-NMR using two-dimensional NOE spectroscopy (NOESY) experiments.[67] With these experiments, ^{1}H–^{1}H coupling constants and through-space NOE-derived distances between the ligand and the DNA can be measured. In contrast to X-ray crystallography, which is performed in the solid state, DNA–ligand complexes are studied in solution (i.e., simulating physiological conditions), which is the main advantage of NMR spectroscopy. NMR gives information of the flexible nature of the DNA or oligonucleotide molecules and the dynamic of the individual groups in motion.[8, 62] However, such experiments have some limitations; first, the NOE is only significant for H atoms. Hence, the phosphate geometry is not directly defined by it, so standard ^{1}H NMR methods provide incomplete information of the nucleotide backbone conformation.[68, 69] Second, the NOE have a short-range effect,

being significant at distances less than 5–6 Å (Note that NOE intensity is proportional to the inverse sixth power of a proton–proton distance).[67]

Nevertheless, both X-ray and NMR techniques should be considered as complementary because they provide different structural information of DNA–ligand complexes.

4.5.2. ^{1}H-NMR studies of compound 3a complexed with AT- and GC-containing oligonucleotides

In this work, we have evaluated the interactions of compound **3a** with oligonucleotides containing $(AT)_4$ and $(CG)_4$ sequences to confirm its mode of binding and selectivity towards the minor groove of AT-rich DNA. We have compared the ^{1}H-NMR spectra of the oligonucleotides with and without **3a** –at different temperatures and concentrations– in order to visualize the effect of ligand binding on the chemical shifts of the DNA bases. Different ^{1}H-NMR spectra of **3a** complexed to $(AT)_4$ oligonucleotide at different Bp/Drug ratios (1:0 to 1:2) were recorded in 90/10 H_2O/D_2O at room temperature (25 ºC). As observed in Figure 4.20, significant shifts in the imino (12.5–14 ppm) and aromatic (7–9 ppm) regions were observed for $(AT)_4$, but not for $(CG)_4$, upon successive additions of **3a** dissolved in DMSO-d_6. This indicates that **3a** binds selectively to the $(AT)_4$ oligonucleotide, which is consistent with the previous data obtained from SPR and CD studies.
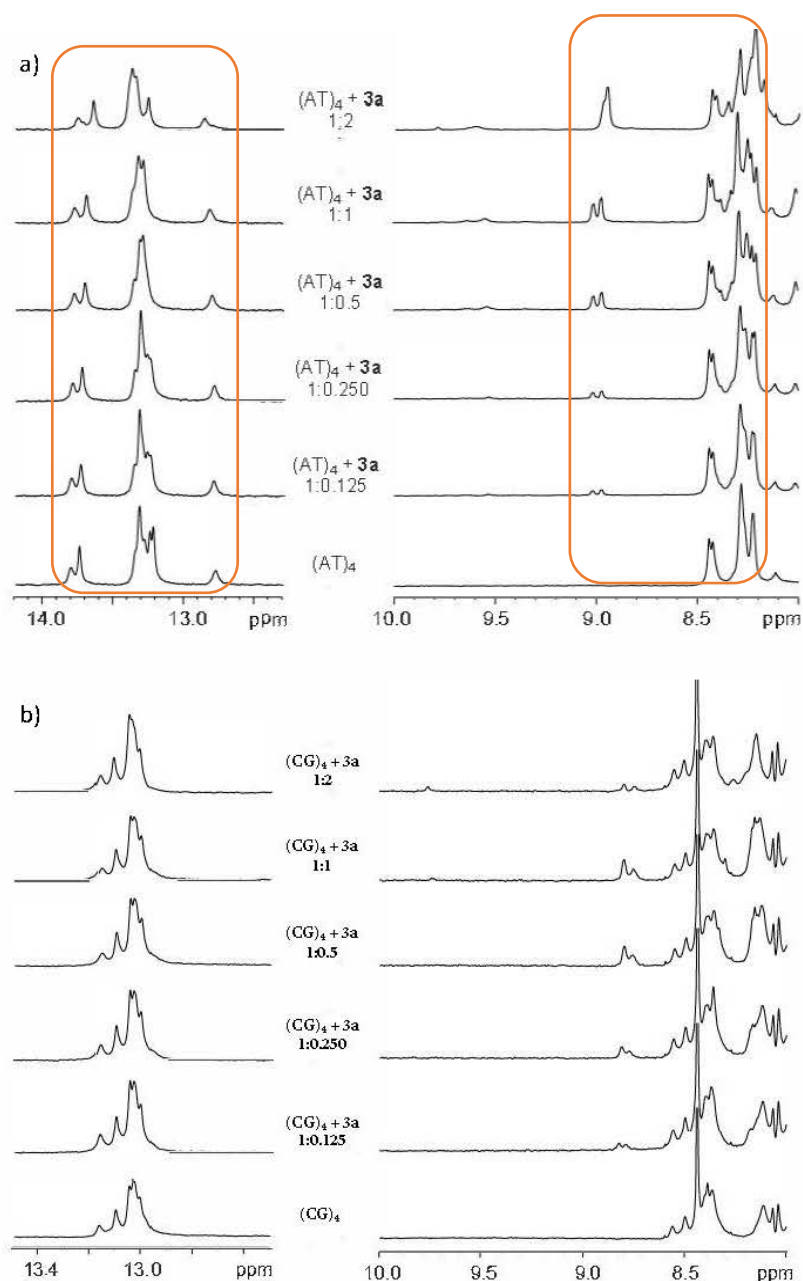
Figure 4.20: Titrations of (a) (AT)$_4$ and (b) (CG)$_4$ (oligonucleotides C = 400 µM, Buffer: 10 mM Na$_2$HPO$_4$, pH 7.1, 100 mM NaCl, 90/10 H$_2$O/D$_2$O) with **3a** (DMSO-d_6) monitored by ^{1}H-NMR spectroscopy at room temperature. Significant changes in the imino (12.5–14 ppm) and aromatic (7–9 ppm) regions are observed for (AT)$_4$, but not for (CG)$_4$, upon successive additions of **3a**.

Melting studies were performed with the oligonucleotide (AT)$_4$ and **3a** using different Bp/Drug ratios (1:1; 1:2). The presence of the imino signals in the ^{1}H-NMR spectra shows the interaction between the oligonucleotide and the ligand (Figure 4.21). These signals disappear between 35 and 45 ºC in all the cases but show slightly higher intensity at 35 ºC in the presence of ligand **3a**. This indicates that bound compound **3a** stabilizes the DNA

double helix on this specific $(AT)_4$ oligonucleotide. This stabilization is consistent with the data previously obtained in the CD and LD experiments (see section 6.4.1. and 6.4.2.). The changes in the imino region supports the hypothesis of initial binding of this drug candidate to AT-rich regions of the minor groove of DNA.
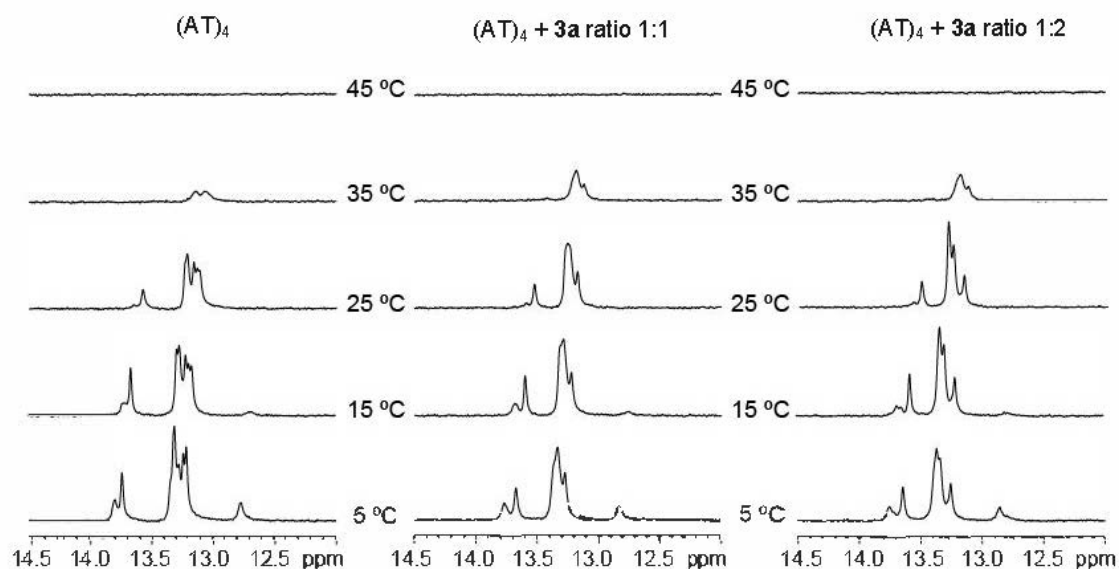
Figure 4.21: Imino region of the ^1H NMR spectra of $(AT)_4$ in the absence (left) and presence of **3a** at 1:1 (middle) and 1:2 (right) DNA:ligand ratios (oligonucleotide C =400 μM, Buffer: 10 mM Na_2HPO_4, pH 7.1, 100 mM NaCl, 90/10 H_2O/D_2O) recorded at different temperatures (5, 15, 25, 35 and 45 ºC). Signals disappear between 35 and 45 ºC in all the cases but show slightly higher intensity at 35 ºC in the presence of ligand **3a**, indicating duplex DNA stabilization.

Once the selectivity to the $(AT)_4$ sequence was set, two-dimensional NOESY experiments were performed to elucidate the interaction of ligand **3a** with DNA at atomic level (Figure 4.22). Clear NOE were detected at $\delta = 9.6$ ppm corresponding to amino groups (NH_2) from the adenine bases. The nature of the NH_2 group was confirmed by performing the same study using deuterated water, in which these interchangeable protons are invisible. NOE signals in the imino proton region ($\delta = 13.4$ ppm) were also detected, indicating the interaction of the ligand even in a 1:1 ratio. The experiments at high ligand concentration (1:2 ratio) NOESY spectra were more difficult to analyse due to the signal overlapping and complexity of the spectra.
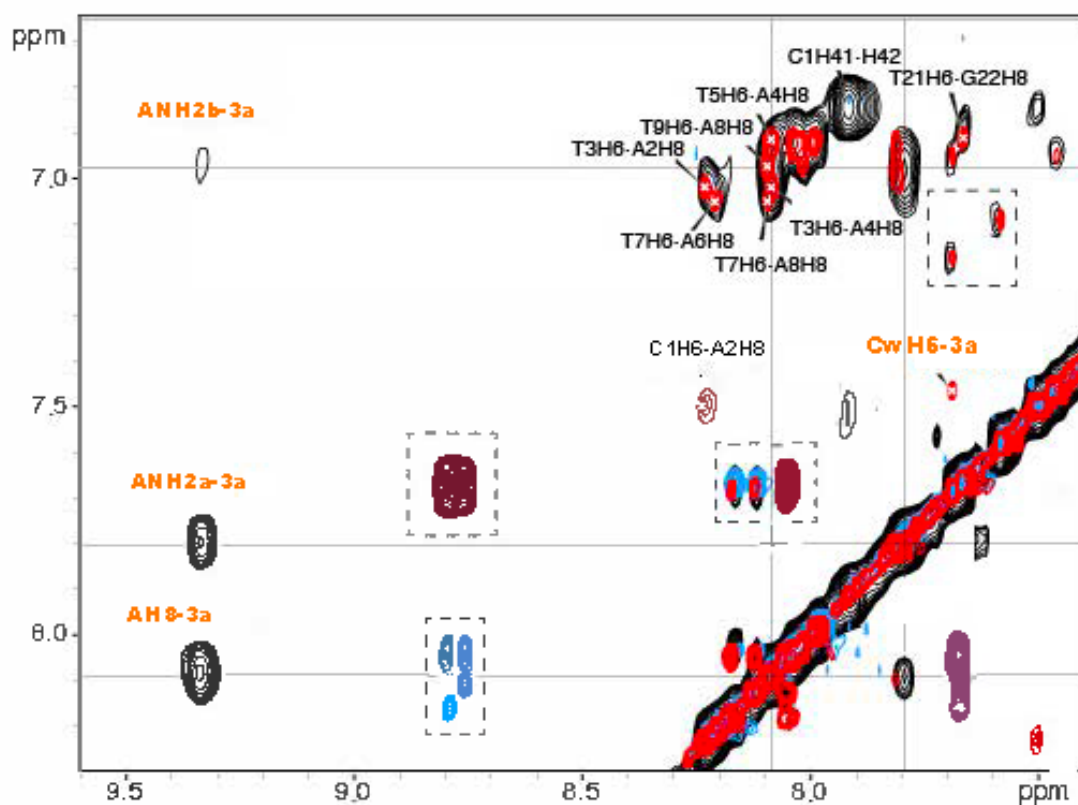
Figure 4.22: Region of the NOESY spectrum of (AT)$_4$:**3a** 1:1 mixture in 90:10 H$_2$O/D$_2$O (black) at 5 °C overlapped with the NOESY (red) and TOCSY (blue) of the same sample acquired in D$_2$O. Cross-peaks between DNA and ligand protons are labelled in orange. Squared signals correspond to intramolecular **3a** cross-peaks.

Altogether, the NMR experiments clearly showed that compound **3a** binds selectively to the (AT)$_4$-containing oligonucleotide, interacting with the NH$_2$ of adenine bases, even at low concentration of ligand. The melting experiments (Figure 4.21) also proved that this interaction increases the stability of the DNA duplex when the complex is formed. The exact interactions as well as the coupling distances for the drug – oligonucleotide complex has yet been solved. Work is still on progress to solve the total spectra.

4.6. Crystallographic studies

The crystallization of macromolecular complexes is an important stage in X-ray crystallographic investigation because it requires well-ordered single crystals of sufficient size. Obtaining crystals does not always indicate that they are well organized and have the proper atomic periodic arrangement required for X-ray crystallography structural resolution. As a result, poor diffraction patterns with low resolution can arise. Getting the correct crystallization conditions for AT-rich DNA to produce diffraction-quality crystals is particularly difficult.[70-72]

The physicochemical properties of the oligonucleotide, the purity of the samples, concentration, pH, temperature, ionic force, precipitants and additives, control of mass transfer (diffusion, convection), and pressure, and the presence of electric and magnetic fields, among other factors, all play a role in the successful crystallization of macromolecules.[71]

The elucidation of the three-dimensional structure of biological macromolecules has contributed enormously to the current understanding of many basic mechanisms involved in life processes. X-ray diffraction from high quality crystals remains the most reliable approach to obtain accurate structural details at atomic resolution. It provides powerful insight into the molecular mechanisms in which macromolecules interact with each other to form complex supramolecular assemblies capable of performing specialized biological functions.[73] Moreover, knowledge of binding sites at atomic detail allows a rational drug design, which is essential for searching of novel drugs. For this reason, X-ray crystallography has been the main technique used for DNA-ligand structure determination up to date.

The following steps are involved in determining the 3D structure using X-ray crystallography: (1) obtaining the target macromolecule (design, synthesis, or expression, and purification), (2) searching for initial crystallization conditions, (3) optimizing crystal quality, (4) diffraction data collection, (5) data analysis and processing, (6) structure determination, (7) 3D model refinement, and (8) validation.

4.6.1. Crystallization Fundaments and Parameters

Macromolecule crystallization is a multi-parametric process that consists of three major steps:

Step 1. **Nucleation**: is the most difficult step since it occurs when a specific number of macromolecules combine to form a critical mass that breaks the energetic barrier of a first-order phase transition and precipitates to the solid state as a nucleus. To avoid amorphous precipitation, this step is performed when the solution is supersaturated and in a meta-equilibrium known as the labile zone (Figure 4.23).[71, 72]

Step 2. **Crystal growth**: Once formed, a nucleus serves as a scaffold centre for the incorporation of macromolecules into a crystal network, typically from a monomeric state. This step occurs in a supersaturated state of metaequilibrium, near the phase boundary known as the metastable zone (Figure 4.23). A solution reaches this state as a result of nucleation, which occurs as the concentration decreases and the solute escapes to the solid state by forming a nucleus. The metastable phase promotes diffusion conditions for ordered molecule incorporation as layer addition over crystallographic faces.

Step 3. **Halt in growth (or cessation of growth)**: concentration decreases after consumption of excess macromolecules during crystal growth, reaching equilibrium when thermodynamic energetics are insufficient for solute to pass to solid state, resulting in the termination of crystal growth.
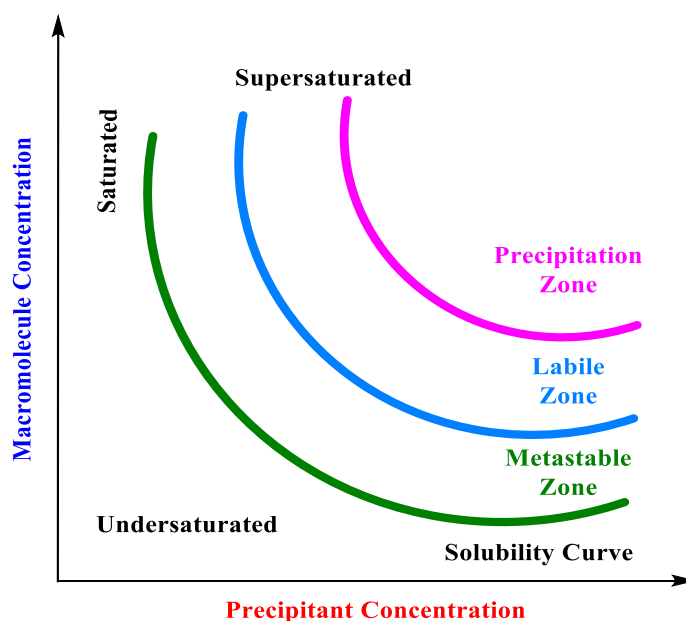
Figure 4.23: Schematic representation of a 2D phase diagram for the crystallization of macromolecules showing the compound solubility as function of precipitant. Labile and metastable zones, where nucleation and crystal growth respectively occur, are indicated.

A two-dimensional phase diagram (Figure 4.23) can be used to depict the entire crystallization process, representing the stable states as a function of two crystallization variables: macromolecule concentration and precipitant concentration. Supersaturation occurs when the concentration of a biomacromolecule solution exceeds its solubility limit. This zone of the diagram can be divided into three regions based on the level of supersaturation: very high supersaturation (precipitation), where molecules form amorphous aggregates; intermediate supersaturation (labile), where nucleation occurs; and lower supersaturation (metastable), where only crystal growth occurs.

The crystallization system in the work presented here is constantly modified as the process evolves by changing the concentrations in the equilibrium solution, particularly for the precipitant. The relationship between macromolecule solubility and precipitant concentration varies depending on the precipitant, but in general, macromolecule solubility decreases proportionally as precipitant concentration increases.[74]

The crystallization of biomacromolecules is a particularly difficult process. The concentration of components in the solution (e.g., macromolecule concentrations and ratio, precipitants, additives), pH, temperature, ionic strength, pressure, electric fields, magnetic

fields, properties that affect mass transfer (e.g., density, viscosity, volume, geometry, diffusion, convection), sample integrity and purity (i.e., heterogeneity of sequence and length, and presence of other molecules) are some variables that influence macromolecule crystallization. There are also experimental contributions and external factors that perturb the system (e.g., vibrations) and influence crystallization. As a result, this multi-variable process is largely empirical in nature and necessitates patience, perseverance, and intuition. The main parameters that are controlled before crystallization are: (1) oligonucleotide concentration; (2) sample purity and homogeneity; (3) pH; (4) drugs (DNA binders); (5) temperature and (6) precipitants.

In the development of this research work, crystallization conditions were based on previous successful conditions reported by us.[10]

4.6.2. Crystallization Method: Vapour Diffusion Technique

Obtaining high-quality single crystals is both the foundation and the limiting step in X-ray structure determination. As a result, numerous macromolecular crystallization methods have been described, each of which employs a unique approach to controlling mass transfer and concentration of all system components in order to achieve supersaturation for crystallization. The method used is determined by the specific requirements and the number of macromolecule(s) available in each case. Vapour diffusion, microbatch, evaporation, micro dialysis, and free-interface diffusion are the most commonly used macromolecular crystallization methods.
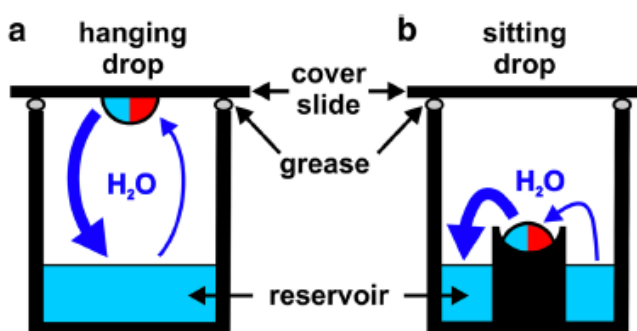
Figure 4.24: Vapour diffusion crystallization techniques. (a) Hanging drop and (b) sitting drop setup. (Taken form *Chem.Texts* **2018**, *4,* 10).[75]

For the purposes of this study, crystallization assays were carried out using the vapour diffusion technique (Figure 4.24), which is the most widely used method for macromolecular crystallization. The two typical vapour diffusion setups are hanging-drop, where a droplet is placed on an inverted cover slip, and sitting-drop, where the droplet is placed on a pedestal. Even though these two methods are in principle similar, the main difference lay on the vapour diffusion path. In sitting-drop method, a droplet of a non-supersaturated solution of macromolecules, precipitants and additives is equilibrated by vapour diffusion against a reservoir containing precipitants and additives in high concentrations, all within a hermetic system. In order to obtain well-ordered crystals, the concentration of all components is gradually changed, bringing the system to a supersaturated state over a period of time.[75, 76]

4.6.3. Crystallization results

Four compounds (**1c**, **1g**, **3a** and **36**) showing promising results as DNA-MGBs in the preliminary biophysical studies were subjected to crystallization. These compounds were selected among the two most active series **1** and **3** (i.e., best binding affinity). Following the hanging drop-protocol, we prepared eight different solutions for each of the five tested AT-rich DNA oligonucleotides (Table 4.8). The crystals were grown by vapour diffusion at 12 ºC on hanging-drops (Figure 4.24). The conditions used for these experiments were previously described by our group[10, 77]: a pre-incubated DNA–compound complex in sodium cacodylate buffer pH 6.5 was added to the drop with final concentrations of 0.2 mM DNA duplex, 0.4 mM compound, 25 mM sodium cacodylate (NaCac) buffer pH 6.5, 10 mM salt, 0.1 mM spermine and 5% 2-methyl-2,4-pentanediol (MPD); equilibrated against a 20% MPD reservoir. MPD acts both as a precipitant and a cryoprotectant. The concentration of the reservoir was increased gradually up to 50% MPD. As crystals were growing and MPD was increased, the samples were moved to 12, 10, 8, 4 and 0 ºC, to avoid degradation. Finally, the crystals obtained with the tested compounds were flash-frozen in the cold room (4 ºC) and stored in liquid Nitrogen. This step is required ato be performed in the cold room as fishing the right crystals require time and temperature can destroy the formed crystals.
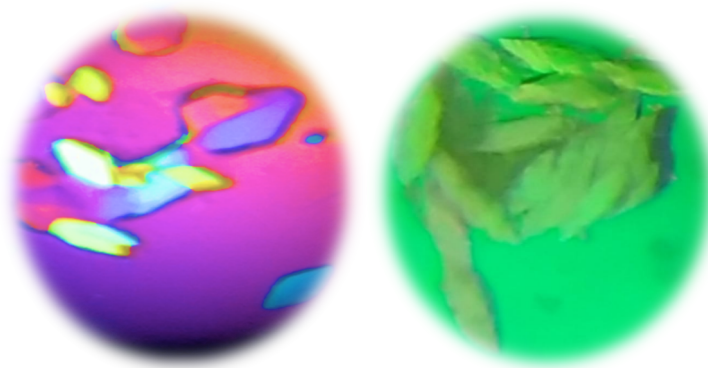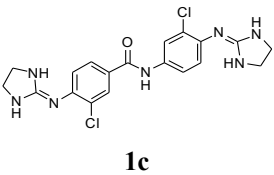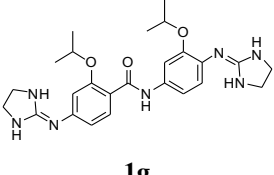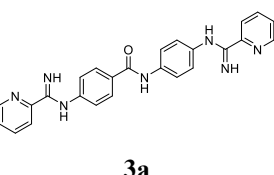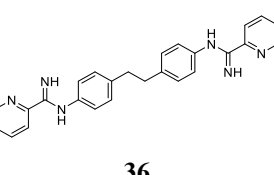
Figure 4.25: Under the right conditions, **3a** crystals grow in the drop as shown in the picture. Crystals with 16 mM $MgCl_2$ (right) and with 6 mM $MnCl_2$ (left).

The crystals obtained were continuously evaluated and scored to monitor their evolution. The best crystals were selected at first based on a visual inspection (size, shape and defects). A second inspection was carried out under polarized light to evaluate the birefringence of the crystal, which is an indicator of the internal order of the crystal (Figure 4.25). It can be used additionally to identify a twinned crystal (macle) by the presence of two polarizing domains. Selected crystals were fished from the droplet using a cryo-loop that catches only one crystal in a thin layer of liquid by surface tension.

As the crystallization conditions already contained MPD - which works as a cryo-protectant - the crystals were directly transferred from the cryo-loop to a Dewar with liquid nitrogen for flash freezing immediately after fishing. Fished crystals were stored and transported at liquid nitrogen temperature until X-ray diffraction.

Additionally, other crystals have been obtained that are growing following the described protocol. The most suitable growing conditions are in the presence of salts like $Mg(CH_3CO_2)_2$, $MnCl_2$ and $MgCl_2$. These new crystals are under evaluation and conserved at the correct temperature until they are in the ideal size to be fished and frozen for X-ray analysis.

Table 4.8: Final concentration of hanging drops.[a]

Drug (0.4 mM)	Oligonucleotide (0.2 mM)	Buffer (25 mM)	Salt Concentration (mM)[a]	
1c	d(CGAATTAATTCG) d(AATAATTATT) d(CGCAAATTTGCG) d(AAATATATTT) d(ATTAATTAAT)	NaCac[b] pH = 6.5	$Mg(CH_3CO_2)_2$	8
				10
			$MnCl_2$	6
				8
			$NH_4CH_3CO_2$	8
				10
				25
			$MgCl_2$	16
1g	d(CGAATTAATTCG) d(AATAATTATT) d(CGCAAATTTGCG) d(AAATATATTT) d(ATTAATTAAT)	NaCac pH = 6.5	$Mg(CH_3CO_2)_2$	8
				10
			$MnCl_2$	6
				8
			$NH_4CH_3CO_2$	8
				10
				25
			$MgCl_2$	16
3a	d(CGAATTAATTCG) d(AATAATTATT) d(CGCAAATTTGCG) d(AAATATATTT) d(ATTAATTAAT)	NaCac pH = 6.5	$Mg(CH_3CO_2)_2$	8
				10
			$MnCl_2$	6
				8
			$NH_4CH_3CO_2$	8
				10
				25
			$MgCl_2$	16
36	d(CGAATTAATTCG) d(AATAATTATT) d(CGCAAATTTGCG) d(AAATATATTT) d(ATTAATTAAT)	NaCac pH = 6.5	$Mg(CH_3CO_2)_2$	8
				10
			$MnCl_2$	6
				8
			$NH_4CH_3CO_2$	8
				10
				25
			$MgCl_2$	16

[a]Spermine 0.2 mM and precipitant 3 % (v/v). [b]Sodium cacodylate.

4.6.4. X-Ray diffraction results

After the X-ray diffraction on the chosen crystals has been completed and the data has been obtained, mathematical analysis is used to investigate the diffraction pattern. The aim behind the examination and translation of the diffraction information is to solve the density function to reveal the structure of the macromolecule(s) under study. The components of the unit cell, the space symmetry and the adequacy for all diffraction directions are data that can be extricated from the diffraction patterns. As it is not possible to determine the diffractions phase directly (i.e., the 3-dimensional arrangement of the atoms), data analysis is done in two stages: (1) data reduction, which involves indexing, parameter refinement and integration; and (2) merge and scaling. Indexing the reflections (i.e., to identify the dimensions) of the unit cell and assigning image peak to correspondent position in reciprocal space is the first stage of the data analysis. In order to perform indexing and integration, Dr. Campos' group runs the analysis using the programs iMOSFLM[78] and XDS,[79] then REFMAC and COOT.

Crystals obtained with compound **1c**, **3a** and **36** were flash-frozen and stored in liquid nitrogen. The sample was transported to the Macromolecules crystallography laboratory to be analysed in the beamline BL13–XALOC at ALBA Synchrotron,[80] Barcelona, Spain. The main data collection detector was PILATUS 6M-Dectris, capable of recording up to 12 images per second. The active area is 424×435 mm, 6M pixels. During data collection, the crystal was cooled with liquid nitrogen all the time (Figure 4.26).
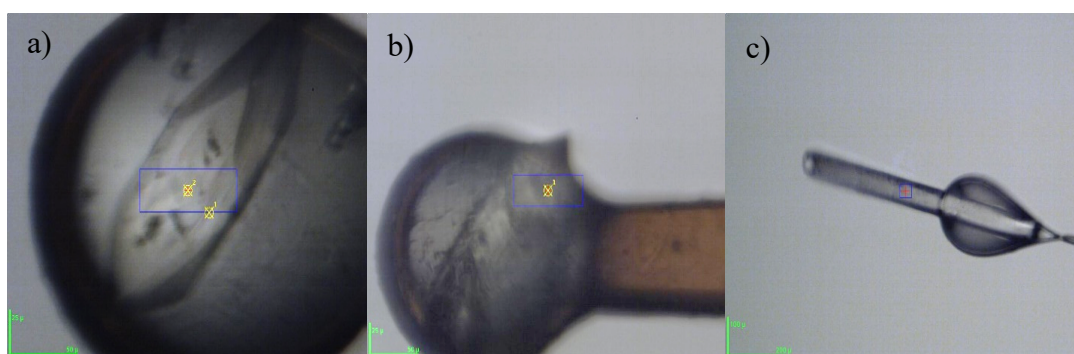
Figure 4.26: Position of the crystal of **3a** and **d(AAATATATTT)** decamer complex centered on the beam just before diffracting, at Alba synchrotron. (a) and (b) crystal at 25×50 µm scale. (c) bladed crystal fished at 100×200 µm scale.

Compounds **1c**, **3a** and **36** produced crystals in different conditions (see Appendix 3) whereas solutions of compound **1g** did not grow any crystal up to the date of writing of this thesis. This could be related to the presence of the hydrophobic isopropoxy groups on the *N*-phenylbenzamide scaffold. Bulky groups tend to hide inside the DNA minor groove avoiding the interaction between the central atoms (O and NH) from the amide linker and the A–T bases. This interaction (H-bond interaction) between the NH of the amide bridge of our compounds and the minor groove is hypothesised as being essential for the binding of our compounds to the oligonucleotide.
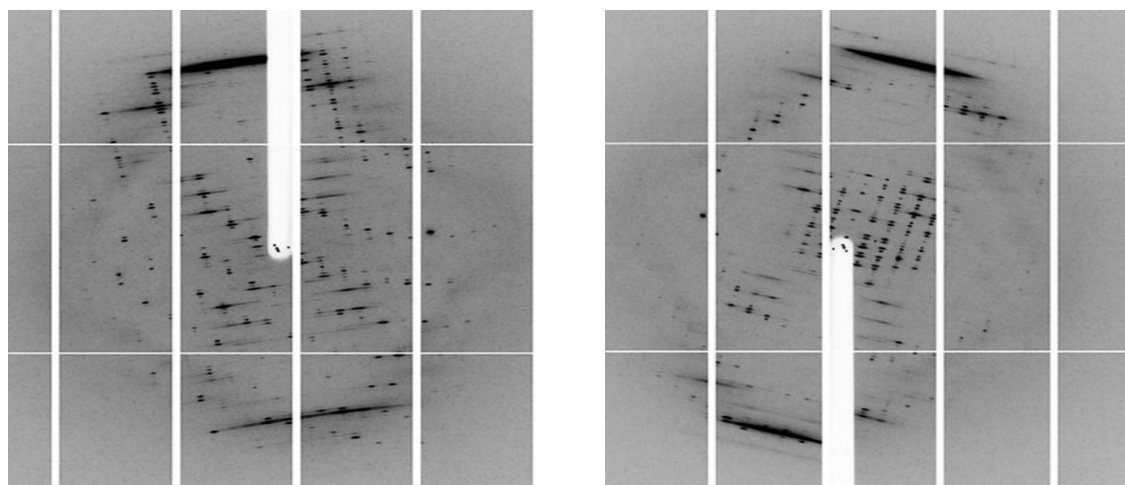
Figure 4.27: X-ray diffraction of complex **3a** and **d(AAATATATTT)** crystallized in the presence of 16 mM MnCl$_2$.

Nevertheless, we were able to obtain some diffraction patterns for compound **3a** crystallized with d(AAATATATTT) oligonucleotide. As shown in Figure 4.27, in this crystal structure the oligonucleotide is better ordered and stacked in columns of six oligonucleotides in a helical arrangement. In this model, the twist in the TA base step between neighbour duplexes is negative (approximately −22°). This is consistent with the information reported by Campos *et al.* showing that the organization of AT duplexes is regular and repetitive, mainly determined by the stacking of the terminal base pairs. As a result, the twist in the virtual TA base step between neighbour duplexes is always negative (∼ −22 °).[70]

The unit cell parameters are: *a* and *b* = 42 Å and *c* = 197 Å; *c* parameter is the length of the six stacked bases on the oligonucleotide forming the helix. Although this structure is stabilized by the interaction with compound **3a**, we were not able to localize it due to the

lack of perfect order in the crystal structure. This crystal can be indexed to a pseudo hexagonal spatial group.

4.6.5. Conclusions

In spite of our efforts, we were not able to elucidate any crystal structure yet. Some crystals grew twinned and other were poorly ordered. The typical X-ray diffraction pattern of B-DNA[81] was observed on fibers obtained with **3a** (Figure 4.27). However, other crystals are still growing at UPC laboratory in Barcelona, under the supervision of Drs. Lourdes Campos and Núria Saperas. The X-ray diffraction of these new crystals will be carried out at ALBA synchrotron in the second semester of 2022.

4.7. Computational studies

The aim of the computational studies was to dock series **3** compounds into the DNA duplex d(AAATTT)$_2$, which crystal structure complexed with lead compound **I** is available from the Protein Data Bank [PDB: 5LIT].[10, 82] The docking results should shed light on the interactions that are important for binding of series **3** compounds with the minor groove of AT-DNA. Computational studies were performed under the supervision of Dr. Cristina Trujillo at Trinity College of Dublin, Ireland. Computational calculations were performed at the Irish Centre for High-end Computing (ICHEC).

4.7.1. Theoretical study - Outcome

The protonation state of the molecule will have a direct influence on its mode of binding to the DNA minor groove via H-bonding interactions. Therefore, we started by studying the different sites of protonation of the synthesised compounds.
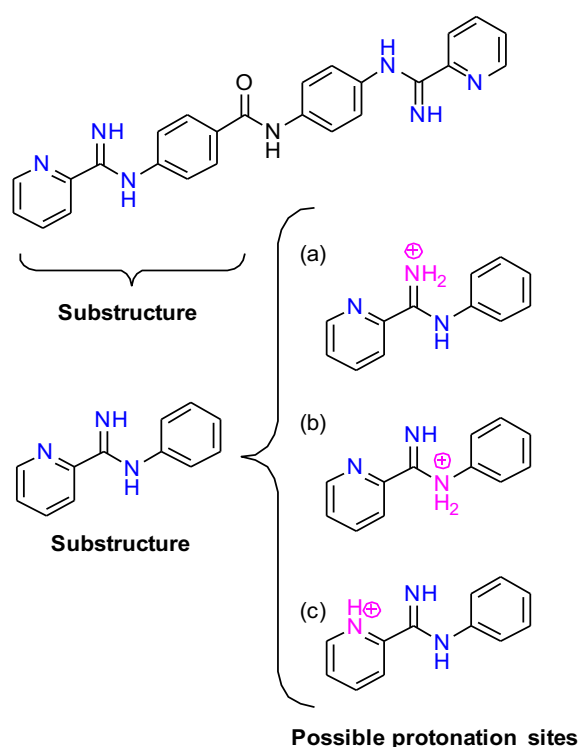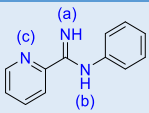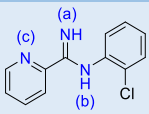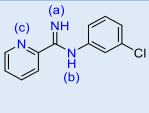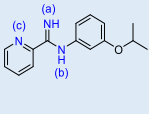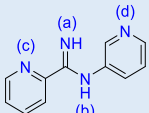
Figure 4.28: Substructures of bis(*N*-phenyl-pyridin-2-carboxamidines) derivatives with possible protonation sites

As bis(*N*-aryl-pyridin-2-carboxamidines) derivatives have three possible protonation centres on each side of the molecule (blue nitrogen atoms), we decided to use the smaller

(i.e., less computationally-demanding) substructures shown in Figure 4.28 (a, b or c) to evaluate where the protonation is most likely to happen in the gas phase.

All possible combinations were evaluated for each compound, taking into account the substituents and the effect it can exert on the pyridine-2-carboxamidine residue. The relative energies of each substructure were calculated, as well as Boltzmann population, in order to rank the most stable and abundant protonated substructure. Results in Table 4.9 show that, in the gas phase, protonation occurs preferably in position (a), in all the cases.

Table 4.9: Relative energy calculated for protonated and non-protonated substructures
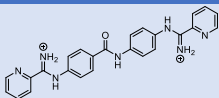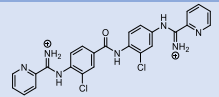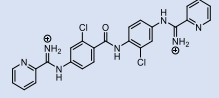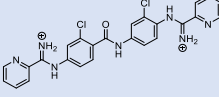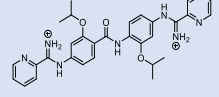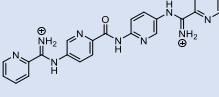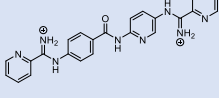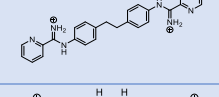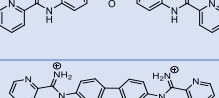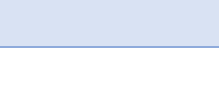
Structure	Protonation	Relative energy (kcal/mol)	Boltzmann population (%)
	Not protonated	a	b
	(a)	0.00	100.0
	(b)	28.71	0.0
	(c)	21.02	0.0
	Not protonated	a	b
	(a)	0.00	100.0
	(b)	28.11	0.0
	(c)	19.56	0.0
	Not protonated	a	b
	(a)	0.00	100.0
	(b)	27.06	0.0
	(c)	26.16	0.0
	Not protonated	a	b
	(a)	0.00	100.0
	(b)	26.75	0.0
	(c)	28.34	0.0
	Not protonated	a	b
	(a)	0.00	100.0
	(b)	37.49	0.0
	(c)	25.08	0.0
	(d)	10.97	0.0

[a] Value not considered in the Boltzmann population calculation. [b] Not calculated

Once the most stable protonation site was found, we built the entire structures of bis(*N*-aryl-pyridin-2-carboxamidines) **3a–i**, **36**, **37**, and **53**. Optimization of these structures was

performed with Gaussian 09[83] using the density functional theory (DFT) with the 6–31+G(d)[84, 85] basis set, to obtain a good starting point for the docking studies. Frequency calculations have been performed at the same computational level to confirm that the resulting optimized structures are energetic minima.

Table 4.10: Conformational analysis of compounds **3a–i**, **36**, **37**, and **53**

Cmpd	Structure	Conformation	Relative energy (kcal/mol)	Boltzmann population (%)
3a		Closed	5.28	0.0135
		Open	0.00	99.9865
3b		Closed	5.15	0.0168
		Open	0.00	99.9832
3c		Closed	5.14	0.0171
		Open	0.00	99.9829
3d		Closed	5.38	0.0114
		Open	0.00	99.9886
3e		Closed	5.00	0.0216
		Open	0.00	99.9784
3g		Closed	5.55	0.0085
		Open	0.00	99.9915
3h		Closed	5.20	0.0154
		Open	0.00	99.9846
3i		Closed	5.09	0.0186
		Open	0.00	99.9814
36		Closed	4.81	0.0298
		Open	0.00	99.9702
37		Closed	6.06	0.0036
		Open	0.00	99.9964
53		Closed	7.65	0.0002
		Open	0.00	99.9998

Conformational analyses were carried out using two conformations for each compound (i.e., closed and open conformations, e.g., Figure 4.29). As shown in Table 4.10, the open

conformations of the dicationic compounds were the most stable. Consequently, they were chosen for the docking studies.
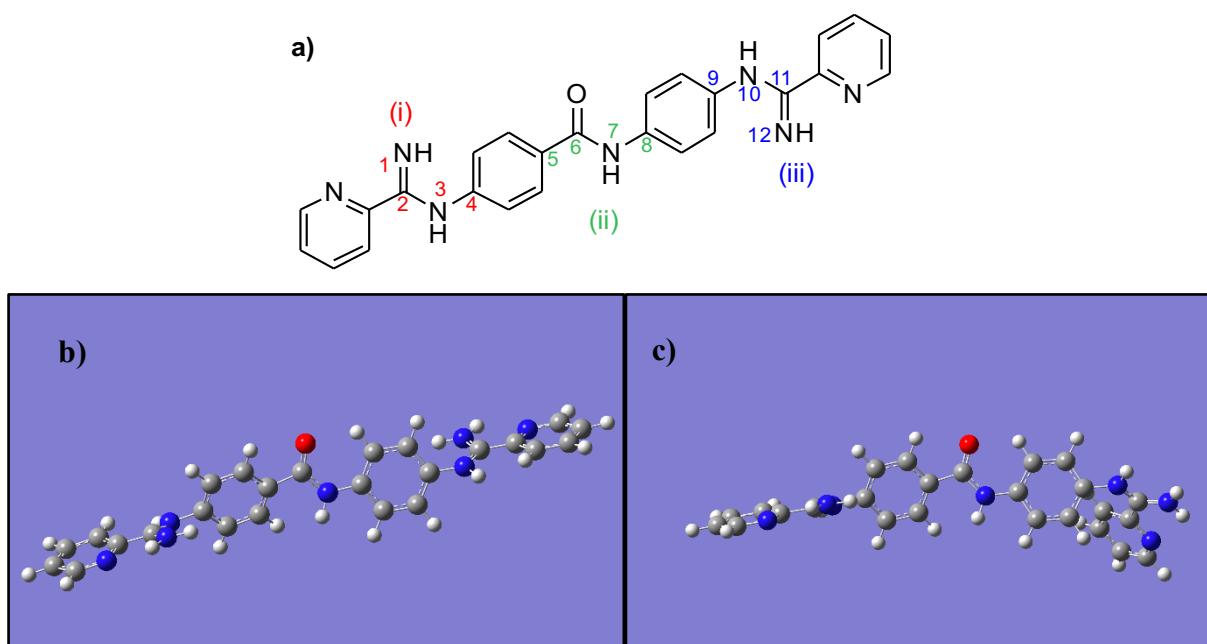
Figure 4.29: Structure of compound **3a** showing atom number labels (a), and optimized open (b) and closed (c) structures. **b)** Open structure refers to a non-constrained structure with the following dihedral values: (i) N1-C2-N3-C4 = -2.98°), (ii) C5-C6-N7-C8 = +179.55° and (iii) C9-N10-C11-N12 = -2.51°. **c)** Closed (or constrained) structures have dihedral values: (i) N1-C2-N3-C4 = -3.59°, (ii) C5-C6-N7-C8 = -179.86°, and (iii) C9-N10-C11-N12 = -163.45°.

4.7.2. Docking studies

Docking studies were performed using the Autodock Vina 1.1.2[86, 87] program in a flexible-rigid approach. The selected compounds (i.e., open conformation) from series **3** (**3a–i, 36, 37**, and **53**) were docked into the DNA duplex d(AAATTT)$_2$, which crystal structure complexed with compound **I** is available from the Protein Data Bank [PDB: 5LIT].[10, 82] The PDB file for DNA–ligand crystal 5LIT[10, 82] was prepared by removing the solvent, salts and metal ions using AutoDockTools 1.5.4.[88] The coordinates of the binding site around the crystallised ligand (compound **I**) were found using the AutoGrid function and the ligand was removed. The macromolecule was saved as a ".pdbqt file". Finally, two sections of the crystal (repeated subunits) were removed and file was recorded as 5LIT-short. To ensure this action does not affect the analysis, a docking simulation using the previous crystallised lead compound **I** was performed. No changes were observed, and the same docking parameters were found. Hence, we decided to use this 5LIT-short to perform

the docking studies. The docking binding scores between the ligands and the target, are shown in Table 4.11

Table 4.11: Docking binding score (in order of decreasing affinity) vs. binding affinity (as determined by thermal melting experiments).

Cmpd.	Structure	Binding score (kcal/mol)	ΔT_m (°C)
53		-9.3	11.0
3i		-9.3	1.8
3d		-8.2	5.1
3h		-8.2	2.3
3a		-8.1	5.9
3b		-8.1	5.2
3e		-8.1	8.9
3c		-8.0	1.6
36		-7.7	8.0
37		-7.7	1.6
3g		-6.9	6.1

[a] Not observed at a maximum concentration of 100 μM

Compounds **53** and **3i** showed the best docking affinities (-9.3 kcal/mol). For DNA minor groove binders, Van der Waals, hydrophobic and electrostatic interactions contribute significantly to the binding affinity of the ligands, as well as polar interactions such as H-bonds.[89] As observed in Figure 4.30a, **53** forms two H-bonds (2.34 Å and 2.35 Å) between the amidino NH_2 groups of the ligand and the oxygen atoms of thymine 4 and sugar backbone (O3'–H310 and O2–H303) at the minor groove floor. In contrast, docking of **3i** reveals only one H-bond interaction (2.40 Å) between the amide NH group (H21) of the ligand and the oxygen atom (O183) of the thymine 1 base (Figure 4.30b). In this case, this strong HB interaction seems to contribute to the stabilization of the DNA-ligand complex.
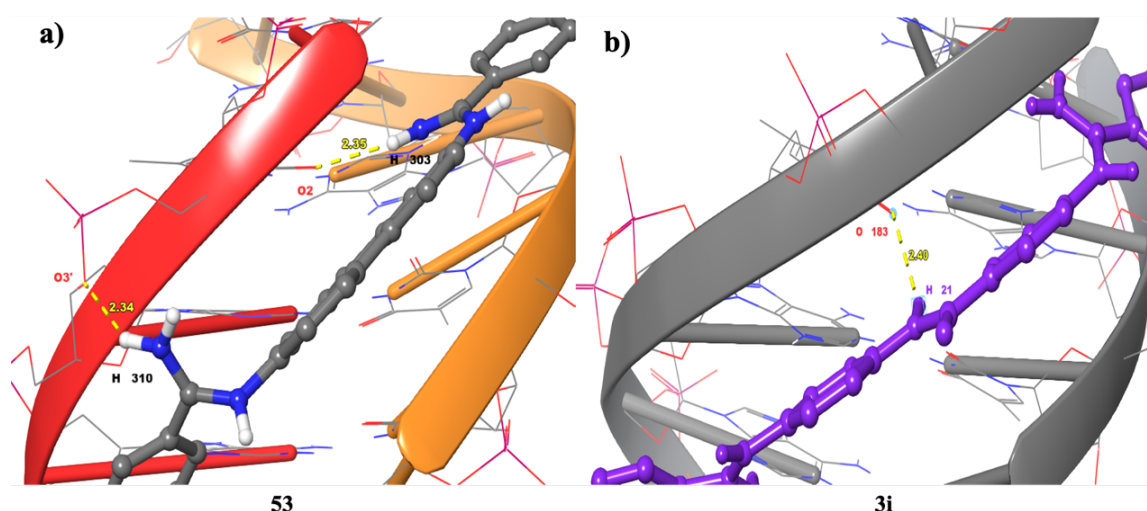
Figure 4.30: Docking of **53** (left) and **3i** (right) showing the main interactions (H-bonds) with the 5LIT crystalline structure. Distances between atoms are reported in Å (yellow dotted lines). **a)** H-bonds: (O3'–H310, distance = 2.34 Å), (O2–H303, distance = 2.35 Å). **b)** H-bond: (O183–H21, distance = 2.40 Å).

Compounds **3d**, **3h**, **3a**, **3b**, **3e** and **3c** present similar docking scores (-8.2 to -8.0 kcal/mol) but a dissimilar binding mode. Among the di-chlorinated derivatives (**3b–e**), only **3b**, **3c** and **3e** share a H-bond between the anilino NH group (H12) linked to the phenyl ring of the scaffold and O176 (**3b** and **3e**) or O79 (**3c**) (from the sugar backbone) from the d(AAATTT)$_2$ oligonucleotide (Figure 4.31).
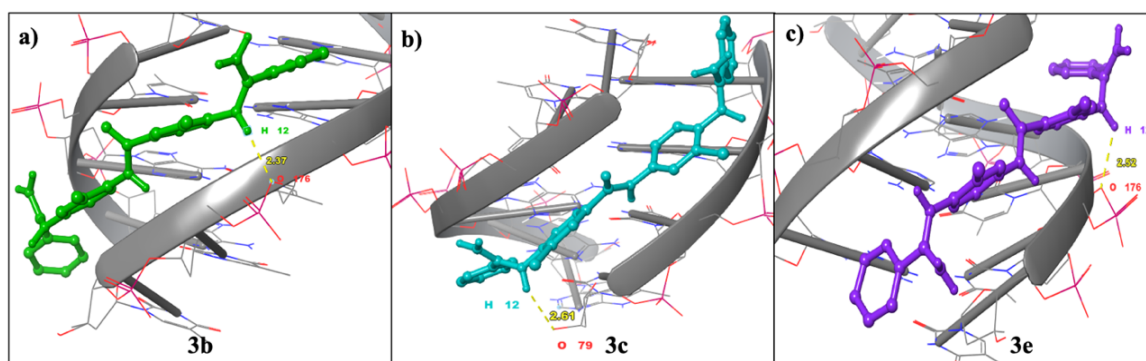
Figure 4.31: Docking of **3b**, **3c**, and **3e** showing the main interactions (H-bonds) with the 5LIT crystalline structure. **a) 3b** (H-bond: O176–H12, distance = 2.37 Å); **b) 3c** (H-bond: O79–H12, distance = 2.61 Å); and **c) 3e** (H-bond: O176–H12, distance = 2.52 Å); H-bond distances between atoms (yellow dotted lines) are reported in Å.

In contrast, chlorinated derivative **3d** shows a different binding mode with two H-bonds (O216–H10, 2.03 Å and O188–H41, 2.52 Å) between the amidino NH_2 groups of the ligand and the oxygen atoms of the sugar backbone of DNA (Figure 4.32a). Remarkably, this is the only derivative that shows two halogen-bond interactions (Cl27–H166, 3.13 Å and Cl27–H84, 3.28 Å) with the adenine 3 and thymine 1 bases (Figure 4.32b).
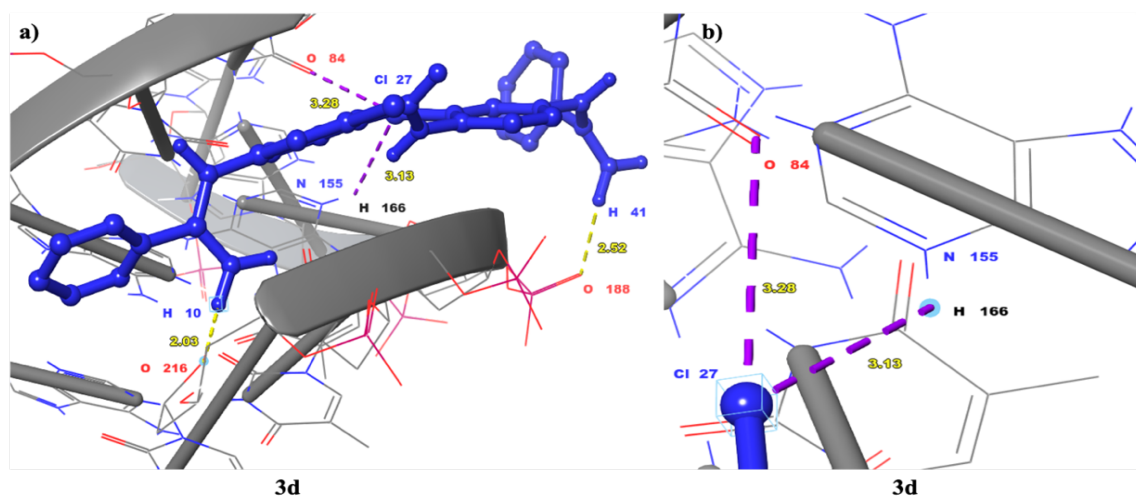
Figure 4.32: Docking of **3d** showing the main interactions with the 5LIT crystalline structure. **a) 3d** (O216–H10, distance = 2.03 Å and O188–H41, distance = 2.52 Å); **b) 3d** (Cl27–H166, distance = 3.13 Å and Cl27–H84, distance = 3.28 Å); Distances between atoms are reported in Å (yellow).

The dipyridine derivative (**3h**) only displays one H-bond (O190–H40, 2.66 Å) between the amidino NH_2 of the ligand (H40) and the oxygen (O190) of thymine 1, indicating a different binding interaction with respect to the chlorinated derivatives **3b–e** (Figure 4.33).
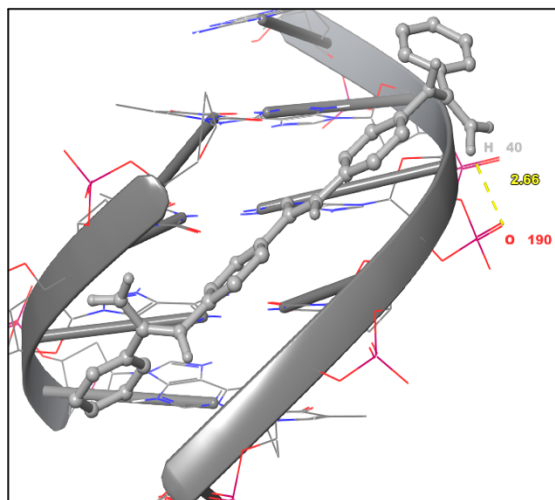
Figure 4.33: Docking of **3h** showing the H-bond interaction (O190–H40, distance = 2.66 Å) with the 5LIT crystalline structure. The distance between atoms is reported in Å (yellow).

Compound **3a** interaction with the minor groove of the DNA duplex is characterized by the presence of a strong H-bond (H44–O434, 1.95 Å) between the amide NH of the *N*-phenylbenzamide scaffold (H44) and the oxygen (O434) of thymine 4 residue (Figure 4.34a). This is different from the chlorinated derivatives **3b–e** where H-bond interactions with DNA occur via the anilino NH group directly linked to the phenyl ring of the scaffold. A second H-bond (O467–H39, 1.43 Å) between the amidine NH_2 of the ligand and the O atom of the sugar backbone also helps to stabilize the complex of **3a** with DNA (Figure 4.34b). Compound **3a** also shows $\pi – \pi$ stacking interaction (ring-to-ring distance of 5.16 Å) between the phenyl ring of the scaffold [C18, C19, C20, C21, C22 & C23] and the adenine 3 residue [C414, C415, C418, C420, N417 & N419] (Figure 4.34c). Additionally, three aromatic H-bond interactions (O434–H45, 1.57 Å), (O314–H43, 2.79 Å) and (O469–H37, 2.77 Å) are observed. Of note, these interactions are only observed in compound **3a**, regardless all of the proposed compounds present the same aromatic scaffold. Altogether, these stabilizing interactions may explain the potent DNA minor groove binding affinity observed for **3a** (ΔT_{m} = 5.9 °C, binding score = -8.1 kcal/mol).
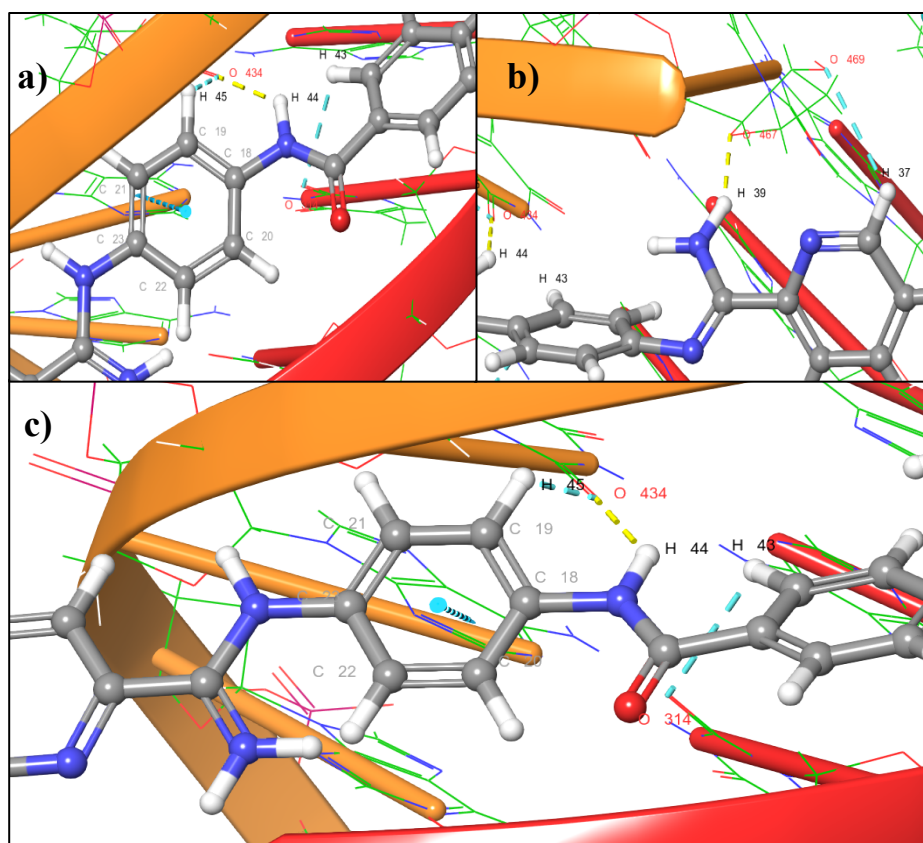
Figure 4.34: Docking of compound **3a** showing the H-bonds, aromatic bonds and $\pi - \pi$ interactions with the 5LIT crystalline structure. **a)** Central H-bond between the amide NH of the scaffold (O434–H44, distance = 1.95 Å) and aromatic H-bond interactions (O434–H45, distance = 1.57 Å; O314–H43, distance = 2.79 Å); **b)** Second H-bond with the amidino NH_2 of the scaffold (O467–H39, distance = 1.43 Å) and aromatic H-bond (O469–H37, distance = 2.77 Å); **c)** $\pi - \pi$ interaction with the phenyl ring of the scaffold (C18, C19, C20, C21, C22 & C23) and the oligonucleotide ring (C414, C415, C418, C420, N417 & N419) with a ring-to-ring distance = 5.16 Å.

Docking and schematic representations of the interactions between **3a** and d[AAATTT]$_2$ are shown in Figures 4.35-4.36. According to the docking results, and based on a previous study in which lead **I** fit the minor groove of the d(AAATTT)$_2$ in a similar way,[10] the presence of the central H-bond between the amide NH of the scaffold and the carbonyl of thymine T4 is, in some way, director of the fitting inside the minor groove (Figure 4.35). In the case of the fluorene derivative **53**, which lacks this H-bond interaction due to the absence of the central amide bridge in its structure, the potent binding affinity (ΔT_{m} = 11 ºC, binding score = -9.3 kcal/mol) may be explained by the interaction of the two amidino NH_2 residues of the *N*-aryl-pyridin-2-carboxamidine groups with the DNA bases and the sugar backbone.
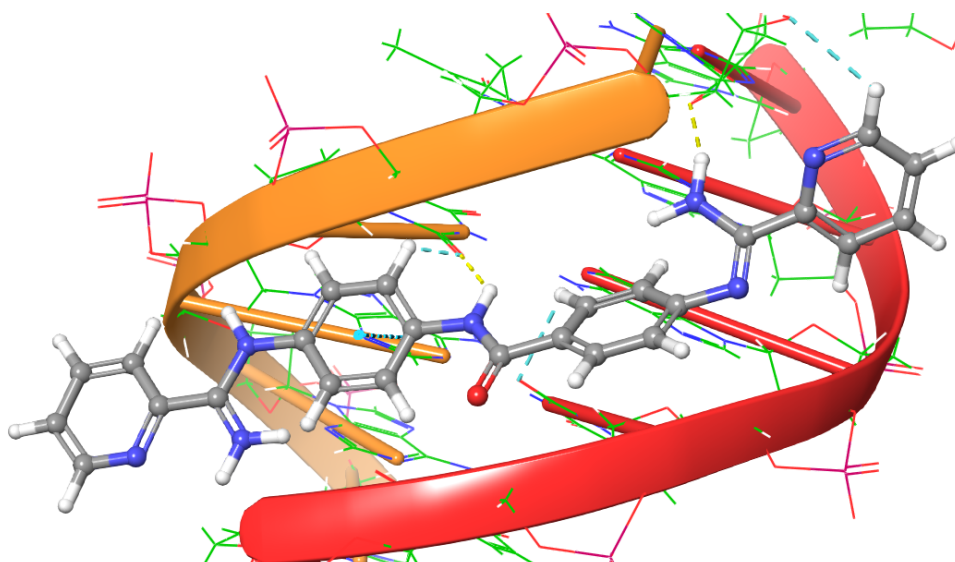
Figure 4.35: Molecular docking of **3a** with d(AAATTT)₂ oligonucleotide (PDB: 5LIT) showing all the interactions.
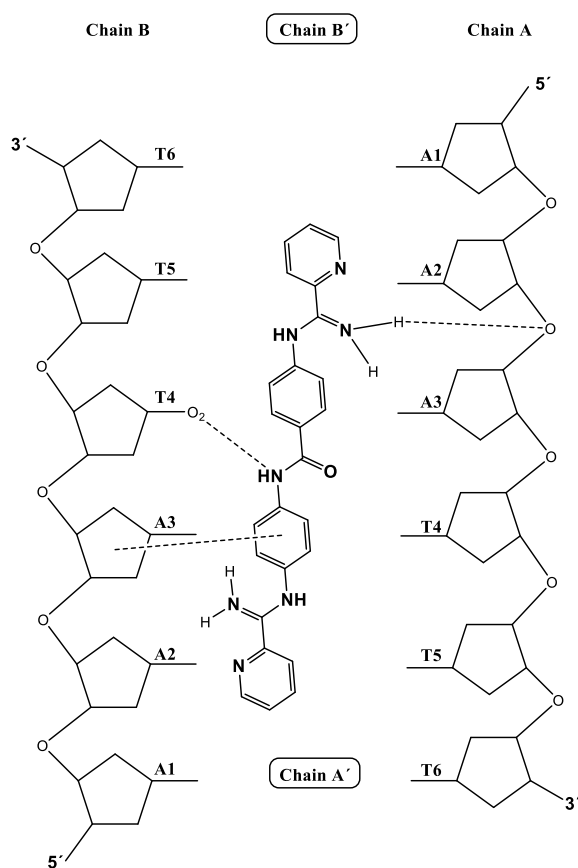
Figure 4.36: Schematic representation of the interactions between **3a** and d[AAATTT]₂, proposed according to the data observed in the docking study. Symmetric chains are indicated with apostrophe. A and T indicates Adenine and Thymine, respectively.

Compounds **36** and **37** have the same binding score (-7.7 kcal/mol). The urea derivative **37** shares only one H-bond (O63–H10, 2.16 Å) between the amidino NH_2 group and the carbonyl oxygen of thymine 5. Apparently, the length and rigid nature of the urea linker does not allow the compound to match the curvature of the groove (Figure 4.37b). In contrast, compound **36** with an ethylene linker of the same length as the original amide bridge (**3a**) seems to fit better into the groove. The docking results show that **36** has two H-bond interactions with the d(AAATTT)$_2$ oligonucleotide (Figure 4.37a): the first one (O223–H28, 1.99 Å) between the anilino NH directly linked to the scaffold is similar to that observed with halogen derivatives **3b**, **3c** and **3e**. The second H-bond (O7–H37, 2.55 Å) occurs between the amidino NH_2 group of the ligand and the oxygen atom of the sugar backbone. Altogether, these observations may explain why **36** displays a much stronger binding affinity to AT-containing DNA than **37** (ΔT_m = 8 °C and 1.6 °C, respectively).
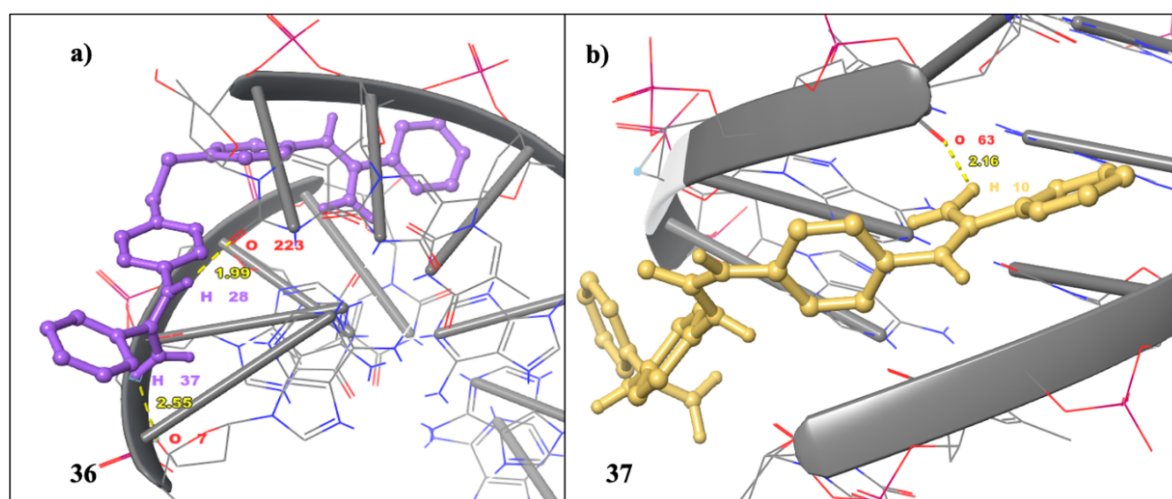
Figure 4.37: Docking of **a) 36** shows two H-bonds (O223–H28, distance = 1.99 Å and O7–H37, distance = 2.55 Å); **b) 37** H-bond (O63–H10, distance = 2.16 Å); with the 5LIT crystalline structure. Distances between atoms are reported in Å (yellow).

As regards to derivative **3g**, the lower docking score (-6.9 kcal/mol) may be due not only to the steric clash of the large isopropoxy substituents with the curvature of the minor groove but also to electronic repulsion. Furthermore, this steric hindrance does not allow the correct interaction of the central amide NH of the scaffold to form an H-bond, as with compound **3a** (Figure 4.38).
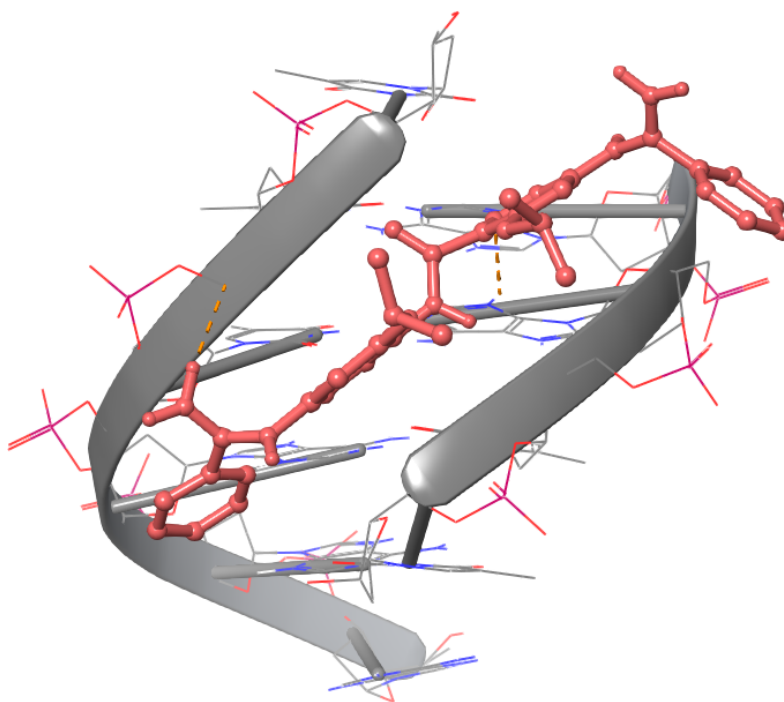
Figure 4.38: Docking of **a) 3g** no interaction with the 5LIT.

4.7.3. Conclusions

The lack of correlation between the binding scores and the DNA binding affinities determined by thermal melting experiments may be due to several factors:

- Docking experiments are performed in absence of solvent, which makes a big difference, as compounds in solution are able to interact forming H-bond using water molecules.[50]
- In this study, the positive charge is fixed on the most stable ligand conformation, offering a limited H-bond capability, even though in real conditions this is delocalized over the surrounding N atoms.[89]
- For DNA binding, some drugs require divalent cations such as Mg^{2+}.[89]

We plan to perform Molecular Dynamics with these compounds in order to get better match between the DNA binding results and the computational calculations.

4.8. References

1. Rahman, A.; O'Sullivan, P.; Rozas, I. Recent developments in compounds acting in the DNA minor groove. *MedChemComm* **2019,** 10, 26-40.

2. Wilson, W. D.; Nguyen, B.; Tanious, F. A.; Mathis, A.; Hall, J. E.; Stephens, C. E.; Boykin, D. W. Dications that target the DNA minor groove: compound design and preparation, DNA interactions, cellular distribution and biological activity. *Curr. Med. Chem.: Anti-Cancer Agents* **2005,** 5, 389-408.

3. Neidle, S. *Principles of Nucleic Acid Structure*. 1st edition ed.; Elsevier: 2008.

4. Neidle, S. DNA minor-groove recognition by small molecules. *Nat. Prod. Rep.* **2001,** 18, 291-309.

5. Nagle, P. S.; Quinn, S. J.; Kelly, J. M.; O'Donovan, D. H.; Khan, A. R.; Rodriguez, F.; Nguyen, B.; Wilson, W. D.; Rozas, I. Understanding the DNA binding of novel non-symmetrical guanidinium/2-aminoimidazolinium derivatives. *Org. Biomol. Chem.* **2010,** 8, 5558-5567.

6. Bailly, C.; Chaires, J. B. Sequence-Specific DNA Minor Groove Binders. Design and Synthesis of Netropsin and Distamycin Analogues. *Bioconjugate Chem.* **1998,** 9, 513-538.

7. Neidle, S.; Kelland, L. R.; Trent, J. O.; Simpson, I. J.; Boykin, D. W.; Kumar, A.; Wilson, W. D. Cytotoxicity of bis(phenylamidinium)furan alkyl derivatives in human tumour cell lines: Relation to DNA minor groove binding. *Bioorg. Med. Chem. Lett.* **1997,** 7, 1403-1408.

8. Francesconi, I.; Wilson, W. D.; Tanious, F. A.; Hall, J. E.; Bender, B. C.; Tidwell, R. R.; McCurdy, D.; Boykin, D. W. 2,4-Diphenyl Furan Diamidines as Novel Anti-*Pneumocystis carinii* Pneumonia Agents. *J. Med. Chem.* **1999,** 42, 2260-2265.

9. Costas-Lago, M. C.; Vila, N.; Rahman, A.; Besada, P.; Rozas, I.; Brea, J.; Loza, M. I.; González-Romero, E.; Terán, C. Novel Pyridazin-3(2H)-one-Based Guanidine Derivatives as Potential DNA Minor Groove Binders with Anticancer Activity. *ACS Med. Chem. Lett.* **2022,** 13, 463-469.

10. Millan, C. R.; Acosta-Reyes, F. J.; Lagartera, L.; Ebiloma, G. U.; Lemgruber, L.; Nué Martinez, J. J.; Saperas, N.; Dardonville, C.; de Koning, H. P.; Campos, J. L. Functional and structural analysis of AT-specific minor groove binders that

disrupt DNA-protein interactions and cause disintegration of the *Trypanosoma brucei* kinetoplast. *Nucleic Acid Res.* **2017,** 45, 8378-8391.

11. Rios Martinez, C. H.; Dardonville, C. Rapid Determination of Ionization Constants (pK_a) by UV Spectroscopy Using 96-Well Microtiter Plates. *ACS Med. Chem. Lett.* **2013,** 4, 142-5.

12. Manallack, D. T.; Prankerd, R. J.; Nassta, G. C.; Ursu, O.; Oprea, T. I.; Chalmers, D. K. A chemogenomic analysis of ionization constants-implications for drug discovery. *ChemMedChem* **2013,** 8, 242-255.

13. Dardonville, C. Automated techniques in pKa determination: Low, medium and high-throughput screening methods. *Drug Discov. Today: Technol.* **2018,** 27, 49-58.

14. ACD/Labs. An Introduction to the Acid Dissociation Constant (pKa). https://www.acdlabs.com/download/docs/Technical-Document-Introduction-to-pKa.pdf (4 November 2021).

15. Manallack, D. T. The pK(a) Distribution of Drugs: Application to Drug Discovery. *Perspect. Medicin. Chem.* **2007,** 1, 25-38.

16. Dardonville, C.; Caine, B. A.; Navarro de la Fuente, M.; Martin Herranz, G.; Corrales Mariblanca, B.; Popelier, P. L. A. Substituent effects on the basicity (pK(a)) of aryl guanidines and 2-(arylimino) imidazolidines: correlations of pH-metric and UV-metric values with predictions from gas-phase ab initio bond lengths. *New J. Chem.* **2017,** 41, 11016-11028.

17. Caine, B. A.; Dardonville, C.; Popelier, P. L. A. Prediction of Aqueous pKa Values for Guanidine-Containing Compounds Using Ab Initio Gas-Phase Equilibrium Bond Lengths. *ACS Omega* **2018,** 3, 3835-3850.

18. Caine, B. A.; Bronzato, M.; Fraser, T.; Kidley, N.; Dardonville, C.; Popelier, P. L. A. Aqueous pK(a) prediction for tautomerizable compounds using equilibrium bond lengths. *Commun. Chem.* **2020,** 3.

19. Rupp, M.; Korner, R.; Tetko, I. V. Predicting the pK_a of small molecule. *Comb. Chem. High Throughput Screen.* **2011,** 14, 307-27.

20. Ming, X.; Ju, W.; Wu, H.; Tidwell, R. R.; Hall, J. E.; Thakker, D. R. Transport of Dicationic Drugs Pentamidine and Furamidine by Human Organic Cation Transporters. *Drug Metab. Dispos.* **2009,** 37, 424-430.

21. De Koning, H. P. The Drugs of Sleeping Sickness: Their Mechanisms of Action and Resistance, and a Brief History. *Trop. Med. Infect. Dis.* **2020,** 5, 14.

22. Hanlon, S.; Wong, L.; Pack, G. R. Proton equilibria in the minor groove of DNA. *Biophys. J.* **1997,** 72, 291-300.

23. Nguyen, B.; Stanek, J.; Wilson, W. D. Binding-linked protonation of a DNA minor-groove agent. *Biophys. J.* **2006,** 90, 1319-28.

24. Nguyen, B.; Hamelberg, D.; Bailly, C.; Colson, P.; Stanek, J.; Brun, R.; Neidle, S.; David Wilson, W. Characterization of a Novel DNA Minor-Groove Complex. *Biophys. J.* **2004,** 86, 1028-1041.

25. Lamm, G.; Pack, G. R. Acidic domains around nucleic acids. *Proc. Natl. Acad. Sci. U. S. A.* **1990,** 87, 9033-9036.

26. Lead, A. M. T., O.; Novikov, A.; Moskalenko, E.; Vysotsky, A.; Volokh, V. *Prism 5 for Windows*, 5.01; GraphPad Software Inc.: 1992-2007.

27. Ríos Martínez, C. H. Synthesis and study of new antiprotozoal agents derivatives of dicationic compounds for the treatment of Human African Trypanosomiasis. PhD Thesis, Universidad Complutense de Madrid, Madrid, Spain, 2013.

28. Fraczkiewicz, R. *In Silico* Prediction of Ionization. In *Reference Module in Chemistry, Molecular Sciences and Chemical Engineering*, Elsevier: 2013.

29. Shedlovsky, T.; Pesce, B. *Electrolytes*. Pergamon Press: New York, 1962.

30. Yasuda, M. Dissociation Constants of Some Carboxylic Acids in Mixed Aqueous Solvents. *Bull. Chem. Soc. Jpn.* **1959,** 32, 429-432.

31. Ríos Martínez, C. H.; Nué Martinez, J. J.; Ebiloma, G. U.; de Koning, H. P.; Alkorta, I.; Dardonville, C. Lowering the pK_a of a bisimidazoline lead with halogen atoms results in improved activity and selectivity against *Trypanosoma brucei in vitro*. *Eur. J. Med. Chem.* **2015,** 101, 806-817.

32. Nguyen, B.; Tanious, F. A.; Wilson, W. D. Biosensor-surface plasmon resonance: Quantitative analysis of small molecule–nucleic acid interactions. *Methods* **2007,** 42, 150-161.

33. Cooper, M. A. Optical biosensors in drug discovery. *Nat. Rev. Drug Discovery* **2002,** 1, 515-528.

34. Freyer, M. W.; Buscaglia, R.; Nguyen, B.; David Wilson, W.; Lewis, E. A. Binding of netropsin and 4,6-diamidino-2-phenylindole to an A2T2 DNA hairpin: A comparison of biophysical techniques. *Anal. Biochem.* **2006,** 355, 259-266.

35. Ríos Martínez, C. H.; Lagartera, L.; Trujillo, C.; Dardonville, C. Bisimidazoline arylamides binding to the DNA minor groove: *N*1-hydroxylation enhances binding affinity and selectivity to AATT sites. *MedChemComm* **2015,** 6, 2036-2042.

36. Ivens, A. C.; Peacock, C. S.; Worthey, E. A.; Murphy, L.; Aggarwal, G.; Berriman, M.; Sisk, E.; Rajandream, M.-A.; Adlem, E.; Aert, R.; Anupama, A.; Apostolou, Z.; Attipoe, P.; Bason, N.; Bauser, C.; Beck, A.; Beverley, S. M.; Bianchettin, G.; Borzym, K.; Bothe, G.; Bruschi, C. V.; Collins, M.; Cadag, E.; Ciarloni, L.; Clayton, C.; Coulson, R. M. R.; Cronin, A.; Cruz, A. K.; Davies, R. M.; Gaudenzi, J. D.; Dobson, D. E.; Duesterhoeft, A.; Fazelina, G.; Fosker, N.; Frasch, A. C.; Fraser, A.; Fuchs, M.; Gabel, C.; Goble, A.; Goffeau, A.; Harris, D.; Hertz-Fowler, C.; Hilbert, H.; Horn, D.; Huang, Y.; Klages, S.; Knights, A.; Kube, M.; Larke, N.; Litvin, L.; Lord, A.; Louie, T.; Marra, M.; Masuy, D.; Matthews, K.; Michaeli, S.; Mottram, J. C.; MuÌ^ller-Auer, S.; Munden, H.; Nelson, S.; Norbertczak, H.; Oliver, K.; O'Neil, S.; Pentony, M.; Pohl, T. M.; Price, C.; Purnelle, B. n. d.; Quail, M. A.; Rabbinowitsch, E.; Reinhardt, R.; Rieger, M.; Rinta, J.; Robben, J.; Robertson, L.; Ruiz, J. C.; Rutter, S.; Saunders, D.; SchaÌ^fer, M.; Schein, J.; Schwartz, D. C.; Seeger, K.; Seyler, A.; Sharp, S.; Shin, H.; Sivam, D.; Squares, R.; Squares, S.; Tosato, V.; Vogt, C.; Volckaert, G.; Wambutt, R.; Warren, T.; Wedler, H.; Woodward, J.; Zhou, S.; Zimmermann, W.; Smith, D. F.; Blackwell, J. M.; Stuart, K. D.; Barrell, B.; Myler, P. J. The Genome of the Kinetoplastid Parasite, *Leishmania major*. *Science* **2005,** 309, 436-442.

37. Wartell, R. M.; Benight, A. S. Thermal denaturation of DNA molecules: A comparison of theory with experiment. *Phys. Rep.* **1985,** 126, 67-107.

38. Mergny, J. L.; Lacroix, L. Analysis of thermal melting curves. *Oligonucleotides* **2003,** 13, 515-37.

39. Barbi, M.; Lepri, S.; Peyrard, M.; Theodorakopoulos, N. Thermal denaturation of a helicoidal DNA model. *Phys. Rev. E* **2003,** 68, 061909.

40. Norden, B.; Kubista, M.; Kurucsev, T. Linear dichroism spectroscopy of nucleic acids. *Q. Rev. Biophys.* **1992,** 25, 51-170.

41. Andrews, S. S.; Tretton, J. Physical Principles of Circular Dichroism. *J. Chem. Educ.* **2020,** 97, 4370-4376.

42. Power, E. A.; Thirunamachandran, T. Circular dichroism: A general theory based on quantum electrodynamics. *J. Chem. Phys.* **1974,** 60, 3695-3701.

43. Ranjbar, B.; Gill, P. Circular dichroism techniques: biomolecular and nanostructural analyses- a review. *Chem. Biol. Drug. Des.* **2009,** 74, 101-20.

44. Vorlickova, M.; Kejnovska, I.; Sagi, J.; Renciuk, D.; Bednarova, K.; Motlova, J.; Kypr, J. Circular dichroism and guanine quadruplexes. *Methods* **2012,** 57, 64-75.

45. Vorlickova, M.; Kejnovska, I.; Bednarova, K.; Renciuk, D.; Kypr, J. Circular dichroism spectroscopy of DNA: from duplexes to quadruplexes. *Chirality* **2012,** 24, 691-8.

46. Kypr, J.; Kejnovská, I.; Bednářová, K.; Vorlíčková, M. Circular Dichroism Spectroscopy of Nucleic Acids. In *Comprehensive Chiroptical Spectroscopy*, 2012; pp 575-586.

47. Wilson, W. D.; Tanious, F. A.; Fernandez-Saiz, M.; Rigl, C. T. *Evaluation of drug-nucleic acid interactions by thermal melting curves*. Humana Press, Totowa, NJ.: 1997; Vol. 90, p 219-40.

48. Nagle, P. S. Synthesis, biophysical and biochemical studies of new guanidine-like derivatives targeting DNA. Doctoral thesis, Trinity College of Dublin, Dublin, Ireland, 2010.

49. Arafa, R. K.; Brun, R.; Wenzler, T.; Tanious, F. A.; Wilson, W. D.; Stephens, C. E.; Boykin, D. W. Synthesis, DNA Affinity, and Antiprotozoal Activity of Fused Ring Dicationic Compounds and Their Prodrugs. *J. Med. Chem.* **2005,** 48, 5480-5488.

50. Nanjunda, R.; Wilson, W. D. Binding to the DNA minor groove by heterocyclic dications: from AT-specific monomers to GC recognition with dimers. *Curr. Protoc. Nucleic Acid Chem.* **2012,** Chapter 8, Unit8.8-Unit8.8.

51. Sapunar, M.; Domcke, W.; Došlić, N. UV absorption spectra of DNA bases in the 350-190 nm range: assignment and state specific analysis of solvation effects. *Phys. Chem. Chem. Phys.* **2019,** 21, 22782-22793.

52. Han, F.; Taulier, N.; Chalikian, T. V. Association of the Minor Groove Binding Drug Hoechst 33258 with d(CGCGAATTCGCG)2: Volumetric, Calorimetric, and Spectroscopic Characterizations. *Biochemistry* **2005,** 44, 9785-9794.

53. Li, H.; Yang, T.; Ding, L.; Wang, W. Synthesis, characterization, fluorescence and DNA-binding studies of europium(III) pirates complexes with amide-based 2,3-dihydroxynaphthalene derivatives. *J. Rare Earths* **2012,** 30, 297-303.

54. Baranovsky, S. F.; Bolotin, P. A.; Evstigneev, M. P.; Chernyshev, D. N. Interaction of ethidium bromide and caffeine with DNA in aqueous solution. *J. Appl. Spectrosc.* **2009,** 76, 132.

55. De Almeida, S. M.; Lafayette, E. A.; Da Silva, L. P.; Amorim, C. A.; De Oliveira, T. B.; Ruiz, A. L.; De Carvalho, J. E.; De Moura, R. O.; Beltrão, E. I.; De Lima, M. D.; Júnior, L. B. Synthesis, DNA Binding, and Antiproliferative Activity of Novel Acridine-Thiosemicarbazone Derivatives. *Int. J. Mol. Sci.* **2015,** 16.

56. Lafayette, E. A.; Vitalino de Almeida, S. M.; Da Rocha Pitta, M. G.; Carneiro Beltrão, E. I.; Gonçalves da Silva, T.; Olímpio de Moura, R.; Da Rocha Pitta, I.; De Carvalho, L. B.; Do Carmo Alves de Lima, M. Synthesis, DNA Binding and Topoisomerase I Inhibition Activity of Thiazacridine and Imidazacridine Derivatives. *Molecules* **2013,** 18, 15035-15050.

57. Zhou, C.-Y.; Xi, X.-L.; Yang, P. Studies on DNA binding to metal complexes of Sal$_2$trien. *Biochemistry (Moscow)* **2007,** 72, 37-43.

58. Kashanian, S.; Dolatabadi, J. E. N. DNA binding studies of 2-tert-butylhydroquinone (TBHQ) food additive. *Food Chem.* **2009,** 116, 743-747.

59. Ihmels, H.; Otto, D. Intercalation of Organic Dye Molecules into Double-Stranded DNA -- GeneralPrinciples and Recent Developments. In *Supermolecular Dye Chemistry*, Würthner, F., Ed. Springer Berlin Heidelberg: Berlin, Heidelberg, 2005; pp 161-204.

60. Norden, B. Applications of linear Dichroism Spectroscopy. *Appl. Spectrosc. Rev.* **1978,** 14, 157-248.

61. Diehl, B. Chapter 1 - Principles in NMR Spectroscopy. In *NMR Spectroscopy in Pharmaceutical Analysis*, Holzgrabe, U.; Wawer, I.; Diehl, B., Eds. Elsevier: Amsterdam, 2008; pp 1-41.

62. de Clairac, R. P. L.; Geierstanger, B. H.; Mrksich, M.; Dervan, P. B.; Wemmer, D. E. NMR Characterization of Hairpin Polyamide Complexes with the Minor Groove of DNA. *J. Am. Chem. Soc.* **1997,** 119, 7909-7916.

63. Reid, B. R. Sequence-specific assignments and their use in NMR studies of DNA structure. *Q. Rev. Biophys.* **1987,** 20, 1-34.

64. Jenkins, T. C.; Lane, A. N. AT selectivity and DNA minor groove binding: modelling, NMR and structural studies of the interactions of propamidine and pentamidine with d(CGCGAATTCGCG)2. *Biochim. Biophys. Acta, Gene Struct. Expression* **1997,** 1350, 189-204.

65. Trotta, E.; Paci, M. Solution structure of DAPI selectively bound in the minor groove of a DNA T·T mismatch-containing site: NMR and molecular dynamics studies. *Nucleic Acid Res.* **1998,** 26, 4706-4713.

66. James, T. L. The nuclear magnetic resonance experiment. In *Fundamentals of NMR*, Department of Pharmaceutical Chemistry, U. o. C., San Francisco, Ed. Department of Pharmaceutical Chemistry, University of California, San Francisco: 1998; pp 1-31.

67. Borgias, B. A.; James, T. L. MARDIGRAS-A procedure for matrix analysis of relaxation for discerning geometry of an aqueous structure. *J. Magn. Reson.* **1990,** 87, 475-487.

68. Sathyamoorthy, B.; Sannapureddi, R. K. R.; Negi, D.; Singh, P. Conformational characterization of duplex DNA with solution-state NMR spectroscopy. *J. Magn. Reson. Open* **2022,** 10-11, 100035.

69. Abi-Ghanem, J.; Heddi, B.; Foloppe, N.; Hartmann, B. DNA structures from phosphate chemical shifts. *Nucleic Acid Res.* **2010,** 38, e18-e18.

70. Campos, L.; Valls, N.; Urpí, L.; Gouyette, C.; Sanmartín, T.; Richter, M.; Alechaga, E.; Santaolalla, A.; Baldini, R.; Creixell, M.; Ciurans, R.; Skokan, P.; Pous, J.; Subirana, J. A. Overview of the Structure of All-AT Oligonucleotides: Organization in Helices and Packing Interactions. *Biophys. J.* **2006,** 91, 892-903.

71. Prasad, M. R.; Deb, P. K.; Chandrasekaran, B.; Maheshwari, R.; Tekade, R. K. Chapter 3 - Basics of Crystallization Process Applied in Drug Exploration. In *Dosage Form Design Parameters*, Tekade, R. K., Ed. Academic Press: 2018; pp 67-103.

72. Aggarwal, A. K. Crystallization of DNA binding proteins with oligodeoxynucleotides. *Methods* **1990,** 1, 83-90.

73. Russo Krauss, I.; Pica, A.; Merlino, A.; Mazzarella, L.; Sica, F. Duplex-quadruplex motifs in a peculiar structural organization cooperatively contribute

to thrombin binding of a DNA aptamer. *Acta Crystallogr. D.* **2013,** 69, 2403-11.

74. Benvenuti, M.; Mangani, S. Crystallization of soluble proteins in vapor diffusion for x-ray crystallography. *Nat. Protoc.* **2007,** 2, 1633-1651.

75. Bijelic, A.; Rompel, A. Polyoxometalates: more than a phasing tool in protein crystallography. *ChemTexts* **2018,** 4, 10.

76. Hou, H.; Shi, M.; Hu, S.-Y.; Ahmad, F.; Zhang, B.; Chen, Z.-H.; Yin, D.-C. A systematic comparison of sitting and hanging-drop crystallization using traditional and cross-diffusion microbatch crystallization plates. *J. Cryst. Growth* **2019,** 521, 1-8.

77. Millan, C. R. Structural and functional studies of AT-rich DNA ligands and their effect on *Trypanosoma brucei*. Doctoral thesis, Universitat Politècnnica de Catalunya, Barcelona, 2017.

78. Battye, T. G.; Kontogiannis, L.; Johnson, O.; Powell, H. R.; Leslie, A. G. iMOSFLM: a new graphical interface for diffraction-image processing with MOSFLM. *Acta Crystallogr. D.* **2011,** 67, 271-81.

79. Kabsch, W. Xds. *Acta Crystallogr. D.* **2010,** 66, 125-32.

80. Juanhuix, J.; Gil-Ortiz, F.; Cuni, G.; Colldelram, C.; Nicolas, J.; Lidon, J.; Boter, E.; Ruget, C.; Ferrer, S.; Benach, J. Developments in optics and performance at BL13-XALOC, the macromolecular crystallography beamline at the ALBA synchrotron. *J. Synchrotron Radiat.* **2014,** 21, 679-689.

81. Langridge, R.; Marvin, D. A.; Seeds, W. E.; Wilson, H. R.; Hooper, C. W.; Wilkins, M. H. F.; Hamilton, L. D. The molecular configuration of deoxyribonucleic acid: II. Molecular models and their fourier transforms. *J. Mol. Biol.* **1960,** 2, 38-IN12.

82. Millan, C. R., Dardonville, C., de Koning, H.P., Saperas, N., Campos, J. L. Structure of the DNA duplex d(AAATTT)$_2$ with the potential antiparasitic drug 6XV at 1.25 Å resolution. DOI: 10.2210/pdb5lit/pdb. In 2016.

83. Frisch, M. J. T., G. W.; Schlegel, H. B.; Scuseria, G. E.; Robb, M. A.; Cheeseman, J. R.; Scalmani, G.; Barone, V.; Mennucci, B.; Petersson, G. A.; Nakatsuji, H.; Caricato, M.; Li, X.; Hratchian, H. P.; Izmaylov, A. F.; Bloino, J.; Zheng, G.; Sonnenberg, J. L.; Hada, M.; Ehara, M.; Toyota, K.; Fukuda, R.; Hasegawa, J.; Ishida, M.; Nakajima, T.; Honda, Y.; Kitao, O.; Nakai, H.; Vreven, T.; Montgomery, J. A., Jr.; Peralta, J. E.; Ogliaro, F.; Bearpark, M.;

Heyd, J. J.; Brothers, E.; Kudin, K. N.; Staroverov, V. N.; Kobayashi, R.; Normand, J.; Raghavachari, K.; Rendell, A.; Burant, J. C.; Iyengar, S. S.; Tomasi, J.; Cossi, M.; Rega, N.; Millam, J. M.; Klene, M.; Knox, J. E.; Cross, J. B.; Bakken, V.; Adamo, C.; Jaramillo, J.; Gomperts, R.; Stratmann, R. E.; Yazyev, O.; Austin, A. J.; Cammi, R.; Pomelli, C.; Ochterski, J. W.; Martin, R. L.; Morokuma, K.; Zakrzewski, V. G.; Voth, G. A.; Salvador, P.; Dannenberg, J. J.; Dapprich, S.; Daniels, A. D.; Farkas, Ö.; Foresman, J. B.; Ortiz, J. V.; Cioslowski, J.; Fox, D. J. . *Gaussian 09, Revision D01*, Wallingford CT., 2009.

84. Petersson, G. A.; Al-Laham, M. A. A complete basis set model chemistry. II. Open-shell systems and the total energies of the first-row atoms. *J. Chem. Phys.* **1991,** 94, 6081-6090.

85. Petersson, G. A.; Bennett, A.; Tensfeldt, T. G.; Al-Laham, M. A.; Shirley, W. A.; Mantzaris, J. A complete basis set model chemistry. I. The total energies of closed-shell atoms and hydrides of the first-row elements. *J. Chem. Phys.* **1988,** 89, 2193-2218.

86. Trott, O.; Olson, A. J. AutoDock Vina: improving the speed and accuracy of docking with a new scoring function, efficient optimization, and multithreading. *J. Comput. Chem.* **2010,** 31, 455-461.

87. Bell, E. W.; Zhang, Y. DockRMSD: an open-source tool for atom mapping and RMSD calculation of symmetric molecules through graph isomorphism. *J. Cheminf.* **2019,** 11, 40.

88. Morris, G. M.; Huey, R.; Lindstrom, W.; Sanner, M. F.; Belew, R. K.; Goodsell, D. S.; Olson, A. J. AutoDock4 and AutoDockTools4: Automated docking with selective receptor flexibility. *J. Comput. Chem.* **2009,** 30, 2785-91.

89. Lauria, A.; Montalbano, A.; Barraja, P.; Dattolo, G.; Almerico, A. M. DNA minor groove binders: an overview on molecular modeling and QSAR approaches. *Curr. Med. Chem.* **2007,** 14, 2136-60.

CHAPTER 5

5. Chapter 5 :   Biological and Pharmacological evaluation

5.1. Introduction

Once the 3 series of molecules were synthesised (Chapter 3) and their DNA binding affinity was analysed by biophysical assays (Chapter 4), the next step was to assess their antiprotozoal activity and cytotoxicity.

Bis(imidazolidin-2-amine) (**1**), bis(2-aminobenzimidazole) (**2**) and bis(arylimidamide) (**3**) derivatives were tested *in vitro* against *Trypanosoma brucei brucei* bloodstream forms (BF) of strain Lister 427/MiTat1.2 (wild-type, Tb427WT) and the drug-resistant strain B48 (i.e., resistant to pentamidine). The compounds were also tested against epimastigotes of *Trypanosoma cruzi* CL Brener strain (DTU TcVI) and promastigotes of *Leishmania donovani* HU3, and intracellular amastigote forms of both parasites members of the Trypanosomatidae family.[1] Additionally, the synthesised compounds were tested *in vitro* against *Trichomonas vaginalis* (Trichomonadidae family). *T. vaginalis* is a monogenetic, anaerobic, amitochondrial parasite and, as such, very different from kinetoplastid parasites such as *Trypanosoma* and *Leishmania* species, which are digenetic, aerobic, and have functional mitochondria that perform essential functions. However, the genome of these parasites has in common a high content in AT base pairs (> 65%).[2-4] Hence, compounds that bind selectively to the DNA at AT-rich sites may potentially generate drugs useful for all these parasites.

The biological assays against *T. cruzi* and *T. vaginalis* were carried out at the Department of Microbiology and Parasitology, Pharmacy College at the Complutense University of Madrid, in collaboration with Prof. Drs. Alicia Gómez Barrio, Cristina Fonseca Berzal and Alexandra Ibáñez Escribano.

Evaluation of the compounds against *L. donovani* was carried out at the Institute of Parasitology and Biomedicine "López-Neyra" (IPBLN) – CSIC, in collaboration with Drs. Francisco Gamarro and Ignacio Manzano.

Biological evaluation against *T. brucei* was performed at the Institute of Infection, Immunity and Inflammation at the University of Glasgow, in collaboration with Dr. Harry De Koning's group (Marzuq A. Ungogo, Maha A. Aloraini).

The nonspecific cytotoxicity of the compounds was assessed with different cell lines according to the standardized models used in each laboratory:

(a) Human embryonic kidney (HEK) cells for *T. brucei*,

(b) L929 murine fibroblasts for *T. cruzi*,

(c) Human myelomonocytic cell line (THP-1) for *L. donovani*, and

(d) African green monkey kidney epithelial cells (Vero CCL-81, ATCC) for *T. vaginalis*.

5.2. Fundamental of the methods for biological assays

5.2.1. Resazurin-based method

This method is based on the evaluation of cell proliferation, using a cell viability dye, resazurin (7-hydroxy-3*H*-phenoxazin-3-one 10 oxide), which is a blue non-fluorescent dye. Under reducing conditions due to the proliferating cells, this dye turns into red highly fluorescent resorufin (Figure 5.1). The amount of fluorescence is proportional to the number of living cells. Hence, it is a good indication of the effect of the tested compounds on cell proliferation.[5-8] Advantageously, this method consists of a simple one step assay and does not need cell lysis, washing or extraction procedures. It is a non-radioactive, reliable, sensitive, reproducible method which is non-toxic to cells.[9]

Resazurin   **Resorufin**
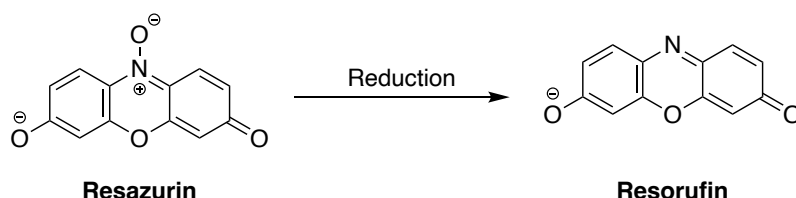
Figure 5.1: Reaction involved in the resazurin assay.

The procedure followed for the resazurin assays consists of the preparation in a 96-well plate of serial drug dilutions to be tested covering a range of concentrations. Then, the parasites or cells are added to each well and the plates are incubated at the correspondent

temperature. Resazurin is then added to each well and the plate is incubated to allow reduction of resazurin to resorufin in the presence of proliferating cells. Hence, the resulting fluorescence is dependent on compound concentration and activity. The plates are read with a microplate fluorometer using an excitation wavelength of 536 nm and an emission wavelength of 588 nm.

5.2.2. MTT method

3-(4,5-Dimethyl-2-thiazolyl)-2,5-diphenyl-2*H*-tetrazolium bromide (MTT) is a dye used to assess cell metabolic activity as an indicator of cell viability. The nicotinamide-adenine-dinucleotide (NAD(P)H)-dependent cellular oxidoreductase enzymes may, under defined conditions, reflect the number of viable cells present in the culture medium. These enzymes are capable of reducing the yellow MTT dye to its insoluble, strongly coloured and lipophilic formazan, which has a purple colour (Figure 5.2).[9-14]

A brief summary of the readout of the assay is as follows: after the cells have been incubated with the test compounds, a solubilisation solution (either dimethyl sulfoxide, an acidified ethanol solution, or a solution of the detergent sodium dodecyl sulphate in diluted hydrochloric acid) is added to dissolve the insoluble purple formazan product. The resulting-coloured solution in the 96-well plates is quantified by measuring absorbance at 500–600 nm using a multi-well spectrophotometer. The degree of light absorbed is dependent on formazan concentration. Hence, a deeper purple colour (i.e., greater formazan concentration) reflects a greater number of viable, metabolically active cells. Tetrazolium dye assays can also be used to measure cytotoxicity or cytostatic activity of potential medicinal compounds.

MTT → Mitochondrial Reductase → **Formazan**
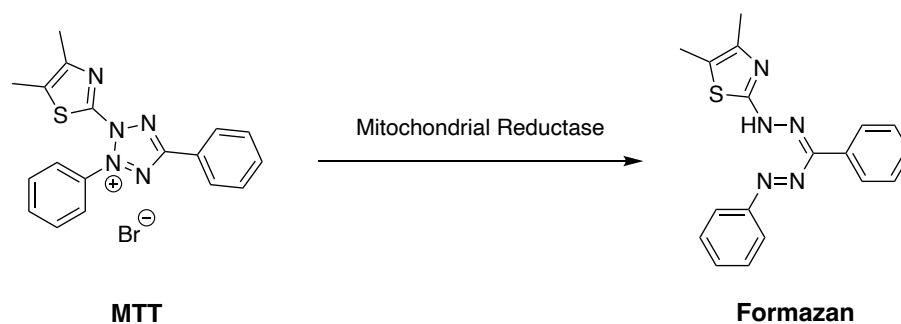
Figure 5.2: Reaction involved in the MTT assay.

5.2.3. ß - D - Galactosidase assay (CPRG)

The β-Galactosidase Assay uses chlorophenol red-β-D-galactopyranoside (CPRG), which is up to 10 times more sensitive than the classic *o*-nitrophenyl-β-D-galactopyranoside method (ONPG).[15] This increased sensitivity makes it simpler to measure β-galactosidase activity in cells that are difficult to transfect or have low β-galactosidase activity expression.

β-galactosidase catalyzes the hydrolysis of the galactoside analog CPRG. Cell lysates are incubated and the β-Galactosidase converts the yellow-orange CPRG substrate into the red chromophore chlorophenol red, yielding a dark red solution (Figure 5.3).
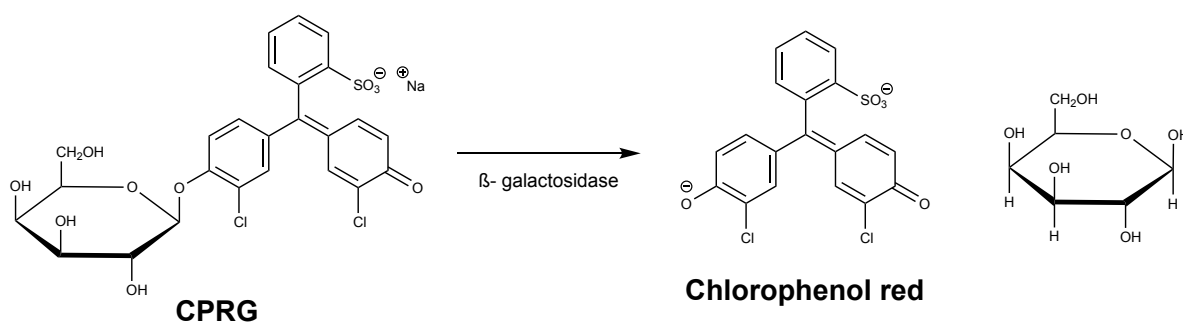
Figure 5.3: Reaction involved in the CPRG assay

The β-galactosidase gene functions well as a reporter gene because the protein product is extremely stable, resistant to proteolytic degradation in cellular lysates, and easily assayed. The colorimetric reaction experienced by CPRG in the presence of β-galactosidase-transfected strains of *T. cruzi* is based on enzyme hydrolyzes the chromogenic substrate (yellow) to chlorophenol red (red) and galactose, providing an absorbance that correlates with the number of live parasites.[16] This activity is measured spectroscopically at 570–595 nm in 48 or 96-well plates to determine the amount of converted substrate, as previously described.[17-19]

.

5.3. Methodology for biological assays

5.3.1. Assays against promastigote and amastigote forms of *Leishmania donovani* and cellular toxicity against human THP-1 cells

The sensitivity of promastigote forms of *L. donovani* HU3 line to the different compounds was determined after incubation for 72 hours at 28 °C in the presence of increasing concentrations of the compounds. The concentration of compound required to inhibit 50% of parasite growth (EC_{50}) was calculated using the MTT colorimetric assay, as described previously (see Chapter 9 for details).[20, 21] Amastigotes of *L. donovani* were grown in mouse peritoneal macrophages as previously reported,[22, 23] using late-stage promastigotes to infect the macrophages at a ratio macrophage/parasite 1:10. Intracellular parasites were detected by nuclear staining with Prolong Gold antifade reagent plus DAPI. Compound activity against intracellular amastigotes was determined from the percentage of infected cells and the number of amastigotes per cell in drug-treated versus non-treated cultures.

For the cellular toxicity of all compounds against THP-1 cells, the colorimetric MTT-based assay was used, as described for *Leishmania* promastigotes, except for the incubation temperature, which was 37 °C in this case. The selectivity index (SI) was calculated as: $SI = EC_{50 \text{ (THP-1)}} / EC_{50 \text{ (}L. donovani\text{)}}$. Each experiment was performed in triplicate. The results are gathered in Tables 5.1–5.3.

5.3.2. Assays against *Trypanosoma brucei brucei* and cytotoxicity against HEK cells

EC_{50} values were determined for bloodstream forms of *T. b. brucei* strain Lister 427[24] and for the multidrug resistant strain B48, which derived from Lister 427 by knockout of the *TbAT1* aminopurine transporter[25] and *in vitro* adaptation to high concentrations of pentamidine.[26] Both strains were cultured in full HMI-9 media (Gibco) supplemented with 10% Fetal Bovine Serum at 37 °C and 5% CO_2 as described.[27] The drug sensitivity was determined using a resazurin-based (AlamarBlue™) assay in 96 wells exactly as described previously,[28] with 23 doubling dilutions and a no drug control for each compound. Each well was seeded with 2000 cells, incubated for 70 hours with the drug before the addition of the resazurin indicator dye and a further incubation of 24 hours. Finally, the results are analysed by plotting obtained fluorescence values against compound concentrations. EC_{50}

values are calculated by non-linear regression using an equation for a sigmoidal dose–inhibition curve with variable slope.

The cytotoxicity of the compounds was determined with human embryonic kidney (HEK) cells, a specific immortalised cell line derived from a spontaneously miscarried or aborted fetus grown in tissue culture.[29] Each well was seeded with 3×10^4 cells, incubated for 24 hours for cytoadhesion, followed by 30 hours of incubation with the drug before the addition of the resazurin (10 µL) indicator dye and a further incubation of 24 hours. Each experiment was performed in triplicate and repeated at least two times.

5.3.3. Assays against epimastigote and amastigote forms of *Trypanosoma cruzi* and cytotoxicity against L929 cells

The activity profile of the compounds was explored on *T. cruzi*, by applying the screening procedure previously described.[18, 30] These assays were performed following a screening protocol in which the activity against epimastigotes (extracellular insect vector stage of the parasite) was firstly evaluated with cultures that had not reached the stationary phase, as previously reported.[31] Cultures of epimastigotes in LIT medium were seeded in 96-well plates at a density of 2.5×10^5 parasites/ml and incubated for 72 hours at 28 °C within the compounds. The plates were then incubated with CPRG at 37 °C for an additional 3 hours and absorbance read at 595 nm. EC_{50} was calculated as previously reported[18] using Benznidazole as the reference drug. Each concentration was tested in triplicate and experiments performed similarly for three.

The cytotoxic properties of the synthetic compounds were evaluated using L929 murine fibroblasts (i.e., amastigotes host cells) simultaneously.[32] The 96-well plates seeded with 10,000 cells/well, were incubated in MEM medium for 3 hours at 37 °C. After cell attachment, culture medium was replaced by compound dilutions and incubated for additional 72 hours. Then, after addition of resazurin, the plates were further incubated for 3 hours at 37 °C and 5% CO_2. Fluorescence intensity was measured with a slight variation, using wavelengths of 535 nm (excitation) and 590 nm (emission). CC_{50} was calculated as indicated in the literature.[18] Each concentration was tested in triplicate and experiments performed three times in similar conditions.

Compounds with selectivity indexes (SI) for epimastigotes (SI = $CC_{50 \, (L929)}$ / $EC_{50 \, (epi)}$.) similar or higher than that of the reference drug benznidazole were selected for further testing against intracellular amastigotes (i.e., mammalian host replicative forms). These assays were carried out by applying the CPRG method. L929 cells were seeded in 48-well plates and infected with CL-B5 tissue culture derived trypomastigotes at 1:6 ratio (cell:parasite). After 24 hours of incubation at 33 °C and 5% CO_2, non-penetrated parasites were removed and compound dilutions in MEM were added to treat the infected cultures and then incubated for seven days at the same previous conditions. Finally, addition of CPRG solution, followed by 3 hours of incubation at 37 ºC allow the reading of the plates at 595 nm. EC_{50} was calculated as previously reported.[18] SI for amastigotes was also calculated: SI = $CC_{50 \, (L929)}$ / $EC_{50 \, (ama)}$. Each concentration was tested in triplicate and experiments performed similarly for three.

5.3.4. *In vitro* screening against urogenital parasite *Trichomonas vaginalis* and unspecific cytotoxicity assays against VERO CCL-81 cells.

The antiparasitic effect of the compounds was evaluated against the *T. vaginalis* isolate JH31A#4 from the American Type Culture Collection (ATCC). The parasite was cultured in TYM (Trypticase-Yeast Extract-Maltose) medium and supplemented with 10% heat inactivated fetal bovine serum (FBS) and antibiotics to avoid contaminations. The *in vitro* screening process was executed following the sequential procedure described previously.[33, 34] The compounds, diluted in DMSO at different concentrations, were added to 1×10^5 *T. vaginalis* cells/mL cultures in exponential growth phase. After 24 hours in contact with the parasites at 37 °C and 5% CO_2, 200 µL of each tube were seeded in sterile 96-well flat-bottomed microplates. Then, culture media was discarded from the plates by centrifugation and the parasites were subsequently resuspended in 200 µL of sterile phosphate buffered saline (PBS).

The antiparasitic activity of each compound was measured by a fluorometric method using the redox dye resazurin. For that, each well was incubated for 1 hour in contact with 20 µL of the redox dye (3 mM stock solution in PBS) at 37 °C and 5% CO_2. Finally, the fluorescence was read in an Infinite 200 TECAN fluorometer at $\lambda_{excitation}$ 535 nm and $\lambda_{emission}$ 590 nm. Each plate included a growth control and a positive control in which the

reference drug metronidazole was evaluated at its MIC_{100} concentration (24 μM). Each experiment was performed in triplicate and repeated at least two times.

The cytotoxicity of the only compound with trichomonacidal effect (**34**) was evaluated at the same concentrations against African green monkey kidney epithelial cells (Vero CCL-81, ATCC). Cells were previously cultured in RPMI-1640 medium supplemented with 10% of heat inactivated FBS and antibiotics in a humidified atmosphere at 37 °C, 5% CO_2.

The cytotoxicity experiments were executed as reported previously.[35] Briefly, 5×10^4 cells/well were incubated in 96-well flat-bottom microplates for 6 h at 37 °C and 5% CO_2. Then, compound **34** was added at the same concentrations used for the susceptibility assays with *T. vaginalis*. After 24 hours of incubation, the plate was read after 3 hours of incubation with the resazurin solution (1 mM stock solution, PBS) in the fluorometer.

5.4. Structure–activity relationships results

5.4.1. SAR studies: bis(imidazolidine-2-imine) derivatives (series 1)

The *in vitro* activity of series **1** compounds against *T. brucei*, *T. cruzi*, *L. donovani*, and *T. vaginalis* is shown in Table 5.1. Similar to lead **I**, most of the new derivatives solely displayed activity against *T. brucei*, with the exception of the isopropoxy derivative **1g** which showed micromolar range activity (7.6 µM), similar to lead **I** (4.3 µM), against *L. donovani* promastigotes. However, **1g** was mostly inactive (> 10 µM) against intracellular amastigotes of *L. donovani*.

As the *in vitro* evaluation against epimastigotes of *T. cruzi* did not show any appreciable activity and thus, they were not progressed to further assays on intracellular amastigote forms.

All the chlorine derivatives (**1c**–**1e**) but **1b** showed activity against both WT and drug-resistant (B48) strains of *T. b. brucei* in the low to medium micromolar range (EC_{50} = 5.71 to 48.4 µM). Compound **1c** (EC_{50} = 5.71 µM), with both chlorine atoms in position *ortho* to the imidazoline rings ($R_1 = R_4 = Cl$), was approximately 2- and 8-times more potent than the analogues with one Cl atom ($R_2 = Cl$) *ortho* to the C=O group (**1d** and **1e**, respectively). In fact, **1c** was the most active and selective compound among the new derivatives, with a selectivity index (SI) > 35.

The introduction of two fluorine (**1f**: $R_1 = R_3 = F$) or chlorine atoms (**1b**: $R_1 = R_3 = Cl$) in position R_1 and R_3 led to a drastic drop (**1f**) or complete loss (**1b**) of anti-*T. brucei* activity with respect to the unsubstituted lead **I**. In contrast, the introduction of hydrophobic isopropoxy moieties (**1g**: $R_2 = R_4 = O^iPr$) in the scaffold led to a micromolar range trypanocide (EC_{50} = 17.6 µM). The replacement of the *N*-phenylbenzamide scaffold of **I** with a *N*-(pyridin-2-yl)picolinamide skeleton (**1h**: X= Y = N) gave a low micromolar range EC_{50} value (25.5 µM, SI > 5.7). The cytotoxicity of these compounds against HEK cells was low (> 100 µM).

None of the compounds of this series showed activity against the *T. vaginalis* parasite.

In summary, the introduction of two substituents (i.e., Cl, F, O^{i}Pr) or N atoms in the scaffold of the bis(imidazolidine-2-imine) series did not improve the *in vitro* antiparasitic activity against extracellular (*T. brucei*) or intracellular (*Leishmania*, *T. cruzi*) kinetoplastid parasites with respect to lead **I** or the mono-chlorinated analogues reported earlier.[28]

Table 5.1. *In vitro* antiprotozoal activity (EC_{50} µM) and cytotoxicity (CC_{50} µM) against mammalian cells of bis(imidazolidine-2-imine) derivatives (series **1**).
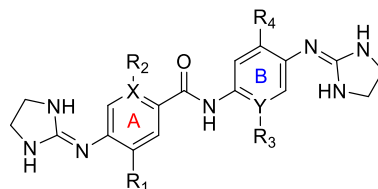
Cmpd.	*T. b. brucei*[a]			HEK[b]		*T. cruzi*[c]	L929[d]	*L. donovani*[e]		THP-1[f]	*T. vaginalis*[g]
	WT[h]	B48[i]	RF[j]		SI[k]			Promast.	Amast.		
I	0.83 ± 0.08[l]	0.87 ± 0.2[l]	1.1	>200	>240	>40	>200	4.3	nt	nt	nt
1b	>100[m]	>100	nt[n]	>200	-	>40	>200	>50	nt	nt	>40
1c	5.7 ± 0.7	6.9 ± 1.5	1.21	>200	>35	>40	>200	>50	nt	nt	>40
1d	10.4 ± 0.8	14.8 ± 0.8	1.42	>200	>19	>40	>200	>50	nt	nt	>40
1e	47.7 ± 13.2	48.4 ± 3.2	1.01	>100	>2.1	>40	>200	>20	nt	38.7 ± 1.5	>40
1f	78.5 ± 6.1	57.4 ± 2.6	0.73	>100	>1.3	>40	>200	>20	nt	>50	>40
1g	17.6 ± 2.1	16.0 ± 0.4	0.91	>100	>5.6	>40	>200	7.6 ± 0.4	>10	>50 (SI >6.5)[o]	>40
1h	25.5 ± 3.2	37.5 ± 4.4	1.47	>200	>7.8	>40	>200	>50	nt	nt	>40

[a] Reference drugs: Pentamidine: 0.00034 ± 0.00002 µM (WT) and 0.111 ± 0.003 µM (B48; RF = 326); Diminazene: 0.010 ± 0.0007 µM (WT) and 0.012 ± 0.0008 µM (B48; RF = 1.2). [b] Human endothelial kidney cells. [c] Epimastigotes of *T. cruzi* strain CL-B5 *lacZ*; reference drug: Benznidazole: 25.3 ± 2.1 µM. [d] Cytotoxicity on L929 fibroblasts; reference drug: Benznidazole: EC_{50} > 200 µM, SI > 7.9. [e] Promastigotes and intracellular amastigotes of *L. donovani* strain HU3; reference drug: Amphotericin B, $EC_{50 \text{ (promastigote)}}$ = 0.07 ± 0.01 µM, $EC_{50 \text{ (amastigote)}}$ = 0.23 ± 0.05 µM. [f] Cytotoxicity on THP-1 cells: Amphotericin B = 28.5 ± 4.5 µM, SI = 122. [g] *Trichomonas vaginalis*; reference drug: Metronidazole: 2.56 ± 0.58 µM. [h] Bloodstream forms trypomastigotes of *T. b. brucei* wild type strain s427. [i] *T. b. brucei* strain resistant to pentamidine. [j] Resistance factor = EC_{50} (B48) / EC_{50} (WT). [k] Selectivity index = EC_{50} (HEK) / EC_{50} (WT). [l] Taken from reference [28]. [m] Not effective, maximum concentration tested. [n] Not tested. [o] Selectivity index versus promastigotes = EC_{50} (THP-1) / EC_{50} (promastigote)

5.4.2. SAR studies: bis(2-aminobenzimidazole) derivatives (series 2)

The activity of the series **2** compounds was tested *in vitro* against four parasites: *T. brucei*, *T. cruzi*, *L. donovani*, and *T. vaginalis* (Table 5.2). Compound **30** was the sole product to show leishmanicidal effect in the low micromolar range against promastigotes of *L. donovani* (EC_{50} = 8.67 µM). However, its cytotoxicity against THP-1 cells was more pronounced than the rest of the series (except **34**) resulting in a poor selectivity index (1.6). Hence, the leishmanicidal effect could reflect a general cytotoxicity for this compound.

None of the tested compounds showed appreciable activity against epimastigotes of *T. cruzi* and thus, they were not progressed to further *in vitro* assays on intracellular amastigote forms. Moreover, only one compound (**34**) displayed marginal trichomonacidal activity (EC_{50} = 33.2 µM). According to the sequential procedure in this antiparasitic model,[33] the unspecific cytotoxicity of compound **34** was tested against Vero CCL-81 cells. After 24 hours in contact with mammalian cells, **34** caused the reduction of about 50% of the cell culture at the highest concentration evaluated (40 µM).

In contrast, the compounds were active in the micromolar range against *T. b. brucei* (Table 2). Six compounds (**2b–e**, **30**, and **34**) displayed EC_{50} values < 6 µM against both the WT and B48 strains, with selectivity indexes ranging from 2.9 (**2d**) to 12.1 (**2c**). This represented a >15-fold increase in activity compared to unsubstituted compound **2a** (EC_{50} = 85.6 µM). Chlorine atoms *ortho* to the 2-aminobenzimidazole moieties (**2c**: R_1 = R_4 = Cl) produced the best anti–*T. brucei* compound of this series (EC_{50} = 1.68 µM, SI = 12.1). In contrast, the presence of one chlorine atom *ortho* to the carbonyl group (**2d**, **2d**, R_2 = Cl) was unfavourable with a loss of activity (1.5-fold and 3.5-fold, respectively) and selectivity (3–4 fold) relative to **2c**. This effect was similar to that observed with the bis(imidazolidine-2-imine) series **1** (see 5.4.1.).

Replacement of the *N*-phenylbenzamide scaffold with *N*-(pyridin-2-yl)picolinamide (**2h**: X =Y = N) also resulted in a loss of activity against *T. brucei*, as well as a decrease of the cytotoxicity against mammalian (HEK) cells (CC_{50} = 80.9 µM). Replacement of the *N*-phenylbenzamide scaffold with a 1,2-diphenylethane (**30**) or 9*H*-fluorene (**34**) skeleton maintained the potency against *T. brucei* compared to the best compound **2c**. In contrast, a 1,3-diphenylurea scaffold (**31**) led to an almost complete loss of activity vs **2c**, as well

as the lowest cytotoxicity against HEK cells. With the exception of **34**, which was marginally more active against B48 (RF 0.71), the compounds were equipotent against the multi-drug resistant strain B48 (i.e., RF ≈ 1) indicating that the P2 and aquaporin-2 transporters are not involved in their uptake, in contrast to diamidine MGBs.[36] This is consistent with the substrate-binding SAR of these transporters, which does not allow substitutions on the terminal imidazole moieties.[37, 38] The non-dependence on the known drug transporters ensures that no cross-resistance with the existing diamidine and melaminophenyl arsenical trypanocidal drugs is likely to occur.[39]

In summary, the replacement of the 2-aminoimidazoline groups by 2-aminobenzimidazole heterocycles afforded compounds that are slightly more active against *T. brucei* but also more cytotoxic, resulting in lower SI. However, this structural modification did not improve the activity against the parasites *Leishmania* (promastigotes and amastigotes) and epimastigotes of *T. cruzi* with respect to lead **I**. Interestingly, the main SAR results seem to apply for both series **1** and **2**. For instance, the effects on the anti-*T. brucei* activity of incorporating Cl atoms in the scaffold were similar in both series.

Table 5.2. *In vitro* antiprotozoal activity (EC$_{50}$ µM) and cytotoxicity (CC$_{50}$ µM) against mammalian cells of bis(2-aminobenzimidazole) derivatives (series **2**).

30: **X** = CH$_2$CH$_2$
31: **X** = NHCONH

34

Cmpd.	*T. brucei*[a]			HEK[b]		*T. cruzi*[c]	L929[d]	*L. donovani*[e]		THP-1[f]	*T. vaginalis*[g]
	WT[h]	**B48**[i]	**RF**[j]		**SI**[k]			Promast.	Amast.		
2a	85.6 ± 2.3	81.9 ± 8.5	0.96	>100	>1.2	nt[l]	nt	nt	nt	nt	nt
2b	1.96 ± 0.03	1.93 ± 0.04	0.99	16.8 ± 0.9	8.6	>40	<50	>20	>20	>500	>40
2c	1.68 ± 0.06	1.81 ± 0.06	1.08	20.3 ± 1.9	12.1	>40	<50	>20	>20	>500	>40
2d	5.56 ± 0.26	5.75 ± 0.11	1.03	16.2 ± 0.5	2.9	>40	<50	>20	>20	>500	>40
2e	2.64 ± 0.09	2.93 ± 0.17	1.11	10.2 ± 0.3	3.9	>40	<50	>20	>20	>500	>40
2h	11.3 ± 0.2	11.6 ± 0.3	1.03	80.9 ± 2.7	7.2	>40	>200	>20	>20	>500	>40
30	2.3 ± 0.2	2.2 ± 0.2	0.95	13.5 ± 0.1	5.9	>40	<50	8.67 ± 3.84	>10	14.1 ± 4.4 (SI=1.6)[m]	>40
31	57.1 ± 1.4	68.8 ± 1.4	1.20	>200	>3.5	>40	>200	>20	>20	>500	>40
34	2.44 ± 0.18	1.73 ± 0.06	0.71	9.15 ± 0.35	3.8	>40	<50	>20	nt	12.1 ± 2.6	33.2

[a] Reference drugs: Pentamidine: 0.00034 ± 0.00002 µM (WT) and 0.111 ± 0.003 µM (B48; RF = 326); Diminazene: 0.010 ± 0.0007 µM (WT) and 0.012 ± 0.0008 µM (B48; RF = 1.2). [b] Human endothelial kidney cells. [c] Epimastigotes of *T. cruzi* strain CL-B5 *lacZ*, reference drug: Benznidazole: 25.3 ± 2.1 µM. [d] Cytotoxicity on L929 fibroblasts; reference drug: Benznidazole: EC$_{50}$ > 200 µM, SI > 7.9. [e] Promastigotes and intracellular amastigotes of *L. donovani* strain HU3; reference drug: Amphotericin B, EC$_{50}$ (promastigote) = 0.07 ± 0.01 µM, EC$_{50}$ (amastigote) = 0.23 ± 0.05 µM. [f] Cytotoxicity on THP-1 cells: Amphotericin B = 28.5 ± 4.5 µM, SI = 122. [g] *Trichomonas vaginalis*; reference drug: Metronidazole: 2.56 ± 0.58 µM. [h] Bloodstream forms trypomastigotes of *T. b. brucei* wild type strain s427. [i] *T. b. brucei* strain resistant to pentamidine. [j] Resistance factor = EC$_{50}$ (B48) / EC$_{50}$ (WT). [k] Selectivity index versus WT = EC$_{50}$ (HEK) / EC$_{50}$ (WT). [l] Not tested. [m] Selectivity index versus promastigotes = EC$_{50}$ (THP-1) / EC$_{50}$ (promastigote).

5.4.3. SAR studies: bis(arylimidamide) derivatives (series 3)

The activity of the series **3** compounds was tested *in vitro* against four parasites: *T. brucei*, *T. cruzi*, *L. donovani*, and *T. vaginalis* (Table 5.3).

Within this series, the anti-*T. brucei* activity was disparate. Three compounds (**3a**: R_1–R_4 = H, **3c**: R_1 = R_4 = Cl, and **3h**: X = Y = N) displayed submicromolar EC_{50} values against *T. brucei* WT (0.4, 0.25 and 0.12 µM, respectively) with SI > 118. The rest of the compounds were either effective in the micromolar range and poorly selective (**3b**, **3d**, **3e**, **3g**, **3i**, and **53**) or inactive (**36**, **37**, and **41**). With the exception of **3a**, **3e**, **3g**, and **36**, which were marginally more active against B48 (RF < 0.81), the rest of the active compounds (**3b**, **3c**, **3d**, and **3h**) were less potent against the multi-drug resistant strain B48 (i.e., RF > 1.2) indicating that the P2 and/or aquaporin-2 transporters are involved in their uptake, although the modest levels of resistance, compared to pentamidine controls (RF = 326), appear to indicate that other, as yet unknown uptake mechanisms are also involved. Compound **3a**, which displayed high efficacy and selectivity (EC_{50} = 0.16 µM, SI>1250) similar to the control drug pentamidine (0.11 µM) against the multi-drug resistant strain B48, emerged as a very interesting lead compound against *T. brucei*.

All of the bis(arylimidamides) but **3d** inhibited the growth of promastigotes of *L. donovani* with EC_{50} values ranging from 0.26 (**3a**) to 3.0 µM (**3g**). This represented an improvement in antileishmanial activity versus lead compound **I** (Table 1, EC_{50} = 4.29 µM). In general, the leishmanicidal activity against intracellular amastigotes was maintained, although with a small loss of potency (approximately 1.5 to 3-fold) for **3a**, **36**, **53**, **3e** and **3g** (EC_{50} = 0.65 – 4.19 µM). These activities were in the same range as the reference drug amphotericin B (0.19 µM). In contrast, the *N*-(pyridin-2-yl)picolinamide derivative **3h** (EC_{50} = 0.55 µM) and the chlorine-containing compounds **3b** (0.91 µM) and **3c** (0.78 µM) were nearly twice as potent against amastigotes vs promastigotes. Apparently, the presence of chlorine atoms *ortho* to the 4-picolinimidamido groups (e.g., **3b**: R_1 = Cl, **3c**: R_1 = R_4 = Cl) or two nitrogen atoms next to the amide linker (**3h**) promoted the antileishmanial activity against intracellular amastigotes. Remarkably, the closely related *N*-(pyridin-2-yl)benzamide analogue **3i** was ineffective (EC_{50} >10 µM) against amastigotes of *L. donovani*. The compounds displayed good selectivity versus THP-1 cells with selectivity indexes from > 11.9 for the least active compound **3g** to > 76.9 for the most effective (**3a**). Thus,

compound **3a**, which displayed submicromolar efficacy against amastigotes of *L. donovani* and excellent selectivity, emerged as a new antileishmanial hit compound.

Regarding the activity on the parasite *T. cruzi* (Table 3), series **3** stands out with activities on epimastigotes in the mid-nanomolar range for the chlorine-containing derivatives **3b**, **3c**, and **3e** (SI from 159 to 3454). Other compounds displayed activities in the submicromolar (**3a**, **3h**, **53**) and low micromolar (**3g**, **36**) range. In general, the anti-*T. cruzi* activity against intracellular amastigotes was maintained, although with a loss of potency of approximately 6 to 20-fold for **3a**–**c** and **3e** (EC$_{50}$ = 0.26 – 1.28 µM). Remarkably, the activity of compound **3g**, which has two large hydrophobic isopropoxy groups (R$_2$ = R$_3$ = O^{i}Pr), was twice as good against intracellular amastigotes vs epimastigotes. On the other hand, the rigid tricyclic fluorene derivative **53** was as almost equally active against epimastigotes and intracellular amastigotes (0.84 and 1.26 µM, respectively). Importantly, all the compounds were selective towards the parasite with selectivity indices between 17.3 (**3c**) and 399 (**3e**) against intracellular amastigotes. Compound **3e**, which is twice as potent as the reference drug benznidazole against amastigotes (0.54 µM), emerged as a new lead compound against *T. cruzi*.

As shown in Table 5.3, none of the tested derivatives from series **3** showed trichomonacidal activity at the highest concentration studied (100 µM). Hence, none of the derivatives passed to the next screening phase and their non-specific cytotoxicity in mammalian cells was not determined.

In summary, the bis(arylimidamide) series are very potent inhibitors of *T. brucei*, *T. cruzi* and *Leishmania* growth, with adequate selectivity. The unsubstituted compound **3a** (close analogue of **I**) is definitely the best in class as is shows excellent activity and selectivity against these 3 kinetoplastid parasites. Compound **3h** is another good lead candidate against *T. brucei* whereas **3e** (but also **3a**, **3b**, and **53**) is the best in terms of activity and selectivity against intracellular amastigotes of *T. cruzi*. As regards to *L. donovani*, **3a**, **36** and **53** (and also **3e**) are the new antileishmanial lead compounds.

Table 5.3. *In vitro* antiprotozoal activity (EC$_{50}$ µM) and cytotoxicity (CC$_{50}$ µM) against mammalian cells of bis(arylimidamide) derivatives (series **3**).

36: X = CH$_2$CH$_2$; Y = NH
37: X = NHCONH ; Y = NH
41: X = CONH ; Y = O
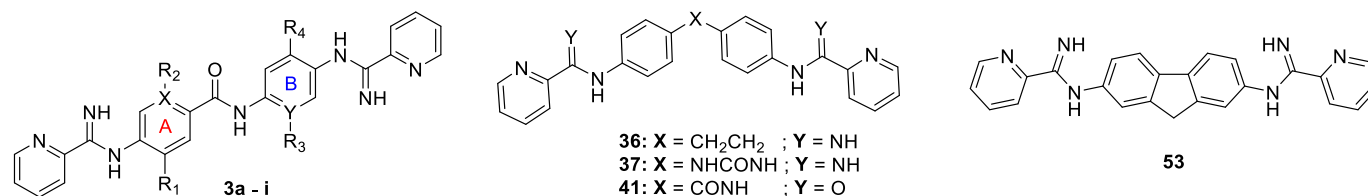
Cpd	T. brucei^a			HEK^b		T. cruzi^c		L929^d	SI^e		L. donovani^f		THP-1^g	SI^h	T. vaginalis^i
	WT^j	B48^k	RF^l		SI^m	Epi.	Ama.		Epi	Ama	Pro.	Ama.		Ama	
3a	0.40 ± 0.02	0.16 ± 0.03	0.4	>200	>500	0.21 ± 0.02	1.28 ± 0.34	89.1 ± 8.3	424.1	69.6	0.26 ± 0.05	0.65 ± 0.20	>50	>76.9	>40
3b	10.5 ± 1.9	12.5 ± 2.0	1.2	46.0 ± 0.1	4.3	0.03 ± 0.00	0.58 ± 0.09	44.9 ± 7.6	1495	77.3	1.63 ± 0.29	0.91 ± 0.30	18.6 ± 2.4	20.4	>40
3c	0.25 ± 0.04	0.69 ± 0.16	2.76	33.4 ± 3.1	134	0.06 ± 0.00	0.55 ± 0.17	9.55 ± 1.50	159.2	17.4	1.44 ± 0.13	0.78 ± 0.11	16.4 ± 1.3	21.1	25.7
3d	15.5 ± 2.7	28.1 ± 2.6	1.81	>100	>6.5	32.7 ± 1.8	nt^n	>200	>6.1		>20		>50		>40
3e	9.4 ± 0.96	7.6 ± 0.8	0.81	35.1 ± 3.5	3.7	0.03 ± 0.00	0.26 ± 0.04	103.6 ± 10.3	3454	398.6	0.89 ± 0.22	2.56 ± 0.41	49.4 ± 6.8	19.3	35.1
3g	5.07 ± 0.03	3.96 ± 0.22	0.78	69.0 ± 1.7	13.6	7.52 ± 0.26	3.51 ± 0.08	85.2 ± 4.8	11.3	24.3	3.00 ± 0.51	4.19 ± 0.57	>50	>11.9	>40
3h	0.12 ± 0.01	0.35 ± 0.02	2.92	14.2 ± 0.8	118	0.35 ± 0.07	nt	0.79 ± 0.08	2.26		0.97 ± 0.24	0.55 ± 0.06	11.2 ± 3.3	20.3	32.5
3i	23.7 ± 0.7	24.0 ± 0.4	1.01	>100	>4.2	>40 epi	nt	>200			1.47 ± 0.46	>10	>50		>40
36	>100	50.1 ± 2.7	<0.51	>100		4.33 ± 0.65	7.66 ± 0.75	>200	>46.2	>26.1	0.33 ± 0.06	1.11 ± 0.23	>50	>45.0	>40
37	>100	>100		nt		nt	nt	nt			nt	nt	nt		nt
41	>100	>100		>100		>40	nt	>200			>20	nt	nt		>40
53	5.4 ± 0.3	5.0 ± 0.3	0.93	58.5 ± 6.2	10.8	0.84 ± 0.13	1.26 ± 0.30	59.8 ± 8.4	71.2	47.5	0.77 ± 0.19	0.98 ± 0.12	46.5 ± 3.5	47.4	>40

^{a} Reference drugs: Pentamidine: 0.00034 ± 0.00002 µM (WT) and 0.111 ± 0.003 µM (B48; RF = 326); Diminazene: 0.010 ± 0.0007 µM (WT) and 0.012 ± 0.0008 µM (B48; RF = 1.2). ^{b} Human endothelial kidney cells. ^{c} Epimastigotes and intracellular amastigotes of *T. cruzi* strain CL-B5 *lacZ*; reference drug: Benznidazole: EC$_{50\ (epimastigote)}$ = 25.3 ± 2.1 µM, EC$_{50\ (amastigote)}$ = 0.54 ± 0.01 µM. ^{d} Cytotoxicity on L929 fibroblasts; reference drug: Benznidazole: EC$_{50}$ > 200 µM, SI > 7.9. ^{e} Selectivity index versus epimastigotes and amastigotes = EC$_{50}$ (L929)/ EC$_{50}$ (epimastigote or amastigote). ^{g} Cytotoxicity on THP-1 cells: Amphotericin B = 28.5 ± 4.5 µM, SI = 122. ^{h} Selectivity index versus amastigotes = EC$_{50}$ (THP-1) / EC$_{50}$ (amastigote). ^{i} *Trichomonas vaginalis*; reference drug: Metronidazole: 2.56 ± 0.58 µM. ^{j} Bloodstream forms trypomastigotes of *T. b. brucei* wild type strain s427. ^{k} *T. b. brucei* strain resistant to pentamidine. ^{l} Resistance factor = EC$_{50}$ (B48) / EC$_{50}$ (WT). ^{m} Selectivity index versus WT = EC$_{50}$ (HEK) / EC$_{50}$ (WT). ^{n} Not tested.

5.5. Preliminary pharmacological studies of lead compound 3a

5.5.1. Microsomal stability assay

5.5.1.1. Background

Liver metabolism is the most important pathway for elimination of most of the drugs in mammals. The hepatic enzyme's native ability for metabolizing a drug is commonly referred to as "intrinsic clearance", used to determine the hepatic clearance. The microsomal stability assay provides a means to measure the rate of disappearance of a test compound over time. This technique is primarily used to investigate the *in vitro* intrinsic clearance or identify the metabolites formed upon first path metabolism (Phase I, metabolism of cytochrome P450 (P450) and reduced nicotinamide adenine dinucleotide phosphate (NADPH) as enzyme co-factor).[40-43] However, liver microsomes can also be used to study Phase II metabolism if the correct incubation conditions are used.[43]

Metabolic and Microsomal stability of **3a** toward metabolism by cytochrome P450 (Phase-I metabolism) and Uridine Glucuronosyl-Transfererase (UGT) (Phase-II metabolism) was studied in the presence of the cofactors NADPH and uridine diphosphate glucuronic acid (UDPGA), respectively. These studies were carried out in collaboration with Dr. Tomás Herraiz at the Institute of Food Science, Technology and nutrition (ICTAN)-CSIC.

5.5.1.2. Results

The results of these studies are reported in Table using diclofenac as a positive control drug.

Compound **3a** was not apparently metabolized by human liver microsomes (HLM) and mouse liver microsomes (MLM), as no significant metabolite was found in the reaction up to 120 minutes. Therefore, **3a** is stable towards hepatic metabolism with a half-life time of more than 2 hours. In comparison, diclofenac was rapidly metabolized by HML (high intrinsic clearance) under the same conditions, with a half-life time of less than 30 minutes. In contrast, MLM (CD-1) slowly metabolized the drug diclofenac (Table 5.4).

Compound **3a** was not apparently modified in human serum and it was stable for 1 hour of incubation. Compound **3a** was not apparently metabolized by enzymes using the cofactor UDPGA (glucuronosyl transfereases) (Phase II enzymes) of mouse liver and human liver microsomes.

Then, it is concluded that under the experimental conditions used, compound **3a** is metabolically stable against microsomal fractions of human and mouse and in human serum.

Table 5.4: Microsomal stability of 3a and diclofenac with mouse (MLM) and human liver microsomes (HLM)

Fraction	Phase I/II	Assay	Cmpd. 3a % Remaining	Diclofenac % Remaining
Microsomal assay MLM CD-1[a] Metabolism	P450-NADPH[b]	Control (without fraction)	100.0	
		Assay (60 min)	92.0	
Microsomal assay HLM[c] Metabolism	P450-NADPH[b]	Control (without fraction)	100.0	
		Assay (60 min)	89.0	
HLM[c] Microsomal stability	P450-NADPH[b]	0 min	100.0	100.0
		15 min	93.2	48.8
		30 min	94.6	24.5
		60 min	100.0	7.16
		120 min	93.8	-
HLM[c] Metabolism	UGT-enzymes (UDPGA)[d]	Control (without UDPGA)	100	-
		Assay (60 min)	95.0	-
MLM CD-1[a] Microsomal stability	P450-NADPH[b]	0 min	100.0	100.0
		15 min	99.2	87.4
		30 min	94.6	75.1
		60 min	94.8	67.3
		120 min	93.3	-
MLM CD-1[a] Metabolism	UGT-enzymes (UDPGA)[d]	Control (without UDPGA)	100.0	
		Assay (60 min)	91.7	
Human serum (20 µL)		Control (without serum)	100.0	
		Assay (60 min)	89.1	

[a]MLM CD-1: Mouse (CD-1) liver microsome. [b]P450-NADPH: Cytochrome P450 monooxigenase - Reduced nicotinamide adenine dinucleotide phosphate. [c]HLM: Human liver microsomes. [d]UGT-enzymes (UDPGA): Uridine Glucuronosyl-Transfererase (Uridine diphosphate glucuronic acid).

5.6. Conclusions

Herein, we have evaluated the biological activity of the three synthesised series (**1**–**3**) against three kinetoplastid parasites (i.e., *T. brucei*, *T. cruzi* and *L. donovani*) and the urogenital parasite *T. vaginalis*. Furthermore, unspecific cytotoxicity against three different mammalian cell lines (i.e., HEK, L929 fibroblasts and THP-1) was tested and the selectivity indexes were determined.

Series **1** showed activity against *T. brucei* only, with EC_{50} values in the micromolar range (5.71 to 78.5 µM) and selectivity indexes (SI) in the range 1.3 to >35. Chlorine derivative **1c** was the most active and selective from this series. The potencies of this compound series against both wild-type (WT) and pentamidine-resistant (B48) strains were in the same range. The cytotoxicity evaluated against HEK cells and L929 fibroblasts showed that the bis(imidazolidin-2-amino) derivatives are non-toxic to mammalian cells as was previously observed.[28, 44, 45] With regard to *Leishmania*, compound **1g** was the only one that was active (EC_{50} = 7.64 µM) against promastigotes of *L. donovani*. Finally, the whole series was inactive against *T. cruzi* and *T. vaginalis.*

Series **2** displayed micromolar activity on *T. brucei* whereas it was mainly inactive against *T. cruzi* and *Leishmania* parasites. Hence, the replacement of the 2-aminoimidazoline groups by 2-aminobenzimidazole heterocycles did not improve the activity against the parasites *Leishmania* (promastigotes and amastigotes) and epimastigotes of *T. cruzi* with respect to lead **I** as hypothesised. Compound **30** was the sole compound to show leishmanicidal effect against promastigotes (EC_{50} = 8.67 µM), albeit with a poor selectivity (SI = 1.6). Thus, a general cytotoxic effect could be related to the leishmanicidal activity of **30**. The rest of this series showed disparate cytotoxicity values against HEK and THP-1 cells. Furthermore, only **34** (EC_{50} = 33.2 µM) had weak trichomonacidal efficacy with poor selectivity ($CC_{50} \approx 50$ µM).

Series **3** compounds are very potent inhibitors of *T. brucei*, *T. cruzi* and *Leishmania* growth, with adequate selectivity. The unsubstituted compounds **3a,** which is the closest analogue of **I**, proved to be the best antiparasitic compound with submicromolar activity and high selectivity against these 3 kinetoplastid parasites. Compound **3h** ($EC_{50\ (WT)}$ = 0.12 µM, SI = 118) emerged as another good candidate against *T. brucei.* In contrast, **3e** (but also **3a**, **3b**, and **53**) displayed better activity and selectivity against intracellular

amastigotes of *T. cruzi* ($EC_{50 \text{ (amastigote)}}$ = 0.26, 1.28, 0.58, and 1.26 µM, respectively). As regards to *L. donovani*, **3a**, **36** and **53** (and also **3e**) can be considered as new antileishmanial lead compounds.

In summary, compound **3a** appears as a new lead compound active in the submicromolar range against BSF trypomastigotes of *T. brucei*, and intracellular amastigotes of *L. donovani* and *T. cruzi*. This compound shows high selectivity indexes against the mammalian cells tested (i.e., HEK, THP-1, and L929) and it is metabolically stable towards liver metabolism (i.e., HLM and MLM) and in human serum. Therefore, **3a** is a good candidate to perform further *in vivo* assays.

5.7. References

1. Gull, K. The biology of kinetoplastid parasites: insights and challenges from genomics and post-genomics. *Int. J. Parasitol.* **2001,** 31, 443-452.

2. Wang, A. L.; Wang, C. C. Isolation and characterization of DNA from *Tritrichomonas foetus* and *Trichomonas vaginalis*. *Mol. Biochem. Parasitol.* **1985,** 14, 323-335.

3. Mandel, M.; Honigberg, B. M. Isolation and Characterization of Deoxyribonucleic Acid of Two Species of *Trichomonas donne*. *J. Protozool.* **1964,** 11, 114-116.

4. Brack, C.; Delain, E.; Riou, G. Replicating, convalently closed, circular DNA from kinetoplasts of *Trypanosoma cruzi*. *Proc. Natl. Acad. Sci. U.S.A.* **1972,** 69, 1642-1646.

5. Voytik-Harbin, S. L.; Brightman, A. O.; Waisner, B.; Lamar, C. H.; Badylak, S. F. Application and evaluation of the alamarBlue assay for cell growth and survival of fibroblasts. *In Vitro Cell. Dev. Biol.: Anim.* **1998,** 34, 239-246.

6. O'Brien, J.; Wilson, I.; Orton, T.; Pognan, F. Investigation of the Alamar Blue (resazurin) fluorescent dye for the assessment of mammalian cell cytotoxicity. *Eur. J. Biochem.* **2000,** 267, 5421-5426.

7. Mikus, J.; Steverding, D. A simple colorimetric method to screen drug cytotoxicity against *Leishmania* using the dye Alamar Blue®. *Parasitol. Int.* **2000,** 48, 265-269.

8. Räz, B.; Iten, M.; Grether-Bühler, Y.; Kaminsky, R.; Brun, R. The Alamar Blue® assay to determine drug sensitivity of African trypanosomes (*T. b. rhodesiense* and *T. b. gambiense*) *in vitro*. *Acta Trop.* **1997,** 68, 139-147.

9. Stockert, J. C.; Horobin, R. W.; Colombo, L. L.; Blázquez-Castro, A. Tetrazolium salts and formazan products in Cell Biology: Viability assessment, fluorescence imaging, and labeling perspectives. *Acta Histochem.* **2018,** 120, 159-167.

10. Vistica, D. T.; Skehan, P.; Scudiero, D.; Monks, A.; Pittman, A.; Boyd, M. R. Tetrazolium-based assays for cellular viability: a critical examination of selected parameters affecting formazan production. *Cancer Res. J.* **1991,** 51, 2515-2520.

11. Maehara, Y.; Anai, H.; Tamada, R.; Sugimachi, K. The ATP assay is more sensitive than the succinate dehydrogenase inhibition test for predicting cell viability. *Eur. J. Cancer Clin. Oncol.* **1987,** 23, 273-276.

12. Slater, T. F.; Sawyer, B.; Sträuli, U. Studies on succinate-tetrazolium reductase systems: III. Points of coupling of four different tetrazolium salts III. Points of coupling of four different tetrazolium salts. *Biochim. Biophys. Acta* **1963,** 77, 383-393.

13. Berridge, M. V.; Tan, A. S. Characterization of the Cellular Reduction of 3-(4,5-dimethylthiazol-2-yl)-2,5-diphenyltetrazolium bromide (MTT): Subcellular Localization, Substrate Dependence, and Involvement of Mitochondrial Electron Transport in MTT Reduction. *Arch. Biochem. Biophys.* **1993,** 303, 474-482.

14. Mosmann, T. Rapid colorimetric assay for cellular growth and survival: Application to proliferation and cytotoxicity assays. *J. Immunol. Methods* **1983,** 65, 55-63.

15. Möckli, N.; Auerbach, D. Quantitative β-galactosidase assay suitable for high-throughput applications in the yeast two-hybrid system. *BioTechniques* **2004,** 36, 872-876.

16. Fonseca-Berzal, C.; Arán, V. J.; Escario, J. A.; Gómez-Barrio, A. Experimental models in Chagas disease: a review of the methodologies applied for screening compounds against *Trypanosoma cruzi*. *Parasitol. Res.* **2018,** 117, 3367-3380.

17. Pavlovic Djuranovic, S.; Erath, J.; Andrews, R. J.; Bayguinov, P. O.; Chung, J. J.; Chalker, D. L.; Fitzpatrick, J. A.; Moss, W. N.; Szczesny, P.; Djuranovic, S. *Plasmodium falciparum* translational machinery condones polyadenosine repeats. *eLife* **2020,** 9.

18. Fonseca-Berzal, C.; Merchán Arenas, D. R.; Romero Bohórquez, A. R.; Escario, J. A.; Kouznetsov, V. V.; Gómez-Barrio, A. Selective activity of 2,4-diaryl-1,2,3,4-tetrahydroquinolines on *Trypanosoma cruzi* epimastigotes and amastigotes expressing β-galactosidase. *Bioorg. Med. Chem. Lett.* **2013,** 23, 4851-4856.

19. Vega Gómez, M. C. *Trypanosoma cruzi* : new colorimetric screening methods and therapeutic alternatives. Doctoral thesis, Universidad Complutense de Madrid. Facultad de Farmacia. , 2006.

20. Kennedy, M. L.; Cortés-Selva, F.; Pérez-Victoria, J. M.; Jiménez, I. A.; González, A. G.; Muñoz, O. M.; Gamarro, F.; Castanys, S.; Ravelo, A. G. Chemosensitization of a Multidrug-Resistant *Leishmania tropica* Line by New Sesquiterpenes from *Maytenus magellanica* and *Maytenus chubutensis*. *J. Med. Chem.* **2001,** 44, 4668-4676.

21. Manzano, J. I.; Cueto-Diaz, E. J.; Olias-Molero, A. I.; Perea, A.; Herraiz, T.; Torrado, J. J.; Alunda, J. M.; Gamarro, F.; Dardonville, C. Discovery and Pharmacological Studies of 4-Hydroxyphenyl-Derived Phosphonium Salts Active in a Mouse Model of Visceral Leishmaniasis. *J. Med. Chem.* **2019,** 62, 10664-10675.

22. Seifert, K.; Pérez-Victoria, F. J.; Stettler, M.; Sánchez-Cañete, M. P.; Castanys, S.; Gamarro, F.; Croft, S. L. Inactivation of the miltefosine transporter, LdMT, causes miltefosine resistance that is conferred to the amastigote stage of *Leishmania donovani* and persists *in vivo*. *Int. J. Antimicrob. Agents* **2007,** 30, 229-235.

23. García-Hernández, R.; Manzano, J. I.; Castanys, S.; Gamarro, F. *Leishmania donovani* develops resistance to drug combinations. *PLoS Negl. Trop. Dis.* **2012,** 6, e1974.

24. de Koning, H. P.; MacLeod, A.; Barrett, M. P.; Cover, B.; Jarvis, S. M. Further evidence for a link between melarsoprol resistance and P2 transporter function in African trypanosomes. *Mol. Biochem. Parasitol.* **2000,** 106, 181-185.

25. Matovu, E.; Stewart Mhairi, L.; Geiser, F.; Brun, R.; Mäser, P.; Wallace Lynsey, J. M.; Burchmore Richard, J.; Enyaru John, C. K.; Barrett Michael, P.; Kaminsky, R.; Seebeck, T.; de Koning Harry, P. Mechanisms of Arsenical and Diamidine Uptake and Resistance in *Trypanosoma brucei*. *Eukaryot. Cell* **2003,** 2, 1003-1008.

26. Bridges, D. J.; Gould, M. K.; Nerima, B.; Mäser, P.; Burchmore, R. J. S.; de Koning, H. P. Loss of the High-Affinity Pentamidine Transporter Is Responsible for High Levels of Cross-Resistance between Arsenical and Diamidine Drugs in African Trypanosomes. *Mol. Pharmacol.* **2007,** 71, 1098.

27. Gudin, S.; Quashie, N. B.; Candlish, D.; Al-Salabi, M. I.; Jarvis, S. M.; Ranford-Cartwright, L. C.; de Koning, H. P. *Trypanosoma brucei*: A survey of pyrimidine transport activities. *Exp. Parasitol.* **2006,** 114, 118-125.

28. Ríos Martínez, C. H.; Nué Martinez, J. J.; Ebiloma, G. U.; de Koning, H. P.; Alkorta, I.; Dardonville, C. Lowering the pK_a of a bisimidazoline lead with halogen atoms results in improved activity and selectivity against *Trypanosoma brucei in vitro*. *Eur. J. Med. Chem.* **2015,** 101, 806-817.

29. Kavsan, V. M.; Iershov, A. V.; Balynska, O. V. Immortalized cells and one oncogene in malignant transformation: old insights on new explanation. *BMC Cell Biol.* **2011,** 12, 23.

30. Fonseca-Berzal, C.; Ibáñez-Escribano, A.; Reviriego, F.; Cumella, J.; Morales, P.; Jagerovic, N.; Nogal-Ruiz, J. J.; Escario, J. A.; da Silva, P. B.; Soeiro, M. d. N. C.; Gómez-Barrio, A.; Arán, V. J. Antichagasic and trichomonacidal activity of 1-substituted 2-benzyl-5-nitroindazolin-3-ones and 3-alkoxy-2-benzyl-5-nitro-2*H*-indazoles. *Eur. J. Med. Chem.* **2016,** 115, 295-310.

31. Rolón, M.; Seco, E. M.; Vega, C.; Nogal, J. J.; Escario, J. A.; Gómez-Barrio, A.; Malpartida, F. Selective activity of polyene macrolides produced by genetically modified *Streptomyces* on *Trypanosoma cruzi*. *Int. J. Antimicrob. Agents* **2006,** 28, 104-109.

32. Buckner, F. S.; Verlinde, C. L.; Flamme, A. C. L.; Voorhis, W. C. V. Efficient technique for screening drugs for activity against *Trypanosoma cruzi* using parasites expressing beta-galactosidase. *Antimicrob. Agents Chemother.* **1996,** 40, 2592-2597.

33. Ibáñez-Escribano, A.; Meneses-Marcel, A.; Marrero-Ponce, Y.; Nogal-Ruiz, J. J.; Arán, V. J.; Gómez-Barrio, A.; Escario, J. A. A sequential procedure for rapid and accurate identification of putative trichomonacidal agents. *J. Microbiol. Methods* **2014,** 105, 162-167.

34. Ibáñez Escribano, A.; Meneses Marcel, A.; Machado Tugores, Y.; Nogal Ruiz, J. J.; Arán Redó, V. J.; Escario García-Trevijano, J. A.; Gómez Barrio, A. Validation of a modified fluorimetric assay for the screening of trichomonacidal drugs. *Mem. Inst. Oswaldo Cruz* **2012,** 107, 637-643.

35. Ibáñez-Escribano, A.; Reviriego, F.; Vela, N.; Fonseca-Berzal, C.; Nogal-Ruiz, J. J.; Arán, V. J.; Escario, J. A.; Gómez-Barrio, A. Promising hit compounds against resistant trichomoniasis: Synthesis and antiparasitic activity of 3-(ω-aminoalkoxy)-1-benzyl-5-nitroindazoles. *Bioorg. Med. Chem. Lett.* **2021,** 37, 127843.

36. Alghamdi, A. H.; Munday, J. C.; Campagnaro, G. D.; Gurvic, D.; Svensson, F.; Okpara, C. E.; Kumar, A.; Quintana, J.; Martin Abril, M. E.; Milić, P.; Watson, L.; Paape, D.; Settimo, L.; Dimitriou, A.; Wielinska, J.; Smart, G.; Anderson, L. F.;

Woodley, C. M.; Kelly, S. P. Y.; Ibrahim, H. M.; Hulpia, F.; Al-Salabi, M. I.; Eze, A. A.; Sprenger, T.; Teka, I. A.; Gudin, S.; Weyand, S.; Field, M.; Dardonville, C.; Tidwell, R. R.; Carrington, M.; O'Neill, P.; Boykin, D. W.; Zachariae, U.; De Koning, H. P. Positively selected modifications in the pore of TbAQP2 allow pentamidine to enter *Trypanosoma brucei*. *eLife* **2020,** 9, e56416.

37. Collar, C. J.; Al-Salabi, M. I.; Stewart, M. L.; Barrett, M. P.; Wilson, W. D.; de Koning, H. P. Predictive Computational Models of Substrate Binding by a Nucleoside Transporter*. *J. Biol. Chem.* **2009,** 284, 34028-34035.

38. Alghamdi, A. H.; Munday, J. C.; Campagnaro, G. D.; Gurvic, D.; Svensson, F.; Okpara, C. E.; Kumar, A.; Quintana, J.; Martin Abril, M. E.; Milic, P.; Watson, L.; Paape, D.; Settimo, L.; Dimitriou, A.; Wielinska, J.; Smart, G.; Anderson, L. F.; Woodley, C. M.; Kelly, S. P. Y.; Ibrahim, H. M.; Hulpia, F.; Al-Salabi, M. I.; Eze, A. A.; Sprenger, T.; Teka, I. A.; Gudin, S.; Weyand, S.; Field, M.; Dardonville, C.; Tidwell, R. R.; Carrington, M.; O'Neill, P.; Boykin, D. W.; Zachariae, U.; De Koning, H. P. Positively selected modifications in the pore of TbAQP2 allow pentamidine to enter *Trypanosoma brucei*. *eLife* **2020,** 9.

39. Munday, J. C.; Settimo, L.; de Koning, H. P. Transport proteins determine drug sensitivity and resistance in a protozoan parasite, *Trypanosoma brucei*. *Front. Pharmacol.* **2015,** 6, 1-10.

40. Paine, M. J. I.; Scrutton, N. S.; Munro, A. W.; Gutierrez, A.; Roberts, G. C. K.; Wolf, C. R. Electron Transfer Partners of Cytochrome P450. In *Cytochrome P450: Structure, Mechanism, and Biochemistry*, Ortiz de Montellano, P. R., Ed. Springer US: Boston, MA, 2005; pp 115-148.

41. Wang, M.; Roberts David, L.; Paschke, R.; Shea Thomas, M.; Masters Bettie Sue, S.; Kim Jung-Ja, P. Three-dimensional structure of NADPH–cytochrome P450 reductase: Prototype for FMN- and FAD-containing enzymes. *Proc. Natl. Acad. Sci. U. S. A.* **1997,** 94, 8411-8416.

42. Guengerich, F. P.; Martin, M. V.; Sohl, C. D.; Cheng, Q. Measurement of cytochrome P450 and NADPH–cytochrome P450 reductase. *Nat. Protoc.* **2009,** 4, 1245-1251.

43. Zhengyin, Y.; Gary, W. C. Metabolism Profiling, and Cytochrome P450 Inhibition & Induction in Drug Discovery. *Curr. Top. Med. Chem.* **2001,** 1, 403-425.

44. Rodríguez, F.; Rozas, I.; Kaiser, M.; Brun, R.; Nguyen, B.; Wilson, W. D.; García, R. N.; Dardonville, C. New Bis(2-aminoimidazoline) and Bisguanidine DNA Minor

Groove Binders with Potent *in Vivo* Antitrypanosomal and Antiplasmodial Activity. *J. Med. Chem.* **2008,** 51, 909-923.

45. Dardonville, C.; Barrett, M. P.; Brun, R.; Kaiser, M.; Tanious, F.; Wilson, W. D. DNA Binding Affinity of Bisguanidine and Bis(2-aminoimidazoline) Derivatives with *in vivo* Antitrypanosomal Activity. *J. Med. Chem.* **2006,** 49, 3748-3752.

CHAPTER 6

## 6. Chapter 6: Drug delivery of compound 3a using nanostructured lipid carriers.

6.1. Introduction

6.1.1. Drug delivery systems using nanoparticles

Nano delivery systems are a relatively new but rapidly evolving science that utilizes materials at nanoscale level. These systems are used not only as diagnostic tools but also to deliver therapeutic agents to specific target sites in a controlled manner.[1, 2] Nanotechnology offers multiple benefits in treating chronic human diseases by site-specific and target-oriented delivery of precise medicines (e.g., antifungal,[3] anti-HIV,[4] antineoplastic drugs,[5] etc.).[1] Drug delivery systems based on nanoparticles (NP) have been successfully employed in the delivery of drugs to its target sites, largely based on enhancing the solubility, absorption, bioavailability, and controlled-release of drugs.[6] Other advantages of such systems include a high drug payload, an extended drug half-life, and an improved therapeutic index along with reduced immunogenicity and toxicity.[7]

Nanostructured lipid carriers (NLC) are versatile nanoparticles made of a mixture of solid lipid, liquid lipid and an aqueous phase containing a surfactant or a mixture of surfactants. They form a lipid matrix that can be loaded with both lipophilic and hydrophilic drugs (Figure 1).[2, 8] NLC present several advantages: their production is relatively simple and scalable, they have long-term stability and they can be sterilized by filtration. Furthermore, NLC can be administered by different routes (e.g., oral, transdermal, ocular, intranasal, intravenous) and show very favourable toxicity profiles.[2] NLC are a second generation of lipid carriers that lack a definite crystalline structure. They have increased loading capacity and improved potential of controlled drug release compared to first generation solid lipid nanoparticles (SLN) which are crystalline nanostructures made of either glycerides or waxes (or mixtures of both) stabilized by a surfactant.[8-10]

After endocytosis, the release of the encapsulated bioactive compound from NLC is believed to occur by simultaneous diffusion from the NLC and degradation of the lipid particles in the late endosome (Figure 6.1). The *in vivo* fate of lipid-based nanoparticles depends on various factors including the particle size, lipid composition and surface decoration.[8] The particle size is determinant in the biodistribution because NPs smaller

than 100 nm are able to escape capture by circulating macrophages. As a consequence, they can circulate in the blood for a longer time.[11-13]
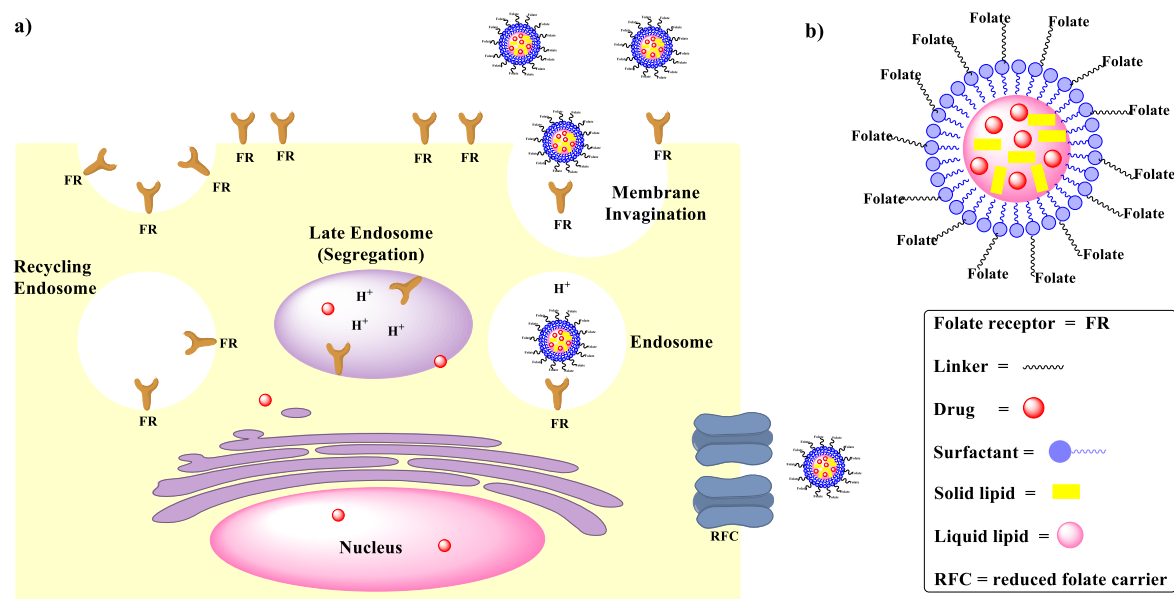
Figure 6.1: a) Folate receptor-mediated endocytosis of NLC folate-drug conjugates. The NLC folate-drug conjugate is taken up into cells by binding of folate to the folate receptor. Invagination of the plasma membrane results in receptor mediated endocytosis. The action of lipases of the endosome results in dissociation of the drug cargo and the folate receptor is recycled to the cell surface once more. b) Design of NLC covered with folate residues (Adapted from *Curr. Med. Chem.* **2018**, *25*, 2675-2708).[14]

Several examples of application of NLC to the delivery of leishmanicidal drugs have been reported.[15-17] For instance, NLC were used to deliver a diselenide leishmanicidal compound in a mouse model of visceral leishmaniasis. In this study, the authors showed that is was possible to control the release of the associated cargo by modification of the NLC lipid matrix.[18]

During the course of this thesis, different families of DNA MGBs were synthesised and tested against different kinetoplastid parasites. Several compounds showed in vitro activity against the trypanosomatid parasites *L. donovani*, *T. cruzi* and *T. b. brucei*. As mentioned in Chapter 1 & 5, a compound targeting the kDNA of *Leishmania* or *T. cruzi* will have to cross 4 membranes to reach its biological target (i.e., host cell plasma membrane, parasitophorous vacuole membrane,[19] *Leishmania* plasma membrane, and mitochondrial membrane). Hence, we envisioned the use of NLC to improve the delivery of these kinetoplast-targeting compounds to the intracellular *Leishmania* parasites. Compound **3a**,

which was the most active and selective compound against *L. donovani* (see Chapter 4 & 5), was chosen as the cargo to be inserted in a nanostructured lipid carrier.

The synthesis of nanoparticles presented in this chapter, was carried out in collaboration with Dr. Ana González Paredes and her research group, at the Medicinal Chemistry Institute – CSIC.

6.1.2. Role of macrophages in *Leishmania* infection

Macrophages are specialized phagocytic cells that attack external agents such as infectious microbes (e.g., parasites) and cancer cells.[20] They are originated by the differentiation of blood monocytes (leaving the circulation and differentiated in different tissues). They have two main functions: (i) innate or non-specific immunity and (ii) adaptive specific-immunity. Macrophages are divided into two categories: pro-inflammatory or traditionally activated macrophages (M_1), and anti-inflammatory or alternatively activated macrophages (M_2). M_1 macrophages are immune effector cells that are aggressive towards microorganisms and have a greater ability to engulf and digest damaged cells, whereas M_2 macrophages help with wound healing, tissue repair, and immune system activation by generating anti-inflammatory cytokines.[7]

Macrophages are important in the course of leishmaniasis infection because resident macrophages of reticulo-endothelial organs such as the spleen and the liver serve as safe havens for *Leishmania* amastigotes in the mammalian hosts.[7, 21] *Leishmania* promastigotes have proven to survive and be able to proliferate within the phagolysosome of macrophages, by differentiating into amastigotes (See Chapter 1). It is this amastigote form which is able to escape from the host cell and reinfect other cells (e.g., macrophages, dendritic cells, fibroblasts, etc). Hence, amastigotes are the main form responsible for spreading the disease and they are accountable for acute disease and chronic infections.[21, 22]

Leishmania amastigotes are able to internalize both low molecular weight molecules and large macromolecules to fulfil their nutritional requirements. Low molecular weight substances are acquired via plasma membrane transporters, used also for the transport of

cations (Fe^{2+}, Mg^{2+}), as well as the phagolysosome membrane transporters. In the case of large macromolecules, they are internalised by endocytosis.[20, 21]

As macrophages are key to the *Leishmania* life-cycle, a targeting approach that uses macrophage's ability to internalize specific biomolecules (e.g., folic acid) appeared as a promising strategy to improve the delivery of anti-leishmanial compounds to the parasite.

6.1.3. Folic acid receptor as a target for drug delivery of DNA minor groove binder drugs to *Leishmania* parasites

Activated macrophages show an over-expression of the folic acid receptor, named folate receptor-β (FR-β), which has high affinity for folic acid (FA). Therefore, folate-based NPs can be exploited to target therapeutic agents (e.g. leishmanicidal drugs) to activated macrophages; NPs functionalized with FA are effectively internalized by macrophages by receptor-mediated endocytosis, without promoting their uptake by other healthy cells and tissues.[7] We rationalized that FA-based NLC loaded with compound **3a** would be taken up effectively in macrophages, which should increase its absorption in the target cell (i.e., *Leishmania* amastigotes). Once internalized into the macrophage, the drug must be released effectively in order to act on the therapeutic target.[14]

As part of this research work, we decided to prepare nanoparticles targeting the folate receptor, which is present in the macrophages. The aim was to improve the cellular penetration of lead compound **3a**, therefore its activity and selectivity against *Leishmania*.

6.2. Methods

6.2.1. Synthesis of Nanostructured Lipid Carriers

As a first step, NLC were prepared with compound **3a** loaded inside the lipid matrix. Due to the use of octadecylamine in their composition, NLC expose free amine residues on its external surface. These amines are able to react with carboxylic acids (e.g., folic acid) and form covalent bonds, resulting in NLC conjugates that carry folate residues (Figure 6.2).
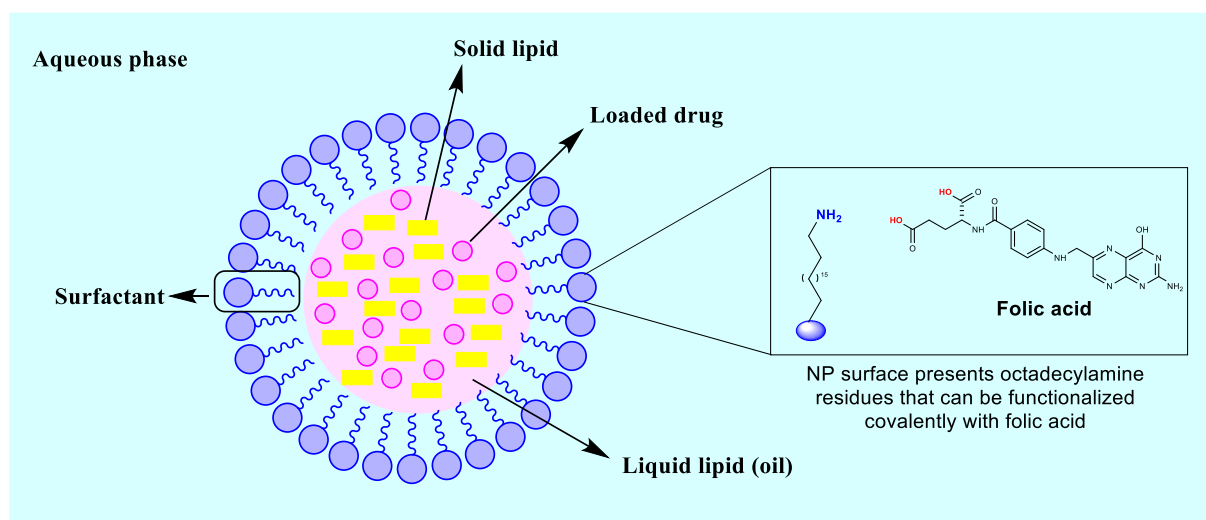
Figure 6.2: Composition of nanostructured lipid carriers (NLC) consisting of solid lipid (yellow), liquid lipid (oil, pink), drug, surfactant and aqueous phase (Adapted from *Molecules* **2022**, *27*, 289)[23]

Nanostructured lipid carriers (Figure 6.2) were synthetized using a microwave reactor by a modification of the warm microemulsion method previously described.[24] Briefly, all components shown in Table 6.1 were weighted in a microwave tube. The reaction was carried out in a microwave reactor (Biotage® Initator+) at 68 °C for 20 minutes, obtaining a clear microemulsion. This was dispersed in water at the same temperature (68 °C) at a ratio 1:20 (v/v) under magnetic stirring (1250 rpm), then it was left to cool down under magnetic stirring. A temperature < 25 °C was achieved after 30 minutes.

Obtained NLC dispersion were then washed 3 times by tangential flow filtration (TFF), using this technique also for NLC concentration by volume reduction up to 10 mL. In the case of NLC synthesized for later functionalization, NLC dispersion was only concentrated by tangential flow filtration (TFF) until reduction of initial volume to 10 mL.

Table 6.1: Microemulsion composition for the synthesis of NLC

Component	Loaded formulation (mg)	Blank formulation (mg)
Lauroglycol 90	20	20
Sunsoft 750C (GML)	60	60
Lipoid S75	5.4	5.4
Octadecylamine	6	6
Tween 20	100	100
Myrj S40	20	20
Compound 3a	1.5	-
H$_2$O milliQ	890	890

The physicochemical characterization of NLC was carried out using a Zetasizer nano ZS90 (Malvern Panalitical, UK). The Hydrodynamic diameter and polydispersity index (PDI) of blank and loaded NLC were assessed by photon correlation spectroscopy (PCS). All measurements were performed in triplicate at room temperature. The determination of zeta potential, NLC's surface charge, were carried out by electrophoretic Light Scattering (ELS) by NLC dilution in sodium chloride 100 mM (1:50) prior to the analyses. Each sample was analyzed in triplicates at room temperature.

6.2.2. Determination of the encapsulation efficiency of 3a

The concentration of 3a in loaded-NLC was determined before and after the purification process via HPLC–MS analysis using a SunFire C18 3.5 μm 2.1 × 50 mm column. The chromatography was carried out at a flow rate 1 mL/min, using a gradient of water/acetonitrile (containing 0.02 % formic acid) from 95/5 to 5/95 in t = 5 minutes. A calibration curve was obtained by dissolving 3a in ethyl acetate and diluting it in acetonitrile at different concentrations (1 μg/mL – 1 mg/mL). The theoretical

concentration of compound **3a** loaded in the NLC is 170 µg/mL (10 mL of reaction volume). **3a**–NLC analytical samples were prepared by dilution (1:50, v/v) of final NLC dispersion (0.02 µL), with acetonitrile (0.98 µL) and then filtered with a 0.2 µm polyethersulfone (PES) filter before analysis. This dilution step is required in first instance to destroy the NLC and release the encapsulated compound **3a** (analyte), using the selected dilution factor in order to fit the concentration of the analytical samples within the concentration range of the calibration curve. Entrapment efficiency (EE %) was calculated using the following formula:

$$\textbf{EE \%} = \frac{C_{AP}}{C_{BP}} \times 100$$

where C_{AP} is the concentration of **3a** obtained after the purification process, and C_{BP} is the concentration of **3a** before the purification process.

6.2.3. Functionalization with folic acid

NLC surface was functionalized with folic acid (FA) by covalent linkage to the amine residues present on the NLC surface.[25, 26] For this, folic acid was added in a molar ratio 2:1 with octadecylamine (ODA) in HEPES 1M (pH 7.5 – 8.0) in the presence of *N*-Ethyl-*N*′-(3-dimethylaminopropyl)carbodiimide hydrochloride (EDC-HCl) and sulfo-*N*-hydroxysuccinimide (sulfo-NHS). The molar ratio between folic acid, EDC and sulfo-NHS was 1:3:3.3. The reaction was left under magnetic stirring (700 rpm) for 4 hours. At pre-established time points (0, 1, 2, 3 and 4 hours), a sample was taken (0.5 mL) to evaluate the incorporation of folic acid. For this, the sample was washed 3 times with Amicon 100 KDa and the zeta potential was measured, because the effective addition of folic acid should cause an inversion of NLC zeta potential, from positive to negative.

At the end of the reaction, FA-functionalized NLC were purified by washing 3 times by tangential flow filtration in order to remove the excess reagents. Finally, the sample was concentrated to obtain a final volume of 10 mL.

The amount of folic acid attached to the NLC was determined spectrophotometrically at 280 nm using a Clariostar Plus Microplate reader with a UV detector. To do so, the FA-functionalized NLC was destroyed by dilution (1:20, v/v) with a polar solvent (i.e.,

methanol) in order to release attached folic acid. Then, the concentration of folic acid in FA-functionalized NLC was calculated with a calibration curve of folic acid in methanol (1 µg/mL – 42 µg/mL).

6.2.4. Stability studies

NLC colloidal stability was evaluated on storage at room temperature and in the culture medium selected for biological studies. For this, measurements of the hydrodynamic diameter, polydispersity index and zeta potential at preestablished time-points were carried out during 60 days.

6.3. Results

6.3.1. Nanostructured Lipid Carriers characterization

The synthesized NLC, either loaded with compound **3a** or blank, showed particles' hydrodynamic size around 200 nm with polydispersity index (PDI) values < 0.3, which indicates quite homogeneous size distribution. As expected, zeta potential was positive confirming the presence of octadecylamine in the surface.

The incorporation of compound **3a** in both loaded (C = 12 µM) and FA-loaded (C = 10 µM) formulations was measured by means of HPLC quantification, showing a small detriment in the concentration ($\approx$ 2 µM) due to the functionalization process. However, these active compound concentrations were >10-fold higher than the EC_{50} value of **3a** against intracellular amastigotes of *Leishmania donovani* (0.65 µM, see Chapter 5), indicating that the loading was adequate to carry out the biological assays against *Leishmania*.
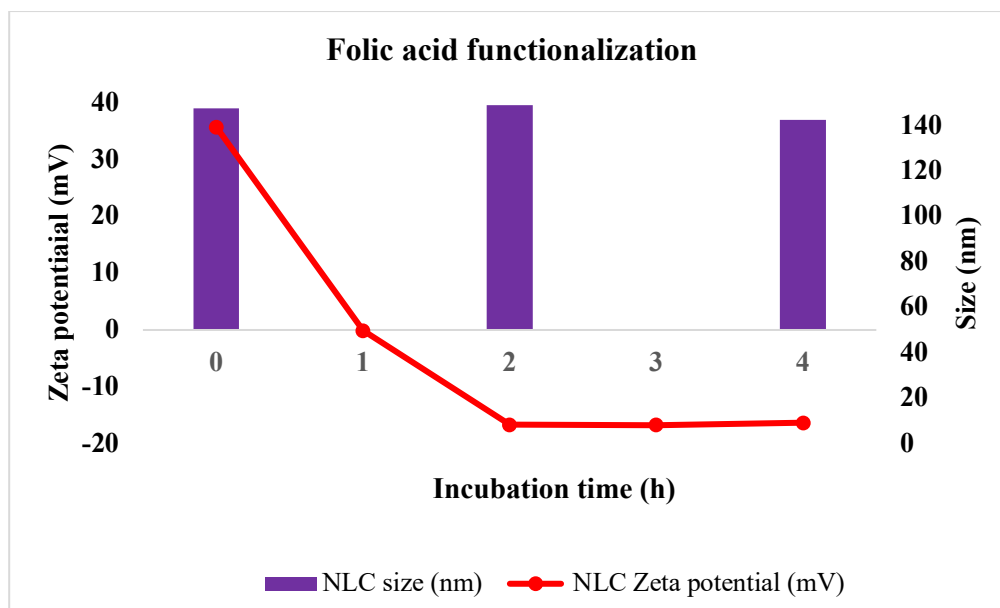
Figure 6.3: Monitoring folic acid functionalization process by changes in zeta potential

The incorporation of folic acid on the NLC surface was achieved by incubation of NLC with folic acid in the presence of EDC and sulfo-NHS at slightly basic pH (7.5 – 8.0). Optimization of the incubation time needed for completing the functionalization was determined by monitoring zeta potential during 4 hours.

As shown in Figure 6.3, the addition of folic acid caused an inversion in zeta potential from positive to negative, reaching a plateau after 2 hours of incubation, whereas the NP size did not change due to the incubation process. The concentration of folic acid on the NLC was determined spectrophotometrically (162 ± 3 µg/mL). Although this concentration represented 15% of the initial amount of folic acid used in the incubation process, it proved to be enough to ensure particle functionalization, as demonstrated by the zeta potential inversion. Table 6.2 shows in detail the characterization data of the formulations synthesized.

Table 6.2: Characterization data of NLC prepared (n = 3–6 ± SD)

NLC type	Name	Size (nm)	PDI	Z potential (mV)
Loaded	**3a**–NP	193 ± 18	0.315 ± 0.035	+35.0 ± 4
Loaded, folic acid functionalized	**3a**–FA-NP	125 ± 18	0.257 ± 0.022	-16 ± 2
Blank	B–NP	160 ± 15	0.289 ± 0.024	+33 ± 3
Blank, folic acid functionalized	B–FA-NP	131 ± 16	0.263 ± 0.039	-18 ± 2

NP: nanoparticle: FA: folic acid: B: blank

6.3.2. Storage stability

Blank NLC showed good colloidal stability during 60 days of storage at room temperature. As shown in **Error! Reference source not found.**, the size did not change over the period of study, whereas positive zeta potential decreased and, after 40 days, turned negative, indicating the denaturation of the NLC. The same behavior was observed for NLC loaded with **3a** (Figure 6.4b).

On the other hand, folic acid-functionalized NLC have limited stability, and after 21 days of storage at room temperature, a yellow precipitate was observed at the bottom of the vial. Storage at room temperature was selected because the composition of the NLC formulation contains fatty acids. Hence, storage at lower temperatures could produce a faster precipitation. However, these are only preliminary results and further studies will be needed to improve the storage stability of these NPs.
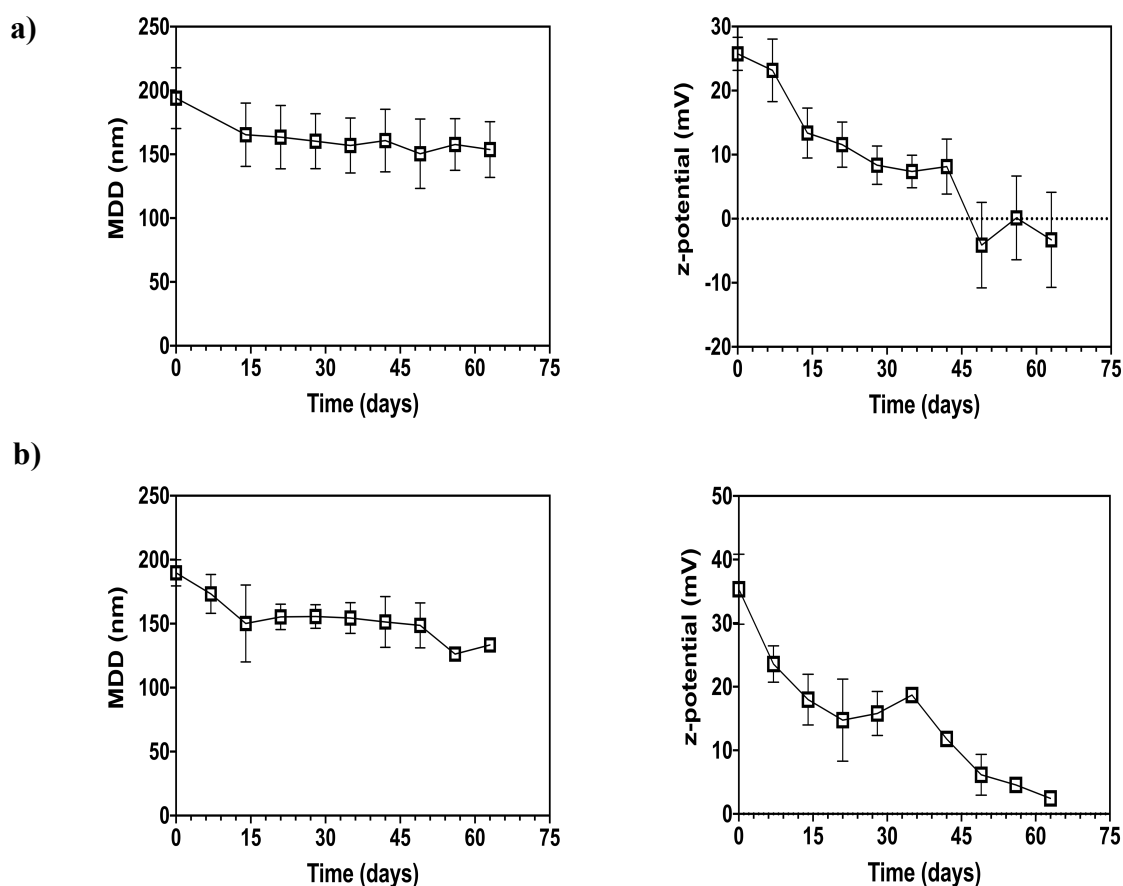
Figure 6.4: (a) Evolution of size and zeta potential of blank NLC over time at room temperature. **(b)** Evolution of size and zeta potential of **3a** loaded NLC over time at room temperature.

6.4. Conclusion and outlook

We successfully prepared NLC loaded with compound **3a**, the storage stability of which depends on the decoration of the NPs. Blank NLC were very stable at room temperature (60 days), whereas folic acid-functionalized NLC displayed limited stability (<21 days). This storage stability should be taken into account for the sake of biological studies. However, the ease of synthesis of these NLC is clearly an advantage that can outweigh this shortcoming.

The biological evaluation of the NCL will be performed at Teesside University (United Kingdom), in collaboration with Dr. Godwin Ebiloma. The synthesized NLC will be evaluated against intracellular amastigotes and axenic amastigotes of *Leishmania* sp. Four series of NLC are going to be tested: (1) Blank NLC, (2) Blank FA-functionalized NLC, (3) **3a**-loaded NLC and (4) **3a**-loaded FA-functionalized NLC. As control, the EC_{50} value of compound **3a** alone will be evaluated.

6.5. References

1. Wilczewska, A. Z.; Niemirowicz, K.; Markiewicz, K. H.; Car, H. Nanoparticles as drug delivery systems. *Pharmacol. Rep.* **2012,** 64, 1020-1037.

2. Salvi, V. R.; Pawar, P. Nanostructured lipid carriers (NLC) system: A novel drug targeting carrier. *J. Drug Delivery Sci. Technol.* **2019,** 51, 255-267.

3. Pandey, R.; Ahmad, Z.; Sharma, S.; Khuller, G. K. Nano-encapsulation of azole antifungals: Potential applications to improve oral drug delivery. *Int. J. Pharm.* **2005,** 301, 268-276.

4. Dev, A.; Binulal, N. S.; Anitha, A.; Nair, S. V.; Furuike, T.; Tamura, H.; Jayakumar, R. Preparation of poly(lactic acid)/chitosan nanoparticles for anti-HIV drug delivery applications. *Carbohydr. Polym.* **2010,** 80, 833-838.

5. Nanjwade, B. K.; Singh, J.; Parikh, K. A.; Manvi, F. V. Preparation and evaluation of carboplatin biodegradable polymeric nanoparticles. *Int. J. Pharm.* **2010,** 385, 176-180.

6. Patra, J. K.; Das, G.; Fraceto, L. F.; Campos, E. V. R.; Rodriguez-Torres, M. d. P.; Acosta-Torres, L. S.; Diaz-Torres, L. A.; Grillo, R.; Swamy, M. K.; Sharma, S.; Habtemariam, S.; Shin, H.-S. Nano based drug delivery systems: recent developments and future prospects. *J. Nanobiotechnol.* **2018,** 16, 1-33.

7. Jain, N. K.; Mishra, V.; Mehra, N. K. Targeted drug delivery to macrophages. *Expert Opin. Drug Delivery* **2013,** 10, 353-367.

8. Patel, P.; Patel, M. Nanostructured Lipid Carriers- A Versatile Carrier for Oral Delivery of Lipophilic Drugs. *Recent Pat Nanotechnol* **2021,** 15, 154-164.

9. Nobari Azar, F. A.; Pezeshki, A.; Ghanbarzadeh, B.; Hamishehkar, H.; Mohammadi, M. Nanostructured lipid carriers: Promising delivery systems for encapsulation of food ingredients. *J. Agric. Food Res.* **2020,** 2, 1-8.

10. Müller, R. H.; Mäder, K.; Gohla, S. Solid lipid nanoparticles (SLN) for controlled drug delivery - a review of the state of the art. *Eur. J. Pharm. Biopharm.* **2000,** 50, 161-177.

11. Hirsjärvi, S.; Sancey, L.; Dufort, S.; Belloche, C.; Vanpouille-Box, C.; Garcion, E.; Coll, J. L.; Hindré, F.; Benoît, J. P. Effect of particle size on the biodistribution of lipid nanocapsules: comparison between nuclear and fluorescence imaging and counting. *Int. J. Pharm.* **2013,** 453, 594-600.

12. Troncoso, E.; Aguilera, J. M.; McClements, D. J. Influence of particle size on the *in vitro* digestibility of protein-coated lipid nanoparticles. *J. Colloid Interface Sci.* **2012,** 382, 110-116.

13. Cabral, H.; Matsumoto, Y.; Mizuno, K.; Chen, Q.; Murakami, M.; Kimura, M.; Terada, Y.; Kano, M. R.; Miyazono, K.; Uesaka, M.; Nishiyama, N.; Kataoka, K. Accumulation of sub-100 nm polymeric micelles in poorly permeable tumours depends on size. *Nat. Nanotechnol.* **2011,** 6, 815-823.

14. Carron, P. M.; Crowley, A.; O'Shea, D.; McCann, M.; Howe, O.; Hunt, M.; Devereux, M. Targeting the Folate Receptor: Improving Efficacy in Inorganic Medicinal Chemistry. *Curr. Med. Chem.* **2018,** 25, 2675-2708.

15. Smith, L.; Serrano, D. R.; Mauger, M.; Bolás-Fernández, F.; Dea-Ayuela, M. A.; Lalatsa, A. Orally Bioavailable and Effective Buparvaquone Lipid-Based Nanomedicines for Visceral Leishmaniasis. *Mol. Pharmaceutics* **2018,** 15, 2570-2583.

16. Monteiro, L. M.; Löbenberg, R.; Cotrim, P. C.; Barros de Araujo, G. L.; Bou-Chacra, N. Buparvaquone Nanostructured Lipid Carrier: Development of an Affordable Delivery System for the Treatment of Leishmaniases. *BioMed Res. Int.* **2017,** 2017, 9781603.

17. Kar, N.; Chakraborty, S.; De, A. K.; Ghosh, S.; Bera, T. Development and evaluation of a cedrol-loaded nanostructured lipid carrier system for *in vitro* and *in vivo* susceptibilities of wild and drug resistant *Leishmania donovani* amastigotes. *Eur. J. Pharm. Sci.* **2017,** 104, 196-211.

18. Etxebeste-Mitxeltorena, M.; Moreno, E.; Carvalheiro, M.; Calvo, A.; Navarro-Blasco, I.; González-Peñas, E.; Álvarez-Galindo, J. I.; Plano, D.; Irache, J. M.; Almeida, A. J.; Sanmartín, C.; Espuelas, S. Oral Efficacy of a Diselenide Compound Loaded in Nanostructured Lipid Carriers in a Murine Model of Visceral Leishmaniasis. *ACS Infect. Dis.* **2021,** 7, 3197-3209.

19. Batista, M. F.; Nájera, C. A.; Meneghelli, I.; Bahia, D. The Parasitic Intracellular Lifestyle of Trypanosomatids: Parasitophorous Vacuole Development and Survival. *Frontiers in Cell and Developmental Biology* **2020,** 8.

20. McConville, M. J.; Saunders, E. C.; Kloehn, J.; Dagley, M. J. *Leishmania* carbon metabolism in the macrophage phagolysosome- feast or famine? *F1000Research* **2015,** 4, 1 -11.

21. McConville, M. J.; de Souza, D.; Saunders, E.; Likic, V. A.; Naderer, T. Living in a phagolysosome; metabolism of *Leishmania* amastigotes. *Trends Parasitol.* **2007,** 23, 368-375.

22. Pearson, R. D.; Anastacio de Queiroz, S. Clinical Spectrum of Leishmaniasis. *Clin. Infect. Dis.* **1996,** 22, 1-11.

23. Syed Azhar, S. N. A.; Ashari, S. E.; Zainuddin, N.; Hassan, M. Nanostructured Lipid Carriers-Hydrogels System for Drug Delivery: Nanohybrid Technology Perspective. *Molecules* **2022,** 27, 1-22.

24. Chinigò, G.; Gonzalez-Paredes, A.; Gilardino, A.; Barbero, N.; Barolo, C.; Gasco, P.; Fiorio Pla, A.; Visentin, S. Polymethine dyes-loaded solid lipid nanoparticles (SLN) as promising photosensitizers for biomedical applications. *Spectrochim. Acta, Part A* **2022,** 271, 120909.

25. Lomant, A. J.; Fairbanks, G. Chemical probes of extended biological structures: Synthesis and properties of the cleavable protein cross-linking reagent [35S]dithiobis(succinimidyl propionate). *J. Mol. Biol.* **1976,** 104, 243-261.

26. Staros, J. V.; Wright, R. W.; Swingle, D. M. Enhancement by *N*-hydroxysulfosuccinimide of water-soluble carbodiimide-mediated coupling reactions. *Anal. Biochem.* **1986,** 156, 220-222.

CHAPTER 7

7. Chapter 7:   Discussion

In this thesis, the synthesis of three new families of asymmetrical dicationic derivatives (i.e., series **1**, **2**, **3**) with structural characteristics related to the trypanocidal lead compounds **I** and **II** (Scheme 7.1)[1] was proposed in order to obtain new DNA minor groove binding molecules active against the intracellular parasites *T. cruzi* and *Leishmania*. Dicationic compounds have a high ability to interact with DNA,[2] especially to the AT-rich double strand of DNA. Because DNA MGB are "sequence-selective" and kinetoplastid parasites have a mitochondrial genome containing a high proportion of AT bases,[3-5] this class of compounds has shown a great promise as anti-kinetoplastid drugs.[2, 5-11]

The rationale behind the chemical modifications proposed was to optimise the access of these compounds to their intracellular target (i.e., kDNA) through the reduction of their highly polar character (e.g., by means of pK_a reduction and lipophilicity increase). Different strategies were proposed using the introduction of two halogen atoms[1] (i.e., Cl or F) or large isopropoxy groups.

Synthesis and physicochemical characterization of series 1–3

The synthesis of the proposed series **1–3** was carried out using the same diamino precursor **15** obtained by reduction of the dinitro precursor **9** (Scheme 7.1). The latter were prepared by coupling commercial anilines with the corresponding acid chlorides following the methodology we had developed previously.[1] The common diamino precursor **15** was connected by a coupling reaction with the respective heterocyclic moiety using previously reported methodologies (i.e., imidazolidine,[12] benzimidazolidine[13, 14]) or a new reagent (**44**) developed during this research project. The latter proved useful for the synthesis of bis(arylimidamidines) from poorly nucleophilic (halogen-containing) anilines. Since some steps involved Boc protected groups, the last step of the synthesis consisted in the deprotection of the molecules to obtain the corresponding salts of the compounds.

As regards to the ionization state, the synthesized series displayed lower pK_a values than the unsubstituted lead **I** ($pK_a = 9.29$).[1, 15] This agreed with previous results on analogous series containing one chlorine atom.[1] Within the bis(imidazolin-2-imino) series **1**, the

percentage of ionization at pH 7.4 ranged from 85.5 to 98.7% indicating that these derivatives are mostly dicationic at physiological pH. As stated earlier (Chapter 4), DNA MGBs tend to be concave in shape, possess several aromatic rings, be cationic in nature and have the ability to form hydrogen bonds.[16] Hence, series **1** compounds fulfil all the criteria to be good DNA MGBs. In contrast, the bisbenzimidazole derivatives (**2a–h**, **30**, **31**, and **34**), showed experimental pK_a values in the range 2.77–5.93, indicating that the compounds are mostly neutral at physiological pH. The predicted pK_a values for this series (6.54–7.70) were discordant with the measured values approximately 3 pK_a units. This data evidenced the limits of certain pK_a prediction tools for compounds containing a large number of possible tautomeric states.[17, 18] The pK_a measurement for the bis(arylimidamide) derivatives (**3a–i**, **36**, **37**, and **41**) was troublesome and only six pK_a could be measured in this series due to inconsistent data (i.e., **3d**, **41**) or the lack of samples to run the analysis (i.e., **3c**, **3h**, **3i**, **37**). The measured pK_a values ranged from 4.76 (**3g**) – 7.18 (**3a**), indicating that this series of compounds is partially charged at physiological pH (percentage of ionization at physiological pH ranging from 0.2% (**3g**) up to 38% for **3a**).

As a whole, the three series of compounds possessed the basic structural features of MGBs including positive charges. Even though series **2** compounds did not fulfil this last criterion, most of the compounds bound to DNA as shown by ΔT_m values > 5 ºC with the (AT)$_4$ hairpin duplex (see below). Hence, the lower *in vitro* antiparasitic activity of series **2** compounds (see below) may be linked to the lack of cationic character which will decrease the uptake of the compounds in the parasite's mitochondrion.

Scheme 7.1: Summary of the synthetic route to prepare series **1–3**.

Cmpd	X	R_1	R_2	R_3	R_4
a	CH	H	H	H	H
b	N	H	H	H	H
c	CH	Cl	H	Cl	H
d	CH	Cl	H	H	Cl
e	CH	H	Cl	Cl	H
f	CH	H	Cl	H	Cl
g	CH	H	Oi-Pr	Oi-Pr	H
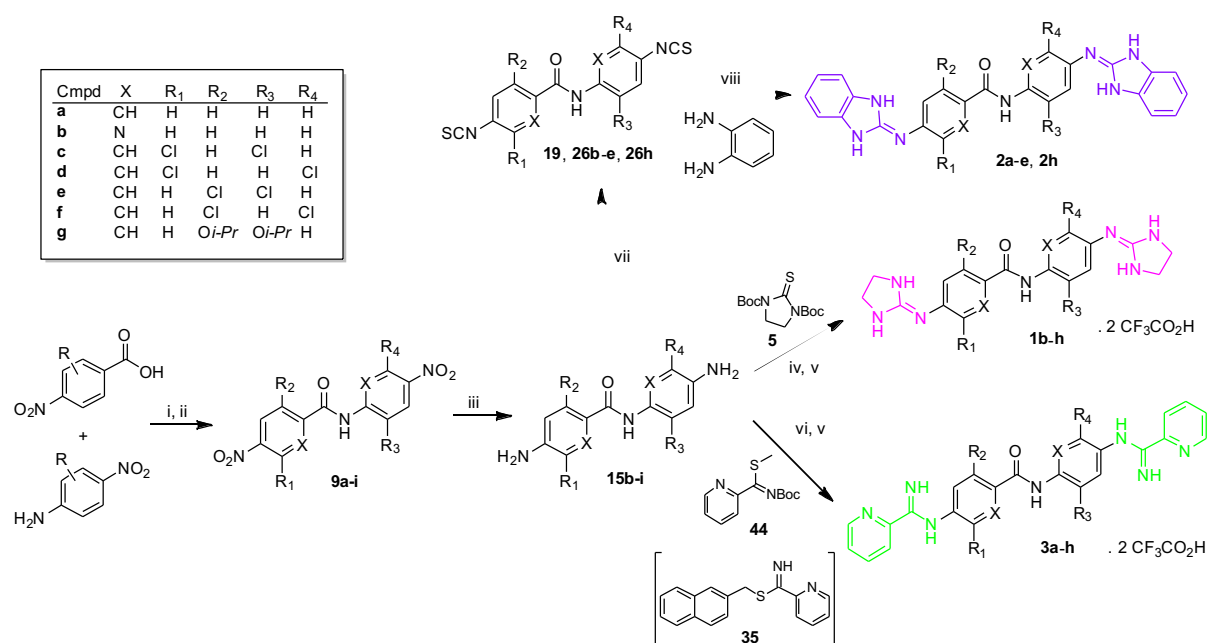
DNA binding affinity

The DNA binding affinity of the three series of compounds was determined with different biophysical methods as reported in Chapter 4. SPR–biosensor assays performed with two oligonucleotides sequences (i.e., CGAATTCG ["AATT"] and CGCGCGCG ["(CG)$_4$"])[19] proved that compounds of series **1** and a few compounds of series **3** bind selectivity to AT-containing DNA, as was observed with related molecules.[1, 20-22] In contrast, the chlorine (**3b–e**), isopropoxy (**3g**), and pyridine-based (**3h**–**i**) bis(arylimidamide) derivatives showed unspecific binding which made it difficult to analyse and interpret the obtained data. Similarly, bis(2-aminobenzimidazole) derivatives (**2a**–**e**, **2h**, **30**, **31**, and **34**) showed no binding to AATT or (CG)$_4$ oligonucleotide hairpin sequences at the highest concentration tested (100 μM). As unspecific binding to the chip dextran matrix (**2a**–**h**) or aggregation/precipitation (**30**, **31**, and **34**) was observed, we conclude that SPR-biosensor assays are not adequate to determine the DNA binding affinity of the bis(2-aminobenzimidazole) class of compounds.

The SPR–biosensor assays on the bis(arylimidamide) derivatives showed that **3a** (K_D = 0.58 μM) was the only compound with the N-phenylbenzamide scaffold that bound to the AT-containing sequence and was selective versus the (CG)$_4$ oligonucleotide. The 1,2-diphenylethane (**36**), and fluorene (**53**) derivatives, none of which possess the same central

scaffold, also bound to DNA. However, **53** was not sequence selective and bound to AT and GC-containing oligonucleotide with similar K_D values (9.82×10^{-6} M and 13×10^{-6} M, respectively). These three compounds (**3a**, **36**, and **53**) displayed a binding stoichiometry (*r*) of two moles of bound compound per mole of DNA hairpin duplex, which is similar to lead **I** and other related bis(imidazolin-2-imine) derivatives.[19, 20, 22] These compounds clearly stabilize the DNA duplex as reported by thermal melting experiments, where the larger thermal increases were obtained for **53**, **36** and **3a**, respectively.

As regard of the bis(imidazolin-2-imine) derivatives (series **1**), compounds holding substituents on the phenyl rings were > 2-fold weaker binders than **I** ($K_D = 0.17$ µM) as shown by primary binding constants (i.e., high affinity site) ranging from 0.38 µM for the dipyridyl derivative **1h** to 45 µM for the dichloro analogue **1c**. On the other hand, derivatives **1f–h** bound selectively to the AATT hairpin sequence with K_D values in the submicromolar to micromolar range. No binding to the (CG)$_4$ oligonucleotide sequence was observed up to 100 µM. These results were consistent with previous results obtained with similar compounds.[1, 20, 23] Importantly, the relative position and size of the substituents (i.e., Cl, O^{i}Pr, F) had a clear influence on the binding mode to the minor groove of the DNA hairpin. We observed that compounds with chlorine (**1b**, **1d**, **1e**) or O^{i}Pr (**1g**) groups in position *ortho* to the amide bond of the scaffold had >40-times weaker binding affinity than the molecules with the Cl atoms next to the 2-aminoimidazoline group (**1c**). This may be due to the conformational restriction and/or steric clash imposed by the presence of chlorine or O^{i}Pr groups near the amide bridge of the molecule. The fact that the fluorine atoms *ortho* to the amide bond (**1f**) hardly affected the binding to DNA ($K_D = 0.55$ µM) compared to **I** is consistent with the hypothesis that small size groups are preferred in this position. It has been reported that even small structural changes can affect the DNA binding affinity of MGBs.[24-26]

Since SPR–biosensor experiments were inconclusive for several compounds of series **2** and **3**, thermal denaturation experiments were performed with an (AT)$_4$-containing DNA hairpin. Significant T_m increases were observed for most of the compounds of series **1–3** indicating that all of these compounds bind to DNA, including the bis(2-aminobenzimidazole) derivatives **2** (see chapter 4.3.2.3 for a detailed discussion of the results). For the bis(imidazolin-2-imine) derivatives **1b–h** (except **1c**: $\Delta T_m = 0.9$ °C), the

T_m increases (from 3.1 ºC (**1g**) to 8.2 ºC (**1h**)) were larger than ΔT_m of lead **I** (1.6 °C) indicating that the introduction of Cl, O^{i}Pr or nitrogen atoms in the scaffold positively affected DNA binding affinity for these molecules. Similar SAR trends were observed with the bis(2-aminobenzimidazoles) **2a**–**e** which showed ΔT_m values in the range 4.0–7.0 °C. The large difference between the value reported for lead **I** with poly(dA·dT)$_2$ (ΔT_m = 47.1 ºC)[27] and our value may be attributed to the different oligonucleotide used in both experiments. DNA containing an A-tract has a narrow minor groove and can bind minor-groove agents without a significant average change in groove width or local helix axis bends in solution. In contrast, straight alternating AT sequences (i.e., (AT)$_4$ used in our assays) require the minor groove to narrow with bending of the helix upon binding minor-groove agents.[8]

It has been reported that optimization of the central linker allows two symmetric bis-benzimidazole motifs to maintain hydrogen-bonded contacts with the DNA minor groove.[10, 28-30] The different T_m increases displayed by the planar fluorene derivative **34**, the urea-bridged (**31**) or the ethylene-bridged scaffold (**30**) with respect to **2a** may reflect this trend.

Mode of binding to DNA

The determination of the mode of binding of compounds from series **1**–**3** was studied by circular (CD) with the (AT)$_4$ oligonucleotide and flow linear dichroism (LD) with unspecific DNA. For the bis(imidazolin-2-imine) derivatives (**I**, **1b**–**h**) and the bis(arylimidamide) **3a**, a substantial positive induced CD signal was observed at ≈ 300–320 nm at 25 ºC, which is characteristic of MGB. Compound **3a** had also shown by LD experiments a positive induced band at 310 nm, been indicative of binding the DNA minor groove. It was also observed by UV-Vis experiments that **3a** has a different binding mode than series **2** derivatives.

Additionally, a weak induced CD signal was perceived for **3b**, **3g**–**i**, **37**, and **53**. In contrast, the bis(2-aminobenzimidazole) series displayed no (**2a**–**d**, **2h**) or an insignificant induced CD signal (**2e**, **30**, **31**, **34**), which could be related to the lower number of hydrogen-bond contacts with the floor of the DNA minor groove for these uncharged analogues.[28] According to the UV titrations results, where a pronounced hypochromic effect was

observed – being different to the slight hypochromic effect observed for the MGB **3** –, this could also indicate that the bis(2-aminobenzimidazole) compounds have a different mode of binding to DNA (e.g., intercalation or mixed MGB/intercalation). However, further experiments will be needed to confirm these findings.

To investigate further the mode of binding to DNA, LD spectra were recorded with two representative compounds from series **1** and **3** following the protocol reported in the literature.[31, 32] Titration of natural DNA (salmon testes) with compounds **1e** and **3a** were recorded at 1:1 and 1:5 Bp/Drug ratios. Positive induced LD signals were observed at 310 nm (where the DNA does not absorb) indicating that compounds **1e** and **3a** bind to the minor groove of DNA. These results were consistent with the data obtained by SPR and CD experiments with specific AT-containing DNA.

The ^{1}H-NMR experiments also confirmed that compound **3a** binds selectively to the minor groove of the $(AT)_4$ oligonucleotide, interacting with the NH_2 of the adenine bases, even at low concentration of ligand. This interaction appears to increase the stability of the DNA duplex as was observed in the melting studies performed by ^{1}H-NMR.

Crystallographic studies were performed using five different AT-containing oligonucleotides [i.e., d(CGAATTAATTCG), d(AATAATTATT), d(CGCAAATTTGCG), d(AAATATATTT) and d(ATTAATTAAT)] to elucidate the mode of binding of the compounds at atomic resolution. Crystallization experiments were conducted using four compounds (**1c**, **1g**, **3a** and **36**) from the bis(imidazolidin-2-imines) and bis(arylimidamides) series that showed good DNA binding affinities in the preliminary biophysical studies. Crystals were obtained with compounds **1c**, **3a** and **36** and the X-ray diffraction was performed at ALBA synchrotron. However, we were not able to elucidate any structure so far.

The docking studies carried out with series **3** derivatives using the crystal structure of **I** complexed with $d(AAATT)_2$ (PDB: 5LIT)[20, 33] showed that **3a** fits the minor groove of the $d(AAATT)_2$ oligonucleotide in a similar way as lead **I**.[20] The presence of the central H-bond between the amide NH of the scaffold and the carbonyl of thymine T4 is, in some way, director of the fitting inside the minor groove. Compound **3a** interaction with the

minor groove of the DNA duplex is characterised by the presence of a strong H-bond (1.95 Å) between the amide NH of the *N*-phenylbenzamide scaffold (H44) and the oxygen (O434) of thymine 4 residue. It shows $\pi - \pi$ stacking interaction (ring-to-ring distance of 5.16 Å) between the phenyl ring of the scaffold and the adenine residues, and three aromatic H-bond interactions (O434–H45, 1.57 Å), (O314–H43, 2.79 Å) and (O469–H37, 2.77 Å). Of note, these interactions were observed with **3a** only; regardless all of the proposed compounds present the same aromatic scaffold. Therefore, these stabilizing interactions may explain the potent DNA minor groove binding affinity of **3a**. The elucidation of the crystal structure of **3a** complexed with AT-containing oligonucleotides would answer this question.

Biological evaluation

The three families of derivatives (i.e., series **1**, **2**, **3**) were tested against the kinetoplastid parasites *T. brucei*, *T. cruzi* and *L. donovani*, and against the urogenital parasite *T. vaginalis*. Unspecific cytotoxicity against three different mammalian cell lines (i.e., HEK, L929 fibroblasts and THP-1) was also tested in order to determine the selectivity indexes. The introduction of two substituents (i.e., Cl, F, O^{i}Pr) or N atoms in the scaffold of the bis(imidazolidine-2-imine) series **1** did not improve the *in vitro* antiparasitic activity against *T. brucei*, *T. cruzi* or *Leishmania* with respect to lead **I** or the mono-chlorinated analogues reported earlier.[1] Series **1** compounds showed EC$_{50}$ values in the micromolar range and selectivity indexes (SI) in the range 1.3 to >35. Thus, this chemical modification appeared to bring no advantage versus the introduction of one chlorine atom in the *N*-phenylbenzamide scaffold. From this series, the chlorine derivative **1c**, which was the most active and selective against both wild-type (WT) and pentamidine-resistant (B48) strains, was approximately 7-times less potent than **I** against *T. brucei*. Importantly, the cytotoxicity assays against HEK cells and L929 fibroblasts showed that the bis(imidazolidin-2-amino) derivatives are non-toxic to mammalian cells as was previously observed.[1, 27, 34]

The replacement of the 2-aminoimidazoline groups by 2-aminobenzimidazole heterocycles afforded series **2** compounds that were active in the micromolar range against *T. brucei* but also more cytotoxic, resulting in lower SI than series **1** compounds. None of series **2** compounds showed activity against *T. cruzi* or *L. donovani*, except **30** which had marginal activity against promastigotes of *L. donovani* (EC$_{50}$ = 8.7 μM), albeit with low selectivity

(SI = 1.6). For lead **I**, the effect of replacing the 2-aminoimidazoline rings with 2-aminobenzimidazole heterocycles was even more dramatic with a 100-fold lower activity against *T. brucei* for analogue **2a** (85.6 µM) with respect to **I** (0.83 µM). Interestingly, the main SAR results seem to apply for both series **1** and **2**. For instance, the effect on the anti-*T. brucei* activity of incorporating Cl atoms in the scaffold were similar in both series. As a whole, the chemical modification 2-aminoimidazoline ↔ 2-aminobenzimidazole provided no improvement in antiprotozoal activity nor in DNA binding affinity. This is probably related to the low pK_a of these compounds, which will be unionized at physiological pH and will not accumulate in the mitochondrion of the parasites. This could finally lead to an insignificant concentration of the drugs, not being able to exert the pharmacological effect.

In contrast, the bis(arylimidamide) series were very potent inhibitors of *T. brucei*, *T. cruzi* and *Leishmania* growth, with excellent selectivity. These results were consistent with the data reported in the literature for molecules sharing the *N*-(pyridine-2-carboxamidine) moiety (i.e., arylimidamide) with different aromatic and heteroaromatic scaffolds.[35-40] In fact, the *N*-(pyridine-2-carboxamidine) group seems to be a privileged scaffold to obtain highly potent anti-trypanosomatid compounds that are effective against intracellular forms of *T. cruzi* and *Leishmania*.[36, 38, 39, 41-47]

The bis(arylimidamide) derivatives were very effective in the *L. donovani*-infected macrophage assay. Derivatives **3a**, **36** and **53** (and also **3h**), which display submicromolar EC$_{50}$ values and SI > 20 against intracellular amastigotes of *L. donovani*, can be considered as new antileishmanial lead compounds. Series **3** compounds also showed the best activity against intracellular amastigotes of *T. cruzi* in the submicromolar (**3b**, **3c**, and **3e**) and single-digit micromolar range (**3a**, **3g**, **53**) with SI indexes between 17.3 (**3c**) and 399 (**3e**). These values are in the same range as bis(arylimidamide) DB766[48] and show superior activity and selectivity to analogues modified on the terminal group[49] (Figure 1.17). Compound **3e**, which is twice as potent as the reference drug benznidazole against intracellular amastigotes (0.54 µM), can be considered as a new lead compound against *T. cruzi*. Among this series, compounds **3a**, **3h**, and **3c** were the most active and selective against *T. brucei* with EC$_{50}$ < 0.4 µM and SI > 118.

All of the compounds were tested against the amitochondriate parasite *T. vaginalis* because its genome has a high content in AT base pairs which may potentially be targeted by DNA MGBs. In previous studies, Crowell *et al.* showed that aromatic diamidines, which are dicationic DNA MGBs at AT sites, have potential as antitrichomonal agents with activities in the micromolar range.[50]

Among all the series synthesised in this Thesis, only the bis(2-aminobenzimidazole) derivative **34** showed a weak trichomonicidal effect (EC_{50} = 33.2 µM) but with poor selectivity ($CC_{50} \approx 50$ µM). Series **1** and **3**, as well as the rest of bis(2-aminobenzimidazoles) derivatives resulted to be inactive against *T. vaginalis* at the highest concentration studied (100 µM). We do not have an explanation for the lack of trichomonacidal activity of these compounds which are DNA MGBs. This may be related to a poor uptake of these dicationic compounds in *Trichomonas*. In kinetoplastid parasites, cationic compounds accumulate in the parasite mitochondrion driven by the plasma and mitochondrial negative transmembrane potential. This will be different in *Trichomonas* which is an amitochondriate parasite.

We did not observe a correlation between the antiparasite activity of the 3 series and the DNA binding affinity as determined by thermal melting experiments. However, such correlation between the cellular activity and the binding affinity for the target depends on several factors (e.g., cell uptake differences, distinct cellular targets) and is not always easy to demonstrate. Soeiro and co-workers showed that the trypanocidal activity of bis(arylimidamide) related to compound DB766 compounds did not correlate with their binding affinity to *Trypanosoma cruzi* kinetoplast.[51] In their study, they observed that a strong affinity with kDNA per se was not sufficient to generate and trigger the trypanocidal activity of the studied diamidines. For lead compound **I**, we were able to confirm that kDNA is the cellular target against *T. brucei* by evaluating the in vitro and in vivo effect of the compound by a combination of flow cytometry, imaging techniques, and biophysical experiments.[20] Work is in progress to try to corroborate kDNA as the cellular target of the compounds of this Thesis.

As a major result of the biological evaluations, the unsubstituted compound **3a** - the closest analogue of **I** - proved to be the best antiparasitic compound with submicromolar activity and high selectivity against these three kinetoplastid parasites, including the intracellular therapeutically-relevant amastigote forms. Thus, **3a** arises as a new lead compound. This

bis(arylimidamide) derivative shows submicromolar activity against BSF trypomastigotes of *T. brucei*, and intracellular amastigotes of *L. donovani* and *T. cruzi*. Compound **3a** has also shown high selectivity against the mammalian cells tested and it proved to be metabolically stable towards liver metabolism (i.e., HLM and MLM) and in human serum. Therefore, **3a** is a suitable candidate to carry out *in vivo* assays of pharmacodynamics and efficacy in mouse models of leishmaniasis and Chagas disease.

An attempt to optimize the delivery of this class of kinetoplast-targeting compounds to the intracellular *Leishmania* parasites using nanostructured lipid carrier (NLC) was carried out. Compound **3a**, the most active and selective compound against *L. donovani*, was chosen as the cargo to be inserted in the NLC. NLC were prepared with compound **3a** loaded inside the lipid matrix, exposing free amine residues on its external surface due to the use of octadecyl amine. These amino groups allowed the functionalization of the NLC surface with folate residues that can be recognized by the folate receptor of macrophages. The incorporation of compound **3a** in both blank and FA-loaded formulations
was achieved successfully with compound concentrations >10-fold the EC$_{50}$ value of **3a** (*L. donovani* amastigotes) in both NLC formulations. A slight loss of **3a** loading was observed with the FA-covered NLC due to the functionalization process. However, the final loading was adequate to carry out the biological assays against *Leishmania*, which are planned in the next months.

7.1. References

1. Ríos Martínez, C. H.; Nué Martinez, J. J.; Ebiloma, G. U.; de Koning, H. P.; Alkorta, I.; Dardonville, C. Lowering the pK_a of a bisimidazoline lead with halogen atoms results in improved activity and selectivity against *Trypanosoma brucei in vitro*. *Eur. J. Med. Chem.* **2015,** 101, 806-817.

2. Wilson, W. D.; Nguyen, B.; Tanious, F. A.; Mathis, A.; Hall, J. E.; Stephens, C. E.; Boykin, D. W. Dications that target the DNA minor groove: compound design and preparation, DNA interactions, cellular distribution and biological activity. *Curr. Med. Chem.: Anti-Cancer Agents* **2005,** 5, 389-408.

3. Wilson, W. D.; Tanious, F. A.; Mathis, A.; Tevis, D.; Hall, J. E.; Boykin, D. W. Antiparasitic compounds that target DNA. *Biochimie* **2008,** 90, 999-1014.

4. Ivens, A. C.; Peacock, C. S.; Worthey, E. A.; Murphy, L.; Aggarwal, G.; Berriman, M.; Sisk, E.; Rajandream, M.-A.; Adlem, E.; Aert, R.; Anupama, A.; Apostolou, Z.; Attipoe, P.; Bason, N.; Bauser, C.; Beck, A.; Beverley, S. M.; Bianchettin, G.; Borzym, K.; Bothe, G.; Bruschi, C. V.; Collins, M.; Cadag, E.; Ciarloni, L.; Clayton, C.; Coulson, R. M. R.; Cronin, A.; Cruz, A. K.; Davies, R. M.; Gaudenzi, J. D.; Dobson, D. E.; Duesterhoeft, A.; Fazelina, G.; Fosker, N.; Frasch, A. C.; Fraser, A.; Fuchs, M.; Gabel, C.; Goble, A.; Goffeau, A.; Harris, D.; Hertz-Fowler, C.; Hilbert, H.; Horn, D.; Huang, Y.; Klages, S.; Knights, A.; Kube, M.; Larke, N.; Litvin, L.; Lord, A.; Louie, T.; Marra, M.; Masuy, D.; Matthews, K.; Michaeli, S.; Mottram, J. C.; Mul̀ ller-Auer, S.; Munden, H.; Nelson, S.; Norbertczak, H.; Oliver, K.; O'Neil, S.; Pentony, M.; Pohl, T. M.; Price, C.; Purnelle, B. n. d.; Quail, M. A.; Rabbinowitsch, E.; Reinhardt, R.; Rieger, M.; Rinta, J.; Robben, J.; Robertson, L.; Ruiz, J. C.; Rutter, S.; Saunders, D.; Schal̀ fer, M.; Schein, J.; Schwartz, D. C.; Seeger, K.; Seyler, A.; Sharp, S.; Shin, H.; Sivam, D.; Squares, R.; Squares, S.; Tosato, V.; Vogt, C.; Volckaert, G.; Wambutt, R.; Warren, T.; Wedler, H.; Woodward, J.; Zhou, S.; Zimmermann, W.; Smith, D. F.; Blackwell, J. M.; Stuart, K. D.; Barrell, B.; Myler, P. J. The Genome of the Kinetoplastid Parasite, *Leishmania major*. *Science* **2005,** 309, 436-442.

5. Bailly, C.; Chaires, J. B. Sequence-Specific DNA Minor Groove Binders. Design and Synthesis of Netropsin and Distamycin Analogues. *Bioconjugate Chem.* **1998,** 9, 513-538.

6. Tidwell, R. R. B., W. D. Dicationic DNA Minor Groove Binders as Antimicrobial Agents. In Small Molecule DNA and RNA Binders: From Synthesis to Nucleic Acid Complexes. In Wiley-VCH: Weinheim, Germany, 2002; Vol. 2, pp 414-460.

7. Acosta-Reyes, F. J.; Dardonville, C.; de Koning, H. P.; Natto, M.; Subirana, J. A.; Campos, J. L. In and out of the minor groove: interaction of an AT-rich DNA with the drug CD27. *Acta Crystallogr. D.* **2014,** 70, 1614-1621.

8. Chai, Y.; Munde, M.; Kumar, A.; Mickelson, L.; Lin, S.; Campbell, N. H.; Banerjee, M.; Akay, S.; Liu, Z.; Farahat, A. A.; Nhili, R.; Depauw, S.; David-Cordonnier, M. H.; Neidle, S.; Wilson, W. D.; Boykin, D. W. Structure-dependent binding of arylimidamides to the DNA minor groove. *ChemBioChem* **2014,** 15, 68-79.

9. Giordani, F.; Khalaf, A. I.; Gillingwater, K.; Munday, J. C.; de Koning, H. P.; Suckling, C. J.; Barrett, M. P.; Scott, F. J. Novel Minor Groove Binders Cure Animal African Trypanosomiasis in an *in vivo* Mouse Model. *J. Med. Chem.* **2019,** 62, 3021-3035.

10. Hegde, M.; Sharath Kumar, K. S.; Thomas, E.; Ananda, H.; Raghavan, S. C.; Rangappa, K. S. A novel benzimidazole derivative binds to the DNA minor groove and induces apoptosis in leukemic cells. *RSC Adv.* **2015,** 5, 93194-93208.

11. Rahman, A.; O'Sullivan, P.; Rozas, I. Recent developments in compounds acting in the DNA minor groove. *MedChemComm* **2019,** 10, 26-40.

12. Dardonville, C.; Goya, P.; Rozas, I.; Alsasua, A.; Martín, M. I.; Borrego, M. J. New aromatic iminoimidazolidine derivatives as α_1-adrenoceptor antagonists: a novel synthetic approach and pharmacological activity. *Bioorg. Med. Chem.* **2000,** 8, 1567-1577.

13. Xie, Y.; Zhang, F.; Li, J.; Shi, X. Novel Synthesis of 2-Aminobenzimidazoles from Isoselenocyanates. *Synlett* **2010,** 2010, 901-904.

14. Carpenter, R. D.; DeBerdt, P. B.; Lam, K. S.; Kurth, M. J. Carbodiimide-Based Benzimidazole Library Method. *J. Comb. Chem.* **2006,** 8, 907-914.

15. Dardonville, C.; Caine, B. A.; Navarro de la Fuente, M.; Martin Herranz, G.; Corrales Mariblanca, B.; Popelier, P. L. A. Substituent effects on the basicity (pK(a)) of aryl guanidines and 2-(arylimino) imidazolidines: correlations of pH-metric and UV-metric values with predictions from gas-phase ab initio bond lengths. *New J. Chem.* **2017,** 41, 11016-11028.

16. Neidle, S. *Principles of Nucleic Acid Structure.* 1st edition ed.; Elsevier: 2008.

17. Caine, B. A.; Bronzato, M.; Fraser, T.; Kidley, N.; Dardonville, C.; Popelier, P. L. A. Aqueous pK(a) prediction for tautomerizable compounds using equilibrium bond lengths. *Commun. Chem.* **2020,** 3.

18. Dardonville, C. Automated techniques in pKa determination: Low, medium and high-throughput screening methods. *Drug Discov. Today: Technol.* **2018,** 27, 49-58.

19. Ríos Martínez, C. H.; Lagartera, L.; Trujillo, C.; Dardonville, C. Bisimidazoline arylamides binding to the DNA minor groove: *N*1-hydroxylation enhances binding affinity and selectivity to AATT sites. *MedChemComm* **2015,** 6, 2036-2042.

20. Millan, C. R.; Acosta-Reyes, F. J.; Lagartera, L.; Ebiloma, G. U.; Lemgruber, L.; Nué Martinez, J. J.; Saperas, N.; Dardonville, C.; de Koning, H. P.; Campos, J. L. Functional and structural analysis of AT-specific minor groove binders that disrupt DNA-protein interactions and cause disintegration of the *Trypanosoma brucei* kinetoplast. *Nucleic Acid Res.* **2017,** 45, 8378-8391.

21. Dardonville, C.; Nué Martinez, J. J. Bis(2-aminoimidazolines) and Bisguanidines: Synthetic Approaches, Antiparasitic Activity and DNA Binding Properties. *Curr. Med. Chem.* **2017,** 24, 3606-3632.

22. Ríos Martínez, C. H.; Lagartera, L.; Kaiser, M.; Dardonville, C. Antiprotozoal activity and DNA binding of *N*-substituted *N*-phenylbenzamide and 1,3-diphenylurea bisguanidines. *Eur. J. Med. Chem.* **2014,** 81, 481-491.

23. Ríos Martínez, C. H.; Miller, F.; Ganeshamoorthy, K.; Glacial, F.; Kaiser, M.; de Koning, H. P.; Eze, A. A.; Lagartera, L.; Herraiz, T.; Dardonville, C. A new nonpolar *N*-hydroxy imidazoline lead compound with improved activity in a murine model of late-stage *Trypanosoma brucei brucei* infection is not cross-resistant with diamidines. *Antimicrob. Agents Chemother.* **2015,** 59, 890-904.

24. Baraldi, P. G.; Bovero, A.; Fruttarolo, F.; Preti, D.; Tabrizi, M. A.; Pavani, M. G.; Romagnoli, R. DNA minor groove binders as potential antitumor and antimicrobial agents. *Med. Res. Rev.* **2004,** 24, 475-528.

25. Karlsson, H. J.; Bergqvist, M. H.; Lincoln, P.; Westman, G. Syntheses and DNA-binding studies of a series of unsymmetrical cyanine dyes: structural influence on the degree of minor groove binding to natural DNA. *Bioorg. Med. Chem.* **2004,** 12, 2369-2384.

26. Ryabinin, V. A.; Butorin, A. S.; Elen, K.; Denisov, A. Y.; Pyshnyi, D. V.; Sinyakov, A. N. Effect of structural factors on the stability of duplexes formed by oligonucleotide conjugates with minor groove binders. *Russ. J. Bioorg. Chem.* **2005,** 31, 146-152.

27. Rodríguez, F.; Rozas, I.; Kaiser, M.; Brun, R.; Nguyen, B.; Wilson, W. D.; García, R. N.; Dardonville, C. New Bis(2-aminoimidazoline) and Bisguanidine DNA Minor Groove Binders with Potent *in Vivo* Antitrypanosomal and Antiplasmodial Activity. *J. Med. Chem.* **2008,** 51, 909-923.

28. Joubert, A.; Sun, X.-W.; Johansson, E.; Bailly, C.; Mann, J.; Neidle, S. Sequence-Selective Targeting of Long Stretches of the DNA Minor Groove by a Novel Dimeric Bis-benzimidazole. *Biochemistry* **2003,** 42, 5984-5992.

29. Bostock-Smith, C. E.; Searle, M. S. DNA minor groove recognition by bis-benzimidazole analogues of Hoechst 33258: Insights into structure—DNA affinity relationships assessed by fluorescence titration measurements. *Nucleic Acid Res.* **1999,** 27, 1619-1624.

30. Nelson, S. M.; Ferguson, L. R.; Denny, W. A. Non-covalent ligand/DNA interactions: Minor groove binding agents. *Mutat. Res., Fundam. Mol. Mech. Mutagen.* **2007,** 623, 24-40.

31. Nagle, P. S.; Rodriguez, F.; Kahvedžić, A.; Quinn, S. J.; Rozas, I. Asymmetrical Diaromatic Guanidinium/2-Aminoimidazolinium Derivatives: Synthesis and DNA Affinity. *J. Med. Chem.* **2009,** 52, 7113-7121.

32. Nagle, P. S.; Quinn, S. J.; Kelly, J. M.; O'Donovan, D. H.; Khan, A. R.; Rodriguez, F.; Nguyen, B.; Wilson, W. D.; Rozas, I. Understanding the DNA binding of novel non-symmetrical guanidinium/2-aminoimidazolinium derivatives. *Org. Biomol. Chem.* **2010,** 8, 5558-5567.

33. Millan, C. R., Dardonville, C., de Koning, H.P., Saperas, N., Campos, J. L. Structure of the DNA duplex d(AAATTT)$_2$ with the potential antiparasitic drug 6XV at 1.25 Å resolution. DOI: 10.2210/pdb5lit/pdb. In 2016.

34. Dardonville, C.; Barrett, M. P.; Brun, R.; Kaiser, M.; Tanious, F.; Wilson, W. D. DNA Binding Affinity of Bisguanidine and Bis(2-aminoimidazoline) Derivatives with *in vivo* Antitrypanosomal Activity. *J. Med. Chem.* **2006,** 49, 3748-3752.

35. Abdelhameed, A.; Feng, M.; Joice, A. C.; Zywot, E. M.; Jin, Y.; La Rosa, C.; Liao, X.; Meeds, H. L.; Kim, Y.; Li, J.; McElroy, C. A.; Wang, M. Z.; Werbovetz, K. A. Synthesis and Antileishmanial Evaluation of Arylimidamide–Azole Hybrids Containing a Phenoxyalkyl Linker. *ACS Infect. Dis.* **2021,** 7, 1901-1922.

36. Banerjee, M.; Farahat, A. A.; Kumar, A.; Wenzler, T.; Brun, R.; Munde, M. M.; Wilson, W. D.; Zhu, X.; Werbovetz, K. A.; Boykin, D. W. Synthesis, DNA binding and antileishmanial activity of low molecular weight bis-arylimidamides. *Eur. J. Med. Chem.* **2012,** 55, 449-454.

37. Reid, C. S.; Farahat, A. A.; Zhu, X.; Pandharkar, T.; Boykin, D. W.; Werbovetz, K. A. Antileishmanial bisarylimidamides: DB766 analogs modified in the linker region and bisarylimidamide structure-activity relationships. *Bioorg. Med. Chem. Lett.* **2012,** 22, 6806-6810.

38. Wang, M. Z.; Zhu, X.; Srivastava, A.; Liu, Q.; Sweat, J. M.; Pandharkar, T.; Stephens, C. E.; Riccio, E.; Parman, T.; Munde, M.; Mandal, S.; Madhubala, R.; Tidwell, R. R.; Wilson, W. D.; Boykin, D. W.; Hall, J. E.; Kyle, D. E.; Werbovetz, K. A. Novel Arylimidamides for treatment of visceral Leishmaniasis. *Antimicrob. Agents Chemother.* **2010,** 54, 2507-2516.

39. Zhu, X.; Farahat, A. A.; Mattamana, M.; Joice, A.; Pandharkar, T.; Holt, E.; Banerjee, M.; Gragg, J. L.; Hu, L.; Kumar, A.; Yang, S.; Wang, M. Z.; Boykin, D. W.; Werbovetz, K. A. Synthesis and pharmacological evaluation of mono-arylimidamides as antileishmanial agents. *Bioorg. Med. Chem. Lett.* **2016,** 26, 2551-2556.

40. Zhu, X.; Liu, Q.; Yang, S.; Parman, T.; Green, C. E.; Mirsalis, J. C.; de Nazare Correia Soeiro, M.; Mello de Souza, E.; da Silva, C. F.; da Gama Jaen Batista, D.; Stephens, C. E.; Banerjee, M.; Farahat, A. A.; Munde, M.; Wilson, W. D.; Boykin, D. W.; Wang, M. Z.; Werbovetz, K. A. Evaluation of arylimidamides DB1955 and DB1960 as candidates against visceral leishmaniasis and Chagas'

disease: *in vivo* efficacy, acute toxicity, pharmacokinetics, and toxicology studies. *Antimicrob. Agents Chemother.* **2012,** 56, 3690-3699.

41. da Silva, C. F.; Batista, D.; de Araújo, J. S.; Cunha-Junior, E. F.; Stephens, C. E.; Banerjee, M.; Farahat, A. A.; Akay, S.; Fisher, M. K.; Boykin, D. W.; Soeiro, M. N. C. Phenotypic evaluation and *in silico* ADMET properties of novel arylimidamides in acute mouse models of *Trypanosoma cruzi* infection. *Drug Des., Dev. Ther.* **2017,** 11, 1095-1105.

42. Guedes-da-Silva, F. H.; Batista, D. G.; Meuser, M. B.; Demarque, K. C.; Fulco, T. O.; Araujo, J. S.; Da Silva, P. B.; Da Silva, C. F.; Patrick, D. A.; Bakunova, S. M.; Bakunov, S. A.; Tidwell, R. R.; Oliveira, G. M.; Britto, C.; Moreira, O. C.; Soeiro, M. N. *In vitro* and *in vivo* Trypanosomicidal Action of Novel Arylimidamides against *Trypanosoma cruzi. Antimicrob. Agents Chemother.* **2016,** 60, 2425-2534.

43. Timm, B. L.; da Silva, P. B.; Batista, M. M.; da Silva, F. H.; da Silva, C. F.; Tidwell, R. R.; Patrick, D. A.; Jones, S. K.; Bakunov, S. A.; Bakunova, S. M.; Soeiro Mde, N. *In vitro* and *in vivo* biological effects of novel arylimidamide derivatives against *Trypanosoma cruzi. Antimicrob. Agents Chemother.* **2014,** 58, 3720-3726.

44. Pandharkar, T.; Zhu, X.; Mathur, R.; Jiang, J.; Schmittgen, T. D.; Shaha, C.; Werbovetz, K. A. Studies on the antileishmanial mechanism of action of the arylimidamide DB766: azole interactions and role of CYP5122A1. *Antimicrob. Agents Chemother.* **2014,** 58, 4682-4689.

45. Liu, Z. Y.; Wenzler, T.; Brun, R.; Zhu, X.; Boykin, D. W. Synthesis and antiparasitic activity of new bisarylimidamides: DB766 analogs modified in the terminal groups. *Eur. J. Med. Chem.* **2014,** 83, 167-173.

46. Da Silva, C. F.; Daliry, A.; PB, D. A. S.; Akay, S.; Banerjee, M.; Farahat, A. A.; Fisher, M. K.; Hu, L.; Kumar, A.; Liu, Z.; Stephens, C. E.; Boykin, D. W.; Correia Soeiro, M. D. The efficacy of novel arylimidamides against *Trypanosoma cruzi in vitro. Parasitology* **2011,** 138, 1863-1869.

47. Batista Dda, G.; Batista, M. M.; de Oliveira, G. M.; do Amaral, P. B.; Lannes-Vieira, J.; Britto, C. C.; Junqueira, A.; Lima, M. M.; Romanha, A. J.; Sales Junior, P. A.; Stephens, C. E.; Boykin, D. W.; Soeiro Mde, N. Arylimidamide DB766, a

potential chemotherapeutic candidate for Chagas' disease treatment. *Antimicrob. Agents Chemother.* **2010,** 54, 2940-2952.

48. Wang, M. Z.; Zhu, X.; Srivastava, A.; Liu, Q.; Sweat, J. M.; Pandharkar, T.; Stephens, C. E.; Riccio, E.; Parman, T.; Munde, M. Novel arylimidamides for treatment of visceral leishmaniasis. *Antimicrob. Agents Chemother.* **2010,** 54, 2507-2516.

49. Liu, Z.-y.; Wenzler, T.; Brun, R.; Zhu, X.; Boykin, D. W. Synthesis and antiparasitic activity of new bis-arylimidamides: DB766 analogs modified in the terminal groups. *Eur. J. Med. Chem.* **2014,** 83, 167-173.

50. Crowell, A. L.; Stephens, C. E.; Kumar, A.; Boykin, D. W.; Secor, W. E. Activities of Dicationic Compounds against *Trichomonas vaginalis*. *Antimicrob. Agents Chemother.* **2004,** 48, 3602-3605.

51. Daliry, A.; Pires, M. Q.; Silva, C. F.; Pacheco, R. S.; Munde, M.; Stephens, C. E.; Kumar, A.; Ismail, M. A.; Liu, Z.; Farahat, A. A.; Akay, S.; Som, P.; Hu, Q.; Boykin, D. W.; Wilson, W. D.; Castro, S. L. D.; Soeiro, M. N. C. The Trypanocidal Activity of Amidine Compounds Does Not Correlate with Their Binding Affinity to *Trypanosoma cruzi* Kinetoplast DNA. *Antimicrob. Agents Chemother.* **2011,** 55, 4765-4773.

CHAPTER 8

8.   Chapter 8 :   Conclusions and Future Work

8.1. Conclusions

- Three series of compounds structurally related to **I** were synthesised

Three new families of derivatives (i.e., series **1**–**3**) structurally related to the dicationic lead compounds **I** and **II** were successfully prepared as potential DNA minor groove binders and its SAR was studied. The synthetic routes, which were carried out from the same dianiline precursors for the 3 series, were successful in spite of the poor nucleophilic character of the starting material dianilines. The synthetic procedure using the classical di-*tert*-butyl 2-thioxoimidazolidine-1,3-dicarboxylate (**5**) was fine-tuned to obtain the bis(imidazolidin-2-imine) analogues (**1b**–**h**) vía their Boc-protected synthetic intermediates (**25b**–**h**) whereas the nine bis(2-aminobenzimidazole) derivatives (**2a**–**e**, **2h**, **30**, **31**, **34**) were successfully synthesised from their isothiocyanate precursors. The most challenging compounds to synthesise were the bis(arylimidamide) derivatives (**3a**–**e**, **3g**–**i**, **36**, **37**, **53**) for which a new synthetic protocol was developed. This procedure, using the novel reagent *N*-(*tert*-butoxycarbonyl)pyridine-2-carbimidothioate (**44**), allowed the access to (electron-poor) halogen-containing bis(arylimidamides) which could not be obtained via other described synthetic strategies. Hence, this protocol complements the synthetic toolbox available for the synthesis of this important class of bioactive compounds.

- Series **1**–**3** bind selectively to AT-rich DNA

The SPR results allowed to rank the compounds as binders/non binders for series **1** and most compounds of series **3**. The measured DNA binding constants ranged from 0.38 to 55×10^{-6} M (series **1**) and 0.58 to $>100 \times 10^{-6}$ M (series **3**). Compounds **3a**, **36**, and **53** displayed a binding stoichiometry (*r*) of two moles of bound compound per mole of DNA hairpin duplex. For series **2**, binding to DNA was not clear from the SPR results due to the precipitation of the compounds or non-specific binding to the chip dextran matrix. The SPR experiments also provided an indication of the sequence selectivity of the compounds. Most of them, except the fluorene derivative **53**, did not bind to $(CG)_4$ hairpin indicating that the compounds are AT-selective like lead compound **I**.

Then, different biophysical techniques were used to confirm the DNA binding affinity of the three series. Thermal melting experiments with the $(AT)_4$-containing DNA hairpin showed that all of the compounds (series **1**–**3**) stabilize the DNA duplex upon binding. The T_m increases measured for the bis(imidazolidin-2-imine) derivatives (**1**) ranged from 3.1 ºC to 8.2 ºC versus 1.6 °C for lead **I**. Bis(2-aminobenzimidazole) **2a**–**e** showed ΔT_m values in the range 4.0–7.0 °C, indicating that these derivatives also bind to AT-rich DNA. For the bis(arylimidamide) series, thermal increases ranged from 1.6 to 11 ºC, with most of the compounds (except **3i**) showing larger T_m increases than **I**. These experiments also confirmed the specificity of binding to AT sequences for this series. The UV-Vis titrations in the presence of unspecific (salmon testes) DNA confirmed that series **2** compounds bind to DNA.

Regarding the crystallization studies, crystals were obtained for **1c**, **3a** and **36** with d(AAATATATTT) oligonucleotide further confirming that these compounds bind to AT-rich DNA. However, no satisfactory diffraction patterns were obtained up to the date of writing this thesis. Hence, no precise structural information could be gained from these studies up to now.

- Series **1** compounds and **3a** are DNA minor groove binders

The binding mode of series **1**–**3** was studied using three techniques: CD, LD and ^{1}H NMR. For series **1**, a substantial positive induced CD signal was observed at ≈ 300–310 nm upon complexation with the $(AT)_4$ hairpin DNA, which is typically indicative of minor groove binding. This result was confirmed unequivocally for **1e** using LD experiments with unspecific DNA. These results were consistent with the SPR data showing AT base-pair specificity versus CG, and hence, minor groove preference for these ligands.

For series **3**, the CD experiments with the $(AT)_4$ oligonucleotide showed a substantial positive induced CD signal at ≈ 320 nm for **3a**, indicative of minor groove binding, and a weak induced CD signal for **3b**, **3g**–**i**, **37**, and **53**. LD experiments with unspecific DNA confirmed the minor groove mode of binding of compound **3a**. ^{1}H-NMR experiments also showed clearly that compound **3a** binds selectively to the $(AT)_4$-containing oligonucleotide, interacting with the NH_2 of adenine bases, even at low concentration of ligand.

In contrast, the mode of binding for the rest of the series (**3b–i**, **36**) was not determined unambiguously. In particular, the fused ring tricyclic fluorene derivative **53**, which is not AT-selective (as shown by SPR) and displays the largest stabilization effect upon binding to DNA (ΔT_m = 11.0 ºC), may have a mixt mode of binding. This was shown earlier with similar guanidinium compounds that have the ability to bind to the minor groove of certain DNA sequences and intercalate to others.[1]

- Serie **2** mode of binding to DNA remains to be determined

The bis(2-aminobenzimidazole) compounds displayed none (**2a–2d**, **2h**) or minor induced CD signal (**2e**, **30**, **31**, **34**) in the experimental conditions used for the thermal assays. However, since the spectral window used in these experiments was not optimal (230–320 nm) to observe the induced CD band, further experiments will be needed to get a better understanding of the binding mode of this series.

For compound **2a**, which showed a T_m increase of 4.9 ºC with the (AT)$_4$ hairpin and none with the (CG)$_4$ oligonucleotide, the intercalative mode of binding – which is sequence-independent – does not seem probable. Hence, **2a** is probably a MGB although further experiments will need necessary to corroborate this hypothesis.

- Bis(imidazolidin-2-imines) (**1**) and bis(arylimidamides) (**3**) are (di)cations whereas bis(2-aminoimidazole) (**2**) are uncharged at physiological pH

The measured pK_a values for bis(imidazolidin-2-imine) series (**1**) are > 8, indicating that they are mostly dicationic at physiological pH (85.5 to 98.7%). Calculated logP ranged from 1.82 to 3.89. Bis(arylimidamide) derivatives show pK_a values in the range 4.76–7.18, with percentages of ionization at pH 7.4 from 0.2% (**3g**) to 38% for **3a**. Calculated logP values were in the range 2.21–5.15. Bis(2-aminobenzimidazole) derivatives have lower pK_a values in the range 2.77–5.93, indicating that the compounds are mostly neutral at physiological pH. This series has the highest calculated logP values (4.3–7.24).

The cationic nature of the molecule is an important feature of DNA MGB but it is not critical for DNA binding. In fact, we did not observe any correlation between the pK_a and the DNA affinities (ΔT_m). For example, series **1–3** display different ionization states at pH 7.4 and they all bind strongly to AT-rich DNA.

On the other hand, the cationic nature of these compounds seems important for their antiparasitic activity because cationic compounds accumulate to high levels into the mitochondrion of kinetoplastid parasites. This accumulation depends in part on the charge and the lipophilic character of the molecule. A subtle equilibrium between the charge, the lipophilicity and the DNA binding affinity seems to determinate the *in vitro* antiparasitic activity of the compounds. This is in illustrated with the bis(2-aminobenzimidazoles) **30** and **31**, for example, which have similar pK_a (5.64 and 5.93), logP (7.24 and 6.23), and DNA binding affinities (ΔT_m = 6.1 and 7.0 ºC, respectively) but very different *in vitro* activity against *T. brucei* (EC$_{50}$ = 2.3 and 57.1 µM) and *L. donovani* promastigotes (EC$_{50}$ = 8.67 and >200 µM, respectively).

- Bis(imidazolidin-2-imines) **1** and bis(2-aminobenzimidazoles) **2** are active against *brucei in vitro*

Series **1** and **2** showed moderate activity against wild-type and pentamidine-resistant strains of *T. brucei* with EC$_{50}$ values in the micromolar range (5.71–78.5 µM and 1.68–88.6 µM, respectively) and modest selectivity indexes (SI) in the range 1.3 to >35 (**1**) and >1.2 to 12.8 (**2**). The cytotoxicity evaluated against HEK cells and L929 fibroblasts showed that the bis(imidazolidin-2-imine) derivatives and, to a lesser extent, the bis(2-aminobenzimidazole are non-toxic to mammalian cells.

With regard to *Leishmania*, compounds **1g** and **30** were the only compounds that were active (EC$_{50}$ = 7.64 and 8.67 µM, respectively) against promastigotes of *L. donovani*. The whole series were inactive against *T. cruzi* and *T. vaginalis*. Hence, the replacement of the 2-aminoimidazoline groups by 2-aminobenzimidazole heterocycles did not improve the activity against the parasites *Leishmania* (promastigotes and amastigotes) and epimastigotes of *T. cruzi* with respect to lead **I** as hypothesised. In fact, all these new derivatives were less active than **I** against the three kinetoplastid parastites.

- Bis(arylimidamide) series (**3**) are very effective antiparasitic agents against the kinetoplastid parasites *T. brucei*, *T. cruzi* and *L. donovani*

These compounds are very potent inhibitors of *T. brucei*, *T. cruzi* and *Leishmania* growth, with adequate SI. Compound **3h** emerged as a good candidate against *T. brucei* (EC$_{50 \text{ (WT)}}$ = 0.12 µM, SI = 118) and *L. donovani* amastigotes (EC$_{50}$ = 0.55 µM, SI = 20.3). Chlorinated compounds **3e** (EC$_{50}$ = 0.26 µM, SI = 399) and **3b** (EC$_{50}$ = 0.58 µM, SI =

77.3), and the fluorene analogue **53** (EC$_{50}$ = 1.26 µM, SI = 47.5) displayed the best activities and selectivity against intracellular amastigotes of *T. cruzi*. As regards to intracellular amastigotes of *L. donovani*, **3a**, **36** (EC$_{50}$ = 1.1 µM, SI > 45), and **53** (EC$_{50}$ = 0.98 µM, SI = 47.4) can be considered as new antileishmanial lead compounds.

- Compound **3a** is an AT-selective MGB active against extracellular (*T. brucei*) and intracellular parasites (*T. cruzi* and *L. donovani*)

The unsubstituted compound **3a**, which is the closest analogue of **I**, was the best antiparasitic compound with submicromolar activity and high selectivity against these three kinetoplastid parasites. Compound **3a** appears as a new lead compound active in the submicromolar range against BSF trypomastigotes of *T. brucei* (EC$_{50}$ = 0.40 µM, SI > 500) and intracellular amastigotes of *L. donovani* (EC$_{50}$ = 0.65 µM, SI > 76.9) and *T. cruzi* (EC$_{50}$ = 1.28 µM, SI = 69.6). This compound shows high selectivity indexes against the mammalian cells tested and it is metabolically stable towards liver metabolism (i.e., HLM and MLM) and in human serum. Therefore, **3a** is a good candidate to perform further *in vivo* assays.

- Series **1**–**3** are inactive against *T. vaginalis*

All of the compounds were tested against the amitochondriate parasite *T. vaginalis* because its genome has a high content in AT base pairs which may potentially be targeted by DNA MGBs. Only one compound (**34**, EC$_{50}$ = 33.2 µM) among the three series had weak trichomonacidal efficacy with poor selectivity (CC$_{50}$ ≈ 50 µM). We do not have an explanation for the lack of trichomonacidal activity of these compounds which are DNA MGBs.

- The effect of the *N*-phenylbenzamide scaffold modification on the antiprotozoal activity depends on the series

For series **1**, the introduction of Cl, O^{i}Pr, pyridine rings, 1,2-diphenylethane,[2] or 1,3-diphenylurea[2] did not improve the antikinetoplastid activity of compound **I**.

For series **2**, modification of the *N*-phenylbenzamide scaffold with Cl, O^{i}Pr, pyridine rings, 1,2-diphenylethane, fluorene or 1,3-diphenylurea led to up to 50-fold increase in anti-*T. brucei* activity with respect to the unmodified *N*-phenylbenzamide analogue **2a**.

For series **3**, the introduction of pyridine rings in the scaffold (**3h**) increase the anti-*T. brucei* and antileishmanial activity very efficiently, as was shown earlier with diamidines.[3] The substitution of the *N*-phenylbenzamide scaffold with two lipophilic groups such as chlorine atoms (**3b**, **3c**, **3e**) or O*i*Pr groups (**3g**) appears as a good strategy to improve the activity against intracellular amastigotes of *T. cruzi* and *Leishmania* parasites. The fluorene (**53**) is another interesting scaffold which displayed excellent activities and selectivity against intracellular amastigotes of *T. cruzi*, whereas the 1,2-diphenylethane (**36**) is adequate for antileishmanial compounds. The latter also worked as *N*-phenylbenzamide surrogate for bis(imidazolidin-2-imines) series.[2, 4]

- Compound **3a** was successfully loader into NLC nanoparticles

We successfully prepared NLC loaded with compound **3a** and evaluated its storage stability which depend on the decoration of the NPs. Blank NLC were very stable at room temperature (60 days), whereas folic acid-functionalized NLC had limited stability (<21 days), and it is possibly due to the functionalization. The ease of synthesis of these NLC is clearly an advantage that can outweigh this shortcoming. Future studies, using different formulation (avoiding or reducing the quantity of fatty acids) should be developed to evaluate different storage temperatures in order to increase the stability periods.

8.2. Future Work

To continue the evaluation of the MGBs which are most active against the kinetoplastid parasites *T. cruzi* and *L. donovani*, further *in vivo* assays should be performed with the bis(arylimidamide) series **3**. Compound **3a** in particular is an excellent candidate for pharmacokinetics and efficacy studies in animal models of leishmaniasis. Compound **3e** is another candidate for *in vivo* efficacy assays against *T. cruzi*.

The biological evaluation of the NLC loaded with **3a** will be performed at Teesside University (United Kingdom) in the next months, in collaboration with Dr. Godwin Ebiloma. The synthesized NLC will be evaluated against intracellular amastigotes and axenic amastigotes of *Leishmania* spp.

As regards to the crystallographic studies, the growing of new crystals is in progress. The X-ray diffraction of these new crystals will be carried out at ALBA synchrotron in the second semester of 2022.

Finally, the synthesis of new kDNA-targeting compounds should continue, especially within the bis(arylimidamide) series which provided DNA MGB with excellent *in vitro* efficacy against the intracellular parasites *L. donovani* and *T. cruzi*. The presence of chlorine atom in ring B (R_4) next to the pyridine-2-carboxamidine rings (similar to **3c**) is observed to have an influence in the biological activity against both parasites (*L. donovani* and *T. cruzi*). Further studies should be performed with new derivatives taking into account these SAR results. For instance, the introduction of different lipophilic substituents next to the pyridine-2-carboxamidine rings (e.g., Me, OR, ...) could be tested.

Taking into consideration that for *L. donovani* the unsubstituted scaffold was the most active and selective (e.g., **3a**, **36**), modifications could be made on the cationic pyridine-2-carboxamidine rings, but preserving the number of H-bond donors (i.e., N atoms) for an optimum binding to DNA.

Importantly, considering that the benzimidazole derivatives were mostly inactive, the new derivatives should have a pK_a that allows their ionization at physiological pH in order to facilitate drug accumulation into the targeted kinetoplastid mitochondrion.

As regard to the synthesis protocol to obtain the bis(arylimidamide) compounds, new synthesis conditions (e.g., number of equivalents of $HgCl$/Et_3N/**44**) and purification conditions should be tested to improve the yields of bis(arylimidamides) obtained with this new methodology set up in this Thesis. Work is ongoing to solve these issues.

8.3. References

1. Nagle, P. S.; McKeever, C.; Rodriguez, F.; Nguyen, B.; Wilson, W. D.; Rozas, I. Unexpected DNA Affinity and Sequence Selectivity through Core Rigidity in Guanidinium-Based Minor Groove Binders. *J. Med. Chem.* **2014,** 57, 7663-7672.
2. Rodríguez, F.; Rozas, I.; Kaiser, M.; Brun, R.; Nguyen, B.; Wilson, W. D.; García, R. N.; Dardonville, C. New Bis(2-aminoimidazoline) and Bisguanidine

DNA Minor Groove Binders with Potent *in Vivo* Antitrypanosomal and Antiplasmodial Activity. *J. Med. Chem.* **2008,** 51, 909-923.

3. Ismail, M. A.; Brun, R.; Easterbrook, J. D.; Tanious, F. A.; Wilson, W. D.; Boykin, D. W. Synthesis and Antiprotozoal Activity of Aza-Analogues of Furamidine. *J. Med. Chem.* **2003,** 46, 4761-4769.

4. Ríos Martínez, C. H.; Miller, F.; Ganeshamoorthy, K.; Glacial, F.; Kaiser, M.; de Koning, H. P.; Eze, A. A.; Lagartera, L.; Herraiz, T.; Dardonville, C. A new nonpolar *N*-hydroxy imidazoline lead compound with improved activity in a murine model of late-stage *Trypanosoma brucei brucei* infection is not cross-resistant with diamidines. *Antimicrob. Agents Chemother.* **2015,** 59, 890-904.

CHAPTER 9

9. Chapter 9: Experimental Section

9.1. Chemistry

All the commercial chemicals were obtained from Sigma-Aldrich, Fluorochem, Acros Organics or Alfa Aesar and were used without further purification. Deuterated solvents for NMR use were purchased from Merck (Sigma-Aldrich). Dry solvents were both obtained from Acros Organics & Sigma Aldrich in SureSeal™ bottles, or were distilled using standard procedures, according to Vogel's Textbook of Practical Organic Chemistry.[1] Solvents for synthesis purposes were used at GPR grade. Reactions heated by microwaves were realized in a Biotage Initiatior™ microwave oven reactor (frequency: 2045 GHz). Chromatographic columns were run using Silica gel 60 (230–400 mesh ASTM) or Aluminium Oxide (activated, Neutral Brockman I STD grade 150 mesh). Analytical TLC was performed using Merck Kieselgel 60 F_{254} silica gel plates or Alugram© Alox N/UV$_{254}$ aluminium oxide plates. TLC plates were visualised under UV light (254 and 365 nm) and/or revealed with staining reagents (i.e., iodine, phosphomolybdic acid (PMA), ninhydrin). Flash chromatography was performed in a Isolera One (Biotage™) with Isolera™ 3.3.0 version, using Biotage Sfär™ columns (silica D, duo 60 μm) or SiliaSep™ Flash cartridges (SiliCycle) 40–63 μm, 60 Å. Reverse-phase chromatography was performed using LiChroprep RP-18 (25–40 μm), Merck, and Claricep Screw-on Flash C18 columns (spherical, 20–35 μm, 100 Å, 122 g). Centrifugal TLC was carried out with Chromatotron™, Harrison Research. Ser. Nº. 498, using circular glass plates prepared with silica gel 60 PF_{254} containing gypsum. NMR spectra were recorded on a Bruker DPX-400 Advance spectrometer, operating at 400.13 MHz and 600.1 MHz for ^{1}H-NMR and 100.6 MHz and 150.9 MHz for ^{13}C-NMR. Shifts are referenced to the internal solvent signals (DMSO-d_6: ^{1}H NMR δ 2.50, ^{13}C NMR δ 39.52; Chloroform-d: ^{1}H NMR δ 7.26, ^{13}C NMR δ 77.16; Methanol-d_4: ^{1}H NMR δ 3.31, ^{13}C NMR δ 49.00). NMR data were processed using MestReNova 14.2.1software. Signals multiplicity for ^{1}H NMR is defined as: singlet (s), doublet (d), triplet (t), quartet (q), multiplet (m), br (broad signal). Coupling constants J are expressed in hertz (Hz). Mass spectra were recorded in negative and positive mode using electrospray ionization technique (ESI$^+$ or ESI) using three different cone voltages. Apparatus: HPLC–MS WATERS integrated with a separation module 2695, detector PDA (photodiode array) 2996 and Micromass ZQ spectrometer. Analytical

liquid chromatography (HPLC) was performed in reverse phase with SunFire C18-3.5 µm column, 100 Å porous size, (2.1 mm × 50 mm). Mobile phase A: CH_3CN + 0.08% formic acid and B: H_2O + 0.05% formic acid. Common gradient used was 15% to 95% of A, unless otherwise indicated, time = 5 min and 1 mL/min flow rate. UV detection was carried over 190 to 440 nm. Melting points were determined using a Mettler Toledo MP70 digital melting point apparatus and are uncorrected. Some of them show a broad melting range due to the low degree of crystallinity. Elemental analysis was carried out at the Microanalysis Laboratory, "Manuel Lora Tamayo" Organic Chemistry Centre – CSIC. High resolution mass spectra were recorded at the Elemental Microanalysis Unity at the Pharmacy College, Complutense University of Madrid. cLogP values have been calculated using the MarvinSketch (ChemAxon method, considering tautomerization/resonance), version 22.9.0.

9.1.1. General procedures

Method A: synthesis of 4-nitro-*N*-(4-nitrophenyl)benzamides (9a–h)

The reactions were carried out in a round-bottom flask sealed with a screw cap. A solution of carboxylic acid (1.5 equiv., 0.5 – 3 g scale) in $SOCl_2$ (5 – 50 mL) was stirred at 80 °C for the time specified in each case. After cooling back to room temperature, the flask was open carefully because of internal pressure of SO_2 and HCl. The solution was concentrated under vacuum to eliminate excess $SOCl_2$. To facilitate the complete elimination of $SOCl_2$, CH_2Cl_2 was added to the oily residue and the solvent was evaporated again. The acid chloride, which was obtained as oil, was added slowly with a syringe over a stirred solution of nitroaniline (1.0 equiv.) and DIPEA (2.0 equiv.) in anhydrous toluene (20 mL) under Argon atmosphere. The reaction mixture was stirred overnight at room temperature.

Workup 1: The solvent was removed under vacuum and the reaction crude was diluted with MeOH allowing the precipitation of a crude solid. The precipitate was filtrated over a filter funnel and washed successively with 0.1 M aq. HCl (10 mL) and MeOH (20 mL) to give the product as solid powder.

Workup 2: few drops of methanol were added to the reaction mixture to precipitate the product. The solid was isolated by filtration and washed successively with 0.1 M HCl and MeOH to yield the pure benzamides.

Method B: microwave synthesis of 4-nitro-*N*-(4-nitrophenyl)benzamides (9i)

A microwave oven glass tube was charged with a solution of aniline (1.0 equiv.), 4-nitrobenzoyl chloride (1.5 equiv.), and DIPEA (5.0 equiv.) in anhydrous toluene (8 mL). The reaction mixture was heated at 100 °C for 30 minutes under Argon atmosphere.

Method C: general procedure for the reduction of 4-nitrobenzamides with Tin(II) chloride (15b−f)

SnCl$_2$.2H$_2$O (10 equiv.) was added to a suspension of nitrobenzamide (1 equiv., 1 – 5.5 g scale) in EtOAc (15 – 60 mL) and a catalytic amount of concentrated HCl (20 drops). The reaction mixture was stirred overnight at 50 °C. The reaction mixture was filtered through a pad of Celite and the filter cake was rinsed with CH$_2$Cl$_2$:MeOH (1:1) (250 mL). The filtrate was evaporated under vacuum and the crude solid was dissolved in EtOAc and extracted with NaHCO$_3$ (pH = 8). The compound was extracted with EtOAc several times. Complete extraction from the aqueous phase was checked by TLC revealed with ninhydrin. The organic phase was washed with brine, dried with MgSO$_4$, and the solvent was evaporated under vacuum. Recrystallization from CHCl$_3$ (**15e**), or EtOAc (**15b, 15c**, **15d**), or EtOAC/MeOH (**15f**) gave the product as solid powder.

Method D: Catalytic hydrogenation with Pd-C (Parr hydrogenation) (15g−i)

A 200 mL Parr hydrogenation flask was charged with the dinitrobenzamide derivative (0.2 – 2.4 g scale) dissolved in EtOAc (15 – 50 mL). The flask was cooled in an ice-bath, and 5% Pd-C catalyst (10% w/w) was added. After air was purged under vacuum, H$_2$ was introduced into the flask (39 Psi). The hydrogenation process was monitored by TLC using ninhydrin as staining agent. The resulting reaction mixture was diluted with MeOH and filtered through a pad of Celite. The organic phase was evaporated under vacuum to give the crude diamino compound.

Method E: General procedure for the synthesis of Boc-protected bis-2-iminoimidazolidinyl benzamides derivatives (25b–h)

Mercury (II) chloride (3 equiv.) was added to a cooled solution (ice-water bath) of di-*tert*-butyl 2-thioxoimidazolidine-1,3-dicarboxylate (**5**) (3 equiv.), diamine compound (1 equiv., 100 - 300 mg scale) and anhydrous triethylamine (7 equiv.) in dry DMF (3 mL / 0.7 mmol) under argon atmosphere. The reaction mixture was stirred 1 hour at 0 ºC. Then, the ice-water bath was removed and the reaction mixture was stirred at 60 °C for the time specified in each case. The reaction mixture was diluted with CH_2Cl_2 and filtered over Celite, using a mixture of CH_2Cl_2:MeOH (1:1, 200 mL). The solvent was removed under vacuum. The filtrate was diluted with EtOAc (100 mL) and extracted with water (3 × 150 mL). The organic phase was washed with brine, dried over $MgSO_4$, and evaporated under vacuum. The pure compounds were obtained by crystallization or by silica centrifugal thin-layer chromatography as specified in each case.

Method F: general method for Boc group hydrolysis using trifluoroacetic acid (1b−h)

Trifluoroacetic acid (2 mL) was added to a cooled solution (ice-water bath) of the Boc-protected compound (1 mmol, 60 – 220 mg scale) dissolved in CH_2Cl_2 (2 – 6 mL). The resulting solution was stirred four hours at the same temperature. Trifluoroacetic acid and dichloromethane excess were evaporated under vacuum. This process was repeated by dissolving the crude residue in CH_2Cl_2 and evaporating the solvents under high vacuum. The sticky solid was crushed with diethyl ether to precipitate the product as a powder.

Method G: general procedure for the formation of isothiocyanates (19, 20, 26b–e, 26h, 29, 33)

The reaction was performed in a KIMAX tube. A solution of diamine (1 equiv., 0.07 – 3.4 g scale) and thiophosgene (2.5 equiv.) in Et_2O:H_2O mixture (3:1) (2 – 50 mL) was stirred at room temperature overnight. After stirring, a solid appeared at the bottom of the tube. The solid precipitate was filtered in a funnel and washed with water (100 mL). The product was dried under vacuum at 40 °C to yield the product.

CAUTION! work in well-ventilated fume-hood and wear adequate protecting clothes. Thiophosgene residues should be disposed off adequately.

Method H: general procedures for the synthesis of bis(2-aminobenzimidazole) derivatives (2a–e, 2h, 30, 31, 34)

The reaction was performed in a KIMAX tube. A solution of isothiocyanate (1 equiv., 50 – 125 mg scale) and *o*-phenylendiamine (2.2 equiv.) in dry DMF (3 – 5 mL) was stirred at 0 ºC (ice–water bath) until complete formation of the thiourea intermediate (verified by TLC and HPLC-MS). Then, EDC hydrochloride (2.5 equiv.) was added in one step and the resulting reaction mixture was stirred at 60 ºC for 24 hours. The reaction was processed by addition of ice-chunks to the crude, and the tube was shaken vigorously. The solid precipitate was purified by silica centrifugal TLC using CH_2Cl_2:MeOH (9:1; 8:2; 7:3; 6:4; 1:1) as elution system.

Method I: general procedure for the synthesis of bis(2-arylimidamides) from methyl *N*-(*tert*-butoxycarbonyl)pyridine-2-carbimidothioate (44)

I.1: A microwave vial was charged with diamine (0.4 mmol, 1 equiv., 90 – 150 mg scale), methyl *N*-(*tert*-butoxycarbonyl)pyridine-2-carbimidothioate **44** (4 equiv.), and $HgCl_2$ (4 equiv.). The vial was sealed with a septum cap and purged with argon. Dry CH_2Cl_2 (2 – 4 mL) was added, followed by dry Et_3N (4 equiv.). The reaction mixture was irradiated for 1 h at 50 ºC. The crude reaction mixture was diluted with CH_2Cl_2 and filtered on Celite. The filter pad was rinsed successively with CH_2Cl_2 and CH_2Cl_2:MeOH (1:1) mixture (50 mL). The solvents were evaporated under vacuum and the product was purified by chromatography as described for each compound.

I.2: Removal of Boc-protecting groups using TFA

To a cooled (ice-water bath) solution of the Boc-protected bis(2-arylimidamide) (scale: 10 – 50 mg) in CH_2Cl_2 (2 – 5 mL) was added slowly TFA (2 mL). The resulting solution was stirred 2 hours at 0 ºC. The solvents were removed under vacuum to give a crude oil which was dried under high-vacuum. The crude solid was triturated with Et_2O to precipitate the product as powder.

Method J: general procedure for the synthesis of bis(2-arylimidamides) from naphthalen-2-ylmethyl pyridine-2-carbimidothioate hydrobromide (35)

To a solution of diamine (0.5 g, 2.2 mmol) in a 3:1 mixture of anhydrous EtOH:CH₃CN (30 mL) stirred at 0 °C (ice-water bath) was added slowly a solution of naphthalen-2-ylmethyl pyridine-2-carbimidothioate hydrobromide (**35**) (1.97 mg, 5.5 mmol, 2.5 eq.) in 6 mL of EtOH:CH₃CN (3:1). The resulting reaction mixture was allowed to stir at room temperature for 48 hours. The solvents were removed under vacuum and the crude product was purified as specified in each case.

9.1.2. Synthesis and characterization of the compounds

9.1.2.1. Synthesis of precursor compounds

Isopropyl 2-isopropoxy-4-nitrobenzoate (11)
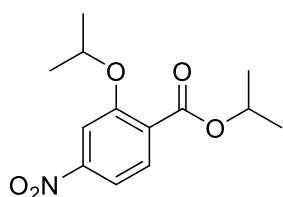
To a round-bottom flask containing a magnetic stir bar was added sequentially 2-hydroxy-4-nitrobenzoic acid (2.8 g, 15.2 mmol), anhydrous *N,N*-dimethylformamide (20 mL), K₂CO₃ (5.24 g, 38 mmol), and 2-iodopropane (3.8 mL, 38 mmol). The reaction was stirred at room temperature for 16 h. The mixture was diluted with dichloromethane and washed successively with distilled water (twice) and aqueous saturated sodium chloride solution (brine). The organic layer was dried over magnesium sulphate, filtered, and the solvent was evaporated under vacuum. Column chromatography was performed using hexane/ethyl acetate: 100/0 → 97/3 as elution system, yielding **11** as yellowish oil (2.9 g, 71.4%).

¹H NMR (400 MHz, DMSO-*d₆*) δ 7.87 (d, *J* = 2.0 Hz, 1H), 7.82 (dd, *J* = 8.4, 2.0 Hz, 1H), 7.75 (d, *J* = 8.4 Hz, 1H), 5.14 (sept, *J* = 6.0 Hz, 1H), 4.87 (sept, *J* = 6.0 Hz, 1H), 1.31 (d, *J* = 6.0 Hz, 6H), 1.30 (d, *J* = 6.0 Hz, 6H).

¹³C NMR (101 MHz, DMSO-*d₆*) δ 164.8, 156.0, 149.9, 130.7, 128.8, 115.0, 108.8, 71.8, 68.9, 21.52, 21.49.

mp.: >184.0 °C.

HPLC (UV) > 95 %.

LRMS (ESI⁺) *m/z* 268.4 [M+H].

Anal. calcd for $C_{13}H_{17}NO_5$: C, 58.42; H, 6.41; N, 5.24. Found: C, 58.00; H, 6.33; N, 5.36.

2-Isopropoxy-4-nitrobenzoic acid (6g)
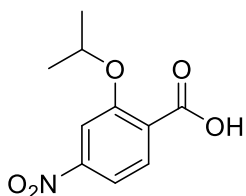
A Kimax tube was loaded with **11** (300.5 mg, 1.1 mmol), LiOH (135.3 mg, 5.7 mmol) and 16 mL THF/H_2O (1:1). The reaction mixture was stirred at room temperature for 12 hours. THF was then evaporated under vacuum and the aqueous solution acidified with 1 M aqueous HCl. The product was extracted with CH_2Cl_2, washed with brine, and dried over magnesium sulphate. Finally, the solvent was removed under vacuum. Recrystallization from ethyl acetate yielded **6g** as a light-yellow solid (212 mg, 83.4%).

¹H NMR (300 MHz, DMSO-*d₆*) δ 7.85 (d, *J* = 2.0 Hz, 1H), 7.81 (dd, *J* = 8.4, 2.0 Hz, 1H), 7.75 (d, *J* = 8.4 Hz, 1H), 4.84 (sept, *J* = 6.0 Hz, 1H), 1.30 (d, *J* = 6.0 Hz, 6H).

¹³C NMR (101 MHz, DMSO-*d₆*) δ 166.7, 156.0, 149.7, 130.8, 129.8, 115.1, 109.4, 71.9, 21.6.

mp.: 142–143 °C (146–147 °C).[2]

HPLC (UV) 100%.

LRMS (ESI⁺) *m/z* 226.1 [M+H].

Anal. calcd for $C_{10}H_{11}NO_5 \cdot 0.5\ H_2O$: C, 51.28; H, 5.16; N, 5.98. Found: 50.89; H, 4.95; N, 5.95.

ALTERNATIVE PROTOCOL FOR THE SYNTHESIS OF 6g (without isolating the benzoate intermediate):

To a stirred solution of 2-hydroxy-4-nitrobenzoic acid **10** (500 mg, 2.7 mmol) in dry DMF (5 mL) was added K_2CO_3 (943 mg, 6.8 mmol) at once. After 5 minutes stirring, 2-iodopropane (0.7 mL, 6.8 mmol) was added dropwise to the mixture. After 16 hours stirring at room temperature, the crude reaction mixture was diluted with EtOAc and extracted with 1M aq. HCl. The organic phase was washed with saturated NaCl solution, dried over Na_2SO_4, filtered and the solvent was evaporated under vacuum to yield a yellowish oil (HPLC > 95%).

The crude oil was diluted in a mixture of THF/H$_2$O (1:1, 10 mL), followed by the addition of LiOH (240 mg, 10 mmol). After 6 hours stirring at room temperature, the crude reaction mixture was diluted with CH$_2$Cl$_2$ and extracted with 1M aq. HCl. The organic phase was washed with brine, dried over Na$_2$SO$_4$ and evaporated under vacuum.

Compound **6g** was obtained as yellowish solid (369 mg, 82 %) by recrystallization from EtOAc.

2-Isopropoxy-4-nitroaniline (8g)
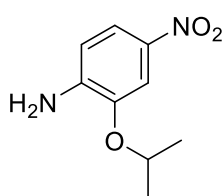
To a pressure round-bottom flask containing a magnetic stir bar was added sequentially 2-amino-5-nitrophenol (1540 mg, 10 mmol), anhydrous *N,N*-dimethylformamide (15 mL), K$_2$CO$_3$ (1380 mg, 10 mmol), and 2-iodopropane (1.2 mL, 12 mmol). The reaction was refluxed for 48 h. After cooling, the mixture was diluted with distilled water (40 mL) and neutralized with 10 mL of 1 N Na$_2$CO$_3$ (until pH = 8). The resulting mixture was extracted with dichloromethane and washed with aqueous saturated sodium chloride solution (brine). The organic layer was dried over magnesium sulphate, filtered, and the solvent was evaporated under vacuum. Column chromatography was performed using hexane/ethyl acetate: 90/10 → 20/80 as elution system, yielding **8g** as yellowish oil (1393 mg, 71%).

^{1}H NMR (500 MHz, Methanol-d_4) δ 7.74 (dd, *J* = 8.8, 2.4 Hz, 1H), 7.66 (d, *J* = 2.4 Hz, 1H), 6.68 (d, *J* = 8.8 Hz, 1H), 4.67 (hept, *J* = 6.1 Hz, 1H), 1.38 (d, *J* = 6.1 Hz, 6H).

^{13}C NMR (126 MHz, Methanol-d_4) δ 147.9, 144.4, 138.3, 120.3, 112.5, 109.3, 72.5, 22.1.

mp.: 58.8–60.1 °C.

HPLC (UV) > 95 %.

LRMS (ESI$^+$) 197.4 *m/z* [M+H].

(Z)-1,2-bis(4-carboxy-3- isopropoxyphenyl)diazene-1-oxide (13)
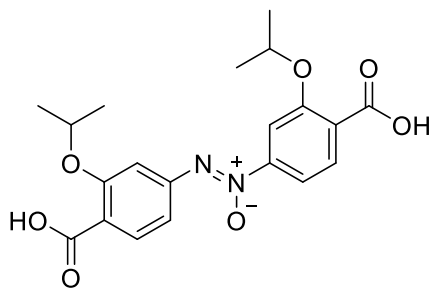
To a round-bottom screw cap pressure flask was added sequentially 2-hydroxy-4-nitrobenzoic acid **10** (1099 mg, 6 mmol), anhydrous *N,N*-dimethylformamide (12.5 mL), K$_2$CO$_3$ (2070 mg, 15 mmol), and 2-iodopropane (1.5 mL, 15 mmol). The flask was capped and the reaction was stirred at 80 °C for 20 hours. After being allowed to cool to room temperature, the mixture was diluted with ethyl acetate and washed successively with water (2×) and brine. The organic layer was dried over magnesium sulphate, filtered, and then the solution was evaporated to dryness to obtain a brownish oil. This material was taken up in tetrahydrofuran (5 mL), to which was added ethanol (12 mL) and 45% aqueous NaOH solution (12 mL). This mixture was allowed to stir at 80 °C (i.e., internal temperature) for 15 hours. The resulting solution was allowed to cool to ambient temperature and then diluted with distilled water and washed twice with ethyl acetate. The aqueous solution was then acidified using 1 M aqueous HCl and extracted twice with diethyl ether. The combined organic layers were washed with an aqueous saturated sodium chloride solution, dried over magnesium sulphate, filtered, and the solvent was removed under vacuum. Recrystallization from ethyl acetate yielded **13** as yellowish solid (1237 mg, 92%). This compound was reported on *Arkivoc* **2021,** viii, 265-276.[3]

¹H NMR (500 MHz, DMSO-*d₆*) δ 12.82 (br, 2H), 7.91 (d, *J* = 2.0 Hz, 1H), 7.86 (dd, *J* = 8.4, 2.0 Hz, 1H), 7.79 (d, *J* = 1.8 Hz, 1H), 7.77 (d, *J* = 8.4 Hz, 1H), 7.74 (d, *J* = 8.3 Hz, 1H), 7.62 (dd, *J* = 8.3, 1.8 Hz, 1H), 4.81 (sept, *J* = 6.1 Hz, 1H), 4.69 (sept, *J* = 6.1 Hz, 1H), 1.32 (d, *J* = 6.1 Hz, 6H),1.31 (d, *J* = 6.1 Hz, 6H).

¹³C NMR (101 MHz, DMSO-*d₆*) δ 167.0, 166.9, 156.3, 156.2, 149.9, 146.3, 130.82, 130.77, 127.4, 124.0, 116.9, 114.0, 111.4, 108.9, 71.7, 71.3, 21.8, 21.7.

mp.: 225.7 °C.

HPLC (UV) >95%.

Anal. calcd. for C$_{20}$H$_{22}$N$_2$O$_7$ (403.14): C, 59.70; H, 5.51; N, 6.96. Found: C, 59.83; H, 5.79; N, 6.76.

IR (solid, v_{max}, cm^{-1}): 2971, 2925, 2869, 2641, 2563, 1682, 1580, 1551, 1485, 1446, 1408, 1387, 1290, 1237, 1178, 1137, 1112, 920.

9.1.2.2. Preparation of the dinitro compounds (9b–i)

3-Chloro-*N*-(2-chloro-4-nitrophenyl)-4-nitrobenzamide (9b)
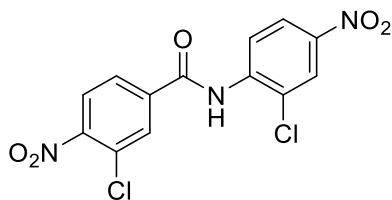
A mixture of 3-chloro-4-nitrobenzoic acid **6b** (850 mg; 1.5 mmol) and SOCl$_2$ (5 mL) reacted following the general Method A. The acid chloride **7b** was obtained as yellowish oil after 12 hours of reaction. The acid chloride **7b** was added over a suspension of 2-chloro-4-nitroaniline **8b** (485 mg; 2.8 mmol) and DIPEA (728 mg; 0.98 mL; 5.6 mmol) in dry toluene (20 mL). The resulting mixture was stirred under argon atmosphere for 16 hours at room temperature. After workup 1, **9b** was obtained as brownish solid (760 mg; 76%).

^{1}H NMR (300 MHz, DMSO-*d$_6$*) δ 10.73 (s, 1H), 8.44 (d, *J* = 2.6 Hz, 1H), 8.32 (d, *J* = 1.8 Hz, 1H), 8.29 (dd, *J* = 8.9, 2.6 Hz, 1H), 8.27 (d, *J* = 8.5 Hz, 1H), 8.13 (dd, *J* = 8.5, 1.8 Hz, 1H), 8.02 (d, *J* = 8.9 Hz, 1H).
^{13}C NMR (101 MHz, DMSO-*d$_6$*) δ 163.2, 149.5, 145.1, 140.7, 138.1, 131.0, 128.7, 128.3, 127.5, 125.9, 125.2, 125.1, 123.0.
mp.: 188.5 – 193.5 °C.
HPLC (UV) > 95 %.
LRMS (ESI⁻) *m/z* 354.3 [M-H].

3-Chloro-*N*-(3-chloro-4-nitrophenyl)-4-nitrobenzamide (9c)
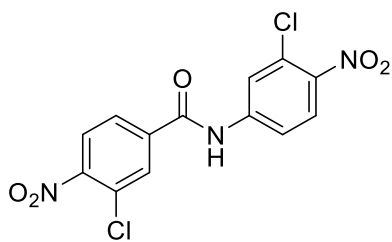
A mixture of 3-chloro-4-nitrobenzoic acid **6b** (3 g; 15 mmol) and SOCl$_2$ (50 mL) reacted following the general Method A. The acid chloride **7b** was obtained as dark yellowish oil after 12 hours of reaction. **7b** was added over a suspension of 3-chloro-4-nitroaniline **8c** (1.7 g; 10 mmol) and DIPEA (2.6 g; 3.5 mL; 20 mmol) in dry toluene (20 mL). The resulting mixture was stirred under argon atmosphere for 16 hours at room temperature. After workup 2, **9c** was obtained as brownish solid (2.7 g; 77%).

¹H NMR (300 MHz, DMSO-*d₆*) δ 11.09 (s, 1H), 8.32 (d, *J* = 1.8 Hz, 1H), 8.27 (d, *J* = 8.4 Hz, 1H), 8.20 (d, *J* = 2.4 Hz, 1H) 8.20 (d, *J* = 8.9 Hz, 1H), 8.12 (dd, *J* = 8.4, 1.8 Hz, 1H), 7.93 (dd, *J* = 8.9, 2.4 Hz, 1H).

¹³C NMR (75 MHz, DMSO-*d₆*) δ 163.5, 149.4, 143.5, 142.2, 138.5, 130.9, 128.3, 127.5, 126.6, 125.9, 125.1, 121.7, 119.0.

mp.: 244.3 – 245.6 °C.

HPLC (UV): > 95 %.

LRMS (ESI⁻): *m/z* 354.3 [M-H].

2-Chloro-*N*-(2-chloro-4-nitrophenyl)-4-nitrobenzamide (9d)
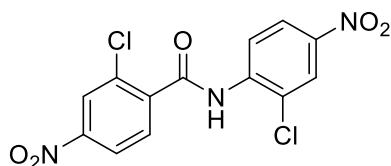
A mixture of 2-chloro-4-nitrobenzoic acid **6d** (1.5 g; 7.5 mmol) and SOCl₂ (30 mL) reacted following the general Method A. The acid chloride **7d** was obtained as yellowish oil after 14 hours of reaction. The acid chloride **7d** was added over a suspension of 2-chloro-4-nitroaniline **8b** (863 mg; 5 mmol) and DIPEA (1.5 g; 11.25 mmol) in dry toluene (10 mL). The resulting mixture was stirred under argon atmosphere for 24 hours at room temperature. After workup 1, **9d** was obtained as brownish solid (1.5 g; 83%).

¹H NMR (300 MHz, DMSO-*d₆*) δ 10.89 (s, 1H), 8.43 (d, *J* = 2.2 Hz, 1H), 8.41 (d, *J* = 2.6 Hz, 1H), 8.32 (dd, *J* = 8.4, 2.2 Hz, 1H), 8.30 (dd, *J* = 9.0, 2.6 Hz, 1H), 8.22 (d, *J* = 9.0 Hz, 1H), 7.96 (d, *J* = 8.4 Hz, 1H).

¹³C NMR (75 MHz, DMSO-*d₆*) δ 164.3, 148.6, 144.6, 141.4, 140.2, 131.3, 130.3, 126.8, 125.9, 125.1, 124.6, 123.1, 122.5.

mp.: 150.7 – 155.7 °C.

HPLC (UV): > 95 %.

LRMS (ESI⁻): *m/z* 354.2 [M-H].

2-Chloro-*N*-(3-chloro-4-nitrophenyl)-4-nitrobenzamide (9e)
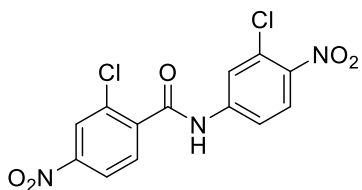
A mixture of 2-chloro-4-nitrobenzoic acid **6d** (1.7 g; 8.4 mmol) and SOCl₂ (20 mL) reacted following the general Method A. The acid chloride was obtained as yellowish oil after 12 hours of reaction. The acid

chloride was added over a suspension of 3-chloro-4-nitroaniline **8c** (970 mg; 5.6 mmol) and DIPEA (1.5 g; 2.0 mL; 11.3 mmol) in dry toluene (10 mL). The resulting mixture was stirred under argon atmosphere for 12 hours at room temperature. After workup 2, **9e** was obtained as yellowish solid (1.3 g; 65%).

^{1}H NMR (300 MHz, DMSO-d_6) δ 11.41 (s, 1H), 8.46 (d, J = 2.2 Hz, 1H), 8.34 (dd, J = 8.4, 2.2 Hz, 1H), 8.20 (d, J = 9.0 Hz, 1H), 8.13 (d, J = 2.2 Hz, 1H), 7.98 (d, J = 8.4 Hz, 1H), 7.79 (dd, J = 9.0, 2.2 Hz, 1H).

^{13}C NMR (75 MHz, DMSO-d_6) δ 164.3, 148.8, 143.1, 142.4, 141.2, 131.2, 130.3, 127.7, 126.9, 124.8, 122.7, 121.1, 118.5.

mp.: 170.7 – 173.2 °C.

HPLC (UV): > 95 %.

LRMS (ESI$^-$): *m/z* 354.3 [M-H].

3-Fluoro-*N*-(2-fluoro-4-nitrophenyl)-4-nitrobenzamide (9f)
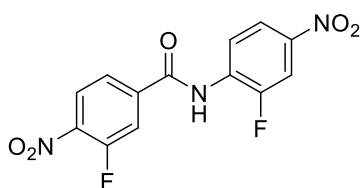
A mixture of 3-fluoro-4-nitrobenzoic acid **6f** (1.13 g, 6.1 mmol) and SOCl$_2$ (5 mL) reacted following the general Method A. The acid chloride **7f** was obtained as yellowish solid after 17 hours of reaction. The acid chloride (610 mg, 3 mmol) was dissolved in THF (2 mL) and added over a suspension 2-fluoro-4-nitroaniline **8f** (312 mg, 2 mmol) and DIPEA (0.7 mL, 4 mmol) in anhydrous THF (5 mL). The resulting mixture was stirred under argon atmosphere for 3 days at room temperature. The colorless precipitate was collected by filtration and rinsed with Et$_2$O to yield **9f** as off-white solid (505 mg). A further crop of the product was obtained from the filtrate as follows; the filtrate was evaporated under vacuum and the crude residue was dissolved in a mixture of MeOH (1 mL) and Et$_2$O (1 mL). The flask was allowed to stand at 4 °C overnight. The precipitate was collected, rinsed successively with MeOH and Et$_2$O, and dried to give another crop of the product as off-white solid (115 mg; 96% overall).

^{1}H NMR (300 MHz, DMSO-d_6) δ 11.06 (s, 1H), 8.43 – 8.12 (m, 5H), 8.00 (dd, J = 7.0, 1.3 Hz, 1H).

^{13}C NMR (75 MHz, DMSO-d_6) δ 162.1, 158.7 (d, J = 253.1 Hz), 152.4 (d, J = 250.9 Hz), 149.7 (d, J = 9.2 Hz), 143.8 (d, J = 8.4 Hz), 132.1 (d, J = 11.4 Hz), 131.5

(d, J = 3.4 Hz), 129.6 (d, J = 15.8 Hz), 123.5 (d, J = 1.7 Hz), 120.6 (d, J = 3.5 Hz), 119.7 (d, J = 3.8 Hz), 112.1 (d, J = 27.3 Hz), 111.9 (d, J = 24.7 Hz).

mp.: 204.3 °C.

HPLC (UV): > 95 %.

LRMS (ESI⁻): *m/z* 322.3 [M-H].

2-Isopropoxy-*N*-(3-isopropoxy-4-nitrophenyl)-4-nitrobenzamide (9g)
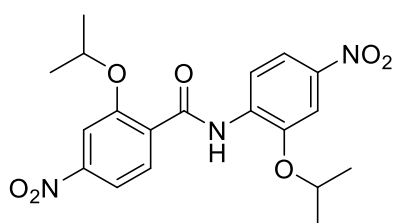
A mixture of 2-isopropoxy-4-nitrobenzoic acid **6g** (0.5 g, 2.2 mmol) and SOCl₂ (5 mL) were reacted according to Method A for 12 hours. The acid chloride **7g** was obtained as yellowish solid. **7g** was added over a stirring suspension of 2-isopropoxi-4-nitroaniline **8g** (291 mg; 1.5 mmol) and DIPEA (383 mg; 0.5 mL; 3.0 mmol) in dry toluene (10 mL). The resulting reaction mixture was stirred at room temperature under argon atmosphere for 48 hours. After workup 2, **9g** was obtained as yellowish solid after recrystallization from MeOH (410 mg; 69%).

¹H NMR (300 MHz, DMSO-*d₆*) δ 10.07 (s, 1H), 8.65 (d, J = 8.9 Hz, 1H), 8.15 (d, J = 8.6 Hz, 1H), 8.00 (d, J = 2.2 Hz, 1H), 7.95 (d, J = 2.2 Hz, 1H), 7.93 – 7.89 (m, 2H), 5.06 (d, J = 6.0 Hz, 1H), 4.95 (d, J = 6.0 Hz, 1H), 1.44 (d, J = 6.0 Hz, 6H), 1.39 (d, J = 6.0 Hz, 6H).

¹³C NMR (75 MHz, DMSO-*d₆*) δ 162.8, 156.0, 150.8, 147.0, 143.6, 134.5, 133.1, 128.9, 120.3, 117.2, 116.1, 110.4, 108.5, 74.3, 73.0, 22.0.

mp.: 179.4 − 180.9 °C.

HPLC (UV): > 95 %.

LRMS (ESI⁻): *m/z* 402.6 [M-H].

5-Nitro-*N*-(5-nitropyridin-2-yl)picolinamide (9h)
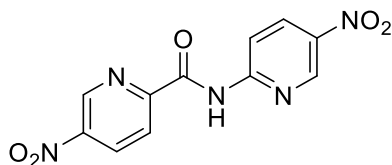
A suspension of 5-nitro picolinic acid **6h** (1.9 g; 11.2 mmol) in dry CH$_2$Cl$_2$ (10 mL) was stirred at 0 °C (ice-water bath), followed by the dropwise addition of a catalytic amount of DMF (10 drops). Oxalyl chloride (1.4 g; 1 mL; 11.2 mmol) was added dropwise, under argon atmosphere, to the stirred mixture, allowing to stir overnight and warming to room temperature. The resulting mixture was cooled to 0 °C (ice-water bath), following by the dropwise addition of Et$_3$N. A solution of 5-nitropyridin-2-amine **8h** (1.1 g; 8 mmol) in dry toluene (15 mL) was slowly added over the stirring mixture. The resulting mixture was stirred for 12 hours at room temperature. The mixture was cooled with an ice-water bath and cold MeOH was added slowly to precipitate the product **9h** as greyish solid (1.9 g; 81%).

^{1}H NMR (300 MHz, DMSO-*d$_6$*) δ 11.02 (s, 1H), 9.51 (d, *J* = 2.4 Hz, 1H), 9.25 (d, *J* = 2.7 Hz, 1H), 8.86 (dd, *J* = 8.6, 2.4 Hz, 1H), 8.74 (dd, *J* = 9.2, 2.7 Hz, 1H), 8.46 (d, *J* = 9.2 Hz, 1H), 8.43 (d, *J* = 8.6 Hz, 1H).

^{13}C NMR (75 MHz, DMSO-*d$_6$*) δ 161.4, 154.5, 152.3, 146.3, 145.0, 144.2, 140.8, 134.8, 134.0, 123.7, 113.1.

mp.: 238.8 – 241.3 °C.

HPLC (UV) > 95 %.

LRMS (ESI⁻) *m/z* 288.3 [M-H].

4-Nitro-*N*-(5-nitropyridin-2-yl)benzamide (9i)
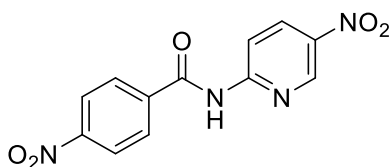
4-nitrobenzoyl chloride **7a** (1.13 g, 6.11 mmol) and 2-amino-5-nitropyridine **8h** (566.4 mg; 4.07 mmol) were reacted with DIPEA (1.05 g;1.42 mL; 8.14 mmol) under argon atmosphere following Method B. **9i** was obtained as whitish solid (930 mg; 80%) after recrystallization from MeOH.

¹H NMR (300 MHz, DMSO-d_6) δ 11.90 (s, 1H), 9.25 (d, J = 2.2 Hz, 1H), 8.69 (dd, J = 9.2, 2.2 Hz, 1H), 8.44 (d, J = 9.2 Hz, 1H), 8.35 (d, J = 8.7 Hz, 2H), 8.24 (d, J = 8.7 Hz, 2H).

¹³C NMR (75 MHz, DMSO-d_6) δ 165.40, 156.11, 149.58, 144.60, 140.39, 139.13, 134.31, 129.92, 123.45, 113.83.

mp.: 209–211 ºC.

HPLC (UV) > 95%.

LRMS (ES⁻) *m/z* 287.4 [M-H].

HRMS (ES⁻) *m/z* 287.0432 [M-H] (Calc. for $C_{12}H_7N_4O_5$: 287.0422).

9.1.2.3. Preparation of the diamino compounds (15b–i)

4-Amino-*N*-(4-amino-2-chlorophenyl)-3-chlorobenzamide (15b)
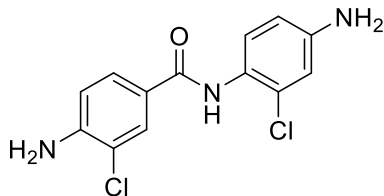
9b (5.5 g; 15.4 mmol) and SnCl$_2$.2H$_2$O (35 g; 154 mmol) reacted following Method C. **15b** was obtained by recrystallization from EtOAc as a brownish powder (4.1 g; 90%).

^{1}H NMR (300 MHz, DMSO-*d$_6$*) δ 9.40 (s, 1H), 7.86 (d, *J* = 2.0 Hz, 1H), 7.67 (dd, *J* = 8.5, 2.0 Hz, 1H), 7.04 (d, *J* = 8.5 Hz, 1H), 6.81 (d, *J* = 8.5 Hz, 1H), 6.68 (d, *J* = 2.5 Hz, 1H), 6.51 (dd, *J* = 8.5, 2.5 Hz, 1H), 5.95 (br s, 2H), 5.33 (br s, 2H).

^{13}C NMR (75 MHz, DMSO-*d$_6$*) δ 164.3, 148.3, 147.7, 130.7, 129.8, 128.8, 127.7, 123.0, 122.1, 116.1, 114.1, 113.4, 112.6.

mp.: 174.8 – 179.3 °C.

HPLC (UV) > 95%.

LRMS (ESI$^+$) *m/z* 296.1 [M+H].

4-Amino-*N*-(4-amino-3-chlorophenyl)-3-chlorobenzamide (15c)
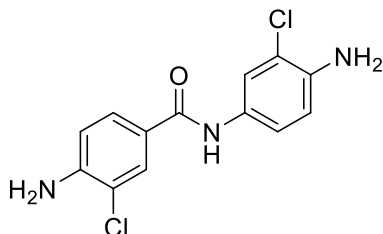
9c (2 g; 5.6 mmol) and SnCl$_2$.2H$_2$O (12.7 g; 56.2 mmol) reacted following Method C. **15c** was obtained by recrystallization from EtOAc as yellowish powder (400 mg; 24%).

^{1}H NMR (400 MHz, Methanol-*d$_4$*) δ 7.84 (d, *J* = 2.1 Hz, 1H), 7.64 (dd, *J* = 8.5, 2.1 Hz, 1H), 7.60 (d, *J* = 2.4 Hz, 1H), 7.27 (dd, *J* = 8.6, 2.4 Hz, 1H), 6.84 (d, *J* = 8.5 Hz, 1H), 6.83 (d, *J* = 8.6 Hz, 1H).

^{13}C NMR (101 MHz, Methanol-*d$_4$*) δ 167.4, 149.2, 142.0, 131.1, 130.1, 128.5, 124.3, 123.8, 122.7, 119.8, 118.7, 117.1, 115.5.

mp.: 190.0 – 192.5 °C.

HPLC (UV) > 95%.

LRMS (ESI$^+$) *m/z* 296.1 [M+H].

4-Amino-*N*-(4-amino-2-chlorophenyl)-2-chlorobenzamide (15d)
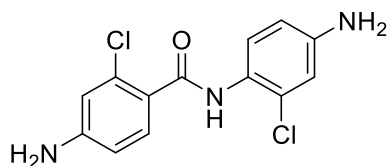
9d (1.4 g; 4.0 mmol) and $SnCl_2.2H_2O$ (9 g; 40 mmol) reacted following Method C. **15d** was obtained by recrystallization from EtOAc as a brownish powder (693 mg; 59%).

¹H NMR (400 MHz, DMSO-*d₆*) δ 9.25 (s, 1H), 7.33 (d, *J* = 8.2 Hz, 1H), 7.16 (d, *J* = 8.4 Hz, 1H), 6.66 (d, *J* = 2.6 Hz, 1H), 6.62 (d, *J* = 2.2 Hz, 1H), 6.56 – 6.47 (m, 2H), 5.75 (s, 2H), 5.32 (s, 2H).

¹³C NMR (126 MHz, DMSO-*d₆*) δ 165.3, 151.5, 148.0, 131.5, 130.8, 129.7, 128.8, 122.9, 122.2, 113.8, 113.4, 112.6, 111.6.

mp.: 180.7 – 183.2 °C.

HPLC (UV) > 95%.

LRMS (ESI⁺) *m/z* 296.1 [M+H].

4-Amino-*N*-(4-amino-3-chlorophenyl)-2-chlorobenzamide (15e)
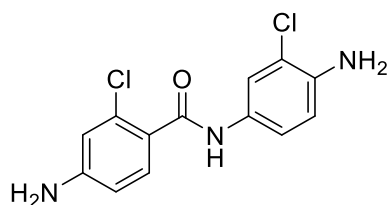
9e (1 g; 2.5 mmol) and $SnCl_2.2H_2O$ (4.75 g; 25 mmol) reacted following Method C. **15e** was obtained by recrystallization from $CHCl_3$ as yellowish powder (520 mg; 71%).

¹H NMR (300 MHz, DMSO-*d₆*) δ 9.83 (s, 1H), 7.68 (d, *J* = 2.4 Hz, 1H), 7.28 (dd, *J* = 8.8, 2.4 Hz, 1H), 7.23 (d, *J* = 8.4 Hz, 1H), 6.75 (d, *J* = 8.8 Hz, 1H), 6.63 (d, *J* = 2.1 Hz, 1H), 6.53 (dd, *J* = 8.4, 2.1 Hz, 1H), 5.74 (s, 2H), 5.12 (s, 2H).

¹³C NMR (126 MHz, DMSO-*d₆*) δ 164.7, 151.3, 140.3, 140.3, 131.3, 130.4, 129.7, 123.1, 120.4, 119.8, 116.8, 115.5, 113.6, 111.6.

mp.: decomposition at 218.2 °C.

HPLC (UV) > 95%.

LRMS (ESI⁺) *m/z* 296.1 [M+H].

4-Amino-*N*-(4-amino-2-fluorophenyl)-3-fluorobenzamide (15f)
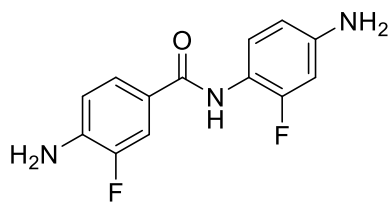
9f (476 mg, 1.47 mmol) was hydrogenated following Method D in presence of Pd-C 5% (86 mg). **15f** was obtained as grey solid (230 mg, 59.4%) by recrystallization from EtOAc/MeOH (98:2).

^{1}H NMR (300 MHz, DMSO-d_6) δ 9.32 (s, 1H), 7.59 (m, 2H), 7.01 (t, J = 8.7 Hz, 1H), 6.77 (t, J = 8.7 Hz, 1H), 6.38 (m, 2H), 5.76 (s, 2H), 5.30 (s, 2H).

^{13}C NMR (75 MHz, DMSO-d_6) δ 164.3, 157.4 (d, J = 243.1 Hz), 149.4 (d, J = 236.9 Hz), 148.5 (d, J = 11.0 Hz), 139.9 (d, J = 13.0 Hz), 128.8 (d, J = 3.5 Hz), 124.7, 121.1 (d, J = 5.5 Hz), 114.7 (d, J = 4.9 Hz), 114.3 (d, J = 19.6 Hz), 113.4 (d, J = 13.5 Hz), 109.3, 100.4 (d, J = 23.0 Hz).

mp.: 144.2 – 147.3 ºC.

HPLC (UV) >95 %.

LRMS (ESI$^+$) *m/z* 264.07 [M + H].

4-Amino-*N*-(4-amino-2-isopropoxyphenyl)-2-isopropoxybenzamide (15g)
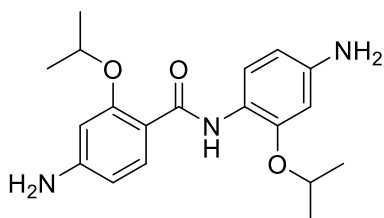
9g (324 mg, 0.8 mmol) was hydrogenated following Method D in presence of Pd-C 5% (65 mg). **15g** was obtained as brownish solid (253 mg, 92.4%) by recrystallization from EtOAc/Hexane.

^{1}H NMR (300 MHz, DMSO-d_6) δ 9.51 (s, 1H), 7.87 (d, J = 8.6 Hz, 1H), 7.72 (d, J = 8.5 Hz, 1H), 6.32 (d, J = 2.3 Hz, 1H), 6.30 (d, J = 2.0 Hz, 1H), 6.23 (dd, J = 8.5, 2.0 Hz, 1H), 6.12 (dd, J = 8.6, 2.3 Hz, 1H), 5.72 (s, 2H), 4.86 (s, 2H), 4.65 (d, J = 6.0 Hz, 1H), 4.49 (d, J = 6.0 Hz, 1H), 1.39 (d, J = 6.0 Hz, 6H), 1.30 (d, J = 6.0 Hz, 6H).

^{13}C NMR (75 MHz, DMSO-d_6) δ 162.3, 157.1, 153.3, 148.0, 145.2, 132.8, 122.6, 118.4, 110.3, 106.8, 105.6, 100.1, 98.4, 71.6, 70.6, 22.2, 22.0.

mp.: > 126.5 ºC.

HPLC (UV) > 95 %.

LRMS (ESI$^+$) *m/z* 343.3 [M+H].

5-Amino-*N*-(5-aminopyridin-2-yl)picolinamide (15h)
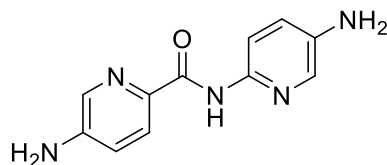
9h (1.5 g; 5.3 mmol) and Pd-C 5% (300 mg; 20% w/w) were reacted under H_2 athmosphere following Method D. **15h** was obtained by recrystallization from EtOAc as brownish powder (1.2 g; 99.8%).

^{1}H NMR (400 MHz, DMSO-d_6) δ 9.80 (s, 1H), 7.96 (d, J = 2.7 Hz, 1H), 7.94 (d, J = 8.7 Hz, 1H), 7.82 (d, J = 8.7 Hz, 1H), 7.70 (d, J = 2.7 Hz, 1H), 7.03 (dd, J = 8.7, 2.7 Hz, 2H), 6.12 (s, 2H), 5.13 (s, 2H).

^{13}C NMR (101 MHz, DMSO-d_6) δ 161.5, 148.0, 141.7, 141.3, 136.4, 134.4, 133.7, 123.1, 122.7, 119.4, 113.3.

mp.: 220.7 – 222.9 °C.

HPLC (UV): > 95%.

LRMS (ESI$^+$): *m/z* 229.1 [M+H].

4-Amino-*N*-(5-aminopyridin-2-yl)benzamide (15i)
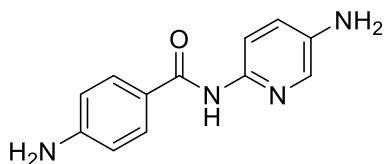
4-nitro-*N*-(5-nitropyridin-2-yl)benzamide **9i** (200 mg, 0.69 mmol) was reduced following Method D. Recrystallization from EtOAc gave **15i** as brown powder (130 mg, 83%).

^{1}H NMR (300 MHz, DMSO-d_6) δ 9.72 (s, 1H), 7.78 (s, 1H), 7.76 – 7.70 (m, 3H), 6.99 (dd, J = 8.7, 2.9 Hz, 1H), 6.55 (d, J = 8.6 Hz, 2H), 5.70 (s, 2H), 5.06 (s, 2H).

^{13}C NMR (75 MHz, DMSO-d_6) δ 164.62, 152.00, 142.50, 141.38, 133.15, 129.30, 122.41, 120.76, 115.63, 112.55.

mp.: 190–191 ºC.

HPLC (UV): 90%.

LRMS (ESI$^+$) *m/z* 229.2 [M+H].

HRMS (ESI$^+$) *m/z* 229.1085 [M+H] (Calc. for $C_{12}H_{13}N_4O$: 229.1084).

1,3-Bis(4-aminophenyl)urea (28)
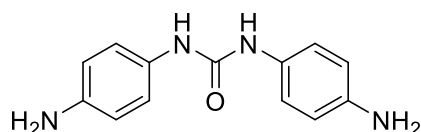
Commercial 1,3-bis(4-nitrophenyl)urea (2.4 g; 8.0 mmol) and Pd-C 5% (213 mg) reacted under H$_2$ atmosphere following Method D. **28** was obtained by recrystallization from MeOH/DMF as a purplish powder (520 mg; 27%). The data were consistent with the literature.[4]

^{1}H NMR (300 MHz, DMSO-d_6) δ 7.91 (s, 2H), 7.04 (d, J = 8.1 Hz, 4H), 6.49 (d, J = 8.1 Hz, 4H), 4.71 (s, 4H).

^{13}C NMR (101 MHz, DMSO-D_6) δ 153.5, 143.1, 129.7, 119.9, 114.3.

HPLC (UV): > 95%.

LRMS (ESI$^+$): m/z 243.3 [M+H].

9.1.2.4. Preparation of imidazolinyl reagents 4 and 5

Methyl 2-(methylthio)-4,5-dihydro-1*H*-imidazole-1-carboxylate (4)
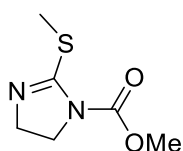
A solution of 2-(methylthio)-4,5-dihydro-1*H*-imidazole hydroiodide **16** (10 g, 41 mmol) and Et₃N (3.2 mL, 22.6 mmol) in dry dichloroethane (20 mL) were stirred at 0 ºC (ice-water bath). Then, methylchloroformiate (4.3 mL, 55.8 mmol) was added dropwise, allowing the resulting reaction mixture to warm to room temperature. Column chromatography using *n*-hexane:EtOAc (2:8) as elution system yielded **4** as whitish solid (6.4 g, 90%). The ¹H-NMR spectrum was consistent with the data previously reported.[5]

¹H NMR (300 MHz, Chloroform-*d*) δ 3.93 – 3.85 (m, 4H), 3.76 (s, 3H), 2.43 (s, 3H).

mp.: 99.6 – 101.0 ºC.

HPLC (UV) > 95%.

LRMS (ESI⁺) *m/z* 175.2 [M+H].

Di-*tert*-butyl 2-thioxoimidazolidine-1,3-dicarboxylate (5)
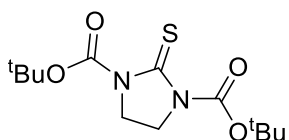
Sodium hydride (6.3 g, 156.8 mmol; 60% in mineral oil, 4 equiv.) was added to a cooled solution (ice-water bath) of imidazolidin-2-thione (**24**) (4 g, 39.2 mmol, 1 equiv.) in anhydrous tetrahydrofuran (500 mL) under argon. After 5 minutes, the ice-bath was removed and the reaction was stirred 10 minutes at room temperature. Then, the reaction mixture was cooled to 0 °C and di-*tert*-butyldicarbonate (18.8 g, 86.2 mmol, 2.2 equiv.) was added neat. After 30 min, the ice-bath was removed and the reaction mixture was stirred another 4 hours at room temperature. The reaction was quenched carefully, drop-by-drop, with a NaHCO₃ saturated aqueous solution. The mixture was poured into 300 mL of water and the aqueous layer was extracted with EtOAc (3×150 mL). The combined organic phases were washed with brine, dried over MgSO₄ and concentrated under vacuum. **5** was obtained by recrystallization from *n*-hexane:EtOAc (8:2) as yellow needles (10.1 g, 85%) according to the previously reported literature.[6]

^{1}H NMR (300 MHz, Methanol-d_4) δ 3.95 (s, 4H), 1.56 (s, 18H).

^{13}C NMR (75 MHz, Methanol-d_4) δ 176.05, 150.61, 83.40, 44.61, 26.82.

mp.: 117 – 119 °C.

HPLC (UV) > 95%.

LRMS (ESI$^+$) *m/z* 303.3 [M+H].

HRMS (ESI$^+$) *m/z* 303.1377 [M+H] (Calc. for $C_{13}H_{23}N_2O_4S$: 303.1373).

9.1.2.5. Preparation of Boc-protected bis(imidazolidin-2-imines) (25b–i)

Di-*tert*-butyl-2-((4-((4-((1,3-bis(*tert*-butoxycarbonyl)imidazolidin-2-ylidene)amino)-2-chlorophenyl)carbamoyl)-2-chlorophenyl)imino)imidazolidine-1,3-dicarboxylate (25b)
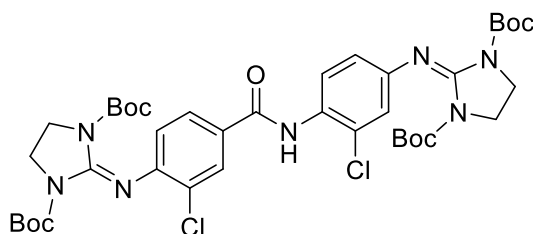
The reaction was performed with **15b** (200 mg; 0.68 mmol), **5** (617 mg; 2.04 mmol), HgCl₂ (553 mg; 2.04 mmol) and Et₃N (482 mg; 4.76 mmol) following the general Method E. The reaction mixture was stirred at 60 °C for 6 days. The crude product was purified by centrifugal TLC using plates previously neutralized with *n*-hexane (235 mL) and Et₃N (15 mL); Petroleum ether:EtOAc was used as elution system (8:2→6:4→0:1). **25b** was obtained as orangish solid (302 mg; 54 %).

¹H NMR (300 MHz, Chloroform-*d*) δ 8.32 (d, *J* = 8.8 Hz, 1H), 8.19 (s, 1H), 7.87 (d, *J* = 2.1 Hz, 1H), 7.61 (dd, *J* = 8.4, 2.1 Hz, 1H), 7.03 (d, *J* = 2.4 Hz, 1H), 6.99 (d, *J* = 8.4 Hz, 1H), 6.90 (dd, *J* = 8.8, 2.4 Hz, 1H), 3.80 (s, 4H), 3.79 (s, 4H), 1.33 (s, 18H), 1.32 (s, 18H).

¹³C NMR (101 MHz, Chloroform-*d*) δ 163.7, 150.2, 150.0, 149.5, 145.2, 140.1, 140.0, 129.6, 128.8, 128.7, 126.2, 125.6, 123.1, 122.1, 121.9, 121.7, 120.8, 83.3, 83.2, 43.3, 42.9, 28.03, 28.02.

mp.: > 115.3 °C.

HPLC (UV) > 95%.

LRMS (ESI⁺) *m/z* 832.7 [M+H].

Di-*tert*-butyl-2-((4-(4-((1,3-bis(*tert*-butoxycarbonyl)imidazolidin-2-ylidene)amino)-3-chlorobenzamido)-2-chlorophenyl)imino)imidazolidine-1,3-dicarboxylate (25c)
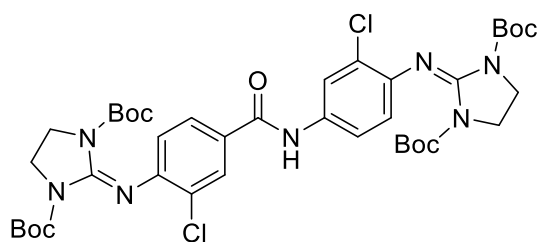
The reaction was performed with **15c** (200 mg; 0.68 mmol), **5** (617 mg; 2.04 mmol), HgCl₂ (553 mg; 2.04 mmol) and Et₃N (482 mg; 4.76 mmol) following the general Method E. The reaction mixture was stirred at 60 °C for 6 days. The crude product was purified by centrifugal TLC using plates previously neutralized with *n*-hexane (235 mL) and Et₃N (15 mL). Petroleum ether:EtOAc was used as elution system (8:2→6:4→0:1) **25c** was obtained as yellowish solid (268 mg; 47.3 %).

¹H NMR (400 MHz, DMSO-*d₆*) δ 10.07 (s, 1H), 8.02 (d, *J* = 2.1 Hz, 1H), 7.91 (d, *J* = 2.4 Hz, 1H), 7.78 (dd, *J* = 8.4, 2.1 Hz, 1H), 7.52 (dd, *J* = 8.7, 2.4 Hz, 1H), 7.01 (d, *J* = 8.4 Hz, 1H), 6.90 (d, *J* = 8.7 Hz, 1H), 3.80 (s, 4H), 3.77 (s, 4H), 1.31 (br s, 36H).

¹³C NMR (101 MHz, DMSO-*d₆*) δ 163.5, 149.6, 149.4, 149.3, 141.7, 140.5, 139.6, 134.1, 128.5, 128.0, 126.8, 125.3, 125.2, 120.9, 120.4, 120.3, 119.2, 81.9, 81.6, 42.8, 42.7, 27.51, 27.50.

mp.: 188.7 – 211.2 °C.

HPLC (UV) > 95%.

LRMS (ESI⁺) *m/z* = 832.7 [M+H].

Di-*tert*-butyl 2-((4-(4-((1,3-bis(*tert*-butoxycarbonyl)imidazolidin-2-ylidene)amino)-2-chlorobenzamido)-3-chlorophenyl)imino)imidazolidine-1,3-dicarboxylate (25d)
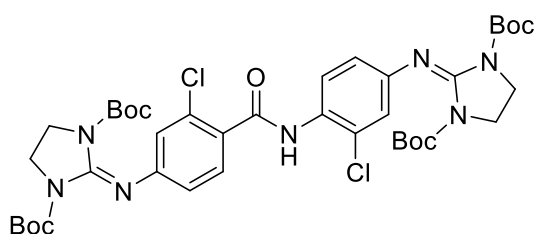
The reaction was performed with **15d** (200 mg; 0.68 mmol), **5** (617 mg; 2.04 mmol), HgCl₂ (553 mg; 2.04 mmol), and Et₃N (482 mg; 4.76 mmol) following the general method E. The reaction mixture was stirred 30 hours at 60 °C. The crude product was purified by centrifugal TLC using a 2 mm plate previously neutralized with *n*-hexane (235 mL)

and Et$_3$N (15 mL); Petroleum ether:EtOAc was used as elution system (8:2→6:4→0:1). **25d** was obtained as whitish solid (440 mg; 78 %).

¹H NMR (400 MHz, DMSO-d_6) δ 9.67 (s, 1H), 7.54 – 7.43 (m, 2H), 6.94 (d, J = 2.4 Hz, 1H), 6.91 (d, J = 1.9 Hz, 1H), 6.87 – 6.79 (m, 2H), 3.78 (s, 4H), 3.77 (s, 4H), 1.32 (s, 18H), 1.31 (s, 18H).

¹³C NMR (101 MHz, DMSO-d_6) δ 165.1, 158.0, 157.3, 157.0, 155.6, 155.5, 152.50, 152.46, 149.3, 148.4, 130.8, 129.8, 128.0, 118.3, 117.1, 116.4, 106.5, 82.5, 82.4, 45.10, 45.07, 27.8, 27.5.

mp.: > 180 °C.

HPLC (UV) > 95%.

LRMS (ESI⁺) m/z 832.7 [M+H].

Di-*tert*-butyl-2-((4-(4-((1,3-bis(*tert*-butoxycarbonyl)imidazolidin-2-ylidene)amino)-2-chlorobenzamido)-2-chlorophenyl)imino)imidazolidine-1,3-dicarboxylate (25e)
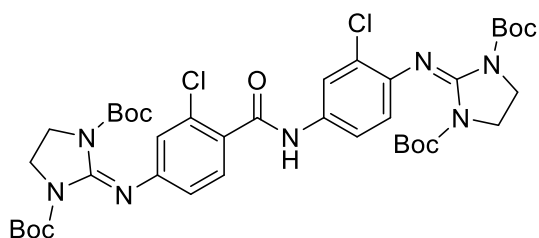
The reaction was performed with **15e** (300 mg; 1.0 mmol), **5** (916 mg; 3.0 mmol), HgCl$_2$ (823 mg; 3.0 mmol), and Et$_3$N (716 mg; 7.1 mmol) in dry DMF (10 mL) following the general Method E. The reaction mixture was stirred at 60 °C for 3 days. The crude product was filtered over florisil. The organic phase was concentrated and centrifugal TLC was performed in a 2 mm plate, using Hexane:EtOAc:MeOH as elution system (80:20:0 → 0:20:10) to yield the product as whitish solid (739 mg; 88%).

¹H NMR (400 MHz, DMSO-d_6) δ 10.27 (s, 1H), 7.88 (d, J = 1.9 Hz, 1H), 7.42 (d, J = 8.2 Hz, 2H), 6.92 – 6.87 (m, 2H), 6.84 (d, J = 8.2 Hz, 1H), 3.78 (br s, 4H), 3.76 (br s, 4H), 1.32 (s, 18H), 1.31 (s, 18H).

¹³C NMR (101 MHz, DMSO-d_6) δ 166.2, 164.7, 151.4, 149.6, 149.4, 141.8, 140.8, 139.7, 134.2, 130.4, 129.5, 129.3, 125.3, 121.3, 120.5, 120.1, 119.3, 118.6, 81.8, 81.7, 43.1, 42.8, 27.5.

mp.: 192.4 – 196.0 °C.

HPLC (UV) 95 %.

LRMS (ESI⁺) m/z = 832.7 [M+H].

Di-*tert*-butyl 2-((4-((4-((1,3-bis(*tert*-butoxycarbonyl)imidazolidin-2-ylidene)amino)-2-fluorophenyl)carbamoyl)-2-fluorophenyl)imino)imidazolidine-1,3-dicarboxylate (25f)
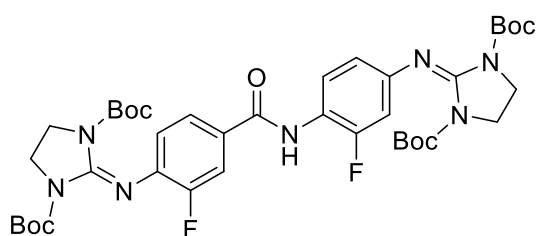
The reaction was performed with 4-amino-*N*-(4-amino-2-fluorophenyl)-3-fluorobenzamide **15f** (108 mg, 0.41 mmol), **5** (371 mg, 1.23 mmol), HgCl$_2$ (334 mg; 1.23 mmol), Et$_3$N (0.285 mL, 2 mmol) and anhydrous DMF (3 mL) following the general Method E. The reaction mixture was stirred 7 days at room temperature. The mixture was diluted with DMF (10 mL) and filtered on Celite. The filter cake was rinsed successively with DMF (20 mL) and CH$_2$Cl$_2$ (20 mL). The filtrate was evaporated under vacuum and the crude yellow oil was partitioned between CH$_2$Cl$_2$ (60 mL) and water (40 mL). The organic phase was washed with brine, dried (MgSO$_4$) and evaporated to give a crude yellow oil. Flash chromatography on neutral alumina eluting with hexane/EtOAc (5:1→1:1→0:1) yielded **25f** as greyish solid (67 mg, 20%).

^{1}H NMR (300 MHz, Chloroform-*d*) δ 8.20 (dd, *J* = 11.0, 6.8 Hz, 1H), 7.81 (d, *J* = 3.4 Hz, 1H), 7.62–7.35 (m, 2H), 7.04 (d, *J* = 8.2 Hz, 1H), 6.80 – 6.60 (m, 2H), 3.78 (s, 4H), 3.77 (s, 4H), 1.31 (s, 18H), 1.30 (s, 18H).
HPLC (UV) 85 %.

Di-*tert*-butyl 2-((4-(4-((1,3-bis(*tert*-butoxycarbonyl)imidazolidin-2-ylidene)amino)-2-isopropoxybenzamido)-2-isopropoxyphenyl)imino)imidazolidine-1,3-dicarboxylate (25g)
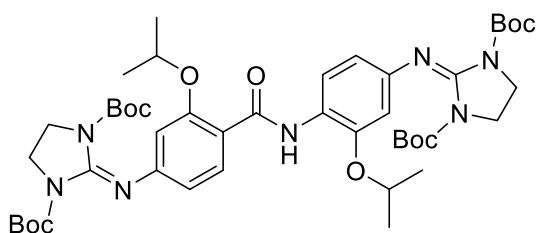
The reaction was performed with **15g** (150 mg; 0.44 mmol), **5** (399 mg; 1.32 mmol), HgCl$_2$ (358 mg; 1.32 mmol) and Et$_3$N (312 mg; 3.08 mmol) in dry DMF (5 mL) following the general Method E. The reaction was stirred at 60 °C for 3 days. The crude product was purified by circular chromatography using plates previously neutralized with *n*-

hexane (235 mL) and Et$_3$N (15 mL). Elution system was prepared with hexane:EtOAc mixture (7:3→4:6). **25g** was obtained as brownish solid (174 mg; 45%).

^{1}H NMR (400 MHz, DMSO-d_6) δ 9.82 (s, 1H), 8.20 (d, J = 8.6 Hz, 1H), 7.85 (d, J = 8.4 Hz, 1H), 6.64 (d, J = 1.8 Hz, 1H), 6.59 (d, J = 2.2 Hz, 1H), 6.55 (dd, J = 8.5, 1.8 Hz, 1H), 6.43 (dd, J = 8.6, 2.2 Hz, 1H), 4.71 (hept, J = 6.2 Hz, 1H), 4.54 (hept, J = 6.2 Hz, 1H), 3.78 (s, 4H), 3.75 (s, 4H), 1.36 (d, J = 6.0 Hz, 12H), 1.29 (s, 18H), 1.28 (s, 18H).

^{13}C NMR (101 MHz, DMSO-d_6) δ 162.3, 156.2, 153.7, 149.7, 149.4, 147.1, 144.8, 140.6, 139.3, 131.8, 123.5, 120.7, 116.5, 114.5, 113.3, 106.9, 106.5, 81.7, 81.4, 72.5, 71.3, 43.0, 42.9, 27.5, 22.1, 21.9.

mp.: > 93.5 °C.

HPLC (UV) > 95%.

LRMS (ESI$^+$) m/z = 880.8 [M+H].

Di-*tert*-butyl-2-((6-(5-((1,3-bis(*tert*-butoxycarbonyl)imidazolidin-2-ylidene)amino)picolinamido)pyridin-3-yl)imino)imidazolidine-1,3-dicarboxylate (25h)
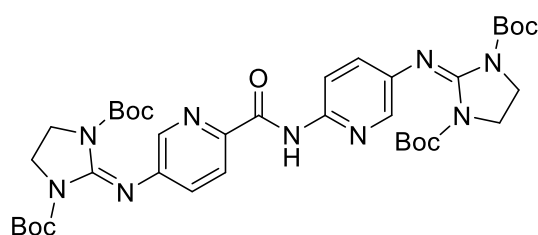
The reaction was performed with **15h** (229 mg; 1.0 mmol), **5** (907 mg; 3.0 mmol), HgCl$_2$ (813 mg; 3.0 mmol) and Et$_3$N (708 mg; 7 mmol) in dry DMF (5 mL) following the general Method E. The reaction mixture was stirred at 60 °C for 6 days. The crude product was purified by circular chromatography using plates previously neutralized with *n*-hexane (235 mL) and Et$_3$N (15 mL). Elution system was prepared with Petroleum ether:EtOAc mixture (8:2→6:4→0:1). **25h** was obtained as brownish solid (358 mg; 47%).

^{1}H NMR (400 MHz, DMSO-d_6) δ 10.13 (s, 1H), 8.19 (d, J = 2.4 Hz, 1H), 8.14 (d, J = 8.8 Hz, 1H), 8.03 (d, J = 8.4 Hz, 1H), 7.89 (d, J = 2.6 Hz, 1H), 7.41 (dd, J = 8.4,

2.4 Hz, 1H), 7.34 (dd, J = 8.8, 2.6 Hz, 1H), 3.81 (s, 4H), 3.78 (s, 4H), 1.30 (br s, 36H).

^{13}C NMR (101 MHz, DMSO-d_6) δ 161.5, 149.4, 149.2, 149.0, 145.2, 142.1, 142.0, 141.5, 141.4, 140.9, 140.6, 129.5, 127.8, 122.5, 112.7, 82.0, 81.7, 43.2, 43.1, 27.5, 27.4.

mp.: 93.0 – 103.0 °C.

HPLC (UV) > 95%.

LRMS (ESI$^+$) m/z = 766.8 [M+H].

9.1.2.6. Synthesis of bis(imidazolidin-2-imine) salts (1b–h)

3-Chloro-*N*-(2-chloro-4-(imidazolidin-2-ylideneamino)phenyl)-4-(imidazolidin-2-ylideneamino)benzamide di-trifluoroacetate salt (1b)
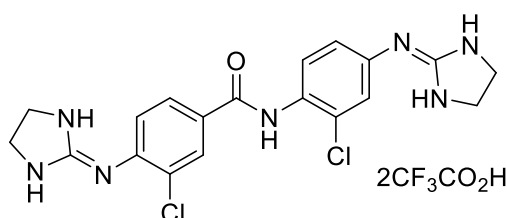
Compound **25b** (64 mg, 0.08 mmol) was reacted with TFA according to the general Method F. **1b** was obtained as whitish solid (14.5 mg, 28%).

^{1}H NMR (400 MHz, DMSO-d_6) δ 10.84 (br s, 2H), 10.37 (s, 1H), 8.67 (br s, 2H), 8.58 (br s, 2H), 8.22 (d, J = 2.0 Hz, 1H), 8.03 (dd, J = 8.3, 2.0 Hz, 1H), 7.66 (d, J = 8.3 Hz, 1H), 7.59 (d, J = 8.6 Hz, 1H), 7.49 (d, J = 2.4 Hz, 1H), 7.28 (dd, J = 8.6, 2.4 Hz, 1H), 3.70 (br s, 8H).

^{13}C NMR (101 MHz, DMSO-d_6) δ 163.5, 158.1, 157.8, 136.2, 135.1, 133.8, 132.5, 130.5, 129.9, 129.6, 129.5, 128.3, 128.0, 124.1, 122.3, 42.8, 42.7.

mp.: 222.4 – 223.8 °C.

HPLC (UV) > 95 %.

LRMS (ESI$^+$) m/z = 432.4 [M+H].

HRMS (ESI$^+$) m/z = 432.1102 [M+H] (Calc. for: $C_{19}H_{20}Cl_2N_7O$: 432.1101).

3-Chloro-*N*-(3-chloro-4-(imidazolidin-2-ylideneamino)phenyl)-4-(imidazolidin-2-ylideneamino)benzamide di-trifluoroacetate salt (1c)
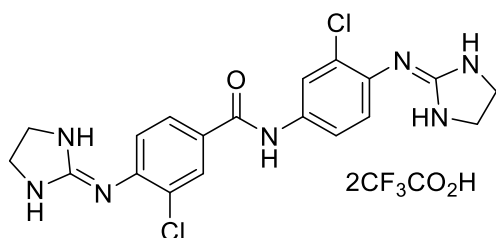
Compound **25c** (212 mg, 0.25 mmol) was reacted with TFA according to the general Method F. **1c** was obtained as a whitish powder (140 mg, 85%).

^{1}H NMR (500 MHz, DMSO-d_6) δ 10.95 (br s, 1H), 10.75 (s, 1H), 10.59 (br s, 1H), 8.70 (br s, 2H), 8.50 (br s, 2H), 8.23 (d, J = 2.1 Hz, 1H), 8.14 (d, J = 2.4 Hz, 1H), 8.03 (dd, J = 8.3, 2.1 Hz, 1H), 7.82 (dd, J = 8.7, 2.4 Hz, 1H), 7.67 (d, J = 8.3 Hz, 1H), 7.48 (d, J = 8.7 Hz, 1H), 3.70 (s, 4H), 3.67 (s, 4H).

^{13}C NMR (126 MHz, DMSO-d_6) δ 163.6, 158.6, 158.1, 139.6, 136.1, 134.2, 130.6, 129.7, 129.4, 129.3, 128.1, 128.0, 127.9, 121.2, 119.9, 42.8, 42.7.

mp.: > 114.0 °C.

HPLC (UV) > 95 %.

LRMS (ESI $^+$) *m/z* 432.3 [M+H].

HRMS (ESI$^+$) *m/z* = 432.1093 [M+H] (Calc. for: $C_{19}H_{20}Cl_2N_7O$: 432.1101).

2-Chloro-4-(imidazolidin-2-ylideneamino)-*N*-(2-chloro-4-(imidazolidin-2-ylideneamino)phenyl)-benzamide di-trifluoroacetate salt (1d)
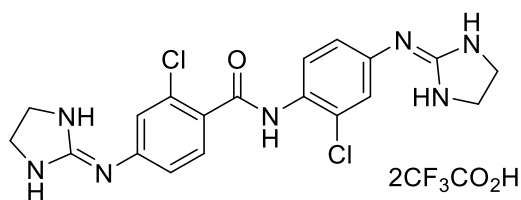
Compound **25d** (98 mg, 0.12 mmol) was reacted with TFA according to the general Method F. Compound **1d** was obtained as a whitish solid (76 mg, 60%).

^{1}H NMR (500 MHz, DMSO-d_6) δ 11.03 (br s, 1H), 10.76 (br s, 1H), 10.27 (s, 1H), 8.74 (br s, 2H), 8.60 (br s, 2H), 7.73 (d, *J* = 8.5 Hz, 1H), 7.68 (d, *J* = 8.3 Hz, 1H), 7.48 (d, *J* = 2.5 Hz, 1H), 7.47 (d, *J* = 2.2 Hz, 1H), 7.32 (dd, *J* = 8.3, 2.2 Hz, 1H), 7.27 (dd, *J* = 8.5, 2.5 Hz, 1H), 3.71 (s, 4H), 3.69 (s, 4H).

^{13}C NMR (126 MHz, DMSO-d_6) δ 165.2, 158.3, 158.0, 138.9, 135.0, 133.6, 132.9, 131.6, 130.7, 129.5, 128.8, 124.9, 124.0, 123.1, 121.7, 43.2, 43.1.

mp.: 196.5 – 207.3 °C.

HPLC (UV) > 95 %.

LRMS (ESI$^+$) *m/z* = 432.3 [M+H].

HRMS (ESI$^+$) *m/z* = 432.1106 [M+H] (Calc. for: $C_{19}H_{20}Cl_2N_7O$: 432.1101).

2-Chloro-4-(imidazolidin-2-ylideneamino)-*N*-(3-chloro-4-(imidazolidin-2-ylideneamino)phenyl)-benzamide di-trifluoroacetate salt (1e)
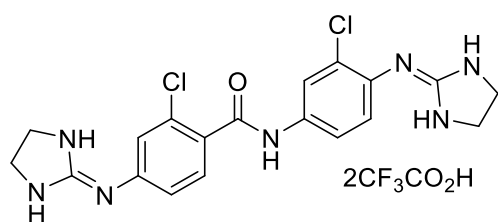
Compound **25e** (159 mg, 0.2 mmol) was reacted with TFA according to general Method F, yielding compound **1e** as whitish solid (102 mg, 81%).

¹H NMR (500 MHz, DMSO-*d*₆) δ 11.08 (s, 1H), 10.87 (s, 1H), 10.44 (s, 1H), 8.75 (s, 2H), 8.39 (s, 2H), 8.08 (d, *J* = 2.4 Hz, 1H), 7.66 (dd, *J* = 8.5, 2.4 Hz, 2H), 7.49 (d, *J* = 2.2 Hz, 1H), 7.47 (d, *J* = 8.5 Hz, 1H), 7.32 (dd, *J* = 8.5, 2.2 Hz, 1H), 3.71 (s, 4H), 3.66 (s, 4H).

¹³C NMR (126 MHz, DMSO-*d*₆) δ 164.7, 158.6, 157.5, 139.5, 138.6, 133.3, 131.0, 130.1, 129.6, 127.9, 123.5, 121.3, 120.3, 119.2, 42.8, 42.7.

mp.: 190.2 – 201.7 °C.

HPLC (UV) 95 %.

LRMS (ESI⁺) *m/z* = 432.3 [M+H].

HRMS (ESI⁺) *m/z* = 431.9160 [M+H] (Calc. for: $C_{19}H_{20}Cl_2N_7O$: 432.1101).

3-Fluoro-*N*-(2-fluoro-4-(imidazolidin-2-ylideneamino)phenyl)-4-(imidazolidin-2-ylideneamino)benzamide di-trifluoroacetate salt (1f)
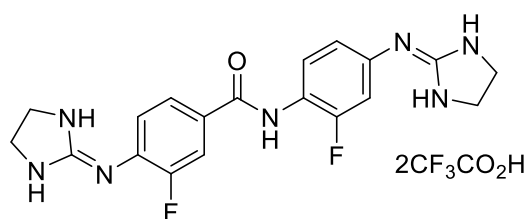
Compound **25f** (53 mg, 0.07 mmol) was reacted with TFA according to the general Method F. **1f** was obtained as beige solid by recrystallization from iPrOH/Et₂O (9.7 mg, 23%).

¹H NMR (400 MHz, Methanol-*d*₄) δ 7.95 – 7.87 (m, 2H), 7.82 (t, *J* = 8.4 Hz, 1H), 7.58 (t, *J* = 8.2 Hz, 1H), 7.24 (dd, *J* = 11.1, 2.4 Hz, 1H), 7.17 (dt, *J* = 8.5, 1.6 Hz, 1H), 3.83 (s, 4H), 3.80 (s, 4H).

¹³C NMR (101 MHz, Methanol-*d*₄) δ 166.5, 160.1 (d, *J* = 4.1 Hz), 158.6 (d, *J* = 17.0 Hz), 156.1 (d, *J* = 16.6 Hz), 136.0 (d, *J* = 6.4 Hz), 135.7 (d, *J* = 9.9 Hz), 128.6 (d, *J* = 2.2 Hz), 128.2 (d, *J* = 13.1 Hz), 128.0, 125.9 (d, *J* = 3.7 Hz), 125.5 (d, *J* =

12.2 Hz), 121.0 (d, J = 3.4 Hz), 117.5 (d, J = 21.8 Hz), 113.1 (d, J = 23.2 Hz), 44.4, 44.2.

HPLC (UV) > 95%.

LRMS (ESI$^+$) m/z = 400.4 [M+H].

HRMS (ESI$^+$) m/z = 200.5887 [M+2H] (Calc. for: $C_{19}H_{21}F_2N_7O$: 200.5883).

4-(Imidazolidin-2-ylideneamino)-*N*-(4-(imidazolidin-2-ylideneamino)-3-isopropoxyphenyl)-2-isopropoxybenzamide di-trifluoroacetate salt (1g)
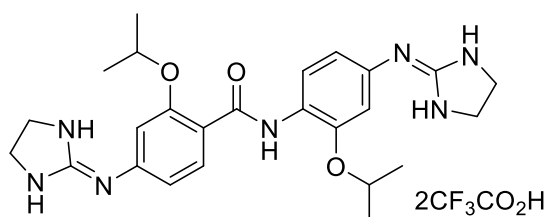
Compound **25g** (114 mg, 0.13 mmol) was reacted with TFA according to the general Method F. **1g** was obtained as whitish solid (47 mg, 51 %).

^{1}H NMR (500 MHz, DMSO-*d$_6$*) δ 10.94 (d, J = 9.0 Hz, 1H), 10.54 – 10.37 (m, 1H), 9.93 (s, 1H), 8.67 (d, J = 4.5 Hz, 1H), 8.52 – 8.39 (m, 1H), 8.35 (s, 1H), 8.09 - 8.06 (m, 1H), 7.37 (br s, 1H), 7.23 – 7.10 (m, 2H), 7.06 – 6.94 (m, 2H), 6.86 (d, J = 8.8 Hz, 1H), 4.94 – 4.79 (m, 1H), 4.77 – 4.66 (m, 1H), 3.72 (s, 4H), 3.66 (s, 4H), 1.56 (s, 12H).

^{13}C NMR (101 MHz, DMSO-*d$_6$*) δ 162.2, 158.2, 157.6, 150.6, 147.3, 140.7, 133.0, 131.6, 126.7, 121.4, 119.6, 116.0, 115.0, 109.8, 109.0, 73.2, 71.7, 42.73, 42.69, 22.0, 21.9.

mp.: > 201.1 °C.

HPLC (UV) > 95%.

LRMS (ESI$^+$) m/z = 480.4 [M+H].

HRMS (ESI$^+$) m/z = 480.2707 [M+H] (Calc. for: $C_{25}H_{34}N_7O_3$: 480.2718).

5-(Imidazolidin-2-ylideneamino)-*N*-(5-(imidazolidin-2-ylideneamino)pyridin-2-yl)picolinamide di-trifluoroacetate salt (1h)
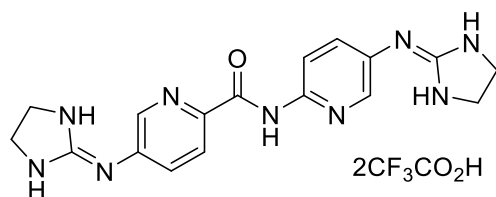
Compound **25h** (64 mg, 0.08 mmol) was reacted with TFA according to the general Method F. **1h** was obtained as whitish solid (16.7 mg, 35 %).

¹H NMR (400 MHz, DMSO-d_6) δ 11.34 (br s, 1H), 10.72 (br s, 1H), 10.44 (s, 1H), 8.95 (br s, 2H), 8.66 (d, J = 2.6 Hz, 1H), 8.60 (br s, 2H), 8.34 (d, J = 2.5 Hz, 1H), 8.33 (d, J = 8.9 Hz, 1H), 8.26 (d, J = 8.5 Hz, 1H), 7.97 (dd, J = 8.5, 2.5 Hz, 1H), 7.85 (dd, J = 8.9, 2.6 Hz, 1H), 3.74 (s, 4H), 3.68 (s, 4H).

¹³C NMR (101 MHz, DMSO-d_6) δ 161.5, 158.5, 157.8, 148.8, 145.1, 144.6, 142.9, 136.7, 135.1, 131.6, 129.1, 123.3, 113.6, 42.8, 42.7.

mp.: 214.0 – 226.8 °C.

HPLC (UV) > 95 %.

LRMS (ESI $^+$) m/z 366.3 [M+H].

HRMS (ESI$^+$) m/z = 366.1781 [M+H] (Calc. for: $C_{17}H_{20}N_9O$: 366.1785).

9.1.2.7.   Preparation of isothiocyanates (**19**, **20**, **26b–e**, **26h**, **29**, **33**)

4-Isothiocyanato-*N*-(4-isothiocyanatophenyl)benzamide (19)
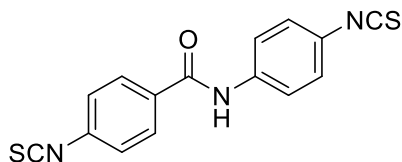
4-amino-*N*-(4-aminophenyl)benzamide (3.4 g, 15 mmol) was reacted with thiophosgene (2.5 mL, 33 mmol) according to the general Method G to yield **19** as grey solid (92%). The spectroscopic data were consistent with the literature.[7]

¹H NMR (300 MHz, Chloroform-*d*) δ 7.88 (s 1H), 7.85 (d, *J* = 8.7, 2H), 7.63 (d, *J* = 8.8, 2H), 7.31 (d, *J* = 8.7, 2H), 7.22 (d, *J* = 8.8, 2H).
mp.: 199–200 °C.
HPLC (UV): > 95%.
LRMS (ES⁺): *m/z* = 312.3 [M+H].

1,3-Bis(4-isothiocyanatophenyl)urea (20)
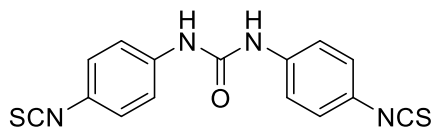
1,3-bis(4-aminophenyl)urea **28** (201 mg, 0.83 mmol.) in Et_2O:H_2O (3:1) (2 mL) was reacted with thiophosgene (0.16 mL, 2.08 mmol) following general Method G to yield **20** as whitish solid (174 mg: 64%). The spectroscopic data were consistent with the literature.[8]

¹H NMR (400 MHz, DMSO-*d₆*) δ 9.03 (s, 2H), 7.52 (d, *J* = 8.9 Hz, 4H), 7.37 (d, *J* = 8.9 Hz, 4H).
¹³C NMR (101 MHz, DMSO-*d₆*) δ 152.1, 139.2, 132.2, 126.7, 123.2, 119.0.
mp.: > 300.0 °C.
HPLC (UV): > 95%.
LRMS (ES⁺): *m/z* = 314.3 [M+H].

3-Chloro-*N*-(2-chloro-4-isothiocyanatophenyl)-4-isothiocyanatobenzamide (26b)
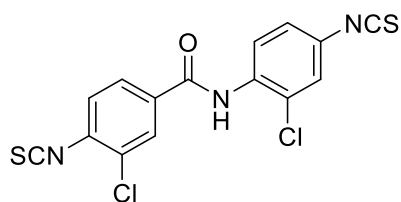
4-amino-*N*-(4-amino-2-chlorophenyl)-3-chlorobenzamide **15b** (100 mg, 0.34 mmol) was reacted with thiophosgene (65 μL, 0.85 mmol) according to the general Method G to yield **26b** as brownish solid (99.6 mg, 44%).

¹H NMR (300 MHz, Chloroform-*d*) δ 8.53 (d, *J* = 8.9 Hz, 1H), 8.31 (s, 1H), 7.98 (s, 1H), 7.74 (d, *J* = 8.3 Hz, 1H), 7.36 (dd, *J* = 8.3, 1.1 Hz, 1H), 7.21 (dd, *J* = 8.9, 1.3 Hz, 1H).

¹³C NMR (126 MHz, DMSO-*d₆*) δ 164.07, 139.00, 138.75, 134.72, 134.34, 131.49, 130.61, 130.19, 128.61, 128.07, 128.04, 126.91, 126.79, 125.20, 122.20.

mp.: 177.4 – 182.8 °C.

HPLC (UV): > 95%.

LRMS (ES⁻): *m/z* = 377.6 [M-H].

3-Chloro-*N*-(3-chloro-4-isothiocyanatophenyl)-4-isothiocyanatobenzamide (26c)
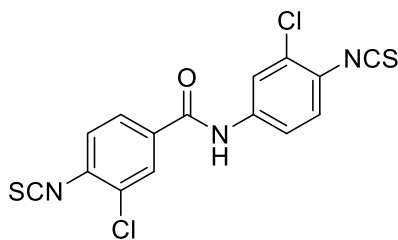
4-amino-*N*-(4-amino-3-chlorophenyl)-3-chlorobenzamide **15c** (150 mg, 0.51 mmol) was reacted with thiophosgene (147 mg, 0.1 mL, 1.28 mmol) according to the general Method G to yield **26c** as whitish solid (160 mg, 83%).

¹H NMR (300 MHz, DMSO-*d₆*) δ 10.63 (s, 1H), 8.15 (d, *J* = 2.0 Hz, 1H), 8.08 (d, *J* = 2.4 Hz, 1H), 7.94 (dd, *J* = 8.4, 2.0 Hz, 1H), 7.73 (dd, *J* = 8.8, 2.4 Hz, 1H), 7.67 (d, *J* = 8.4 Hz, 1H), 7.51 (d, *J* = 8.8 Hz, 1H).

¹³C NMR (75 MHz, DMSO-*d₆*) δ 163.2, 139.1, 138.7, 136.7, 134.0, 131.4, 130.5, 130.4, 129.2, 128.0, 127.5, 127.3, 123.3, 120.7, 119.7.

mp.: 186.3 – 187.6 °C.

HPLC (UV): > 95%.

LRMS (ES⁻): *m/z* = 377.7 [M-H].

2-Chloro-*N*-(2-chloro-4-isothiocyanatophenyl)-4-isothiocyanatobenzamide (26d)
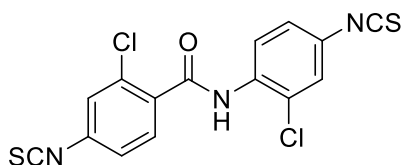
2-chloro-*N*-(2-chloro-4-nitrophenyl)-4-nitrobenzamide **15d** (100 mg, 0.34 mmol) was reacted with thiophosgene (98 mg, 65 µL, 0.85 mmol) according to the general Method G. Column chromatography using Petroleum ether: EtOAc (100:0 → 25:75) was performed to yield **26d** as whitish solid (85 mg, 66%).

¹H NMR (500 MHz, DMSO-*d₆*) δ 10.42 (s, 1H), 7.79 (d, *J* = 8.5 Hz, 1H), 7.74 (d, *J* = 2.0 Hz, 1H), 7.73 (d, *J* = 2.4 Hz, 1H), 7.68 (d, *J* = 8.2 Hz, 1H), 7.53 (dd, *J* = 8.2, 2.0 Hz, 1H), 7.48 (dd, *J* = 8.5, 2.5 Hz, 1H).

¹³C NMR (126 MHz, DMSO-*d₆*) δ 164.4, 135.7, 135.1, 134.7, 133.9, 132.3, 131.2, 130.4, 128.2, 127.8, 127.0, 126.9, 125.4, 125.3, 124.9.

mp.: 226.8 – 228.0 °C

HPLC (UV): > 95%.

LRMS (ES⁻): *m/z* = 377.8 [M-H]

2-Chloro-*N*-(3-chloro-4-isothiocyanatophenyl)-4-isothiocyanatobenzamide (26e)
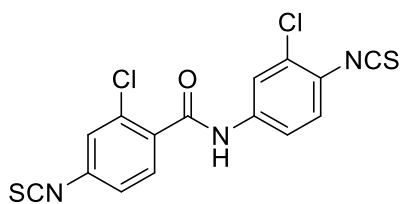
4-amino-*N*-(4-amino-3-chlorophenyl)-2-chlorobenzamide **15e** (310 mg, 1.05 mmol) was reacted with thiophosgene (303 mg, 0.2 mL, 2.63 mmol) according to the general Method G to yield **26e** as whitish solid (94 mg, 24%).

¹H NMR (300 MHz, Chloroform-*d*) δ 8.15 (s, 1H), 7.86 (d, *J* = 2.3 Hz, 1H), 7.74 (d, *J* = 8.2 Hz, 1H), 7.45 (dd, *J* = 8.6, 2.3 Hz, 1H), 7.28 (d, *J* = 2.0 Hz, 1H), 7.22 (d, *J* = 8.6 Hz, 1 H), 7.20 (dd, *J* = 8.2, 2.0 Hz, 1 H).

¹³C NMR (75 MHz, Chloroform-*d*) δ 163.3, 140.1, 139.1, 136.8, 135.4, 132.6, 132.6, 132.0, 131.8, 127.4, 127.1, 126.3, 124.8, 121.5, 119.1.

mp.: 115.6 – 118.0 °C.

HPLC (UV): > 95%.

LRMS (ES⁻): m/z = 377.8 [M-H].

5-Isothiocyanato-*N*-(5-isothiocyanatopyridin-2-yl)picolinamide (26h)
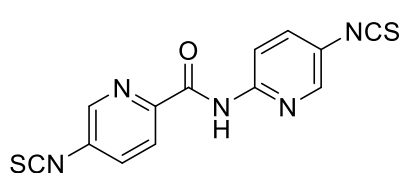
5-amino-*N*-(5-aminopyridin-2-yl)picolinamide **15h** (74.5 mg, 0.32 eq.) was reacted with thiophosgene (62 µL, 0.81 eq.) according to Method G. Purification by column chromatography on silica was performed using Petroleum ether:EtOAc as elution mixture (100:0 → 50:50) to yield **26h** as brownish solid (52 mg, 52%).

¹H NMR (300 MHz, DMSO-*d₆*) δ 10.43 (s, 1H), 8.81 (s, 1H), 8.63 – 8.43 (m, 1H), 8.37 – 8.12 (m, 3H), 8.00 (m, 1H).

¹³C NMR (75 MHz, DMSO-*d₆*) δ 181.4, 172.1, 165.0, 162.2, 153.8, 146.3, 139.9, 136.2, 129.7, 126.3, 124.6, 123.6.

mp.: 117.7 – 122.8 °C.

HPLC (UV): > 95%.

LRMS (ES⁺): m/z = 314.3 [M+H].

1,2-Bis(4-isothiocyanatophenyl)ethane (29)
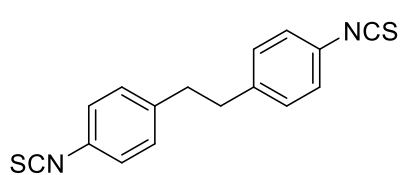
4,4'-diaminobibenzyl (1.28 g, 6 mmol) was reacted with thiophosgene (1.73 g: 1.15 mL, 15 mmol) according to the general Method G. Silica column chromatography using *n*-hexane:EtOAc (100:0 → 80:20) yielded **29** as whitish solid (1.4 g: 79%). The spectroscopic data were consistent with the literature.[4, 8]

¹H NMR (400 MHz, Chloroform-*d*) δ 7.12 (d, *J* = 8.6 Hz, 4H), 7.07 (d, *J* = 8.6 Hz, 4H), 2.89 (s, 4H).

¹³C NMR (101 MHz, Chloroform-*d*) δ 140.6, 135.1, 129.8, 129.3, 125.8, 37.3.

mp.: 130.3 – 130.9 °C.

HPLC (UV): > 95%.

LRMS (ES⁺): *m/z* = 297.3 [M+H].

2,7-Diisothiocyanato-9*H*-fluorene (33)
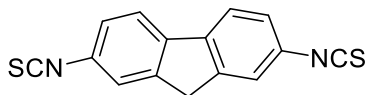
2,7-diaminofluorene (137 mg, 0.7 mmol) was reacted with thiophosgene (201 mg: 130 µL, 1.75 mmol) according to the general Method G to yield **33** as brownish solid (169 mg; 86%).

¹H NMR (400 MHz, DMSO-*d₆*) δ 8.01 (d, *J* = 8.1 Hz, 2H), 7.69 (d, *J* = 2.0 Hz, 2H), 7.49 (dd, *J* = 8.1, 2.0 Hz, 2H), 3.98 (s, 2H).

¹³C NMR (101 MHz, DMSO-*d₆*) δ 145.1, 139.6, 133.4, 128.7, 125.1, 123.0, 121.7, 36.4.

mp.: decomposes at 213.6 °C.

HPLC (UV): > 95%.

LRMS (ES⁻): *m/z* = 279.4 [M-H].

9.1.2.8.   Synthesis of bis(2-aminobenzimidazoles) (2a–e, 2h, 30, 31, 34)

4-((1*H*-benzo[*d*]imidazol-2(3*H*)-ylidene)amino)-*N*-(4-((1*H*-benzo[*d*]imidazol-2(3*H*)-ylidene)amino)phenyl)benzamide (2a)
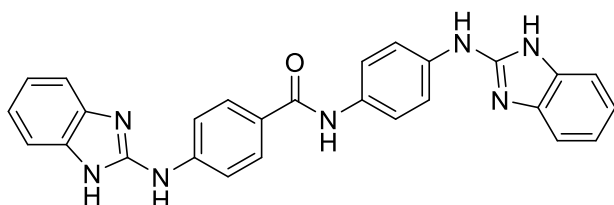
A solution of **19** (200 mg, 0.64 mmol) and *o*-phenylendiamine (151 mg, 1.4 mmol) in dry DMF (10 mL) was stirred at room temperature for two hours until complete starting material consumption. Metallic iodine (405 mg, 1.6 mmol) was added, followed by the addition of potassium carbonate (221 mg, 1.6 mmol). The resulting reaction mixture was allowed to stir overnight at room temperature. The reaction was quenched with 5% aq. $Na_2S_2O_3$ solution (3.5 mL), diluted brine (50 mL), and extracted with CH_2Cl_2 (3 × 30 mL) to yield a yellowish oil. Column chromatography using silica (Hexane: EtOAc, 100:0→40:60) yielded **2a** as a brownish solid (178 mg, 61%).

¹H NMR (500 MHz, DMSO-*d₆*) δ 12.97 (br s, 1H), 11.72 (s, 1H), 11.37 (s, 1H), 10.57 (s, 1H), 8.21 (d, *J* = 8.2 Hz, 2H), 8.02 (d, *J* = 8.5 Hz, 2H), 7.65 (d, *J* = 8.2 Hz, 2H), 7.51 (dd, *J* = 5.9, 3.2 Hz, 2H), 7.49 – 7.42 (m, 4H), 7.27 (m, 4H).

¹³C NMR (126 MHz, DMSO-*d₆*) δ 164.6, 147.9, 146.9, 139.9, 137.6, 131.3, 129.7, 129.6, 123.7, 123.53, 123.46, 121.7, 120.6, 112.3, 112.3, 111.9.

mp.: > 300 °C.

HPLC (UV) > 95%.

LRMS (ESI⁺) *m/z* = 460.2 [M+H].

HRMS (ESI⁺) *m/z* = 460.1872 [M+H] (Calc. for: $C_{27}H_{22}N_7O$: 460.1881).

4-((1*H*-benzo[*d*]imidazol-2(3*H*)-ylidene)amino)-*N*-(4-((1*H*-benzo[*d*]imidazol-2(3*H*)-ylidene)amino)-2-chlorophenyl)-3-chlorobenzamide (2b)
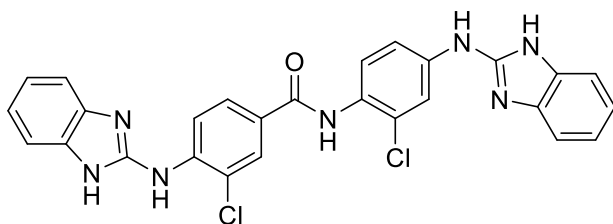
A solution of **26b** (125 mg, 0.33 mmol) and *o*-phenylendiamine (78 mg, 0.72 mmol) were reacted according to general Method H. EDC hydrochloride

(157 mg, 0.82 mmol) was added to the solution and the mixture was stirred at 60 °C for 12 hours. Centrifugal TLC (CH$_2$Cl$_2$: MeOH, 100:0→70:30) yielded **2b** as yellowish solid (75 mg, 43%).

^{1}H NMR (500 MHz, DMSO-d_6) δ 10.04 (s, 1H), 9.04 (t, J = 5.7 Hz, 1H), 8.86 (d, J = 8.9 Hz, 1H), 8.17 (d, J = 2.1 Hz, 1H), 8.12 (d, J = 2.5 Hz, 1H), 8.05 (dd, J = 8.7, 2.1 Hz, 1H), 7.61 (dd, J = 8.6, 2.5 Hz, 1H), 7.50 (d, J = 8.7 Hz, 1H), 7.45 (dd, J = 5.9, 3.2 Hz, 1H), 7.38 (td, J = 6.2, 3.2 Hz, 3H), 7.21 (dd, J = 5.9, 3.2 Hz, 1H), 7.09 (td, J = 6.2, 3.2 Hz, 4H), 3.46 – 3.40 (m, 2H).

^{13}C NMR (126 MHz, DMSO-d_6) δ 163.9, 150.0, 149.5, 149.3, 139.6, 139.1, 130.4, 129.9, 129.4, 128.8, 128.5, 127.7, 127.4, 123.0, 121.0, 120.7, 118.6, 118.4, 117.2, 111.2.

mp.: 209.8 – 219.8 °C.

HPLC (UV): > 95%.

LRMS (ESI$^+$): m/z = 528.2 [M+H].

HRMS (ESI$^+$) m/z = 528.1170 [M+H] (Calc. for: C$_{27}$H$_{20}$Cl$_2$N$_7$O: 528.1101).

4-((1H-benzo[d]imidazol-2(3H)-ylidene)amino)-N-(4-((1H-benzo[d]imidazol-2(3H)-ylidene)amino)-3-chlorophenyl)-3-chlorobenzamide (2c)
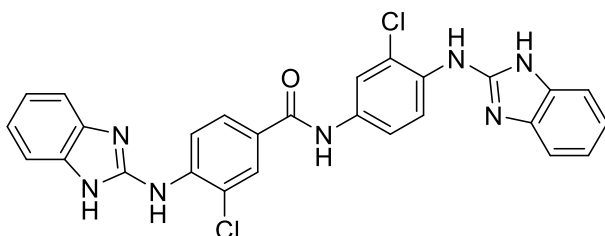
A solution of **26c** (102 mg, 0.27 mmol) and *o*-phenylendiamine (64 mg, 0.60 mmol) were reacted according to general Method H. EDC·HCl (131 mg, 0.68 mmol) was added to the solution and the mixture was stirred at 60 °C for 48 hours. Centrifugal TLC (CH$_2$Cl$_2$: MeOH, 100:0→70:30) yielded **2c** as yellowish solid (21 mg; 15%).

^{1}H NMR (400 MHz, DMSO-d_6) δ 10.93 (br s, 3H), 9.50 (br s, 2H), 9.23 (br s, 2H), 8.85 (d, J = 9.8 Hz, 2H), 8.72 (d, J = 9.8 Hz, 2H), 8.59 – 8.30 (m, 6H), 3.16 (br s, 2H).

^{13}C NMR (101 MHz, DMSO-d_6) δ 161.1, 154.2, 152.1, 146.1, 144.6, 143.8, 140.7, 134.4, 133.6, 123.4, 112.9.

mp.: 211.4 – 224.9 °C.

HPLC (UV): > 95%.

LRMS (ESI⁺): *m/z* 528.1 [M+H].

HRMS (ESI⁺) *m/z* = 528.1102 [M+H] (Calc. for: $C_{27}H_{20}Cl_2N_7O$: 528.1101).

4-((1*H*-benzo[*d*]imidazol-2(3*H*)-ylidene)amino)-*N*-(4-((1*H*-benzo[*d*]imidazol-2(3*H*)-ylidene)amino)-2-chlorophenyl)-2-chlorobenzamide (2d)
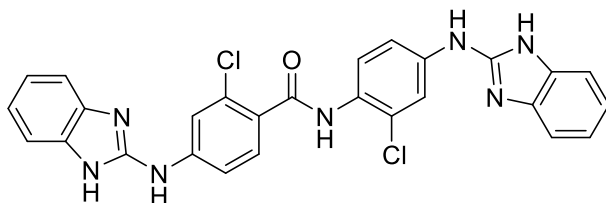
A solution of **26d** (50 mg, 0.13 mmol) and *o*-phenylendiamine (31 mg, 0.29 mmol) were reacted according to general Method H. EDC hydrochloride (63 mg, 0.33 mmol) was added to the solution and the mixture was stirred at 60 °C for 48 hours. Centrifugal TLC (CH₂Cl₂: MeOH–NH₃(saturated), 100:0→80:20) yielded **2d** as yellowish solid (21 mg; 31%).

¹H NMR (400 MHz, DMSO-*d₆*) δ 11.17 (s, 1H), 11.06 (s, 1H), 9.92 (s, 1H), 9.84 (s, 1H), 9.70 (s, 1H), 8.23 (d, *J* = 2.4 Hz, 1H), 8.21 (d, *J* = 2.4 Hz, 1H), 7.69 (dd, *J* = 2.2, 8.1 Hz, 1H), 7.59 – 7.53 (m, 3H), 7.43 (d, *J* = 7.1 Hz, 1H), 7.40 (d, *J* = 7.1 Hz, 1H), 7.32 (t, *J* = 8.7 Hz, 2H), 7.04 (m, 4H).

¹³C NMR (101 MHz, DMSO-*d₆*) δ 165.2, 150.0, 149.5, 143.2, 142.8, 142.6, 139.9, 132.6, 132.6, 131.0, 130.1, 129.2, 128.2, 127.5, 127.2, 120.7, 120.6, 120.3, 120.0, 117.0, 117.0, 116.3, 116.1, 115.9, 115.0, 109.8, 109.6.

mp.: 195.5 °C.

HPLC (UV): > 95%.

LRMS (ESI⁺): *m/z* = 528.2 [M+H].

HRMS (ESI⁺) *m/z* = 528.1088 [M+H] (Calc. for: $C_{27}H_{20}Cl_2N_7O$: 528.1101).

4-((1*H*-benzo[d]imidazol-2(3*H*)-ylidene)amino)-*N*-(4-((1*H*-benzo[*d*]imidazol-2(3*H*)-ylidene)amino)-3-chlorophenyl)-2-chlorobenzamide (2e)
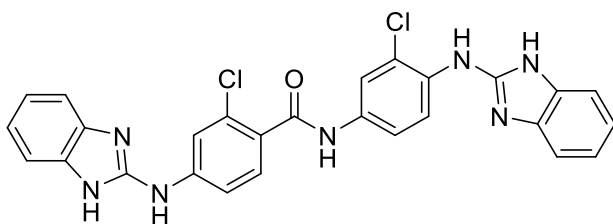
A solution of **26e** (83 mg, 0.22 mmol) and *o*-phenylendiamine (52 mg, 0.48 mmol) were reacted according to general Method H. EDC hydrochloride (106 mg, 0.55 mmol) was added to the solution and the mixture was stirred at 60 °C for 72 hours. Centrifugal TLC (CH$_2$Cl$_2$: MeOH–NH$_{3(saturated)}$, 100:0→90:10) yielded **2e** as yellowish solid (68 mg; 59%).

^{1}H NMR (500 MHz, Methanol-*d$_4$*) δ 8.07 (d, *J* = 8.8 Hz, 1H), 8.02 (d, *J* = 2.4 Hz, 1H), 7.85 (d, *J* = 2.1 Hz, 1H), 7.57 (dd, *J* = 8.8, 2.4 Hz, 1H), 7.56 (d, *J* = 8.5 Hz, 1H), 7.53 (dd, *J* = 8.5, 2.1 Hz, 1H), 7.43 – 7.29 (m, 4H), 7.12 (m, 2H), 7.07 (m, 2H).

^{13}C NMR (126 MHz, Methanol-*d$_4$*) δ 168.0, 152.4, 151.1, 144.9, 135.9, 134.5, 133.2, 131.0, 129.9, 125.5, 123.0, 122.5, 122.4, 122.2, 120.8, 119.1, 116.7.

mp.: >300 °C.

HPLC (UV): 94.2%.

LRMS (ESI$^+$): *m/z* = 528.2 [M+H].

HRMS (ESI$^+$) *m/z* = 528.1073 [M+H] (Calc. for: C$_{27}$H$_{20}$Cl$_2$N$_7$O: 528.1101).

5-((1*H*-benzo[*d*]imidazol-2(3*H*)-ylidene)amino)-*N*-(5-((1*H*-benzo[*d*]imidazol-2(3*H*)-ylidene)amino)pyridin-2-yl)picolinamide (2h)
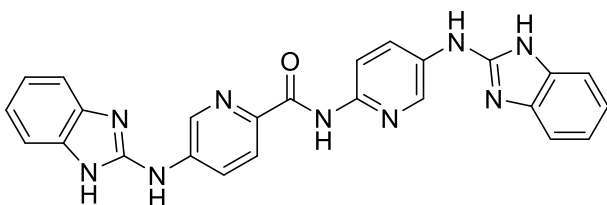
A solution of **26h** (20 mg, 64 µmol) and *o*-phenylendiamine (15 mg, 140 µmol) in dry CH$_3$CN (1 mL) was stirred at 0 °C for 48 hours until complete starting material consumption. EDC hydrochloride (30.6 mg, 160 µmol) was added to the solution and the mixture was stirred at 60 °C overnight. Ice was added to the crude to facilitate product precipitation. The precipitate was filtered on a fritted plate and washed with cold water to yield **2h** as brownish solid (13 mg, 44%).

¹H NMR (300 MHz, DMSO-*d₆*) δ 11.32 (s, 1H), 11.07 (s, 1H), 10.26 (s, 1H), 10.19 (s, 1H), 9.60 (s, 1H), 8.96 (d, *J* = 2.5 Hz, 1H), 8.77 (d, *J* = 2.6 Hz, 1H), 8.66 (dd, *J* = 8.5, 2.2 Hz, 1H), 8.33 (dd, *J* = 9.0, 2.6 Hz, 1H), 8.26 (d, *J* = 8.9 Hz, 1H), 8.19 (d, *J* = 8.7 Hz, 1H), 7.52 – 7.23 (m, 4H), 7.11 – 6.93 (m, 4H).

¹³C NMR (75 MHz, DMSO-*d₆*) δ 161.5, 150.3, 149.2, 144.5, 142.9, 142.5, 140.8, 140.4, 137.5, 137.4, 134.4, 132.9, 132.7, 126.7, 123.7, 123.0, 120.9, 120.6, 119.9, 116.5, 116.0, 113.0, 110.0, 109.5.

mp.: 210.6 °C.

HPLC (UV) > 95%.

LRMS (ESI⁺) *m/z* = 462.2 [M+H].

HRMS (ESI⁺) *m/z* = 462.1773 [M+H] (Calc. for: $C_{25}H_{20}N_9O$: 462.1785).

4,4'-(Ethane-1,2-diyl)bis(*N*-(1*H*-benzo[*d*]imidazol-2(3*H*)-ylidene)aniline) (30)
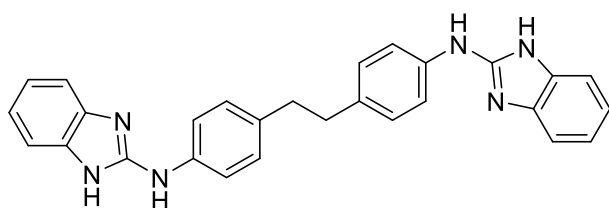
A solution of **29** (225 mg; 0.76 mmol) and *o*-phenylendiamine (180 mg; 1.67 mmol) were reacted according to general Method H. After 15 minutes, the brownish transparent solution turned into a turbid pallid yellow one. After 3 hours, starting materials consumption was revealed by TLC. EDC hydrochloride (364 mg, 1.93 mmol) was added, and the resulting mixture was heated at 60 °C. The crude reaction mixture was extracted with H_2O, and the combined organic phase was washed with brine, dried, and concentrated under vacuum to yield a brownish oil. The product was purified by column chromatography in silica using CH_2Cl_2:MeOH (100:0 →92:8) to yield **30** as whitish solid (182 mg, 54%).

¹H NMR (400 MHz, DMSO-*d₆*) δ 9.29 (s, 2H), 7.63 (d, *J* = 8.5 Hz, 4H), 7.29 (dd, *J* = 5.8, 3.2 Hz, 4H), 7.16 (d, *J* = 8.5 Hz, 4H), 6.97 (dd, *J* = 5.8, 3.2 Hz, 4H), 2.83 (s, 4H).

¹³C NMR (101 MHz, DMSO-*d₆*) δ 162.4, 150.8, 138.7, 133.8, 128.7, 120.0, 117.2, 36.7.

mp.: > 177.3 °C.

HPLC (UV): > 95%.

LRMS (ESI⁺): *m/z* = 445.3 [M+H].

HRMS (ESI⁺) *m/z* = 445.2125 [M+H] (Calc. for: $C_{28}H_{25}N_6$: 445.2135).

1,3-Bis(4-((1*H*-benzo[*d*]imidazol-2(3*H*)-ylidene)amino)phenyl)urea (31)
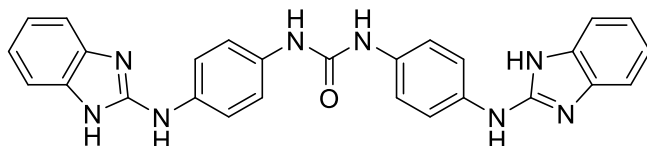
A solution of **20** (103 mg, 0.32 mmol) and *o*-phenylendiamine (756 mg, 0.7 mmol) were reacted according to general Method H. EDC hydrochloride (154 mg, 0.8 mmol) was added to the solution and the mixture was stirred at 60 °C for 48 hours. The precipitate was filtered on a fritted plate and washed with cold water. Circular chromatography (CH₂Cl₂: MeOH–NH₃(saturated) (98.75:1.25 → 80:20) gave the product **31** as yellowish solid (38 mg: 25%).

¹H NMR (400 MHz, DMSO-*d₆*) δ 10.86 (br s, 2H), 9.25 (br s, 2H), 8.47 (s, 2H), 7.65 (d, *J* = 8.9 Hz, 4H), 7.39 (d, *J* = 8.9 Hz, 4H), 7.28 (dd, *J* = 5.8, 3.3 Hz, 4H), 6.97 (dd, *J* = 5.8, 3.3 Hz, 4H).

¹³C NMR (101 MHz, DMSO-*d₆*) δ 171.4, 152.9, 152.9, 151.0, 135.3, 133.3, 119.8, 119.1, 117.9.

mp.: > 207.6 °C.

HPLC (UV): > 95%.

LRMS (ESI⁺): *m/z* 475.5 [M+H].

HRMS (ESI⁺) *m/z* = 475.1980 [M+H] (Calc. for: $C_{27}H_{23}N_8O$: 475.1989).

***N²,N⁷*-bis(1*H*-benzo[*d*]imidazol-2-yl)-9*H*-fluorene-2,7-diamine (34)**
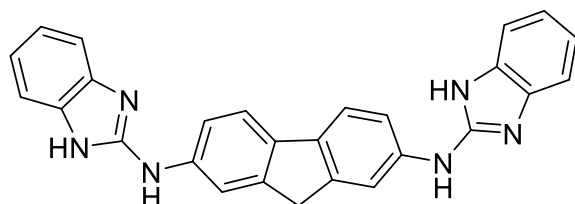
A solution of **33** (100 mg; 0.36 mmol) and *o*-phenylendiamine (86 mg; 0.8 mmol) were reacted according to general Method H.

EDC hydrochloride (173 mg; 0.9 mmol) was added, and the resulting mixture was heated at 60 °C. Ice was added to the crude to facilitate product precipitation. The precipitate was collected by filtration and purified by circular chromatography using silica (CH$_2$Cl$_2$:MeOH (100:0 → 70:30) to yield the product as whitish solid (94 mg; 61%).

^{1}H NMR (500 MHz, DMSO-d_6) δ 10.95 (br s, 2H), 9.52 (s, 2H), 8.12 (d, J = 2.0 Hz, 2H), 7.69 (d, J = 8.2 Hz, 2H), 7.61 (dd, J = 8.2, 2.0 Hz, 2H), 7.33 (br s, 4H), 7.07 – 6.92 (m, 4H), 3.95 (s, 2H).

^{13}C NMR (126 MHz, DMSO-d_6) δ 150.7, 143.6, 143.6, 139.1, 134.4, 120.0, 119.2, 115.9, 113.8, 36.8.

mp.: 196.3 – 210.2 °C.

HPLC (UV): > 95%.

LRMS (ESI$^+$): m/z = 429.2 [M+H].

HRMS (ESI$^+$) m/z = 429.1811 [M+H] (Calc. for: C$_{27}$H$_{21}$N$_6$: 429.1822).

9.1.2.9. Preparation of the pyridine carboxamide reagents (35, 44) used for the synthesis of bis(arylimidamides)

Naphthalen-2-ylmethyl pyridine-2-carbimidothioate hydrobromide (35)
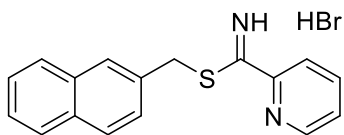
A solution of commercial pyridine-2-carbothioic acid amide (2-pyridinethioamide) (6 g, 1 eq.) and 2-(bromomethyl)-naphthalene (9.6 g, 1 eq.) in dry CHCl$_3$ (75 mL) was heated to reflux (65 ºC) for 1.5 hour. Then, the reaction mixture was cooled immediately in an ice-water bath and poured into cool Et$_2$O (350 mL). The resulting suspension was filtered and the organic phase was concentrated until dryness to yield **35** as white solid. The spectroscopic data were consistent with the literature.[9]

^{1}H NMR (300 MHz, DMSO-d_6) δ 8.85 – 8.77 (m, 1H), 8.32 (dd, J = 8.0, 0.9 Hz, 1H), 8.19 – 8.10 (m, 1H), 8.08 (d, J = 1.7 Hz, 1H), 8.03 – 7.89 (m, 3H), 7.80 (ddt, J = 7.7, 4.7, 0.9, 0.9 Hz, 1H), 7.62 (dd, J = 8.4, 1.8 Hz, 1H), 7.59 – 7.51 (m, 2H), 4.86 (s, 2H).

mp.: decomposes at 192 °C.

Anal. (C$_{17}$H$_{15}$BrN$_2$S) Calcd. C: 56.83, H: 4.21, N: 7.80, S: 8.92 Found: C: 56.51, H: 4.26, N: 7.82, S: 9.03.

tert-Butyl (imino(pyridin-2-yl)methyl)carbamate (43)
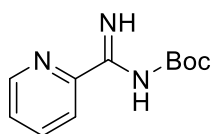
A solution of pyridine-2-carboximidamide hydrochloride (3 g; 25 mmol) in a mixture of dry MeOH/THF (2/3; 50 mL) was stirred at room temperature. Di-_tert_-butyl dicarbonate (8.2 g; 8.6 mL; 37.5 mmol) and NaHCO$_3$ (4.2 g; 50 mmol) were added successively. The purple heterogeneous reaction mixture turned to a whitish solution. After 12 hours, the reaction was stopped and filtered using paper filter. The filtrate was evaporated under vacuum and the resulting sticky product was diluted with EtOAc and washed successively with aqueous saturated ammonium chloride and brine. The organic phase was dried over MgSO$_4$ to yield the **43** as yellowish oil. Finally, compound **43** was obtained as whitish solid after lyophilisation (4.1 g; 73.6%).

¹H NMR (400 MHz, DMSO-*d₆*) δ 9.03 (s, 1H), 8.87 (s, 1H), 8.68 (dd, *J* = 4.7, 1.7 Hz, 1H), 8.24 (d, *J* = 8.2 Hz, 1H), 7.97 (td, *J* = 7.6, 1.7 Hz, 1H), 7.62 (ddd, *J* = 7.6, 4.7, 1.2 Hz, 1H), 1.46 (s, 9H).

¹³C NMR (101 MHz, DMSO-*d₆*) δ 163.8, 162.7, 150.0, 148.7, 137.7, 126.9, 122.2, 78.1, 27.9.

mp.: 93.8 – 96.0 ºC.

tert-Butyl (pyridine-2-carbonothioyl)carbamate (45)
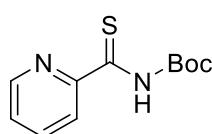
A suspension of NaH (7.64 g; 60% in mineral oil; 191 mmol) in dry THF (200 mL) was stirred at 0 ºC (ice-water bath) under argon atmosphere. Commercially available pyridine-2-carbothioic acid amide (2-pyridinethioamide) (12 g, 86.8 mmol) was slowly added to the stirring solution. **CAUTION**! Use an appropriate 1 L round-bottom flask as H_2 is liberated from the reaction. After 15 minutes, di-*tert*-butyl-dicarbonate (19 g; 20 mL, 86.8 mmol) was added dropwise at room temperature, and the resulting reaction mixture was stirred for 20 hours. The reaction was quenched by the dropwise addition of aq. saturated $NaHCO_3$ solution (100 mL). The crude was extracted with EtOAc and the organic phase was washed with brine. The organic phase was dried over $MgSO_4$ and evaporated to dryness. Compound **45** was obtained as pinkish solid by precipitation from MeOH (19.4 g, 93.7%).

¹H NMR (400 MHz, DMSO-*d₆*) δ 11.88 (s, 1H), 8.60 (dd, *J* = 4.7, 1.0 Hz, 1H), 8.29 (d, *J* = 8.0 Hz, 1H), 8.01 (td, *J* = 7.7, 1.8 Hz, 1H), 7.67 (ddd, *J* = 7.7, 4.7, 1.0 Hz, 1H), 1.47 (s, 9H).

¹³C NMR (101 MHz, DMSO-*d₆*) δ 194.7, 160.0, 149.5, 147.4, 138.0, 127.1, 124.2, 82.3, 27.5.

mp.: 111.4 – 112.1 °C.

HRMS (ESI⁺) *m/z* = 239.0844 [M+H] (Calc. for: $C_{11}H_{15}N_2O_2S$: 239.0849).

Methyl-*N*-(*tert*-butoxycarbonyl)pyridine-2-carbimidothioate (44)
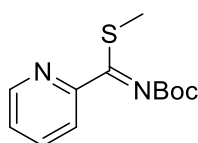
A suspension of NaH (6.7 g; 60% in mineral oil; 167.4 mmol) in dry THF (200 mL) was stirred at 0 ºC (ice-water bath) under argon atmosphere. *Tert*-butyl (pyridine-2-carbonothioyl)carbamate (**45**)

was slowly added to the stirring reaction mixture. After 15 minutes, iodomethane (22.6 g; 9.9 mL; 159.5 mmol) was slowly added to the stirring reaction mixture. The reaction was quenched after 12 hours stirring at room temperature by adding aq. sat. NaHCO$_3$ (100 mL). The crude product was extracted with EtOAc and the organic phase was washed with brine and dried over MgSO$_4$. The organic phase was evaporated under vacuum to obtain a yellowish oil. Silica column chromatography using *n*-hexane:EtOAc (100:0 → 97:3) yielded **44** as transparent oil. The product was obtained as whitish solid after lyophilisation using CH$_3$CN:H$_2$O (10.9 g; 54%).

^{1}H NMR (400 MHz, DMSO-*d$_6$*) δ 8.64 (dd, *J* = 4.7, 1.6 Hz, 1H), 7.97 (td, *J* = 7.7, 1.6 Hz, 1H), 7.73 (dd, *J* = 7.7, 1.1 Hz, 1H), 7.56 (ddd, *J* = 7.7, 4.7, 1.1 Hz, 1H), 2.43 (s, 3H), 1.38 (s, 9H).

^{13}C NMR (101 MHz, DMSO-*d$_6$*) δ 169.4, 159.3, 150.9, 149.1, 137.8, 126.3, 121.9, 80.9, 27.5, 13.6.

mp.: 46.0 – 50.0 °C.

HRMS (ESI$^+$) *m/z* = 253.1002 [M+H] (Calc. for: C$_{12}$H$_{17}$N$_2$O$_2$S: 253.1005).

Anal. calcd for C$_{12}$H$_{16}$N$_2$O$_2$S: C, 57.12; H, 6.39; N, 11.10; O, 12.68; S, 12.71 Found: C, 57.26; H, 6.29; N, 11.11; S, 12.64.

9.1.2.10. Synthesis of Boc-protected bis(arylimidamides) (52a–e, 52h–h, 54)

***tert*-Butyl-((4-((4-(-*N*'-(*tert*-butoxycarbonyl)picolinimidamido)-2-chlorophenyl)carbamoyl)-2-chlorophenyl)amino)(pyridin-2-yl)methylene)carbamate (52a)**
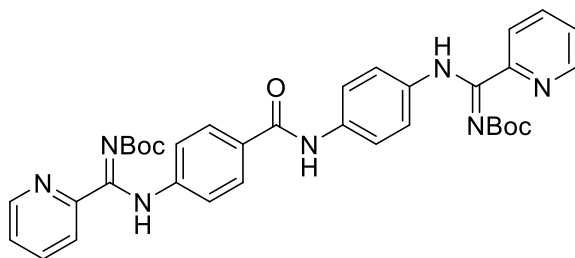
The reaction was performed following the general Method I.1 with commercial 4,4'-diaminobenzanilide (100 mg, 0.44 mmol), **44** (444 mg, 1.8 mmol), HgCl$_2$ (478 mg, 1.8 mmol) and Et$_3$N (0.25 mL, 1.8 mmol). The crude solid was purified by reverse phase chromatography with a C18 (12 g) cartridge using H$_2$O: CH$_3$CN (100:0 → 0:100) as elution system. The product was obtained as yellowish solid (33 mg, 12%).

^{1}H NMR (500 MHz, DMSO-d_6) δ 10.18 (s, 1H), 10.06 (s, 1H), 9.81 (s, 1H), 8.75 – 8.61 (m, 2H), 8.04 – 7.96 (m, 3H), 7.88 (d, *J* = 8.4 Hz, 2H), 7.79 – 7.66 (m, 6H), 7.58 (m, 2H), 1.24 (s, 9H), 1.22 (s, 9H).

^{13}C NMR (126 MHz, DMSO-d_6) δ 164.7, 160.4, 160.1, 156.4, 156.3, 151.9, 151.4, 149.1, 149.0, 142.3, 137.2, 137.1, 135.2, 135.1, 129.5, 128.4, 125.6, 125.4, 123.1, 123.0, 121.3, 121.1, 120.6, 119.8, 119.5, 112.5, 79.0, 78.5, 27.59, 27.57.

mp.: 143.6 – 145.3 °C.

HPLC (UV) > 94%.

LRMS (ESI$^+$) *m/z* 636.0 [M+H].

HRMS (ESI$^+$) m/z 636.2913 [M+H] (Calc. for C$_{35}$H$_{38}$N$_7$O$_5$: 636.2929).

tert-Butyl-((4-((4-(-_N'_-(_tert_-butoxycarbonyl)picolinimidamido)-2-chlorophenyl)carbamoyl)-2-chlorophenyl)amino)(pyridin-2-yl)methylene)carbamate (52b)
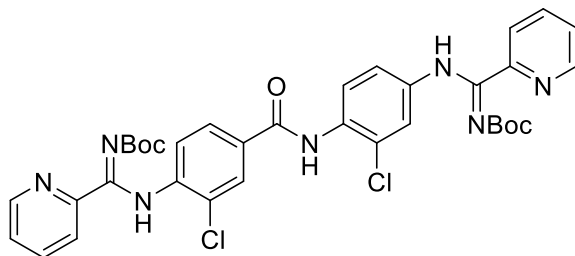
The reaction was performed following the general Method I.1 with diamine **15b** (150 mg, 0.5 mmol), **44** (515 mg, 2 mmol), HgCl$_2$ (554 mg, 2 mmol) and Et$_3$N (0.3 mL, 2 mmol). The crude solid (800 mg) was purified by reverse phase chromatography with a C18 (12 g) cartridge using H$_2$O: CH$_3$CN (100:0 → 0:100) as elution system. The product was obtained as yellowish solid (159 mg, 44%).

¹H NMR (500 MHz, DMSO-_d₆_) δ 10.04 (s, 1H), 9.99 (br s, 2H), 8.70 (ddd, _J_ = 4.8, 1.7, 1.0 Hz, 2H), 8.62 (ddd, _J_ = 3.6, 1.7, 1.0 Hz, 1H), 8.08 – 7.98 (m, 3H), 7.96 – 7.83 (m, 1H), 7.74 – 7.67 (m, 3H), 7.59 (ddd, _J_ = 7.7, 4.8, 1.0 Hz, 2H), 7.50 (d, _J_ = 8.7 Hz, 2H), 1.24 (s, 9H), 1.22 (s, 9H).

¹³C NMR (126 MHz, DMSO-_d₆_) δ 163.9, 160.1, 156.3, 151.4, 151.1, 149.3, 149.1, 148.5, 138.5, 137.2, 130.2, 129.6, 128.9, 128.8, 127.0, 125.6, 125.0, 123.2, 123.1, 120.8, 119.5, 80.4, 79.0, 27.6, 27.5.

mp.: 188.7 – 211.2 °C.

HPLC (UV) > 92%.

LRMS (ESI⁺) _m/z_ 704.3 [M+H].

tert-Butyl-((4-((4-(-N'-(tert-butoxycarbonyl)picolinimidamido)-3-chlorophenyl)carbamoyl)-2-chlorophenyl)amino)(pyridin-2-yl)methylene)carbamate (52c)
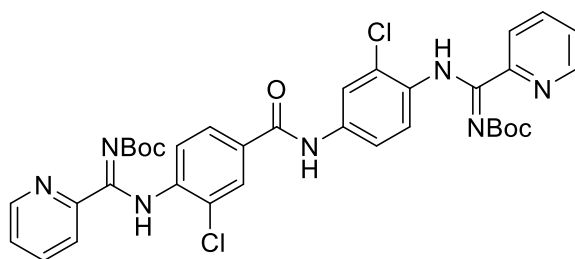
The reaction was performed following the general Method I.1 with diamine **15c** (79 mg, 0.3 mmol), **44** (273 mg, 1.1 mmol), $HgCl_2$ (293 mg, 1.1 mmol) and Et_3N (0.2 mL, 1.1 mmol). The crude solid obtained (512 mg) was purified by reverse phase chromatography with a C18 (12 g) cartridge using H_2O: CH_3CN (100:0 → 0:100) as elution system. The product was obtained as yellowish solid (61 mg, 32%).

^{1}H NMR (500 MHz, DMSO-d_6) δ 10.28 (s, 1H), 9.38 (s, 1H), 8.86 – 8.57 (m, 3H), 8.55 – 8.39 (m, 1H), 8.19 – 7.79 (m, 4H), 7.76 – 7.46 (m, 4H), 7.37 – 7.21 (m, 1H), 7.18 – 6.92 (m, 2H), 1.22 (br s, 18H).

^{13}C NMR (126 MHz, DMSO-d_6) δ 163.6, 151.1, 148.5, 148.3, 141.6, 137.1, 128.6, 127.0, 125.5, 124.9, 123.1, 121.2, 120.7, 119.2, 80.4, 80.1, 27.6, 27.5.

mp.: 244.1 – 269.7 °C.

HPLC (UV) > 95%.

LRMS (ESI$^+$) *m/z* 704.3 [M+H].

***tert*-Butyl-((4-((4-(-*N'*-(*tert*-butoxycarbonyl)picolinimidamido)-2-chlorophenyl)carbamoyl)-3-chlorophenyl)amino)(pyridin-2-yl)methylene)carbamate (52d)**
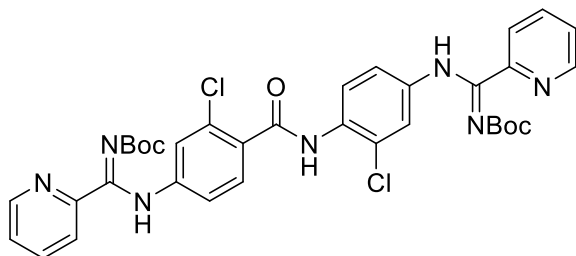
The reaction was performed following the general Method I.1 with diamine **15d** (112 mg, 0.38 mmol), **44** (240 mg, 0.95 mmol) and HgCl$_2$ (248 mg, 0.91 mmol) and Et$_3$N (154 mg, 1.5 mmol). The crude solid (372 mg) was purified by circular chromatography using a 2 mm silica plate previously neutralized with *n*-hexane (235 mL) and Et$_3$N (15 mL); hexane:EtOAC (6:4 → 4:6) was used as elution system. The product was obtained as yellowish solid (181 mg, 67%).

H NMR (300 MHz, DMSO-*d$_6$*) δ 10.09 (s, 1H), 9.99 (s, 1H), 9.81 (s, 1H), 8.70 (s, 1H), 8.56 (s, 1H), 8.14 – 7.92 (m, 4H), 7.79 – 7.50 (m, 6H), 7.26 – 7.13 (m, 1H), 7.13 – 6.99 (m, 1H), 1.24 (d, *J* = 4.1 Hz, 18H).

**^{13}C NMR (126 MHz, DMSO-*d$_6$*) δ** 162.3, 160.1, 160.0, 156.3, 156.3, 151.4, 151.1, 149.1, 149.1, 147.1, 139.8, 138.8, 138.2, 137.3, 137.2, 129.8, 129.7, 127.8, 125.7, 125.6, 124.2, 123.4, 123.1, 123.1, 120.9, 119.6, 118.6, 79.2, 79.0, 27.6, 27.6.

mp.: 157.5 – 170.0°C.

HPLC (UV) > 95%.

LRMS (ESI⁺) *m/z* 704.2 [M+H].

tert-butyl-((4-((4-(-N'-(tert-butoxycarbonyl)picolinimidamido)-3-chlorophenyl)carbamoyl)-3-chlorophenyl)amino)(pyridin-2-yl)methylene)carbamate (52e)
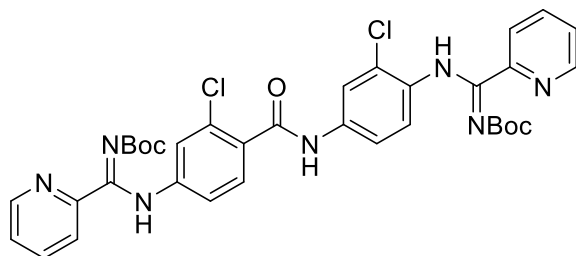
The reaction was performed following the general Method I.1 with diamine **15e** (109 mg, 0.37 mmol), **44** (235 mg, 0.93 mmol), HgCl$_2$ (242 mg, 0.89 mmol) and Et$_3$N (150 mg, 1.5 mmol). The crude solid (539 mg) was purified by circular chromatography using a 2 mm silica plate previously neutralized with n-hexane (235 mL) and Et$_3$N (15 mL); CH$_2$Cl$_2$:EtOAC (95:5 → 90:10) was used as elution system. The product was obtained as yellowish solid (32 mg, 12%).

^{1}H NMR (300 MHz, DMSO-d_6) δ 10.53 (s, 1H), 10.10 (br s, 2H), 9.58 (m, 1H), 9.37 (m, 1H), 8.75 – 8.66 (m, 2H), 8.67 – 8.57 (m, 1H), 8.15 – 7.93 (m, 3H), 7.85 – 7.76 (m, 1H), 7.73 – 7.66 (m, 1H), 7.65 – 7.52 (m, 3H), 7.06 – 6.92 (m, 1H), 1.24 (s, 9H), 1.22 (s, 9H).

^{13}C NMR (101 MHz, DMSO-d_6) δ 165.7, 160.8, 160.0, 156.3, 153.2, 151.1, 144.8, 141.7, 138.5, 137.3, 133.6, 129.5, 125.7, 123.1, 120.6, 119.9, 118.8, 113.6, 113.1, 80.1, 79.2, 27.51, 27.47.

mp.: > 300 ºC.

HPLC (UV) > 95%.

LRMS (ESI$^+$) *m/z* 704.2 [M+H].

***tert*-Butyl-((4-(4-(-*N'*-(*tert*-butoxycarbonyl)picolinimidamido)-2-isopropoxyphenyl)carbamoyl)-3-isopropoxyphenyl)amino)(pyridin-2-yl)methylene)carbamate (52g)**
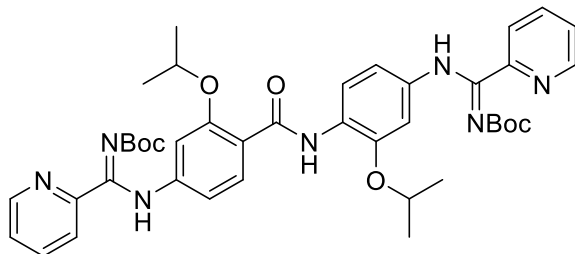
A solution of **15g** (50 mg, 0.15 mmol), **44** (96 mg, 0.38 mmol), and $HgCl_2$ (98 mg, 0.36 mmol), in dry CH_2Cl_2 (3 mL) was stirred at room temperature, followed by the dropwise addition of Et_3N (61 mg, 0.6 mmol). The reaction mixture was stirred 6 days at room temperature. The crude was filtered through a pad of florisil rinsing with CH_2Cl_2 and MeOH. The filtrate was extracted with H_2O, washed with brine and dried over Na_2SO_4. The organic phase was concentrated and purified by circular chromatography using a 2 mm silica plate previously neutralized with *n*-hexane (235 mL) and Et_3N (15 mL); hexane:EtOAc (2:3) was used as elution system. The product was obtained as yellowish solid (56 mg, 50%).

¹H NMR (500 MHz, DMSO-*d₆*) δ 10.06 (s, 1H), 9.91 (s, 1H), 9.80 (s, 1H), 8.70 (dd, J = 9.9, 4.8 Hz, 2H), 8.33 (d, J = 8.8 Hz, 1H), 8.10 – 7.95 (m, 3H), 7.77 – 7.65 (m, 3H), 7.59 (ddd, J = 12.4, 7.9, 5.1 Hz, 3H), 7.48 (s, 1H), 7.37 (d, J = 7.5 Hz, 1H), 4.72 (hept, J = 6.0 Hz, 1H), 4.59 (hept, J = 6.0 Hz, 1H), 1.47 (d, J = 6.0 Hz, 6H), 1.39 (d, J = 6.0 Hz, 6H), 1.25 (s, 9H), 1.22 (s, 9H).

¹³C NMR (126 MHz, DMSO-*d₆*) δ 162.3, 160.1, 160.0, 156.3, 156.3, 151.4, 151.1, 149.1, 149.1, 147.1, 139.8, 138.8, 138.2, 137.3, 137.2, 129.8, 129.7, 127.8, 125.7, 125.6, 124.2, 123.4, 123.1, 123.1, 120.9, 119.6, 118.6, 79.2, 79.0, 27.6, 27.6.

mp.: 96.3 – 102.0 ºC.

HPLC (UV) > 95%.

LRMS (ESI⁺) *m/z* 752.45 [M+H].

***tert*-Butyl-(-((6-((5-(-*N'*-(*tert*-butoxycarbonyl)picolinimidamido)pyridin-2-yl)carbamoyl)pyridin-3-yl)amino)(pyridin-2-yl)methylene)carbamate (52h)**
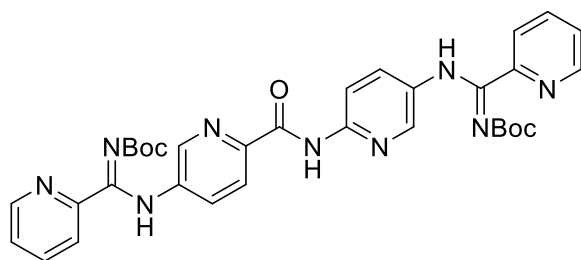
The reaction was performed following the general Method I.1 with diamine **15h** (99 mg, 0.43 mmol), **44** (436 mg, 1.73 mmol), HgCl₂ (469 mg, 1.73 mmol) and Et₃N (1.75 mL, 1.73 mmol) Purification by medium pressure chromatography (4g silica cartridge) using hexane:EtOAc (100:0 → 80:20) gave **52h** as yellowish solid (97 mg; 36%).

¹H NMR (300 MHz, DMSO-*d₆*) δ 10.49 (br m, 8H), 9.78 (s, 1H), 8.03 – 7.88 (m, 2H), 7.81 (d, *J* = 8.5 Hz, 1H), 7.70 (d, *J* = 2.7 Hz, 1H), 7.03 (dd, *J* = 8.7, 2.7 Hz, 2H), 6.16 (s, 1H), 5.14 (s, 1H), 1.20 (m, 18H).

¹³C NMR (126 MHz, DMSO-*d₆*) δ 161.5, 148.1, 141.7, 141.3, 136.3, 134.4, 133.7, 123.1, 122.6, 119.3, 113.3, 57.7, 8.4.

mp.: 187.6 °C.

HPLC (UV) > 95%.

LRMS (ESI⁺): *m/z* = 638.4 [M+H].

***tert*-Butyl-(*N,N''*-(ethane-1,2-diylbis(4,1-phenylene))dipicolinimidamide) carbamate (54)**
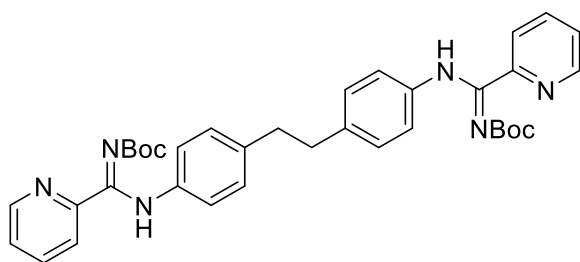
The reaction was performed following the general Method I.1 with commercial 4,4´-diaminobibenzyl (51 mg, 0.24 mmol), **44** (110 mg, 0.43 mmol), HgCl₂ (118 mg, 0.43 mmol) and Et₃N (61 µL, 0.44 mmol). Purification by medium pressure chromatography (12g C18 cartridge) using H₂O:CH₃CN (100:0 → 0:100) gave **54** as yellowish solid (126 mg, 85%).

¹H NMR. (300 MHz, DMSO-*d₆*) δ 9.74 (s, 2H), 8.67 (d, J= 5.1 Hz, 2H), 8.08-7.90 (m, 2H), 7.70 – 7.46 (m, 8H), 7.19 (d, J= 8.2 Hz, 4H), 2.86 (s, 4H). 1.21 (s, 18H).

^{13}C NMR (126 MHz, DMSO-d_6)) δ 160.3, 156.4, 151.8, 149.0, 137.2, 137.1, 136.9, 128.5, 125.3, 123.0, 120.8, 78.4, 36.6, 27.6.

mp.: 158.5 − 160.2 °C.

HPLC (UV) > 92%.

LRMS (ESI$^+$): *m/z* = 621.0 [M+H].

9.1.2.11. Synthesis of bis(arylimidamides) (3a–e, 3g–i, 36–41, 53)

4-(Picolinimidamido)-*N*-(4-(picolinimidamido)phenyl)benzamide (3a)
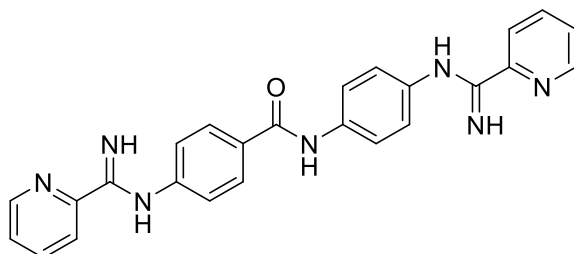
The reaction was performed following the general Method J with 4,4'-diaminobenzanilide (0.5 g, 2.2 mmol) and naphthalen-2-ylmethyl pyridine-2-carbimidothioate hydrobromide **35** (1.97 g, 5.5 mmol), in 6 mL of EtOH:CH$_3$CN (3:1). The resulting reaction mixture was allowed to stir at room temperature for 48 hours. The solvents were removed under vacuum and the crude product was purified by silica gel column chromatography using *n*-hexane:EtOAc (20:80 → 0:100). The free base product was obtained as yellowish solid (220 mg, 23%).

¹H NMR (400 MHz, DMSO-*d₆*) δ 10.05 (s, 1H), 8.65 (ddt, *J* = 6.7, 4.9, 1.4 Hz, 2H), 8.33 (d, *J* = 8.0 Hz, 2H), 8.07 – 7.88 (m, 4H), 7.79 (d, *J* = 8.7 Hz, 2H), 7.56 (dddd, *J* = 9.0, 7.5, 4.8, 1.3 Hz, 2H), 7.05 (d, *J* = 8.0 Hz, 2H), 6.95 (d, *J* = 8.2 Hz, 2H), 6.90 – 6.00 (m, 4H).

¹³C NMR (101 MHz, DMSO-*d₆*) δ 164.8, 153.7, 151.8, 151.6, 151.2, 148.1, 148.0, 145.6, 137.2, 137.1, 134.2, 129.0, 128.6, 125.6, 125.4, 121.6, 121.5, 121.4, 121.2, 113.7, 112.5.

mp.: 246.9 – 259.4 °C.

HPLC (UV) > 95 %.

LRMS (ESI⁺) *m/z* 436.4 [M+H].

HRMS (ESI⁺) *m/z* = 436.1881 [M+H] (Calc. for: C$_{26}$H$_{23}$N$_6$O: 436.1880).

ALTERNATIVE PROTOCOL FOR THE SYNTHESIS OF 3a (using **44**)

4-(Picolinimidamido)-*N*-(4-(picolinimidamido)phenyl)benzamide di-trifluoroacetate salt (3a)

2CF$_3$CO$_2$H
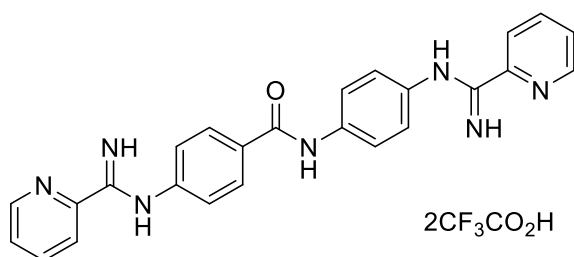
The reaction was performed with **52a** (13 mg, 0.02 mmol) following the general procedure I.2. Compound **3a** was obtained as yellowish solid (11 mg, 99%).

¹H NMR (400 MHz, DMSO-*d₆*) δ 10.67 (s, 1H), 10.14 (br s, 1H), 10.00 (s, 1H), 9.46 (br s, 1H), 9.25 (s, 1H), 8.95 – 8.84 (m, 1H), 8.40 – 8.33 (m, 2H), 8.27 – 8.17 (m, 4H), 8.03 (d, J = 8.9 Hz, 2H), 7.91 – 7.82 (m, 2H), 7.67 (d, J = 7.2 Hz, 2H), 7.49 (d, J = 8.9 Hz, 2H).

¹³C NMR (126 MHz, DMSO-*d₆*) δ 164.8, 159.6, 149.9, 144.6, 139.2, 138.5, 138.4, 129.5, 129.5, 129.4, 128.7, 128.6, 126.4, 125.8, 124.0, 123.8, 121.4.

mp.: 246.8 – 259.4 °C.

HPLC (UV) > 90 %.

LRMS (ESI⁺) *m/z* 436.2 [M+H].

3-Chloro-*N*-(2-chloro-4-(picolinimidamido)phenyl)-4-(picolinimidamido)benzamide di-trifluoroacetate salt (3b)

2CF$_3$CO$_2$H
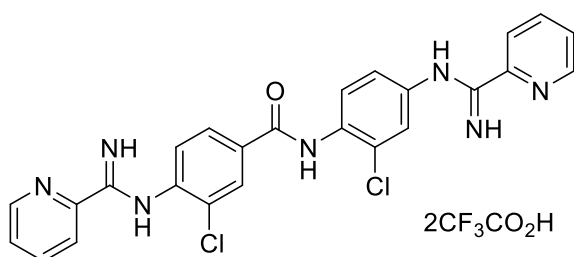
The reaction was performed with **52b** (50 mg, 70 µmol) following the general procedure I.2. Compound **3b** was obtained as yellowish solid (45 mg, 88%).

¹H NMR (500 MHz, DMSO-*d₆*) δ 10.41 (s, 1H), 10.09 (br s, 1H), 9.56 (br s, 1H), 8.91 (d, *J* = 4.4 Hz, 1H), 8.84 (d, *J* = 5.3 Hz, 1H), 8.42 – 8.32 (m, 2H), 8.32 – 8.20 (m, 2H), 8.17 (t, *J* = 7.8, 7.8 Hz, 1H), 8.09 (dd, *J* = 8.3, 2.0 Hz, 1H), 7.87 (dd, *J* = 8.3, 4.7 Hz, 1H), 7.82 – 7.73 (m, 3H), 7.61 – 7.46 (m, 2H), 3.63 (br s, 2H).

¹³C NMR (126 MHz, DMSO-*d₆*) δ 163.8, 159.6, 149.9, 149.4, 144.6, 138.5, 138.2, 134.9, 130.1, 129.6, 129.3, 128.7, 128.1, 127.2, 125.2, 123.9, 123.1.

mp.: 118.1 – 120.0 °C.

HPLC (UV) > 95%.

LRMS (ESI⁺) *m/z* 504.32 [M+H].

HRMS (ESI⁺) *m/z* = 504.1087 [M+H] (Calc. for: C₂₅H₂₀Cl₂N₇O: 504.1101).

3-Chloro-*N*-(3-chloro-4-(picolinimidamido)phenyl)-4-(picolinimidamido)benzamide di-trifluoroacetate salt (3c)
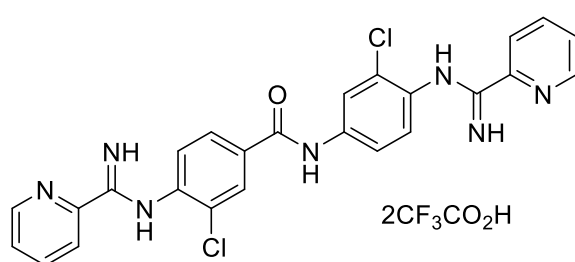
The reaction was performed with **52c** (25 mg, 36 µmol) following the general procedure I.2. Compound **3c** was obtained as yellowish solid (20 mg, 76%).

¹H NMR (500 MHz, DMSO-*d₆*) δ 10.49 (br s, 3H), 9.14 – 8.78 (m, 3H), 8.61 – 8.28 (m, 3H), 8.25 – 8.04 (m, 3H), 8.03 – 7.68 (m, 3H), 7.36 – 7.17 (m, 3H).

**¹³C NMR (101 MHz, DMSO-*d₆*) δ** 164.1, 158.0, 150.0, 149.2, 144.2, 138.7, 138.4, 129.4, 128.8, 128.1, 123.7, 122.9, 121.3, 120.1.

mp.: 130.7 °C.

HPLC (UV) > 95%.

LRMS (ESI⁺) *m/z* 504.3 [M+H].

HRMS (ESI⁺) *m/z* = 504.1087 [M+H] (Calc. for: C₂₅H₂₀Cl₂N₇O: 504.1101).

2-Chloro-*N*-(2-chloro-4-(picolinimidamido)phenyl)-4-picolinimidamido)benzamide di-hydrochloride (3d)
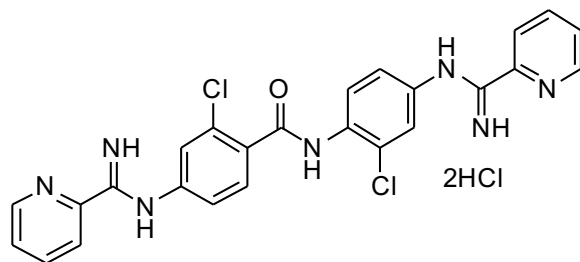
A solution of **52d** (57 mg, 80 µmol) in dry CH₂Cl₂ (1.5 mL) was stirred at 0 °C (ice-bath), followed by the dropwise addition of 4 M HCl in dioxane. After one hour, the solvent and HCl excess was removed under vacuum. The crude product was crushed with Et₂O to yield **3d** as brownish solid (31 mg, 67%).

¹H NMR (400 MHz, DMSO-*d₆*) δ 10.46 (s, 1H), 10.02 (br s, 1H), 9.41 (br s, 1H), 8.90 (br s, 2H), 8.37 (d, *J* = 7.8 Hz, 2H), 8.28 – 8.18 (m, 2H), 7.99 – 7.78 (m, 4H), 7.72 (m, 2H), 7.50 (d, *J* = 9.1 Hz, 2H), 7.38 – 7.30 (m, 2H).

¹³C NMR (101 MHz, DMSO-*d₆*) δ 164.9, 154.3, 149.9, 149.8, 138.6, 131.2, 130.5, 128.8, 128.7, 128.5, 128.1, 127.9, 127.6, 127.4, 125.3, 123.9.

mp.: > 130.2 °C.

HPLC (UV) > 95%.

LRMS (ESI⁺) *m/z* 504.1 [M+H].

HRMS (ESI⁺) *m/z* = 504.1098 [M+H] (Calc. for: $C_{25}H_{20}Cl_2N_7O$: 504.1101).

2-Chloro-*N*-(3-chloro-4-(picolinimidamido)phenyl)-4-(picolinimidamido)benzamide di-trifluoroacetate salt (3e)
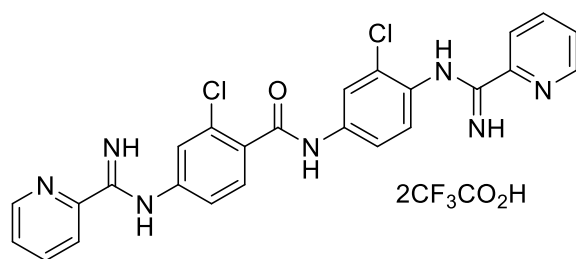
The reaction was performed with **52e** (30 mg, 40 µmol) following the general procedure I.2. After two hours, excess TFA was removed under vacuum. The crude product was dissolved in MeOH and the solvent was evaporated to give a solid that was dried under high vacuum. The purplish solid was crushed with Et₂O to yield pure **3e** as whitish solid (24 mg, 82%).

¹H NMR (400 MHz, DMSO-*d₆*) δ 11.01 (s, 1H), 8.92 – 8.90 (m, 1H), 8.89 – 8.87 (m, 1H), 8.46 – 8.31 (m, 2H), 8.29 – 8.15 (m, 3H), 7.90 – 7.81 (m, 2H), 7.81 – 7.75 (m, 2H), 7.69 (br s, 1H), 7.58 (d, *J* = 8.6 Hz, 1H), 7.50 (br s, 1H), 3.52 (br s, 4H).

¹³C NMR (101 MHz, DMSO-*d₆*) δ 164.9, 159.8, 150.0, 149.9, 149.7, 149.5, 144.3, 140.3, 138.5, 138.3, 131.0, 130.9, 130.2, 129.6, 128.7, 128.3, 124.5, 123.6, 120.6, 119.5.

mp.: 214.0 – 222.9 °C.

HPLC (UV) > 95%.

LRMS (ESI⁺) *m/z* 504.1 [M+H].

HRMS (ESI⁺) *m/z* = 504.1089 [M+H] (Calc. for: $C_{25}H_{20}Cl_2N_7O$: 504.1101).

2-Isopropoxy-*N*-(2-isopropoxy-4-(picolinimidamido)phenyl)-4-(picolinimidamido)benzamide di-hydrochloride (3g)
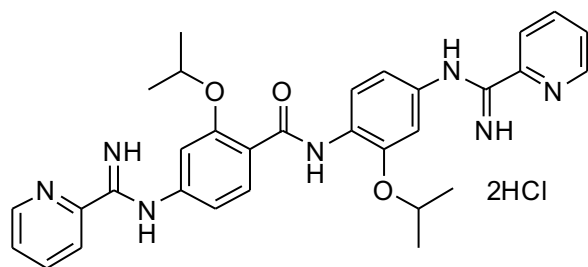
A solution of **52g** (45 mg; 60 µmol) in dry CH_2Cl_2 (3 mL) was stirred at 0 °C (ice-bath), followed by the dropwise addition of 4 M HCl in dioxane. After two hours, the reaction was stopped and the excess of HCl was removed under vacuum. The crude product was crushed with Et_2O to yield **3g** as brownish solid (24 mg, 65%).

¹H NMR (400 MHz, DMSO-*d*₆) δ 9.83 (s, 1H), 9.21 (s, 1H), 8.89 (d, *J* = 4.8 Hz, 1H), 8.74 – 8.61 (m, 1H), 8.40 (dd, *J* = 8.5, 4.6 Hz, 1H), 8.22 (m, 1H), 8.17 – 7.97 (m, 1H), 7.85 (dd, *J* = 7.7, 4.8 Hz, 1H), 7.77 (dd, *J* = 9.9, 8.5 Hz, 2H), 7.14 (d, *J* = 2.3 Hz, 1H), 6.93 (dd, *J* = 8.5, 2.3 Hz, 1H), 6.45 – 6.41 (m, 1H), 6.36 – 6.32 (m, 1H), 4.75 – 4.58 (m, 4H), 3.73 – 3.64 (m, 1H), 3.52 – 3.43 (m, 1H), 1.44 – 1.36 (m, 12H).

¹³C NMR (101 MHz, DMSO-*d*₆) δ 163.2, 159.5, 157.3, 149.8, 149.0, 148.6, 148.3, 147.4, 147.1, 144.5, 138.5, 138.4, 137.9, 133.1, 129.1, 128.6, 128.0, 126.5, 123.8, 122.6, 122.0, 121.4, 114.9, 108.6, 107.8, 72.2, 71.9, 22.0, 21.9.

mp.: 142.9 – 150.0 °C.

HPLC (UV) >95%.

LRMS (ESI⁺) *m/z* 552.2 [M+H].

HRMS (ESI⁺) *m/z* = 552.2712 [M+H] (Calc. for: $C_{31}H_{34}N_7O_3$: 552.2718).

5-(Picolinimidamido)-*N*-(5-(picolinimidamido)pyridin-2-yl)picolinamide di-trifluoroacetate salt (3h)
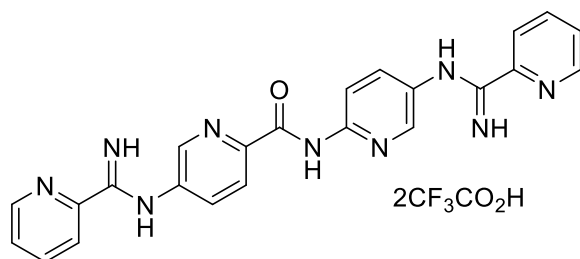
The reaction was performed with **52h** (80 mg, 0.13 mmol) was reacted following the general procedure I.2. Compound **3h** was obtained as brownish solid (78 mg, 90%).

¹H NMR (500 MHz, DMSO-d_6) δ 11.68 (br s, 1H), 10.55 (s, 1H), 9.44 (br s, 1H), 8.95 – 8.87 (m, 2H), 8.85 – 8.79 (m, 2H), 8.48 – 8.40 (m, 5H), 8.27 (d, J = 8.1 Hz, 2H), 8.22 (d, J = 9.9 Hz, 1H), 7.98 – 7.80 (m, 4H).

¹³C NMR (101 MHz, DMSO-d_6) δ 163.0, 162.2, 150.2, 150.0, 149.2, 148.9, 144.7, 135.0, 129.3, 129.2, 124.3, 124.2, 123.9, 119.8, 114.2, 113.6.

mp.: 135.0 – 138.0 °C.

HPLC (UV): > 95 %.

LRMS (ESI⁺): m/z 438.3 [M+H].

HRMS (ESI⁺) m/z = 219.0932 [M+2H] (Calc. for: $C_{24}H_{22}N_8O$: 219.0953).

4-(Picolinimidamido)-*N*-(5-(picolinimidamido)pyridin-2-yl)benzamide (3i)
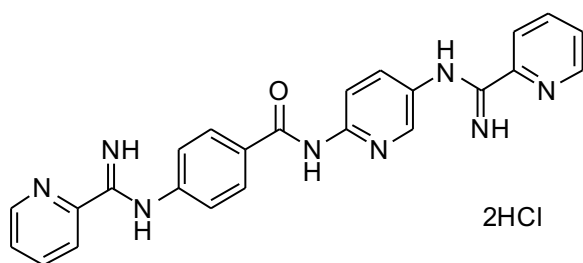
The diamine **15i** (86 mg, 0.38 mmol) was suspended in anhydrous acetonitrile (2 mL) and anhydrous EtOH (6 mL). The flask was cooled with an ice-water bath and the solid naphthalen-2-ylmethyl pyridine-2-carbimidothioate hydrobromide **35** (284 mg, 0.79 mmol) was added at once to the suspension. The thick yellowish slurry was stirred at 0 ºC and allowed to warm up to room temperature. After 5 days stirring at room temperature, Et₂O was added to the reaction mixture. The precipitate was collected on a fritted plate and rinsed with Et₂O. The precipitate was dissolved in EtOH (20 mL) and the cooled solution (ice-water bath) was basified with 1N NaOH until pH ≈ 10. The solution was concentrated under vacuum and the product was partitioned between water (25 mL) and EtOAc (40 mL). The aqueous phase was extracted with EtOAc (2×50 mL) and the combined organic extracts were washed with brine, dried (Na₂SO₄) and evaporated to give a crude yellow residue. Silica chromatography (5 g SI cartridge) with CHCl₃/ NH₃(sat.)-MeOH: 0→5% yielded a mixture (≈75/25, 38 mg) of the expected product **3i** (M = 436) and the monosubstituted product **39** (M = 332). The mixture was dissolved in CH₂Cl₂/MeOH (2 mL), cooled with an ice-bath, and treated with HCl(sat.)-dioxane solution for 1 h with gentle stirring. The mono-substituted product **39** that precipitated from the reaction mixture was collected by filtration and rinsed with Et₂O to give **39** as colorless solid (20 mg, 12.2%). The filtrate was evaporated under

vacuum and the product **3i** was recrystallized from CH$_2$Cl$_2$/MeOH at -20 ºC. The product was rinsed with Et$_2$O to yield **3i** as yellowish solid (10 mg, 6.1%).

^{1}H NMR (400 MHz, DMSO-d_6) δ 11.99 (brs, 1H), 11.84 (brs, 1H), 11.27 (s, 1H), 10.22 (brs, 1H), 10.20 (brs, 1H), 9.50 (brs, 2H), 8.92 (d, J = 4.7 Hz, 2H), 8.55 (d, J = 2.7 Hz, 1H), 8.50 (d, J = 8.0 Hz, 1H), 8.47 (d, J = 9.2 Hz, 1H), 8.41 (d, J = 8.8 Hz, 1H), 8.31-8.20 (m, 4H), 8.01 (dd, J = 8.8, 2.7 Hz, 1H), 7.92 – 7.84 (m, 2H), 7.65 (d, J = 8.1 Hz, 2H).

^{13}C NMR (126 MHz, DMSO-d_6) δ 165.3, 160.2, 151.8, 149.9, 148.5, 145.9, 144.3, 138.5, 138.4, 138.3, 136.5, 130.0, 129.8, 129.0, 128.7, 125.7, 124.1, 123.9, 122.6, 119.8, 119.5, 115.3.

mp.: > 130 ºC.

HPLC (UV): > 95%.

LRMS (ESI$^+$) *m/z* 437.3 [M+H].

HRMS (ESI$^+$) *m/z* = 437.1824 [M+H] (Calc. for C$_{24}$H$_{21}$N$_8$O: 437.1833).

N-(5-aminopyridin-2-yl)-4-(picolinimidamido)benzamide hydrochloride salt (39)
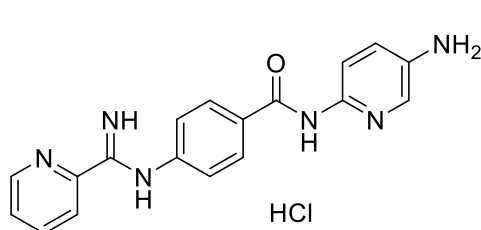
^{1}H NMR (400 MHz, DMSO-d_6) δ 11.18 (s, 0.1H), 10.31 (s, 0.2H), 9.58 (s, 0.2H), 8.90 (dd, J = 4.7, 2.7 Hz, 1H), 8.56 (dd, J = 5.7, 2.7 Hz, 2H), 8.53 (d, J = 2.6 Hz, 1H), 8.39 (d, J = 9.1 Hz, 1H), 8.31 – 8.24 (m, 1H), 8.25 – 8.19 (m, 2H), 8.07 – 8.00 (m, 2H), 7.89 – 7.83 (m, 1H), 7.17 (d, J = 8.2 Hz, 1H), 5.10 (br s, 2H).

^{13}C NMR (101 MHz, DMSO-d_6) δ 165.6, 160.1, 151.7, 149.9, 144.8, 144.0, 138.5, 138.4, 137.4, 129.9, 129.8, 128.8, 127.0, 125.7, 124.1, 118.8, 115.3.

HPLC (UV): 91% (contains 9% of **3i**).

LRMS (ESI$^+$) *m/z* 333[M+H].

N,*N''*-(ethane-1,2-diylbis(4,1-phenylene))dipicolinimidamide (36)
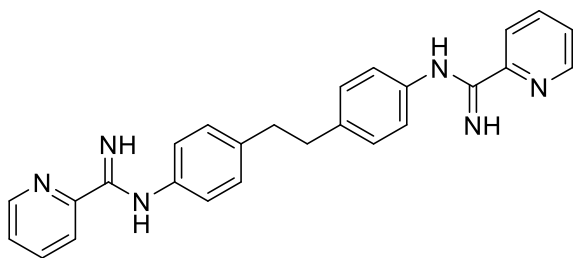
The reaction was performed following the general Method J with commercial 4,4′-diaminobibenzyl (106 mg, 0.5 mmol) and naphthalen-2-ylmethyl pyridine-2-carbimidothioate hydrobromide **35** (449 mg, 1.25 mmol) suspended in a 3:1 mixture of anhydrous EtOH:CH₃CN (16 mL). The mixture was allowed to stir at room temperature overnight. The solvent was eliminated under vacuum and the solid crude was purified by silica column chromatography using hexane:EtOAc (100:0 → 10:90) as elution system. The product was obtained as yellowish solid (51 mg, 24%).

¹H NMR (300 MHz, DMSO-*d₆*) δ 11.68 (s, 2H), 10.02 (s, 2H), 9.25 (s, 2H), 8.89 (d, J= 4.7 Hz, 2H), 8.36 (d, J= 8.0 Hz, 2H), 8.21 (t, J= 7.7 Hz, 2H), 7.85 (dd, J= 7.6, 4.7 Hz, 2H), 7.51 (d, J= 8.1 Hz, 3H), 7.42 (d, J= 8.4 Hz, 3H), 3.02 (s, 4H).

¹³C NMR (126 MHz, DMSO-*d₆*) δ 151.8, 151.4, 148.0, 147.5, 137.1, 135.6, 129.2, 125.4, 121.4, 121.3, 36.9.

mp.: 174.7 – 180.0 °C.

HPLC (UV) > 95%.

LRMS (ESI⁺) *m/z* 421.2 [M+H].

HRMS (ESI⁺) *m/z* = 421.2132[M+H] (Calc. for: $C_{26}H_{25}N_6$: 421.2135).

N,*N′*-((carbonylbis(azanediyl))bis(4,1-phenylene))dipicolinimidamide (37)
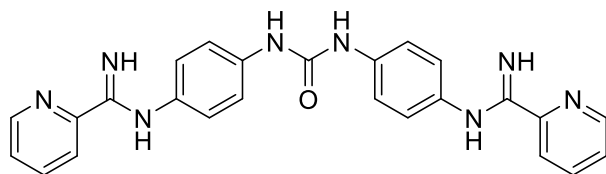
The reaction was performed following the general Method J with **28** (300 mg; 1.24 mmol) and **35** (1.12 g; 3.1 mmol) suspended in a 3:1 mixture of EtOH:CH₃CN (24 mL). The reaction mixture was stirred at room temperature for 3 days. The precipitate was collected by filtration,

rinsed with MeOH, and dried. The resulting solid was dissolved in CH_2Cl_2 and MeOH was added to precipitate the product as whitish solid (220 mg, 39.4%).

^{1}H NMR (400 MHz, DMSO-d_6) δ 7.90 – 7.88 (m, 4H), 7.88 – 7.86 (m, 4H), 7.86 – 7.84 (m, 2H), 7.83 – 7.81 (m, 4H), 7.80 – 7.77 (m, 2H), 7.66 – 7.64 (m, 2H), 7.53 – 7.48 (m, 4H).

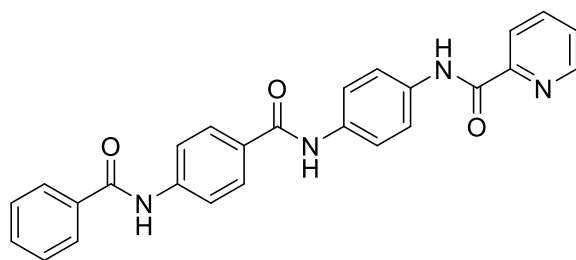**^{13}C NMR (101 MHz, DMSO-d_6) δ** 150.9, 139.7, 133.0, 128.0, 127.5, 127.5, 127.4, 126.9, 126.2, 126.0, 125.7.

mp.: > 300 °C.

HPLC (UV) > 95%.

LRMS (ESI$^+$) *m/z* 451.3 [M+H].

HRMS (ESI$^+$) *m/z* = 451.1981 [M+H] (Calc. for: $C_{25}H_{23}N_8O$: 451.1989).

N-(4-(4-(picolinamido)benzamido)phenyl)picolinamide(41)

A suspension of 4,4′-diaminobenzanilide (150 mg, 0.7 mmol) and picolinyl chloride (294 mg, 1.7 mmol) in dry THF (8 mL) was stirred at room temperature. Et$_3$N (140 mg, 1.4 mmol) was added dropwise, turning the brown into a whitish solution. After two hours, the reaction mixture was diluted with CH_2Cl_2 whereupon a whitish precipitate appeared. The product was collected by filtration as whitish solid (271 mg, 94%).

^{1}H NMR (500 MHz, DMSO-d_6) δ 10.91 (s, 1H), 10.62 (s, 1H), 10.18 (s, 1H), 8.79 – 8.73 (m, 2H), 8.22 – 8.15 (m, 2H), 8.12 – 8.05 (m, 4H), 8.00 (d, *J* = 8.9 Hz, 2H), 7.89 (d, *J* = 8.9 Hz, 2H), 7.77 (d, *J* = 8.9 Hz, 2H), 7.73 – 7.65 (m, 2H).

^{13}C NMR (126 MHz, DMSO-d_6) δ 164.7, 162.9, 162.2, 150.0, 149.7, 148.5, 148.4, 141.3, 138.2, 138.1, 135.3, 134.0, 129.9, 128.4, 127.2, 126.9, 122.6, 122.3, 120.6, 120.5, 119.5.

HPLC (UV) >95%.

LRMS (ESI$^+$) *m/z* 438.2 [M+H].

***N*-(7-benzimidamido-9H-fluoren-2-yl)picolinimidamide dihydrochloride salt (53)**

2HCl
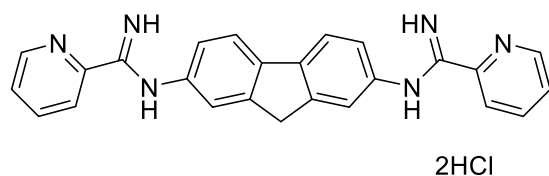
A solution of **54** (59 mg, 0.1 mmol) in dry CH_2Cl_2 (2 mL) was stirred with 4 M HCl in dioxane (2 mL) for two hours. After removal of solvents, the solid crude was crushed with Et_2O. Compound **53** was obtained as yellowish solid (33.4 mg, 83%). Spectroscopic data is consistent with literature.[10]

¹H NMR (400 MHz DMSO-*d₆*) δ 10.18 (br s, 2H), 9.39 (br s, 2H), 8.89 (d, *J* = 7.2 Hz, 2H), 8.58 (d, *J* = 8.0 Hz, 2H), 8.14−8.24 (m, 4H), 7.83−7.87 (m, 2H), 7.74 (s, 2H), 7.53 (d, *J* = 8.0 Hz, 2H), 4.08 (s, 2H),

¹³C NMR (101 MHz DMSO-*d₆*) δ 159.8, 149.7, 144.0, 143.9, 140.4, 138.5, 133.5, 128.6, 124.9, 124.2, 122.9, 121.8, 36.8

HPLC (UV) >95%.

LRMS (ESI⁺) *m/z* 405.38 [M+H].

HRMS (ESI⁺) *m/z* = 203.0943[M+2H] (Calc. for: $C_{26}H_{21}N_5$: 203.0948).

9.2. Physicochemical and biophysical experiments

9.2.1. pK_a Determination

The pK_a values were determined by UV spectroscopy in 96-well microtiter plates as described by Drs. Ríos Martinez and Dardonville.[11, 12]

The buffers used in the experiments were prepared at 25 °C in the laboratory (see http://www.biomol.net/en/tools/buffercalculator.htm for buffer recipes). The following buffers were used: pH 3.0 (phosphate buffer), pH 4.0 to 5.0 (acetate buffer), pH 5.5 to 6.8 (MES buffer), pH 7.0 to 8.2 (phosphate buffer), pH 8.5 to 10.5 (ethanolamine buffer), pH 11.0 (piperidine buffer) and pH 12.0 (phosphate buffer). The pH of the buffers was measured with a glass electrode (METTLER TOLEDO SevenCompact pH-meter: InLab® Expert Pro-ISM) at 25 ºC.

9.2.1.1. Experimental procedure

A small quantity (1–2 mg) of each compound was weighted in an eppendorf tube using a high precision analytical balance (Mettler Toledo XS105). The compound was dissolved in DMSO to a concentration of 5 mM (stock solution). The UV transparent 96-well microplate (Thermo Scientific Nunc) was loaded, each line of the plate was loaded with 196 µL of buffer solutions of increasing pH (pH ranging from 3 to 12.6). Then, 4 µL of the compound stock solutions were added to each well with a micropipette (the resulting analyte solution was premixed with the micropipette). The final concentration of the analyte compound in each well was 200 µM. One blank solution was prepared for each buffer by adding 4 µL of DMSO to 196 µL of the corresponding buffer solution (i.e., free of analyte compounds) in the well. The 96-well plate was loaded into the UV-spectrophotometer (CLARIOstar Plus apparatus), incubated at room temperature and shaken at 700 rpm for 5 min in a double orbital mode, before the reading was performed. UV-spectra scans were recorded between 200 nm and 600 nm (2 nm resolution).

It should be noted that the number and range of buffer solutions needed to determine the pK_a (e.g., every 0.2, 0.5 or 1 pH units) was adjusted depending on the compound tested. In general, a first screening with 12 buffers ranging from 3 to 12 should give an approximate

pK_a value which can be refined when repeating the experiment using buffers within ± 2 pH units of the pK_a value.

9.2.1.2. Data Analysis

In the present study we have used a similar data analysis as described by Tomsho et al.[13] for the determination of ionization constants by spectral analysis.[11] The raw UV-spectra scans were imported to the Excel program and processed as follows using the template provided in Dardonville *et al. New J. Chem.* **2017**, 41, 11016-11028.[12]

i) UV-spectra of the analyte compounds were corrected by subtracting the UV- spectra of the blank solutions;

ii) The raw scans were normalized by subtracting from the UV spectra the absorbance at which the compound does not absorb (e.g., λ = 400 or 500 nm in most cases);

iii) The spectral difference between the acid spectra and the spectra at every other pH was plotted;

iv) The wavelengths of maximum positive and negative absorbance were determined graphically from the spectral difference plot;

v) The total absorbance difference at the chosen wavelengths (that is: the sum of the absolute values of the maximum positive and negative absorbance in the spectral difference plot) was plotted against the pH.

vi) These data were imported to the Prism program and the pK_a values were worked out by non-linear regression using equation 2.

$$Absorbance\ total = \frac{\varepsilon_{HA} - \varepsilon_A * [10^{(pH - pK_a)}]}{1 + 10^{(pH - pK_a)}} * [S_t]$$

ε_{HA} and ε_A- are the extinction coefficients of the acid and base forms of the compound, respectively (i.e., the minima and maxima of the absorbance difference curve, respectively), and [S_t] is the total compound concentration.

9.2.2. DNA and oligonucleotides used in the biophysical studies

Deoxyribonucleic acid sodium salt from salmon testes (i.e., unspecific DNA containing 41.2 % GC) was purchased from Sigma Aldrich (Ref. D1626). This DNA was employed in UV–Vis and LD experiments.

Oligonucleotides used in the SPR–biosensor assays were acquired from Sigma Aldrich, with reverse-phase HPLC purification: [Biotin]CGAATTCGTCTCCGAATTCG [i.e., (AATT)] and [Biotin]CGCGCGCGTTTTCGCGCGCG [i.e., (CG)$_4$].

Oligonucleotides used in the CD and NMR experiments were purchased from Integrated DNA Technologies (IDT), with HPLC purity.

5'- CAT ATA TAT CCC CAT ATA TAT G -3' [i.e., (AT)$_4$] and 5'- CGC GCG CGT TTT CGC GCG CG-3' [i.e., (CG)$_4$].

For crystallization experiments, oligonucleotides were provided by Drs. Núria Saperas and Lourdes Campos, from Polytechnic University of Catalonia. DNA samples for crystallography must comply high purity standards. The oligonucleotides used for crystallographic essays must be in the range of 95 to 98% purity. All the oligonucleotides used were synthesized at the Genomic Platform of the Pasteur Institute as the ammonium salt on an automatic synthesizer by the phosphoramidite method and purified by gel filtration and reverse-phase HPLC. These oligonucleotides were: d(CGAATTAATTCG), d(AATAATTATT), d(CGCAAATTTGCG), d(AAATATATTT) and d(ATTAATTAAT).

9.2.3. UV spectroscopy

UV titration experiments were performed by adding aliquots of salmon testes DNA to a fixed concentration of the ligand dissolved in phosphate-buffered saline (PBS, pH = 7). After each addition, an equilibration time of 1 min was allowed and the UV spectra were recorded.

All UV-visible absorbance spectra were recorded on a Perkin Elmer Lambda 35 UV/VIS spectrometer. A quartz cell with a 1 cm path length was used for all absorbance studies. All concentrations were determined using the appropriate extinction coefficients. Phosphate buffer solutions contained 10 mM Na_2HPO_4/NaH_2PO_4 adjusted to pH = 7 were prepared using MilliQ ultrapure water. Compound stock solutions were 20 mM in DMSO.

An aliquot was transferred to an Eppendorf and diluted with 10 mM sodium phosphate buffer (pH = 7) to obtain a 25 μM solution.

The DNA at increasing ratios was then titrated into the compound solution and the corresponding absorption spectra were recorded under the same conditions. UV titration plots of each compound with increasing aliquots of salmon sperm DNA were obtained and processed with Excel.

9.2.4. Circular Dichroism Spectroscopy

Frozen samples of lyophilized DNA oligonucleotides (IDT) were removed from the fridge and warmed to room temperature over 5 min. These oligonucleotides were dissolved in 1 mL of buffer sodium phosphate 10 mM/ NaCl 100 mM pH = 7.0 (stock solution). The DNA concentration was measured using a Nanodrop 2000 spectrophotometer.

CD spectra were recorded on a Jasco 8 J-810 Spectropolarimeter using a 1-mm path-length quartz cuvette. The non-annealed oligonucleotide $(AT)_4$ or $(CG)_4$ was diluted at 60 μM concentration in a volume of 200 μL, of 10 mM NaPi/100 mM NaCl pH =7 buffer. Test compounds were prepared as 120 μM stock solutions in DMSO. Scans from 320 to 220 nm were performed with a 50 nm/min scanning speed. For each spectrum, an average of three spectra was taken and the spectrum of the corresponding buffer was subtracted for baseline correction. The melting curves were obtained by recording the change of the molar ellipticity at 270 nm in a range of temperatures from 5 ºC to 85 ºC. The temperature was controlled using a Jasco peltier, being the rate of temperature rising 40 ºC/h. The resulting melting temperatures were calculated by fitting the denaturing curves with the program Origin Pro 6.0.

9.2.5. Linear Dichroism

Salmon testes DNA was purchased from Sigma Aldrich. Phosphate buffer solutions containing 10 mM Na_2HPO_4/NaH_2PO_4 adjusted to pH = 7 were prepared using MilliQ ultrapure water. Stock solutions of the compounds were prepared in DMSO with a 20 mM concentration and dissolved with phosphate buffer. LD spectra were collected with a JASCO J-810 spectrometer at different ratios of compound to DNA at 25 ºC in 10 mM phosphate buffer. Each flow LD spectrum was acquired from 200 nm to 400 nm and

reflects the average of two scans. A Couette flow cell was used for sample orientation for all LD studies. The DNA solutions were 378.8 µM with a compound to DNA base pair ratio of 1 to 5.

9.2.6. Surface plasmon resonance (SPR-biosensor experiments)

The oligomers and compounds from series **1** were dissolved directly in 10 mM HEPES, 150 mM NaCl, pH 7.4. Compounds from series **2** and **3** were dissolved in DMSO and diluted with 10 mM HEPES, 150 mM NaCl, pH 7.4.

SPR binding experiments were performed at 25 °C with a Biacore X100 apparatus (Biacore GE). HEPES 1 buffer containing 10 mM HEPES, 3 mM EDTA, 200 mM NaCl, and surfactant P-20 at 0.05% (v/v) pH 7.4. The DNA hairpins were immobilized on a streptavidin-derivatized gold chip (SA chip from Biacore) by injection of a 25 nM hairpin DNA solution with a flow rate of 1 µL/min until ~400 RU were reached. Flow cell 1 was used as reference while flow cell 2 was immobilized with the hairpins in different chips. Direct binding was measured by injection of increasing concentrations of each compound over the immobilized DNA surfaces at a flow rate of 50 µL/min for a period of 60 s followed by a dissociation period of 120 s. Regeneration of the surface was made with NaCl 200 mM/NaOH 10 mM using a flow rate of 10 µL/min during 30 s. The binding affinity was determined by fitting the results to a two-sites binding model according to the equation:

$$r = \frac{(K_1 C_f + 2 K_1 K_2 C_f^2)}{(1 + K_1 C_f + K_1 K_2 C_f^2)}$$

where r is the moles of bound compound per mole of DNA hairpin duplex, C_f is the free concentration at the equilibrium, and K_1 and K_2 the microscopic binding constants.

The regeneration conditions were similar to the binding experiments described above. The binding responses (RU) at steady state were averaged and normalized by setting the RU with the compound alone as 100% binding to DNA and the RU with saturation by the inhibitor as 0%.

9.2.7. Crystallographic studies

These studies were carried out following the protocol previously described by Campos et al.[14] A pre-incubated DNA-compound complex in sodium cacodylate buffer pH 6.5 was added to the drop with final concentrations of 0.2 mM DNA duplex, 0.4 mM compound, 25 mM sodium cacodylate buffer pH 6.5, 10 mM salt (Sigma-Aldrich), 0.1 mM spermine (Fluka) and 5% 2-methyl-2,4-pentanediol (MPD; Sigma-Aldrich); equilibrated against a 20% MPD reservoir. MPD acts both as a precipitant and a cryoprotectant. Once the drops were prepared, and according to observation of the crystals the concentration of the reservoir was increased gradually up to 50% MPD. As crystals were growing and MPD was increased, the samples were moved to 12, 10, 8, 4 and 0 ºC, to avoid degradation.[14, 15] Finally, the crystals obtained with the tested compounds were flash-frozen in the cold room (4 ºC) and stored in liquid Nitrogen.

9.2.8. Nuclear magnetic resonance studies

All the ^{1}H-NMR spectra were acquired in Bruker spectrometers. ^{1}H NMR spectra were recorded in spectrometers operating at 600 and 800 MHz, equipped with cryoprobes. All spectra were processed with TOPSPIN 2.1 software.

a) Titration experiments with **3a** and oligonucleotide (AT)$_4$

NMR samples of interacting compound was prepared at 400 µM in buffer 10 mM NaPi/ 100 mM NaCl pH 7.1, containing 10% D$_2$O. ^{1}D-NMR spectra were acquired at 5 ºC and 25 ºC before the addition of the oligo. (AT)$_4$ oligonucleotide was added to the hit sample from non-annealed 1.5 mM stock solutions in 15 mM NaPi pH 7 buffer. Two additions of the oligo were performed reaching oligo:compound ratios of 1:0, 1:0.125, 1:0.5, 1:1 and 1:2, and ^{1}D NMR spectra were recorded after each addition.

9.3. Biological and biochemical evaluation

As indicated in Chapter 5, the biological assays were perfomed in collaboration with Dr. Francisco Gamarro (IPLN-CSIC) for evaluation against *L. donovani*, Dr. De Koning (U. of Glasgow) for evaluation against *T. brucei* and Drs. Gómez Barrio, Fonseca and Ibáñez (UCM) for evaluation against *T. cruzi* and *T. vaginalis*.

9.3.1. *In vitro* Activity against *Leishmania donovani*

9.3.1.1. *Leishmania* culture conditions

The *L. donovani* promastigotes (MHOM/ET/67/HU3) used in this study were grown at 28°C in RPMI 1640-modified medium (Invitrogen) supplemented with 20% or 10% heat-inactivated fetal bovine serum (HIFBS, Invitrogen).

9.3.1.2. Promastigote and amastigote sensitivity testing *in vitro*

The assays against *L. donovani* were performed following the reported protocol as described by Manzano *et al*.[16]: The sensitivity of *Leishmania* promastigote lines to the different compounds was determined after incubation for 72 h at 28 °C in the presence of increasing concentrations of the compounds. The concentration of the compound required to inhibit 50% of parasite growth (EC_{50}) was calculated using the MTT colorimetric assay, as described previously.[17] For the intracellular *Leishmania* amastigotes assays, stationary-phase promastigotes were used to infect macrophage-differentiated THP-1 cells at a macrophage/ parasite ratio of 1:10, as described previously.[17] After overnight infection at 35 °C with 5% CO_2 in RPMI 1640 medium plus 5% hiFBS, extracellular parasites were removed by washing with serum-free medium. Infected macrophages were incubated with different concentrations of compounds in RPMI 1640 medium plus 10% hiFBS at 37 °C and a 5% CO_2 atmosphere, for 96 h. Following incubation, samples were fixed for 20 min at 4 °C with 2.5% paraformaldehyde in PBS buffer and then permeabilized with 0.1% TX100 in PBS for 10 min. Infection level and mean number of intracellular parasites/cell were detected by nuclear staining with Prolong-Gold antifade agent with DAPI (Invitrogen). The percentage of infection and mean number of amastigotes per infected macrophage were determined in 200 macrophages/well. The median effective concentration (EC_{50}) values were calculated by sigmoidal analysis using MicroSoftxlfit (ID Business Solution). Three separate experiments were performed *in vitro*.

9.3.1.3. Cytotoxicity against human myelomonocytic cell line

Human myelomonocytic cell line THP-1 was grown in RPMI-1640 supplemented with 10% heat-inactivated fetal bovine serum (hiFBS), 2 mM glutamate, 100 U/mL penicillin, and 100 mg/ mL streptomycin at 37 °C and 5% CO_2. 5×10^5 THP-1 cells per well in 24-

well plates were differentiated to macrophages with 20 ng/mL of PMA treatment for 48 h followed by 24 h of culture in complete fresh medium.

The cellular toxicity of all compounds was determined using the colorimetric MTT-based assay,[18] as described for *Leishmania* promastigotes, except for the incubation temperature, which was 37 °C in this case.

9.3.2. *In vitro* Activity against *Trypanosoma brucei* Lister 427 and multidrug resistant strain B48

The assays against *T. brucei* were performed following the reported protocol of De Koning *et al.*[19]: For each test compound a doubling dilution series was prepared in HMI9+10% fetal bovine serum (FBS) over two rows of a 96 well- plate, resulting in 23 concentrations as the last well received only 100 µL HMI9/FBS as drug-free control. An equal volume (100 µL) of HMI9/FBS containing 2000 bloodstream forms of *Trypanosoma brucei brucei* strain Lister 427 or B48 was added to each well. For each test compound the highest concentration was 200 µM whereas the lowest concentration was 4.8×10^{-5} µM. Plates were incubated for 70 h at 37 °C/5% CO_2 before the further addition of 20 µL of 125 µg/mL resazurin sodium salt (Sigma, St Louis, MO) in sterile phosphate-buffered saline (PBS, pH = 7.4) to each well, followed by a further incubation of 24 h.

Fluorescence was determined in a FLUOstar Optima plate reader (BMG Labtech, Durham, NC) at λ_{exc} 536 nm and λ_{em} 588 nm, and plotted to an equation for a sigmoid curve with variable slope using Prism 5.0 (GraphPad) for the determination of EC_{50} values. All EC_{50} values were determined at least 3 – 4 times independently.

9.3.2.1. Cytotoxicity against human embryonic kidney cells

Human embryonic kidney cells (HEK) were maintained and used for Alamar Blue drug sensitivity assays as described, but the Alamar Blue protocol was adapted from that described previously[20] to allow longer incubation times. Briefly, wells of a 96-well microtiter plate were each seeded with 3×10^4 cells in 100 µL DMEM and allowed to adhere for 24 h. Doubling drug dilutions were then added (100 µL per well), resulting in a maximum concentration of 200 µM test compound, and after 30 h incubation 10 mL

resazurin solution (125 µg/mL in PBS) was added; the plate was read and analysed after another 24 h incubation as described above for trypanocidal activity.

9.3.3. *In vitro* Activity against *Trypanosoma cruzi*

The assays against *T. brucei* were performed following the reported protocol of Fonseca *et al*.[21, 22]

9.3.3.1. Source of compounds

Stock solutions of the pulverized compounds were prepared in DMSO (Panreac) to obtain concentrations ranging from 256 µM to 1 µM when they finally dissolved in each media. In fact, final DMSO concentration in cultures never exceeded 0.2% (v/v).[23] Benznidazole (raw product, kindly provided by LAFEPE, Pernambuco, Brazil) was included in all the experiments as reference drug.

9.3.3.2. Biological procedures

9.3.3.2.1. *Mammalian cell line*

L929 murine fibroblasts were grown in plastic culture flasks, using Minimal Essential Medium (MEM) without phenol-red (Sigma), supplemented with 10% heat-inactivated foetal bovine serum (FBS) (Gibco) (30 min., 56 ºC) and antibiotics (penicillin 100 U/mL and streptomycin 100 µg/mL). Cell cultures were maintained in a humidified 5% CO_2 atmosphere at 37 ºC and subpassaged once a week.

9.3.3.2.2. *Parasites*

Cultures of *Trypanosoma cruzi* epimastigotes of the CL Brener strain stably transfected with *Escherichia coli* β-galactosidase gene *(lacZ)*[24, 25], were grown at 28 ºC in liver infusion tryptose (LIT) medium, supplemented with 10% heat-inactivated FBS and axenized with penicillin (100 U/mL) and streptomycin (100 µg/mL). Parasites were continuously maintained in logarithmic growth by weekly passages.

9.3.3.2.3.   *Cell infection*

Axenic cultures of epimastigotes reaching their stationary phase of growth (14 day-old cultures) were used to infect non-confluent monolayers of L929 fibroblasts to obtain tissue culture derived trypomastigotes (TCT).[26] After 24 h at 33 ºC in a humidified 5% CO_2 atmosphere, the infected cultures were washed with phosphate buffer saline (PBS) to removed non-penetrated epimastigotes. TCT were harvested from the supernatant of the cultures after one week of incubation in these conditions of temperature and humidity.

9.3.3.2.4.   *Epimastigote susceptibility assay*

Log-phase cultures of epimastigotes were seeded in 96-well microplates at a density of 2.5 $\times 10^{27}$ parasites/mL in a final volume of 200 μL/well and then, stock solutions of the compounds added to the cultures. Growth, medium and drug controls were also included in all the plates. Each concentration was assayed by triplicate. The plates were incubated at 28 ºC for 72 h. Afterwards, 50 μL of the β-galactosidase substrate chlorophenol red β-D-galactopyranoside (CPRG) (Roche) in 0.9% Triton X-100 (Panreac) solution were added to each well (200 μM, pH 7.4) and the plates incubated at 37 ºC for 3 h. Percentages of anti-epimastigote activity (%AE) were obtained by reading absorbance at 595 nm and calculated as follows:

$$\%AE = 100 - [(A_E - A_{EM}) / (A_C - A_M)] \times 100$$

where A_E, A_{EM}, A_C and A_M represent the mean value of absorbance for the experimental wells, compound in medium, growth control wells and medium alone, respectively.

IC_{50} (concentration that inhibits the 50% of epimastigote growth) was estimated to each compound by plotting drug concentrations *versus* percentages of anti-epimastigote activity.

9.3.3.2.5.   *Unspecific cytotoxicity assay*

Unspecific cytotoxicity against L929 murine fibroblasts was evaluated by measuring the metabolic cell function in presence of the redox indicator resazurin (Sigma).[5] Briefly, 100 μL of MEM medium containing 15×10^3 cells were seeded per well in 96-well plates and

incubated for 3 h at 37 ºC in a humidified 5% CO_2 atmosphere to allow their attachment. Then, the medium was replaced by 200 μL of compound solutions in fresh medium as previously cited. Each concentration was evaluated by triplicate. Growth, medium and drug controls were also included in each plate. The cells were exposed to the compounds for 48 h at 37 ºC with 5% CO_2. Afterwards, 20 μL of a resazurin in PBS solution (2 mM, pH 7) were added to each well and the plates incubated at the same conditions for another 3 h. Fluorescence intensities were finally read at 530 nm of excitation and 590 nm of emission. Unspecific cytotoxicity (%C) was calculated with the following formula:

$$C = 100 - [(FI_E-FI_{EM}) / (FI_C-FI_M)] \times 100$$

where FI_E, FI_{EM}, FI_C and FI_M are the mean values of fluorescence intensity for the experimental wells, compound in medium, growth control wells and only medium, respectively.

LC_{50} (concentration that produces 50% of cellular inhibition) was estimated to each compound by plotting drug concentrations *versus* percentages of cytotoxicity.

9.3.3.2.6.   *Amastigote susceptibility assay*

L929 fibroblasts/well were seeded in 48-well plates and after their attachment, infected with TCT in a ratio 1:6 (cell: parasite) and incubated at 33 ºC and 5% CO_2 overnight. After the infection, experimental wells were washed with PBS to eliminate non-penetrated TCT and solutions of each compound in fresh medium added in a final volume of 450 μL/well. Each concentration was evaluated by triplicate. Infection, growth, medium and drug controls were also included in each plate. The plates were incubated for 7 days in similar conditions of temperature and humidity and then, 50 μL of a CPRG solution in 3% Triton X-100 (pH 7.4) added to each well in a final concentration of 400 μM. Subsequent to 3 h of incubation at 37 ºC, absorbance was read at 595 nm and percentages of antiamastigote activity (%AA) estimated as follows:

$$\%AA = 100 - [(A_E - A_{EM}) / (A_{CI} - A_M)] \times 100$$

where each value represents the mean absorbance of the experimental wells (A_E), compound in medium (A_{EM}), control of infection (A_{CI}), and only medium (A_M),

respectively. Absorbance of non-infected wells (only L929 cells) was subtracted to both groups (experimental and control of infection) as background.

IC$_{50}$ (concentration that inhibits the 50% of amastigote proliferation) was estimated to each compound by plotting drug concentrations *versus* percentages of anti-amastigote activity.

9.3.4. *In vitro Activity against Trichomonas vaginalis*

The assays against *T. vaginalis* were performed following the reported protocol of Ibáñez *et al*.[28, 29]

9.3.4.1. *T. vaginalis culture.*

The *in vitro* assays were conducted with two different isolates from the American Type Culture Collection (ATCC, Maryland, USA): JH31A#4 (metronidazole-sensitive) and IR78 (metronidazole-resistant). Trophozoites were cultivated in TYM (Tripticase-Yeast-Maltose) medium supplemented with 10% fetal bovine serum (FBS) and 5% of antibiotic solution (100 IU penicillin and 100 mg/mL streptomycin), in a humified chamber at 37 °C and 5% CO$_2$.

9.3.4.2. *Mammalian cell cultures.*

The cellular line employed for the unspecific cytotoxic assays were Vero CCL-81 (ATCC, Maryland, USA). The cells were cultured in RPMI medium (Sigma Aldrich), supplemented with 10% FBS and antibiotics solution (100 IU penicillin and 100 µg/mL streptomycin) in a humidified 95% air/5% CO$_2$ atmosphere at 37 °C.

9.3.4.3. *Trophozoites susceptibility assays.*

Initially, the studied compounds were evaluated against the sensitive isolate JH31A#4. Stock solutions of the studied compounds were prepared in DMSO and added to glass tubes containing log-phase growth cultures after 5 h of seeding 10^5 trophozoites/mL, to achieve 9.37 – 300 µM final concentrations of the products. Final concentration of DMSO was always <0.2% v/v. The biological activity was determined after 24 h of incubation at 37 °C by fluorometric determination using resazurin (Sigma Aldrich) as redox dye as

previously described by Ibañez and col.[28] Metronidazole (Sigma Aldrich) at 25 µM concentration was used as the reference drug.

Trichomonacidal activity against the resistant isolate IR78 was evaluated only for compounds showing a relevant activity against JH31A#4 isolate and absence of unspecific cytotoxic effect against Vero cells.[29]

The experiments were performed at least two times in triplicate. EC_{50} values and the 95% confidence limits were calculated by probit analysis (SPSS v20, IBM).

9.3.4.4. *Unspecific cytotoxicity assays.*

Vero cells were seeded (50,000 cells/well) in 96-well flat-bottom microplates (Nunc) with 100 µL of medium. After cell attachment for 6 h at 37 °C, 100 µL of medium containing the studied products were added. The unspecific toxicity was determined after 24 h of incubation with the compounds. Resazurin (1 mM stock solution) was used as redox dye. After 3 h of incubation, fluorescence was measure in a fluorimeter (Infinite 200, Tecan) (λ_{exc} 535 nm, λ_{em} 590 nm) following a method previously published by Ibañez and col.[29]

Each concentration was assayed per triplicate and in two independent assays. The concentration causing 50% of Vero cells growth inhibition (EC_{50}) and the 95% confidence limits was determined by probit analysis (SPPS v20, IBM).

9.3.5. *Microsomal stability of 3a*

Commercially available compounds were used for these experiments. Benzamidine (Alfa Aesar), benzamidoxime (Thermo Fisher Scientific), and NADH (Sigma Aldrich). The employed enzymatic fractions were obtained from human liver microsomes and human liver mitochondrias. These assays were performed by Dr. Tomás Herraiz at the Institute of Food Science, Technology and Nutrition (ICTAN - CSIC).

9.3.5.1. *Procedures:*

Metabolic and Microsomal stability of **3a** toward metabolism by cytochrome P450 (Phase I metabolism) and Uridine Glucuronosyl-Transfererase (UGT) (Phase II metabolism) was studied in presence of the cofactors NADPH and UDPGA, respectively. Incubation media (100–400 µL, final reaction volume) containing 1 mg/mL protein of human liver microsomes (HLM) (Gentest; Corning) or mouse (CD-1) liver microsomes, in 80 mM potassium phosphate buffer (pH = 7.4) and NADPH (1 mM) were added with **3a** (5 µM final concentration) or diclofenac (25 µM) and incubated in a water bath at 37 ºC during time 0–2 hours.

On the other hand, incubation media (100 µL of final reaction volume) containing human or mouse liver microsomes (1 mg/mL protein) or mouse liver microsomes (1 mg/mL protein) in 80 mM potassium phosphate buffer (pH = 7.4) were added with $MgCl_2$ 4 mM, UDPGA (2 mM), and sonicated for 3 minutes with the tubes placed in an ice-bath, and subsequently added with **3a** (5 µM) and incubated at 37 ºC for 1 hour. The stability in serum was assessed with fractions of 100 µL (final reaction volume) with 5 µM of **3a** and 20 µL of human serum (Sigma-Aldrich) and incubated at 37 ºC for 1 hour**.**

9.3.5.2. *Sampling:*

Aliquots (60–100 µL) were withdrawn at 0, 15, 30, 60 or 120 minutes and added to 60–100 µL of acetonitrile, vortexed and centrifuged at 10000 rpm. Controls without microsomal fraction and/or cofactors were also carried out. A solution of the compound **3a** was prepared in water.

9.3.5.3. *Analysis:*

An aliquot of supernatant (20 µL) was analysed by RP-HPLC (Agilent 1100 apparatus with a 1100 diode array detector (DAD) using a reversed phase 3.9 × 150 mm, 4 µm, Nova-pak C18 column (Waters, Milford, MA, USA) under the following chromatographic conditions: eluent A: 50 mM ammonium phosphate buffer (pH = 3) and eluent B: 20 % A in acetonitrile. A linear gradient was used from 0 to 32 % B in 8 minutes, and then 100% B for 12 minutes. Under these conditions **3a** eluted at 6.5 minutes. Chromatographic areas

of **3a** and diclofenac were determined by absorbance at 280 nm. Assays were carried out at least in duplicate.

9.1. References

1. Furniss, B. S. H., Anthony J.; Smith, Peter W.G.; Tatchell, Austin R. *Vogel's Textbook of Practical Organic Chemistry*. New York, N.Y. 10158, 1989; p 1513.

2. Azzarito, V.; Prabhakaran, P.; Bartlett, A. I.; Murphy, N. S.; Hardie, M. J.; Kilner, C. A.; Edwards, T. A.; Warriner, S. L.; Wilson, A. J. 2-O-Alkylated para-benzamide α-helix mimetics: the role of scaffold curvature. *Org. Biomol. Chem.* **2012,** 10, 6469-6472.

3. Nué Martínez, J. J.; Alkorta, I.; Dardonville, C. High yield synthesis of trans-azoxybenzene versus 2-isopropoxy-4-nitrobenzoic acid: influence of temperature and base concentration. *Arkivoc* **2021,** viii, 265-276.

4. Ríos Martínez, C. H. Synthesis and study of new antiprotozoal agents derivatives of dicationic compounds for the treatment of Human African Trypanosomiasis. PhD Thesis, Universidad Complutense de Madrid, Madrid, Spain, 2013.

5. Mundla, S. R.; Wilson, L. J.; Klopfenstein, S. R.; L. Seibel, W.; Nikolaides, N. N. A novel method for the efficient synthesis of 2-arylamino-2-imidazolines. *Tetrahedron Lett.* **2000,** 41, 6563-6566.

6. Dardonville, C.; Goya, P.; Rozas, I.; Alsasua, A.; Martín, M. I.; Borrego, M. J. New aromatic iminoimidazolidine derivatives as α₁-adrenoceptor antagonists: a novel synthetic approach and pharmacological activity. *Bioorg. Med. Chem.* **2000,** 8, 1567-1577.

7. Ríos Martínez, C.; Miller, F.; Ganeshamoorthy, K.; Glacial, F.; Kaiser, M.; de Koning, H.; Eze, A.; Lagartera, L.; Herraiz, T.; Dardonville, C. A new non-polar *N*-hydroxy imidazoline lead compound with improved activity in a murine model of late stage *T. b. brucei* infection is not cross-resistant with diamidines. *Antimicrob. Agents Chemother.* **2015,** 59, 890-904.

8. Ríos Martínez, C. H.; Miller, F.; Ganeshamoorthy, K.; Glacial, F.; Kaiser, M.; de Koning, H. P.; Eze, A. A.; Lagartera, L.; Herraiz, T.; Dardonville, C. A new nonpolar *N*-hydroxy imidazoline lead compound with improved activity in a

murine model of late-stage *Trypanosoma brucei brucei* infection is not cross-resistant with diamidines. *Antimicrob. Agents Chemother.* **2015,** 59, 890-904.

9. Stephens, C. E.; Tanious, F.; Kim, S.; Wilson, W. D.; Schell, W. A.; Perfect, J. R.; Franzblau, S. G.; Boykin, D. W. Diguanidino and "Reversed" Diamidino 2,5-Diarylfurans as Antimicrobial Agents. *J. Med. Chem.* **2001,** 44, 1741-1748.

10. Arafa, R. K.; Brun, R.; Wenzler, T.; Tanious, F. A.; Wilson, W. D.; Stephens, C. E.; Boykin, D. W. Synthesis, DNA Affinity, and Antiprotozoal Activity of Fused Ring Dicationic Compounds and Their Prodrugs. *J. Med. Chem.* **2005,** 48, 5480-5488.

11. Rios Martinez, C. H.; Dardonville, C. Rapid Determination of Ionization Constants (pK_a) by UV Spectroscopy Using 96-Well Microtiter Plates. *ACS Med. Chem. Lett.* **2013,** 4, 142-145.

12. Dardonville, C.; Caine, B. A.; Navarro de la Fuente, M.; Martin Herranz, G.; Corrales Mariblanca, B.; Popelier, P. L. A. Substituent effects on the basicity (pK(a)) of aryl guanidines and 2-(arylimino) imidazolidines: correlations of pH-metric and UV-metric values with predictions from gas-phase ab initio bond lengths. *New J. Chem.* **2017,** 41, 11016-11028.

13. Tomsho, J. W.; Pal, A.; Hall, D. G.; Benkovic, S. J. Ring Structure and Aromatic Substituent Effects on the pKa of the Benzoxaborole Pharmacophore. *ACS Med. Chem. Lett.* **2012,** 3, 48-52.

14. Campos, L.; Valls, N.; Urpí, L.; Gouyette, C.; Sanmartín, T.; Richter, M.; Alechaga, E.; Santaolalla, A.; Baldini, R.; Creixell, M.; Ciurans, R.; Skokan, P.; Pous, J.; Subirana, J. A. Overview of the Structure of All-AT Oligonucleotides: Organization in Helices and Packing Interactions. *Biophys. J.* **2006,** 91, 892-903.

15. Millan, C. R.; Acosta-Reyes, F. J.; Lagartera, L.; Ebiloma, G. U.; Lemgruber, L.; Nué Martinez, J. J.; Saperas, N.; Dardonville, C.; de Koning, H. P.; Campos, J. L. Functional and structural analysis of AT-specific minor groove binders that disrupt DNA-protein interactions and cause disintegration of the *Trypanosoma brucei* kinetoplast. *Nucleic Acid Res.* **2017,** 45, 8378-8391.

16. Manzano, J. I.; Cueto-Diaz, E. J.; Olias-Molero, A. I.; Perea, A.; Herraiz, T.; Torrado, J. J.; Alunda, J. M.; Gamarro, F.; Dardonville, C. Discovery and Pharmacological Studies of 4-Hydroxyphenyl-Derived Phosphonium Salts

Active in a Mouse Model of Visceral Leishmaniasis. *J. Med. Chem.* **2019,** 62, 10664-10675.

17. Kennedy, M. L.; Cortés-Selva, F.; Pérez-Victoria, J. M.; Jiménez, I. A.; González, A. G.; Muñoz, O. M.; Gamarro, F.; Castanys, S.; Ravelo, A. G. Chemosensitization of a Multidrug-Resistant *Leishmania tropica* Line by New Sesquiterpenes from *Maytenus magellanica* and *Maytenus chubutensis*. *J. Med. Chem.* **2001,** 44, 4668-4676.

18. Gómez-Pérez, V.; Manzano, J. I.; García-Hernández, R.; Castanys, S.; Campos Rosa, J. M.; Gamarro, F. 4-Amino bispyridinium derivatives as novel antileishmanial Agents. *Antimicrob. Agents Chemother.* **2014,** 58, 4103-4112.

19. Ríos Martínez, C. H.; Nué Martinez, J. J.; Ebiloma, G. U.; de Koning, H. P.; Alkorta, I.; Dardonville, C. Lowering the pK_a of a bisimidazoline lead with halogen atoms results in improved activity and selectivity against *Trypanosoma brucei in vitro*. *Eur. J. Med. Chem.* **2015,** 101, 806-817.

20. Rodenko, B.; van der Burg Alida, M.; Wanner Martin, J.; Kaiser, M.; Brun, R.; Gould, M.; de Koning Harry, P.; Koomen, G.-J. 2,N^6-Disubstituted Adenosine Analogs with Antitrypanosomal and Antimalarial Activities. *Antimicrob. Agents Chemother.* **2007,** 51, 3796-3802.

21. Fonseca-Berzal, C.; Arán, V. J.; Escario, J. A.; Gómez-Barrio, A. Experimental models in Chagas disease: a review of the methodologies applied for screening compounds against *Trypanosoma cruzi*. *Parasitol. Res.* **2018,** 117, 3367-3380.

22. Fonseca-Berzal, C.; Merchán Arenas, D. R.; Romero Bohórquez, A. R.; Escario, J. A.; Kouznetsov, V. V.; Gómez-Barrio, A. Selective activity of 2,4-diaryl-1,2,3,4-tetrahydroquinolines on *Trypanosoma cruzi* epimastigotes and amastigotes expressing β-galactosidase. *Bioorg. Med. Chem. Lett.* **2013,** 23, 4851-4856.

23. Rolón, M.; Seco, E. M.; Vega, C.; Nogal, J. J.; Escario, J. A.; Gómez-Barrio, A.; Malpartida, F. Selective activity of polyene macrolides produced by genetically modified Streptomyces on *Trypanosoma cruzi*. *Int. J. Antimicrob. Agents* **2006,** 28, 104-109.

24. Buckner, F. S.; Verlinde, C. L.; La Flamme, A. C.; Van Voorhis, W. C. Efficient technique for screening drugs for activity against *Trypanosoma cruzi* using

parasites expressing beta-galactosidase. *Antimicrob. Agents Chemother.* **1996,** 40, 2592-2597.

25.	Le-Senne, A.; Muelas-Serrano, S.; Fernández-Portillo, C.; Escario, J. A.; Gómez-Barrio, A. Biological characterization of a beta-galactosidase expressing clone of *Trypanosoma cruzi* CL strain. *Mem. Inst. Oswaldo Cruz* **2002,** 97, 1101-1105.

26.	Saraiva, J.; Vega, C.; Rolon, M.; da Silva, R.; e Silva, M. L. A.; Donate, P. M.; Bastos, J. K.; Gomez-Barrio, A.; de Albuquerque, S. *In vitro* and *in vivo* activity of lignan lactones derivatives against *Trypanosoma cruzi*. *Parasitol. Res.* **2007,** 100, 791-795.

27.	Rolón, M.; Vega, C.; Escario, J. A.; Gómez-Barrio, A. Development of resazurin microtiter assay for drug sensibility testing of *Trypanosoma cruzi* epimastigotes. *Parasitol. Res.* **2006,** 99, 103-107.

28.	Ibáñez Escribano, A.; Meneses Marcel, A.; Machado Tugores, Y.; Nogal Ruiz, J. J.; Arán Redó, V. J.; Escario García-Trevijano, J. A.; Gómez Barrio, A. Validation of a modified fluorimetric assay for the screening of trichomonacidal drugs. *Mem. Inst. Oswaldo Cruz* **2012,** 107, 637-643.

29.	Ibáñez-Escribano, A.; Meneses-Marcel, A.; Marrero-Ponce, Y.; Nogal-Ruiz, J. J.; Arán, V. J.; Gómez-Barrio, A.; Escario, J. A. A sequential procedure for rapid and accurate identification of putative trichomonacidal agents. *J. Microbiol. Methods* **2014,** 105, 162-167.

APPENDIX 1

Appendix 1

UV-Vis spectra of compounds from series **2**

Compound 2c
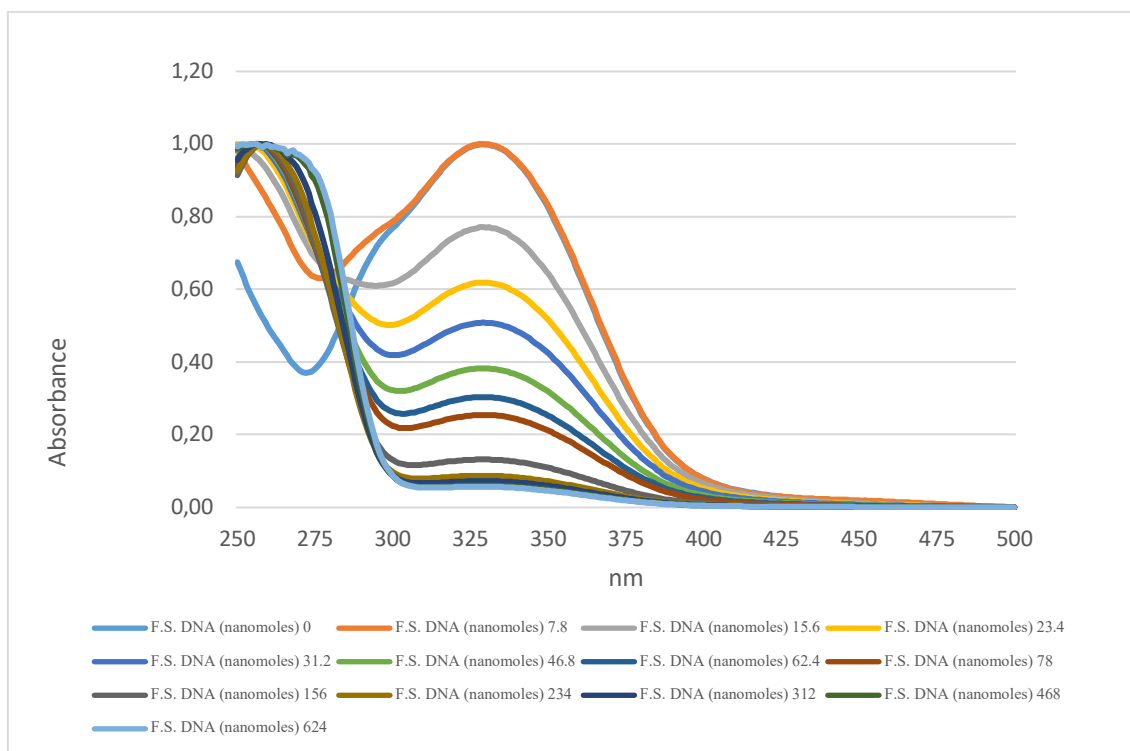
Compound 2d
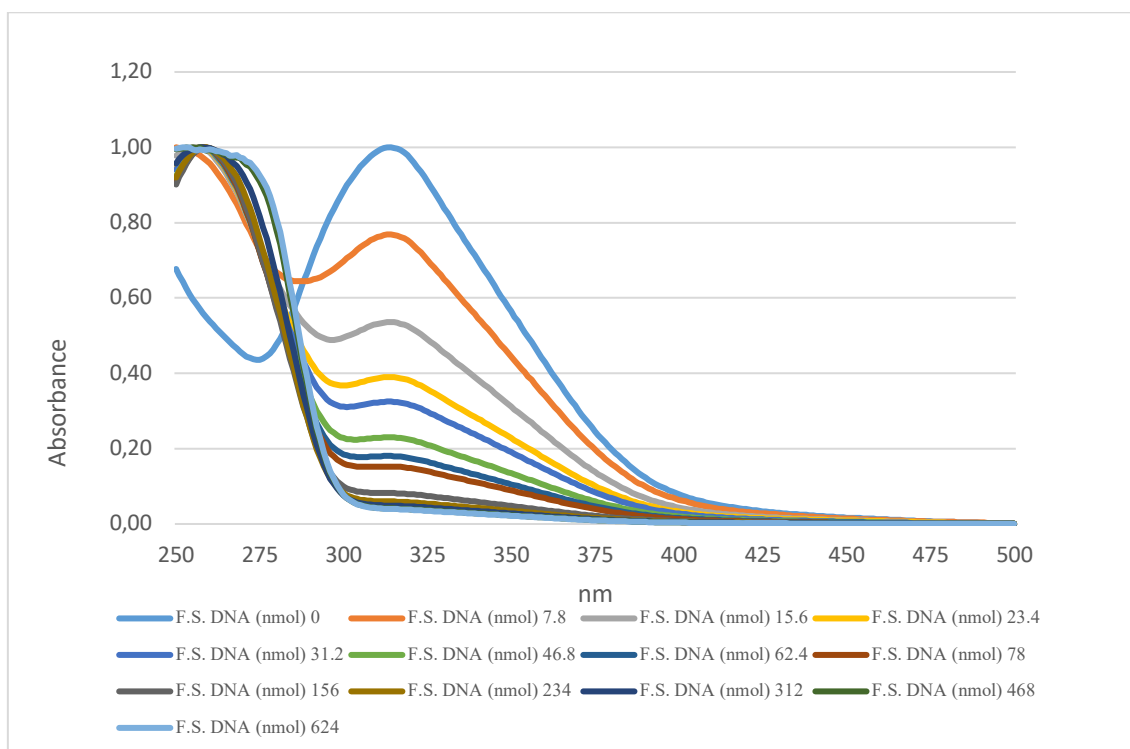
Compound 2e
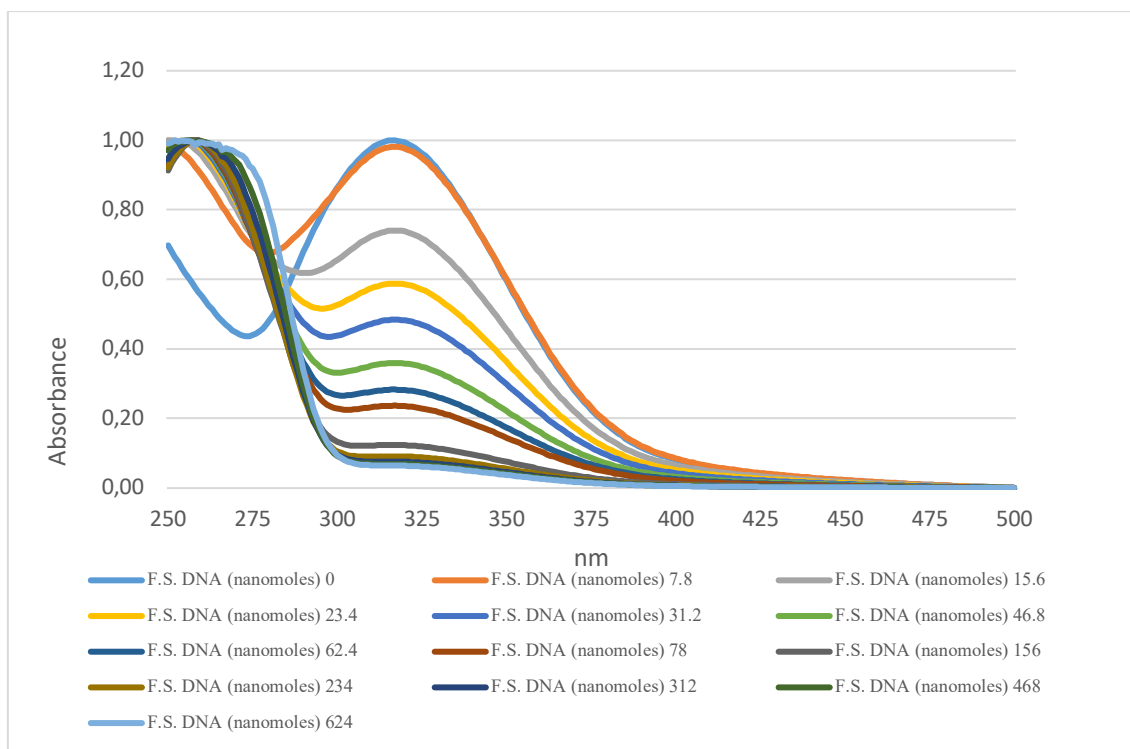
Compound 2h
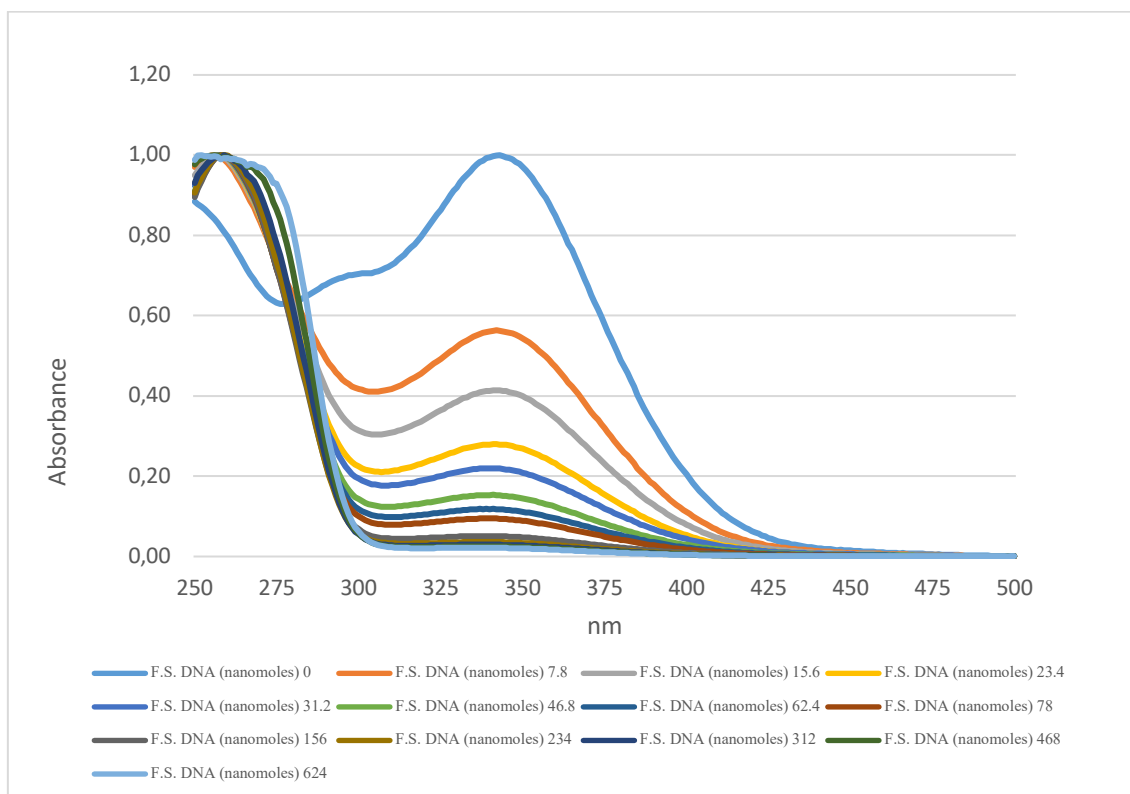
Compound 30
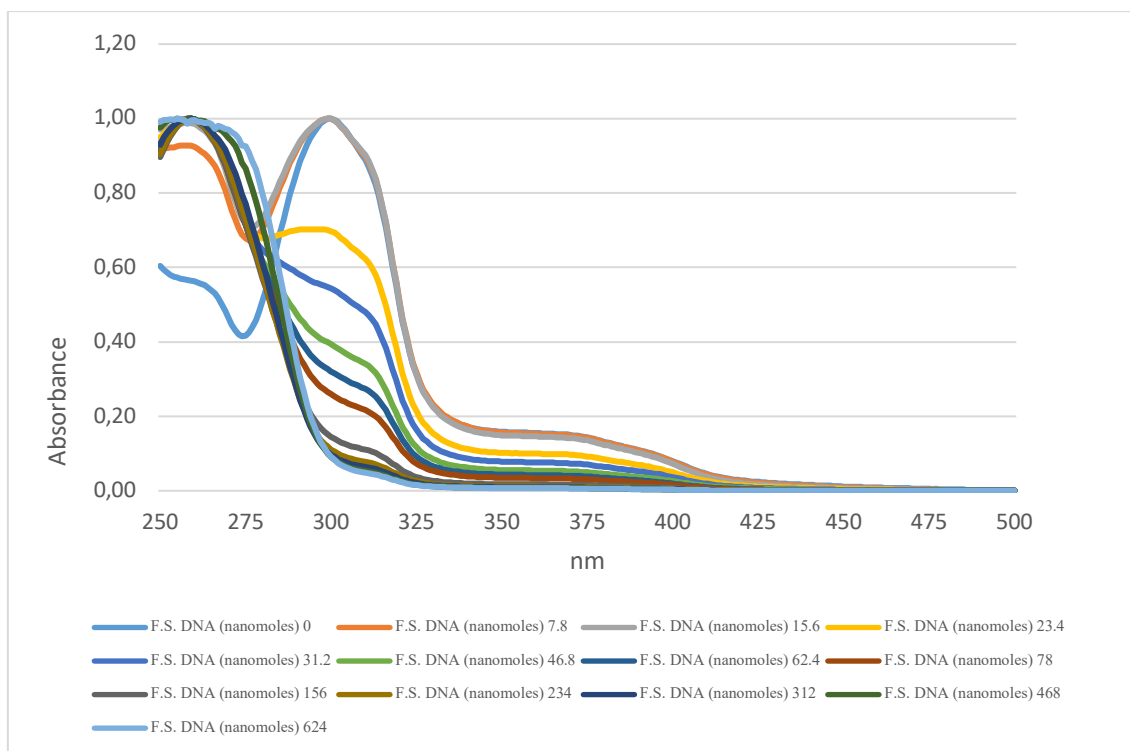
Compound 31
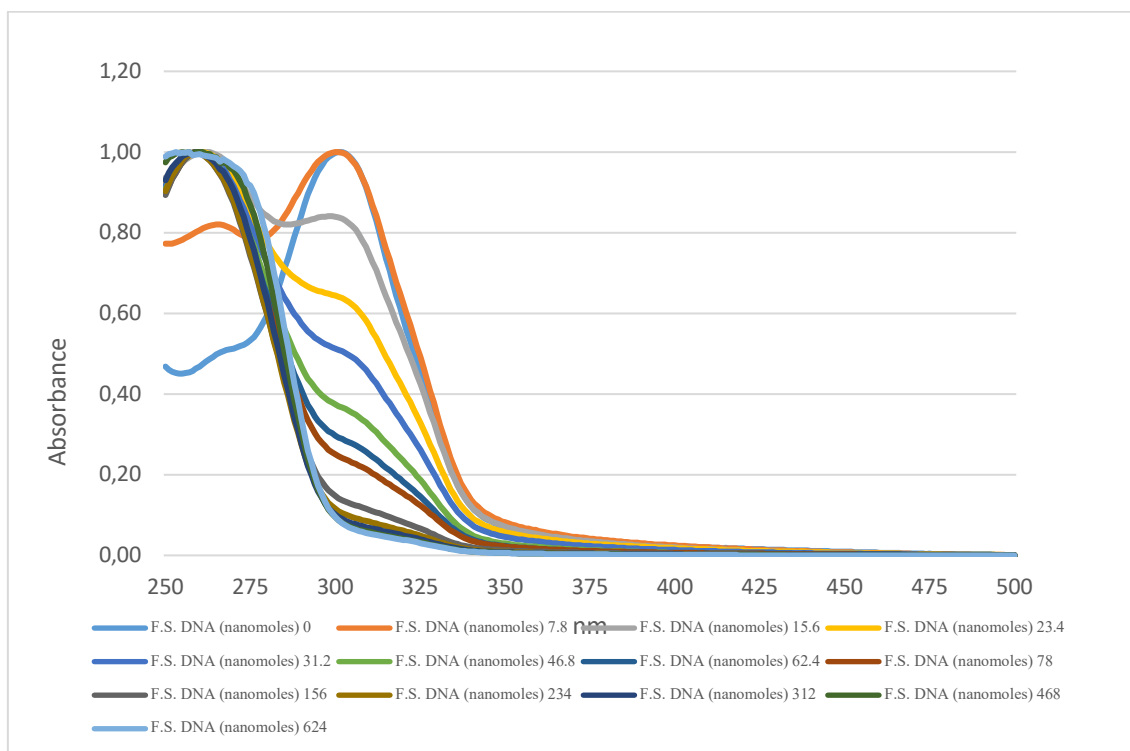
Compound 34
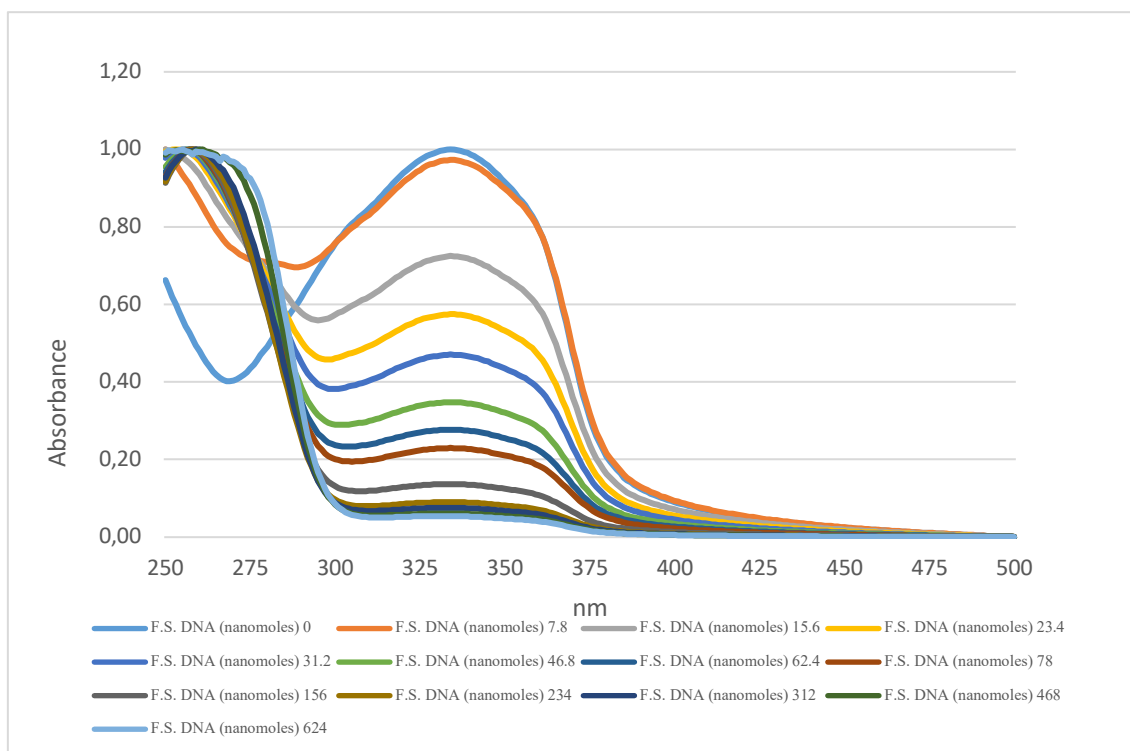
APPENDIX 2

Appendix 2

Circular Dichroism spectra of compounds from series **1.**
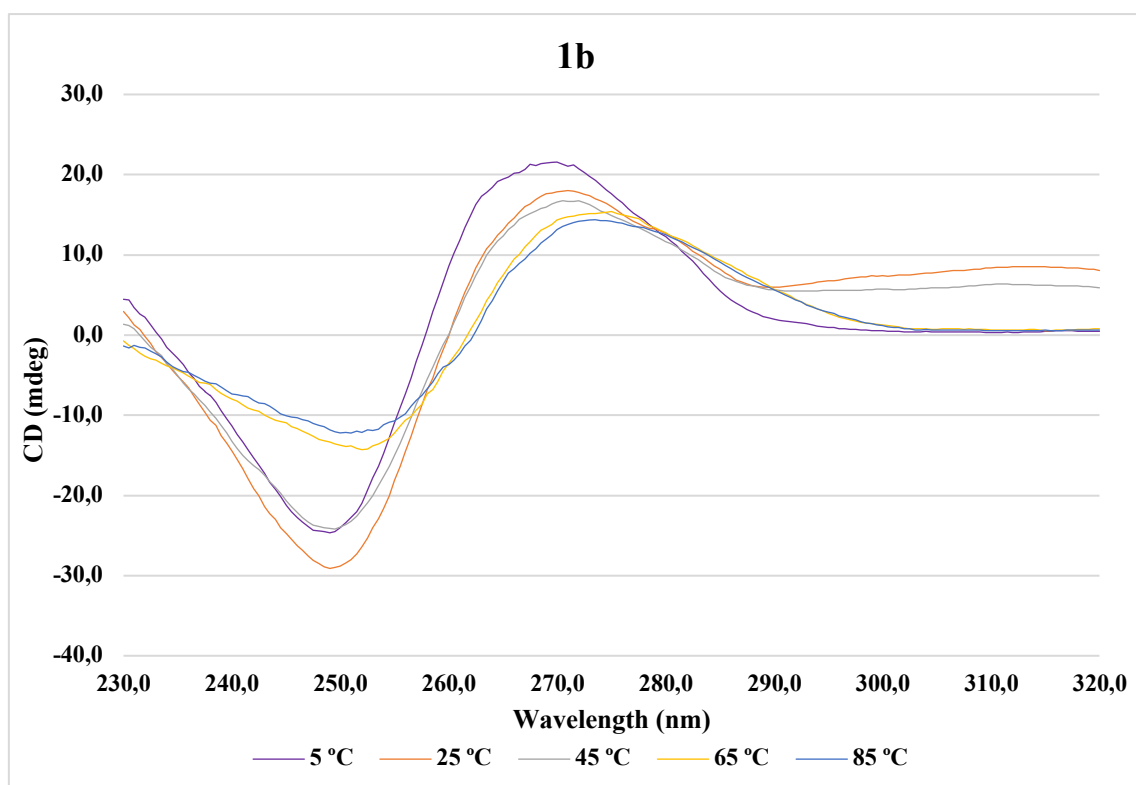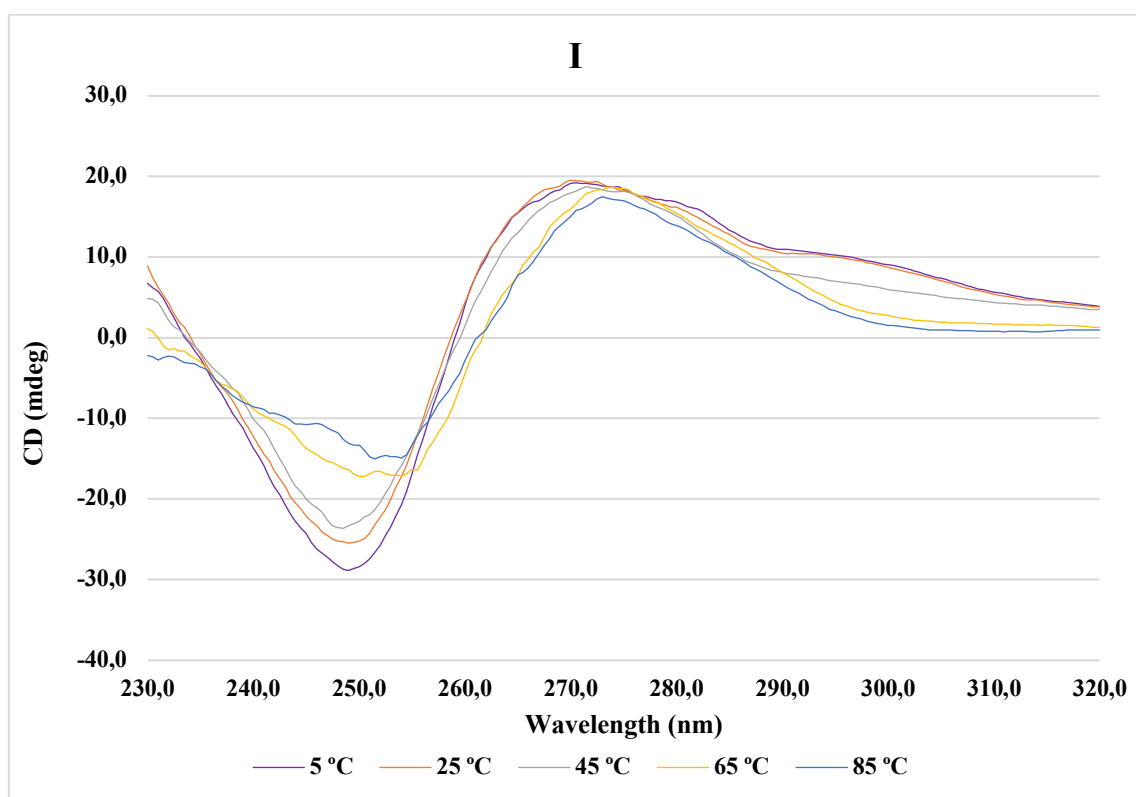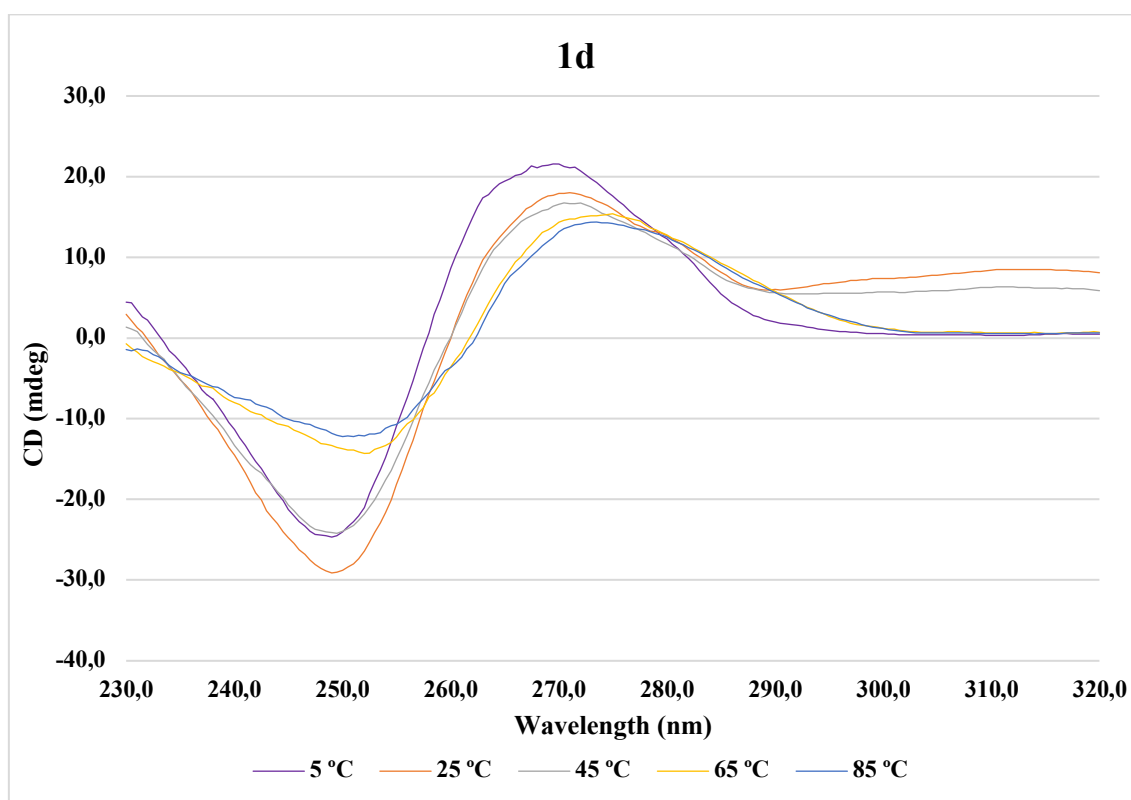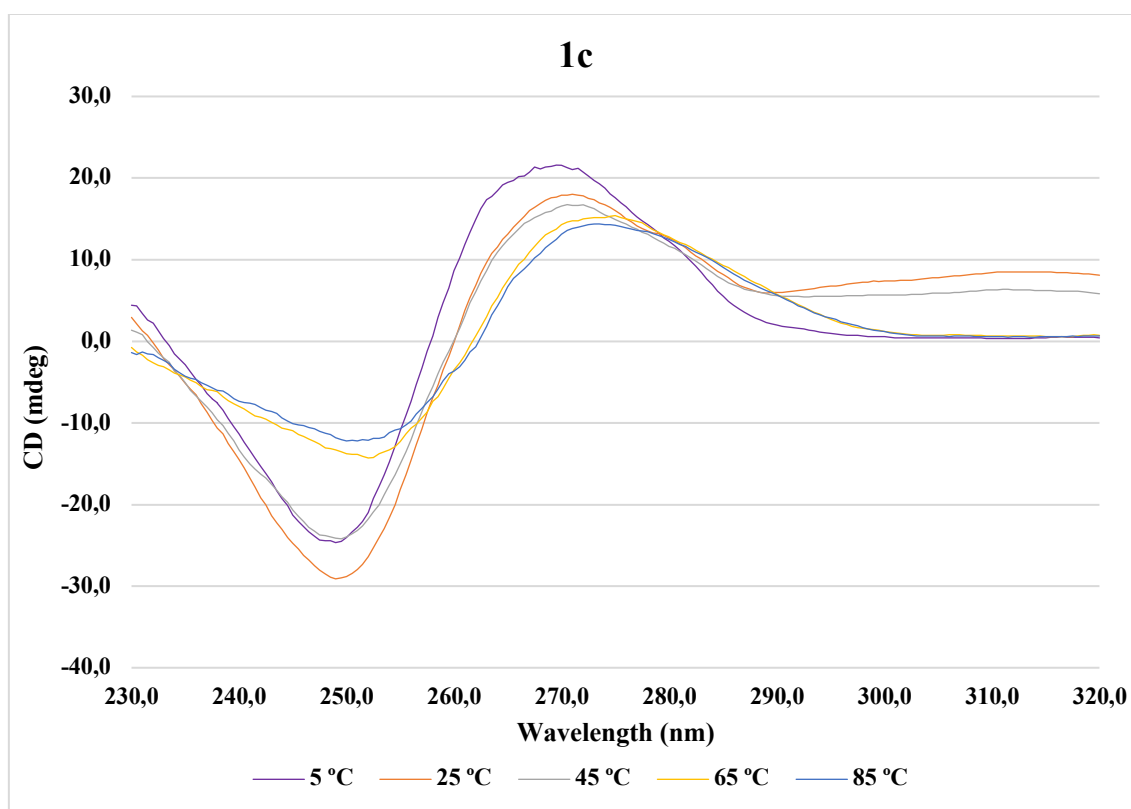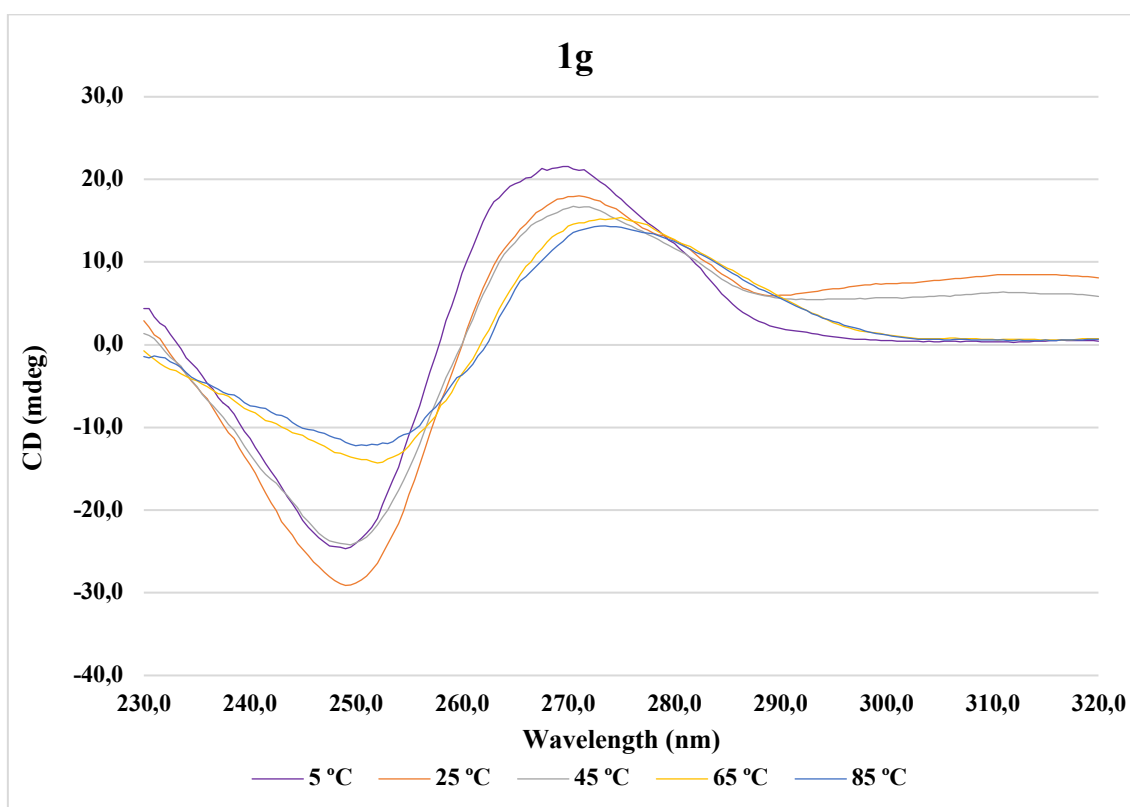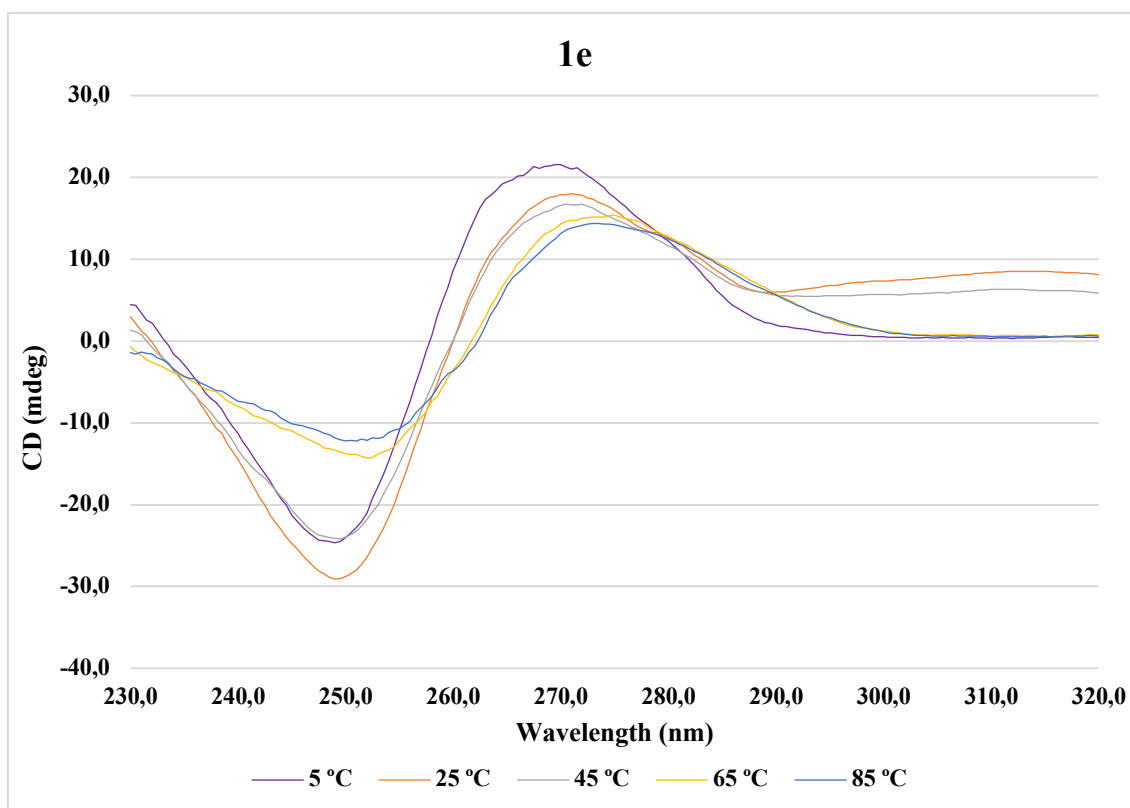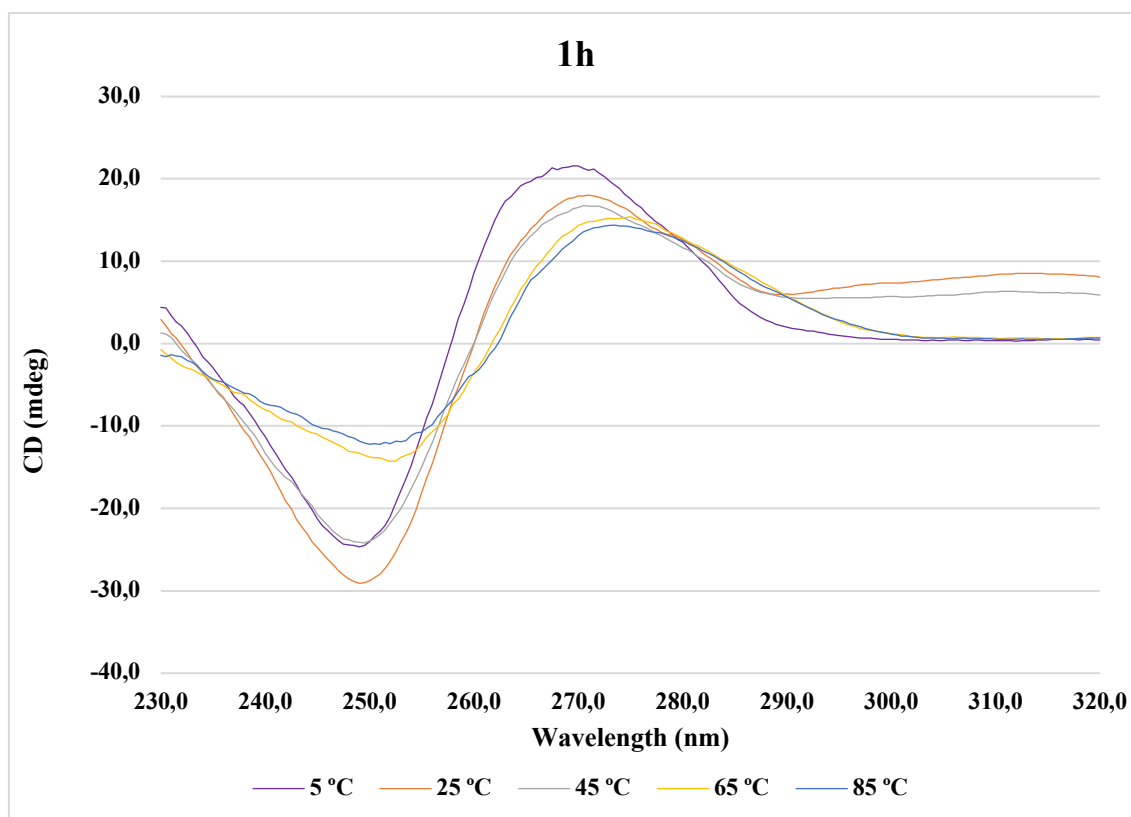
1c

1d

1h
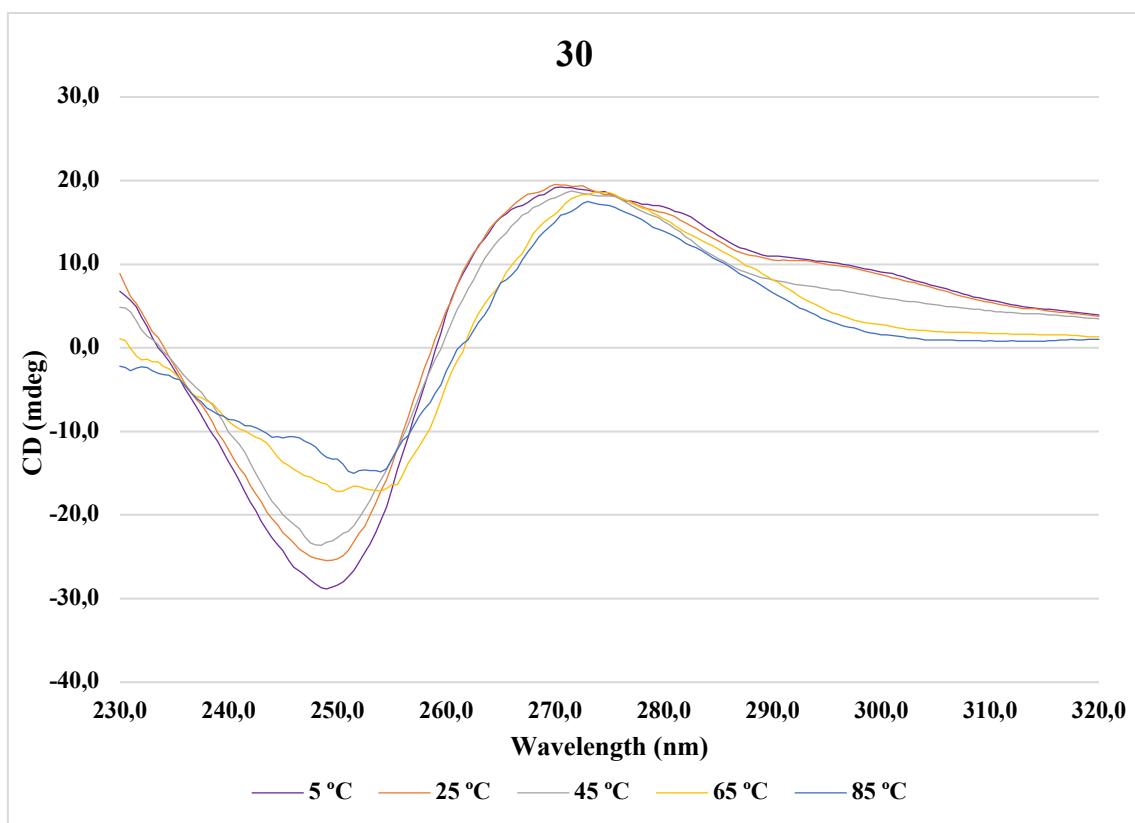
Circular Dichroism spectra of compounds from series **2.**

2c

2d

2e

2h

34
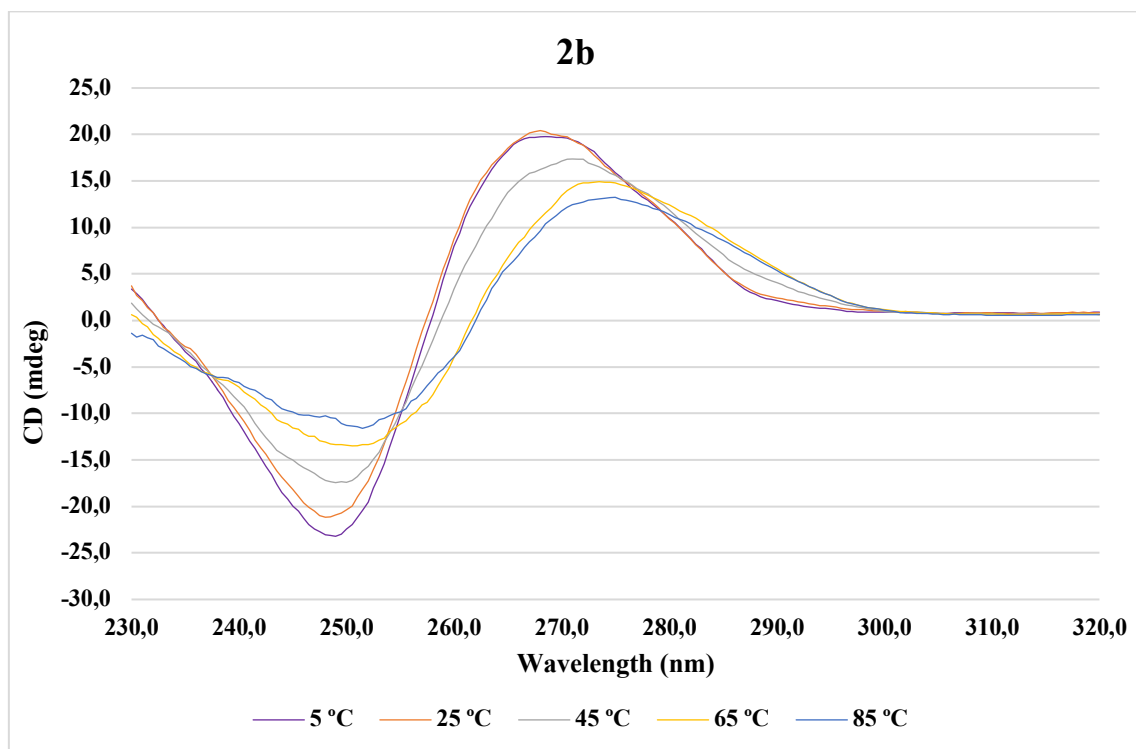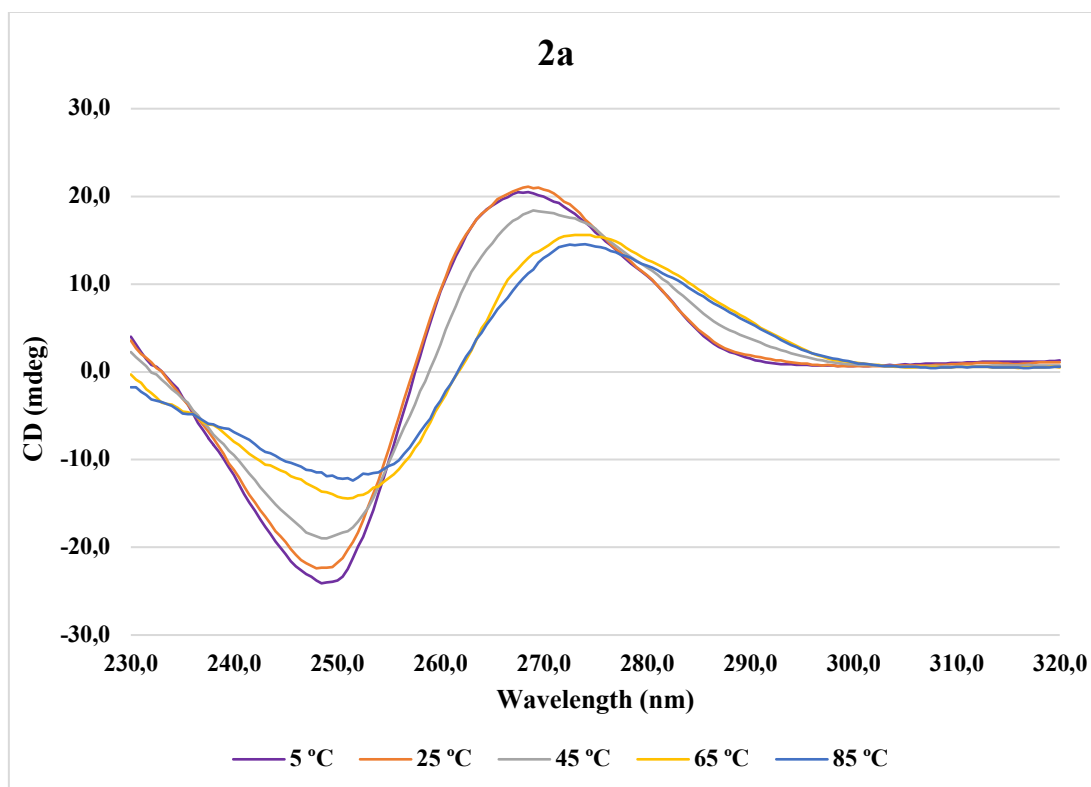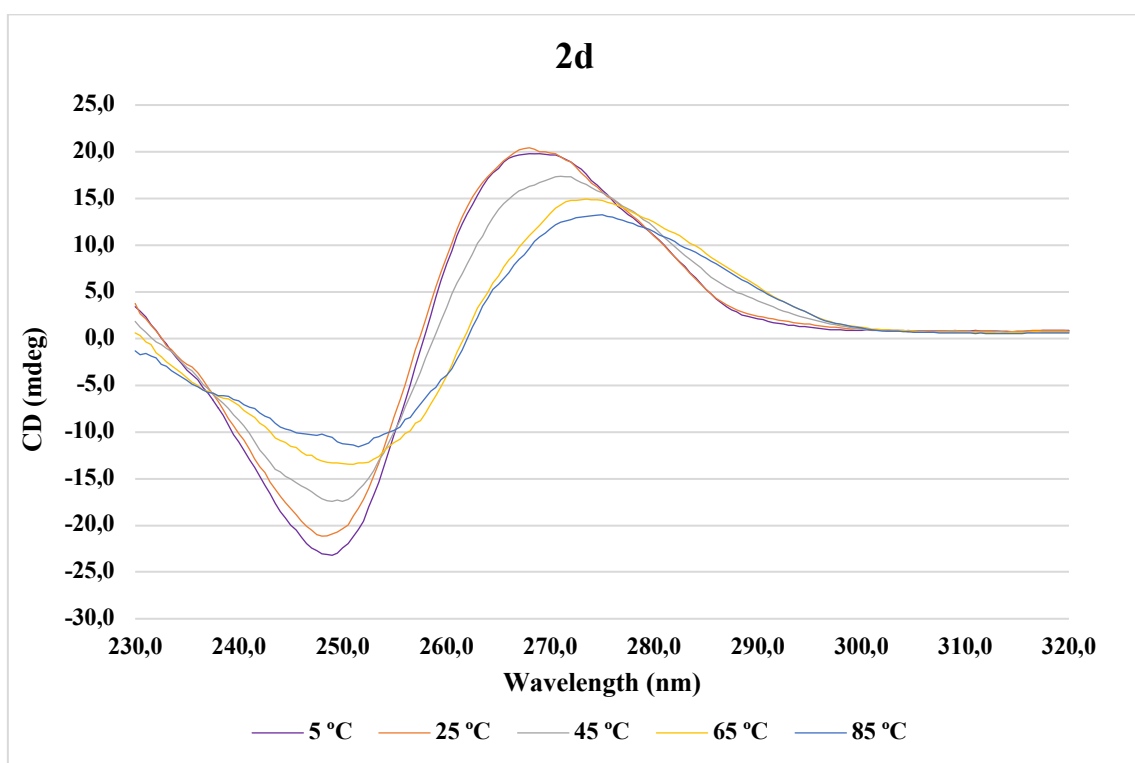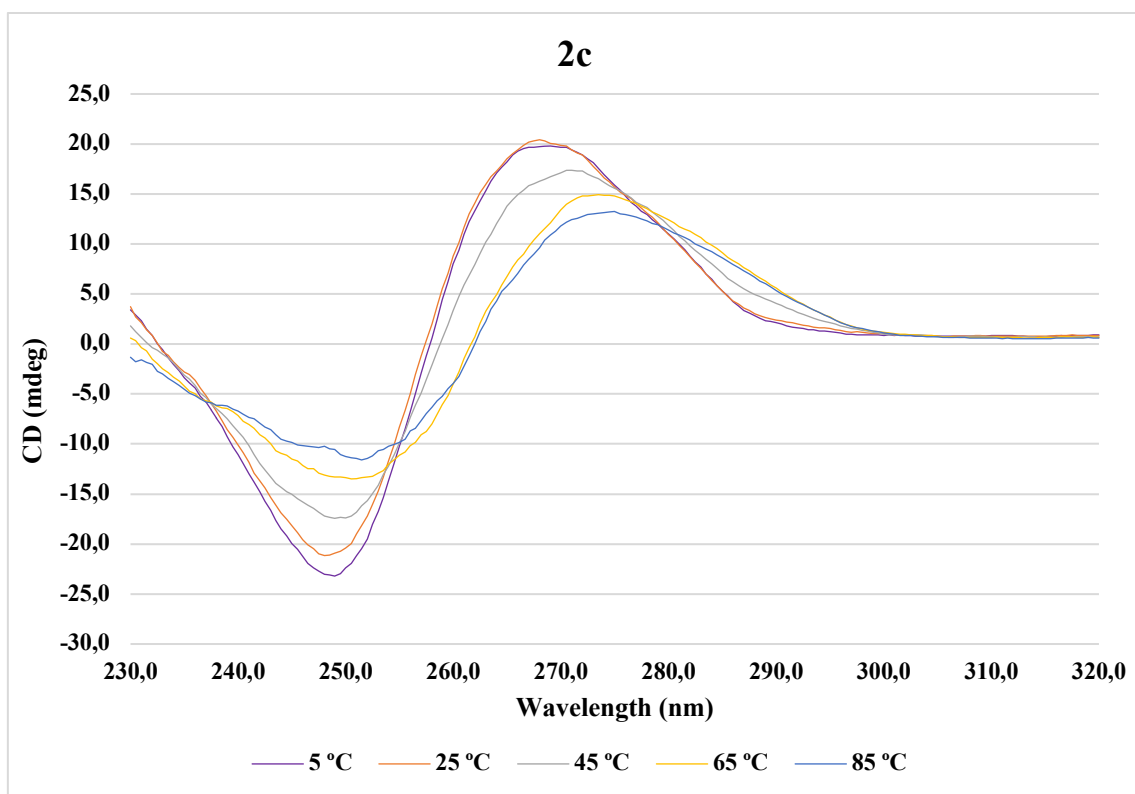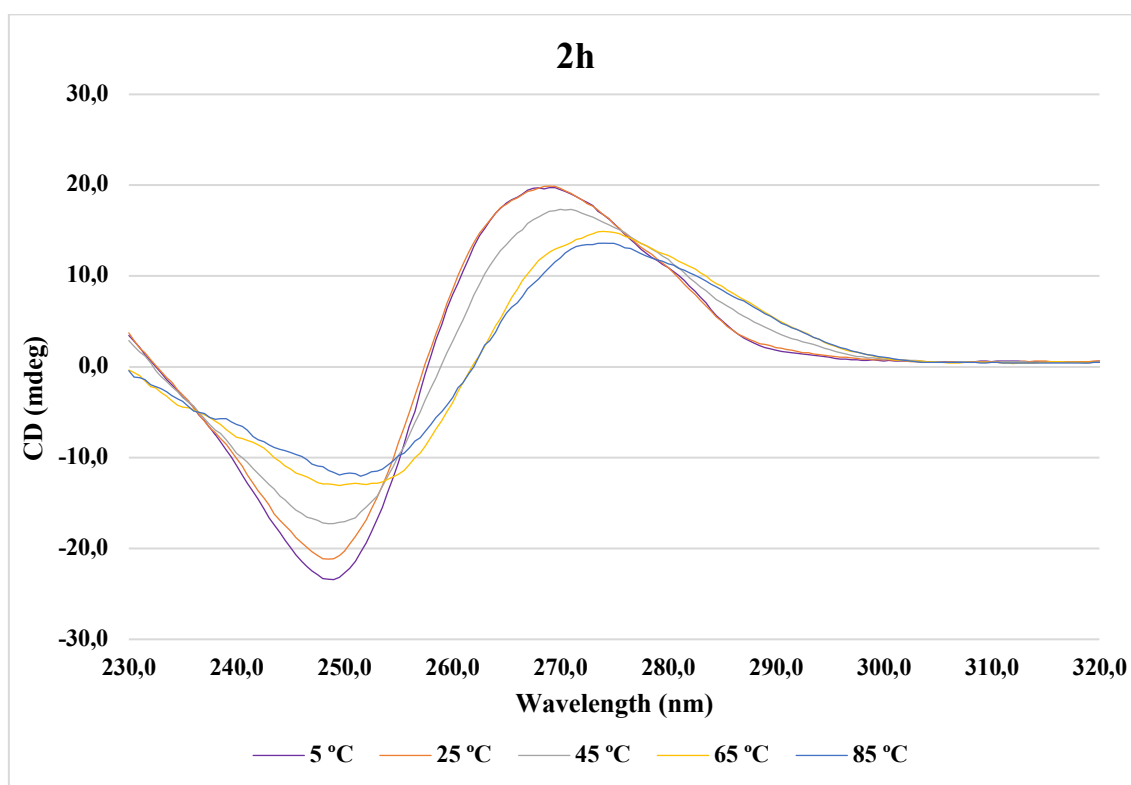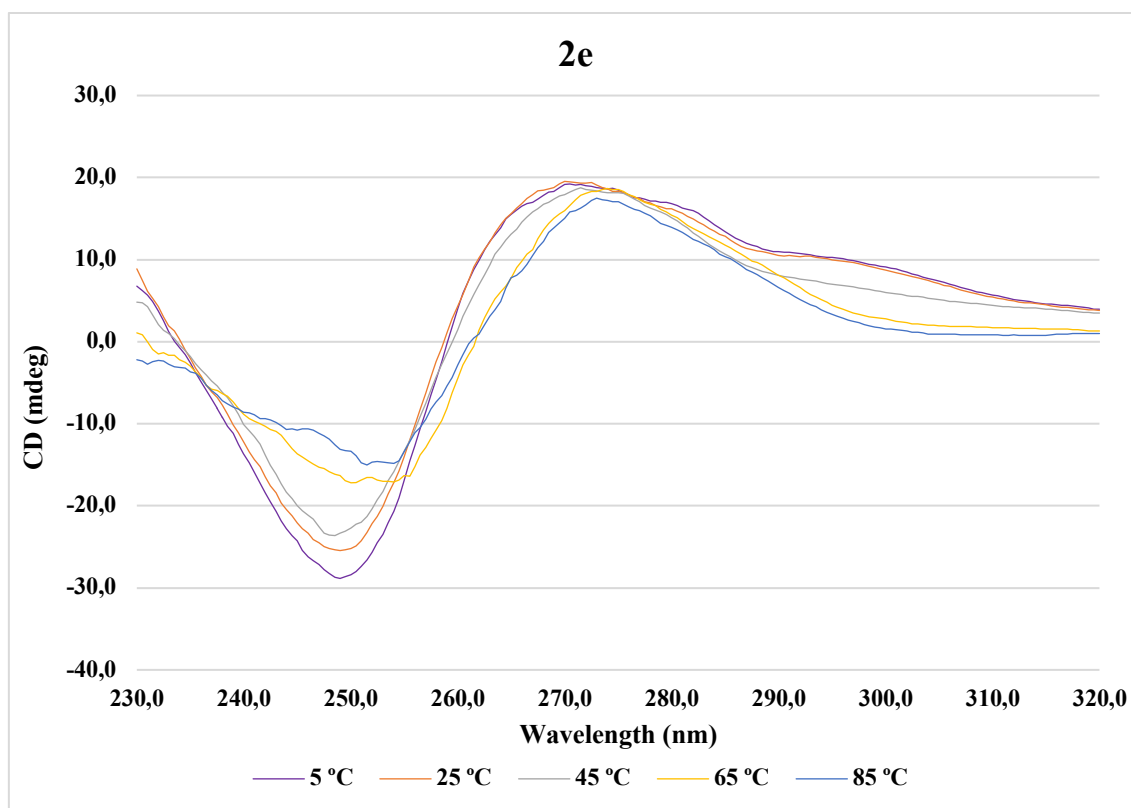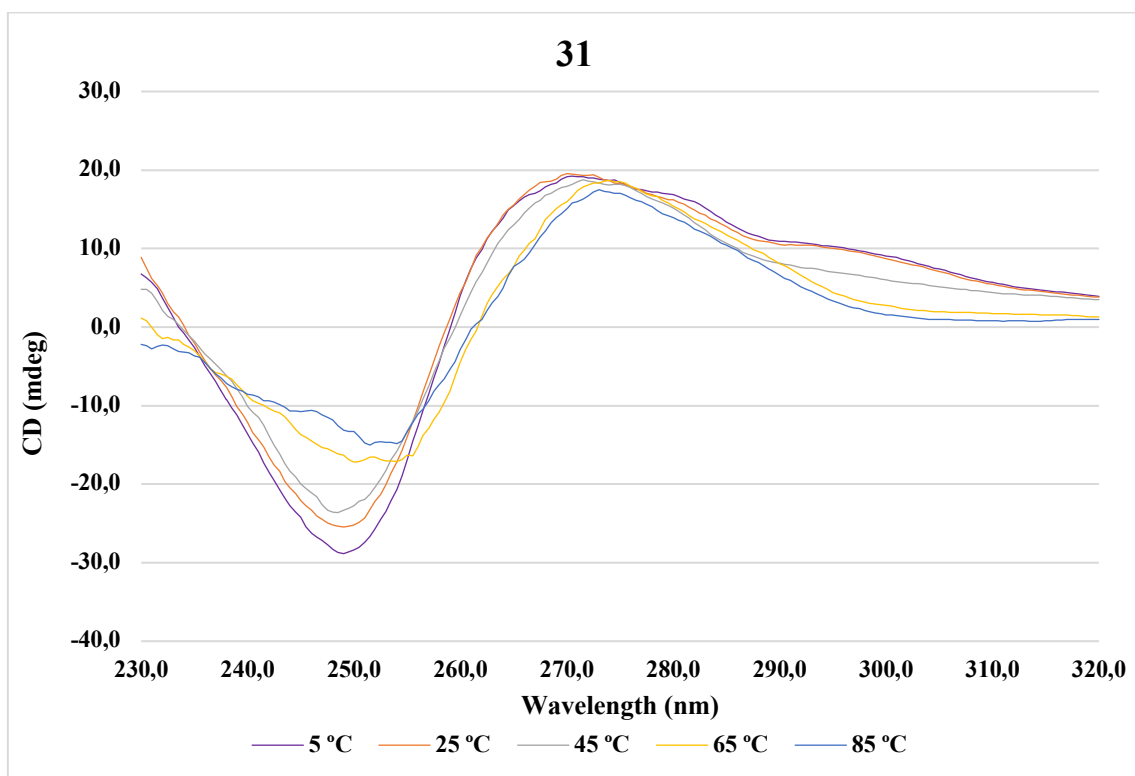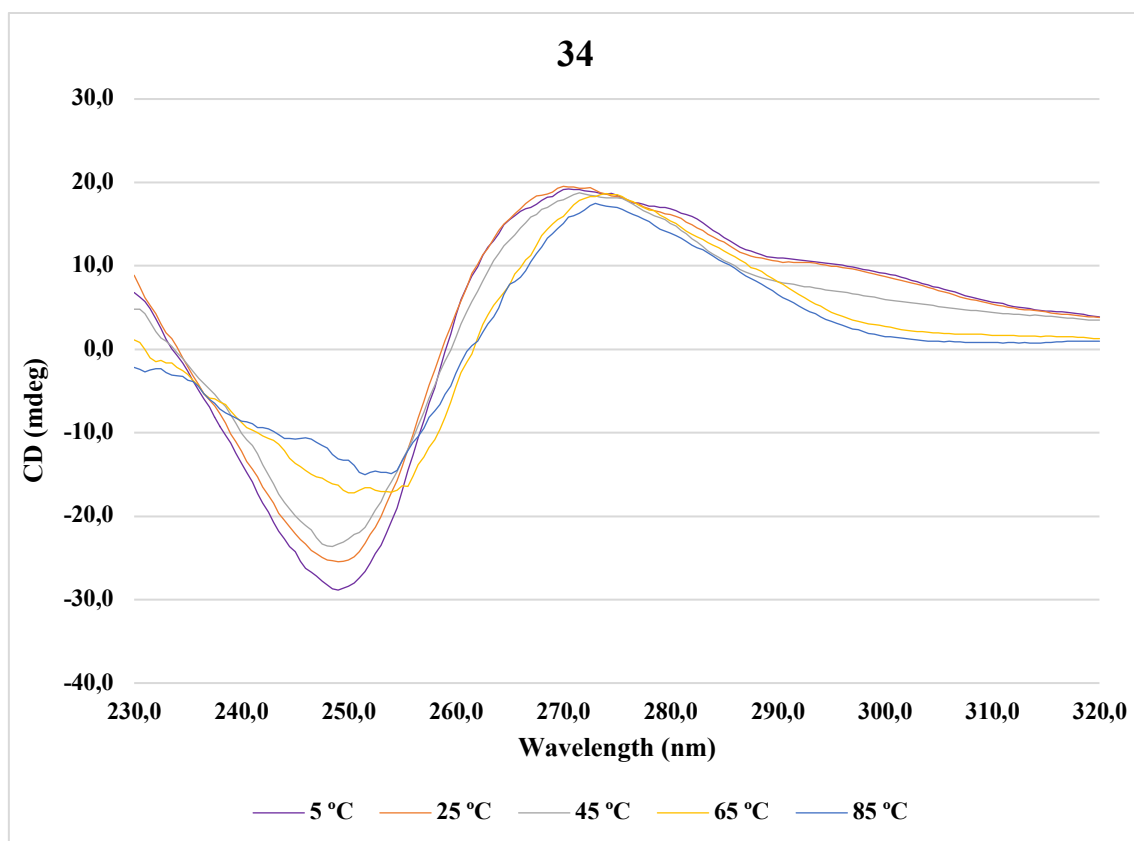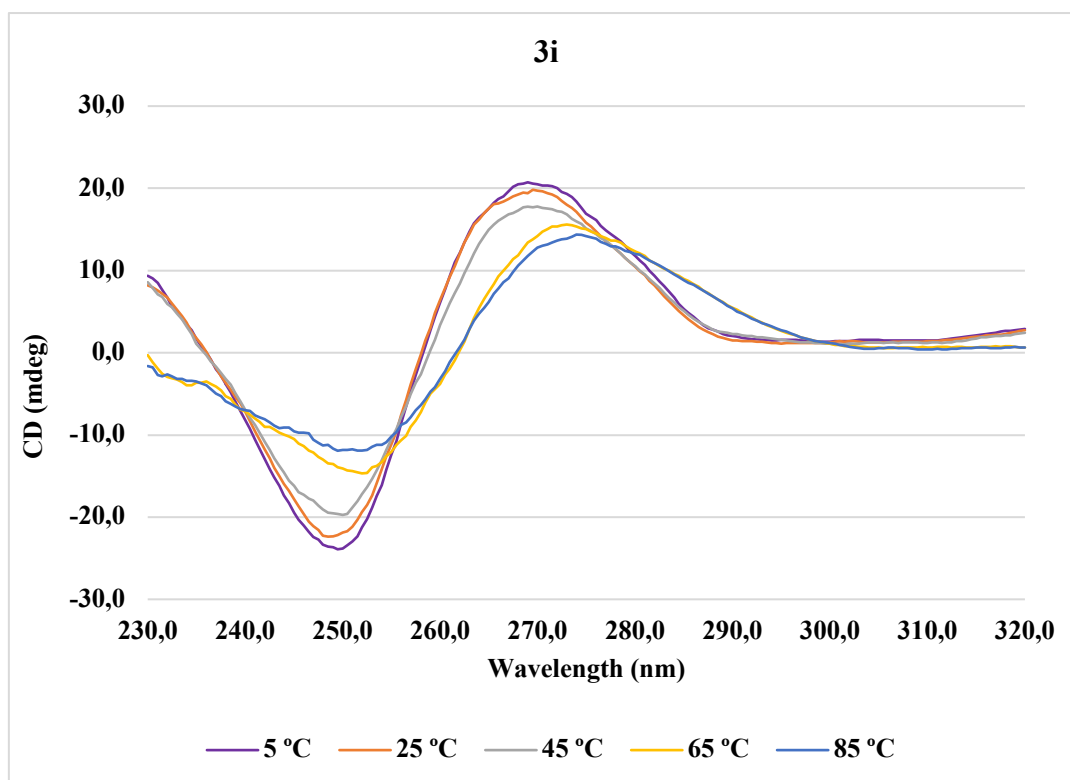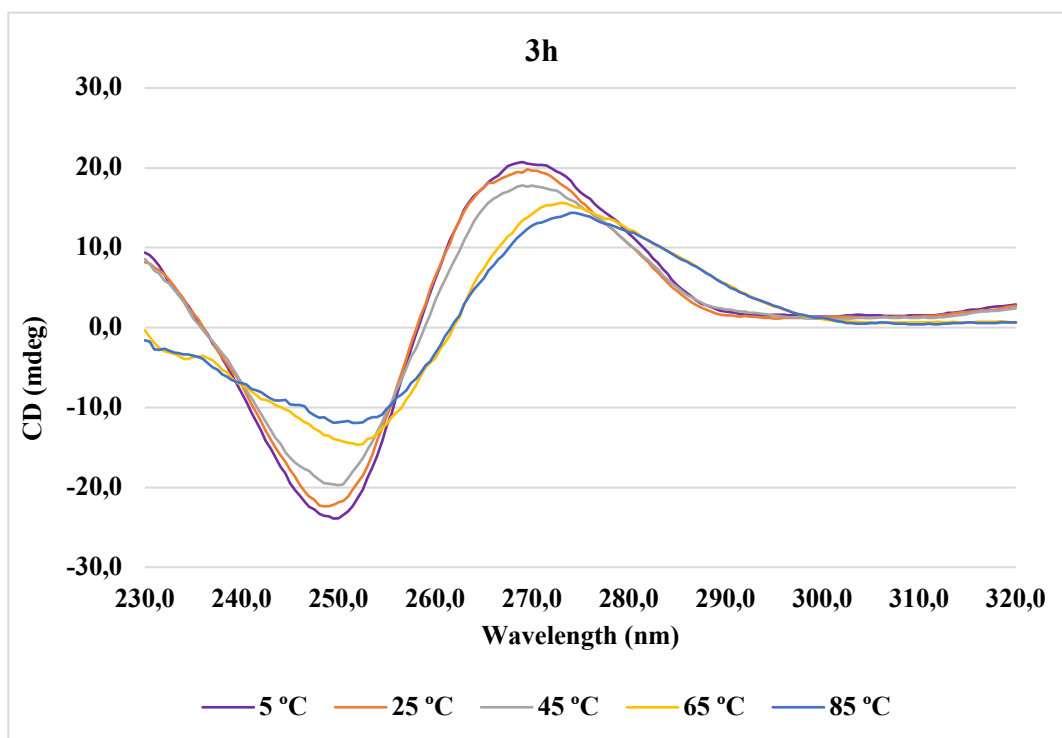
Circular Dichroism spectra of compounds from series **3.**

3e

3g

3h

3i

36

37

53
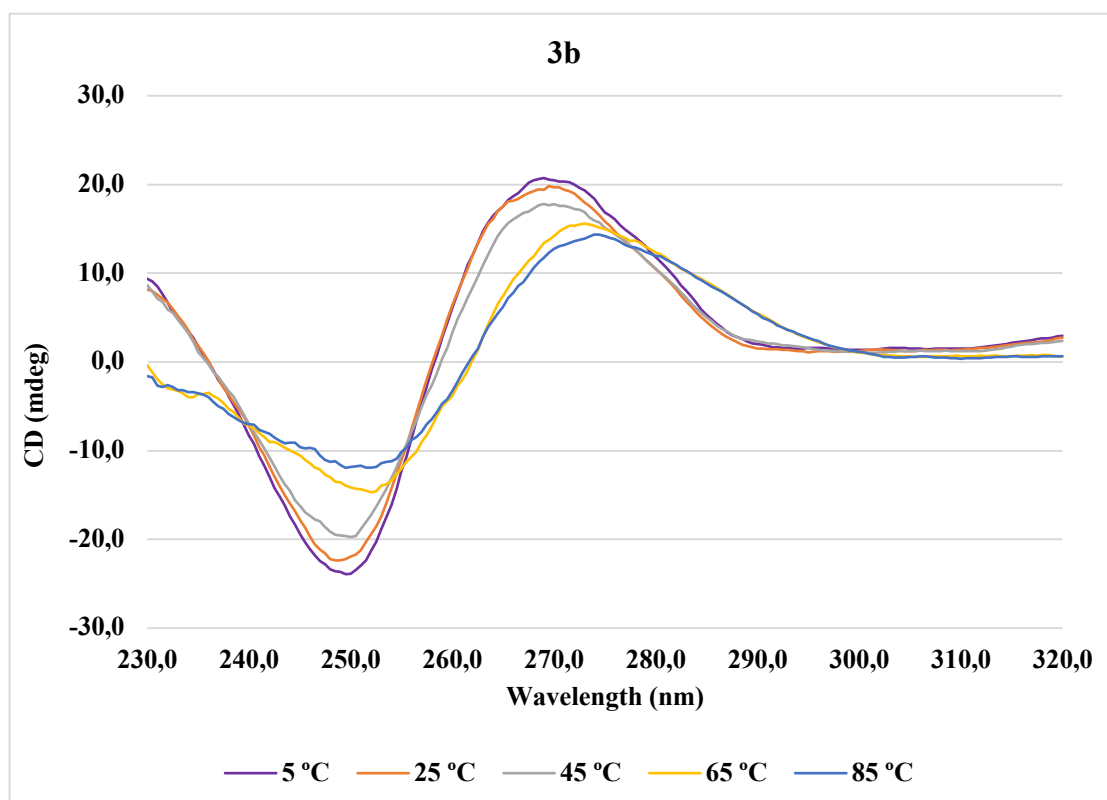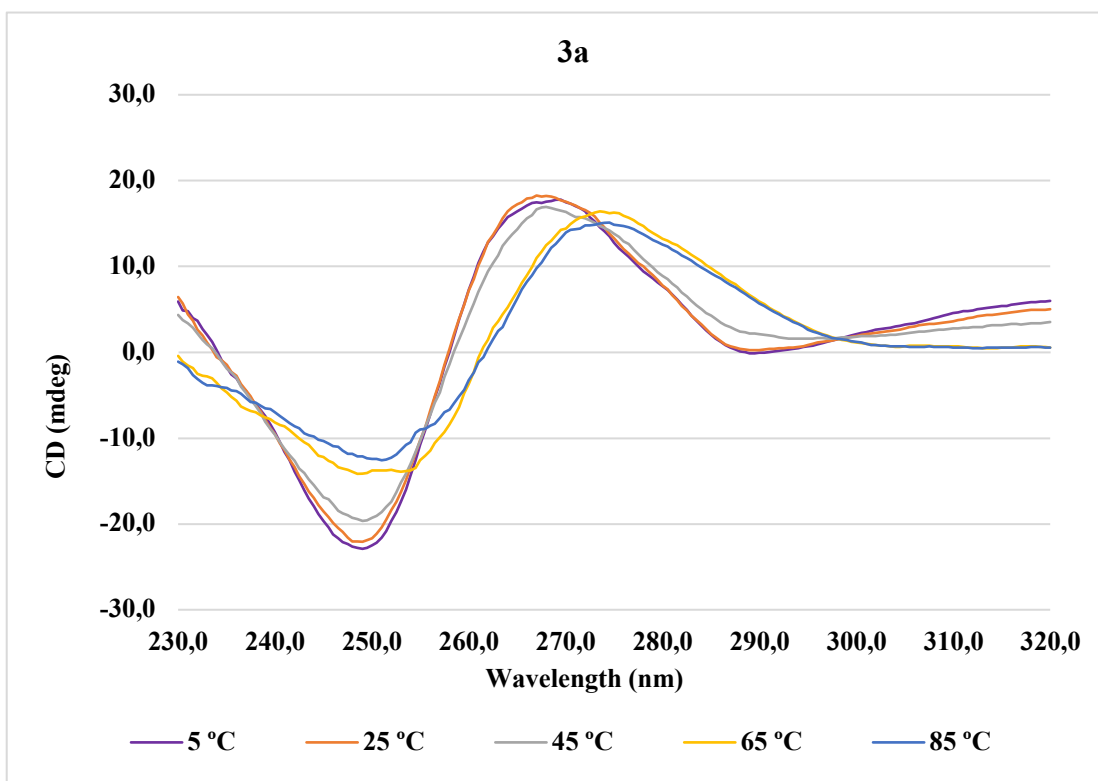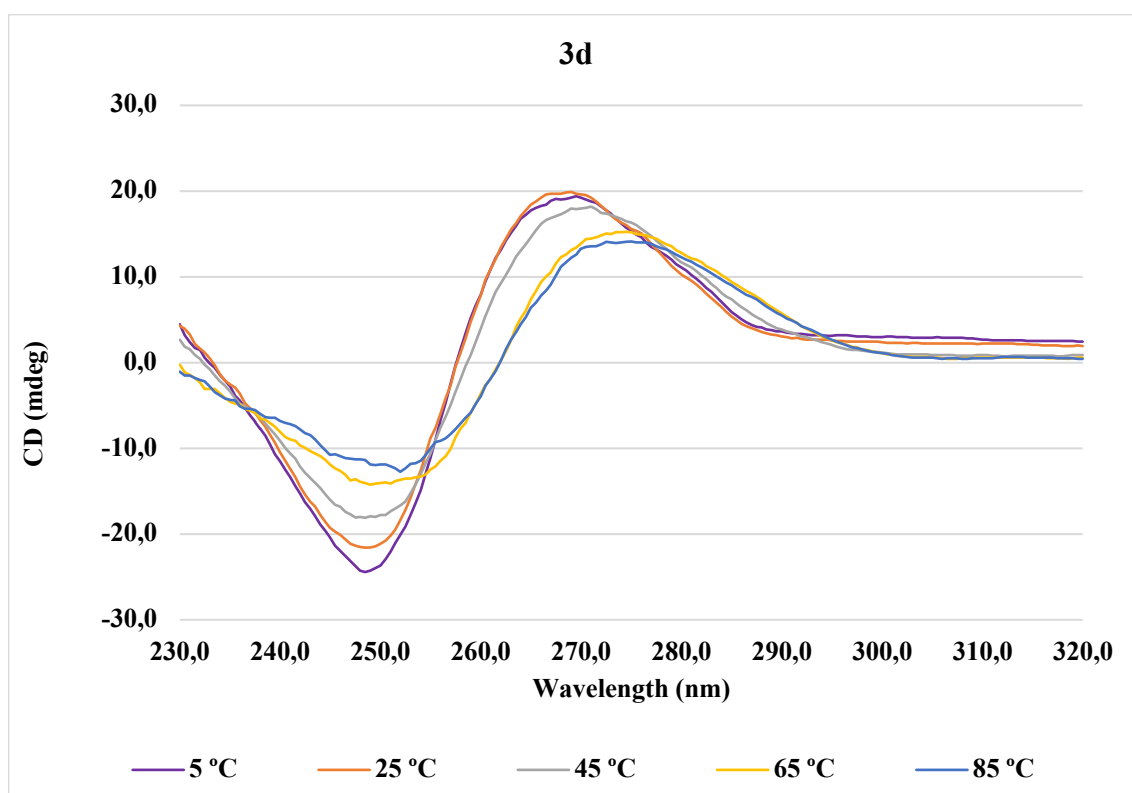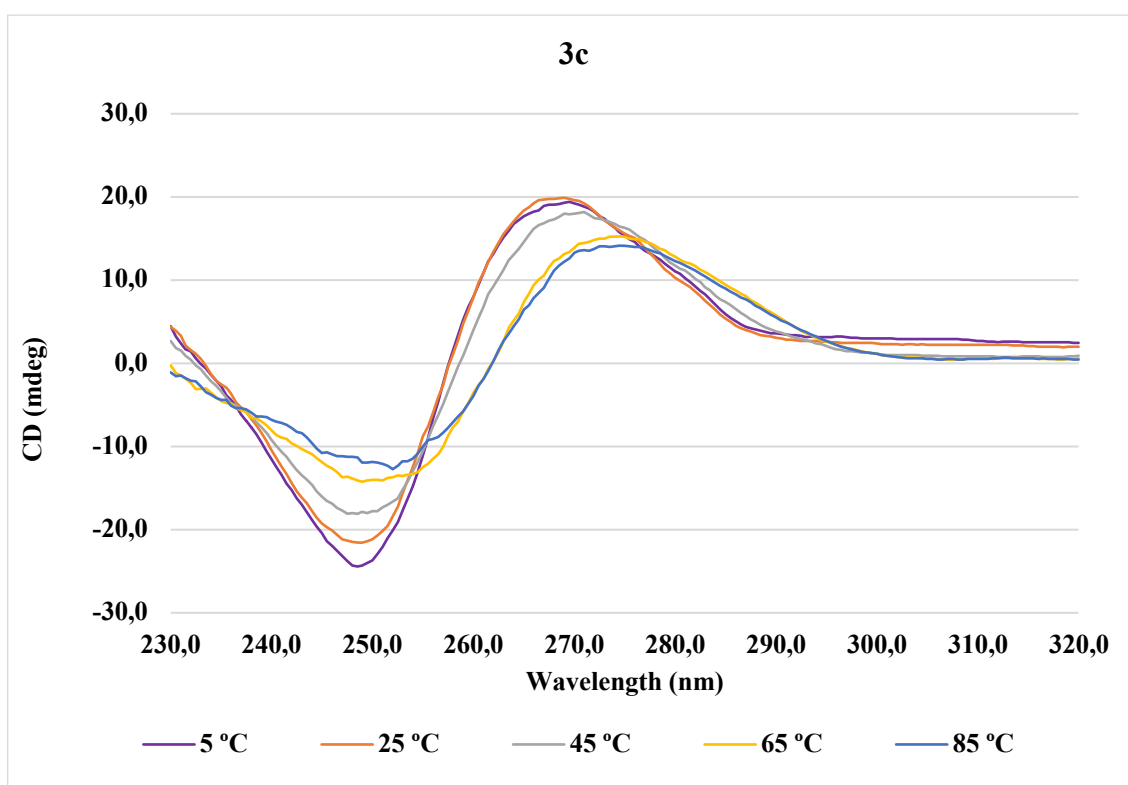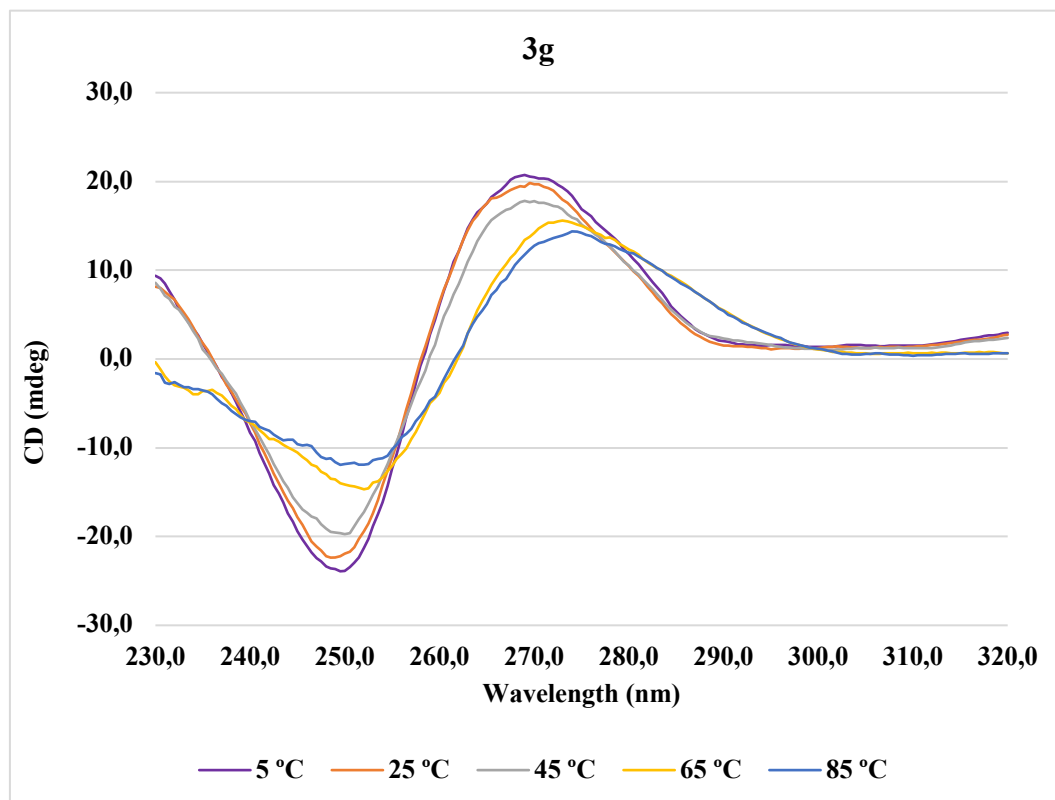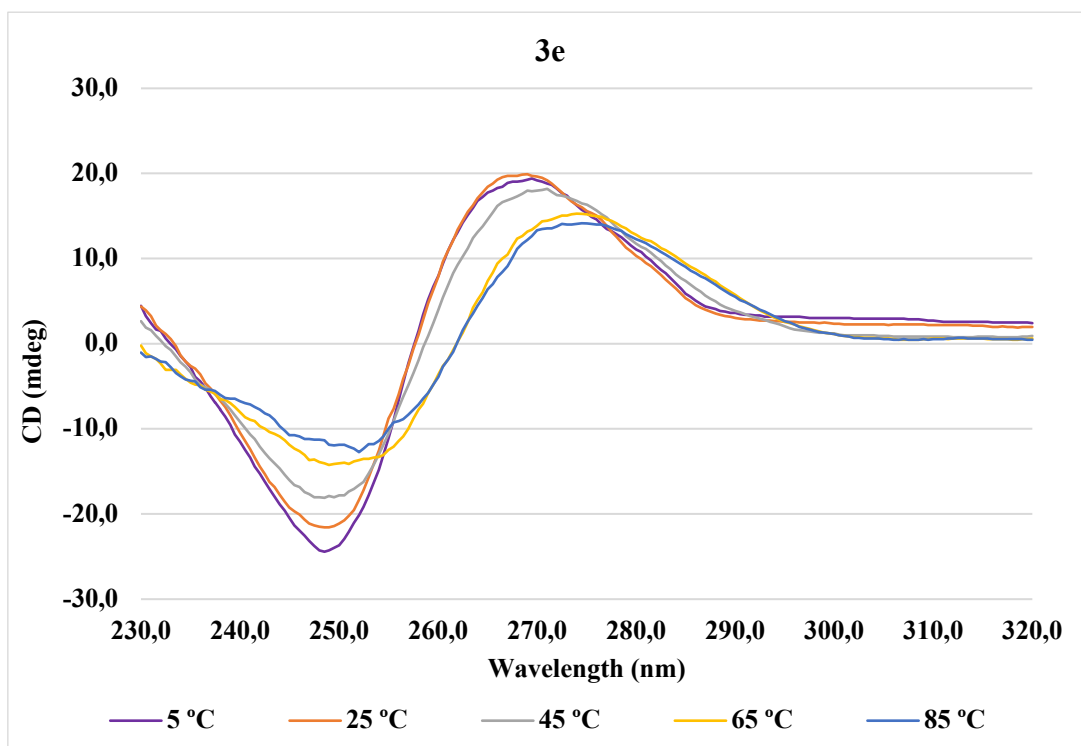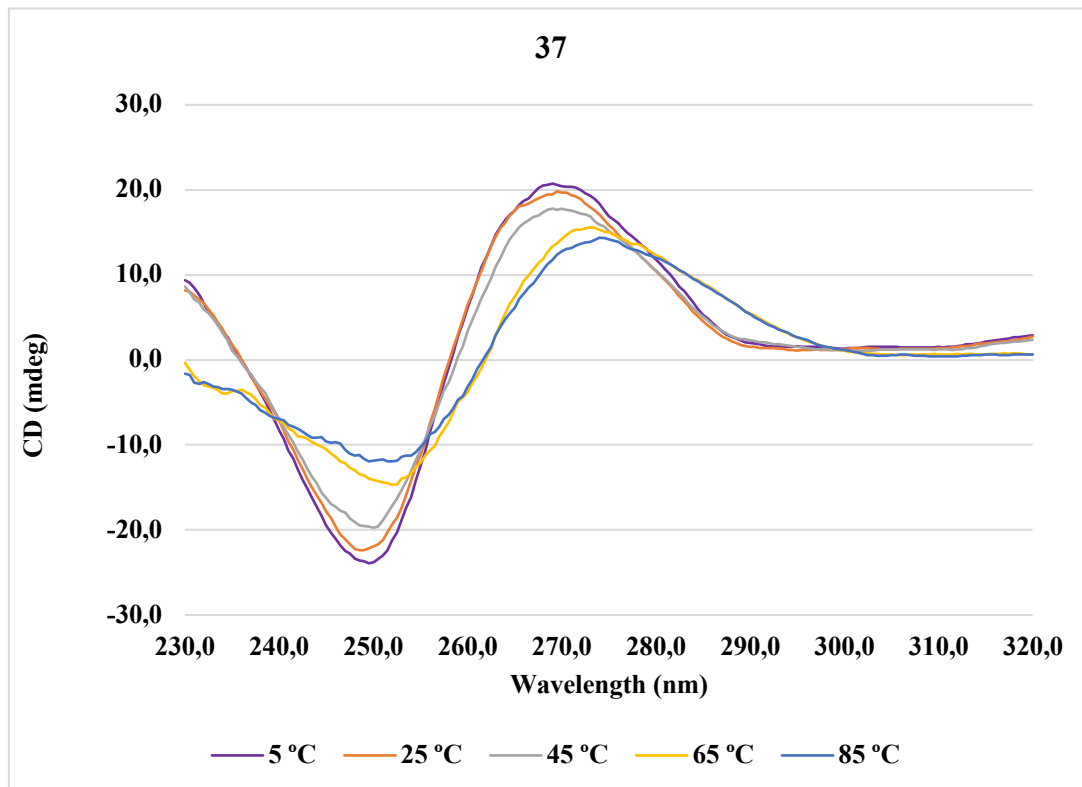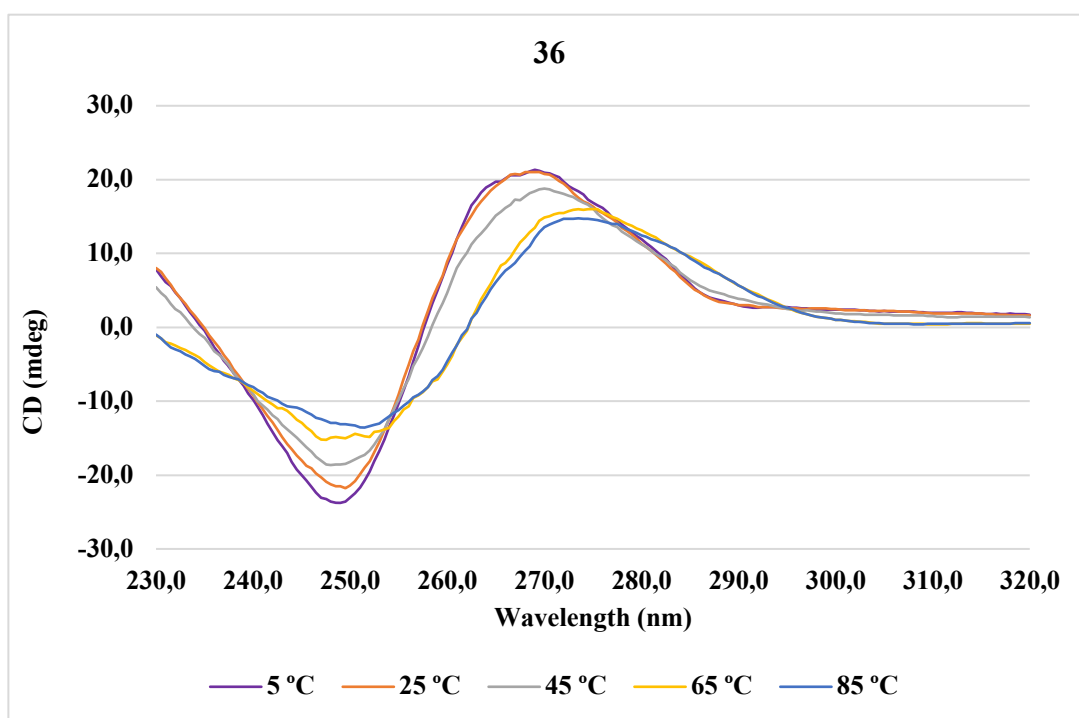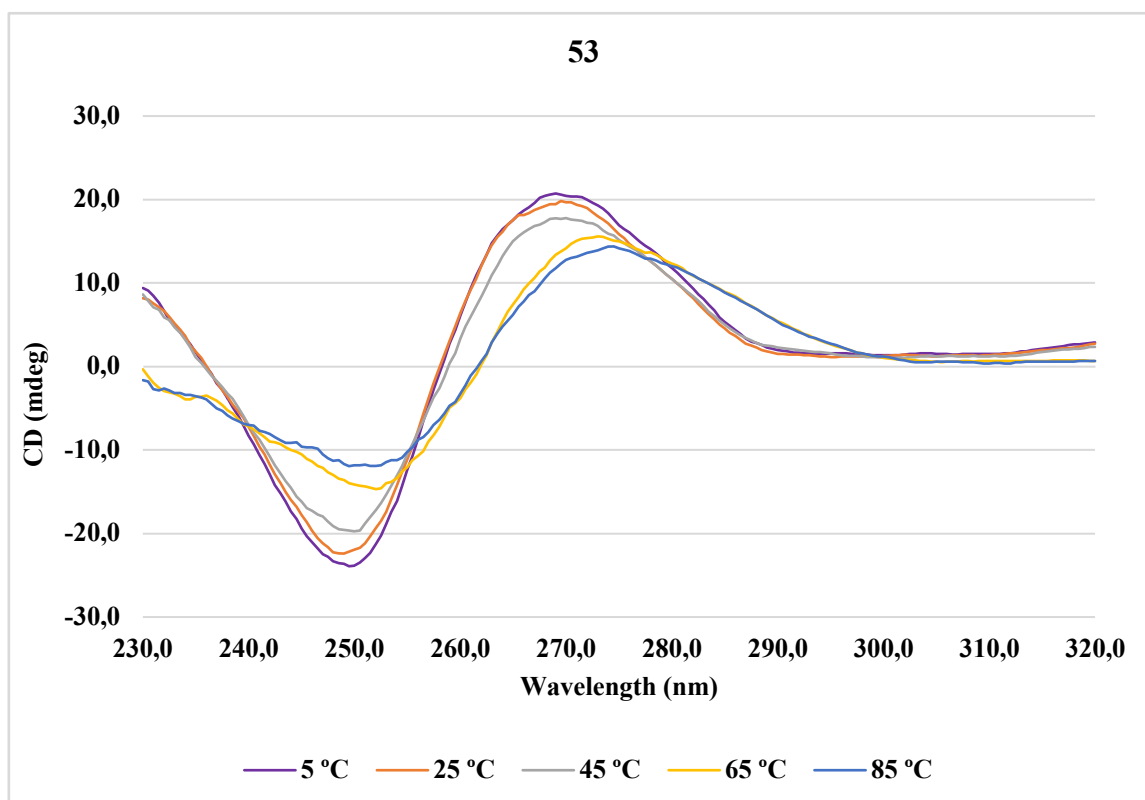
APPENDIX 3

Appendix 3

Crystallographic conditions for the growth of crystalls

	pH	Compound	Oligo
J.I.A.	pH=6.5	**1g**	CGA2T2
J.I.B.	pH=6.5	**1g**	CGA2T2
J.I.D.	pH=6.5	**1g**	CGA3
J.I.F.	pH=6.5	**1g**	A3TA
J.II.B	pH=6.5	**1c**	CGA2T2
J.II.D	pH=6.5	**1c**	CGA3
J.II.F	pH=6.5	**1c**	A3TA
J.III.B.	pH=6.5	**3a**	CGA2T2
J.III.C.	pH=6.5	**3a**	A2TA2
J.III.D.	pH=6.5	**3a**	CGA3
J.III.E.	pH=6.5	**3a**	AT2A2
J.III.F.	pH=6.5	**3a**	A3(TA)2T3
J.III.G.	pH=6.5	**3a**	ATA2T
J.III.H.	pH=6.5	**3a**	AT2AT2
J.III.E.BIS	pH=6.5	**3a**	AT2A2
J.III.F.BIS	pH=6.5	**3a**	A3TA
J.IV.B	pH=6.5	**36**	CGA2T2
J.IV.C.	pH=6.5	**36**	A2TA2
J.IV.D.	pH=6.5	**36**	CGA3
J.IV.E.	pH=6.5	**36**	AT2A2
J.IV.F.	pH=6.5	**36**	A3TA